

THE JOURNAL OF PHYSICAL CHEMISTRY

Volume 69, Number 8 August 1965

Diffusion in Carbon Tetrachloride-Cyclohexane Solutions	M. V. Kulkarni, G. F. Allen, and P. A. Lyons	2491
Hydrogen-Bonding Properties of Alcohols	Asish Kumar Chandra and Abani Bhusan Sannigrahi	2494
Sites for Hydrogen Adsorption on Zinc Oxide	Richard Narvaez and H. Austin Taylor	2500
The Thermodynamics of the Yttrium-Hydrogen System	L. N. Yannopoulos, R. K. Edwards, and P. G. Wahlbeck	2510
Rates of Decay of Phosphorescence from Triphenylene in Acrylic Polymers	F. C. Unterleitner and E. I. Hormats	2516
Scaling in Isoelectronic Molecules	Jerry Goodisman	2520
Radiation Chemistry of Some Cyclic Fluorocarbons	D. R. MacKenzie, F. W. Bloch, and R. H. Wiswall, Jr.	2526
Mass Spectrometric Study of Zirconium Diboride	O. C. Trulson and H. W. Goldstein	2531
Equilibria in Ethylenediamine. III. Determination of Absolute pK Values of Acids and Silver Salts. Establishment of a pH and pAg Scale	L. M. Mukherjee, Stanley Bruckenstein, and F. A. K. Badawi	2537
The Photochemical and Thermal Isomerization of <i>trans</i> - and <i>cis</i> - α -Cyano- α -phenyl-N-phenylnitrones	Kinko Koyano and Ikuzo Tanaka	2545
Thermodynamics of the Higher Oxides. I. The Heats of Formation and Lattice Energies of the Superoxides of Potassium, Rubidium, and Cesium	L. A. D'Orazio and R. H. Wood	2550
Thermodynamics of the Higher Oxides. II. Lattice Energies of the Alkali and Alkaline Earth Peroxides and the Double Electron Affinity of the Oxygen Molecule	R. H. Wood and L. A. D'Orazio	2558
Thermodynamics of the Higher Oxides. III. The Lattice Energy of Potassium Ozonide and the Electron Affinity of Ozone	R. H. Wood and L. A. D'Orazio	2562
Nuclear Magnetic Resonance Dilution Shifts for Carboxylic Acids in Rigorously Dried Solvents. I. Acetic Acid in Acetic Anhydride, Acetone, and 1,4-Dioxane	Norbert Muller and Philip I. Rose	2564
Hindered Rotation and Carbon-13-Hydrogen Coupling Constants in Amides, Thioamides, and Amidines	Robert C. Neuman, Jr., and L. Brewster Young	2570
Electrolyte-Solvent Interaction. XVI. Quaternary Salts in Cyanoethylsucrose-Acetonitrile Mixtures	Claude Treiner and Raymond M. Fuoss	2576
The Conductance of Symmetrical Electrolytes. V. The Conductance Equation	Raymond M. Fuoss, Lars Onsager, and James F. Skinner	2581
The Effect of Pressure on the Dissociation of Manganese Sulfate Ion Pairs in Water	F. H. Fisher and D. F. Davis	2595
Adsorption of Nonylphenoxyacetic Acid by Metals	Jerry E. Berger	2598
Surface Tension of Liquid Alkali Halide Binary Systems	G. Bertozzi	2606
Solubilities of Argon and Nitrogen in Sea Water	Everett Douglas	2608
Thermodynamic Properties of Nonaqueous Solutions. I. Heats of Solution of Selected Alkali Metal Halides in Anhydrous N-Methylformamide	Robert P. Held and Cecil M. Criss	2611
Calculation of the Hall Effect in Ionic Solutions	Harold L. Friedman	2617
Radiolysis of Heavy Water in the pD Range 0-14	E. Hayon	2628
Kinetics of the Ethyl Chlorophyllide Sensitized Photoreduction of Phenosafranine by Hydrazobenzene	G. R. Seely	2633

The Radiation-Induced <i>cis-trans</i> Isomerization of Polybutadiene. IV	Morton A. Golub	2639
The 300- μ Band of NO_3^-	Eitan Rotlevi and Avner Treinin	2645
The Acidity Function, H_0 , of Hydrogen Bromide in Acetic Acid-Water Mixtures	Walter W. Zajac, Jr., and Robert B. Nowicki	2649
A Thermodynamic Study of the Ionization of 3-Amino-4-methylbenzenesulfonic Acid	Paul J. Conn and D. F. Swinehart	2653
Thermal Properties of Atactic and Isotactic Polystyrene	F. E. Karasz, H. E. Bair, and J. M. O'Reilly	2657
Specific Heat of Synthetic High Polymers. XII. Atactic and Isotactic Polystyrene	Ismat Abu-Isa and Malcolm Dole	2668
Desorption of Olefins from Silica-Alumina Catalysts	Yutaka Kubokawa	2676
The Effect of Aromatic Solvents on Proton Magnetic Resonance Spectra	Theodore L. Brown and Kurt Stark	2679
Vaporization, Thermodynamics, and Dissociation Energy of Lanthanum Monosulfide	E. David Cater, Thomas E. Lee, Ernest W. Johnson, Everett G. Rauh, and Harry A. Eick	2684
A Differential Vapor Pressure Study of the Self-Association of Acids and Bases in 1,2-Dichloroethane and Certain Other Solvents	J. F. Coetzee and Rose Mei-Shun Lok	2690
Properties of Organic-Water Mixtures. III. Activity Coefficients of Sodium Chloride by Cation-Sensitive Glass Electrodes	R. D. Lanier	2697
The Radiation Chemistry of Cyclopentane	B. Mason Hughes and Robert J. Hanrahan	2707
An Infrared Study of the Dimerization of Trimethylacetic Acid in Carbon Tetrachloride Solution	T. C. Chiang and R. M. Hammaker	2715
The Effect of Urea on the Structure of Water and Hydrophobic Bonding	Mohammad Abu-Hamdiyyah	2720
Electrical Conductances of Aqueous Solutions at High Temperature and Pressure. II. The Conductances and Ionization Constants of Sulfuric Acid-Water Solutions from 0 to 800° and at Pressures up to 4000 Bars	Arvin S. Quist, William L. Marshall, and H. R. Jolley	2726
Mass Spectrometric Study of the Reaction of Nitrogen Atoms with Ethylene	John T. Herron	2736
Effect of Adsorbed Polyelectrolytes on the Polarographic Currents. I	I. R. Miller	2740
The Vapor Pressure and Enthalpy of Arsenic Triiodide and Its Absolute Entropy at 298°K.	Daniel Cubicciotti and Harold Eding	2743
On the Unification of the Thermal and Chain Theories of Explosion Limits	B. F. Gray and C. H. Yang	2747
Dissociation Constant of Acetic Acid in Deuterium Oxide from 5 to 50°. Reference Points for a pD Scale	Robert Gary, Roger G. Bates, and R. A. Robinson	2750
Excess Properties of Some Aromatic-Alicyclic Systems. I. Measurements of Enthalpies and Volumes of Mixing	A. E. P. Watson, I. A. McLure, J. E. Bennett, and G. C. Benson	2753
Excess Properties of Some Aromatic-Alicyclic Systems. II. Analyses of H^E and V^E Data in Terms of Three Different Theories of Molecular Solutions	I. A. McLure, J. E. Bennett, A. E. P. Watson, and G. C. Benson	2759
Solvent Effects on Charge-Transfer Complexes. II. Complexes of 1,3,5-Trinitrobenzene with Benzene, Mesitylene, Durene, Pentamethylbenzene, or Hexamethylbenzene	C. C. Thompson, Jr., and P. A. D. de Maine	2766
Kinetics of the Reactions of Elemental Fluorine. IV. Fluorination of Graphite	A. K. Kuriakose and J. L. Margrave	2772
The Reaction of Triphenylphosphine with Alkali Metals in Tetrahydrofuran	A. D. Britt and E. T. Kaiser	2775

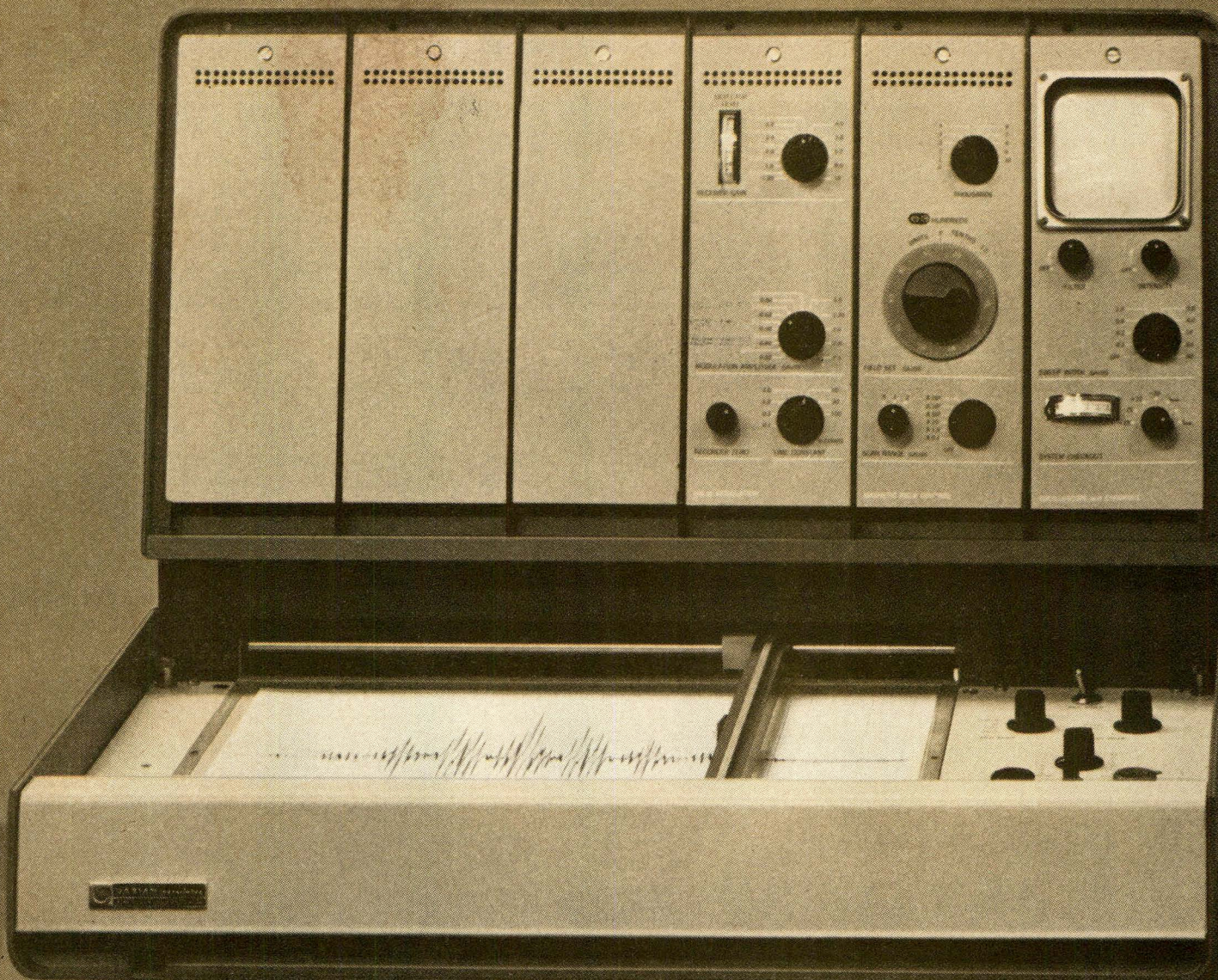
NOTES

On the Chlorophyllide-Sensitized Reduction of Azobenzene and Other Compounds	G. R. Seely	2779
Diffusion in Deuterio-Normal Hydrocarbon Mixtures	J. D. Birkett and P. A. Lyons	2782
Diffusion in the System Cyclohexane-Benzene	L. Rodwin, J. A. Harpst, and P. A. Lyons	2783
On the Compressibility of Molten Alkali Halides	E. L. Heric	2785

The Association of Cesium Chloride in Anhydrous Methanol at 25°	Robert L. Kay and James L. Hawes	2787
Solubility Behavior of Polyoxyethylene Nonylphenol Ethers in Cyclohexane and the Effect of Water by a Light-Scattering Method	Ayao Kitahara	2788
The Proton Magnetic Resonance Study of the Protonation of Pyrazine	Hirotake Kamei	2791
The Behavior of the Silver-Silver Iodide Electrode in the Presence of Tetraalkylammonium Ions	R. Fernández-Prini and J. E. Prue	2793
Effects of Experimental Parameters on the (n, γ)-Activated Reactions of Bromine with Liquid Cyclohexane	Joseph A. Merrigan and Edward P. Rack	2795
Hydrogen Bonding of Amide Groups in Dioxane Solution	H. Susi	2799
Ion-Pair Formation in Aqueous Solutions of Butylammonium Isobutyrate	Irving M. Klotz and Henry A. DePhillips, Jr.	2801

COMMUNICATIONS TO THE EDITOR

The Reaction of Methylene with CF ₂ H ₂	G. O. Pritchard, J. T. Bryant, and R. L. Thommarson	2804
The Radiolysis of Monodisperse Colloidal Sulfur	F. J. Johnston	2805
Evidence for Bromine-82m Isomeric Transition Activated Reactions in Saturated Hydrocarbons and Alkyl Halides	Joseph Andrew Merrigan and Edward Paul Rack	2806
The Volume Change on Neutralization of Strong Acids and Bases	L. A. Dunn, R. H. Stokes, and L. G. Hepler	2808
A Suggested Mechanism for the Hydrogen-Fluorine Reaction. II. The Oxygen-Inhibited Reaction	Richard S. Brokaw	2808
Parachor and Surface Tension of Amorphous Polymers	Ryong-Joon Roe	2809



ANOTHER FIRST FROM VARIAN
NEW TABLE-TOP,
LOW-PRICED EPR

Diffusion in Carbon Tetrachloride-Cyclohexane Solutions

by M. V. Kulkarni, G. F. Allen, and P. A. Lyons

Department of Chemistry, Yale University, New Haven, Connecticut (Received March 31, 1965)

Binary diffusion coefficients for the system carbon tetrachloride-cyclohexane have been measured over the entire concentration range at 25° using the Gouy interferometric technique. Sufficient data have been collected at 35° to compare activation energies for diffusive and viscous flow. Tracer diffusion coefficients for each pure component and for each component in mixtures have been measured using the stirred diaphragm cell with C¹⁴ as the tagging agent. It is demonstrated that binary diffusion data may be computed by evaluating frictional coefficients for each compound by a linear interpolation of values for each end of the concentration scale. It is shown that these computed frictional coefficients also agree with tracer diffusion values at intermediate concentrations.

Introduction

One of the difficulties associated with the prediction of binary diffusion coefficients using a reasonable guide such as that of Hartley and Crank¹

$$D = \frac{RT}{N\eta} \frac{d \ln f_1 x_1}{d \ln x_1} \left[\frac{x_1}{\sigma_2} + \frac{x_2}{\sigma_1} \right]$$

is the evident nonconstancy of their intrinsic frictional coefficients, σ_i . $D\eta/[(d \ln f_1 x_1)/(d \ln x_1)]$ is, except in the possible case of interdiffusion of labeled and non-labeled compounds, not a linear function of x_2 . (f_i is the rational activity coefficient of species i at x_i and the other quantities have their usual physicochemical meanings.) Harpst² has proposed that a sensible first-order approximation would be to assume the frictional coefficients to vary linearly between their limiting values at $x_i = 0$ and 1. He further discusses nonideal systems in terms of deviations from this approximation. Confidence in this approach would appear to depend

upon the validity of the first-order approximation for cases where it might be expected to hold.

The system carbon tetrachloride-cyclohexane provides such a test. Thermodynamic departure from ideality is small and well established.^{3,4} The molecules are not too different in size and are compact. A test of Harpst's approximation was made to compare with existing diaphragm cell binary diffusion data.⁵ The average agreement was good but the comparison showed systematic, and hence, discouraging trends.

To discover whether or not the deviation was real it was decided to redetermine the binary diffusion coefficients using the more precise Gouy optical procedure

- (1) G. S. Hartley and J. Crank, *Trans. Faraday Soc.*, **45**, 801 (1949).
- (2) J. A. Harpst, Thesis, Yale University, 1962.
- (3) G. Scatchard, S. E. Wood, and J. M. Mochel, *J. Am. Chem. Soc.*, **61**, 3206 (1939).
- (4) I. Brown and A. H. Ewald, *Australian J. Sci. Res.*, **3**, 306 (1950).
- (5) B. R. Hammond and R. H. Stokes, *Trans. Faraday Soc.*, **52**, 781 (1956).

and to remeasure tracer diffusion coefficients for each component across the concentration scale using C^{14} tagging in conjunction with the stirred diaphragm cell procedure.

Experimental

Binary diffusion coefficients at 25 ± 0.01 and $35 \pm 0.02^\circ$ were measured using the Gouy interferometric technique. The method is well described in the literature and small changes in the procedure as used in this laboratory have been detailed.⁶⁻⁸

The stirred diaphragm cell technique as perfected by Stokes is an ideal procedure for tracer studies.⁹ Several minor variations were used in this laboratory. Both Corning Pyrex disks of fine porosity and Schott Jena (Duran 50) disks of D-4 porosity were used with equal success. The stirring speed for all experiments was 60 r.p.m. The cell compartment volumes of about 30 ml. were known to 0.1%. Each compartment was fitted with a Teflon stopcock with a 2-mm. bore to accommodate syringes for the final filling and all sampling of each compartment. Aliquots of the samples were added to the vials containing scintillation liquid with a Hamilton microsyringe equipped with a Chaney adaptation. Reproducibility of aliquot samples (ranging from 0.5 ml. for cyclohexane-rich to 0.3 ml. for carbon tetrachloride-rich samples) was better than $\pm 0.1\%$ as indicated by delivered weight calibration. The vials were counted in a Packard Tri-Carb liquid scintillation spectrometer optimized in gain for each set of counting conditions. Each vial was counted ten times for 10-min. periods in sequence with the other samples in the run. The number of counts in 10 min. varied from about 10,000 (for an initial "top" compartment sample) to about 400,000 (for an initial "bottom" sample). The error in the experiments was not dependent on counting statistics. Runs in which the total initial and final counts (corrected for sampling) differed by 0.4% were eliminated.

Fisher ACS reagent grade CCl_4 and Fisher Certified reagent C_6H_{12} were used in this work without purification. C^{14} -Labeled compounds used were obtained from the New England Nuclear Corp.

Results and Discussion

Table I includes the measured binary diffusion coefficients and tracer diffusion coefficients. (The tracer values are based on cell calibrations which assume the limiting value of the binary diffusion coefficient for CCl_4 in C_6H_{12} as listed in Table II.) In Table II, rounded values for all the quantities which are useful for comparison of experiment with theory are tabulated. Activation energies for both diffusive and

viscous flows calculated from these data are, within experimental error, linear functions of mole fraction.

Table I

Binary diffusion, 25°		Binary diffusion, 35°	
Mole fraction, x_{CCl_4}	$D \times 10^5$	Mole fraction, x_{CCl_4}	$D \times 10^5$
0.01655	1.481	0.0237	1.768
0.02510	1.481	0.4750	1.633
0.07134	1.476	0.9764	1.515
0.1739	1.447		
0.3002	1.417		
0.3988	1.393		
0.4868	1.374		
0.6053	1.351		
0.6975	1.328		
0.7958	1.311		
0.9333	1.295		
0.9744	1.285		
0.9853	1.287		

Self and tracer diffusion, 25°	
	$D^* \times 10^5$
$D^*_{CCl_4}$	1.282
$D^*_{C_6H_{12}}$	1.433
$D^*_{CCl_4}$	1.412 ^a
$D^*_{C_6H_{12}}$	1.42 ^b
$D^*_{CCl_4}^{0.5}$	1.45 ^c
$D^*_{C_6H_{12}}^{0.5}$	1.42 ^c

^a Capillary method, H. Watts, B. J. Alder, and J. H. Hildebrand, *J. Chem. Phys.*, **23**, 659 (1955). ^b Rayleigh interferometric value, J. D. Birkett, Thesis, Yale University, 1962. ^c Superscript 0.5 designates the mole fraction at which the tracer studies were made.

Table II

Mole fraction, x_{CCl_4}	$\left[1 + \frac{\partial \ln f}{\partial \ln x}\right] \eta \times 10^3$	$\sigma_{C_6H_{12}} \times 10^3$	$\sigma_{CCl_4} \times 10^3$	$D_{calcd} \times 10^5$	$D_{obed} \times 10^5$	
0.0	1.000	0.900	31.91 ^a	30.80 ^b	1.484	1.484 ^b
0.1	0.982	0.882	32.25	31.22	1.463	1.468
0.2	0.967	0.869	32.61	31.70	1.436	1.443
0.3	0.956	0.863	32.96	32.17	1.407	1.417
0.4	0.948	0.858	33.32	32.65	1.381	1.393
0.5	0.944	0.856	33.67	33.12	1.359	1.371
0.5	33.85 ^a	33.15 ^a	1.355	...
0.6	0.944	0.860	34.02	33.60	1.334	1.350
0.7	0.950	0.864	34.38	34.08	1.320	1.330
0.8	0.960	0.871	34.73	34.55	1.307	1.311
0.9	0.977	0.886	35.09	35.03	1.293	1.296
1.0	1.000	0.904	35.47 ^b	35.51 ^a	1.283	1.283 ^b
1.0						1.283 ^c

^a Directly calculated from self- and tracer-diffusion data of Table I using $D^* = RT/\eta\sigma^*N$. ^b Obtained by Sandquist extrapolation, graph of $D\eta/[1 + (\partial \ln f)/(\partial \ln x)]$ vs. $\Delta\eta$. ^c Diaphragm cell tracer diffusion value based on a calibration using $\lim D = 1.484 \times 10^{-5}$ ($x_{CCl_4} \rightarrow 0$).

- (6) L. G. Longworth, *J. Am. Chem. Soc.*, **69**, 2510 (1947).
 (7) L. J. Gosting, E. Hanson, G. Kegeles, and M. S. Morris, *Rev. Sci. Instr.*, **20**, 209 (1949).
 (8) C. L. Sandquist and P. A. Lyons, *J. Am. Chem. Soc.*, **76**, 4641 (1954).
 (9) R. H. Stokes, *ibid.*, **72**, 763 (1950).

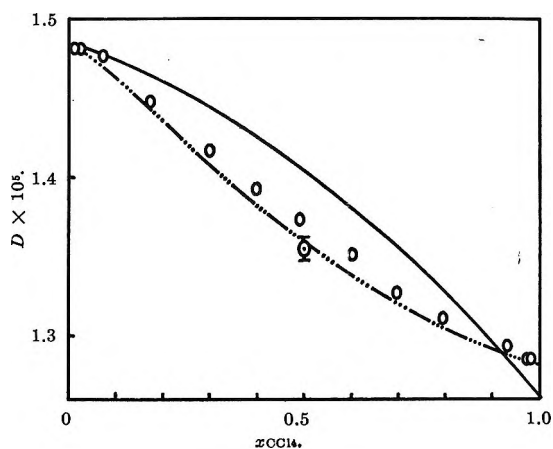


Figure 1. Diaphragm cell,⁵ —; Gouy method, O; tracer diffusion, Φ ; calculated, - - -.

In Figure 1 the binary diffusion values are plotted together with the earlier diaphragm cell results and the values predicted by Hartley and Crank's expression

$$D = \frac{RT}{N\eta} \frac{d \ln f_1 x_1}{d \ln x_1} \left[\frac{x_1}{\sigma_2} + \frac{x_2}{\sigma_1} \right]$$

where the σ -terms are taken from a straight line between the limiting values in Table II. The average agreement of the two sets of experimental data is good and within the accuracy claimed for the diaphragm method. The trend mentioned earlier is apparent.

The agreement of the Gouy results with the values calculated from the linear estimation of the σ -terms is

excellent, probably within the accuracy of the $d \ln f_1 x_1 / d \ln x_1$ term which had earlier been computed from Scatchard's fit of vapor pressure data.^{3,5}

In Figure 1 the value of D computed from the tracer frictional coefficients is also included. Although the limiting binary diffusion coefficients and the corresponding tracer values are consistent within 0.1% (see Table II), a more realistic estimate of the possible error in the tracer experiments would be $\pm 1\%$. As is seen in Table II, the measured tracer frictional coefficients agree very well with the linear approximation. This agreement suggests a criterion which might be used with some confidence to compute the activity coefficients from the Hartley-Crank equation. Thus with the values of σ from the straight line approximation and measured values of D at finite concentrations

$$\int_{x_1=1}^{x_1>0} \left(\frac{DN\eta}{\left[\frac{x_1}{\sigma_2} + \frac{x_2}{\sigma_1} \right] RT} - 1 \right) \frac{1}{x_1} dx_1 = \int_{x_1=1}^{x_1} d \ln f_1 = \ln f_1$$

It is anticipated that very few systems will conform to these simple and convenient rules. However, if systematic and predictable departures from the rules can be rationalized for less ideal systems, they may prove to be very useful.

Acknowledgment. The work was supported by Atomic Energy Commission Contract AT (30-1)-1375.

Hydrogen-Bonding Properties of Alcohols

by Asish Kumar Chandra and Abani Bhusan Sannigrahi

*Department of Chemistry, University Colleges of Science and Technology, Calcutta-9, India
(Received September 4, 1964)*

The hydrogen-bonding properties of primary, secondary, and tertiary butyl alcohols both as proton donors and as proton acceptors were studied with crotonaldehyde, cyclohexanone, and α -naphthol. The equilibrium constants were estimated from the $n \rightarrow \pi^*$ blue shift and the $\pi \rightarrow \pi^*$ red shift and optical density measurements. The results show that the proton-donating power of the alcohols decreases in the order primary > secondary > tertiary while the proton-accepting power of the alcohols decreases in the reverse order. A method has been suggested to account for the association of the alcohols in the estimation of the equilibrium constant.

The phenomenon of intermolecular hydrogen formation is evident in the changes of many physical properties, *e.g.*, melting point, sublimation energy, dielectric constant, and spectral behavior, of the molecules involved. However, the nature of the forces operative in hydrogen bond formation have been understood only recently. It is generally argued that the hydrogen bond is essentially electrostatic and the exchange forces make only a small contribution to its formation. Ignoring the dispersive force, the strength of a hydrogen bond is mainly determined (as in the case of the $-O-1-H-O-2<$ system) by the attraction between the proton and the approaching nonbonding electrons of the O-2 atom, and by the repulsions between these electrons and those of the covalent O-1-H bond and those of the proton and the O-2 nucleus.

Very few systematic attempts have been made to investigate how the hydrogen bond energy varies with the chemical nature of the proton acceptor and/or the proton donor. One such systematic investigation of the hydrogen-bonding effect of various aliphatic alcohols on some organic molecules was made by Chandra and Basu.¹ In their investigation they reported the relative extent to which the different aliphatic alcohols could donate a proton to a given acceptor. Since the oxygen atom of alcohols has a lone pair of electrons and the alcohols associate considerably among themselves, it would be interesting to examine the relative extent to which they can accept the proton from a given proton donor such as phenol. The present investigation was undertaken in order to obtain a better understanding of

the hydrogen-bonding properties of simple alcohols, both as proton donors and acceptors.

The hydrogen-bonding effects on the electronic spectra of organic molecules are of two types. In the first type, the $\pi \rightarrow \pi^*$ bands of the proton donors such as phenols, carbazole, etc., move towards longer wave lengths as a result of hydrogen bonding.²⁻⁴ In the other type, the absorption bands of ketones, aldehydes, pyridiazine, etc. (arising from the singlet-singlet $n \rightarrow \pi^*$ transitions), undergo a blue shift as a result of hydrogen bonding.⁵ From the spectral measurement of the $\pi \rightarrow \pi^*$ and the $n \rightarrow \pi^*$ shifts for a continuous solvent change from a pure hydrocarbon to a pure alcohol, one can calculate the equilibrium constant in the hydrogen bond forming reaction, hence the free-energy change. We have followed this method in the present investigation.

Experimental

Crotonaldehyde, cyclohexanone, and α -naphthol were chosen for the present study. They were purified as follows. Commercial crotonaldehyde was first dried with anhydrous calcium chloride and then distilled before use. Cyclohexanone was purified first by prepara-

- (1) A. K. Chandra and S. Basu, *Trans. Faraday Soc.*, **56**, 632 (1960)
- (2) N. D. Coggeshall and G. M. Lang, *J. Am. Chem. Soc.*, **70**, 3285 (1948).
- (3) S. Nagakura and H. Baba, *ibid.*, **74**, 5693 (1952).
- (4) A. B. Sannigrahi and A. K. Chandra, *J. Phys. Chem.*, **67**, 1106 (1963).
- (5) G. J. Brealy and M. Kasha, *J. Am. Chem. Soc.*, **77**, 4462 (1955)

tion of its bisulfite derivative which was later treated with 80% aqueous caustic soda solution. The liberated ketone layer was dried with anhydrous sulfate and then distilled. α -Naphthol (E. Merck) was recrystallized before use.

The *n*-, iso-, *sec*-, and *t*-butyl alcohols were first refluxed over solid caustic soda for about 2 hr., then dried with anhydrous sodium sulfate, and finally distilled.

The solvent employed was British Drug Houses *n*-heptane which was purified by chromatographic adsorption on alumina. The purified solvent showed cutoff at 220 $m\mu$.

α -Naphthyl methyl ether was prepared from α -naphthol and dimethyl sulfate by a standard method.

All solutions were made gravimetrically and the spectral measurements were made in a Beckman Model DU spectrophotometer using 1-cm. silica cells at 25°.

Results

In Figures 1 and 2 are shown the low-intensity absorption bands of crotonaldehyde and cyclohexanone, respectively, and also the progressive change on addition of *n*-butyl alcohol. These bands, which moved towards shorter wave lengths upon addition of alcohol, were attributed to the $n \rightarrow \pi^*$ transition in the solute molecules. The blue shift of these bands by a solvent such as alcohol were attributed to the formation of an external hydrogen bond, since the hydrogen bond was disrupted by a transition of the nonbonding electron to the excited state. The absorption bands of α -naphthol move gradually toward the longer wave lengths on increasing addition of *n*-butyl alcohol as shown in Figure 3. The intensities of the bands also increase progressively with addition of increasing amount of alcohol. Since neither the position of the peak nor the intensity of the corresponding absorption bands of α -methoxynaphthalene changed on addition of alcohol (Figure 4), we concluded that in the interaction of α -naphthol with alcohol the hydrogen bond was formed between the phenolic hydroxyl group and the oxygen atom of the alcohol. The anomaly in the spectrum of α -naphthol alcohol mixture was therefore

Table I: The Peak of the $n \rightarrow \pi^*$ and $\pi \rightarrow \pi^*$ Absorption Bands of Some Compounds in *n*-Heptane and in *n*-Butyl Alcohol

Compd.	λ , $m\mu$	
	<i>n</i> -Heptane	<i>n</i> -Butyl alcohol
Crotonaldehyde	328	305
Cyclohexanone	290	284
α -Naphthol	290, 308, 322	298, 314, 324
α -Methoxynaphthalene	290, 307, 320	290, 307, 320

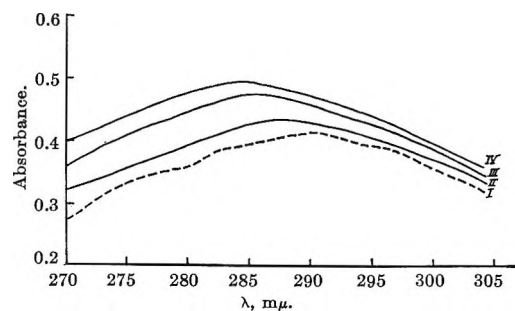


Figure 1. Absorption spectra of cyclohexanone in 0 (I), 0.547 (II), 1.094 (III), and 2.188 (IV) *M* *n*-butyl alcohol. Concentration of cyclohexanone is 3.104×10^{-2} *M* for all absorption curves.

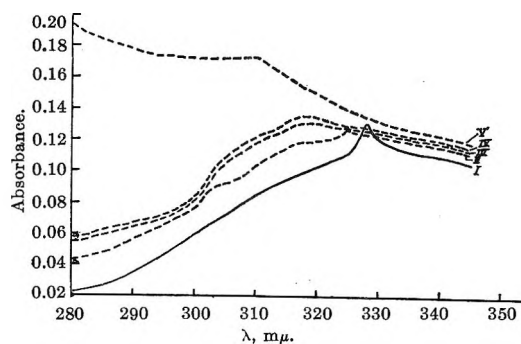


Figure 2. Absorption spectra of crotonaldehyde in 0 (I), 0.219 (II), 0.875 (III), 1.094 (IV), and 3.182 (V) *M* *n*-butyl alcohol. Concentration of crotonaldehyde is 2.45×10^{-3} *M* for all absorption curves.

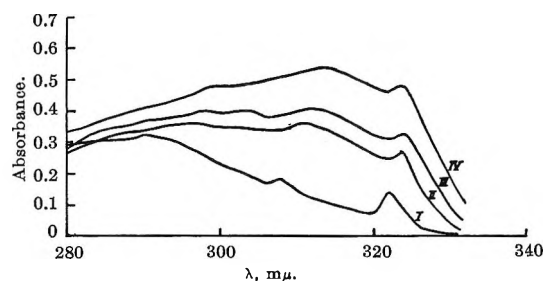


Figure 3. Absorption spectra of α -naphthol in 0 (I), 0.547 (II), 1.094 (III), and 2.188 (IV) *M* *n*-butyl alcohol. Concentration of α -naphthol is 6.611×10^{-5} *M* for all absorption curves.

mainly due to the hydrogen-bonding effect. The positions of the peaks of the complexed solutes observed in the present series of experiments are reported in Table I.

The optical density measurements were made on *n*-heptane solutions of mixtures of solute with different alcohols at several wave lengths near the absorption peak of the complexed solutes. The physicochemical basis of the method of calculating the equilibrium con-

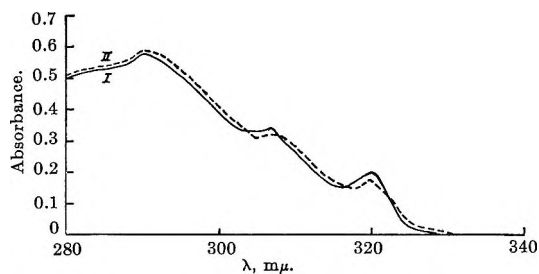


Figure 4. Absorption spectra of α -methoxynaphthalene in *n*-heptane (I) and in *n*-butyl alcohol (II). Concentration of α -methoxynaphthalene is $1.201 \times 10^{-4} M$ for both curves.

stant has been described in details in our previous communications.^{1,4} Using eq. 1 bearing the same notations

$$\frac{[A]}{\bar{\epsilon} - \epsilon_0} = \frac{1}{(\epsilon_1 - \epsilon_0)K} + \frac{[A]}{\epsilon_1 - \epsilon_0} \quad (1)$$

as before, the plot of $[A]/\bar{\epsilon} - \epsilon_0$ vs. $[A]$, where $[A]$ is the formal concentration of the nonabsorbing species, was found to be linear in all cases and at all wave lengths. Figures 5-7 show the plots for complexes at one such wave length. From the slope and the intercept of the curves the equilibrium constant of the hydrogen-bonded complexes was evaluated. The equilibrium constant for each hydrogen-bonded complex was measured similarly at several wave lengths and was found to be constant within 10%. The results are summarized in Table II where the mean values of the equilibrium constants measured at several wave lengths are given.

Discussion

It is evident from Table II that the equilibrium constants for the hydrogen-bonded complexes of crotonal-

Table II: Equilibrium Constants of the Hydrogen-Bonded Complexes

Solute	Concentration of solute, M	Alcohol	Range of alcohol concn., M	Equilibrium constant, M^{-1}
Crotonaldehyde	2.45×10^{-3}	<i>n</i> -Butyl	0.2188-0.8752	0.63
	2.45×10^{-3}	Isobutyl	0.3266-1.3664	0.69
	2.45×10^{-3}	<i>sec</i> -Butyl	0.4368-2.6208	0.30
	4.90×10^{-3}	<i>t</i> -Butyl	1.066-4.2640	0.09
Cyclohexanone	3.104×10^{-2}	<i>n</i> -Butyl	0.2188-1.0940	2.58
		Isobutyl	0.2178-1.0890	2.65
		<i>sec</i> -Butyl	0.4364-2.1820	1.66
		<i>t</i> -Butyl	0.6396-3.1980	0.65
α -Naphthol	6.611×10^{-6}	<i>n</i> -Butyl	0.2188-1.0940	5.33
		Isobutyl	0.2178-1.0890	5.17
		<i>sec</i> -Butyl	0.2184-1.0920	10.43
		<i>t</i> -Butyl	0.1066-1.2790	17.00

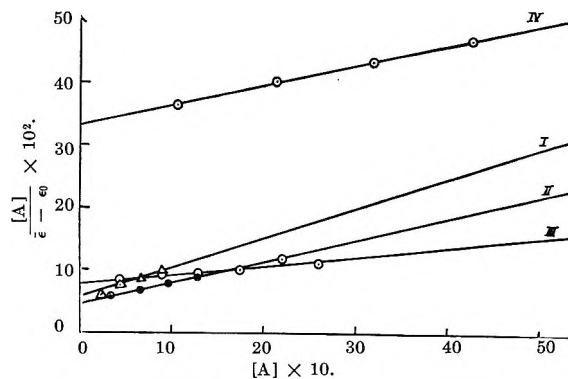


Figure 5. Plot of $[A]/(\bar{\epsilon} - \epsilon_0)$ vs. $[A]$: I, crotonaldehyde and *n*-butyl alcohol; II, crotonaldehyde and isobutyl alcohol; III, crotonaldehyde and *sec*-butyl alcohol; IV, crotonaldehyde and *t*-butyl alcohol. All the spectral measurements in this figure were made at 300 $m\mu$.

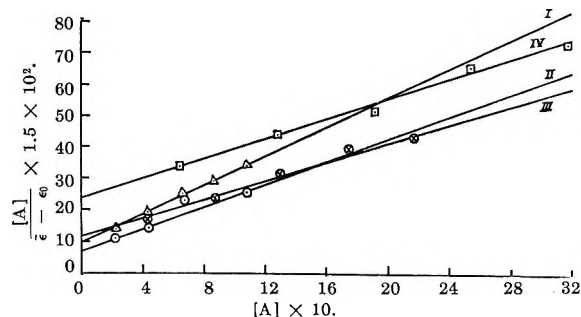


Figure 6. Plot of $[A]/(\bar{\epsilon} - \epsilon_0)$ vs. $[A]$: I, cyclohexanone and *n*-butyl alcohol; II, cyclohexanone and isobutyl alcohol; III, cyclohexanone and *sec*-butyl alcohol; IV, cyclohexanone and *t*-butyl alcohol. All the spectral measurements were made at 282 $m\mu$.

dehyde and cyclohexanone with the alcohols decrease in the order primary > secondary > tertiary. The same conclusion was arrived at by Chandra and Basu¹ in regard to the proton-donor character of the homologous alcohols. The intensity measurements⁶ in the infrared region of *n*-, *sec*-, and *t*-butyl alcohols with ether and trimethylamine also support this conclusion.

There is, however, one difficulty in drawing a definite conclusion immediately from the recorded data in Table II. In order to make the O.D. measurements very accurate near the shifted peaks of the carbonyl-alcohol system, the concentration of the alcohol, especially that of *t*-butyl alcohol, must be kept very large compared to that used in the α -naphthol-alcohol system. At high alcohol concentrations the association of the alcohols will be fairly large. Becker⁷ has deter-

(6) G. M. Barrow, *J. Phys. Chem.*, **59**, 1129 (1955).

(7) E. D. Becker in "Hydrogen Bonding," D. Hadzi, Ed., Pergamon Press Ltd., London, 1959.

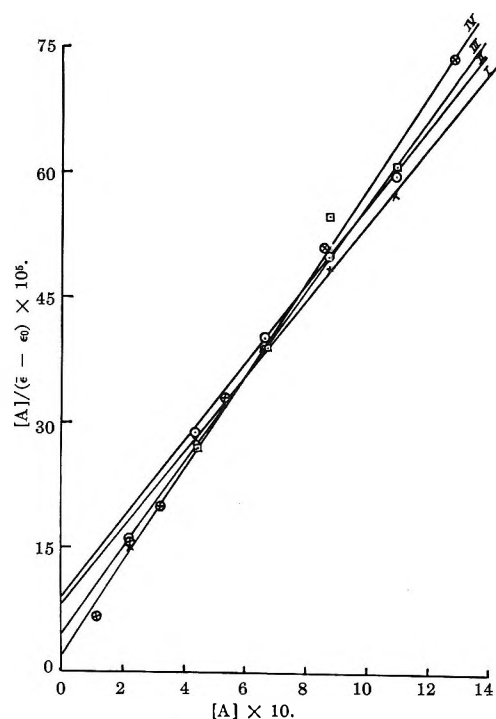


Figure 7. Plot of $[A]/(\bar{\epsilon} - \epsilon_0)$ vs. $[A]$: I, α -naphthol and *n*-butyl alcohol; II, α -naphthol and isobutyl alcohol; III, α -naphthol and *sec*-butyl alcohol; IV, α -naphthol and *t*-butyl alcohol. All the spectral measurements were made at 314 $m\mu$.

mined the dimerization constant of *t*-butyl alcohol from measurements in the infrared region and has shown that association in *t*-butyl alcohol is higher than that in ethyl or methyl alcohol. Coggeshall and Sair⁸ reported earlier the dimerization constant of *n*- and *t*-butyl alcohols, but their value for *t*-butyl alcohol is different from that obtained by Becker and, moreover, they have shown that association in *n*-butyl alcohol is higher than that in *t*-butyl alcohol. As the magnitude of the association constant of these two butyl alcohols differ very little, it would be practically of no significance in the present investigation whether the association in *t*-butyl alcohol is greater or less than that in *n*-butyl alcohol. Using the dimerization constant of *t*-butyl alcohol as reported by Becker⁷ and that of *n*-butyl alcohol as reported by Coggeshall and Sair,⁸ both at 25°, we have determined the monomer concentration in the range of concentration of the alcohols used in the present study of crotonaldehyde and cyclohexanone systems.

The stability constants of the crotonaldehyde- and cyclohexanone-butyl alcohol systems have been determined using eq. 2 in which $D = \text{O.D.} - \epsilon_B[B]_0$ where

$$\frac{[A]}{D} = \frac{1}{K_2[B]_0\bar{\epsilon}} + \frac{[A]}{[B]_0\bar{\epsilon}} \quad (2)$$

O.D. is the optical density of a mixture, ϵ_B and $[B]_0$ are the molar extinction coefficient and the formal concentration of the carbonyl compound, respectively, $[A]$ is the monomer concentration of alcohol, and K_2 is the new equilibrium constant of the complex AB. The detailed derivation of eq. 2 is shown in the Appendix. The plot $[A]/D$ vs. $[A]$ always gives a straight line as shown in Figure 8 except for the crotonaldehyde-*t*-butyl alcohol system where the slope of the curve is negative. The results are reported in Table III.

Table III: Equilibrium Constant of Some Hydrogen-Bonded Complexes after Making Correction for Alcohol Association

Proton acceptors	Concn. of proton acceptors $\times 10^3$ M	Alcohols	Range of alcohol concn., M	Range of monomer alcohol concn. used, M	Equilibrium constant, M^{-1}
Crotonaldehyde	2.45	<i>n</i> -Butyl	0.2188-0.8752	0.1719-0.4890	0.42
	4.9	<i>t</i> -Butyl	1.066-4.225	0.5215-1.225	...
Cyclohexanone	31.04	<i>n</i> -Butyl	0.2188-1.0946	0.1719-0.5720	2.00
	31.04	<i>t</i> -Butyl	0.6396-3.198	0.3685-1.038	0.75
Benzophenone	7.83	<i>n</i> -Butyl	0.2162-2.7027	0.1703-1.024	0.44
	5.84	<i>t</i> -Butyl	1.064-3.195	0.5215-1.0380	... ^a
	4.46	<i>n</i> -Butyl	0.5425-3.243	0.3418-1.1460	0.41

^a The equilibrium constant was found to be 0.06 when the association of alcohol was neglected.

In a previous communication, Chandra and Basu¹ reported the hydrogen-bonding stability constants of the primary, secondary, and tertiary butyl alcohols with benzophenone. In those measurements too high alcohol concentration had to be used and the self-association of the alcohols was completely neglected. We can now re-evaluate the stability constants of benzophenone-alcohol systems after making correction for the alcohol association by the method suggested here. The results for benzophenone are also shown in the Figure 8 and Table III. In order to study any effect due to solute concentration, the system benzophenone-*n*-butyl alcohol was examined at two different concentrations of benzophenone. No significant variation in the stability constant was observed. However, it is seen that like the crotonaldehyde-*t*-butyl alcohol systems the plot of $[A]/D$ vs. $[A]$ for benzophenone-*t*-butyl alcohol gives rise to a negative slope. Since both the previous measurements for the benzophenone-*t*-butyl alcohol system and the present investigation of crotonalde-

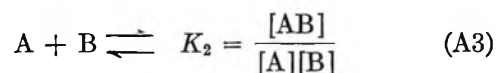
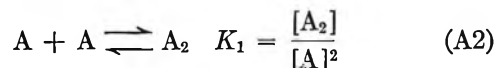
(8) N. D. Coggeshall and E. L. Sair, *J. Am. Chem. Soc.*, **73**, 5414 (1951).

Appendix

If $[A]_0$ is the concentration of alcohol, then

$$[A]_0 = [A] + 2[A_2] + [AB] \quad (A1)$$

where $[A]$, $[A_2]$, and $[AB]$ are the equilibrium concentrations of the monomer alcohol, its dimer, and the hydrogen-bonded complex AB, respectively. There are two competitive equilibria as follows



The concentration of the complex AB is very small compared to the first two terms in A1 where $[B]_0 \ll [A]_0$ ($[B]_0$ is the formal concentration of the component B) and the complex is very weak. $[A]$ is determined from the following quadratic equation (A4). As only

$$2K_1[A]^2 + [A] - [A]_0 = 0 \quad (A4)$$

B and AB are the absorbing species in the ultraviolet region of interest, the optical density of a mixture is given by

$$\text{O.D.} = \epsilon_C[AB] + \epsilon_B([B]_0 - [AB])$$

Let

$$D = \text{O.D.} - \epsilon_B[B]_0 = (\epsilon_C - \epsilon_B)[AB] = \bar{\epsilon}[AB] \quad (A5)$$

where ϵ_C and ϵ_B are the molar extinction coefficient of the complex AB and B, respectively. The equilibrium constant (A3) may then be written as

$$K_2 = \frac{[AB]}{[A]([B]_0 - [AB])} \quad (A6)$$

Substituting for AB, $D/\bar{\epsilon}$ from eq. A5 into eq. A6 we have

$$\frac{[A]}{D} = \frac{1}{K_2[B]_0\bar{\epsilon}} + \frac{[A]}{[B]_0\bar{\epsilon}} \quad (A7)$$

Sites for Hydrogen Adsorption on Zinc Oxide

by Richard Narvaez¹ and H. Austin Taylor

Nichols Chemistry Laboratory, New York University, New York 53, New York (Received November 27, 1964)

Two kinds of experiments were performed. In one, the extent of hydrogen adsorption on ZnO was studied as a function of a stepwise increase in temperature. The effect of pre-adsorbed water on these $q-T$ curves was followed. Four maxima at 55, 130, 170, and 245° are taken to correspond to four processes labeled A-I to A-IV. In the second kind of experiment, the volume of H₂ desorbed after each 20° rise in temperature between 0 and 400° is measured as a function of the temperature at which H₂ had been adsorbed and as a function of pre-adsorbed water. Four desorption maxima occur at 60, 150, 250, and 400° corresponding to four desorption processes D-I to D-IV which are shown to pair, respectively, with A-I to A-IV and correspond to hydrogen adsorption on Zn⁺O⁻², Zn⁺, O⁻², and ·H·O⁻. These assignments satisfy the data found, as well as prior infrared and conductivity results. The end product of A-IV is the same as that produced by direct water adsorption, accounting for the inhibition of hydrogen adsorption and both the inhibition and enhancement of hydrogen desorption in differing temperature ranges. The desorption technique has widespread application.

It has been known for many years that the adsorption of hydrogen on zinc oxide is not a simple process. Taylor and Strother² were the first to show the presence of two maxima in isobars of hydrogen adsorption on zinc oxide as a function of temperature. Many workers³⁻⁶ have reinvestigated this system and all seem agreed that two processes are involved, one associated with zinc in some form, and the other, with oxygen. There has been considerable disagreement on the nature of the sites in each case and on the processes involved. Examination of the temperatures of the maximum adsorption given by the various investigators shows lack of concordance. Taylor,² Cimino,⁴ and Nagarjunan⁶ give the first maximum at 55°; Low^{3b} and Wicke^{3a} as 70-73°. Taylor gives the second maximum as 180°; Cimino, Low, and Nagarjunan give it as 200°, but Wicke gives 273°. Nagarjunan has a minimum at 72°, Taylor, Wicke, and Low, at 107, 109, and 105°, respectively, while Cimino's minimum is at 120°. While there are minor differences in the pressures of hydrogen used and in the duration of the exposure of the surface to hydrogen justifying the "isobars," it is obvious that the differences, almost 100° in the extremes, can only be attributed to major differences in the adsorbents

used. Alternatively, the chemisorption may be more complex than dual processes, perhaps three or four processes may be involved, and one or the other may be suppressed by a surface contaminant. It is known that zinc oxide is poisoned by oxygen⁷ and by water vapor.^{2,8} The present work was undertaken to determine the effect of the pre-adsorption of water in the hydrogen adsorption onto and desorption from zinc oxide.

Experimental

Materials. Zinc Oxide. Two preparations of zinc

(1) Abstract of a dissertation in the Department of Chemistry submitted to the faculty of the Graduate School of Arts and Science in partial fulfillment of the requirements for the degree of Doctor of Philosophy at New York University, 1963.

(2) H. S. Taylor and C. O. Strother, *J. Am. Chem. Soc.*, **56**, 589 (1934).

(3) (a) E. Wicke, *Z. Elektrochem.*, **53**, 279 (1949); (b) M. J. D. Low, *Can. J. Chem.*, **37**, 1916 (1959).

(4) A. Cimino, E. Cipollini, E. Molinari, G. Liuti, and E. L. Manes, *Gazz. chim. ital.*, **90**, 91 (1960).

(5) V. Kesavulu and H. A. Taylor, *J. Phys. Chem.*, **64**, 1124 (1960).

(6) T. S. Nagarjunan, M. V. C. Sastri, and J. C. Kuriacose, *Proc. Natl. Inst. Sci. India*, **27A**, 496 (1961).

(7) J. Aigueperse and S. J. Teichner, *Ann. Chim.*, **7**, 13 (1962).

(8) M. J. D. Low and H. A. Taylor, *J. Phys. Chem.*, **63**, 1317 (1959).

oxide from zinc oxalate were used. The first zinc oxalate was obtained from zinc nitrate and oxalic acid. The oxalate was heated in air for several hours at 100° and for 4 hr. at 400°. The second preparation of zinc oxalate from zinc nitrate and ammonium oxalate was converted to the oxide in the reaction chamber at 400° under vacuum for 9 days. Five samples were derived from these preparations as follows: ZnO I, a 17.9-g. portion of the first preparation exposed to 1 atm. of oxygen for 1 hr. at 400°; ZnO II, a 22.3-g. portion of the first preparation exposed to oxygen at 660 mm. and 400° overnight; ZnO III was ZnO I after considerable use, re-exposed to 1 atm. of oxygen at 400° for 16 hr.; ZnO IV was ZnO III again exposed to oxygen overnight at 400° and 600 mm.; ZnO V was a 10.8-g. portion of the second preparation exposed to oxygen at 600 mm. and 400° overnight. This sample was evacuated until it was almost "clean." Throughout this work, "clean" will be defined as the condition of the surface when the desorption of gases produces a pressure of no more than 10×10^{-5} mm. in 1 min. in a system volume of ~ 0.5 l. Surface area B.E.T. measurements, using nitrogen, of these samples lay in the following ranges: I, 25.4 to 19.0 m.²/g.; II, 17.6 to 16.6 m.²/g.; III, 15.9 to (undetermined) m.²/g.; IV, 12.1 to 11.4 m.²/g.; V, 27.1 to 13.1 m.²/g. The ranges indicate deterioration of the surfaces through use.

The gases, oxygen, helium, and nitrogen, were taken directly from commercial cylinders and used after passage through a liquid nitrogen trap. Tank hydrogen was purified by diffusion through hot palladium.

Procedure. A conventional adsorption system was modified to permit a continuous study of the amount of gas adsorbed as a function of a slowly rising temperature. Pressure changes were measured on a dibutyl phthalate (DBP) manometer. Catalyst temperatures were measured by a chromel-alumel thermocouple and oven temperatures could be maintained with a Thermo-cap control. Gold traps were suitably placed to prevent access of mercury vapor to the zinc oxide sample.

Results

Adsorption Experiments. For comparison with results given later and to indicate how real a two-maximum curve may appear, an example is given in Table I of the hydrogen adsorption, q , as a function of a step-wise increase in temperature of ZnO I. This catalyst had been used in many kinetic measurements prior to this run during which it had been exposed to hydrogen at temperatures as high as 300° and had been evacuated at temperatures up to 350° for many hours. The de-

tails of these runs are not significant here, though the history of the catalyst is significant. For the data in Table I, hydrogen at P_0 of 60.4 mm. was introduced to the catalyst which had been exposed to hydrogen and then thoroughly evacuated at 150°, and the accumulative amounts adsorbed at various temperatures calculated from the pressure changes in the DBP manometer. The sample was left at each temperature for the times given, required to achieve a pressure change of less than ~ 1 mm. of DBP/hr. The data show two maxima, around 50 and 200°, separated by a minimum around 130°. Beyond 200° there is a steady decrease in hydrogen adsorption. The data are plotted as ZnO I in Figure 1.

Table I: Adsorption of Hydrogen as a Function of Temperature, q - T

T , °C.	q , ml. (STP)	t , min. at T
0	2.68	52
25	2.78	29
47	3.89	420
65	3.76	349
92	2.77	144
134	2.35	122
160	2.43	40
198	2.50	310
212	2.33	105
240	2.06	150
274	1.77	185
319	1.34	130
361	1.24	130

The effect of presorbed water vapor, and its subsequent desorption, on the catalyst's ability to adsorb hydrogen is illustrated in Figure 2. These data were obtained using ZnO II which had been evacuated overnight at 400°, a treatment demonstrated sufficient to remove the poisoning effect of oxygen, and then subjected to the following sequence of operations: (1) adsorption of 2.4 ml. (STP) of H₂O at 51°; (2) evacuation at room temperature for 40 hr.; (3) H₂ at 53.9 mm. admitted and q - T determination made, the catalyst being held 1 hr. at each temperature. These data are labeled I in Figure 2; (4) evacuation at 82° for 4 hr.; (5) a further adsorption of 5.5 ml. of H₂O at 51°; (6) evacuation at room temperature for 8.5 hr.; (7) a heating curve, q - T , determination as before with $P_0 = 53.3$ mm., labeled II; (8) evacuation at room temperature for 12.5 hr.; (9) a repeat of (7) at $P_0 = 53.2$ mm., labeled III (the dotted curves here and in II resulted from a plugged stopcock and are intended only to join consecutive observations for

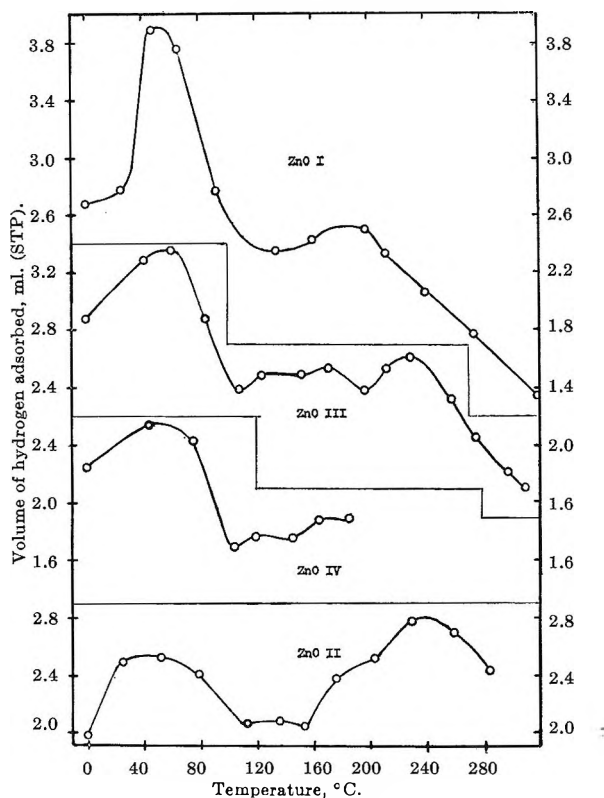


Figure 1. Comparison of q - T plots for different ZnO samples under differing experimental details.

clarity; (10) evacuation for 4 hr. at 283° ; (11) q - T determination at $P_0 = 54.3$ mm., labeled IV; (12) evacuation for 11.5 hr. at 313° ; (13) q - T , V with $P_0 = 54.5$ mm.; (14) evacuation for 12 hr. at 287° ; (15) a kinetics run at 0° followed by exposure to hydrogen for 4 hr. at 325° ; (16) evacuation for 16 hr. at 325° ; (17) q - T , VII determination at $P_0 = 53.6$ mm.; (18) evacuation at 324° for 9.5 hr. and at 367° for 4 hr.; (19) q - T , VIII determination at $P_0 = 54.0$ mm.; (20) evacuation at 353° for 3 hr.

The first result of significance is the difference between curve I and the data in Table I. There is a maximum around 50° in each case but the maximum at 200° in Table I appears only as a shoulder on curve I and is followed by increased hydrogen adsorption to a maximum around 260° . The relative heights of the maxima are inverted in curve I from those in Table I.

The steady increase in hydrogen adsorption at all temperatures, shown in the sequence of curves III to VIII, correlates with the increase in temperature of evacuation. Such evacuation may remove either hydrogen or water or both. The decline especially of the higher maximum between curves II and III must reflect the lack of removal of hydrogen by the low

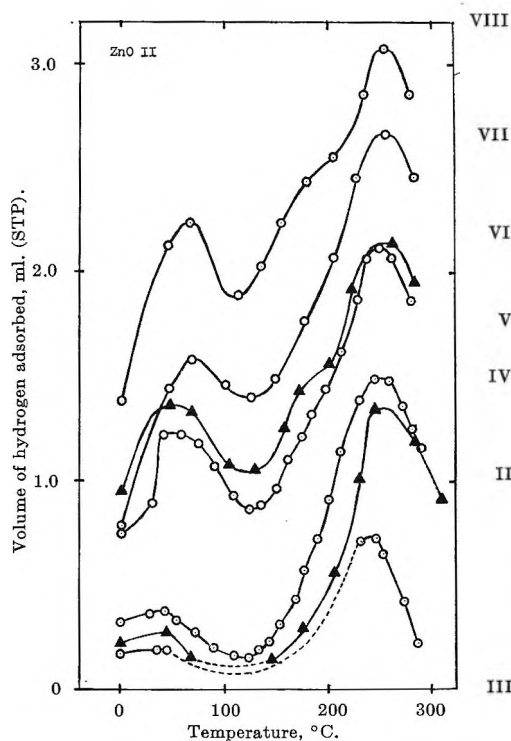


Figure 2. Heating curves for H_2 on ZnO II: I, after 2.4 ml. of H_2O presorbed; II, after 7.9 ml. of H_2O presorbed; III, a repeat of II after evacuation at room temperature; IV, after evacuation at 325° ; VIII, after evacuation at 367° .

temperature evacuation, since no additional water was adsorbed for III after II. Now, if hydrogen alone was removed by the evacuation and if water did not affect hydrogen adsorption, the hydrogen adsorption would be expected to return to that of curve I. That it goes beyond it in curves VII and VIII shows the effect of water removal from the surface, demonstrating the inhibition of hydrogen adsorption by adsorbed water. It is to be noted that the two major maxima in each curve grow in a roughly parallel manner as water is removed.

In order to confirm this desorption of water, its presence in the vapor phase during evacuation was tested by placing liquid nitrogen around a bulb in the manifold line with examination for an accompanying pressure decrease. No such pressure decrease was observed up to 310° . However, when a trap in liquid nitrogen was left in the evacuation line, condensables were trapped out after considerable evacuation and from the pressure registered in a known volume when they were re-evaporated, the amounts could be determined. It is apparent that desorption of water is occurring slowly at 283° at a low partial pressure. At higher temperatures of evacuation, the on-stream pressure is higher and a pressure change accompanies sudden cooling. After step 14, 0.4 ml. (STP) was trapped;

step 16 produced 3.4 ml.; step 18 gave 1.5 ml. in the first part and 1.9 ml. in the second; step 20 produced 1.3 ml., a total of 8.5 ml. This is larger than the recorded 7.9 ml. of water initially adsorbed and shows that these recorded values are minimum values arising from the method of introducing water. The water source was allowed to equilibrate with the manifold system, excluding the catalyst chamber, for 0.5 hr. before the pressure was observed. On opening the catalyst chamber, water was immediately adsorbed and the pressure change was noted. The recorded values of water adsorbed were calculated from this pressure change. However, the decrease in pressure permits a desorption from glass and subsequent unmeasured adsorption on the catalyst. On the other hand, in the determination of condensables by warming the trap, the maximum pressure change was measured because the pressure subsequently decreased, adsorption on the manifold becoming significant.

The shape of the q - T curves depends also on the completeness of hydrogen desorption between successive runs. In Table II are listed the data for two q - T runs using ZnO II each at $P_0 \simeq 54$ mm. Prior to the first, XI, the sample was evacuated for 7 hr. at 343° . After the last measurement at 257° , the sample was cooled to 152° and then evacuated for 1 hr. The sample was cooled to 45° and run XII was begun. It is obvious from a comparison of XI and XII that hydrogen adsorption was definitely inhibited throughout the whole temperature range for XII, but more so in the region of the second major maximum; the q values decrease steadily beyond the 70° value.

Table II: Hydrogen Adsorption after Incomplete Desorption. ZnO II

XI		XII	
$T, ^\circ\text{C.}$	$q, \text{ml. (STP)}$	$T, ^\circ\text{C.}$	$q, \text{ml. (STP)}$
45	1.79	45	1.44
67	1.88	70	1.50
98	1.74	108	1.30
126	1.61	132	1.14
150	1.70	158	1.06
175	1.94	182	1.03
197	2.10	203	0.94
223	2.27	229	0.87
257	2.43	254	0.74

Anticipating later results, it may be pointed out that 152° is too low a temperature at which to desorb the hydrogen adsorbed on the sites responsible for the high temperature process; these sites, therefore, remained largely occupied after run XI. The same explanation

applies to the data in Table I where no maximum occurs in the region beyond 200° ; the prior evacuation had been made only at 150° . This means, further, that the maximum in Table I around 200° is distinct from that in Figure 2 since they are at least 50° apart and since it appears as a shoulder on curves I and VIII. Attention must therefore be focused on three possible maxima and not just two. Further experiments show that probably four maxima are involved.

In Figure 1, a comparison is given of four q - T plots obtained on different samples of zinc oxide under different experimental conditions. The upper curve labeled ZnO I follows the data in Table I. The lowest curve labeled ZnO II was obtained after run XII in Table II. The sample was evacuated for 6 hr. at 350° and the q - T experiment performed as before. Seven hours was allowed for the first point, 4 hr. for the second, and 3 hr. each for the other points. Three maxima obviously appear around $50, 135,$ and 240° but there is a shoulder around 170° on the curve rising to the 240° maximum. Taken alone, this evidence for a fourth maximum would not be convincing since ZnO I had shown only two maxima. ZnO I was reoxidized in oxygen and subsequently labeled ZnO III. It was evacuated for 34 hr. at 385° and the q - T run was made in the usual manner but with the time interval between successive points being 2 hr. Four maxima appear in the curve labeled ZnO III and although the relative heights of the maxima in III are unlike those in II, the temperatures agree remarkably. ZnO III was again reoxidized and then evacuated for more than 2 days at 400° until a desorption rate of 7×10^{-5} mm./min. was attained. The curve labeled ZnO IV is the first experiment performed on this sample, a q - T experiment using 1-hr. intervals between temperature changes. Again the maximum around 170° appears.

The coincidence of the maxima temperatures is striking, considering the different samples with different histories and the differences in the details of the q - T experiments. Analysis of data shows that the sum of the experimental uncertainties is ± 0.03 ml. (STP). Thus, the point at 171° in ZnO III, though only 0.04 ml. higher than the preceding value, is significant because of the improbability that the error contributions in each run would tend to maximize this value while at the same time minimize the preceding value. Since the q - T plots represent net adsorption, it is possible that the four apparent maxima around $55, 130, 170,$ and 245° need not represent four distinct chemisorption processes. A combination of the descending portion of one process with the ascending portion of the following process, provided that the sign of the second derivative of each process is negative, could give an

apparent maximum or a shoulder. It was in an effort to settle this that the succeeding work on desorption was undertaken.

Desorption Experiments. The purpose of these experiments was to correlate the desorption characteristics of hydrogen from zinc oxide, as a function of the amount of presorbed water and as a function of the temperature of the initial hydrogen adsorption, with the adsorption maxima. Data are presented as d - T values, that is, amounts of hydrogen desorbed at a given temperature as a function of temperature. Since the first adsorption maximum is around 55° , it was only necessary to measure the relative amounts desorbed from the catalyst, degassed at some lower temperature, and 0° was chosen. When the catalyst sample had been exposed to hydrogen at a temperature higher than 0° , the sample was cooled to 0° in ice water for about 1 hr. The gas external to the sample chamber was evacuated. Residual gas in the chamber was then expanded into the newly evacuated portion of the system. After recording the pressure, the sample chamber was closed and the gas external to the chamber again evacuated. This process was repeated until the pressure recorded after the gas expansion was less than ~ 1.5 mm. of DBP. The sample chamber was removed from the ice bath and placed in an electric oven. The oven was used to raise the temperature about 20° every 0.5 hr. When the sample temperature was raised about 20° , more gas was desorbed. This gas was released to the evacuated part of the system and its pressure recorded. The sample chamber was isolated, the external gas evacuated, and the sample temperature raised an additional 20° . The process was repeated until a temperature of 400° was attained. The sample chamber had a free volume slightly less than one-tenth that of the entire system. The data, for convenience, are plotted as a continuous curve. The first point, at about 20° , is the volume of gas in milliliters (STP) desorbed at this temperature by raising the temperature from 0 to 20° ; the second point, at about 40° , is the new volume desorbed at this temperature resulting from the temperature rise from 20 to 40° and so on. The point at 40° does not represent the total amount of gas desorbed at this temperature. In contrast, the q - T plots represent the total net volume adsorbed at each temperature. In the d - T plots the total volume desorbed would be given by the sum of the ordinates at all the temperatures used. In a sense, the d - T plots have a rate of desorption connotation. Thus, a d value at $T + 20$, lower than the d value at T , does not signify a re-adsorption, but rather that the desorption between T and $T + 20$ is slower than that below T . Maxima

in the plots, then, indicate peaks in relative desorption rates. The curves between peaks correspond to the net of two processes, both of which may involve hydrogen, or one of hydrogen and one of water.

The effect of the temperature at which the hydrogen had been adsorbed on the d - T plots is shown in the three curves in Figure 3. For the top curve, 1.7 ml. (STP) of water vapor was first adsorbed on ZnO V at 0° . The adsorption was complete. The sample was exposed to hydrogen at 0° for 0.5 hr. at P_i of 740 mm. of DBP. All subsequent adsorptions were performed at the same initial pressure prior to opening the sample stopcock. After the 0.5 hr., the desorption process described was begun at 0° and carried through to 400° . The sample was cooled to room temperature without further desorption before beginning the next run. For this run, the middle curve, the sample was exposed to hydrogen at the same P_i but at 130° for 1 hr. The sample was cooled in 10 min. to 0° and

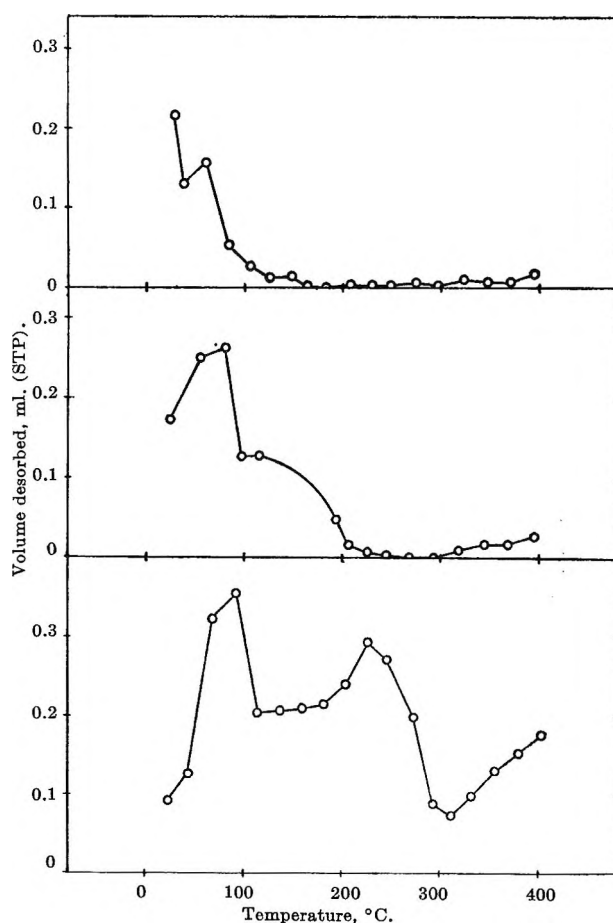


Figure 3. d - T curves of H_2 desorbed as a function of temperature from ZnO V with 1.7 ml. (STP) of H_2O presorbed, after H_2 adsorption at (top) 0° ; (middle) 130° ; (bottom) 240° .

left for an additional 40-min. exposure to the hydrogen. The desorption run followed. For the lowest curve, hydrogen adsorption was at 240° for 1 hr. The cooling to 0° was slow, taking 8 hr., after which the desorption measurements were taken.

It is apparent in Figure 3 that there is a peak desorption, around 80° in all cases, and around 240° when hydrogen had been adsorbed at that temperature. There is evidence of a smaller peak at about 130° in the upper curves. The surprising result is the increasing desorption in the lowest curve at the higher temperatures. That this desorption was mainly hydrogen was proved by the absence of any condensation on cooling a bulb in the gas phase with liquid nitrogen. Since this desorption might interfere in subsequent experiments, desorption was continued at 403° until the residual pressure was 1 mm. of DBP. The sample was then cooled to room temperature.

The effect of additional presorbed water on hydrogen desorption is shown in Figure 4. Comparison should be made with the lowest curve in Figure 3 since the hydrogen adsorption in all these cases was at 240°. For the top curve, an additional 1.9 ml. (STP) of water vapor was adsorbed at 0°. The sample was exposed to hydrogen at 740 mm. of DBP and 240° for 1 hr., cooled to 0° in 4 hr., and the desorption study made. This d - T plot differs from the lowest curve in Figure 3 in that the two large peaks are unequally diminished while the high temperature desorption shows a substantial increase. The first peak is diminished ~ 0.1 ml.; the second, ~ 0.05 ml., and the 400° value is increased ~ 0.1 ml. The ratio of these values is expressed as 2:1:-2. After this run, desorption at 400° was continued until a residual pressure of only ~ 1.5 mm. of DBP was obtained. During the entire desorption process the gas evacuated was drawn through a trap in liquid nitrogen to trap any condensables. After the completion of the run, these condensables were measured and amounted to 0.44 ml. (STP). Recall that 3.6 ml. of water vapor had been presorbed.

The middle curve in Figure 4 was obtained after a further 2.0 ml. (STP) of water vapor was added to the sample and completely adsorbed at 0°. Again hydrogen was adsorbed at the usual pressure and at 240° for 1 hr., the sample cooled rapidly to 0°, and was left for 0.5 hr. before the desorption run was made. Again the two large peaks were unequally reduced, the low temperature peak being the more affected, while the high temperature desorption showed a further increased slope. Tests for condensables were made at 288, 399, and 422° and showed condensable fractions of 0.00, 0.17, and 0.28, respectively. The total amount of condensables trapped throughout this desorption was

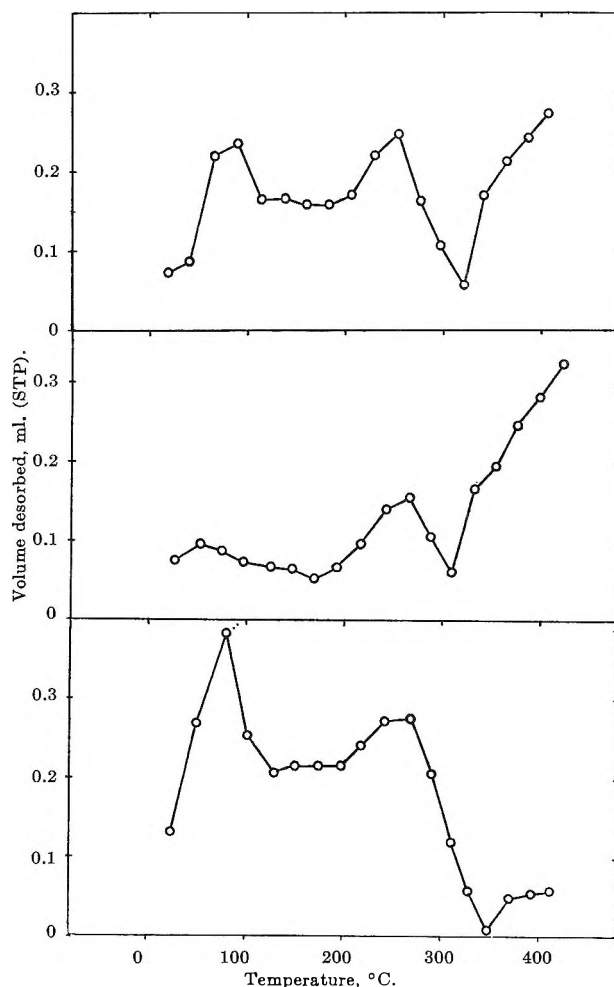


Figure 4. Effect of H_2O presorption on d - T curve after H_2 adsorption at 240°: (top) 3.6 ml. (STP) of H_2O ; (middle) 5.6 ml. H_2O ; (bottom) after thorough evacuation at $>400^\circ$.

0.33 ml. (STP) out of the total 5.6 ml. (STP) presorbed, of which only 0.44 ml. had been previously desorbed.

The bottom curve in Figure 4 shows the d - T relations for hydrogen adsorbed at 240° on a "clean" surface. To this end the sample was evacuated at 432°, the condensables being collected. After 11.5 hr., 5.6 ml. had been trapped, which, by coincidence, is exactly the amount of presorbed water. After a further 47-hr. evacuation, another 4.1 ml. had been collected. Most of this seems probably the product of surface chemical reduction. After further evacuation at around 400° for 26.5 hr., a desorption rate of 20×10^{-5} mm./min. was attained and the sample temperature was lowered to 240°. At this temperature it was exposed to hydrogen as in the previous runs for 1 hr. The sample was gradually cooled to 0° in 5 hr., left at 0° for 1 hr., and then desorbed at 0° until a residual pressure of 1.3 mm. of DBP was obtained. The

d-T experiment followed giving the data for the bottom curve. This indicates the restoration of the two large peaks and the diminution of the high temperature desorption process. There was no measurable condensable fraction at the last temperature studied and the total condensable desorption product amounted only to 0.09 ml. (STP). This, again, must be derived from chemical reduction of the surface. A subsequent surface area measurement yielded a value of 13.6 m.²/g., considerably less than the value found before the series of runs.

In order to demonstrate that the water desorbed around 400° could result from a surface chemical reduction by hydrogen adsorbed around the adsorption maximum at 240°, the two runs shown in Figure 5 were made. The surface of ZnO V was evacuated at 445° until a desorption rate of 1×10^{-5} mm./min. was achieved. The specific surface area was 12.4 m.²/g. Hydrogen was adsorbed at 740 mm. of DBP initial pressure and 130° for 1 hr., the sample cooled rapidly to 0° and left in the hydrogen for another hour before the desorption study. The total condensables collected during the desorption were determined as 0.01 ml. (STP). The sample was evacuated at 435° for 16.5 hr. and showed a desorption rate of 42×10^{-5} mm./min. An attempt at a surface reduction was made by introducing hydrogen at 240° and the usual pressure of 740 mm. of DBP for 9 hr. The sample was evacuated for 24 hr. at temperatures in the range 436 to 455°. The desorption rate was 14×10^{-5} mm./min. and the trapped condensables amounted to 0.4 ml. (STP). This was taken as evidence of reduction. The second *d-T* run in Figure 5 was then performed. The catalyst was cooled to 130°, exposed to hydrogen exactly as before, cooled rapidly and so on, duplicating the conditions of the *d-T* run before reduction. A specific surface area of 12.1 m.²/g. was found. The data in Figure 5 are plotted for unit area. The effect of the reduction is to increase the desorption, especially at temperatures below 300°.

Discussion

Desorption Processes. The sharpness and reproducibility of the various desorption peaks are taken as evidence for the existence of different desorption processes. For convenience in referring to these peaks, let the first desorption maximum occurring in the general vicinity of 60° be called D-I; the small maximum around 150° in Figure 5, D-II; the larger maximum at about 250° in Figure 3 and 4, D-III. Another desorption is evident, beginning at about 350° whose maximum has not been established but is suspected to be around 400°. This desorption is not condensable

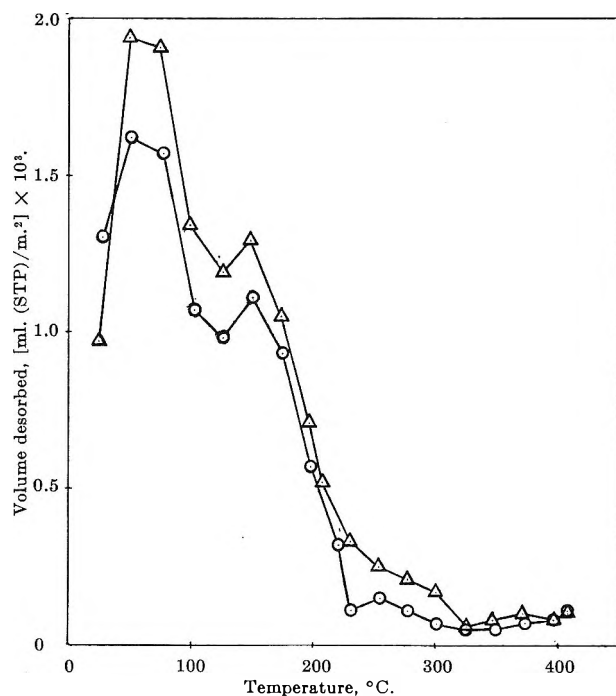


Figure 5. Effect of chemical reduction of ZnO on *d-T* curve; circles before, triangles after reduction.

and is therefore mainly a hydrogen desorption. Let it be referred to as D-IV. Finally, there is a desorption which is condensable occurring even when the original sample was water-free prior to hydrogen adsorption. Let this be labeled D-V. That the maximum of this process was not established definitely though exploratory work suggests that it is around 450°.

It is characteristic of D-I that there is a gradual increase in magnitude with increase in temperature of the adsorption. The same trend is suspected for D-II although its effect is masked by the rapid growth of D-III, particularly from 130 to 240°, implying that the adsorption process initially responsible for D-III must take place above 130°. The characteristic of D-IV is its increase with the amount of presorbed water and by an amount similar to the decrease in D-I. The ratio of changes in peak height, previously referred to, may be extended to 2:1:1:−2 in D-I, II, III, and IV with respect to inhibition by water, suggesting that, whatever may be the mechanism by which water blocks adsorption sites eventually responsible for these desorptions, a two-center site is blocked for D-I and one-center site each for D-II and D-III.

Such distinct desorption processes presuppose distinct adsorption processes. Adsorption maxima have been found around 55, 130, 170, and 245°. Let these be labeled A-I, A-II, A-III, and A-IV. To pair these

directly with the desorption maxima in the same order of increasing temperature requires justification. Since D-I occurs with adsorption temperatures as low as 0° and, at this temperature, the other desorption processes are practically nonexistent, while experiment has shown a direct relationship between the extent of adsorption at 0° and the size of A-I, it seems justifiable to pair A-I with D-I. Figure 2 shows that A-I and A-IV have a parallel growth as water is desorbed from the surface. If D-I, and thereby A-I, involves a two-center site, it appears that A-IV may also involve a two-center site excluding its pairing with either D-II or D-III. Thus, D-IV is left as the desorption for A-IV. There are now left the two adsorption maxima at 130 and 170° to be paired with the two desorptions at 150 and 250°. It is not reasonable, though not impossible, that a process adsorbing at 170° be paired with a process desorbing at 150°, since the two types of experiments are not entirely equivalent. It seems more logical to pair A-II and D-II, A-III and D-III. Further, if the processes I through IV, both in adsorption and desorption, occur in the order of increasing temperature, it would appear that the energies of activation of both adsorption and desorption increase with increasing temperature. The continued widening of the gap between the desorption and adsorption maximum temperatures, $\Delta T = 5, 20, 80, \text{ and } 155^\circ$ for processes I through IV, respectively, may be interpreted as due to an increasing heat of adsorption in the same order.

The recognition of the actual sites and the processes occurring thereon must satisfy not only the data found here but the earlier results from infrared and conductivity investigations. Eischens⁹ and co-workers examined the infrared spectrum of hydrogen chemisorbed on ZnO concluding that at 30°, bands attributable to OH and ZnH stretching vibrations occur and the ratio of the intensities of these bands remains constant with increasing hydrogen pressure. In addition, there is a slow chemisorption at 30° that does not produce detectable infrared bands, which is attributed to H⁺. When the ZnO is heated above 80° in hydrogen both bands decrease, maintaining a constant ratio of OH and ZnH intensities. Above 80° a general decrease in background transmission is taken to indicate an increase in electrical conductivity.

From the temperatures used in the infrared studies, it is apparent that it is process I that is referred to as involving the two covalent stretching vibrations and that there is little if any electrical conductivity during process I; the noninfrared active adsorption is attributable to process II.

Cimino¹⁰ has summarized the electrical conductivity

data of ZnO with hydrogen chemisorbed and desorbed, through a wide range of temperature. Below 100°, where process A-I is dominant, the change in conductivity with hydrogen adsorption is very small. It begins to increase as the temperature is raised. Experiments at 107 and 122°, the region of A-II, show only very slight conductivity. From 157° upward in temperature, electron donation becomes an increasingly important factor in the responsible adsorption processes, A-III and A-IV.

The desorption experiments of Cimino are more interesting. After permitting adsorption of hydrogen to occur for 100 min. while noting the conductivity changes, the sample was evacuated for 100 min. again noting the conductivity changes. Whereas the increases in conductivity with time of exposure to hydrogen increased uniformly with increase in temperature, there appears to be no regular order with respect to temperature in the desorption. Thus, after 75 min. desorption, the sample had the highest conductivity when hydrogen had been adsorbed at 204°, the next highest for adsorption at 259°, the next for 178°, and in order of decreasing conductivity, 312, 232, and 349°. No regular order is apparent. Detailed examination shows, however, that the results are determined by the question of whether the temperature is high enough to desorb the hydrogen which had adsorbed at that temperature. This is difficult, as has been shown for processes III and IV having ΔT of 80 and 155°, respectively, between desorption and adsorption.

In attempting to assign the particular surface species responsible in each of the four processes, six possible species, three each for Zn and O, the neutral atom, univalent and divalent ions must be considered and the new species produced by hydrogen adsorption must satisfy the infrared and conductivity evidence as well as the evidence on the initial activity of a clean virgin sample and the effects of a chemical reduction of the surface.

Taking process I as involving a two-center site adsorbing a molecule of hydrogen, the infrared evidence calls for a zinc-hydrogen covalent bond. The conductivity results show that the adsorption must not produce an electron. The data reported here show an increased adsorption after a chemical reduction of the surface but appreciable activity before such a reduction. Examination of the various possibilities shows that only the site Zn^+O^{-2} satisfies all the requirements.

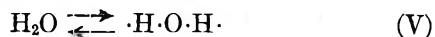
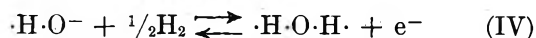
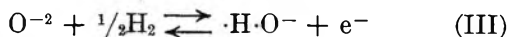
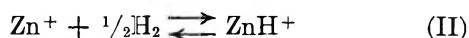
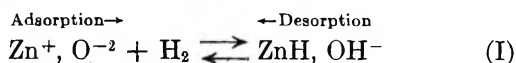
(9) R. P. Eischens, W. A. Pliskin, and M. J. D. Low, *J. Catalysis*, **1**, 180 (1962).

(10) A. Cimino, E. Molinari, F. Cramarossa, and G. Ghersini, *ibid.*, **1**, 275 (1962).

For process II, consideration must be given to the absence of any new infrared evidence, to the absence of conductivity in the temperature range of A-II, to the fact that the site probably combines with only one atom of hydrogen, judging from the 2:1:1:-2 desorption ratio, and finally, that the site should not be improbable in the absence of a chemical reduction of the surface. In view of these considerations, Zn^+ appears to be the most probable site. As an n-type semiconductor, the site would normally be present, would be increased by surface reduction, while adsorption of a hydrogen atom would produce a protonated zinc: $Zn^+ + \frac{1}{2}H_2 \rightarrow ZnH^+$, as suggested by Eischens and co-workers.

Since the processes responsible for A-III, A-IV, D-III, and D-IV seem closely interrelated, the sites for processes III and IV can best be discussed together. The following facts must be rationalized. D-III is inhibited and D-IV is enhanced in the ratio 1:-2 as the amount of presorbed water is increased. A-I and A-IV increase in a parallel manner as water presorption is decreased. At the higher temperatures of these processes there is considerable conductivity. For processes III and IV there are large differences in temperature between the respective adsorption and desorption maxima, implying a stronger binding than those encountered at sites I and II. Finally, the adsorption of hydrogen in the temperature range of A-IV has been shown to be retarded by illumination with a mercury arc.¹¹ This illumination excites electrons from the valence band into the conduction band, impeding the discharge of an electron into the conduction band by adsorption.

In order to explain these phenomena as well as the general effect of water the following processes are postulated.



In reactions III, IV, and V there appear "half-bonded" hydrogens, written with dots to represent this. In this state the hydrogen is located between two adjacent oxygens. The calculated O-O distance in zinc oxide is 3.18 Å., which may be compared with the corresponding distance for ice, of 2.76 Å., known to be hydrogen bonded. It is probably the strength of this bond that is responsible for the large ΔT values found for types

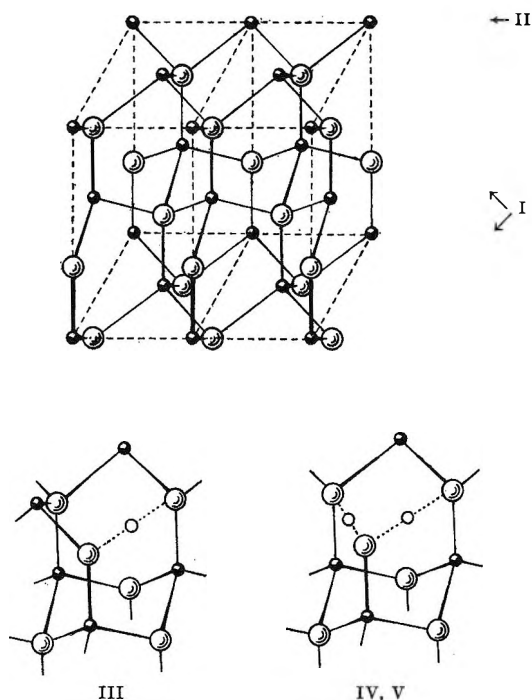


Figure 6. Arrangement of zinc (small black circles), oxygen (large open circles), and hydrogen (small open circles) in adsorption processes I, II, III, IV, and V.

III and IV. Certainly, the hydrogen adsorption on oxygen must be significantly different in A-III and IV from that in A-I to account for the observed maximum temperature difference. Figure 6 shows the proposed arrangement of zinc, oxygen, and hydrogen for the several processes.

The effect of temperature on the electrical conductivity is accounted for, since after A-IV two electrons pass to the conduction band for each one after A-III. The reverse desorptions will have the reverse effect.

The inhibition of hydrogen adsorption by water follows, since water adsorbs by orienting its oxygen toward zinc and sharing its hydrogens with neighboring oxide or hydroxide ions. The result is identical with the form of the species obtained by successively proceeding from A-III to A-IV. This is the link between the adsorption of water and that of hydrogen. In water poisoning of the surface all the positions between oxide ions are occupied and A-III and A-IV cannot occur. Similarly, all the zinc ions are blocked and there can be no A-I and A-II. As water is successively desorbed, A-I and A-IV show a parallel growth each accounting for two hydrogen atoms in the adsorbed state. The ratio 2:1:1:-2 for the four desorption processes follows directly for the first three proc-

(11) V. Kesavulu and H. A. Taylor, *J. Phys. Chem.*, 66, 54 (1962).

esses from the equations. For D-IV, however, as water presorption is increased, the $\cdot\text{H}\cdot\text{O}\cdot\text{H}\cdot$ form is increased and the probability of D-IV is increased. At the high temperatures of this process, D-IV produces the species $\cdot\text{H}\cdot\text{O}^-$ which immediately decomposes to yield another hydrogen. Hence, two hydrogens are released and an oxide ion remains; the conductivity is decreased and the surface is oxidized. Chemical reduction of zinc oxide proceeds in the reverse manner. There is first A-III followed by A-IV to form $\cdot\text{H}\cdot\text{O}\cdot\text{H}\cdot$. At about 450° this species can desorb as water more effectively than at lower temperatures. Both water and hydrogen could be produced as the final adsorbed species could desorb by D-IV or D-V. The ratio of these products is determined by the temperature and the partial pressures of hydrogen and water.

It should be noted that not all surface oxide sites could successfully accommodate two hydrogen atoms. For an $\cdot\text{H}\cdot\text{O}^-$ species to accommodate another hydrogen it must have an available neighboring oxide or hydroxide with which to share the incoming hydrogen. If such were not available, $\cdot\text{H}\cdot\text{O}\cdot\text{H}\cdot$ could not form. A corollary would be that type III adsorption is a

function of the density of surface oxygen pairs while type IV is a function of oxygen triplets.

The stabilization of the proton in ZnH^+ in process II is probably due to the negative potential well formed by three neighboring oxide ions.

It may be asked why previous investigations have shown only two maxima in the isobars. The answer lies in the technique used, where each point of the isobar is derived from a separate kinetic experiment at a given temperature, performed in a sequence independent of the temperature, and separated by evacuation at temperatures above 400° . Some scatter of the points could easily mask a small maximum. In addition, since considerable time is required to obtain one point of an isobar plot, investigators have limited the number of experiments and consequently large temperature gaps occur between points, increasing the probability of missing a small maximum. The desorption technique used here is relatively rapid and provides valuable information on inhibition and enhancement of adsorption and desorption. It should have widespread application in similar studies of other systems.

The Thermodynamics of the Yttrium-Hydrogen System¹

by L. N. Yannopoulos, R. K. Edwards, and P. G. Wahlbeck

Department of Chemistry, Illinois Institute of Technology, Chicago 16, Illinois (Received December 23, 1964)

Isothermal equilibrium hydrogen pressure measurements were carried out as a function of composition for the yttrium-hydrogen system in the temperature ranges 250 to 350° and 650 to 950°, up to a pressure of 1 atm. The existence of three solid solution phases in this system is indicated by the data. The primary solid solution range extends to about $\text{YH}_{0.55}$. The other two solid solution phases can be described as yttrium hydride phases deficient in hydrogen with respect to YH_2 and YH_3 . The phase boundaries were evaluated in the temperature ranges 650 to 950° and 250 to 350°, respectively. The experimental relative partial molal and integral thermodynamic quantities were calculated.

Introduction

Although the position of yttrium metal in the periodic table is significant in regard to the correlation of the properties of the hydrogen compounds with those of the alkaline earth, transitional, and rare earth hydrides, the lack of available high-purity metal has been a hindrance to accurate work on the Y-H system.

Lundin and Blackledge² recently published pressure-temperature-composition curves for the Y-H system in the temperature range 900 to 1350°. They reported the existence of a stable hydrogen-deficient yttrium dihydride in this temperature range and determined the solubility limits of hydrogen in yttrium and yttrium dihydride. They also reported the existence of YH_3 from 300° down to room temperature but gave no isothermal equilibrium pressure measurements for this low temperature range. Their findings have been substantiated also by X-ray data of Dialer and Frank.³ Flotow, Osborne, and Otto^{4,5} have also reported the preparation of YH_2 and YH_3 and the measurement of low-temperature heat capacities.

The purpose of the work reported here was the determination of thermodynamic data and the elucidation of the yttrium-hydrogen phase diagram.

Experimental

Apparatus. A modified type of the Sieverts' apparatus used in this research is described in detail elsewhere.¹ The equilibrium pressures were measured by a McLeod gauge, a small Octoil-S manometer, or an adjustable-level mercury manometer according to the pressure range. The yttrium metal was contained

in a small mullite crucible placed in a quartz cell which was connected to the section of the vacuum system leading to the equilibrium pressure-measuring devices. The sample was heated by means of an HDT-812-Model Hevi-Duty electric furnace, and the temperature was controlled to better than $\pm 1^\circ$ with a West JSB Model saturable-core reactor controller. A chromel-alumel thermocouple served as the sensing element, and a separate calibrated chromel-alumel thermocouple was used for measuring the temperature. Both thermocouples were placed outside the quartz tube cell in which the sample had been positioned.

Materials. The yttrium metal used was obtained from Lindsay Chemical Division of American Potash and Chemical Corp. The purity designation was given as 99.9 wt. %. The metal was received in an ingot form, and small size turnings were obtained through the use of a very carefully cleaned lathe. The turnings were cleaned with pure distilled benzene and allowed to dry. Gas vacuum fusion analyses of yttrium showed oxygen and nitrogen contamination of

(1) Based on a thesis by L. N. Yannopoulos, submitted to the Illinois Institute of Technology in partial fulfillment of the requirements for the Ph.D. Degree, June 1963. Presented before the Physical Chemistry Division at the 145th National Meeting of the American Chemical Society, New York, N. Y., Sept. 1963.

(2) C. E. Lundin and J. P. Blackledge, *J. Electrochem. Soc.*, **109**, 838 (1962).

(3) K. Dialer and B. Z. Frank, *Z. Naturforsch.*, **15b**, 58 (1960).

(4) E. H. Flotow, D. W. Osborne, and K. Otto, *J. Chem. Phys.*, **36**, 866 (1962).

(5) E. H. Flotow, D. W. Osborne, K. Otto, and B. M. Abraham, *ibid.*, **38**, 2620 (1963).

0.179 and 0.0033 wt. %, respectively. Similar analyses for a yttrium sample, first hydrided at 850° and subsequently at 250° up to the composition $\text{YH}_{2.7}$ and then dehydrided at around 900° down to a pressure of 10^{-5} mm., showed 0.269 and 0.0070 wt. % for oxygen and nitrogen, respectively. This second sample was held in the furnace for about 24 hr. A new yttrium sample was used for each isotherm in order to avoid cumulative oxygen contamination. The hydrogen used was obtained from the Matheson Co. with reported gas impurities of nitrogen, oxygen, carbon dioxide, and carbon monoxide less than 25, 5, 5, and 25 p.p.m., respectively. Helium, supplied from the Matheson Co., was used in calibrations, and its purity was reported to be 99.99%.

Both gases, before being used, were passed first through liquid nitrogen traps to remove condensable impurities and then through zirconium turnings at 800° to remove reactive impurities.⁶ Furthermore, the zirconium turnings served as a storage for hydrogen since pure zirconium absorbs large quantities of hydrogen at this temperature. The stored hydrogen was released as desired by raising the temperature of the furnace surrounding the zirconium turnings.

Procedure. A typical run was made as follows. Approximately 0.9 to 1.0 g. of cleaned yttrium turnings was placed in a small mullite crucible which was degassed in the quartz cell to a pressure of 10^{-6} mm. at ca. 900° and allowed to anneal under vacuum at this temperature for approximately 2 additional hr. A separate auxiliary furnace core was used for this preliminary treatment of the metal. After the degassing and annealing were completed, the quartz cell was cooled *in vacuo* to room temperature and was transferred, without exposure to the atmosphere, to the Hevi-Duty electric furnace which was set at the desired temperature. The cell was degassed at this experimental temperature to a pressure of less than 10^{-5} mm. prior to the initiation of the procedure for the equilibrium measurements.

Following the degassing treatment, a calibration of the effective residual gas volume of the system with helium gas was performed for each new sample, both in the high and low pressure ranges (which involve different effective volumes). After the calibration was completed, the helium gas was pumped out.

Successive amounts of hydrogen were added to the reaction zone, and the equilibrium pressures were measured. When the equilibrium pressures were high enough to be measured by the small Octoil-S manometer, the stopcock leading to the McLeod gauge was closed, and the higher pressure equilibrium points were obtained. The equilibrium pressures, which cycled

with temperature fluctuations, were read at the mean point of each temperature fluctuation cycle, thus ensuring an actual temperature definition better than $\pm 1^\circ$. The measurements were continued until the equilibrium pressures approached 1 atm. In the high pressure region several desorption points were also obtained in order to establish the reversible nature of the yttrium-hydrogen reaction.

Results

The isothermal equilibrium data for the yttrium-hydrogen system are represented in Figure 1 for the temperature range from 601.4 to 949.4°. From the shape of the isotherms of Figure 1, one can infer for the condensed state the existence of two single-phase regions separated by a two-phase field. In the dilute region of the Y-H system up to 0.1 g.-atom of hydrogen/g.-atom of yttrium, Sieverts' general law for the metal-hydrogen systems was assumed to hold; *i.e.*, $C = KP^{1/2}$, where C is the hydrogen gram-atom per cent, P is the equilibrium hydrogen pressure, and K is a constant dependent on temperature. Based on this assumption, the dotted extrapolation isotherms shown in Figure 2 were drawn as straight lines through the low composition points to the origin. The analogous system, scandium-hydrogen, has been demonstrated by Lieberman and Wahlbeck⁷ to follow Sieverts' law behavior, for low compositions up as far as 0.10 (H/Sc) unit.

Reversibility of the measurements for the composition range shown in Figure 1 is demonstrated by the fit of the isothermal desorption points in the right-hand portion and the "desorption" points in the left of the figure. The latter were taken by successively raising the temperature of a given sample to check the fit to the previously established curves.

In the composition range approximating YH_2 - YH_3 , it was necessary to work at lower temperatures to stay within the pressure limits of the apparatus. The data, shown in Figure 3, show a definite hysteresis loop in the absorption *vs.* desorption measurements. Moreover, these isothermal loops were found to be reproducible. This was tested in some cases by isothermal absorption followed by desorption and followed by reabsorption measurements. Further tests showed that a desorption point at a higher temperature would move to fit naturally on the absorption curve for a lower temperature when the furnace temperature was lowered; the converse was also observed.

Phase boundary estimates are indicated by the

(6) R. K. Edwards and E. Veleckis, *J. Phys. Chem.*, **66**, 1657 (1962).

(7) M. L. Lieberman and P. G. Wahlbeck, private communication.

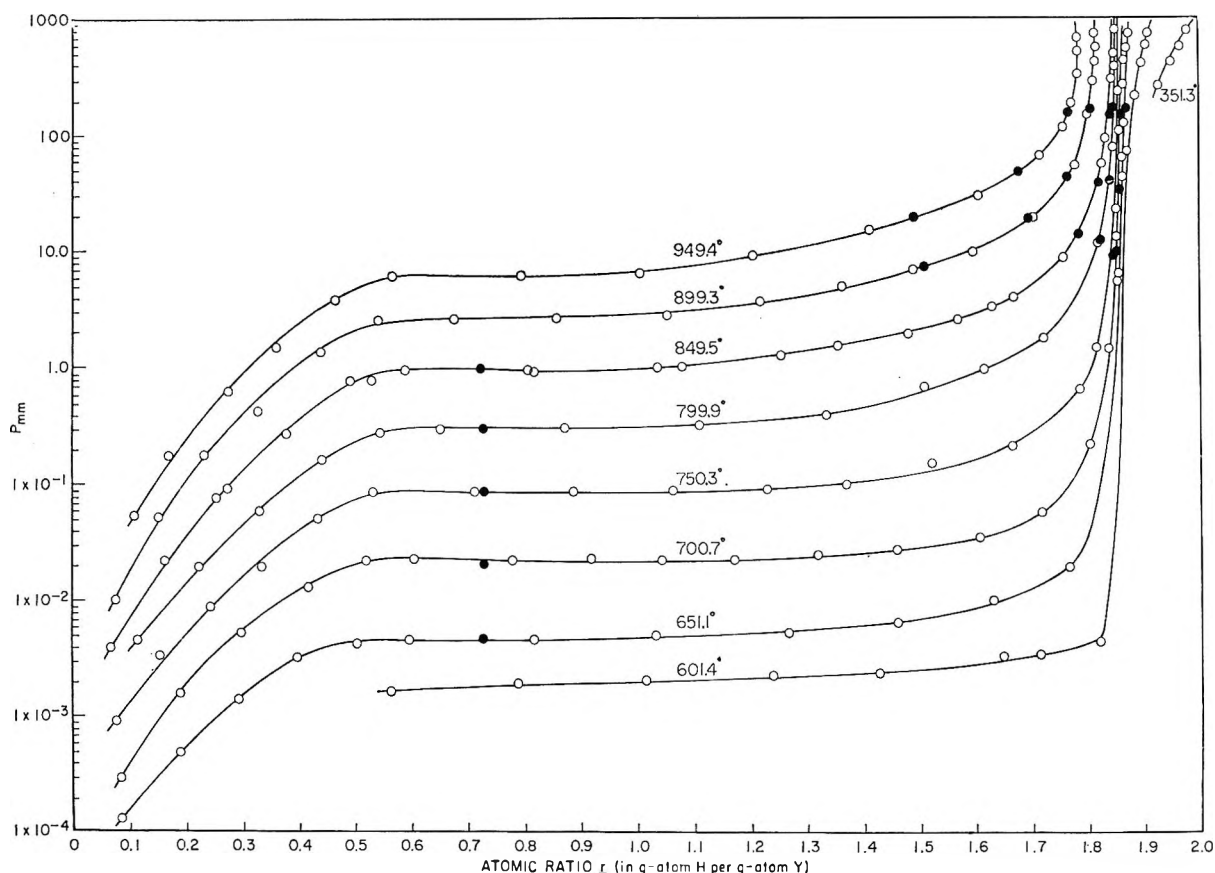


Figure 1. Experimental isotherms for the system yttrium-hydrogen: O, absorption points; ●, desorption points.

dashed lines in Figures 2 and 3. The estimated uncertainty in visually defining these boundaries are ± 0.05 (H/Y) and ± 0.10 (H/Y) units, respectively. In the latter case, it is assumed that a two-phase field exists even though thermodynamic irreversibility is demonstrated.

The thermodynamic data appropriate to the temperature ranges studied are presented in Table I. The procedure for obtaining the thermodynamic results from the experimental data is reported elsewhere.¹ The integral quantities ΔH_f and ΔS_f in the table were obtained by graphical integration of the $(\bar{H}_H - \frac{1}{2}H^\circ_{H_2})$ and $(\bar{S}_H - \frac{1}{2}S^\circ_{H_2})$ values by means of the equation

$$\Delta H_f = \frac{1}{1+r} \int_0^r (\bar{H}_H - \frac{1}{2}H^\circ_{H_2}) dr$$

for the enthalpy and the similar form for the entropy. Here, ΔH_f and ΔS_f correspond to the standard heat and entropy of formation of 1 g.-atom of solution from solid yttrium and gaseous diatomic hydrogen at a pressure of 1 atm., while $(\bar{H}_H - \frac{1}{2}H^\circ_{H_2})$ and $(\bar{S}_H - \frac{1}{2}S^\circ_{H_2})$ refer to the relative partial molal quantities per gram-

atom of hydrogen in the solid solution. Ideal behavior for hydrogen gas has been assumed. The integration in the dilute region where no experimental data are available was performed by using the assumption that Sieverts' law was applicable up to 0.10 (H/Y). Such an assumption implies a constant $(\bar{H}_H - \frac{1}{2}H^\circ_{H_2})$ value in this composition interval. Furthermore, the calculation of the contribution for this dilute region to the integral entropies is simply obtained.⁸ The relative partial molal quantities for the composition range $YH_{2.0}$ - $YH_{2.6}$ are of questionable significance since irreversible behavior prevailed in this range. They are presented only for purposes of comparison of the absorption and desorption behavior of the system.

Discussion

The special position of yttrium between the alkaline metals, which form ionic hydrides, and the transition and the rare earth metals, which form intermetallic type hydrides, does not seem to lead to an obvious intermediate character for the yttrium hydrides inso-

(8) E. Veleckis, Ph.D. Thesis, Illinois Institute of Technology, 1960.

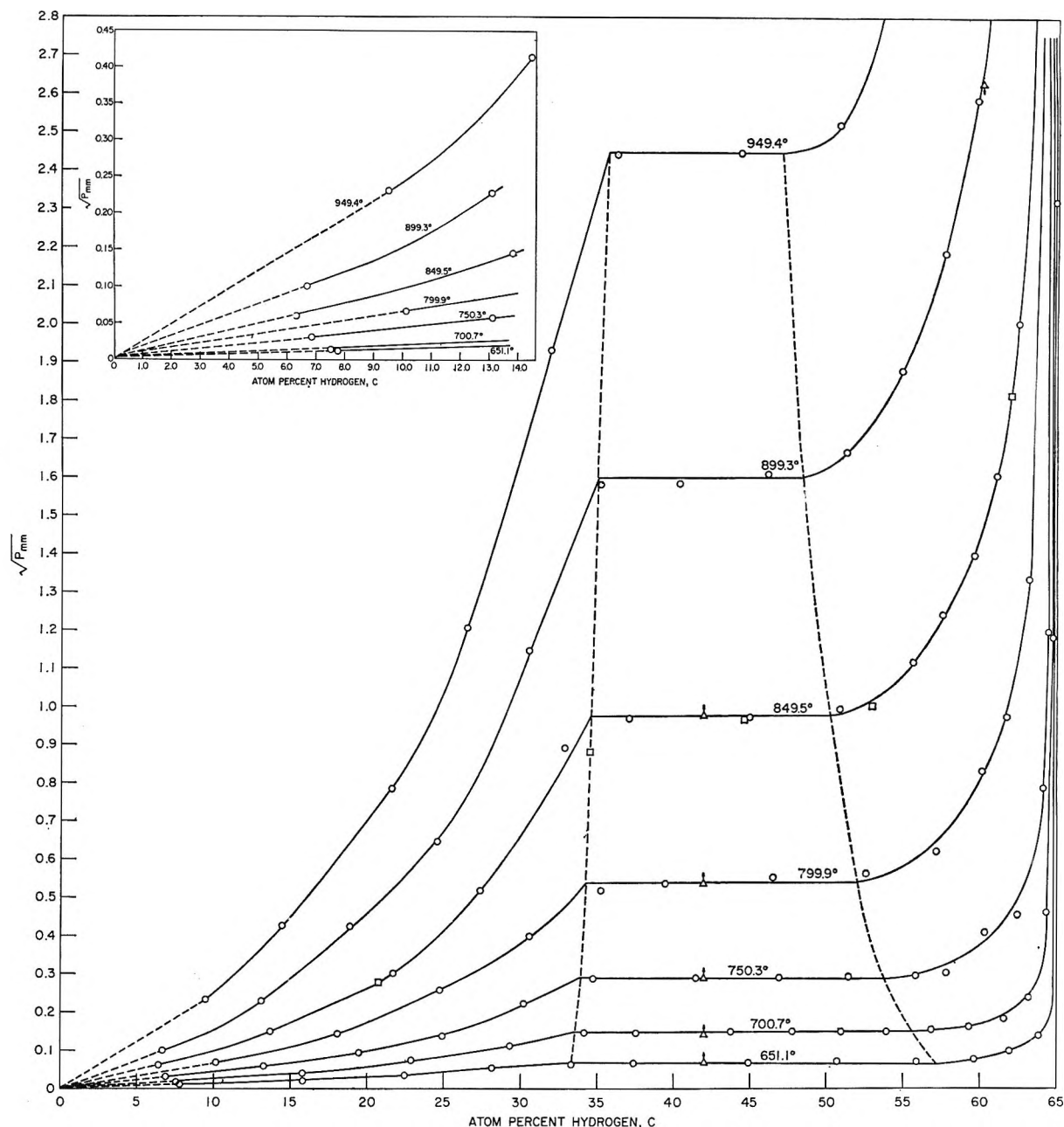


Figure 2. Experimental isotherms for the system yttrium-hydrogen: O, absorption points; □, repeat absorption points; \triangle , "desorption" points obtained by raising the temperature; ∇ , "desorption" point obtained by lowering the temperature from the 949.4° isotherm.

far as the thermodynamic results can be revealing. The latter seem to fall rather clearly in the intermetallic class.

The existence of yttrium dihydride and trihydride phases reported in this study is supported by the X-ray data and pressure-composition isotherms of Lundin and Blackledge,² the hydride preparations of Dialer and Frank³ and Flotow, Osborne, and Otto,^{4,5} and the limited X-ray studies of Pebler and Wallace.⁹ Al-

though Lundin and Blackledge² covered a higher temperature range in their apparatus, two of their isothermal curves fall within our temperature range and show reasonable agreement with our curves. It is to be noted that the absence of experimental points on their published isotherms limits direct comparison with this study. The highest reported hydride com-

(9) A. Pebler and W. E. Wallace, *J. Phys. Chem.*, **66**, 148 (1962).

Table I: Thermodynamic Quantities for the System Hydrogen-Yttrium

Atomic ratio, g.-atom of H/g.-atom of Y	$-(\bar{H}_H - 1/2H^\circ_{H_2})$, cal./g.-atom of H	$-(\bar{S}_H - 1/2S^\circ_{H_2})$, cal./°K. g.-atom of H	$-\Delta H_f$, cal./g.- atom	$-\Delta S_f$, cal./°K. g.-atom
0	(21,150) ^a	$-\infty$	0	0
0.10	21,399 ± 500	7.76 ± 0.42	1,927	0.533
0.15	22,896 ± 310	9.57 ± 0.29	2,748	0.889
0.20	23,028 ± 310	10.77 ± 0.30	3,583	1.283
0.25	23,436 ± 310	11.77 ± 0.30	4,400	1.680
0.30	23,820 ± 300	11.65 ± 0.28	5,144	2.087
0.35	23,987 ± 300	13.17 ± 0.28	5,825	2.453
0.40	24,497 ± 320	14.19 ± 0.31	6,486	2.856
0.45	25,619 ± 180	15.60 ± 0.18	7,119	3.132
0.50	26,407 ± 190	16.61 ± 0.18	7,746	3.713
(0.55-0.90) ^b	27,151 ± 180	17.47 ± 0.17
1.10	27,450 ± 990	18.01 ± 0.09	13,314	7.678
1.15	27,892 ± 850	18.28 ± 0.08	13,638	7.924
1.20	28,229 ± 710	18.66 ± 0.07	13,969	8.158
1.25	28,531 ± 110	18.99 ± 0.11	14,279	8.415
1.30	28,935 ± 150	19.43 ± 0.14	14,598	8.647
1.35	29,241 ± 180	19.79 ± 0.17	14,927	8.863
1.40	29,822 ± 250	20.42 ± 0.24	15,216	9.118
1.45	30,142 ± 300	20.84 ± 0.28	15,516	9.343
1.50	30,536 ± 350	21.34 ± 0.34	15,709	9.579
1.55	30,874 ± 410	21.81 ± 0.38	16,111	9.816
1.60	31,196 ± 430	22.28 ± 0.41	16,393	10.012
1.65	31,681 ± 490	22.95 ± 0.46	16,691	10.285
1.70	32,251 ± 490	23.77 ± 0.46	16,980	10.529
1.75	33,438 ± 360	25.39 ± 0.34	17,265	10.764
Absorption				
2.00	9,865 ± 250	15.63 ± 0.45		
2.10	10,175 ± 360	16.24 ± 0.06		
2.20	10,449 ± 200	16.75 ± 0.35		
2.30	10,653 ± 240	17.17 ± 0.43		
2.40	10,739 ± 320	17.39 ± 0.56		
2.50	11,086 ± 180	18.09 ± 0.33		
2.60	11,376 ± 280	18.83 ± 0.50		
Desorption				
2.00	9,867 ± 370	14.59 ± 0.63		
2.10	10,365 ± 250	15.60 ± 0.43		
2.20	10,411 ± 190	15.70 ± 0.34		
2.30	10,622 ± 150	16.09 ± 0.26		
2.40	10,816 ± 130	16.46 ± 0.22		
2.50	11,090 ± 830	17.02 ± 0.14		
2.60	11,851 ± 450	18.56 ± 0.78		

^a Graphically extrapolated value in the infinite dilution range. ^b Two-phase region approximate composition limits. It is to be noted that the listed relative partial molal quantities for the two-phase region correspond to the heat and entropy for the reaction $1/(r'' - r')YH_{r'} + 1/2H_2 \rightarrow 1/(r'' - r')YH_{r''}$, where r' and r'' are the atom ratios (H/Y) for the two-phase boundaries.

position, $YH_{2.7}$, obtained by Dialer and Frank³ at a pressure of 1 atm. in a quartz-glass apparatus similar to the one used here, is in good agreement with the

highest composition reached in the present study as may be seen in Figure 3. Also, it may be seen from Figure 3 that the composition, $YH_{1.999}$, reported by Flotow, Osborne, and Otto^{4,5} at 350° and 760 mm. is consistent with the highest composition $YH_{1.972}$ obtained at 351.3° and 717 mm. Kost¹⁰ reported a single hydride phase of limiting composition $YH_{1.6}$, but this is not in agreement with X-ray observations^{2,9} nor with a reasonable extrapolation of the phase boundaries (Figure 2). A comparison of the enthalpy value $(\bar{H}_H - 1/2H^\circ_{H_2}) = -54.30 \pm 0.36$ kcal./mole of H_2 for the reaction (see footnote *b* in the table) in the two-phase regions with the value -44.42 ± 0.40 kcal./mole of H_2 reported by Lundin and Blackledge² and the value -54.2 kcal./mole of H_2 reported¹¹ from the unpublished work of Bradshaw indicates that the value -54.3 kcal./mole of H_2 is to be preferred. A linear extrapolation of the integral entropy values for stoichiometric YH_2 and YH_3 from the heat capacity data of Flotow, Osborne, and Otto^{4,5} gives agreement, within the experimental error, with the value for $YH_{1.75}$ given in the table.

The Y-H system shows a decided similarity to the rare earth M-H system, in particular Gd-H¹² and Yb-H,¹⁵ although the wide homogeneity range of the hydrogen-deficient yttrium dihydride phase found in this study seems to be a characteristic difference from those of the rare earth metal hydrides.¹¹⁻¹³

As a part of an unsuccessful attempt to fit the data to the modified⁸ Lacher's¹⁴ statistical model, it was found possible to fit the data of the two single-phase regions in the composition range Y- $YH_{1.75}$, for the relative partial molal enthalpy of hydrogen to a fourth-order polynomial in r , the hydrogen to yttrium atomic ratio; *i.e.*

$$(\bar{H}_H - 1/2H^\circ_{H_2}) = R(-9631 - 11,733r + 12,144r^2 - 5150r^3 + 406r^4)$$

where R is the gas constant. Using this equation and the integral form

$$\Delta H_f = \frac{1}{1+r} \int_0^r (\bar{H}_H - 1/2H^\circ_{H_2}) dr$$

the ΔH_f values were also calculated. The calculated $(\bar{H}_H - 1/2H^\circ_{H_2})$ and ΔH_f values were found to be in

(10) M. E. Kost, *Dokl. Akad. Nauk SSSR*, **143**, 119 (1962).

(11) P. M. S. Jones and J. Southall, *AWRE-0-24/64*, 1964.

(12) G. E. Sturdy and R. N. R. Mulford, *J. Am. Chem. Soc.*, **78**, 1083 (1956).

(13) C. J. Warf and K. Hardcastle, Office of Naval Research Reports 1 and 2, Contract No. 228 (15), Project No. NR-052-39.

(14) J. R. Lacher, *Proc. Roy. Soc. (London)*, **A161**, 525 (1937).

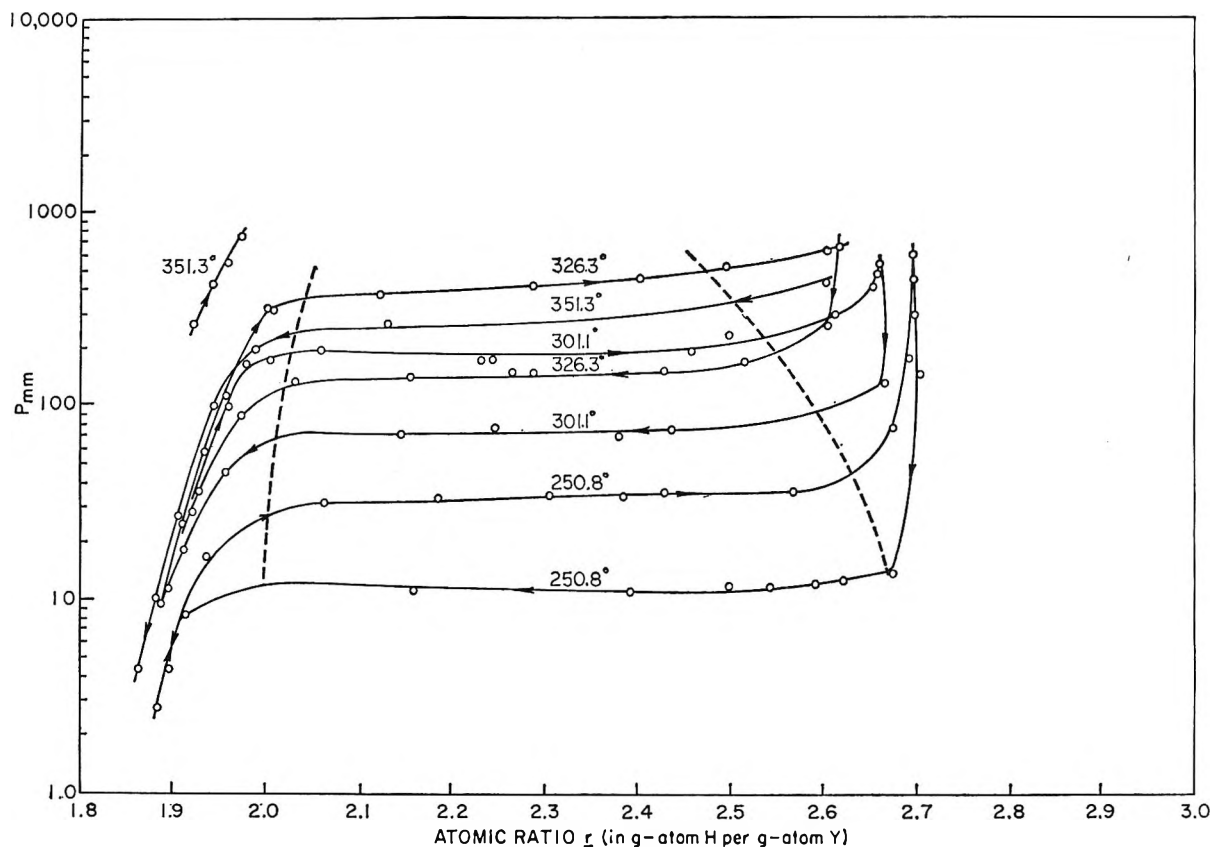


Figure 3. Experimental isotherms for the system yttrium-hydrogen. Absorption and desorption reproducible, irreversible curves are designated by the right- and left-hand arrows, respectively.

good agreement with the observed values given in the table, within the average per cent deviation of ± 2.4 and $\pm 0.5\%$, respectively. Use of the Gibbs-Duhem equation and the above polynomial expression yielded relative partial molal enthalpies for the yttrium metal in solution in good agreement with those obtained by means of the Gibbs-Duhem equation and values of $(\bar{H}_H - \frac{1}{2}H^\circ_{H_2})$ and ΔH_f from the table, except at low hydrogen compositions where small differences in large numbers are involved.

Recent attempts¹⁵ have been made to elucidate the phenomenon of hysteresis, in general, and, in particular, the Pd-H behavior is critically reviewed.¹⁶ The reproducible hysteresis observed in the YH_2 - YH_3 region may serve as a further example for testing Everett's¹⁷ theory.

Acknowledgment. The support of the A.F.O.S.R. and the A.E.C. during the course of this work is gratefully acknowledged. L. N. Y. wishes to thank the Illinois Institute of Technology for a fellowship for 1962-1963. R. K. E. and L. N. Y. acknowledge the support of the Chemical Engineering Division of Argonne National Laboratory during the preparation of the manuscript.

(15) N. A. Scholtus and K. W. Keith, *J. Chem. Phys.*, **39**, 868 (1963).

(16) D. H. Everett and P. Nordon, *Proc. Roy. Soc. (London)*, **A259**, 341 (1960).

(17) (a) D. H. Everett and W. I. Whitton, *Trans. Faraday Soc.*, **48**, 749 (1952); (b) D. H. Everett and F. W. Smith, *ibid.*, **50**, 187 (1954); (c) D. H. Everett, *ibid.*, **50**, 1077 (1954); (d) D. H. Everett, *ibid.*, **51**, 1551 (1955).

Rates of Decay of Phosphorescence from Triphenylene in Acrylic Polymers

by F. C. Unterleitner and E. I. Hormats

Quantum Physics Laboratory, General Dynamics/Electronics, Rochester, New York 14601
(Received December 28, 1964)

The rates of decay of phosphorescence from triphenylene molecules dissolved in polymethyl methacrylate and polybutyl acrylate have been studied between -120 and 100° . In both materials the decay is found to be nonexponential and independent of pump intensity, implying a distribution of sites within the polymer. The knee in the temperature dependence of integrated phosphorescence intensity from polybutyl acrylate coincides with the glass-rubber phase transition. Evidence for the existence of glassy regions in the rubber phase is presented.

Introduction

The luminescent properties of aromatic organic materials dissolved in transparent plastics have been used to study energy transfer,¹ lifetimes of triplet states,² and molecular polarization³ of aromatic compounds. This luminescence may also be used to study properties of the plastic matrix itself; for example, the rate of diffusion of oxygen in polymethyl methacrylate has been measured by use of oxygen quenching at this laboratory,⁴ and the internal structure of polymer solutions has been studied by fluorescence polarization.⁵ This paper indicates the possibility of utilizing the integrated intensity of phosphorescence and the time dependence of phosphorescence decay rate after short flash excitation to obtain information on the temperature dependence of polymer microstructure.

The intensity and decay time of phosphorescence decrease markedly as the matrix turns from a glass to a viscous liquid.⁶ Since this change from glass to viscous liquid is somewhat analogous to the change in a polymer from a hard form to a rubbery one, it was thought that the change in intensity might be used as a measure for the glass transition temperature, T_g . Many temperature-dependent properties of polymers undergo abrupt changes and discontinuities at T_g . Most of these are macroscopic in nature, such as the density, elasticity, or gas permeability, and show only a gradual change in the vicinity of T_g . Thus it was hoped that a property depending on the internal structure, such as the phosphorescence quenching, might give a more serviceable and accurate measurement of the glass transition temperature of polymers.

With this in mind, an investigation into the decay time and intensity of phosphorescent organic compounds above and below the glass transition was undertaken. Triphenylene was chosen as the indicator since it has a relatively long decay time, has quite intense phosphorescence, and is soluble in monomeric materials.

Experimental measurements have been made using two acrylic polymers that are similar chemically but have quite different physical properties. One is polymethyl methacrylate (PMMA) which has been used extensively. The second is polybutyl acrylate (PBA) which was chosen because it has a low glass transition temperature of -56° .⁷

Experimental

Materials. The methyl methacrylate and butyl acrylate monomers (Rohm and Haas) were inhibited by MEHQ and contained other trace impurities which produced strong phosphorescence in the polymer, especially at low temperatures. The monomers were therefore purified by successive washings with 5% sodium nitrite, 5% sodium bisulfite, 5% sodium hydroxide, and three with distilled water. The mono-

(1) K. B. Eisenthal, *J. Chem. Phys.*, **39**, 2108 (1963).

(2) W. H. Melhuish and R. Hardwick, *Trans. Faraday Soc.*, **58**, 1908 (1962).

(3) M. A. El-Sayed, *J. Opt. Soc. Am.*, **53**, 797 (1963).

(4) E. Hormats and F. Unterleitner, to be published.

(5) Y. Nishijima, "Luminescence of Organic and Inorganic Materials," John Wiley and Sons, Inc., New York, N. Y., 1962, p. 235.

(6) G. Porter and L. J. Stiet, *Nature*, **195**, 991 (1962).

(7) F. Bueche, "Physical Properties of Polymers," Interscience Publishers, Inc., New York, N. Y., 1962, p. 110, Table 4.

mers were then dried over Drierite and vacuum distilled. These materials, when outgassed and polymerized with α, α -azodiisobutyronitrile (Azo) catalyst, had barely detectable phosphorescence even at 77°K. For the samples reported here, 0.10% w./w. triphenylene and 0.033% w./w. Azo were dissolved in the methyl methacrylate and 0.098% w./w. triphenylene and 0.011% w./w. Azo were dissolved in the butyl acrylate. The monomer solutions were then transferred to 8-mm. Pyrex tubes, sealed to a vacuum rack, and outgassed by several cycles of freezing with liquid nitrogen and warming under vacuum. The tubes were then filled with dry nitrogen and sealed off. Experiments on oxygen diffusion in similar polymethyl methacrylate samples have been carried out in this laboratory and the results indicate that this procedure is very effective in removing molecular oxygen from the samples, perhaps because the polymerization process assists in scavenging the residual molecular oxygen. The samples were slowly polymerized in order to ensure uniform polymerization; the temperature cycle started at 45° and final cure was 1 day at 110°. The PBA was quite rubbery with a sticky surface when cooled and removed from the Pyrex tube. Upon removal from the tubes, test samples were cut to 5-cm. length and immediately placed in the test cell with a dry nitrogen atmosphere.

Transition Temperature. The glass transition temperature of the PBA sample used for the phosphorescent measurements was measured by dilatometry using denatured 95% alcohol as the working fluid. This was done to determine whether the phosphor acted as a plasticizer or if any unpolymerized material remained to plasticize the material. The glass transition temperature, as determined by the break in the volume-temperature plot, was found to be -55°, in excellent agreement with Bueche.⁷

Phosphorescence Measurements. The phosphorescent spectrum emitted by these samples was measured with a phosphoroscope having a 1-msec. delay time. It consists of a strong peak centered at 21,500 cm^{-1} at room temperature with about seven subsidiary peaks. A slight blue shift and considerable sharpening of the spectrum occurs as the temperature is lowered to 77°K. The spectrum correlates well with that reported for triphenylene in EPA glass at 77°K. by Clar and Zander.⁸ Since no measurable phosphorescent intensity was noted aside from the triphenylene peaks, decay time measurements were made without a monochromator in order to increase the intensity range available for the measurements. Plastic samples were placed in a quartz tube sample holder (Figure 1) and were flash-pumped with a xenon flashlamp having

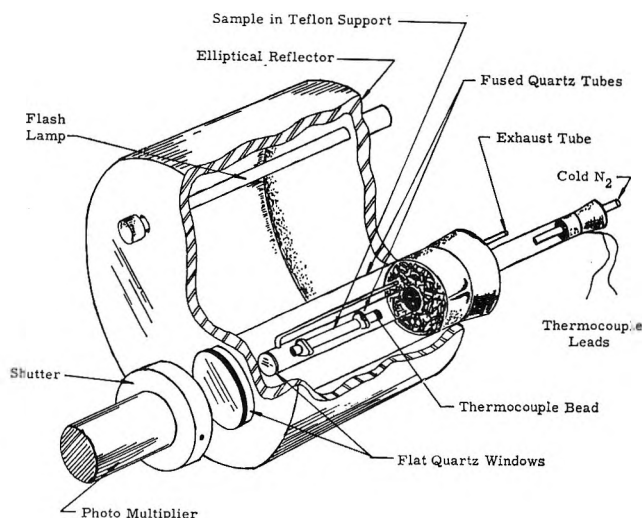


Figure 1. Flash apparatus.

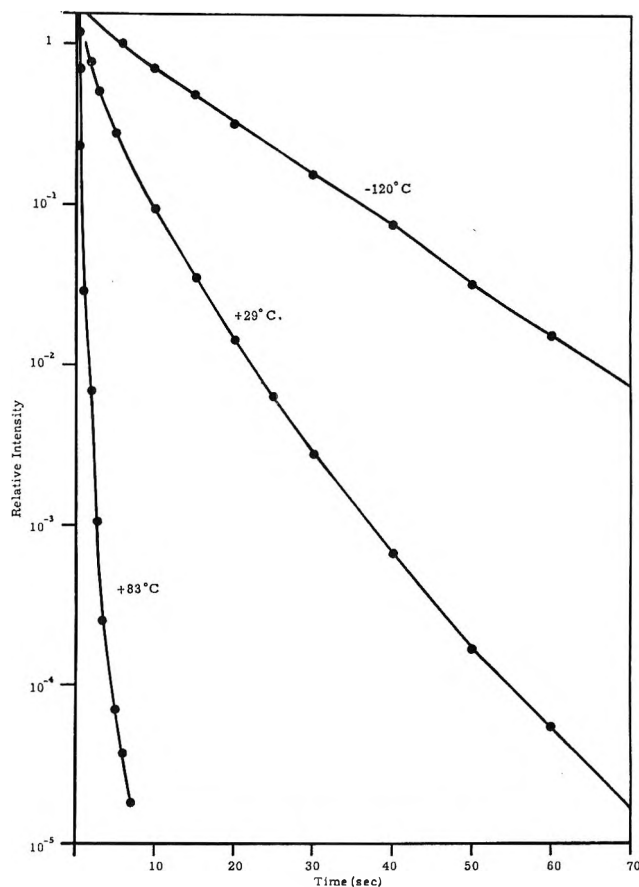


Figure 2. Intensity of phosphorescence from triphenylene in polymethyl methacrylate as a function of time after pump flash at three temperatures.

(8) E. Clar and M. Zander, *Chem. Ber.*, 89, 749 (1956).

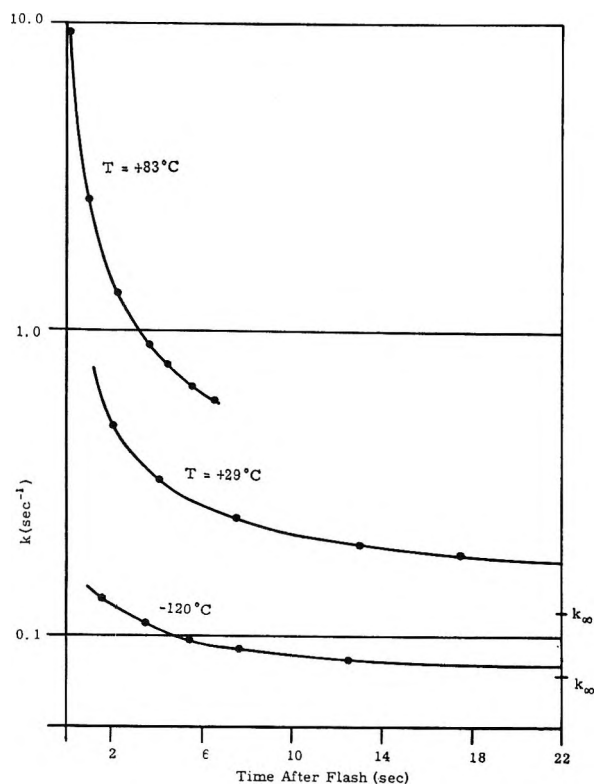


Figure 3. Rate constants for triphenylene in polymethyl methacrylate at three temperatures.

a 100- μ sec. flash duration. The total phosphorescence was measured by an EMI 6256B photomultiplier without intervening optical elements, aside from the quartz windows of the cooling cell and a shutter. Care was taken not to exceed 10^{-5} amp. anode current in the photomultiplier, as recommended by the manufacturer for stable linear operation, and peak luminous flux was maintained below photocathode saturation levels. Photomultiplier current was recorded on an Offner strip chart recorder except for times less than 0.1 sec. after the flash, for which oscilloscope photographs were used.

The sample was cooled with cold gaseous nitrogen obtained by evaporation of liquid nitrogen. The rate of gas flow and hence the sample temperature could be controlled by the electrical power passed through a 100-w. heater in the liquid nitrogen dewar. Tank nitrogen passed over a hot nichrome ribbon was used to heat the sample above room temperature. Again control of the gas flow and the power input to the heater controlled the sample temperature. The sample temperature was measured by a copper-constantan thermocouple, held onto the surface of the sample by a strip of Mylar tape, and a Rubicon portable potentiometer.

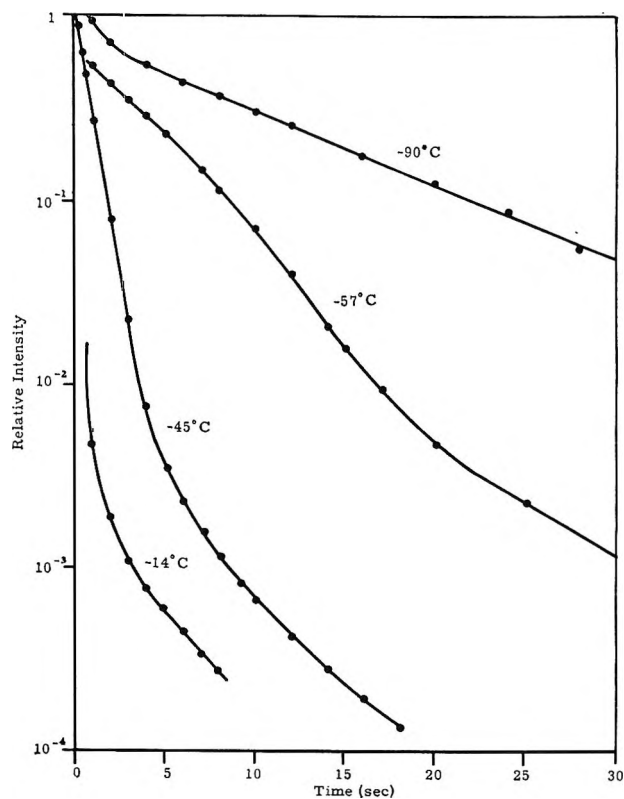


Figure 4. Intensity of phosphorescence from triphenylene in polybutyl acrylate as a function of time after pump flash at four temperatures.

Results

The intensity of phosphorescence as a function of time after flash is plotted in Figure 2 for three different temperatures of PMMA containing 0.1% triphenylene by weight. Within the error of the measurements the initial intensity, extrapolated to $t = 0$, is the same for all temperatures up to 80° , implying that efficiency of internal conversion into triplet excitation is independent of temperature over this temperature range. We define the instantaneous rate constant $k(t)$ by the relation

$$k(t) = -\frac{d}{dt} \ln (I(t)/I_0)$$

which reduces to the normal rate constant for the case of exponential decay. The rate constants for the three intensity curves shown in Figure 2 are plotted in Figure 3. The indicated k_∞ values were obtained by plotting $k(t)$ vs. $1/t$ and extrapolating to zero. It is clear that even at -120° there is still appreciable departure from exponential decay. The glass-rubber transition in PMMA takes place at about 105° ,⁷ so that all of these decay curves are representative of the glass phase of the material.

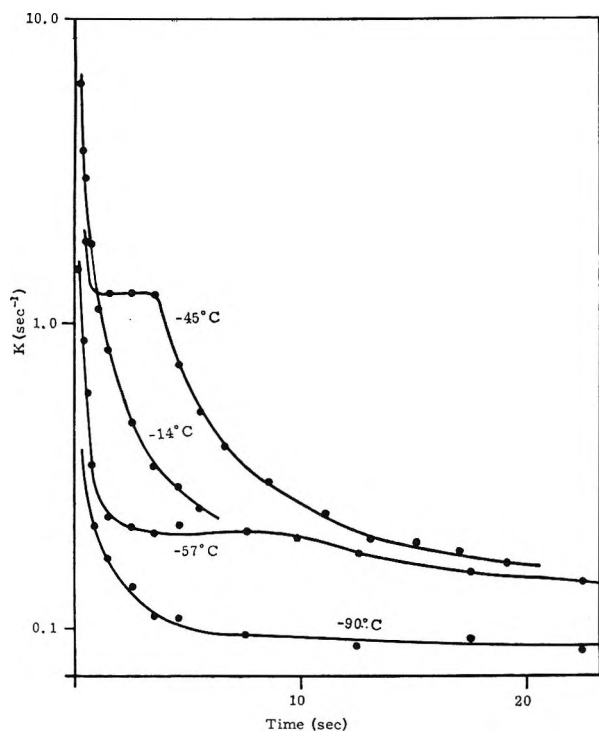


Figure 5. Rate constants for triphenylene in polybutyl acrylate at four temperatures.

The phosphorescence intensity after flash of PBA with 0.10% w./w. triphenylene is shown in Figure 4. It is evident that the intensity drops off rapidly with temperature above $T_g = -55^\circ$. The instantaneous rate constants derived from these data are shown in Figure 5. Well below T_g the curves match those for PMMA quite closely. At -57° ($\sim T_g$) the rate has a plateau considerably above the rate for PMMA, and at -45° (10° above T_g) the plateau is still noticeable, but it is at a much higher value of rate constant. By -14° the plateau may have shifted to rate constants too short to be observed in these experiments, and only the residual slow decay is observed. At room temperature, $k(t)$ vs. t is almost identical with that in PMMA at the same temperature for $0.5 \text{ sec.} < t < 5 \text{ sec.}$, but the intensity is down by about five orders of magnitude.

If the integrated phosphorescent emission is plotted as a function of temperature, Figure 6, there is a knee in the PBA curve which corresponds within experimental error to the glass transition temperature. If this can be shown to be generally valid, it could prove to be a relatively simple method for determining T_g .

The dependence of the rate constant on time after the pump flash proved to be quite reproducible for different samples and pump flash energies. The independence of flash energy, as clearly shown in Figure

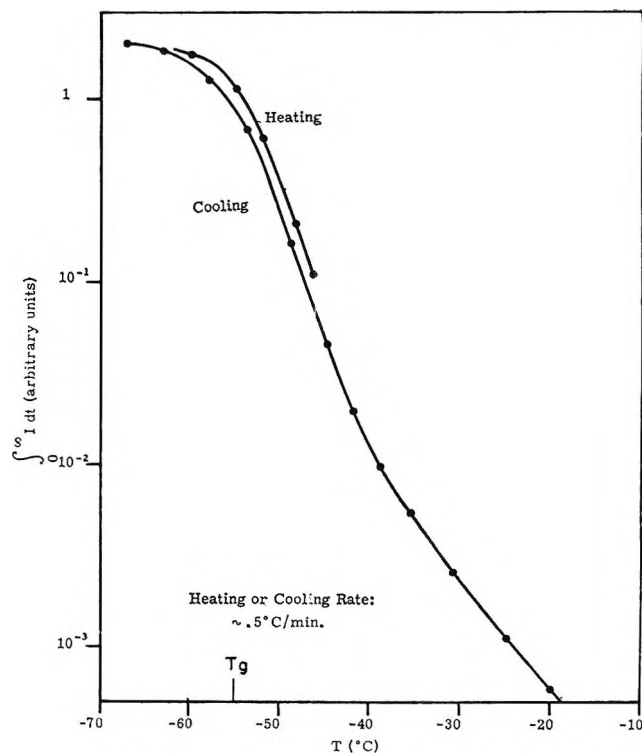


Figure 6. Integrated phosphorescence emission from triphenylene in polybutyl acrylate as a function of temperature.

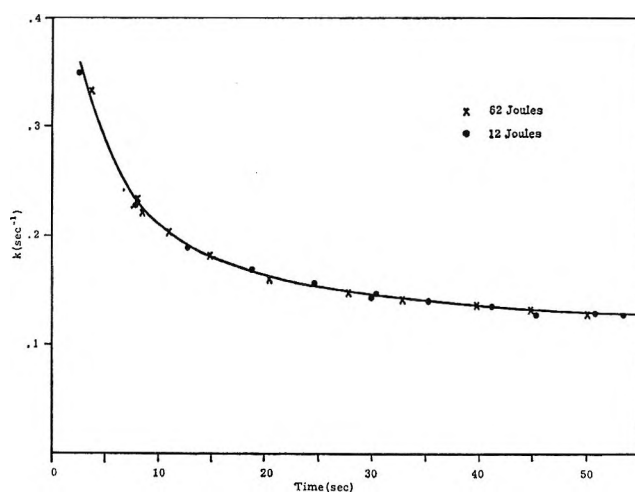


Figure 7. Rate constants for triphenylene and polymethyl methacrylate at two different flash energies.

7, indicates that the effect is not due to the interaction between molecules in the excited state, which has been observed in crystalline and liquid environments, and is strongly dependent on triplet state concentration (that is, pump intensity). The most reasonable explanation appears to be that there is a distribution of sites in the polymer in which the triphenylene (or other

phosphor) molecules may be located and that these sites differ in local vibrational properties and hence in thermal quenching coefficient. Although this view does not seem to conflict with any of the experimental evidence presented, the relationship between the thermal quenching of phosphorescence and the polymer environment does not appear to be understood on a theoretical level; therefore comparisons with theory cannot be made.

Conclusions

Several conclusions can be drawn from these data without further analysis. The time dependence of decay rate in PBA in the rubbery phase is seen to have a plateau of uniform rate followed by a tail of varying rate extending to the limits of observability. The existence of a plateau in $k(t)$ implies that there are a large number of sites having the same rate constant, if the statistical interpretation of the previous section is

valid. The "tail" coincides almost perfectly with that observed in PMMA at corresponding temperatures, implying that glass-like regions continue to exist in the rubbery phase. A comparison of residual intensity leads to the conclusion that perhaps 10^{-5} part by volume of PBA maintains the glassy phase microstructure at 20° . The temperature dependence of rate constants in PMMA clearly indicates that considerable variations in microstructure exist even at -120° , but more work needs to be done to clarify the nature of the interaction which leads to nonradiative quenching of the triplet state in such an environment before specific deductions based on these observations can be made.

Acknowledgments. The authors wish to acknowledge the many helpful discussions with Dr. Ernest Brock and Dr. Jack Taylor, and the valuable assistance of Mr. Kermit Mercer with the experimental work.

Scaling in Isoelectronic Molecules

by Jerry Goodisman¹

Department of Chemistry, University of Illinois, Urbana, Illinois 61803 (Received December 30, 1964)

A modification of a scaling method introduced for atoms by Ellison enables one to use expectation values calculated for one molecule in calculations of the energy of a second molecule isoelectronic to the first. In going from H_2 to He_2^{2+} , the results are only fair, but in going from LiF to BeO, the results are sufficiently good to allow prediction of equilibrium distance and several expectation values as well as energy. The dipole moment is a notable exception, which reveals one basic dissimilarity between the two molecules, the ionic character. LiF dissociates to ions, BeO to neutral atoms, causing our method to break down at large internuclear distance. The inverse scaling transformation, from BeO to LiF, is also accomplished, with similar results.

In an *a priori* molecular calculation, physical intuition may help in choosing the form for a trial wave function for variation, but one is very rarely in the position of being able to use the wave function for one system for a calculation on another, however closely they are related physically. For atoms, one can use

such fundamental theorems as the virial and Hellman-Feynman theorems to elucidate relations between wave functions for various different systems.² Ellison

(1) Part of research supported by National Science Foundation.

(2) For example, P.-O. Löwdin, *J. Mol. Spectry.*, **3**, 46 (1959).

and Huff³ have taken advantage of a scaling procedure, closely related to that used in Fock's proof of the virial theorem,⁴ to calculate the energy of an atomic system from one isoelectronic to it. Tests of the method for various cases^{3b} show impressive agreement.

It is well known that, for molecules, when the usual Born-Oppenheimer separation is used and electronic wave functions are calculated with the nuclei fixed, the virial theorem does not hold in its simple form.⁵⁻⁷ Hirschfelder and Kincaid⁶ have given one way of modifying this theorem, and this suggests a corresponding modification of Ellison's procedure for use in molecules. We first sketch out the arguments of Hirschfelder-Kincaid and Ellison, then formulate the new procedure and apply it to simple cases.

Let $\psi_1(r;R)$ be a wave function for a molecule. We denote all the electronic coordinates by small r and all the nuclear coordinates, which enter as parameters in the usual treatment, by capital R . If we scale (*i.e.*, multiply) *all* coordinates by a parameter, s , we get the scaled wave function $\psi_{1s}(r;R) = s^{3n/2}\psi_1(sr,sR)$. The $s^{3n/2}$ is the correct normalizing factor where n is the number of electrons. We do not integrate over nuclear coordinates in computing norms and expectation values. It is straightforward to show by changing variables in the integrals^{2,3a,6} that $T_s(R) = s^2T_1(sR)$ and $V_s(R) = sV_1(sR)$, where the T 's are expectation values of the kinetic energy and the V 's expectation values of the potential energy. The R or sR in parentheses means this is computed with the internuclear distance held fixed at R or sR , while the subscript 1 or s indicates the use of ψ_1 or ψ_{1s} for the calculation. We find the value of s , s_0 , which minimizes $E_s(R) = T_s(R) + V_s(R)$. If ψ_1 is the exact wave function, s_0 must equal 1. Then, at the equilibrium R , the simple virial theorem holds⁶; at some other R , Slater's modification⁵ will hold.

Now the potential energy consists of three parts

$$V_s(R) = C_s(R) + L_s(R) + M_s(R)$$

and similarly for V_1 , where the three parts are the expectation values of the electron-electron, electron-nucleus, and nucleus-nucleus Coulombic interactions. We want to use the scaled wave function for one molecule for calculation on another molecule isoelectronic with it and related to it by having all nuclear charges multiplied by a constant Z . Then $C_s(R)$ is unchanged, $L_s(R)$ is multiplied by Z , and $M_s(R)$ is multiplied by Z^2 . The expectation value of the energy, using the scaled wave function for the first molecule and the Hamiltonian for the second, is

$$\bar{E}_s(R) = s^2T_1(sR) + sC_1(sR) + ZsL_1(sR) + Z^2sM_1(sR)$$

If we minimize $E_s(R)$ with respect to s , holding sR fixed equal to a constant R_0 , Hirschfelder and Kincaid⁶ note that we will always get an improvement on the energy, but, with sR fixed and s in general different from 1, we will be calculating the energy for the system at $R = R_0/s_0$. This is also true if we minimize $\bar{E}_s(R)$. One finds easily

$$s_0 = [2T_1(sR)]^{-1}[-C_1(sR) - ZL_1(sR) - Z^2M_1(sR)]$$

and the new energy equals

$$\bar{E}_{s_0}(R) = -[4T_{s_0}(R_0)]^{-1}[C_{s_0}(R_0) + ZL_{s_0}(R_0) + Z^2M_{s_0}(R_0)]^2 = -T_{s_0}(R)$$

The last relation expresses the fact that the virial theorem is being satisfied by the scaled function with the Hamiltonian for the second molecule. The case $Z = 1$ is of course the usual case, where a molecular wave function is improved by scaling.

We consider as our unscaled function that for H_2 at its equilibrium internuclear distance, $1.4a_0$. According to the Kolos-Roothaan 40-term function⁸ the total energy in atomic units here is -1.174440 , the total potential energy is -2.349279 (electron-electron potential energy = 0.58737 , nucleus-nucleus potential energy = 0.714286 , electron-nucleus potential energy = -3.65094), and the electronic kinetic energy = 1.174839 . We use this for the He_2^{2+} ion, for which good wave functions are also available.⁸ By the above equations, we find $s_0 = 1.64165$ so that $R = R_0/s_0 = 0.85280$. The new energy is calculated as -3.16621 atomic units. Kolos and Roothaan⁸ do not give the energy at this distance, but by fitting the first five points in their Table XI, $\alpha = 1.75$, to a parabola, we find that the correct answer is -3.433 atomic units.

Note that the variational principle holds here; our answer must be too high. A series of similar calculations with H_2 data for different internuclear distances would yield a series of results for He_2^{2+} , but there is not sufficient data in ref. 8 to make this possible. The agreement is not very good; Ellison^{3b} found, however, that agreement for atoms was better for smaller ratios of nuclear charges, which is reasonable.

There is no reason to limit this kind of treatment to

(3) (a) F. O. Ellison, *J. Chem. Phys.*, **37**, 1414 (1962); (b) F. O. Ellison and N. T. Huff, *ibid.*, **39**, 2051 (1963).

(4) V. Fock, *Z. Physik*, **63**, 855 (1930).

(5) J. C. Slater, *J. Chem. Phys.*, **1**, 687 (1933).

(6) J. O. Hirschfelder and J. F. Kincaid, *Phys. Rev.*, **52**, 658 (1937).

(7) C. A. Coulson and R. P. Bell, *Trans. Faraday Soc.*, **41**, 141 (1945); A. C. Hurley, *Proc. Roy. Soc. (London)*, **A226**, 170 (1954).

(8) W. Kolos and C. C. J. Roothaan, *Rev. Mod. Phys.*, **32**, 219 (1960).

Table I: Calculations for LiF \rightarrow BeO^a

$sR(a_0)$	$T_1(sR)$	$C_1(sR)$	$L_1^A(sR)$	$L_1^B(sR)$	$M_1(sR)$	s_0	$\frac{sR(a_0)}{s_0}$	\bar{E}_{s_0}
1.60	109.52710	59.46506	-34.37385	-257.7301	16.87500	0.892291	1.79314	-87.2036
2.10	107.92227	56.59302	-30.44886	-253.7509	12.85714	0.900295	2.33257	-87.4744
2.35	107.47837	55.49567	-28.99485	-252.3926	11.48936	0.902024	2.60525	-87.4495
2.60	107.19787	54.60136	-27.79869	-251.3504	10.38461	0.902903	2.87960	-87.3914
2.85	107.02626	53.87033	-26.80035	-250.5460	9.47368	0.903254	3.15526	-87.3193

^a Expectation values in columns 1-5 obtained from calculation VIII.A of McLean, ref. 9. All energies in atomic units. See text for abbreviations.

cases where the isoelectronic molecules are related by symmetric scaling of the nuclear charges. Let us increase the charge on nucleus A by a factor Z_A and the charge on nucleus B by Z_B (generally, one of these will be >1 and the other <1). Minimizing the energy with respect to the scaling parameter s while holding $sR = R_0$ fixed yields

$$s_0 = [2T_1(sR)]^{-1}[-C_1(sR) - Z_A L_1^A(sR) - Z_B L_1^B(sR) - Z_A Z_B M_1(sR)]$$

where we write L_1^A for the expectation value of the interaction of the electrons with nucleus A, and L_1^B for that for nucleus B. The energy obtained is equal to $-s_0^2 T_1(sR)$.

In attempting to apply this to molecules, one finds that the literature offers a paucity of published calculations with sufficient data for our procedure. We require the expectation values of total energy, kinetic energy, and electron-nucleus interaction for each nucleus. McLean⁹ has performed a series of LCAO-SCF calculations on the LiF molecule and tabulated many important expectation values. We employ these for calculations on the isoelectronic BeO molecule. Furthermore, Yoshimine¹⁰ has performed limited basis SCF calculations for BeO, and we can use his results in several ways, to be indicated below. Here, Z_A (referring to Li \rightarrow Be) is $4/3$ and Z_B (referring to F \rightarrow O) is $8/9$. The expectation values used come from McLean's calculation VIII.A and appear, with the results, in Table I. We have used only values of sR ($=R_{\text{LiF}}$) such that R ($=R_{\text{BeO}}$) falls near the equilibrium value.

From data in Herzberg,¹¹ we estimate the true total energy of BeO at the equilibrium distance as -89.784 a.u. Our energy at the minimum, -87.478 , is off by 2.5%. We have fitted the five calculated energies to a parabola in the internuclear distance.¹² The result is an equilibrium distance of $2.55 \pm 0.01a_0$ and a force constant of 0.88 ± 0.20 a.u./ a_0^2 or 13.7×10^5 dynes/cm.², to be compared with the experimental¹¹ $2.5147a_0$ and 7.5089×10^5 dynes/cm.².

Now we refer to the calculations of Yoshimine¹⁰ on BeO, similar in scope to McLean's for LiF. This enables us, first, to decide whether the errors in the quantities calculated above are to be considered large and, second, to compare a wider variety of scaled expectation values (whose calculation we discuss below), for some of which experimental data are not available, with their values as predicted by an *a priori* calculation on BeO. Finally, the expectation values furnished by Yoshimine allow us to accomplish the scaling transformation from BeO to LiF.

With reference to the first point, we note that Yoshimine's calculated equilibrium internuclear distance for BeO is $2.4378a_0$, *i.e.*, 3% too low, whereas ours is about 1.05% too high. His calculated force constant (proportional to the square of the frequency) is high by a factor of 1.2, ours by a factor of 1.8.

The calculation of expectation values with the scaled function is straightforward. Let $f(r_e)$ be a function homogeneous of degree i in the electronic coordinates, *i.e.*, $f(sr_e) = s^i f(r_e)$. The electron-electron potential energy, for instance, is homogeneous of degree -1 ; the kinetic energy operator for the electrons may be

(9) A. D. McLean, *J. Chem. Phys.*, **39**, 2653 (1963).

(10) M. Yoshimine, *ibid.*, **40**, 2970 (1964).

(11) G. Herzberg, "Spectra of Diatomic Molecules," D. Van Nostrand Co., Inc., New York, N. Y., 1950, pp. 458, 509.

(12) Strictly speaking, these are not the points we should be fitting to get the equilibrium distance and force constant. What we really would like to have is a contour map, giving calculated energy as a function of both scaling parameter s and BeO internuclear distance R . We should then obtain the best scaling parameter and minimum energy for each internuclear distance and fit these points to a parabola. The path through the minima would not, in general, be parallel to either the s or the R axis. What we are doing now is finding the best scaling parameter and minimum energy on the hyperbolae $sR = 1.60, 1.85, 2.10$, etc., and fitting *these* minima to a parabola. We could, in principle, interpolate on each hyperbola to get energies at any value of R , then use these to find the best energy and scaling parameter for each R . This interpolation turns out to be far from reliable and seems to lead to only small changes in the equilibrium distance and force constant for LiF \rightarrow BeO.

Table II: Expectation Values for LiF \rightarrow BeO

$R_{\text{LiF}} = sR(a_0)$	$R_{\text{BeO}} = \frac{sR(a_0)}{s_0}$	E in a.u. by scaling	E by direct calcn. ^a	$\langle r^2 \rangle_{\text{Be}}$ by scaling, a_0^2	$\langle r^2 \rangle_{\text{Be}}$ by calcn. ^a	$\langle 3z^2 - r^2 \rangle_{\text{Be}}$ by scaling	$\langle 3z^2 - r^2 \rangle_{\text{Be}}$ by calcn. ^a	Dipole moment in a.u., by scaling	Dipole moment in a.u., by calcn. ^a
1.60	1.79314	-87.204		49.3824		61.9975		2.9337	
	1.80		-89.153	48.3478	55.4156	2.1593			
	2.150		-89.404	61.1407	79.4192	2.5121			
2.10	2.33257	-87.474		71.2409		104.4469		4.1735	
	2.400		-89.444	71.4815	99.2673	2.7467			
	2.476		-89.444	74.8265	105.7250	2.8114			
	2.550		-89.440	78.1726	112.1944	2.8697			
2.35	2.60525	-87.449		84.3566		130.445		4.6928	
	2.800		-89.412	90.0982	135.2481	3.0072			
2.60	2.87960	-87.391		98.9682		159.618		5.2015	
	3.050		-89.373	102.8409	159.5814	2.9401			
2.85	3.15526	-87.319		115.6269		191.976		5.7099	
	3.800		-89.300	145.1189	238.7916	1.7578			

^a SCF-LCAO calculations by M. Yoshimine, *J. Chem. Phys.*, **40**, 2970 (1964).

considered as homogeneous with $i = -2$. Note that the complete potential energy function is not homogeneous in the electronic coordinates alone. Denoting by $\langle f \rangle_s^R$ the expectation value of f at an internuclear distance R , calculated with the scaled wave function, and $\langle f \rangle_1^{sR}$ the expectation value calculated with the unscaled function at internuclear distance sR , we have

$$\langle f \rangle_s^R = \langle f \rangle_1^{sR} / s^i$$

This is shown by a simple change of variables in the integral, as in the proofs of the virial theorem itself.^{4,6}

In Table II, we have used this to calculate $\langle r_{\text{Be}}^2 \rangle_s^R$ and $\langle 3z_{\text{Be}}^2 - r_{\text{Be}}^2 \rangle_s^R$ from $\langle r_{\text{Li}}^2 \rangle_1^{sR}$ and $\langle 3z_{\text{Li}}^2 - r_{\text{Li}}^2 \rangle_1^{sR}$. The values of R and s from Table I have been employed. For $\langle r^2 \rangle_{\text{Be}}$, we get good agreement with Yoshimine's calculations,¹¹ to a few per cent. The average or expectation value of the square of a distance of an electron from a nucleus is a measure of the size of a molecule. It is the size which a scaling factor can adjust, so that we probably should expect good results here. On the other hand, the expectation value of $\langle 3z_{\text{Be}}^2 - r_{\text{Be}}^2 \rangle = 2(z_{\text{Be}}^2 - x_{\text{Be}}^2)$, which is essentially the electronic contribution to the molecular quadrupole moment, is a measure of the shape of the electron distribution. The agreement here is not nearly as good, but still satisfactory. We should expect the agreement in both cases to get progressively worse at large R . For example, with $sR = R_{\text{LiF}} = 4.85$, we calculate an optimum value of $s = 0.90126$. The predicted values of $\langle r_{\text{Be}}^2 \rangle_s^R$ and $\langle 3z_{\text{Be}}^2 - r_{\text{Be}}^2 \rangle_s^R$ are then $302.173a_0^2$ and $565.955a_0^2$. $R = 4.85/0.90126 = 5.38134a_0$. Interpolating in Yoshimine's results, we estimate the correct values to be, respectively,

$250a_0^2$ and $450a_0^2$. The per cent errors are about the same in both, since, for large internuclear distance, $\langle z^2 \rangle \rightarrow \langle r^2 \rangle$.

The dipole moment consists of an electronic part and a nuclear part. The latter can be separated out and calculated exactly, while the former's operator is homogeneous of degree 1. It is, in fact, $\sum_j z_j$, where z_j is the distance of electron j along the internuclear axis from some origin. For an electrically neutral molecule, the origin may be chosen arbitrarily, as long as it is used consistently for both the electronic and nuclear parts. Taking it on the Li nucleus, we have $\langle z_{\text{Li}} \rangle = \mu - 9R_{\text{LiF}}$ in atomic units, where μ represents the total dipole moment. Scaling to obtain the expectation value for BeO, we have $\langle z_{\text{Be}} \rangle = \langle z \rangle_{\text{Li}} / s$, to which we must add $3R_{\text{BeO}}$ to get the predicted dipole moment for BeO at an internuclear distance of R_{BeO} . The next to the last column in Table II was obtained in this manner. One can, in fact, show that, for our case, the same answer is obtained for any origin, provided that this origin is defined relative to the internuclear distance and not to some space-fixed system of coordinates. Note that we change the internuclear distance in scaling from LiF to BeO. Thus, take the distance from nucleus 1 to the origin as f times the internuclear distance ($1 = \text{Li, Be}$ and $2 = \text{F, O}$). We find

$$\langle z \rangle = \mu - q_2(1 - f)sR + q_1fsR$$

with q_1 and q_2 the charges on 1 and 2. This gives the dipole moment for the scaled molecule with charges q_1' and q_2' as

$$\langle z \rangle / s + q_2(1-f)R - q_1'fR = \mu/s -$$

$$(q_2 - q_2')(1-f)R + (q_1 - q_1')fR = \mu/s +$$

$$fR(q_2 - q_2' + q_1 - q_1') - (q_2 - q_2')R$$

The term depending on f vanishes as long as $q_1 + q_2 = q_1' + q_2'$, *i.e.*, no change in the total nuclear charge between the two isoelectronic molecules. Only for neutral molecules, however, is the dipole moment expected to be independent of origin in the first place.

The agreement for the dipole moment (last two columns of Table II) is poor and gets worse at larger R . This comes from the fact that $\mu_{\text{LiF}} \rightarrow eR$ as $R \rightarrow \infty$, while $\psi_{\text{BeO}} \rightarrow 0$ as $R \rightarrow \infty$. In chemical terms, LiF dissociates into ions and BeO into neutral atoms. The molecules are thus completely different at large R . We see this reflected also in the increasing errors in $\langle r^2 \rangle_{\text{Be}}$ and $\langle 3z^2 - r^2 \rangle_{\text{Be}}$ as R gets large. The dipole moment, which has often been used as the measure of ionic character, is more sensitive to the qualitative differences in bonding between LiF and BeO than either of the above so that errors set in earlier.

Finally, we turn to the problem of rescaling Yo-

shimine's BeO wave function for LiF. Here, $Z_A = 3/4$, $Z_B = 9/8$. Table III, whose construction is similar to that of Table I, shows the results of these calculations. Fitting the points here to a parabola in R , we find the minimum (equilibrium internuclear distance) at $R = 2.387 \pm 0.1a_0$, and a force constant of $0.8194 \text{ a.u./}a_0^2$.¹² The energy at the minimum is -104.4927 . To this we must compare the experimental results— $R_{\text{min}} = 2.955a_0$, $k_f = 0.2069 \text{ a.u./}a_0^2$, $E(R = R_{\text{min}}) = -107.435 \text{ a.u.}$ —as well as the calculated results of McLean— $R_{\text{min}} = 2.8877a_0$, $E(R = R_{\text{min}}) = -106.977 \text{ a.u.}$, $(d^2E/dR^2)_{R=R_{\text{min}}} \cong 0.194 \text{ a.u./}a_0^2$.

In Table IV, the scaling parameters determined in Table III are used for the calculation of expectation values. These are compared to McLean's results. Agreement for $\langle r^2 \rangle_{\text{Li}}$ is good, agreement for $\langle 3z^2 - r^2 \rangle_{\text{Li}}$ is a bit less good, and agreement for the dipole moment is poor. As one might have anticipated, the pattern is inverse to that for LiF \rightarrow BeO (Table II). In this case, the dipole is consistently too low. Here, all the expectation values are too small and get worse at larger R , as the difference in the ionic character of the bonds

Table III: Calculations for BeO \rightarrow LiF^a

$sR(a_0)$	$T_1(sR)$	$C_1(sR)$	$L_1^A(sR)$	$L_1^B(sR)$	$M_1(sR)$	s_0	$\frac{sR}{s_0}(a_0)$	\bar{E}_{s_0}
2.150	90.06195	49.1080	-48.7540	-194.7040	14.8837	1.076711	1.99682	-104.4094
2.400	89.5418	47.7527	-47.0152	-193.0560	13.3333	1.080203	2.22180	-104.4809
2.476	89.4268	47.3844	-46.5520	-192.6264	12.9241	1.080938	2.29060	-104.4887
2.55	89.3307	47.0420	-46.1272	-192.2352	12.5490	1.081542	2.35774	-104.4931
2.80	89.1056	45.9732	-44.8616	-191.0576	11.4286	1.082816	2.58585	-104.4755
3.05	89.0246	44.9570	-43.8372	-190.0088	10.4918	1.083006	2.81624	-104.4171

^a Expectation values in columns 1-5 obtained from calculation c of Yoshimine, ref. 10. Energies in atomic units. See text for abbreviations.

Table IV: Expectation Values for BeO \rightarrow LiF

$R_{\text{BeO}} = sR(a_0)$	$R_{\text{LiF}} = sR/s_0(a_0)$	$E, \text{ a.u.}$		$\langle r^2 \rangle_{\text{Li}}, a_0^2$		$\langle 3z^2 - r^2 \rangle_{\text{Li}}, a_0^2$		Dipole moment, a.u.	
		Scaling	Calcn. ^a	Scaling	Calcn. ^a	Scaling	Calcn. ^a	Scaling	Calcn. ^a
	1.60		-106.2368		39.3174		49.3614		1.0177
2.150		-104.4094		52.7390		68.5058		0.3363	
	2.10		-106.8273		57.7430		84.6575		1.6574
2.400	2.22180	-104.4809		61.2608		85.0737		0.3210	
2.476	2.29060	-104.4887		64.0404		90.4849		0.3103	
	2.350		-106.9240		68.6366		106.1365		1.8830
2.550	2.35774	-104.4931		66.8294		95.9145		0.2956	
2.800	2.58585	-104.4755		76.8434		115.3511		0.1914	
	2.60		-106.9652		80.6820		130.1258		2.0964
3.05	2.81624	-104.4171		87.6807		136.0569		0.1015	
	2.85		-106.9768		93.9270		156.6269		2.3075

^a Calculation is that of A. D. McLean, *J. Chem. Phys.*, **39**, 2653 (1963).

in LiF and BeO gains in importance. The BeO wave function, scaled for LiF, must lead to a dipole moment approaching 0 as R gets very large. This is of course totally unsuited to a description of the ionic LiF molecule.

In fact, BeO and LiF would certainly be considered by a chemist as almost totally dissimilar molecules. This makes it all the more surprising that our scaling allowed us to do so well on the various molecular constants. It is tempting to think that this sort of calculation suffers from disadvantages opposite to those of simple variational calculations; that is, it allows one to do well on the inner shells but describes the valence, or chemical, electrons less adequately.

We must remember that the wave functions we used for LiF and BeO are not exact—errors in the energies run about 0.5%—and that we require several expectation values which are more sensitive than the energy to errors in the wave function.^{8,13} In this connection, the self-consistent field wave function (to which McLean's and Yoshimine's wave functions are approximations) is most suitable for a starting point in the present calculations. Brillouin's theorem¹⁴ guarantees

that one-electron operators, as well as the total energy, have second-order errors when the wave function is in error in first order. The kinetic energy and the electron-nucleus potential energies are one-electron, while the electron-electron repulsion is a difference between the total energy and one-electron operators.

It is unfortunate that there are not more published calculations giving expectation values other than total energy to allow more calculations like those above. An interesting case would be $\text{CO} \rightarrow \text{N}_2$, as the two are often considered to be very similar.¹⁵ If we consider the scaling process to change the "size" of the wave function but not its "shape," we do not anticipate very good results when the nuclear charges are changed too radically.

(13) For instance, P.-O. Löwdin, *Ann. Rev. Phys. Chem.*, **11**, 107 (1960); C. Eckart, *Phys. Rev.*, **36**, 878 (1930). Note, as an example of this, Table XVI of ref. 8.

(14) L. Brillouin, *Actualités Sci. Ind.*, **71**, 159, 160 (1933-1934); C. Möller and M. S. Plesset, *Phys. Rev.*, **46**, 618 (1937); J. Goodisman and W. Klemperer, *J. Chem. Phys.*, **38**, 711 (1963); G. G. Hall, *Phil. Mag.*, **6**, 249 (1961).

(15) For example, Y. K. Syrkin and M. E. Dyatkina, "Structure of Molecules and the Chemical Bond," Dover Publications, New York, N. Y., 1964, pp. 136-138.

Radiation Chemistry of Some Cyclic Fluorocarbons^{1,2}

by D. R. MacKenzie, F. W. Bloch, and R. H. Wiswall, Jr.

Brookhaven National Laboratory, Upton, New York (Received December 31, 1964)

Radiolysis experiments have been carried out on a series of highly purified cyclic fluorocarbons—hexafluorobenzene, perfluorobiphenyl, and perfluoronaphthalene, and their saturated analogs perfluorocyclohexane, perfluorobicyclohexyl, and perfluorodecalin (perfluorodecahydronaphthalene). Irradiations were done in nickel cells using a 1.5-Mev. Van de Graaff electron beam. Temperatures were chosen so that materials were irradiated in the liquid phase and were room temperature where possible, otherwise around 100°. Radiation doses were of the order of 10⁹ rads. Radiation stability of the aromatic compounds is less than that of the corresponding hydrocarbons, whereas the alicyclic fluorocarbons are more stable than their hydrocarbon analogs. Total *G* values for destruction of starting material range from 1.3 to 2.4 and are very similar for aromatic and alicyclic compounds. The aromatic fluorocarbons under irradiation yield polymeric material almost exclusively. Only traces of gaseous and low molecular weight compounds are formed. Polymeric material is colored yellow to dark brown depending on the dose. Radiolysis of the alicyclic fluorocarbons causes appreciable breakdown into gases and products of lower molecular weight than the starting material, as well as polymer formation. Polymeric material is colorless. No free fluorine has been detected in any of the irradiations.

I. Introduction

Several alicyclic and aromatic fluorocarbons have been known for some time to be extremely stable thermally. In particular, perfluorobiphenyl³ and perfluorobenzene, perfluorocyclobutane, and perfluorocyclohexane^{4,5} are stable to over 600°, a performance unmatched by any other completely organic compound, with the possible exception of some aromatic hydrocarbons such as biphenyl.³

Although the radiolysis of perfluoroalkanes has been investigated by several authors⁶⁻⁸ little information concerning cyclic fluorocarbons is available. Two studies have been carried out on perfluorocyclobutane, perfluorocyclopentane, and perfluorocyclohexane under electron impact in a mass spectrometer.^{9,10} More recently, Hanrahan and Fallgatter have studied the radiolysis of perfluorocyclohexane under γ -irradiation.¹¹ The only work on aromatics has been done at the National Bureau of Standards on perfluorobenzene.^{7,12} In view of the very great thermal stability exhibited by some of the cyclic fluorocarbons, the problem of their radiation stability is of some importance. If their stability approached that of the aromatic hydro-

carbons, for example, they would constitute a group of compounds of considerable interest in nuclear technology. In any case, a study of their interaction with ionizing radiation would be interesting in its own right in helping to provide further insight into the radiation

(1) This work was performed under the auspices of the U. S. Atomic Energy Commission.

(2) Presented in part at the 148th National Meeting of the American Chemical Society, Chicago, Ill., Sept. 1964.

(3) L. A. Wall, R. E. Donadio, and W. J. Pummer, *J. Am. Chem. Soc.*, **82**, 4846 (1960).

(4) I. B. Johns, E. A. McElhill, and J. O. Smith, *Ind. Eng. Chem., Prod. Res. Develop.*, **1**, 2 (1962).

(5) I. B. Johns, E. A. McElhill, and J. O. Smith, *J. Chem. Eng. Data*, **7**, 277 (1962).

(6) J. H. Simons and E. H. Taylor, *J. Phys. Chem.*, **63**, 636 (1959).

(7) L. A. Wall, R. E. Florin, and D. W. Brown, National Bureau of Standards Report 6126, Sept. 1958, and *J. Res. Natl. Bur. Std.*, **64A**, 269 (1960).

(8) R. F. Heine, *J. Phys. Chem.*, **66**, 2116 (1962).

(9) P. Natalis, *Bull. Soc. Roy. Sci. Liege*, **29**, 94 (1960).

(10) F. L. Mohler, V. H. Dibeler, and R. M. Reese, *J. Res. Natl. Bur. Std.*, **49**, 343 (1952).

(11) R. J. Hanrahan and M. B. Fallgatter, *J. Phys. Chem.*, **69**, 2059 (1965).

(12) V. H. Dibeler, R. M. Reese, and F. L. Mohler, *J. Chem. Phys.*, **26**, 304 (1957).

chemistry of organic compounds. We are currently engaged in such a study and present here the results of radiolysis experiments carried out between room temperature and 120° on three typical aromatic fluorocarbons and their saturated analogs—perfluorobenzene, C₆F₆; perfluorobiphenyl, C₁₂F₁₀; perfluoronaphthalene, C₁₀F₈; perfluorocyclohexane, C₆F₁₂; perfluorobicyclohexyl, C₁₂F₂₂; and perfluorodecalin, C₁₀F₁₈.

II. Experimental

Purification of Materials. All compounds were purchased from Imperial Smelting Corp. Ltd. of Avonmouth, England, and were usually 95 to 98% pure as received.

Evidence from preliminary experiments with C₆F₆ indicated that relatively small amounts of impurities increased the decomposition yield appreciably over that of highly purified material. (See Table I.) Thus, we decided to purify all the compounds to be used in this study, and chose preparative-scale gas-liquid chromatography (g.l.c.) as the most suitable method. The particular procedures are described elsewhere.¹³

Table I: Results of Irradiating C₆F₆ Samples of Varying Degree of Purity

Material	% im-purity	Nature of impurity	Dose, rads × 10 ⁸	G _{gas}	G _{polymer}
Imperial smelting ^a	1.9	~1% C ₆ F ₅ H, remainder fluorocarbon	9.5	0.02	2.6
Sperry ^b	1.5	No C ₆ H ₅ H, some Cl-containing impurity	8.3	0.04	2.4
BNL ^c purified	<0.01		7.8	0.001	2.15

^a Obtained commercially. ^b Sample provided by Sperry Gyroscope Co. ^c Brookhaven National Laboratory.

Purification was carried out, with one exception, until no impurities could be detected by analytical g.l.c. (<0.01% with our thermal conductivity detector). The one exception, perfluorodecalin, contained a minor impurity whose chromatographic peak was a shoulder on the leading edge of the main peak. "Complete" removal of this impurity involved such lengthy procedures that a measurable amount (0.04%) was tolerated in the final sample.

After g.l.c. purification, the only known contaminant of any significance was water formed by condensation while trapping the products from the column. One treatment used to remove water was to shake the liquefied fluorocarbon with P₂O₅ in an evacuated container with a break-seal. This method proved unsuitable for those fluorocarbons which are solids at

room temperature, such as C₁₀F₈, since a slight amount of reaction occurred when contacting the melt with P₂O₅ at 100°. Preliminary tests with J. T. Baker's "dri-Na"¹⁴ as a desiccant revealed similar—sometimes violent—side reactions. Finally, vapor phase contact of the fluorocarbon with P₂O₅ was adopted as the most satisfactory drying method. It involved the vacuum transfer of fluorocarbon vapor through a bed of P₂O₅, retained between two frits. These procedures were shown by spectrophotometric Karl Fischer determinations to yield material containing <10 p.p.m. water, the method's limit of detection. The purified and dried compounds were transferred to the reaction vessel by vacuum distillation, if liquid at room temperature, or loaded in an inert atmosphere drybox, if solid. Outgassing was accomplished by evacuation during several melt-freeze cycles.

Procedure. The outgassed compounds were irradiated as liquids under vacuum with an incident beam of 1.5-Mev. electrons. A dose rate of approximately 2 × 10⁶ rads/sec. was used. The samples were contained in 4-ml. cylindrical all-nickel vessels made of cold drawn seamless "A" nickel tubing. End plates and connecting tube were welded on by fused nickel only. The window face was machined down to 0.12 mm. and then further reduced in thickness to about 0.07 mm. by electropolishing. A thermocouple well was provided in the face opposite the window.

Nickel was chosen as the container material because of its resistance to fluorine attack at moderate temperatures. The present work has been extended to include irradiations in the temperature range 400 to 500° where some such metal as nickel is required for inertness. Glass is undesirable at any temperature because of the formation of SiF₄ during radiolysis. In order to build up an inert metal fluoride layer on the inner faces of the cells, they were prefluorinated by heating for 1 hr. at 500 to 550° with several atmospheres of fluorine.

Characterization of Products. While g.l.c. analysis afforded accurate insight into the number and distribution of radiolysis products, a detailed characterization was severely hampered by the absence of analytical standards. Identification of specific compounds had therefore to be limited to those products for which chromatographic standards could be made available. As a first step, products have been classified and reported as gases and polymer, with an intermediate molecular weight fraction between these two groups, if one was formed. "Polymer" is arbitrarily defined as

(13) D. R. MacKenzie, paper submitted to *J. Chromatog.*

(14) A sodium-lead alloy containing 9.5% minimum active sodium.

product of a higher molecular weight than the starting compound. G_{polymer} is expressed in terms of destruction of monomer, whereas G values for the gaseous products are given in terms of formation of the individual gases or groups of gases. G_{total} , the G value for total destruction of starting compound, is a measure of the over-all radiation stability of the latter. In the aromatic series, this is virtually identical with G_{polymer} .

Product Analysis. Gas analysis has been carried out by a combination of several methods, some of which were described previously.¹⁵ A Ward low-temperature still¹⁶ was used for partial separation and measurement of fractions which were then further analyzed by mass spectrometer and by g.l.c. with a silica gel column. Since fluorine was not detected in our preliminary work,¹⁷ the only gases considered were fluorocarbons of carbon numbers 1 to 4.

Volatile products from C_6 up were removed from the reaction cell by vacuum transfer at room temperature. Solids of molecular weight comparable to perfluorobiphenyl were then collected by vacuum distillation or sublimation at 100° . The bulk of the unreacted starting compound came over with this or the previous fraction, depending on the material irradiated. Fractions were analyzed using a Perkin-Elmer Model 154 vapor fractometer, or F & M Model 500 chromatograph, with a printing integrator.

The material remaining in the cell after the last vacuum transfer constituted the polymer residue. Adequate methods for analysis of such residues, which were largely composed of high molecular weight products, are still under study. Thus far, elemental analyses have been carried out, and average molecular weights have been determined for the "aromatic" polymers, but no other characterization has been accomplished.

III. Results

The data are presented in Tables II to V. In Table III, Wall's results for γ -irradiation of C_6F_6 are given for comparison.

Table II: Elemental Analysis of Polymers from Radiolysis of Aromatic Fluorocarbons

Compd. irradiated	Polymeric product (exptl.)		Starting material (theoret.)	
	% C	% F ^a	% C	% F ^a
C_6F_6	39.9	56.1	38.7	61.3
$C_{12}F_{10}$	43.8	53.4	43.1	56.9
$C_{10}F_8$	45.0	54.6	44.1	55.9

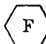

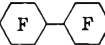
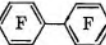

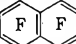
^a Experimental values determined for fluorine are usually less than theoretical owing to difficulty of analysis.

Table III: Summary of Irradiation Results

Compd.	Temp., °C.	Dose, rads $\times 10^6$	G_{total}	G_{gas}	G_{polymer}	Av. mol. wt. of polymer
Aromatics						
C_6F_6	Room ^a	7.8	2.15	0.001	2.15	1140 ^b 1225 ^c
C_6F_6 (ref. 7)	25	2.3		0.01	2.01	
$C_{12}F_{10}$	105	7.7	1.4	~ 0.0001	1.4	1230
$C_{10}F_8$	108	8.6	1.31 ^d	~ 0.0001	1.28	770
Alicyclics						
C_6F_{12}	90	6.2	2.4	0.204	2.1	
$C_{12}F_{22}$	122	8.9	1.6	0.096	0.9	
$C_{10}F_{18}$	Room ^a	7.5	1.7	0.12	1.4	

^a Temperature about 10° above ambient owing to heating by the electron beam. ^b Ether-soluble fraction. ^c Ether-insoluble fraction. ^d Value includes 0.03 for liquid products lighter than starting material.

Table IV: Summary of G Values for Total Destruction of Starting Material in Irradiation of Cyclic Fluorocarbons

Alicyclic	Aromatic
 2.4	 2.1
 1.6	 1.4
 1.7	 1.3

The usual corrections for electron absorption and scattering in the cell window could be calculated quite accurately. When these corrections (10 to 15%) were applied, the relative precision of the dose measurements was ± 2 to 3%. Thus, it is felt that most of the G values should be good to 5% relative to one another, especially values of G_{total} which were based on weighed amounts of recovered starting material.

Absolute G values, of course, depend on the accuracy of the Van de Graaff beam current and voltage readings. These were probably good to well within 5% since, whenever calibrations have been made in the past, the measurements have been in error by only 1

(15) F. W. Bloch, D. R. MacKenzie, and R. H. Wiswall, Jr., TID-7622, 109-20, USAEC, July 1962.

(16) D. J. LeRoy, *Can. J. Res.*, B28, 492 (1950).

(17) Amounts of elemental fluorine as low as 1 mg. could be determined with a precision of about $\pm 10\%$. After finding no fluorine in a number of irradiations of both alicyclic and aromatic fluorocarbons, the procedure was usually omitted.

Table V: Irradiation of Perfluoroalicyclics: Products and G Values

	C ₆ F ₁₂	C ₁₂ F ₂₂	C ₁₀ F ₁₈
CF ₄	0.070	0.020	0.06
C ₂ F ₆	0.065	0.0125	0.04 ^a
C ₂ F ₄	0	0.0005	
C ₃ F ₈	0.035	0.014	0.01 ^a
C ₃ F ₆	0	0.009	
<i>c</i> -C ₃ F ₆	0	0.008	
C ₄ F ₁₀	0.034	0.024	0.01 ^a
C ₄ F ₈ (butene-2)	0	0.008	
Total gas	0.204	0.096	0.12
C ₁₂ F ₂₂	0.30 ^b
Intermediate products ^c	0.09	0.67	0.27
Polymer	2.1	0.9	1.4
G_{total}	2.4	1.6	1.7

^a These values are the sums of C₂, C₃, and C₄ compounds, respectively. ^b Included in value of G polymer. ^c Products of molecular weight between the gas fraction (C₁ to C₄) and the starting material.

or 2%. A number of separate experiments have shown no evidence of possible stray currents associated with the use of a metal cell. Thus, we conclude that the absolute values of the yields are subject to an uncertainty of not more than $\pm 10\%$, and probably significantly less.

Some generalizations can be made from the tables and from other experimental observations.

(1) No free fluorine was detected in the products of any of the irradiations.

(2) All aromatic fluorocarbons showed strikingly low gas yields. For perfluorobiphenyl and perfluoronaphthalene, these were barely measurable. Whatever gas was found was in the C₂ fraction. No CF₄ or C₂F₆ was detected for any member of the series.

(3) The material recovered from aromatic irradiations consisted predominantly of unreacted starting compound and a resinous polymer of high viscosity and yellow-brown color. Elemental analysis (Table II) showed the C:F ratio essentially unchanged from that of the respective starting materials.

(4) G.l.c. work on these polymers showed negligible amounts of material in the range below at least quaterphenyl and probably quinquephenyl. Molecular weight determinations (Table III) showed that the polymers consisted, on the average, of 6 and 7 monomer units for the two fractions from the perfluorobenzene irradiation, 4 monomer units in the case of perfluorobiphenyl, and 3 in the case of perfluoronaphthalene.

(5) In the alicyclic irradiations, products of molec-

ular weight higher than the starting compound were peaked at carbon numbers which were integral multiples of the monomer number, with dimers predominating. Intermediate carbon numbers were, however, well represented. Amounts of the higher products tapered off much more rapidly than in the case of the aromatics, where dimers were not detectable.

(6) The alicyclic fluorocarbons show much higher gas yields than the corresponding aromatics, but overall stabilities are of the same order.

(7) In both the alicyclic and aromatic series there was no marked difference in stability between the fused-ring compounds and those with the rings joined by a C-C bond.

(8) Table IV shows that the two-ring compounds gave G values lower than the one-ring values by almost a factor of 2. Table V indicates that this is true for C₆F₁₂ and C₁₂F₂₂, both with respect to gas production and to total loss of starting material.

(9) It can also be seen from Table V that no trace of any olefinic or cycloalkane gases was found in the radiolysis of C₆F₁₂, in contradistinction to the two-ring compound C₁₂F₂₂ where appreciable quantities of both were formed.

IV. Discussion

The observation in this work which has been most interesting to us is the similarity in stability of the aromatic and the corresponding alicyclic fluorocarbons. The alicyclics are perhaps more stable than one might expect. The aromatics, on the other hand, while extremely stable toward fragmentation, seem almost eager to polymerize. By contrast, the alicyclic and aromatic hydrocarbons which have been studied show almost an order of magnitude difference in radiation stability. Cyclohexane, for example, has a G value for destruction of starting material of >6 ,¹⁸ whereas that of benzene under similar conditions is 0.9,¹⁹ and that of biphenyl is 0.26.²⁰

The experiments performed to date have been in the nature of a survey, with more detailed work on representative compounds to follow. In order to try to obtain quantities of products sufficient for characterization, since almost no standards were available to us, we have worked at relatively high conversions. This approach permits no detailed mechanisms to be deduced. However, there are several aspects of the

(18) A. J. Swallow, "Radiation Chemistry of Organic Compounds," Pergamon Press, Inc., New York, N. Y., 1960, p. 67.

(19) S. Gordon, A. R. Van Dyken, and T. F. Doumani, *J. Phys. Chem.*, **62**, 20 (1958).

(20) R. O. Bolt and J. G. Carroll, "Radiation Effects on Organic Materials," Academic Press, Inc., New York, N. Y., 1963, p. 85.

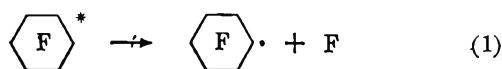
mechanisms which we wish to mention in the light of our experiments.

Wall, Florin, and Brown⁷ comment that the radiolysis of perfluorobenzene offers few novelties beyond that of its hydrocarbon analog, as described by Gordon, Van Dyken, and Doumani.¹⁹ One difference on which Wall did not comment is the very low gas yield. Absence of gaseous fluorine in such a system is understandable because of its reactive nature. A similar argument may also explain the absence of C_2F_2 . However, it is quite possible that no C_2F_2 is formed, thus indicating a certain difference in reaction mechanism between C_6F_6 and C_6H_6 .

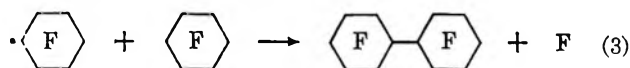
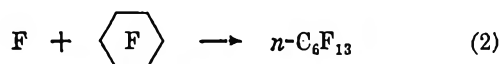
Burns²¹ has observed in the irradiation of benzene that the gas yields of hydrogen and acetylene increase dramatically on going from radiations of low LET (fast electrons and γ -rays) to radiation of high LET (low energy α -particles). This, he feels, is because these gases are formed by interaction of excited molecules, and the local concentration of excited molecules is much increased with radiations of high LET. Investigation of the effect of LET, particularly on gaseous products, should be helpful in further elucidation of the mechanism involved in C_6F_6 radiolysis.

For the alicyclic compounds, as for the aromatic, we have no way of choosing among a free-radical, excited-state, or ionic mechanism, or any combination of the three. A free-radical mechanism is consistent with the results we obtained and seems the logical choice for the predominant type of mechanism in the radiolysis of the saturated ring compounds

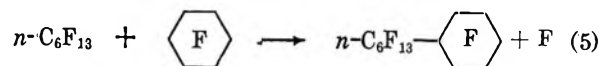
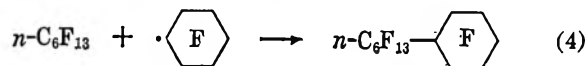
Taking perfluorocyclohexane as an example, the free-radical mechanism would result from an initial step such as



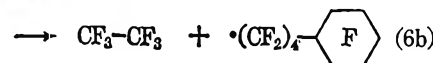
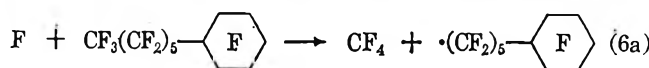
In the early stages of the reaction, the F atoms and perfluorocyclohexyl radicals have mostly molecules of starting material to react with.



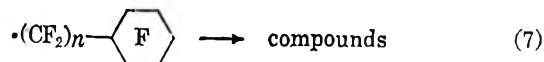
The secondary radical $n\text{-C}_6\text{F}_{13}$ could undergo reaction with starting compound or other radicals to form compounds consisting of rings with side chains



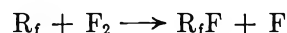
This type of mechanism is consistent with the observation that at low doses the amount of gas formed is too small to analyze properly, almost the only products being perfluorobicyclohexyl and other C_{12} fluorocarbons containing side chains.¹¹ At high doses such as we used, the latter compounds build up to such concentrations that they can react with radicals and F atoms to form saturated fluorocarbon gases and compounds of carbon number other than a multiple of 6, *e.g.*



\rightarrow etc.



The fact that we did not detect fluorine gas in the products does not necessarily mean that none was formed, as for example in three-body recombination of F atoms (abstraction of F being thermodynamically out of the question). Although elemental fluorine is well known not to react with saturated fluorocarbons under normal conditions, reaction with radicals



should be very efficient in removing F_2 molecules.

Acknowledgments. We wish to express our appreciation to A. O. Allen and H. A. Schwarz for allowing us to use their Van de Graaff electron accelerator and for their interest in and discussions of the problems associated with this work.

(21) W. G. Burns, *Trans. Faraday Soc.*, **58**, 961 (1962); W. G. Burns and C. R. V. Reed, *ibid.*, **59**, 101 (1963).

Mass Spectrometric Study of Zirconium Diboride¹

by O. C. Trulson and H. W. Goldstein

Union Carbide Research Institute, Tarrytown, New York (Received December 31, 1964)

A mass spectrometer has been used with a high-temperature Knudsen effusion source to obtain vapor pressure data for zirconium diboride in the temperature range 2267 to 2445°K. The heat of vaporization at 298°K. determined from a third-law analysis of the data is $\Delta H_{298}^v = 474.5 \pm 5.3$ kcal./mole. Vapor pressure data for zirconium and boron were also obtained: the third-law heats of vaporization are $\Delta H_{298}^v = 141.8 \pm 3.3$ kcal./mole, for zirconium, and $\Delta H_{298}^v = 130.3 \pm 3.3$ kcal./mole, for boron. The corresponding heat of formation of zirconium diboride at 298°K. is $\Delta H_{298}^f = -72.1$ kcal./mole. Separate vapor pressure measurements made on zirconium diboride mixed with graphite in a graphite crucible gave the result $\Delta H_{298}^f = -74.5$ kcal./mole.

I. Introduction

Current interest in transition metal borides has been stimulated by the requirements of space technology for materials which will withstand temperature extremes without decomposition. Thermodynamic data for these materials have been difficult to obtain because of uncertainties in composition and the difficulty of finding suitable high-temperature containers. This study concerns the vaporization of zirconium diboride including results for its vapor pressure, heat of vaporization, and heat of formation; the vapor pressure and heat of sublimation of zirconium are also presented.

By considering reactions of boron and metal nitrides Brewer and Haraldsen^{2a} estimated the heat of formation of zirconium diboride to be about -78 kcal./mole, in agreement with Huber, Head, and Holley's^{2b} unpublished calorimetric value of -77 kcal./mole. Recently, Hubbard, *et al.*,³ have determined the heat of combustion of $ZrB_{2.00}$ in a fluorine bomb calorimeter; they obtain $\Delta H_{298}^f = -73.0 \pm 1.6$ kcal./mole for the heat of formation. High-temperature vapor pressure data have been reported by Leitnaker, Bowman, and Gilles,⁴ for $ZrB_{1.906}$; from the measured partial pressures of zirconium and the assumption of congruent vaporization, they obtained $\Delta H_{298}^v = 458.3 \pm 6.5$ kcal./mole for the heat of vaporization.

A mass spectrometer was used with a Knudsen cell effusion source in the present study to obtain vapor pressure data for the systems zirconium in a ZrC-lined graphite crucible, boron in graphite, ZrB_2 in

tungsten, and $ZrB_2 + C$ in graphite. The heats of sublimation of elemental boron and zirconium were combined with the heat of vaporization of ZrB_2 to yield its heat of formation at 298°K. In addition, measurements of the boron vapor pressure were made over the system $ZrB_2 + C$ in a graphite crucible to determine the free energy of the reaction $ZrB_2 + C \rightarrow ZrC + 2B(g)$, which, combined with tabulated thermodynamic data for the solid phases, also yields the heat of formation of ZrB_2 at 298°K.

II. Apparatus

The mass spectrometer is a standard high-temperature instrument constructed by Nuclide Analysis Associates, State College, Pa. In addition to the two-pump vacuum station, a 75-l./sec. Varian Vac-Ion pump was used to evacuate the high-temperature housing to provide three stages of differential pumping for the mass spectrometer. Normal operating pressures with this system were 5×10^{-7} to 5×10^{-6} torr in the high-temperature housing and 5×10^{-8} in the

(1) This research was supported by the Advanced Research Projects Agency Propellant Chemistry Office and was monitored by the Army Missile Command under Contract DA-30-069-ORD-2787.

(2) (a) L. Brewer and H. Haraldsen, *J. Electrochem. Soc.*, **102**, 399 (1955); (b) E. J. Huber, Jr., E. L. Head, and C. E. Holley, Jr., unpublished work.

(3) W. Hubbard, private communication, March 1964. Results from a Master's Thesis by Gerald K. Johnson, University of Wisconsin, *ca.* 1963.

(4) J. M. Leitnaker, M. G. Bowman, and P. W. Gilles, *J. Chem. Phys.*, **36**, 350 (1962).

analyzer section. Defining slits were adjusted to provide resolution near 1/700 over the mass range of interest. Voltage across the 20-dynode multiplier detector was adjusted to provide a gain near 10^6 ; the gain was measured for each of the species considered in the thermodynamic calculations.

The high-temperature heating unit was a modified version of that supplied by the manufacturer. During preliminary testing, considerable high-temperature relaxation in the supporting structures was observed. To prevent the relative movement of the crucible, shields, and supporting structures at high temperatures, most of the unit was reinforced by increasing the size and modifying the shapes of the supporting structures. A tungsten crucible (1.27 cm. in diameter, 1.91 cm. long) heated to 2400° after reconstruction did not shift position over repeated temperature cycling.

Temperatures were measured with a Pyro optical pyrometer calibrated against a standard pyrometer which had been calibrated by the National Bureau of Standards. Crucible temperature measurements were made by sighting into small holes drilled in the crucible wall. For measurements with a tungsten cell a large hole (0.16 cm. in diameter) was first drilled into the wall, and a snug tantalum cap was peened into the hole. A small hole in the cap provided a large inside surface to blackbody hole area ratio of *ca.* 50, necessary because of the low emissivity of tungsten. The walls of the graphite crucibles had blackbody holes with a depth to diameter ratio of *ca.* 3, as was adequate in view of the high emissivity of graphite. All data were corrected for window absorption.

Early runs with the Knudsen effusion source showed poor consistency. A thorough investigation of the instrument, particularly the high-temperature oven, revealed considerable temperature gradients in the crucible, which was heated by electron bombardment from a single spiral filament. Consequently, independent circular filaments were installed near the top and bottom of the crucible and concentric with it. When equal power was fed to the two filaments, four blackbody holes along the length of the crucible showed a total temperature gradient of more than 100° (top hotter than bottom). Such a situation would be the natural consequence of using a single spiral filament. For all the results presented in the following sections this temperature gradient was held to less than $\pm 10^\circ$ by adjusting the separate filament power supplies.

III. Procedure

Standard techniques⁵ have evolved for high-temperature, mass spectrometric, vapor pressure measurements for solid samples heated in Knudsen effusion cells.

Molecules vaporize from the sample and effuse through an orifice in the cell into the source section of the mass spectrometer, where a fraction of them is ionized by a crossed electron beam. The ions are then focused by means of an electrostatic lens system into a well-defined monoenergetic ion beam, directed into the analyzer section of the mass spectrometer where they are separated according to mass-to-charge ratio; the ones desired, preselected by a magnet setting, then pass through a slit system to the first stage of a 20-stage multiplier preamplifier. The current collected at the anode of the multiplier is fed into a vibrating-reed electrometer whose output is displayed continuously on a strip-chart recorder.

The partial pressure developed in the Knudsen cell by an individual molecular species is proportional to the collected ion current for a particular isotope of this molecular species according to the equation

$$P_x = \frac{I_x T}{K_c} \left(\frac{\sigma_c}{\sigma_x} \right) \left(\frac{G_c}{G_x} \right) \left(\frac{i_c}{i_x} \right) \quad (1)$$

where P_x is the unknown pressure of molecular species x , I_x is the measured ion current, and T is the crucible temperature. The factor K_c is a calibrating factor for the mass spectrometer which is assumed to be independent of the mass of the molecular species and which is determined from an independent measurement with a sample of known vapor pressure or known weight.⁵ The factors σ_c/σ_x , G_c/G_x , and i_c/i_x are the ratios of cross sections, multiplier detector gains, and isotopic abundances, respectively, for the calibration material (silver) and the molecular species being measured.

Since zirconium diboride vaporizes to the elements, the standard free energy of vaporization is obtained from $\Delta F^\circ_T = -RT \log P_{Zr} P_B^2$; no complex molecular species containing zirconium and boron were observed. The standard heat of vaporization ΔH°_{298} is determined by combining the free energy of vaporization with appropriate free energy data for $ZrB_2(s)$, $Zr(g)$, and $B(g)$.

$$\Delta H^\circ_{298} = \Delta F^\circ_T + T \left\{ -\frac{F^\circ - H^\circ_{298}}{T} \right\}_{Zr(g)} + 2T \left\{ -\frac{F^\circ - H^\circ_{298}}{T} \right\}_{B(g)} - T \left\{ -\frac{F^\circ - H^\circ_{298}}{T} \right\}_{ZrB_2(s)} \quad (2)$$

The heat of formation of ZrB_2 results from combining

(5) W. A. Chupka and M. G. Inghram, *J. Phys. Chem.*, **59**, 100 (1955).

the heats of vaporization of the compound and of the elements

$$\Delta H_{298}^f = \Delta H_{298}^v(\text{Zr}) + 2\Delta H_{298}^v(\text{B}) - \Delta H_{298}^v(\text{ZrB}_2) \quad (3)$$

In his doctoral thesis, Leitnaker⁶ described investigations of several crucible materials for use with ZrB₂. Tungsten, which Leitnaker found least reactive at high temperatures, was chosen for the present work; a ZrB₂ sample, heated inductively for several hours in an auxiliary system, showed no visible reaction with the crucible confirming Leitnaker's observations. Measurements were made with two samples of ZrB₂. The first sample was prepared here by direct reaction of zirconium hydride and boron powders in a graphite container and subsequent heating for several hours in high vacuum to distil volatile impurities. Spectroscopic analysis of this sample indicated Ti, Fe, and V as major impurities (less than 0.2% total by weight), and chemical analysis showed 1.6% of carbon and the relative composition B/Zr = 2.00. The residue from the mass spectrometer runs was too small for such an analysis, and none was made. Debye-Scherrer X-ray photographs showed only the ZrB₂ phase before running but afterward also showed the lines of ZrC.⁷ In view of the large carbon impurity in the original powder and the preferential loss of boron during the earlier stages of running, we conclude that ZrC was formed by the reaction $\text{ZrB}_2(\text{s}) + \text{C}(\text{s}) \rightarrow \text{ZrC}(\text{s}) + 2\text{B}(\text{g})$. A later experiment showed that the reverse reaction goes with B(s).

A second sample of ZrB₂ was obtained from A. D. Little, Inc. This sample was prepared by vacuum melting at high temperature and was relatively free of carbon (0.66%) and oxygen (0.09%). Spectroscopic and chemical analyses of the sample indicated Ti (0.024%), Fe (0.082%), and Cu (0.001%) as the major metallic impurities. The relative composition B:Zr = 2.00:1 was determined by chemical analysis.

In a preliminary experiment, ZrB₂ and graphite powders were heated together under vacuum in a closed graphite crucible, near 2000° for 2 hr. after which no phases other than a trace amount of ZrC were found in addition to the starting materials. Conversely, powders of the possible products ZrC and B₄C were heated together under vacuum in a closed graphite container for 2 hr. near 2000°. The products of reaction contained the original phases and a large amount of ZrB₂. These results provide the bound $\Delta F^\circ(\text{ZrB}_2) \leq \Delta F^\circ(\text{ZrC}) + \frac{1}{2}\Delta F^\circ(\text{B}_4\text{C}) = -50 \text{ kcal./mole}$. The rate of reaction evidently was too slow to allow complete reaction in 2 hr.

Measurements of the zirconium vapor pressure were made over the solid and liquid phases in a graphite crucible containing ZrB₂ powder, which appeared to inhibit the ordinarily catastrophic reaction between liquid zirconium metal and graphite. Reaction with the graphite, we think by zirconium vapor, was evident, however, and an X-ray analysis of the interior surface of the crucible after several hours of heating near the melting point of zirconium showed the lines of zirconium carbide. The vapor pressure measurements were made after the system had been preheated to allow a surface layer of ZrC to be formed throughout the interior of the crucible. Measurements of the boron vapor pressure were made in a graphite crucible in much the same manner as has been used by Chupka,⁸ Schissel and Williams,⁹ and Verhaegen and Drowart.¹⁰ The results agreed favorably with mass spectrometric data obtained by the above authors.

The reaction $\text{ZrB}_2(\text{s}) + \text{C}(\text{s}) \rightarrow \text{ZrC}(\text{s}) + 2\text{B}(\text{g})$ was also studied. Measurements of boron pressure were made with ZrB₂ and graphite powders intimately mixed in a graphite crucible. A ZrB₂ sample intentionally rich in zirconium (B/Zr = 1.93) prepared here was used to ensure that the boron vapor resulted from the reaction and not as a consequence of the nearly free boron normally found in a stoichiometric phase. The standard free energy of vaporization ($\Delta F^\circ_r = -2RT \log P_B$) was appropriately combined with tabulated free energy functions for ZrB₂, C, ZrC, and B(g) to give twice the heat of vaporization of boron for this system. The enthalpy change for the reaction to yield solid boron, $\text{ZrB}_2(\text{s}) + \text{C}(\text{s}) \rightarrow \text{ZrC}(\text{s}) + 2\text{B}(\text{s})$, was obtained by subtracting twice the average heat of vaporization of elemental boron from this result. The enthalpy of reaction combined with the tabulated heat of formation of ZrC yielded the heat of formation of ZrB₂. In all of the computations pertaining to this reaction, the stoichiometric composition of ZrB₂ was assumed, and free energy functions for ZrB₂ were used even though the starting phase was known to be deficient in boron. Improved computations assuming ZrB_{1.93} as the condensed boride phase were not attempted because thermodynamic data

(6) J. M. Leitnaker, Ph.D. Thesis, University of Kansas, Lawrence, Kan., 1960.

(7) X-Ray Powder Data File Card No. 11-110, ASTM Technical Publication 48-L, American Society for Testing and Materials, Philadelphia, Pa., 1962.

(8) W. A. Chupka, private communication to P. O. Schissel of this laboratory, 1960.

(9) P. O. Schissel and W. S. Williams, *Bull. Am. Phys. Soc.*, **4**, 139 (1959).

(10) G. Verhaegen and J. Drowart, *J. Chem. Phys.*, **37**, 1367 (1962).

for $ZrB_{1.93}$ are not available and because the results are presented only to support the earlier results.

IV. Results

The measurements on ZrB_2 in a tungsten crucible were made over the temperature range 2267 to 2445°K. Partial pressures of zirconium and boron were calculated from the intensities of the respective ion signals according to eq. 1. The relative ionization cross sections $\sigma_{Ag}/\sigma_B = 6.9$ and $\sigma_{Ag}/\sigma_{Zr} = 0.60$ were taken from the compilation of Otvos and Stevenson.¹¹ The detector gain for each of the three species, silver, boron, and zirconium, was measured with the results $G_{Ag}/G_B = 0.70 \pm 0.10$ and $G_{Ag}/G_{Zr} = 0.80 \pm 0.10$, where the error represents the standard deviation in the mean as calculated from quadruplicate measurements.

The partial pressures, free energies of vaporization, free energy functions, and the calculated heat of vaporization for ZrB_2 are given in Table I. The free energy functions were taken from the JANAF tabulation¹² for zirconium and boron vapors and for ZrB_2 solid. Results were obtained from four separate loadings of ZrB_2 powder in the tungsten crucible; a silver calibration was made with each loading and no apparent differences were noticed in the average heats of vaporization obtained for each of the loadings. The relative pressures of zirconium and boron varied slightly with temperature; the pressure ratio P_B/P_{Zr} varied considerably with the starting sample (Table I) from near 300:1 for the powdered sample to near 5:1 for the vacuum-melted sample. Yet the heat of vaporization derived does not appear to be affected by the relative concentrations of the two vapor species over the range studied.

The determination of $\Delta H^f(ZrB_2)$ from vaporization measurements requires that the heats of vaporization of the elements be known. Pressure measurements over elemental boron led to an average heat of vaporization $\Delta H^v_{298} = 130.3 \pm 3.3$ kcal./mole, reconfirming previous results. Measurements of the vapor pressure of zirconium have been made by a Langmuir weight-loss method for temperatures below the melting point by Skinner, Edwards, and Johnston.¹³ The objective of the present mass spectrometric work on zirconium was to check on the accuracy of the estimated ionization cross sections and to provide data which, when used with the vaporization data for ZrB_2 , would cancel the instrumental constants in the heat of formation of ZrB_2 .

The preparation of the crucible to contain zirconium is described in section III. The vapor pressures were calculated according to eq. 1 with the same rela-

Table I: Thermodynamic Data for $ZrB_2(s) \rightarrow Zr(g) + 2B(g)$

T , °K.	P_{Zr} , atm.	P_B , atm.	ΔF°_r , kcal./ mole	$\Delta \left\{ \frac{-T \times}{T} \left(\frac{F^\circ - H^\circ_{298}}{T} \right) \right\}$, kcal./mole	ΔH^v_{298} , kcal./mole
2289 ^a	1.12×10^{-8}	1.36×10^{-7}	227.1	249.0	476.1
2339	2.54×10^{-8}	3.09×10^{-7}	220.7	254.3	475.0
2377	3.87×10^{-8}	4.51×10^{-7}	218.7	258.4	477.1
2364 ^b	4.05×10^{-8}	1.40×10^{-6}	217.4	257.0	474.4
2354	6.02×10^{-8}	5.98×10^{-7}	222.6	255.9	478.5
2398	1.54×10^{-8}	1.10×10^{-6}	216.5	260.7	477.2
2420	1.98×10^{-8}	1.70×10^{-6}	213.1	263.0	476.1
2312	4.34×10^{-8}	3.27×10^{-7}	225.7	251.4	477.1
2354 ^c	6.54×10^{-8}	9.73×10^{-7}	217.7	255.9	473.6
2302	4.16×10^{-8}	3.86×10^{-7}	223.4	250.4	473.8
2337	6.50×10^{-8}	6.45×10^{-7}	220.0	254.1	474.1
2356	1.28×10^{-8}	9.73×10^{-7}	214.7	256.1	470.8
2390	1.59×10^{-8}	1.32×10^{-6}	213.9	259.8	473.7
2356	1.18×10^{-8}	7.63×10^{-7}	217.4	256.1	473.5
2405	2.50×10^{-8}	1.35×10^{-6}	212.9	261.4	474.3
2242 ^d	1.05×10^{-8}	5.59×10^{-8}	230.7	243.9	474.6
2292	2.06×10^{-8}	1.46×10^{-7}	224.0	249.3	473.3
2355	4.69×10^{-8}	3.91×10^{-7}	217.1	256.0	473.1
2307	2.43×10^{-8}	2.11×10^{-7}	221.3	250.9	472.2
2338	3.83×10^{-8}	3.11×10^{-7}	218.6	254.2	472.8
2393	5.89×10^{-8}	5.76×10^{-7}	215.8	260.1	475.9
2413	8.48×10^{-8}	7.84×10^{-7}	212.9	262.3	475.2
2267	1.10×10^{-8}	8.75×10^{-8}	229.0	246.6	475.6
2436	1.42×10^{-7}	1.28×10^{-6}	207.7	264.7	472.4
2445	1.58×10^{-7}	1.46×10^{-6}	206.7	265.7	472.4
					Av. 474.5 ± 0.4

^a First loading vacuum-melted sample. ^b First loading powder sample. ^c Second loading powder sample. ^d Second loading vacuum-melted sample.

tive instrumental constants as were given in section IV, and the free energies of vaporization were appropriately combined with free energy functions for zirconium vapor and solid zirconium taken from the JANAF¹² tabulation. Table II summarizes the vaporization results for zirconium metal over the temperature range 2003 to 2274°K. The slope of the least-squares line for the $\log P$ vs. $1/T$ plot of the data taken above the melting point (2128°K.) yields the value $\Delta H^v_{2200} = 129.5 \pm 5.4$ kcal./mole, which reduced to 298°K. becomes $\Delta H^v_{298} = 137.5$ kcal./mole. The data taken below the melting point similarly yield the average heat of sublimation $\Delta H^v_{2060} = 139.1 \pm 9.7$ kcal./mole, which reduces to $\Delta H^v_{298} = 142.0$ kcal./mole. These

(11) J. W. Otvos and D. P. Stevenson, *J. Am. Chem. Soc.*, **78**, 546 (1956).

(12) "JANAF Interim Thermochemical Tables," The Dow Chemical Co., Midland, Mich. Data for zirconium were taken from the tabulation of June 30, 1961; for boron, December 31, 1964; for ZrB_2 , March 31, 1963. Original references from which these data were obtained are given in the tabulation.

(13) G. B. Skinner, J. W. Edwards, and H. L. Johnston, *J. Am. Chem. Soc.*, **73**, 174 (1951).

results are to be compared to the third-law value $\Delta H_{298}^{\nu} = 141.8 \pm 3.3$ kcal./mole (Table II).

Table II: Thermodynamic Data for the Vaporization of Zirconium

$T, ^\circ\text{K.}$	$P_{\text{Zr}}, \text{ atm.}$	$\Delta F_{T, \text{ kcal./mole}}^{\circ}$	$\Delta \left\{ \frac{-T \times (F^{\circ} - H_{298}^{\circ})}{T} \right\}, \text{ kcal./mole}$	$\Delta H_{298}^{\nu}, \text{ kcal./mole}$
2093	2.33×10^{-8}	73.11	68.89	142.00
2033	9.60×10^{-9}	74.59	67.00	141.59
2003	5.78×10^{-9}	75.51	67.04	142.55
1968	2.83×10^{-9}	76.98	64.95	141.93
2080	1.97×10^{-8}	73.34	68.48	141.82
2092	2.24×10^{-8}	73.23	68.86	142.09
2024	8.32×10^{-9}	74.83	66.71	141.54
1984	4.50×10^{-9}	75.78	65.45	141.23
2070	1.70×10^{-8}	73.60	68.16	141.76
2047	1.06×10^{-8}	74.70	67.44	142.14
2047	1.06×10^{-8}	74.70	67.44	142.14
2082	2.06×10^{-8}	73.23	68.54	141.77
2112	3.52×10^{-8}	72.03	69.48	141.51
2148	5.58×10^{-8}	71.30	70.62	141.92
2148	6.10×10^{-8}	70.91	70.62	141.53
2171	9.36×10^{-8}	69.83	71.34	141.17
2198	1.22×10^{-7}	69.54	72.19	141.73
2216	1.45×10^{-7}	69.35	72.76	142.11
2236	2.05×10^{-7}	68.43	73.38	141.81
2257	2.60×10^{-7}	68.01	74.04	142.05
2274	3.09×10^{-7}	67.74	74.58	142.32
2067	1.70×10^{-8}	73.50	68.07	141.56
				Av. 141.8 \pm 0.1

The heat of formation of ZrB_2 is calculated from the vaporization data according to eq. 3. Using the third-law heats of vaporization, the heat of formation determined from the results presented above is $\Delta H_{298}^f = -474.5 + 141.8 + 2 \times 130.3 = -72.1$ kcal./mole. This result is independent of the assumed cross sections and measured multiplier gain. The data for the reaction $\text{ZrB}_2(\text{s}) + \text{C}(\text{s}) \rightarrow \text{ZrC}(\text{s}) + 2\text{B}(\text{g})$ are reduced to $\Delta H_{298} = 289.7$ kcal./mole (Table III). This result combined with twice the heat of sublimation of boron yields $\Delta H_{298} = 29.1$ kcal. for the reaction $\text{ZrB}_2(\text{s}) + \text{C}(\text{s}) \rightarrow \text{ZrC}(\text{s}) + 2\text{B}(\text{s})$, and this when combined with the heat of formation of zirconium carbide given in the literature,¹² $\Delta H_{298}^f = -45.0$ kcal./mole, gives $\Delta H_{298}^f(\text{ZrB}_2) = -74.1$ kcal./mole.

The experimental errors associated with the ΔH values arise principally as a result of errors in estimated ionization cross sections, multiplier gains, and temperature. The random errors are manifested in the statistical fluctuations of the experimental values and are taken as the standard deviations of the mean ΔH values reported. The Otvos and Stevenson relative ionization

Table III: Thermodynamic Data for the Reaction $\text{ZrB}_2(\text{s}) + \text{C}(\text{s}) \rightarrow \text{ZrC}(\text{s}) + 2\text{B}(\text{g})$

$T, ^\circ\text{K.}$	$P_{\text{B}}, \text{ atm.}$	$\Delta F_{T, \text{ kcal./mole}}^{\circ}$	$\Delta \left\{ \frac{-T \times (F^{\circ} - H_{298}^{\circ})}{T} \right\}, \text{ kcal./mole}$	$\Delta H_{298}^{\nu}, \text{ kcal./mole}$
2092	9.17×10^{-8}	134.8	155.3	290.1
2110	1.21×10^{-7}	133.6	156.6	290.2
2120	1.39×10^{-7}	133.0	157.3	290.3
2144	1.96×10^{-7}	131.6	159.1	290.7
2154	2.76×10^{-7}	129.3	159.9	289.2
2182	4.19×10^{-7}	127.4	161.9	289.3
2223	8.54×10^{-7}	123.5	165.0	288.5
2247	1.17×10^{-6}	122.0	166.7	288.7
1961	7.14×10^{-9}	146.2	145.6	291.8
2099	1.15×10^{-7}	133.3	155.8	289.1
2221	7.91×10^{-7}	124.0	164.8	288.8
				Av. 289.7 \pm 0.3

cross section $\sigma_{\text{B}}/\sigma_{\text{Ae}}$ is assigned an error of $\pm 50\%$ based on a previous measurement; the relative cross section $\sigma_{\text{Zr}}/\sigma_{\text{Ae}}$ taken from the same tabulation is assigned an error of $\pm 50\%$ based on measurements made in this study. Errors of $\pm 10\%$ are estimated for the relative multiplier gains, $G_{\text{Ae}}/G_{\text{B}}$ and $G_{\text{B}}/G_{\text{Zr}}$. A temperature error of $\pm 15^\circ$ is used; this error results from the calibration error, the error in the standard pyrometer, and the error in the window absorption correction.

The net experimental error is taken as the square root of the sum of the squared errors due to each of these uncertainties, including the standard deviation of the mean. Results are ± 5.3 kcal./mole for the heat of vaporization of ZrB_2 , ± 3.3 kcal./mole for the heats of sublimation of the elements, and ± 3.5 kcal./mole for the heat of formation of ZrB_2 . Since the heat of formation of the compound is the algebraic sum of the heats of vaporization of the compound and the elements, the cross sections effectively cancel. This is why the error in the heat of formation is less than the error in the heat of vaporization. The net experimental error in $\Delta H^f(\text{ZrB}_2)$ as deduced from the reaction of ZrB_2 with C is more difficult to analyze since the composition of the ZrC formed is inherently uncertain. If the ZrC is stoichiometric, the experimental error in $\Delta H^f(\text{ZrC})$ and that due to temperature have to be combined; the result is ± 3.0 kcal./mole.

V. Discussion

Many of the refractory carbides and borides of the transition metals have a range of homogeneity near the stoichiometric composition. Kaufman¹⁴ has investigated the thermodynamics of stability of the diborides based on a two-sublattice model proposed by Wagner.¹⁵

Based on considerations of TiB_2 which indicate that the principal defects are boron vacancies, Kaufman has specialized the model to include only vacancies of either kind and interstitial boron atoms. He extended the treatment to consider compositions of congruent vaporization and concluded that at high temperatures the congruently vaporizing phases of TiB_2 , ZrB_2 , and HfB_2 are all boron deficient. Leitnaker, Bowman, and Gilles⁴ found $ZrB_{1.906}$ to vaporize congruently and determined a heat of vaporization from measurements of the zirconium pressure and a boron pressure calculated assuming congruent vaporization. In the present study the condensed phase was assumed stoichiometric as analyzed, and the boron and zirconium pressures were used in the equilibrium constant on this basis. This composition was clearly on the boron-rich side of the congruently vaporizing composition since a boron/zirconium flux ratio greater than 2 was observed in all experiments.

No discrete phases other than ZrB_2 were observed for this system from room temperature X-ray measurements made with several samples. For example, in the mixtures of zirconium metal and ZrB_2 used for measurement of the zirconium vapor pressure, the molten metal formed a skin which neither penetrated the diboride nor reacted with it to form a monoboride detectable by X-ray at room temperature. Since the zirconium pressure observed at a fixed temperature above the zirconium melting point did not decrease with time, one concludes that ZrB is not formed near $2000^\circ K$. This does not rule out the possibility that a subboride is stable at higher or lower temperatures.

The $\Delta H^f(ZrB_2)$ values determined from the systems ZrB_2 and $ZrB_2 + C$ agree within experimental error. Recently the JANAF tabulation has been revised to give -47 kcal./mole for the heat of formation of ZrC compared to -45 kcal./mole used in this study. However, accompanying changes in the free energy functions for ZrC nearly compensate for this difference such that the heat of formation of ZrB_2 deduced from the $ZrB_2 + C$ reaction remains essentially unaltered.

Although it is not the purpose of this work to resolve the literature controversy regarding the heat of sublimation of boron,¹² a few words must be said in support of the use of the value 130.3 kcal./mole in these calculations. The controversy essentially involves the experimental method used to generate boron vapor pressure data. Standard weight loss or torsion effusion measurements, carefully done, yield vapor pressures lower than mass spectrometric results for elemental boron, resulting in heats of sublimation averag-

ing near 135 kcal./mole compared to 130 kcal./mole from mass spectrometric measurements. In either case internal consistency between second- and third-law results is obtained; this anomaly has not been explained. In deriving the heat of formation of $ZrB_2(s)$ from the free energy of vaporization determined mass spectrometrically here, use of the heat of vaporization of boron determined concurrently by the same technique in the same instrument should have the virtue of at least partially compensating for any possible instrumental influence on the results.

The use of our heat of sublimation of zirconium, which differs from a previous value¹² by 3.6 kcal./mole would be similarly justified. Moreover, a claim to improvement in accuracy seems reasonable since the Knudsen technique used here is less sensitive to contamination of the sample surface by residual gases in the vacuum system than is the Langmuir technique used previously. That it was possible to cycle through the liquid range without significant change in the measured solid vapor pressures would seem to eliminate surface contamination as a possible source of error.

The vaporization data for zirconium diboride do not agree with the results of Leitnaker, Bowman, and Gilles. If one treats their data assuming a stoichiometric condensed phase (as was assumed here) their heat of vaporization would be near 487 kcal./mole compared to 474.5 kcal./mole obtained in this study. The reason for this difference is not readily apparent but may be the same as the reason for the discrepancy in boron. Their heat of formation does not differ within experimental error from the present results, provided one uses as sublimation energies $\Delta H_{298} = 145.5$ kcal./mole for zirconium and $\Delta H_{298} = 134.5$ kcal./mole for boron in reducing their data or $\Delta H_{298} = 141.8$ kcal./mole for zirconium and $\Delta H_{298} = 130.3$ kcal./mole for boron in reducing our data, thereby being consistent in the use of nonmass spectrometric and mass spectrometric experimental data for each reduction.

Acknowledgments. The authors are indebted to Dr. Joan Berkowitz-Mattuck of A. D. Little, Inc., who supplied some of the high-purity zirconium diboride samples used in this study. Special thanks are given to Dr. Verner Schomaker for his several helpful discussions during the course of this study.

(14) L. Kaufman, "Compounds of Interest in Nuclear Reactor Technology," J. T. Waber and P. Chiotti, Ed., the Metallurgical Society of AIME, IMD Special Report No. 13, 1964.

(15) C. Wagner, "Thermodynamics of Alloys," Addison-Wesley Press, Inc., Cambridge, Mass., 1952.

Equilibria in Ethylenediamine. III. Determination of Absolute pK Values of Acids and Silver Salts. Establishment of a pH and pAg Scale¹

by L. M. Mukherjee,² Stanley Bruckenstein, and F. A. K. Eadawi

School of Chemistry, University of Minnesota, Minneapolis, Minnesota (Received January 4, 1965)

The dissociation constant for the reaction $HCl \rightleftharpoons H^+ + Cl^-$ in ethylenediamine has been determined by spectrophotometric and cryoscopic measurements. The mean value of pK_{HCl} , 4.01, has been used to calculate the potential of the saturated corrosive sublimate electrode (s.c.s.e.) and $E^{\circ}_{Ag^+, Ag}$ using electrodes of the first and second kinds. E.m.f. values obtained with the hydrogen electrode in solutions of acids and in solutions of salts were used to calculate pK values of acids. Similarly, from e.m.f. values obtained using the silver electrode in silver salt solutions, the corresponding pK values were evaluated. Cryoscopic determination of the pK value for hydrobromic acid in ethylenediamine is also reported.

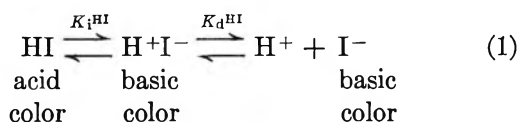
Introduction

In earlier papers^{3,4} concerning equilibria in ethylenediamine (EDA) the potentiometric determination of relative dissociation constants of some silver salts, other uni-univalent salts, and a few acids were reported.

In this work, a spectrophotometric study of solutions of the indicator acid, 3-methyl-4-phenylazophenol (HI), and mixture of the indicator with hydrochloric acid in EDA is described. Also, a cryoscopic investigation of dissociation of hydrochloric and hydrobromic acids is reported. Results obtained from these measurements are used to calculate the potential of the saturated corrosive sublimate reference electrode (s.c.s.e.)^{3,4} and the standard potential of silver-silver ion electrode.

Theory

Spectrophotometry. Pure Indicator Solutions. An indicator acid, HI, dissociates in EDA in the following way



where both the ion pair $H+I^-$ and the dissociated anion I^- have the same molar absorptivities. Accordingly, the over-all dissociation constant, K_{HI} , is given by⁵

$$K_{HI} = \frac{\alpha_{H+I^-}}{\alpha_{HI} + \alpha_{H+I^-}} = \frac{K_i^{HI} K_d^{HI}}{1 + K_i^{HI}} \quad (2)$$

where

$$K_i^{HI} = \frac{c_{H+I^-}}{\alpha_{HI}} \cong \frac{[H+I^-]}{[HI]} \quad (3)$$

and

$$K_d^{HI} = \frac{\alpha_{H+I^-}}{\alpha_{H+I^-}} \quad (4)$$

The bracketed quantities represent equilibrium concentrations. The observed absorbance, A , at a particular wave length is

$$A = b(\epsilon_{HI}[HI] + \epsilon_{I^-}[H+I^-] + \epsilon_{I^-}[I^-]) \quad (5)$$

where b is the light path in centimeters, ϵ_{HI} is the molar absorptivity of the molecular species HI, and ϵ_{I^-} is the molar absorptivity of all species ($H+I^-$ and I^-) containing an I^- ion.

(1) Taken, in part, from a thesis submitted by L. M. Mukherjee in partial fulfillment for the degree of Doctor of Philosophy (Aug. 1961) and by F. A. K. Eadawi in partial fulfillment of the requirements for the degree of Master of Science (Aug. 1964) to the Graduate School of the University of Minnesota.

(2) Chemistry Department, Polytechnic Institute of Brooklyn, Brooklyn, N. Y.

(3) S. Bruckenstein and L. M. Mukherjee, *J. Phys. Chem.*, **64**, 1601 (1960).

(4) S. Bruckenstein and L. M. Mukherjee, *ibid.*, **66**, 2228 (1962).

(5) I. M. Kolthoff and S. Bruckenstein, *J. Am. Chem. Soc.*, **78**, 1 (1956).

Defining the apparent molar absorptivity, ϵ_{app} , as

$$\epsilon_{\text{app}} = \frac{A}{bC_t} \quad (6)$$

where C_t , the total analytical concentration of the indicator, is given by

$$C_t = [\text{HI}] + [\text{H}^+\text{I}^-] + [\text{I}^-] = C_{\text{HI}} + [\text{I}^-] \quad (7)$$

and substituting eq. 3, 4, 5, and 7 into eq. 6 yields

$$\epsilon_{\text{app}} = \frac{\epsilon_{\text{HI}} + \epsilon_{\text{I}^-} K_i^{\text{HI}}}{1 + K_i^{\text{HI}}} \frac{C_{\text{HI}}}{C_t} + \epsilon_{\text{I}^-} \frac{[\text{I}^-]}{C_t} \quad (8)$$

Defining

$$\alpha = [\text{I}^-]/C_t \quad (9)$$

yields

$$1 - \alpha = C_{\text{HI}}/C_t \quad (10)$$

Substituting eq. 9 and 10 into eq. 8, one obtains

$$\alpha = \frac{\epsilon_{\text{app}} - \epsilon'}{\epsilon_{\text{I}^-} - \epsilon'} \quad (11)$$

where

$$\epsilon' = \frac{\epsilon_{\text{HI}} + \epsilon_{\text{I}^-} K_i^{\text{HI}}}{1 + K_i^{\text{HI}}} \quad (12)$$

From the rule of electroneutrality

$$[\text{H}^+] = [\text{I}^-] \quad (13)$$

Assuming

$$f_{\text{H}^+} = f_{\text{I}^-} = f \quad (14a)$$

and

$$f_{\text{HI}} = f_{\text{H}^+\text{I}^-} = 1 \quad (14b)$$

substitution of eq. 7, 11, 13, 14a, and 14b into eq. 8 yields

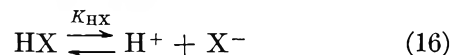
$$\epsilon_{\text{app}} = \epsilon_{\text{I}^-} - \frac{(\epsilon_{\text{app}} - \epsilon')^2 f^2 C_t}{\epsilon_{\text{I}^-} - \epsilon'} \frac{1}{K_{\text{HI}}} \quad (15a)$$

Thus, a plot of ϵ_{app} vs. $[(\epsilon_{\text{app}} - \epsilon')^2 / (\epsilon_{\text{I}^-} - \epsilon')] f^2 C_t$ at any wave length permits evaluation of K_{HI} . Equation 15a differs from a similar expression derived by Bruckenstein and Osugi⁶ in that it takes into account the presence of two undissociated species with different absorptivities. For evaluation of f , we have used the Debye-Hückel limiting law. In terms of the experimental quantities

$$-\log f = 7.608 \sqrt{\frac{\epsilon_{\text{app}} - \epsilon'}{\epsilon_{\text{I}^-} - \epsilon'} C_t} \quad (15b)$$

Mixture of the Indicator Acid and a Nonabsorbing

Acid HX. In an EDA solution containing both the indicator acid, HI, and a nonabsorbing acid, HX, whose over-all dissociation is given by



the rule of electroneutrality yields

$$[\text{H}^+] = [\text{X}^-] + [\text{I}^-] \quad (17)$$

Assuming $f_{\text{H}^+} = f_{\text{X}^-} = f_{\text{I}^-} = f$ and $f_{\text{HX}} = f_{\text{HI}} = f_{\text{H}^+\text{I}^-} = 1$, one obtains

$$\frac{[\text{H}^+]}{[\text{I}^-]} = \frac{K_{\text{HX}}[\text{HX}]}{K_{\text{HI}}C_{\text{HI}}} + 1 \quad (18)$$

where $[\text{HX}]$ denotes the equilibrium concentration of the undissociated HX, and C_{HI} represents the sum $[\text{HI}] + [\text{H}^+\text{I}^-]$ pertaining to the indicator acid HI.

By transposing terms in eq. 18 and substituting $[\text{H}^+] = K_{\text{HI}}C_{\text{HI}}/f^2[\text{I}^-]$ eq. 19 results

$$\frac{[\text{HX}]}{C_{\text{HI}}} = -\frac{K_{\text{HI}}}{K_{\text{HX}}} + \frac{K_{\text{HI}}^2}{K_{\text{HX}} f^2} \frac{C_{\text{HI}}}{[\text{I}^-]^2} \quad (19)$$

It is convenient to express eq. 19 in terms of α (given above by eq. 11) to yield

$$\frac{[\text{HX}]}{(1 - \alpha)C_t} = -\frac{K_{\text{HI}}}{K_{\text{HX}}} + \frac{K_{\text{HI}}^2(1 - \alpha)}{K_{\text{HX}} f^2 \alpha^2 C_t} \quad (20)$$

where C_t is the total analytical concentration of the indicator present in the mixture used. The activity coefficient f can be obtained, as before, from the Debye-Hückel limiting law, $-\log f = 7.608\sqrt{\mu}$, μ being given by

$$\mu = \frac{C_{\text{HX}}}{1 + \frac{K_{\text{HI}}(1 - \alpha)}{K_{\text{HX}}\alpha}} + \alpha C_t \quad (21)$$

where C_{HX} is the total analytical concentration of the acid, HX, in the mixture.

If $[\text{HX}]$ were known, a plot of $[\text{HX}]/(1 - \alpha)C_t$ vs. $(1 - \alpha)/f^2\alpha^2 C_t$ would permit evaluation of K_{HX} and K_{HI} . However, $[\text{HX}]$ cannot be obtained directly, and we have used a trial and error procedure. First, we assume a value for $K_{\text{HI}}/K_{\text{HX}}$ and calculate μ from eq. 21 and $[\text{HX}]$ from

$$[\text{HX}] = C_{\text{HX}} \left(1 - \frac{1}{1 + \frac{K_{\text{HI}}(1 - \alpha)}{K_{\text{HX}}\alpha}} \right)$$

using the experimental value of α . A least-squares treatment is made according to eq. 20. The least-

(6) S. Bruckenstein and J. Osugi, *J. Phys. Chem.*, **65**, 1868 (1961).

squares value of the intercept yields another value of $K_{\text{HI}}/K_{\text{HX}}$. The above procedure is repeated and a plot made of assumed value of $K_{\text{HI}}/K_{\text{HX}}$ vs. the value of $K_{\text{HI}}/K_{\text{HX}}$ found from the least-squares treatment. Inspection of this plot yields the best value of $K_{\text{HI}}/K_{\text{HX}}$ (see Figure 4).

Cryoscopic Measurements. It has been demonstrated experimentally that cryoscopy in EDA⁷ (f.p. 11.3°) is suitable for studying dissociation of the type represented by eq. 16. The equilibrium constant, K_{HX} , may be expressed in the form

$$K_{\text{HX}} = \frac{[\Sigma m - m_s]f^2}{2m_s - \Sigma m} \quad (22)$$

where m_s is the analytical concentration (molal) of HX, and Σm the sum of the equilibrium concentration of HX, H⁺, and X⁻. Σm is approximated, at low concentrations of a solute, by dividing the observed freezing point depression by the molal freezing point depression constant. This treatment assumes that the activity coefficient of the solvent is not affected significantly by the variation in the ionic strengths of the acid solutions studied.

Potentiometry. Our previous potentiometric studies^{3,4} in EDA have yielded only relative dissociation constants, *i.e.*, differences in pK values, rather than absolute dissociation constants. A knowledge of the reference electrode potential vs. the hydrogen electrode in EDA is necessary to obtain the absolute pK values of acids. Similarly, the standard potential of the silver electrode must be known to obtain absolute pK values of compounds studied using the silver electrode. Classical aqueous techniques to evaluate the standard potentials are difficult to apply to EDA solutions since complete dissociation of even the strongest electrolyte would occur only at analytical concentrations approaching $\sim 10^{-5} M$.

Evaluation of Reference Electrode Potential. To avoid the above problem, use was made of the spectrophotometric and cryoscopic values of K_{HCl} to evaluate the reference electrode potential from e.m.f.-concentration data obtained from the cell

Cell I: reference s.c.s.e. || HX(C_{HX}) | H₂ (1 atm.), Pt

At 25°, the e.m.f. of cell I is given by

$$E_{\text{HX}} = E_{\text{scse}} + 0.0296 \log K_{\text{HX}} + 0.0296 \log C_{\text{HX}} \quad (23)$$

taking $E_{\text{H}^+, \text{H}_2}$ as zero. (We shall use the same notation as in ref. 3 and 4.)

Evaluation of $E_{\text{Ag}^+, \text{Ag}}$. Cells I, II, and III were used to evaluate $E_{\text{Ag}^+, \text{Ag}}$.

Cell II: reference s.c.s.e. || AgX(C_{AgX}) | Ag

Cell III: reference s.c.s.e. || AgX(C_{AgX}) + HX(C_{HX}) | Ag

The difference in e.m.f. values between cell I and cell II is

$$E_{\text{AgX}} - E_{\text{HX}} = E_{\text{Ag}^+, \text{Ag}}^\circ + \frac{RT}{2\mathcal{F}} \ln \frac{K_{\text{AgX}} C_{\text{AgX}}}{K_{\text{HX}} C_{\text{HX}}} \quad (24)$$

As was shown earlier³ the difference in e.m.f. values of cells II and III is represented by

$$E_{\text{AgX}} - E_{\text{AgX}, \text{HX}} = \frac{RT}{2\mathcal{F}} \ln \left(1 + \frac{K_{\text{HX}} C_{\text{HX}}}{K_{\text{AgX}} C_{\text{AgX}}} \right) \quad (25)$$

Thus, solving eq. 24 and 25 simultaneously yields $E_{\text{Ag}^+, \text{Ag}}^\circ$.

$$E_{\text{Ag}^+, \text{Ag}}^\circ = E_{\text{AgX}} - E_{\text{HX}} +$$

$$\frac{RT}{2\mathcal{F}} \ln (e^{(E_{\text{AgX}} - E_{\text{AgX}, \text{HX}})/RT/2\mathcal{F}} - 1) \quad (26)$$

Therefore, from the expression for the potential of cell II

$$E = E_{\text{scse}} + E_{\text{Ag}^+, \text{Ag}}^\circ + \frac{RT}{2\mathcal{F}} \ln (K_{\text{AgX}} C_{\text{AgX}}) \quad (27)$$

and from the known values of E_{scse} and $E_{\text{Ag}^+, \text{Ag}}^\circ$ it is possible to determine K_{AgX} .

It is of interest to note that the determination of E° for a half-reaction in a solvent such as EDA does not require the knowledge of any absolute pK values, provided appropriate electrodes of second or third kind can be devised and used in conjunction with electrodes of the first kind.

Experimental

Reagents. Ethylenediammonium bromide was prepared by a method analogous to that described earlier⁴ for the corresponding chloride; a 40% aqueous hydrobromic acid solution was used instead of concentrated hydrochloric acid as was used for the preparation of the chloride. Analysis of the recrystallized sample gave a purity of 100.0%.

Sodium Ethanolamine. Pure sodium metal was slowly reacted in a closed chamber with slight excess of freshly distilled ethanolamine. The excess ethanolamine was removed under vacuum; the solid residue was treated with small amount of pure EDA and again dried under vacuum at $\sim 80^\circ$. The latter treatment was repeated two more times to remove any remaining ethanolamine. A saturated EDA solution (0.00265 M) of sodium ethanolamine was used in the indicator experiments.

(7) L. D. Pettit and S. Bruckenstein, *J. Inorg. Nucl. Chem.*, **13**, 1478 (1962).

Purification of the solvent and other reagents are described elsewhere.^{3,4}

Spectrophotometric Technique. A battery-operated Beckman Model DU spectrophotometer equipped with a photomultiplier attachment was used. The cell compartment was maintained at $25 \pm 0.5^\circ$. All cells were calibrated, and the constancy of calibration was checked periodically by measuring the absorbance of standard potassium chromate solutions in 0.05 *M* potassium hydroxide. The experimental solutions were made by dilution of concentrated stock solutions with the help of a Gilmont ultramicroburet (Model No. G 15401). All manipulations were carried out in a glove box free from water and carbon dioxide.

Cryoscopic Technique. A VECO A 5902 Type thermistor (100,000 ohms resistance at 25° ; temperature coefficient = $-4.6\%/^\circ\text{C}$.) was used as the temperature-sensing device in an equal-arm Wheatstone bridge. The unbalanced bridge voltage was amplified by a Keathly 150 AR microvolt amplifier and recorded using a Sargent potentiometric strip chart recorder. The freezing point cell was the same as that used previously.⁷ Cooling curves were recorded following the previously reported procedure.⁷ The mean deviation of a freezing point measurement was always less than 0.001° . The limiting factor appeared to be the reproducibility of initiating nucleation, not the temperature measurement.

Potentiometric Techniques. These have been described previously.^{3,4}

Results and Discussion

Molar absorptivities of the indicator acid, HI, are given in Figure 1. In the pure indicator solutions (curve A, Figure 1) there is a single maximum at $490 \text{ m}\mu$, followed by a shoulder at $430 \text{ m}\mu$. The $490\text{-m}\mu$ peak is also present in the completely ionized form of the indicator (Na^+I^-) (curve B, Figure 1). On acidification, the peak tends to shift to $470 \text{ m}\mu$ (compare curves C and D, Figure 1) accompanied by reduction of absorbances at $490 \text{ m}\mu$. Plots of molar absorptivities of the indicator *vs.* the concentrations of an added nonabsorbing acid, *e.g.*, acetic (or hydrochloric) acid, at 470 and $490 \text{ m}\mu$ are given in Figure 2. These plots are linear over ~ 0.1 to $\sim 0.5 \text{ M}$ acetic acid added and correspond to the equilibrium mixture of HI and H^+I^- governed by eq. 3; at very high acid concentrations heteroconjugate ions of the type $(\text{IHX})^-$ may form. The linear portions of Figure 2 are extrapolated to zero acid concentration and the extrapolated values of ϵ_{app} so obtained are taken to give ϵ' (eq. 12) for the particular wave lengths used. The value of ϵ' is found to be 2.00×10^4 at $470 \text{ m}\mu$ and 1.74×10^4 at $490 \text{ m}\mu$.

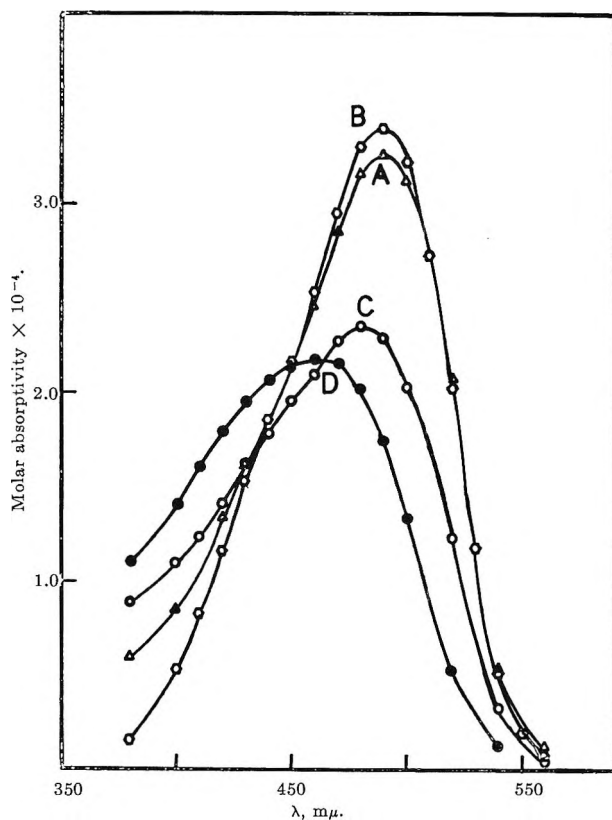


Figure 1. Spectra of 3-methyl-4-phenylazophenol: curve A, $2.23 \times 10^{-6} \text{ M}$ HI in EDA; curve B, $2.028 \times 10^{-6} \text{ M}$ Na^+I^- (HI + 0.00265 *M* sodium ethanalamine); curve C, $3.325 \times 10^{-5} \text{ M}$ HI in 0.00455 *M* acetic acid; curve D, $2.65 \times 10^{-6} \text{ M}$ HI in 0.4720 *M* acetic acid.

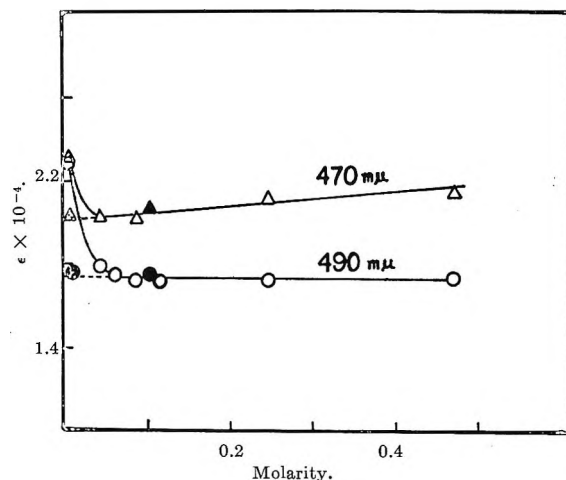


Figure 2. Determination of ϵ' : $470 \text{ m}\mu$, Δ acetic acid, \blacktriangle , HCl; $490 \text{ m}\mu$, \circ acetic acid; \bullet HCl.

Beer's law is valid at 470 and $490 \text{ m}\mu$ for solutions of Na^+I^- (HI + sodium ethanalamine or the sodium salt of HI) over the range of concentration of in-

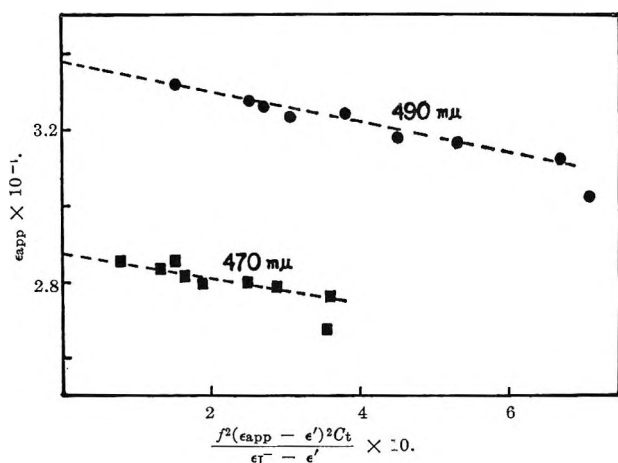


Figure 3. Plot of eq. 15a. Least-squares constants and standard deviations are given in the format: λ (m μ), intercept (standard deviation), and slope \pm (standard deviation) are 470, 2.874×10^4 (0.013×10^4), -0.3297×10^4 (0.013×10^4); 490, 3.378×10^4 (0.025×10^4), -0.3870×10^4 (0.061×10^4). Least-squares lines are shown in the figure.

terest. The ϵ_I - values obtained are 2.90×10^4 at 470 m μ and 3.37×10^4 at 490 m μ .

Plotting the data given in Tables I and II according to eq. 15a yields straight lines as shown in Figure 3. Least-squares constants for these data are given in the legend to Figure 3. K_{HI} equals 2.58×10^{-4} (standard deviation = 0.41×10^{-4}) on the basis of the 490-m μ data and equals 3.04×10^{-4} (standard deviation = 0.55×10^{-4}) using the 470-m μ data. The internal consistency of approach is shown by excellent agreement of the intercept (ϵ_I - in eq. 15a) with the experimental value of ϵ_I -.

Table I: Spectrophotometry with 3-Methyl-4-phenylazophenol in EDA at 470 m μ ^a

Concn., $M \times 10^5$	A	ϵ_{app470} $\times 10^{-4}$	f^2	$\frac{f^2(\epsilon_{app470} - \epsilon'_{470})^2 C_t}{(\epsilon_I - \epsilon')^2} \times 10$
1.125	0.640 ^b	2.85	0.8920	0.807
2.015	0.570 ^c	2.83	0.8598	1.326
2.23	0.191 ^d	2.85	0.8513	1.525
2.675	0.225 ^d	2.81	0.8420	1.642
3.33	0.279 ^d	2.79	0.8273	1.913
4.44	0.369 ^d	2.795	0.8028	2.505
5.47	0.456 ^d	2.78	0.7857	2.903
7.58	0.625 ^d	2.76	0.7568	3.589
9.60	0.769 ^d	2.67	0.7435	3.563

^a $\epsilon_I - 470 = 2.90 \times 10^4$ and $\epsilon'_{470} = 2.00 \times 10^4$. ^b Light path = 2.00 cm. ^c Light path = 1.00 cm. ^d Light path = 0.301 cm. [0.3009 cm. (1.00-cm. cell + 0.70-cm. spacer used; whole calibrated against standard K_2CrO_4 in 0.05 N KOH)]; slit width < 0.015 mm.

Table II: Spectrophotometry with 3-Methyl-4-phenylazophenol in EDA at 490 m μ ^a

Concn., $M \times 10^5$	A	ϵ_{app490} $\times 10^{-4}$	f^2	$\frac{f^2(\epsilon_{app490} - \epsilon'_{490})^2 C_t}{(\epsilon_I - \epsilon')^2} \times 10$
1.125	0.745 ^b	3.32	0.8908	1.519
2.015	0.660 ^c	3.275	0.8585	2.497
2.23	0.219 ^d	3.26	0.8525	2.687
2.675	0.2595 ^d	3.23	0.8410	3.061
3.33	0.324 ^d	3.24	0.8237	3.785
4.40	0.420 ^d	3.18	0.8036	4.503
5.47	0.520 ^d	3.16	0.7852	5.307
7.58	0.710 ^d	3.14	0.7551	6.691
9.60	0.870 ^d	3.02	0.7379	7.119

^a $\epsilon_I - 490 = 3.37 \times 10^4$ and $\epsilon'_{490} = 1.74 \times 10^4$. ^b Light path = 2.00 cm. ^c Light path = 1.00 cm. ^d Light path = 0.301 cm. [0.3009 cm. (1.00-cm. cell + 0.70-cm. spacer used; whole calibrated against standard K_2CrO_4 in 0.05 N KOH)]; slit width < 0.015 mm.

Table III: Spectrophotometry of Mixtures of 3-Methyl-4-phenylazophenol and Hydrochloric Acid in EDA at 490 m μ ^a

Concn. of HI $\times 10^5$	Concn. of HCl $\times 10^5$	ϵ_{app} $\times 10^{-4}$	f^2	[HCl]/ [CHI] ^b	$\frac{C_{HI}^b}{f^2(I^-)^2} \times 10^{-4}$
1.99	1.04	3.14	0.8403	1.034	1.132
1.97	2.575	3.025	0.8219	2.40	2.081
2.015	5.25	2.99	0.7889	4.70	2.49
2.015	10.50	2.88	0.7526	8.73	4.09

^a $\epsilon_I - 490 = 3.37 \times 10^4$, $\epsilon'_{490} = 1.74 \times 10^4$, and $K_{HI}/K_{HCl} = 2.38$. ^b See eq. 19.

Table III presents the results of the HI-HCl mixture experiments obtained at 490 m μ . Using the trial and error procedure outlined in the second section of Theory, a plot of assumed K_{HI}/K_{HX} vs. the corresponding least-squares values was made (Figure 4). The shape of this plot makes the determination of K_{HI}/K_{HX} very precise and yields a value of 2.38 for K_{HI}/K_{HX} . The standard deviation of this ratio for the best least-squares fit is 0.49. The calculated value of K_{HI} from these data is 1.13×10^{-4} with a standard deviation of 0.23×10^{-4} .

The difference between the various estimates of K_{HI} is not outside the range of our experimental error. Therefore, we have averaged all values of K_{HI} weighting inversely as the square of the standard deviation of each value. The average K_{HI} is equal to 1.68×10^{-4} ; and, using the average value of the ratio K_{HI}/K_{HX} equal to 2.38, K_{HCl} calculates to 7.06×10^{-5} .

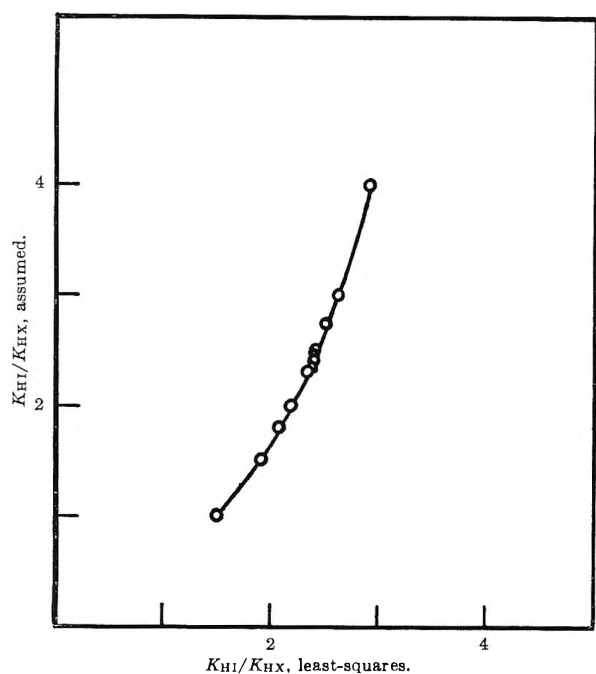


Figure 4. Plot of assumed values of $K_{\text{HI}}/K_{\text{HX}}$ vs. the corresponding least-squares values (eq. 20).

The cryoscopic results obtained with HCl and HBr are given in Table IV. The molar concentration scale has been used to permit comparison between the spectrophotometric and cryoscopic results. The Marshall-Grunwald equation⁸ has been used to evaluate the activity coefficients. K_{HCl} is found to be $1.1 \times 10^{-4} \pm 0.38 \times 10^{-4}$ and K_{HBr} , $1.9 \times 10^{-4} \pm 0.25 \times 10^{-4}$ at $\sim 11.2^\circ$. The uncertainty of these K values is probably larger than that due to change in temperature from ~ 11 to 25° .

Schaap and co-workers⁹ have reported a conductometric value for pK_{HCl} of 3.98 while a value of 3.935 was found by Fowles,¹⁰ *et al.*, from similar measurements. The difference between these values and our values is not large, and we have averaged our mean spectrophotometric result, cryoscopic result, and the above conductometric results^{9,10} to obtain a grand mean of 4.01 ± 0.07 for pK_{HCl} . This value of pK_{HCl} was used below to calculate E_{scse} from potentiometric experiments using cell I.

On repeating our previous potentiometric experiments involving hydrochloric acid in cell I and silver chloride in cell II, lines of theoretical slope were obtained, but these lines were displaced 34 mv. for hydrochloric acid and 10 mv. for silver chloride, as compared to our previously reported values.^{3,4} For other cases, substantial agreement with previously reported e.m.f. data was obtained. The difficulty was found to be the time dependence of the reference electrode potential.

Table IV: Cryoscopic Data for Hydrochloric Acid and Hydrobromic Acid in EDA

HX	Concn., C^a	$\Delta T^b \times 10^3, ^\circ\text{C.}$	ΣC^c	f	$K_{\text{HX}} \times 10^4$
HCl	7.18	22	8.0	0.682	0.49
	14.90	46	17.3	0.566	1.46
	19.53	59	22.1	0.560	1.22
	24.02	74	27.4	0.529	1.55
	43.50	119	46.7	0.534	0.724
Mean $K_{\text{HCl}} \times 10^4 = 1.1 \pm 0.38$					
HBr	1.41	5	1.9	0.732	1.40
	7.54	25	9.3	0.601	1.97
	15.78	49	18.9	0.536	2.21
	17.17	54	20.0	0.549	1.683
	24.06	75	28.0	0.512	2.025

$$\text{Mean } K_{\text{HBr}} \times 10^4 = 1.86 \pm 0.25$$

^a Analytical concentration of HX (mmoles/liter). ^b Freezing point depression, average of three cooling curves on same sample, rounded to 0.001° . Mean deviation is always less than 0.001° . ^c Concentration of HX (mmoles/liter) as determined from freezing point depression using naphthalene as standard.

Cell IV was used to study this effect together with cells I and II containing freshly prepared hydrochloric

Cell IV: (new) reference s.c.s.e. || reference s.c.s.e. (old)

acid and silver chloride solutions, respectively, vs. a s.c.s.e. electrode aged over different periods of time. The results are shown in Figure 5.

Stock¹¹ has also observed similar drifts. Apparently, unsuspected drifts in the s.c.s.e. potential occurred in our previous hydrochloric acid and silver chloride study. In all e.m.f. experiments reported in this paper, the s.c.s.e. electrode was between 1 and 2 days old. We can offer no explanation for the drift in the s.c.s.e. potential.

In Table V, least-squares constants for eq. 23 (cell I), on fitting E_{HX} vs. $\log C_{\text{HX}}$, obtained for hydrochloric acid and hydrobromic acid dilution experiments and for eq. 27 (cell II) on fitting E_{AgX} vs. $\log C_{\text{AgX}}$ obtained for silver chloride, silver bromide, and silver iodide experiments are given. In the least-squares treatment the numerical value of $0.0296 (= 2.303RT/2F$ at 25°) was not adjusted since the two-parameter fit including the adjustment of $2.303RT/2F$ did not fit the data

(8) H. P. Marshall and E. Grunwald, *J. Chem. Phys.*, **21**, 2143 (1953).

(9) W. B. Schaap, R. E. Bayer, J. R. Siefkar, J. Y. Kim, P. W. Brewster, and F. C. Schmidt, *Record Chem. Progr.*, **22**, 197 (1961).

(10) G. W. A. Fowles and W. R. McGregor, *J. Phys. Chem.*, **68**, 1342 (1964).

(11) J. T. Stock, private communication.

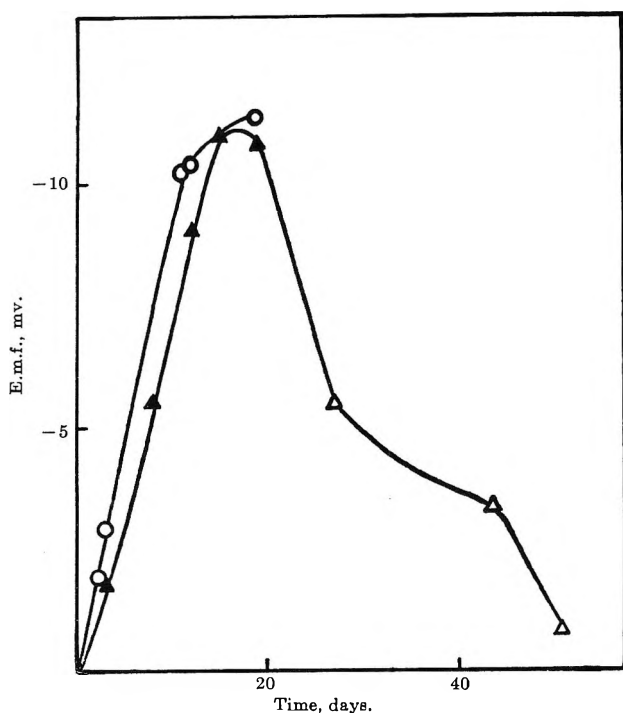


Figure 5. Time dependence of the reference electrode (s.c.s.e.) potential: O, cell I (with HCl); ▲, cell II (with AgCl); △, cell IV.

significantly better. Aside from the hydrochloric acid and silver chloride data, agreement with our previously reported data is good. We calculate E_{scse} to be -0.5272 v. using the mean value of $\text{p}K_{\text{HCl}} = 4.01$.

Data obtained using cell III are given in Table VI. The two sets of hydrochloric acid-silver chloride mixture data were obtained independently by two of the authors some 3 years apart. The value of $\text{p}K_{\text{AgCl}} - \text{p}K_{\text{HCl}}$ calculated from eq. 25 for these two sets of hydrochloric acid-silver chloride data are shown in Table VI. The value of $E_{\text{Ag}^+, \text{Ag}}^\circ$ calculated from the present set of data using eq. 26 is equal to 0.7571 ± 0.0030 v. as compared to 0.7339 v. given by previous HCl-AgCl data.^{3,4}

We have taken previously reported data^{3,4} along with data obtained in this study of cells I and II and calculated absolute $\text{p}K$ values using $E_{\text{scse}} (= -0.5272$ v.) and $E_{\text{Ag}^+, \text{Ag}}^\circ (= 0.7571$ v.) obtained above. These values are listed in Table VII; also listed in Table VII are the acid dissociation constants obtained using cell V.

Cell V: reference s.c.s.e. || MX | H₂ (1 atm.), Pt

where M = Li or Na. Salts investigated included chloride, bromide, nitrate, and perchlorate of lithium and sodium, and sodium phenylacetate.

Table V: Potentiometric Results Obtained Using Cells I and II*

HX or AgX	C_{HX} or C_{AgX}, M	$E, v.$
HCl	0.1192	-0.6718
	0.0597	-0.6814
	0.0264	-0.6924
	0.0130	-0.7013
	0.0035	-0.7214
HBr	0.1490	-0.6602
	0.1011	-0.6651
	0.0508	-0.6721
	0.0254	-0.6824
	0.0108	-0.6908
	0.0051	-0.7043
AgCl	0.4948	0.1006
	0.3947	0.0980
	0.2036	0.0907
	0.1565	0.0874
	0.0947	0.0802
	0.0620	0.0736
	0.0333	0.0669
	0.0148	0.0553
	0.0019	0.0322
	AgBr	0.3332
0.1663		0.0800
0.1065		0.0737
0.0214		0.0567
0.0123		0.0484
AgI	0.2259	0.0584
	0.0988	0.0490
	0.0502	0.0408
	0.0187	0.0302
	0.0101	0.0227
	0.0048	0.0187

* Cell I: $E_{\text{HCl}} = -0.6459 (\pm 0.0015) + 0.0296 \log C_{\text{HCl}}$
 $E_{\text{HBr}} = -0.6349 (\pm 0.0013) + 0.0296 \log C_{\text{HBr}}$

Cell II: $E_{\text{AgCl}} = 0.1105 (\pm 0.0010) + 0.0296 \log C_{\text{AgCl}}$
 $E_{\text{AgBr}} = 0.1039 (\pm 0.0014) + 0.0296 \log C_{\text{AgBr}}$
 $E_{\text{AgI}} = 0.0810 (\pm 0.0032) + 0.0296 \log C_{\text{AgI}}$

As was shown earlier,⁴ in an EDA solution of a pure salt $a_{\text{H}^+} = \sqrt{K_{\text{HX}}K_{\text{S}}/K_{\text{MS}}}$; thus, relative $\text{p}K$ values for a series of acids may be calculated from the e.m.f. values of cell V with the corresponding solutions of lithium and sodium salts. Alternatively, the relative dissociation constant of LiS and NaS (HS denotes EDA) may be obtained by comparing the e.m.f. values found with cell V using the lithium and sodium salts of the same acid. Such comparisons yield $\text{p}K_{\text{NaS}} - \text{p}K_{\text{LiS}} = 0.22 \pm 0.01$.

We have not included the e.m.f. data obtained with any sodium salt of a phenolic compound. Experi-

mentally, for such compounds no change in a_{H^+} is observed with varying concentrations of salt, but we have evidence, both cryoscopic and conductometric, that for sodium *o*-phenylphenolate, for example, a simple monomeric dissociation, $MX \rightleftharpoons M^+ + X^-$, is not sufficient to explain the observed behavior.

Table VI: Results Obtained Using Cell III. Calculation of $E^\circ_{Ag^+,Ag}$ According to Eq. 26

C_{AgCl}, M	C_{HCl}, M	$\Delta E, v.^a$	$pK_{AgCl} - pK_{HCl}$	$E^\circ_{Ag^+,Ag}, v.$
0.01085	0.2410	0.0419	0.055	
0.01085	0.1200	0.0337	0.06	
0.01085	0.0525	0.0236	0.04	
		Mean	0.05 ± 0.01	0.7339 ^b
0.0108	0.2410	0.0408	0.014	
0.0108	0.2076	0.0395	0.03	
0.0108	0.1222	0.0328	0.025	
		Mean	0.023 ± 0.01	0.7571 ^c

^a ΔE = E.m.f. difference between cell II and cell III both containing the same C_{AgCl} . ^b Previous measurements (*cf.* ref. 3 and 4).

Cell I: $E_{HCl} = -0.6122 (\pm 0.0019) + 0.0296 \log C_{HCl}$

Cell II: $E_{AgCl} = 0.1202 (\pm 0.0015) + 0.0296 \log C_{AgCl}$

^c This paper (Table V).

With the exception of HCl and AgCl the agreement between the pK values calculated from the previously reported results^{3,4} and the present ones is as close as can be expected. (As mentioned earlier, this discrepancy in the case of HCl and AgCl has been traced to the accidental drift of the potential of the reference electrode used in the previous measurements.) It should also be mentioned in this connection that our absolute pK values of HCl, HBr, HNO₃, AgBr, and AgI reported in this paper compare favorably with those obtained by conductance measurements.^{9,10}

Table VII: Absolute pK Values of Acids and Silver Salts in EDA

HX or AgX	Present authors	Others (conductometric values)
HCl	2.87, ^{a,b} 4.01 ^{c,d}	3.98, ^e 3.935 ^f
HBr	3.76, ^{b,g} 3.64 ^{c,d} 3.73, ^{g,h} 3.73 ^{d,i}	3.62 ^e
Hydriodic acid	2.97 ^{b,o}	
HNO ₃	3.20 ^{o,h}	3.48 ^e
HClO ₄	3.10 ^{o,h}	
Acetic acid	5.19 ^{b,i}	
Phenylacetic acid	5.19, ^{b,j} 4.48 ^{b,o}	
3-Methyl-4-phenylazophenol	3.77 ^{d,k}	
<i>p</i> -Phenylphenol	7.02, ^{a,b,l} 7.02 ^{a,h,l}	
<i>o</i> -Phenylphenol	7.13, ^{a,b,l} 7.02 ^{a,h,l}	
Phenol	7.13 ^{a,b,l}	
Thymol	8.21 ^{a,b,l}	
AgCl	3.70, ^{m,n} 4.04 ^{d,o}	
AgBr	4.23, ^{m,n} 4.26 ^{d,o}	4.08 ^e
AgI	5.06, ^{m,n} 5.03 ^{d,o}	4.95 ^f

^a Cell I; $E_{scce} = -0.5272 v.$ ^b See ref. 4. ^c Grand mean of spectrophotometric, cryoscopic, and conductance values (see text). ^d This paper. ^e See ref. 9. ^f See ref. 10. ^g Cell V; $pK_{HCl} = 4.01$. ^h F. A. K. Badawi, M.S. Thesis, University of Minnesota, 1964. ⁱ Cryoscopic value (see text). ^j Cell I; pK based on comparison of calculated e.m.f. for $C_{HX} = 0.01 M$ using the corresponding least-squares constants, given in the legend to Figure 2 of ref. 4, *vs.* $E_{HCl} = -0.7051 v.$ at $C_{HCl} = 0.01 M$ (*cf.* footnote to Table V); $pK_{HCl} = 4.01$. This pK value is only approximate. ^k Weighted average (see text). ^l See eq. 5d in ref. 4. ^m Cell II; $E_{scce} = -0.5272 v.$; $E^\circ_{Ag^+,Ag} = 0.7571 v.$

$$E_{AgCl} = 0.1202 (\pm 0.0015) + 0.0296 \log C_{AgCl}$$

$$E_{AgBr} = 0.10445 (\pm 0.0022) + 0.0296 \log C_{AgBr}$$

$$E_{AgI} = 0.0801 (\pm 0.0012) + 0.0296 \log C_{AgI}$$

ⁿ See ref. 3. ^o Cell II; $E_{scce} = -0.5272 v.$; $E^\circ_{Ag^+,Ag} = 0.7571 v.$ Equations for E_{AgX} are given in the footnote to Table V.

Acknowledgment. This work was sponsored by the Army Research Office.

The Photochemical and Thermal Isomerization of *trans*- and *cis*- α -Cyano- α -phenyl-N-phenylnitrones

by Kinko Koyano and Ikuzo Tanaka

Laboratory of Physical Chemistry, Tokyo Institute of Technology, Ohokayama, Meguro-ku, Tokyo, Japan
(Received January 9, 1965)

In order to improve our understanding of the photochemical nitrone \rightarrow oxazirane isomerization, *trans* and *cis* forms of α -cyano- α -phenyl-N-phenylnitronone were photochemically and thermally examined. Thermal *cis* \rightarrow *trans* isomerization was observed in butanol solution; activation energy = 24.6 kcal./mole, frequency factor = 2×10^{11} sec.⁻¹. By irradiation at 3130 Å, both of these forms isomerized to α -cyano- α -phenyl-N-phenyloxazirane without *cis*-*trans* isomerization. The oxaziranes decomposed thermally in concentrated solution; hence their infrared spectra were taken at 77°K. The quantum yields were determined in cyclohexane and ethanol solutions. The *cis* \rightarrow *trans* as well as *trans* \rightarrow *cis* isomerization took place by eosine and uranine photosensitizations, to which reaction triplet nitrone is considered to contribute. Iodine catalyzed only *cis* \rightarrow *trans* isomerization thermally and photochemically. It is concluded that the nitrone in the excited singlet state isomerizes to the oxazirane by oxygen-atom rearrangement and that the nitrone in the triplet state leads to *cis* \rightleftharpoons *trans* isomerization.

Introduction

In the previous paper,¹ it was shown that α ,N-diphenylnitronone isomerized into α ,N-diphenyloxazirane by 3130-Å irradiation. The quantum yield of the photoisomerization was independent of irradiation time, concentration of the nitrone, presence of oxygen, and temperature, but was affected by hydrogen-bond formation. The *trans* \rightarrow *cis* isomerization of the nitrone with irradiation could not be observed. A mechanism was proposed which considered the mobility of the oxygen attached to nitrogen and the *trans* \rightarrow *cis* isomerization, in which the reaction was rapidly performed in the excited singlet state of the nitrone by the movement of oxygen atom to α -carbon atom before the two phenyl rings twisted around the double bond.

Hence, in this report, in order to confirm the mechanism of the photochemical nitrone \rightarrow oxazirane isomerization, α -cyano- α -phenyl-N-phenylnitronone in the *trans* and *cis* forms was examined in the thermal *cis* \rightarrow *trans* isomerization, the photochemical nitrone \rightarrow oxazirane reaction, and the *cis* \rightleftharpoons *trans* isomerization induced by photosensitization.

Experimental

The *trans* and *cis* forms of α -cyano- α -phenyl-N-phenylnitronone were synthesized and purified according to Barrow and Thorneycroft.^{2,3} Cyclohexane and *n*-heptane were purified by passing through silica gel and by distillation. *n*-Butyl alcohol was purified with acidic sodium sulfite. Eosine was Wako Pure Chemical Industries reagent grade, and uranine was Nichiri Co. reagent grade, and these were recrystallized from ethanol. Iodine was resublimed. The experimental procedures of irradiation at 3130 Å, measurements of ultraviolet absorption spectra at room temperature, infrared absorption spectra at 77°K., and determinations of quantum yields were all similar to those de-

(1) K. Shinzawa and I. Tanaka, *J. Phys. Chem.*, **68**, 1205 (1964).

(2) F. Barrow and F. J. Thorneycroft, *J. Chem. Soc.*, 722 (1934).

(3) The melting points of *trans* and the *cis* forms were 143 and 158°, respectively. The latter value was lower by 10° than that obtained by Barrow and Thorneycroft. In spite of the discrepancy we considered it to be the *cis* form by the nitrogen analysis, its thermal isomerization to the *trans* form, and its infrared absorption spectra (Figure 2), which showed characteristic bands due to cyano, mono-substituted benzene, and C=N groups. *Anal.* Calcd. for C₁₄H₁₀N₂O: N, 12.86. Found: N, 12.61.

scribed previously.¹ Ultraviolet absorption spectra at -50° were taken with a Beckman spectrophotometer, Model DU, equipped with a special cell designed for low temperature measurements.⁴ Infrared absorption spectra at room temperature were taken with a Shimadzu IR-27 spectrophotometer. A 250-w. tungsten bulb with a Hoya-crystal Y-44 filter was used for the light source of wave lengths longer than $430\text{ m}\mu$.

Results and Discussion

As is shown in Figure 1, the ultraviolet absorption bands of the *cis* form of α -cyano- α -phenyl-N-phenyl-nitrone (abbreviated to the nitrone) are located at longer wave length than those of its *trans* form, and their intensities are smaller than those of the latter in cyclohexane and in ethanol. Figure 2 shows the infrared absorption spectra of two forms in KBr.

1. *Thermal cis* \rightarrow *trans* Isomerization. The ultraviolet spectra of *cis*-nitrone in butanol solution changed gradually with three isosbestic points when the solution was heated at 117.5° , as illustrated in Figure 3. The change was concluded to be due to the *cis* \rightarrow *trans* isomerization by comparison with the spectra in Figure 1. The rate constants of the reaction at several temperatures were determined by measuring the change in optical density at $320\text{ m}\mu$. The activation energy and the frequency factor were calculated as 24.6 kcal./mole and $2 \times 10^{11}\text{ sec.}^{-1}$, respectively, by the specific rates at several temperatures. These values are about the same magnitude as those for azobenzene *cis* \rightarrow *trans* isomerization.⁵

2. *Nitrone* \rightarrow *Oxazirane* Photoisomerization. The ultraviolet absorption spectra of *trans*- and *cis*-nitrones

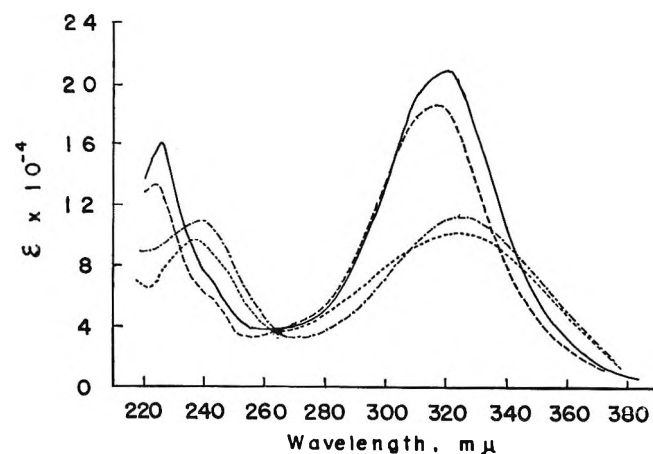


Figure 1. Ultraviolet spectra of *trans* and *cis* forms of the nitrone at 25° : —, *trans* in cyclohexane; ---, *trans* in ethanol, ·····, *cis* in cyclohexane; -·-·-·, *cis* in ethanol.

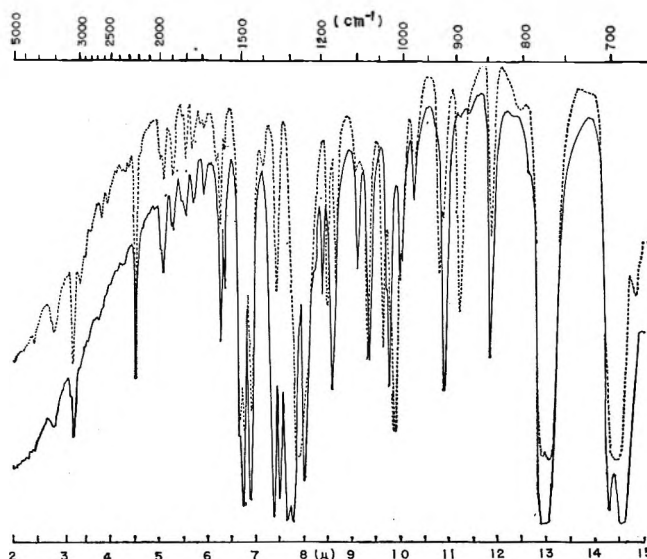
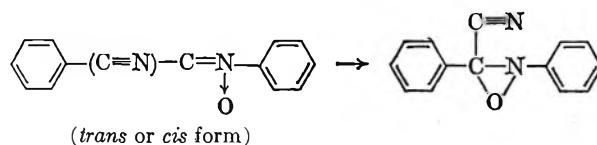


Figure 2. Infrared of *trans* and *cis* forms of the nitrone in KBr at room temperature: —, *trans*; ·····, *cis*.

in cyclohexane solution changed by irradiation with $3130\text{-}\text{\AA}$. light at room temperature, as shown in Figures 4 and 5, respectively. The dotted lines in the figures indicate the spectra of the irradiation products, in which after enough irradiation no reactant bands were superposed. The main product from both isomers was concluded to be an oxazirane, since its properties were the same as those of α ,N-diphenyloxazirane.¹ Supporting evidence was as follows: (1) The ultraviolet absorption spectrum of the product, being below $230\text{ m}\mu$, showed a break of conjugation between the α -carbon and nitrogen. (2) The product liberated iodine from acidic potassium iodide. (3) Ring vibrations of oxazirane in the infrared absorption spectrum were detected as described in the following section. Furthermore, it can be concluded from the existence of isosbestic points as shown in Figures 4 and 5 that no *trans* \rightleftharpoons *cis* isomerization occurs, for there should be no distinct isosbestic point as a result of the two-stage reaction, *i.e.*, *cis* \rightarrow *trans* \rightarrow oxazirane or *trans* \rightarrow *cis* \rightarrow oxazirane. Thus, the reaction is formulated as



The nitrone was isomerized to oxazirane through oxygen transfer rearrangement by $3130\text{-}\text{\AA}$. irradiation,

(4) The authors were indebted to Mr. K. Hirota, Tokyo Institute of Technology, for taking these spectra.

(5) G. S. Hartley, *J. Chem. Soc.*, 633 (1938).

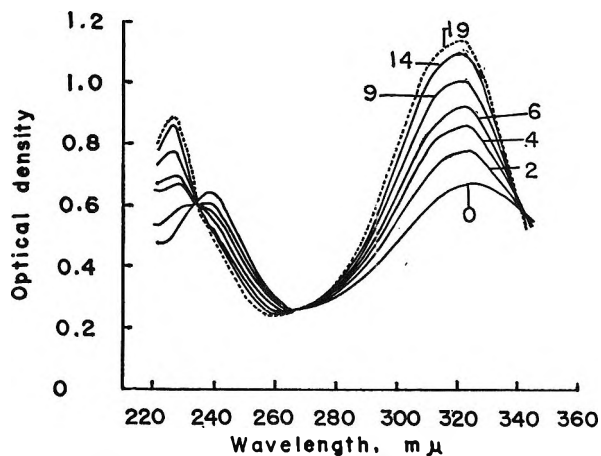


Figure 3. The spectral change of the *cis*-nitron in butanol solution caused by heating the solution at 117.5°; numbers refer to heating time in minutes.

although *trans* forms of azobenzene,⁵ stilbene,⁶ benzylidenephénylimine,⁷ and azoxybenzene⁸ were isomerized to the *cis* form by irradiation.

The oxazirane was not only unstable in concentrated solution at room temperature, but also was susceptible to heat in dilute cyclohexane solution.

3. *Ultraviolet and Infrared Absorption Spectra of the Irradiation Products at Low Temperatures.* As was seen in Figures 4 and 5, the spectrum of the irradiation product from *trans*-nitron was slightly different from that of the *cis* isomer at room temperature. In order to obtain a spectrum of pure oxazirane, the *cis*- and *trans*-nitrones were irradiated at -50°. The spectra obtained at -50° were absolutely the same as those in cyclohexane at room temperature. Therefore, the slight difference may be due to the small amounts of other products from the photochemical side reaction.⁹

The oxazirane in concentrated solution was so unstable at room temperature that the irradiation and the infrared absorption measurement were performed at 77°K. The results are given in Table I. The color of the sample disks in KBr were pale yellow both before and after irradiation for 2.5 hr. at 77°K., but the irradiated disks suddenly darkened and hardly transmitted the infrared ray when brought to room temperature.

As shown in Table I, most of the bands of the irradiation products correspond with each other in frequency and intensity. Although several bands are found to have no corresponding ones, they are attributable to those of the unreacted nitrones, which are denoted by the symbols *t* (*trans*-nitron) and *c* (*cis*-nitron). Thus, most of the common bands among these two spectra can be assigned to those of the oxazirane. Ring vibrations of oxazirane are con-

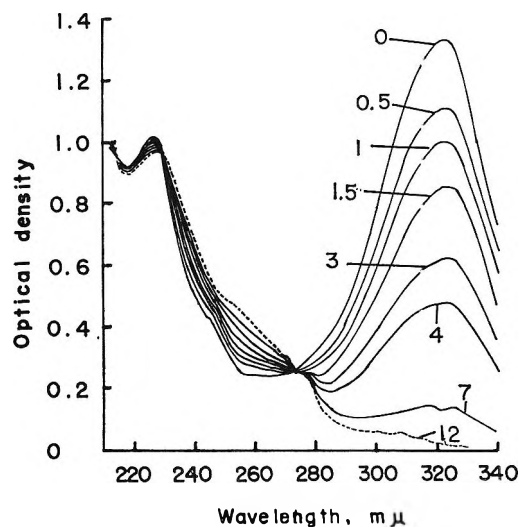


Figure 4. The progressive decrease of the spectrum of the *trans*-nitron on 3130-Å irradiation in cyclohexane solution. Numbers refer to irradiation time in minutes, and the dotted line denotes a spectrum of the product at room temperature.

sidered to be frequencies at 1296¹⁰ and 737-724 cm.⁻¹, which correspond to those at 1250 and 734-715 cm.⁻¹ in α ,N-diphenyloxazirane.¹ These bands appeared with irradiation and disappeared with the thermal decomposition. The bands at 1687 and 1684 cm.⁻¹, due to carbonyl vibration, should be ascribed to the side-reaction product in the photochemical process, because their intensities were weak (from *trans*-nitron) or medium (from *cis*-nitron) at 77°K. but they become extremely strong when observed at room temperature.

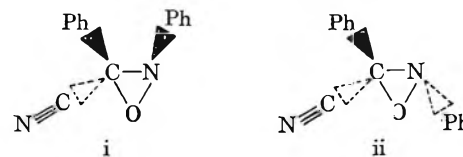
4. *Quantum Yields of the Nitron \rightarrow Oxazirane Reaction.* The quantum yields of the *trans*- and *cis*-nitron \rightarrow oxazirane reaction at 3130 Å. were obtained by measuring the decrease of the nitron absorption.

(6) A. Smakula, *Z. physik. Chem.*, B25, 90 (1934).

(7) E. Fisher and Y. Frei, *J. Chem. Phys.*, 27, 80E (1957).

(8) E. Müller, *Ann.*, 493, 166 (1932).

(9) The discrepancy might be due to difference in content of steric isomers of the oxazirane. Possible structures of the isomers are:



and ii. (C-N rings are placed in the paper, \blacktriangleright bonds stretch upward.)

and bonds \blacktriangleleft stretch downward.)

(10) In the case of *trans*-nitron, the band is hidden by the nitron bands at 1305 and 1289 cm.⁻¹.

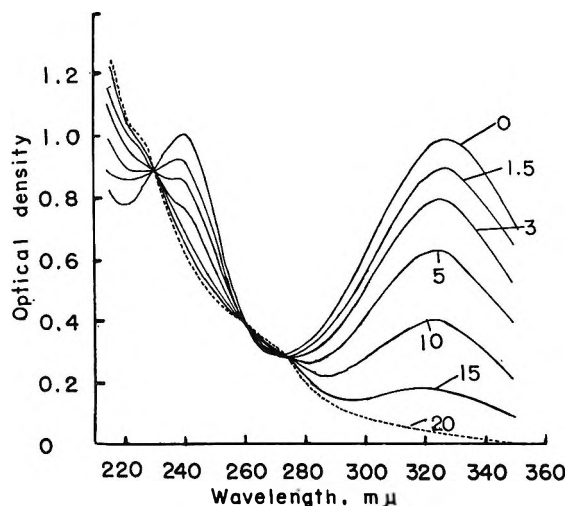


Figure 5. The progressive decrease of the spectrum of the *cis*-nitron on 3130-Å irradiation in cyclohexane solution. Numbers refer to irradiation time in minutes, and the dotted line denotes a spectrum of the product at room temperature.

Table I: Infrared Absorption Spectra of the Irradiation Products at 77°K.

From <i>trans</i> -nitron		From <i>cis</i> -nitron		From <i>trans</i> -nitron		From <i>cis</i> -nitron	
Cm. ⁻¹	Intensity	Cm. ⁻¹	Intensity	Cm. ⁻¹	Intensity	Cm. ⁻¹	Intensity
3368	m, sh	3361	m, sh	1162	w	1156	w
3244	s	3234	s	1103	vw (<i>t</i>)		
3076	m, sh	3071	m, sh	1076	w	1078	w
2225	w	2216	w	1026	w	1025	w
1971	w	1963	w	1007	s	1011	s
1899	w	1893	w	998	sh	999	sh
1806	vw	1810	vw	975		975	w
1687	w	1684	m	924	m	930	m
1597	s	1595	s	917	m	920	w
1505	s (<i>t</i>)	1511	s (<i>c</i>)	908	m	909	w
1487	s	1488	s			894	m (<i>c</i>)
1454	s	1453	s	876	m	879	w
1354	m	1351	w	847	m, sh (<i>t</i>)	846	m (<i>c</i>)
1336	m (<i>t</i>)			843	m (<i>t</i>)		
1305	sh (<i>t</i>)	1296	s	822	w	828	m
1289	s (<i>t</i>)			785	s	783	s
1250	m (<i>t</i>)	1268	s (<i>c</i>)	771-764	vs	772-750	vs
1236	m, sh			737-724	vs	737-724	vs
		1219	w	690-680	vs	690-680	vs
1189	w	1182	w				

The results are listed in Table II. The values obtained from *trans*-nitron were nearly equal to those from *cis*-nitron in the same solvents. The values with α ,N-diphenylnitron in ethanol were smaller than those in cyclohexane.¹ The decrease was attributed to hydrogen-bond formation.

5. Photosensitized *cis*-*trans* Isomerization. The photochemical reaction of the nitron was the isomerization to the oxazirane, while its thermal reaction was

Table II: The Quantum Yields of the *trans*- and *cis*-Nitron \rightarrow Oxazirane Reaction with 3130-Å Irradiation^a

Expt.	<i>trans</i> -Nitron		<i>cis</i> -Nitron	
	In cyclohexane	In ethanol	In cyclohexane	In ethanol
1	0.33	0.23	0.35	0.17
2	0.33	0.24	0.34	0.21
3	0.27	0.25	0.36	0.21
Av.	0.31	0.24	0.35	0.20

^a A high-pressure mercury lamp with a filter was used. Light intensity at 3130 Å. was 2.34×10^{18} photons/sec.

the *cis* \rightarrow *trans* isomerization. Since the oxazirane was postulated as formed without having passed through a triplet state, it is interesting to consider the reaction of the nitron in the triplet state produced by energy transfer from sensitizers.¹¹⁻¹⁴

Eosine, uranine, and iodine were used as sensitizers, since their absorption spectra do not overlap that of nitron, and besides, the lowest singlet excited states of the former two are well known to undergo intersystem crossing to the triplet with high efficiency.¹⁵ The irradiation of the mixtures of eosine and *trans*- or *cis*-nitron in ethanol with light of longer wave length than 430 m μ , which was absorbed only by the sensitizer, resulted in the *trans* \rightarrow *cis*, or *cis* \rightarrow *trans*, isomerization at room temperature. After irradiation for 1 hr., the photostationary state was established. The concentration of *cis* isomer was 44%, as calculated by both isomerization equilibria (Table III).

The case with uranine in ethanol was similar.¹⁶ The concentration of *cis* isomer at photoequilibrium was almost the same value as that of eosine (Table III).

In the presence of iodine, *cis*-nitron in *n*-heptane isomerized thermally to *trans*-nitron rapidly at room temperature. No reaction occurred in the case of *trans*-nitron. The iodine absorption had a maximum at 520 m μ and showed no change with nitron concentration ranging from 0 to 10^{-3} M, so in this range the complex between the nitron and an iodine molecule is

(11) A. Terenin and V. Ermolaev, *Trans. Faraday Soc.*, **52**, 1042 (1956).

(12) G. Porter and F. Wilkinson, *Proc. Roy. Soc. (London)*, **A264**, 1 (1961).

(13) See G. S. Hammond, J. Saltiel, A. A. Lamola, N. J. Turro, J. S. Bradshaw, D. O. Cowan, R. C. Counsell, V. Vogt, and C. Dalton, *J. Am. Chem. Soc.*, **86**, 3197 (1964), in which a series of their work on sensitized *cis*-*trans* isomerization is reviewed.

(14) S. Malkin and E. Fisher, *J. Phys. Chem.*, **68**, 1153 (1964).

(15) G. N. Lewis and M. Kasha, *J. Am. Chem. Soc.*, **66**, 2100 (1944).

(16) Although a very high pH value was favorable for uranine to be completely in the luminescent form, a pH value of 7-8 was used to prevent the nitron from being decomposed at a higher pH range.

Table III: Stationary States of the Nitron with Different Sensitizers by Irradiation with Light of Longer Wave Length than 430 $m\mu$

Sensitizer	Concn. of sensitizer, <i>M</i>	Concn. of nitron, <i>M</i>	Solvent	Initial % <i>cis</i>	% <i>cis</i> at photo-stationary state	Irradiation time for equilibrium, min.	Temp., °C.
Eosine	6.2×10^{-6}	6.3×10^{-5}	Ethanol	100	43	35	Room temp.
Eosine	4.5×10^{-6}	4.7×10^{-5}	Ethanol	0	44	35	Room temp.
Uranine	5.0×10^{-6a}	4.5×10^{-5}	Ethanol	100	42	60	Room temp.
Uranine	4.5×10^{-6a}	4.0×10^{-5}	Ethanol	0	44	60	Room temp.
Iodine	6.6×10^{-4}	3.8×10^{-5b}	<i>n</i> -Heptane	100	0	15	-50
Iodine	5.3×10^{-4}	3.8×10^{-5}	<i>n</i> -Heptane	0	0	..	Room temp.

^a Analytical concentration, a large part of uranine molecules was not the luminescent form for the reason described in ref. 16.

^b Concentration at room temperature.

considered not to be formed.¹⁷ The rate of iodine-catalyzed *cis* \rightarrow *trans* isomerization was accelerated by the increase of temperature, suppressed by the decrease of the temperature, and did not take place at -50° .

The irradiation of the mixtures of iodine and *cis*-nitron in *n*-heptane with light of wave length longer than 430 $m\mu$ resulted in the *cis* \rightarrow *trans* isomerization at -50° . No change was observed in the case of *trans*-nitron. The concentration of the *cis* isomer at photoequilibrium was zero (Table III).

The fact that the uranine- or eosine-sensitized photoequilibria of nitron are different from the thermal equilibrium indicates that the isomerization is caused by triplet-triplet energy transfer. In this case, the equilibrium concentration is not determined by the energy difference of the ground states of isomers but by the efficiencies of excitation energies and the crossing rate from triplet to ground state, in contrast to the thermal isomerization.^{13,14}

In the case of iodine sensitization, where the equilibrium is the same as thermal one, the isomerization is caused by formation of a complex of the nitron with an iodine atom induced by irradiation. A complex between an ethylene-type molecule and iodine is considered to have a low potential barrier between *cis* and *trans* isomers.

6. *Characteristics of the Lowest Singlet Excited State and the Triplet State of the Nitron.* As described above, the nitron \rightarrow oxazirane reaction was not caused by the sensitization from triplet-triplet energy transfer, but only by the singlet-singlet direct excitation. It confirms the mechanism that the reaction takes place in the lowest excited singlet state of nitron, which was already concluded in the previous paper.¹ The first excited singlet state may cross the oxazirane state, because this state consists mainly of the charge transfer from the oxygen atom to the conjugated sys-

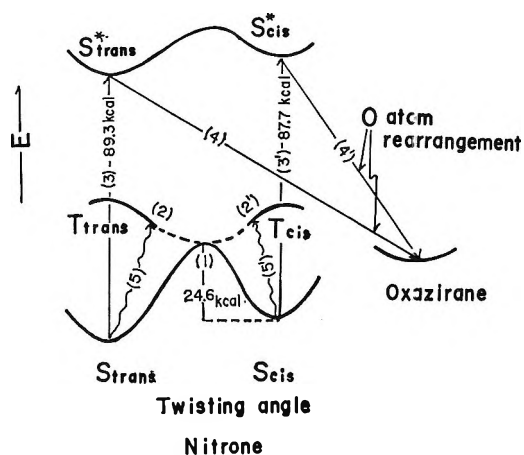


Figure 6. A schematic representation of potential curves. See the text.

tem.¹ This interpretation coincides with the result that almost the same values of quantum yield were obtained for *trans*- and *cis*-nitron in cyclohexane as in ethanol, because the quantum yield should depend largely on the electronic structure of the $>C=N\rightarrow O$ and not on the steric configuration. The decreased quantum yields in ethanol can also be recognized as due to hydrogen-bond formation with the solvent which has an equal effect on their electronic states.

The triplet state of nitron formed by eosine and uranine photosensitizations is indicated to have a configuration similar to the triplet states of stilbene, which play an important part in *cis*-*trans* isomerization.¹⁸

(17) According to T. Kubota [*J. Am. Chem. Soc.*, **87**, 458 (1965)], α -phenyl-N-methylnitron forms a complex with an iodine molecule at higher concentrations.

(18) *trans*- and *cis*-nitron formation were not observed in the case of oxazirane by eosine excitation. This may suggest that the sensitizer does not effect oxazirane-nitron conversion.

Figure 6 represents a scheme of energy levels involved in nitrone \rightarrow oxazirane and *cis-trans* isomerization. The potential curve for thermal rotation around the C-N double bond is denoted by the curve 1. Excited singlet nitrone produced by $S \rightarrow S^*$ transition, 3 and 3', isomerizes to singlet oxazirane directly, 4 and 4'. The triplet nitrone formed by transfer of triplet excitation, 5 and 5', is deactivated to the ground state along the curves 2 and 2', twisting about the C-N bond.¹⁹

It is concluded that the nitrone gives one of the most distinct examples in which reactions from singlet excited states are entirely different from triplet states.

Acknowledgment. The authors wish to express their gratitude to Dr. Y. Mori for his valuable discussions and to Mr. C. Shin for preparation of the isomers of the nitrone.

(19) The sensitization using tetracene (triplet energy is known to be 28 kcal.) was also carried out. With tetracene excitation, *cis* \rightarrow *trans* isomerization was observed, accompanied with some side reaction. *trans* \rightarrow *cis* isomerization could not be distinguished from the side reaction. This sensitized *cis* \rightarrow *trans* isomerization suggests that the energy difference between triplet state and *cis* ground state (nonvertical) is lower than 28 kcal., and the triplet function might fall below the maximum of the ground singlet function.

Thermodynamics of the Higher Oxides. I. The Heats of Formation and Lattice Energies of the Superoxides of Potassium, Rubidium, and Cesium¹

by L. A. D'Orazio and R. H. Wood

Department of Chemistry, University of Delaware, Newark, Delaware (Received January 12, 1965)

The heats of formation of KO_2 , RbO_2 , and CsO_2 were determined at 25.0°. They were -68.0 ± 0.4 , -68.0 ± 0.6 , and -69.2 ± 0.5 kcal./mole, respectively. The lattice energies of these compounds and the electron affinity of molecular oxygen ($EA = 14.9$ kcal./mole) were calculated using various approximations. The accuracy resulting from the use of the approximations is assessed. The heats of formation ($\Delta H_f^\circ = -62$ kcal./mole) and decomposition of hypothetical lithium superoxide are estimated. The results indicate that this compound should be very unstable.

Introduction

The alkali metals and, to a lesser extent, the alkaline earth metals have the tendency of forming higher oxides. Several of the alkali metals are capable of existence as the peroxide, superoxide, and ozonide. All of the alkaline earth metals can exist as the peroxide and there is evidence that some of them can exist as the superoxide. The thermodynamic data available for these compounds are rather meager and generally old. The following series of papers reports the results of a systematic investigation of some of the thermodynamic properties of these compounds, particularly the lattice

energies and the heats of formation of the oxygen anions.

The alkali superoxides are examples of compounds containing the simplest possible complex ion: that is, a complex ion with a covalent bond between two identical atoms. This presents the opportunity of investigating the accuracy of various approximations used in calculating the lattice energy of crystals containing complex ions. In particular, it offered the opportunity of

(1) This study was supported by the Air Force Office of Scientific Research Grant No. AF-AFOSR-325-63.

investigating whether alternate methods of calculating the repulsion energy are equally acceptable. This paper is concerned with the experimental determination of the heats of formation of the superoxides of potassium, rubidium, and cesium together with calculations of the lattice energy using various assumptions.

Experimental

Preparation of the Superoxides. The superoxides were prepared by oxidizing the liquid ammonia solutions of the alkali metals with oxygen at -78° . The ammonia used as the solvent was distilled from a storage cylinder into a glass holding vessel and then slowly redistilled through dry potassium hydroxide pellets into the reaction chamber. Alkali metal (99.9% pure) was added to the liquid ammonia under the protection of an atmosphere of dry argon. Oxygen, which was successively passed through anhydrous sodium carbonate, calcium chloride, and phosphorus pentoxide was rapidly bubbled through the solution. As the oxidation proceeded, the dark blue metal-ammonia solutions gradually turned white owing to the formation of the peroxides. For the potassium and rubidium solutions, the white precipitates rapidly became yellow as the superoxides were formed. In the case of the cesium solution, a brown precipitate (giving the solution the appearance of chocolate milk) followed the white precipitate and persisted for a relatively long time before finally giving way to the yellow precipitate characteristic of the superoxide. The ammonia was evaporated from the reaction flask in a stream of dry oxygen. The superoxide remained behind as the residue. The superoxide was baked at 100° under 0.1 mm. pressure for 16 hr. The samples were then divided and loaded into weighed fragile glass ampoules in a drybox and stored in a desiccator until ready for analysis and calorimetry. One preparation of potassium superoxide and two each of rubidium and cesium superoxide were made.

Analysis of the Superoxides. Five different analyses were carried out in order to characterize the samples. (1) The total metal was determined gravimetrically by precipitation as the tetraphenylborate salt.² (2) Combined superoxide and peroxide content was determined by measuring the volume of oxygen evolved in the decomposition of the sample with water. A palladium-on-charcoal catalyst was used to ensure complete decomposition. (3) Superoxide content was determined by the method of Seyb and Kleinberg.³ (4) and (5) The samples were titrated with standard hydrochloric acid solution to the phenolphthalein and methyl orange end points. The results are given in Table I. The data have been adjusted according to the usual pro-

cedure for conditioned measurements⁴ and the error limits are the standard deviations of the average values.

Table I: Analytical Results

	MO ₂ , %	MHCO ₃ , %	M ₂ CO ₃ , %
KO ₂	94.7	2.0	3.3
RbO ₂ (1)	95.5	3.8	0.7
RbO ₂ (2)	95.0	5.0	...
CsO ₂ (1)	94.6	2.0	3.4
CsO ₂ (2)	93.5	...	6.5

Calorimetry. The superoxide samples were decomposed in water in a twin-vessel solution calorimeter. This apparatus has been described elsewhere.⁵ The calorimeter reaction proceeds quantitatively in the presence of a palladium catalyst to form the products, aqueous alkali hydroxide and oxygen. Fragile glass ampoules containing from 1 to 3 mmoles of the superoxide sample were submerged and broken in 675 cc. of 10^{-3} M, carbonate-free sodium hydroxide solutions. In order for the final state of the evolved oxygen to be accurately known, it was necessary to saturate the solutions with oxygen. A blanket of oxygen was kept over the solutions at all times. Errors in the sample weight were negligible since 85–400-mg. samples were used. The uncorrected calorimetric results for each sample are listed in column 1 of Table II as calories per gram of sample. The average values and their standard deviations are also given.

The heat of ampoule breaking (0.02 cal.) and the correction to infinite dilution were negligible. The corrections for the heat effects due to the impurities and the vaporization of water by the evolved oxygen were not negligible. The corrected results are given in columns 2 and 3 of Table II in kilocalories per mole of superoxide. The error limits are the standard deviations of the average values. The heat of formation of water was taken from Circular 500.⁶ The heats of formation of potassium hydroxide ($\Delta H_f^\circ = -115.32$) and cesium hydroxide ($\Delta H_f^\circ = -117.6$) are taken from

(2) H. Flaschka and A. J. Barnard, "Advances in Analytical Chemistry and Instrumentation," Vol. I, Interscience Publishers, Inc., New York, N. Y., 1960.

(3) E. Seyb and J. Kleinberg, *Anal. Chem.*, **23**, 115 (1951).

(4) A. G. Worthing and J. Geffner, "The Treatment of Experimental Data," John Wiley and Sons, Inc., New York, N. Y., 1943.

(5) H. S. Jongenburger, Thesis, University of Delaware, Newark, Del., 1963.

(6) F. D. Rossini, D. D. Wagman, W. H. Evans, S. Levine, and I. Jaffe, "Selected Values of Chemical Thermodynamic Properties," National Bureau of Standards Circular 500, U. S. Government Printing Office, Washington, D. C., 1952.

Table II: Calorimetric Results at 25°

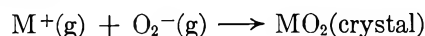
	Uncor. heat of reaction of sample, cal./g.	ΔH of reaction, ^a kcal./mole	Value adopted, kcal./mole	Heat of formation, kcal./mole
KO ₂	-170.2 ± 5.1 (5 runs)	-13.0 ± 0.4	-13.0 ± 0.4	-68.0 ± 0.4
RbO ₂ (1)	-111.0 ± 0.7 (2 runs)	-14.0 ± 0.2	-14.1 ± 0.2	-68.0 ± 0.6
RbO ₂ (2)	-111.2 ± 1.5 (4 runs)	-14.2 ± 0.2		
CsO ₂ (1)	-80.3 ± 2.2 (3 runs)	-14.1 ± 0.5	-14.1 ± 0.2	-69.2 ± 0.5
CsO ₂ (2)	-80.9 ± 1.0 (3 runs)	-14.1 ± 0.2		

^a The calorimetric reaction was $\text{MO}_2(\text{s}) + \frac{1}{2}\text{H}_2\text{O}(\text{l}) \rightarrow \text{MOH}(\text{aq}) + \frac{3}{4}\text{O}_2(\text{g})$.

Gunn and Green^{7a} and Friedman and Kahlweit,^{7b} respectively. The Circular 500 value for cesium hydroxide is not used because it is based on uncertain cell measurements. The value for rubidium hydroxide ($\Delta H_f^\circ = -116.3$) is based on a comparison of Rengade's measurements of the heats of solution of the alkali metals⁸ with the more recent data for potassium and cesium. All other heat data are taken from Circular 500.⁶ The standard heats of formation of the superoxides calculated from the above data are tabulated in column 4 of Table II. The limits of error are the standard deviations.

Lattice Energy Calculations

The lattice energy of interest in this work is the energy change at absolute zero for the process



where M^+ is the alkali metal ion. The reactants are considered to be noninteracting ions at infinite separation and the product is the stable tetragonal alkali superoxide crystal. The energy of the process is equivalent to the enthalpy by virtue of the absolute zero condition. The calculated energy is inserted in the thermodynamic cycle outlined in Figure 1 and the electron affinity of molecular oxygen is deduced.

The lattice energy was calculated by the classical

Born-Mayer method where the energy per molecule, $\phi(r)$, is given by the equation

$$\phi(r) = -\frac{Me^2}{r} - \frac{C}{r^6} + B(r) + \phi_0 \quad (1)$$

M is the Madelung constant, C the van der Waals constant, ϕ_0 the zero point vibrational energy, and $B(r)$ the repulsive potential. In the alkali superoxide system, the repulsive potential can be expressed as

$$B(r) = 4c_{+-}b \exp(r_+ + r_{-\text{min}} - a/2)1/\rho + 2c_{+-}b \exp(r_+ + r_{-\text{maj}} - c/2)1/\rho + (4/2)c_{++}b \exp(2r_+ - \sqrt{2}a/2)1/\rho + (8/2)c_{++}b \exp(2r_+ - \frac{1}{2}\sqrt{a^2 + c^2})1/\rho + (4/2)c_{--}b \exp(2r_{-\text{min}} - \sqrt{2}a/2)1/\rho + (8/2)c_{--}b \exp(r_{-\text{min}} + r_{-\text{maj}} - \frac{1}{2}\sqrt{a^2 + c^2})1/\rho \quad (2)$$

where the first two terms represent the interaction of nearest neighbors and the remaining terms give the interaction of next-nearest neighbors. The c_{ij} are the Pauling factors,⁹ b is a constant evaluated from the equilibrium condition

$$\left(\frac{dU}{dV}\right)_{V=V_0} = 0 \quad (\text{where } U = -N\phi(r)) \quad (3a)$$

r_+ is the cation radius, and $r_{-\text{min}}$ and $r_{-\text{maj}}$ are the ionic radii of the ellipsoidal superoxide ion. The parameters c and a are the crystallographic unit cell dimensions equal to $2\gamma r$ and $2r$, respectively, where r is the nearest neighbor distance and $\gamma = c/a$. The repulsion constant, ρ , is determined from the relation

$$\left(\frac{d^2U}{dV^2}\right)_{V=V_0} = \frac{1}{\beta V} \quad (3b)$$

(7) (a) S. R. Gunn and L. G. Green, *J. Am. Chem. Soc.*, **80**, 4782 (1958); (b) H. L. Friedman and M. Kahlweit, *ibid.*, **78**, 4243 (1956).

(8) E. Rengade, *Ann. chim. phys.*, **14**, 540 (1908).

(9) L. Pauling, *Z. Krist.*, **67**, 377 (1928).

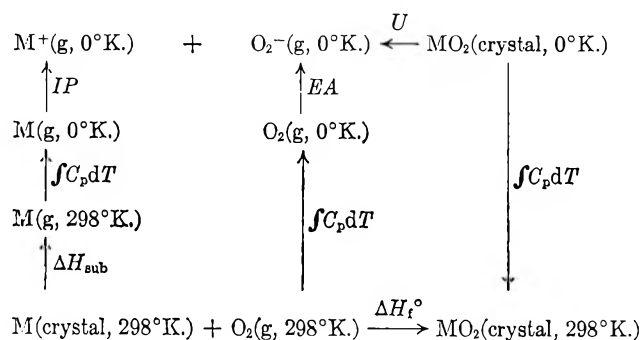


Figure 1. Born-Haber cycle.

The resulting equation is

$$\phi(r) = -\frac{Me^2}{r_0} - \frac{C}{r_0^6} + \phi_0 + \frac{(A + B + C + D + E + F)[A + \gamma^2 B + \tau^2]}{\sigma [A + \gamma B + \sqrt{2}(C + E) + (1 + \gamma^2)^{1/2}(D + F)]^2} \quad (4)$$

where $A = 4c_+ b \exp(r_+ + r_- - a/2)/\rho$, $B =$ next term in $B(r)$ of eq. 2, etc., and

$$\tau = -r_0 \frac{dB(r_0)}{dr_0} = \frac{Me^2}{r_0} + \frac{6C}{r_0^6}$$

$$\sigma = r_0^2 \frac{d^2B(r_0)}{dr_0^2} = 2\frac{Me^2}{r_0} + 42\frac{C}{r_0^6} + \frac{9V}{N\beta}$$

The zero point energy is considered to be independent of r . This approximation does not appreciably affect the results.

The lattice energy was also calculated from a potential function containing a much simpler expression for the repulsion energy. Ladd and Lee¹⁰ have expressed the repulsion potential as

$$B(r) = b \exp\left(-\frac{r}{\rho}\right) \quad (5)$$

After applying conditions (3a) and (3b), the Ladd and Lee potential function reduces to

$$\phi(r_0) = -\frac{Me^2}{r_0} - \frac{C}{r_0^6} + \frac{\tau^2}{\sigma} + \phi_0 \quad (6)$$

Since the higher alkali superoxides have tetragonal crystal structures and are therefore anisotropic, we have used an alternate repulsion potential which will allow us to take advantage of anisotropic equilibrium conditions. The repulsion may be expressed as

$$B(r) = B(a,c) = 2b \exp\left(-\frac{c}{2\rho}\right) + 4b' \exp\left(-\frac{a}{2\rho}\right)$$

where the first term corresponds to the repulsive interaction between an ion and its two nearest neighbors along the crystallographic c axis and the second term corresponds to the interaction of the ion with its four nearest neighbors along the a axes. After applying the conditions

$$\left(\frac{\partial\phi}{\partial a}\right)_{a=a_0} = 0$$

$$\left(\frac{\partial\phi}{\partial c}\right)_{c=c_0} = 0 \quad (7)$$

and also applying eq. 3b (with the assumption of isotropic compressibility), we find

$$B(r) = \frac{1}{\sigma} \left(\frac{\tau_c}{\gamma} + \tau_a \right) (\gamma\tau_c + \tau_a) \quad (8)$$

where

$$\tau_a = -a \left(\frac{\partial B(a,c)}{\partial a} \right)_c; \quad \tau_c = -c \left(\frac{\partial B(a,c)}{\partial c} \right)_a$$

Now, expanding eq. 8 in terms of $(\gamma - 1)$ and ignoring terms higher than $(\gamma - 1)^2$, we find that

$$B(r) = \frac{1}{\sigma} [\tau^2 + \tau_a \tau_c (\gamma - 1)^2] \quad (9)$$

where $\tau = \tau_a + \tau_c$. It is shown, then, that our modification reduces to the Ladd and Lee equation for a cubic crystal and that for a tetragonal system the deviation in the repulsion is only second order in $(\gamma - 1)$. It can also be shown that the coefficient of the τ^2/σ term in eq. 4 takes on values close to unity for systems with cubic symmetry and small like-ion repulsions. We should, therefore, predict little difference in the various calculations for the lattice energies of the superoxides.

The technique reported by Baughan¹¹ for calculating lattice energies was unsuccessfully applied to the superoxide system. Only data for three salts were used for solving his eq. 29 and these showed considerable scatter about the least-squares solution. This fact, coupled with the long extrapolation required to deduce the electron affinity, makes his method unsuited to the present study.

Data

Table III contains the data used for the calculations along with references to the sources of this data.

The Madelung constant, M_δ , was interpolated from the data reported by Wood.¹² The characteristic distance, δ , is the cube root of the molecular volume. It was evaluated for an O-O bond distance of 1.28 Å. and a charge distribution of 0.5 electronic unit per oxygen atom. This charge distribution corresponds to a quadrupole moment of -1.97 e.s.u. Errors in the quadrupole moment of 50% result in errors in M_δ of only 1%. This Madelung constant, based on a given charge distribution in the superoxide ion, includes higher pole interactions and eliminates the need for calculating separate summation constants for quadru-

(10) M. F. C. Ladd and W. H. Lee, *J. Inorg. Nucl. Chem.*, **11**, 264 (1959).

(11) E. C. Baughan, *Trans. Faraday Soc.*, **55**, 736 (1959).

(12) R. H. Wood, *J. Chem. Phys.*, **37**, 598 (1962).

Table III: Data for the Calculations

	KO ₂	RbO ₂	CsO ₂	Ref.
M_{δ}	2.1888	2.1917	2.1929	a
M_{δ} at $z = 0$	2.2287	2.2280	2.2232	a
a , 10 ⁻⁸ cm., at 298°K.	5.704	6.00	6.28	b
c , 10 ⁻⁸ cm., at 298°K.	6.699	7.03	7.24	b
a_0 , 10 ⁻⁸ cm., at 0°K.	5.654	5.95	6.23	c
c_0 , 10 ⁻⁸ cm., at 0°K.	6.641	6.97	7.18	c
r_+ , 10 ⁻⁸ cm., at 0°K.	1.32	1.47	1.68	d
r_{-maj} , 10 ⁻⁸ cm., at 0°K.	2.00	2.00	2.00	e
r_{-min} , 10 ⁻⁸ cm., at 0°K.	1.51	1.51	1.51	e
z (i.e., c/a)	1.1744	1.1717	1.1529	b
γ	0.0955	0.0910	0.0884	b, m
α , 10 ⁻⁵ deg. ⁻¹ (expansivity)	10.5	10.1	9.8	l
β , 10 ⁻¹² cm. ² /dyne	3.86	4.80	5.70	l
c_{++} (Pauling factor)	1.05	1.05	1.05	f
c_{--} (Pauling factor)	1.25	1.25	1.25	f
c_{+-} (Pauling factor)	0.85	0.85	0.85	f
C_{--} , 10 ⁻⁶⁰ erg cm. ⁶	26.5	26.5	26.5	l
C_{++} , 10 ⁻⁶⁰ erg cm. ⁶	24.3	59.4	152	l
C_{+-} , 10 ⁻⁶⁰ erg cm. ⁶	23.3	37.4	48.7	l
S_{--} (van der Waals sum)	8.67	8.46	8.32	l
S_{++} (van der Waals sum)	3.65	3.64	3.76	l
S_{+-} (van der Waals sum)	59.5	59	59	l
ΔH_f° , kcal./mole	-67.9	-68.0	-69.2	l
IP , kcal./mole	100.0	96.3	89.7	g
ΔH_{sub} , kcal./mole	21.5	20.5	18.8	h
$\int_0^{298} C_{PMO_2,c} dT$, kcal./mole	3.9	3.9	3.9	i
$\int_0^{298} C_{PM,g} dT$, kcal./mole	1.5	1.5	1.5	j
$\int_0^{298} C_{PO_2,g} dT$, kcal./mole	2.1	2.1	2.1	k

^a See ref. 12. M_{δ} is the Madelung constant defined in terms of $V^{1/3}$, the cube root of the molecular volume. ^b S. C. Abrahams and J. Kalnajs, *Acta Cryst.*, **8**, 503 (1955); L. I. Kazarnovskaya, *Russ. J. Phys. Chem.*, **20**, 1403 (1946). ^c Calculated from the expansivity. ^d Goldschmidt radii. ^e Estimated from the differences between the interatomic distances and the Goldschmidt cation radii. ^f The Pauling factors were calculated from the approximation formula $c_{ij} = 1 + (Z_i/N_i) + (Z_j/N_j)$, where Z_i = valence of i th ion and N_i = number of electrons in the outer shell of the i th ion. ^g W. Finkelnburg and W. Humbach, *Naturwiss.*, **42**, 35 (1955). ^h W. H. Evans, *et al.*, *J. Res. Natl. Bur. Std.*, **55**, 83 (1955). ⁱ Estimated from the data of S. S. Todd, *J. Am. Chem. Soc.*, **75**, 1229 (1953). ^j Assumed to be the ideal value, $5/2R$. ^k H. W. Woolley, *J. Res. Natl. Bur. Std.*, **40**, 163 (1948). ^l See text. ^m The definition of z is in terms of the O-O distance, $R(O-O) = 2zc$.

pole-point and quadrupole-quadrupole interactions. The Madelung constant for the superoxide ion considered as a point charge was also taken from the same paper. The difference between these two constants enables the calculation of the higher pole interaction energy.

The equation of Slater and Kirkwood¹³ has been used to estimate the van der Waals interaction coefficients

$$E = \frac{3e\hbar}{4\pi m^{1/2}R^6} \frac{\alpha_A\alpha_B}{\left(\frac{\alpha_A}{N_A}\right)^{1/2} + \left(\frac{\alpha_B}{N_B}\right)^{1/2}} = -\frac{C_{AB}}{R^6} \quad (10)$$

where N , the effective number of electrons, is used as an empirical constant.

Huggins and Sakamoto¹⁴ have used a procedure which is equivalent to assuming that $N^{1/2}$ is a linear function of the nuclear charge in an isoelectronic series. Morris¹⁵ assumed that N is the same for chloride and sulfide. For polyatomic systems it has been shown that the assumption of an independent center of attraction at each nucleus gives reasonable results.¹⁶ Accordingly, the equation of Slater and Kirkwood has been used to calculate the interaction of the oxygen atoms using a polarizability of each oxygen atom ($\alpha = 1.32$) taken from Kazarnovskii's value of the polarizability of the superoxide ion ($\alpha = 2.64$).¹⁷ The number of effective electrons for each O^{-1/2} group ($N = 1.93$) was calculated for the values for the fluoride ion ($N = 1.61$) and the sodium ion ($N = 3.13$) assuming that $N^{1/2}$ is a linear function of charge. The fluoride and sodium ion values were calculated from Mayer's accurate evaluation of the van der Waals energy¹⁸ and Pauling's values of the polarizabilities.¹⁹ The interaction constants for the positive ions were taken from Mayer while the interactions of the positive and negative ions were calculated from the above values and eq. 10. The final values are given in Table III.

The van der Waals sums were calculated using an IBM 1620¹¹ computer to perform a direct sum.²⁰ A sum over shells of unit cells was used following the electrostatic energy method of Wood.²¹ The program calculates the sum of R^{-6} for a series of nonequivalent atoms. The van der Waals energy is then

$$E = 1/2 \sum_j \sum_i n_j c_{ij} \sum_k \left(\frac{1}{R_k}\right)^6 \quad (11)$$

where the sums are over-all types of atoms j and i and over-all radii, R_k , between a central atom j and an atom of type i in the shells being calculated. These sums are grouped according to the coefficients of the van der Waals interaction C_{++} , C_{+-} , and C_{--} to give

- (13) J. C. Slater and J. G. Kirkwood, *Phys. Rev.*, **37**, 682 (1931).
 (14) M. L. Huggins and Y. Sakamoto, *J. Phys. Soc. Japan*, **12**, 241 (1957).
 (15) D. F. C. Morris, *Acta Cryst.*, **11**, 163 (1958).
 (16) L. Pauling and M. Simonetta, *J. Chem. Phys.*, **20**, 29 (1952); K. Pitzer and E. Catalano, *J. Am. Chem. Soc.*, **78**, 4844 (1956); K. Pitzer in "Advances in Chemical Physics," Vol. II, I. Prigogine, Ed., Interscience Publishers, Inc., New York, N. Y., 1959, p. 59; S. Kimel, A. Ron, and D. F. Hornig, *J. Chem. Phys.*, **40**, 3351 (1964).
 (17) I. A. Kazarnovskii and S. I. Raikhsheine, *Russ. J. Phys. Chem.*, **21**, 245 (1947).
 (18) J. E. Mayer, *J. Chem. Phys.*, **1**, 270 (1933).
 (19) L. Pauling, *Proc. Roy. Soc. (London)*, **A114**, 191 (1927).
 (20) The authors wish to thank the University of Delaware Computing Center for the use of their facilities. A Fortran listing of the program and a set of directions can be obtained by writing to R. H. Wood.
 (21) R. H. Wood, *J. Chem. Phys.*, **32**, 1690 (1960).

$$E = \sum_{1,m} C_{1,m} (S_{1,m}/\delta^6)$$

where the sum is taken over all pairs of atoms and $S_{1,m}$ is a reduced sum using the cube root of the molecular volume, δ , as a characteristic distance. The results of the calculations are given in Table III.

The zero point energy of interest in this work does not include the internal vibrational energy of the superoxide ion and is given by the relation²²

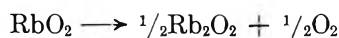
$$\phi_0 = \frac{9}{8} k\theta \quad (12)$$

where ϕ_0 is the energy per constituent ion and θ is the Debye temperature. The compressibility and zero point energy were obtained from the Debye temperature using Blackman's equation²³ and eq. 12, respectively. The compressibility agrees to within 3% with the value calculated from Huggins' equation.²⁴ The fact that these equations apply to cubic crystals was neglected. The Debye temperature ($\theta = 279^\circ\text{K}$.) was calculated from the specific heat measurements of Todd.²⁵

The expansivity of potassium superoxide was estimated from a consideration of its size, binding energy, and heat capacity. The estimated value is in agreement with the value calculated from the equation of Joshi and Mitra.²⁶ The expansivities of rubidium and cesium superoxide were then estimated from the change in expansivities in the K-Rb-Cs series of the isostructural, homologous families in the alkali halides. The hypothetical lattice distances at absolute zero were then calculated, the slight decrease in expansivity with temperature being considered.

Results and Discussion

The heat of formation of potassium superoxide has been accurately determined by Kazarnovskaya²⁷ ($\Delta H_f^\circ = -67.9 \pm 0.1$ kcal./mole) and by Gilles and Margrave²⁸ (-67.6 ± 0.8 kcal./mole). The result of this work (-68.1 ± 0.4 kcal./mole) is in excellent agreement with these values. The present results are also very close to the results of de Forcrand,²⁹ but this is fortuitous since corrections for changes in supplementary data reveal differences of 5 to 10 kcal./mole.⁷ Kraus and Petrocelli³⁰ have calculated the heats of the reactions



from equilibrium pressure measurements at 280 to 360°. Calculation of the standard heat of formation of rubidium superoxide from these data and estimated heat capacities yielded $\Delta H_f^\circ(\text{RbO}_2) = 51$ kcal./mole, a figure which is irreconcilable with the result of this work. It is interesting to note that the entropy of the

first reaction reported by Kraus and Petrocelli, 2 e.u., is considerably smaller than the value for the same reaction of the sodium analogs, 19 e.u.

The individual value for the Coulomb energies, higher-pole interaction energies, London energies, and zero point vibrational energies are given in Table IV. The lattice energies and electron affinity are also given in Table IV.

Kazarnovskii³¹ has calculated the lattice energies and found values 6 to 9 kcal./mole lower. Kazarnovskii's values were based on a quadrupole moment for the O_2^- ion of 3×10^{-26} e.s.u. cm.². This corresponds to a +0.76 charge on the oxygens and a -1.52 charge at the center of the molecule. Recent measurements of the quadrupole moment of the oxygen molecule³² give a charge of less than 0.1 on the oxygens. This indicates that a $-1/2$ charge on each oxygen in a much better estimate of the charge distribution on O_2^- since O_2^- has one more antibonding electron than O_2 .

Table IV: Results of Calculation

	KO ₂	RbO ₂	CsO ₂
Coulomb energy, kcal./mole	197.0	187.1	179.5
Higher pole interaction energy, kcal./mole	-3.6	-3.0	-2.5
London dispersion energy, kcal./mole	8.7	10.0	10.9
Zero point energy, kcal./mole	-1.2	-1.1	-1.0
Repulsion energy, eq. 5, kcal./mole	-23.8	-24.3	-24.7
Repulsion exponent, eq. 5, Å.	0.274	0.296	0.317
Lattice energy, eq. 6, kcal./mole	177.1	168.7	162.2
Electron affinity of oxygen, kcal./mole	12.6	16.4	15.8

Evans and Uri's³³ value for the lattice energy is based on an incorrect Madelung constant and a spherically symmetric O_2^- ion. Yatsimirskii's³⁴ values for the lattice energies were calculated using Kapustinskii's equation. Both results differ by +2 to -5

(22) R. H. Fowler, "Statistical Mechanics," 2nd Ed., Cambridge University Press, London, 1936, p. 123.

(23) M. Blackman, *Proc. Roy. Soc. (London)*, **A151**, 58 (1942).

(24) M. L. Huggins, *J. Chem. Phys.*, **5**, 143 (1937).

(25) S. S. Todd, *J. Am. Chem. Soc.*, **75**, 1229 (1953).

(26) S. K. Joshi and S. S. Mitra, *Z. Physik. Chem.*, **29**, 95 (1961).

(27) L. I. Kazarnovskaya and I. A. Kazarnovskii, *Zh. Fiz. Khim.*, **25**, 293 (1951).

(28) P. W. Gilles and J. L. Margrave, *J. Phys. Chem.*, **60**, 1333 (1956).

(29) de Forcrand, *Compt. rend.*, **150**, 1399 (1910); **158**, 991 (1914).

(30) D. L. Kraus and A. W. Petrocelli, *J. Phys. Chem.*, **66**, 1225 (1962).

(31) I. A. Kazarnovskii, *Dokl. Akad. Nauk SSSR*, **59**, 67 (1948).

(32) W. V. Smith and R. Howard, *Phys. Rev.*, **79**, 132 (1950); R. S. Anderson, W. V. Smith, and W. Gordy, *ibid.*, **82**, 264 (1951).

(33) M. G. Evans and N. Uri, *Trans. Faraday Soc.*, **45**, 224 (1949).

(34) K. B. Yatsimirskii, *Khim. i Khim. Tekhnol.*, **4**, 480 (1959).

kcal./mole from the present values. This is surprisingly close for approximate equations.

It is instructive to examine the dependency of the total lattice energy on its various components. Equation 6 can be rewritten in the form

$$\phi(r_0) = -\frac{Me^2}{r_0} - \frac{C}{r_0^6} + \frac{\rho}{r_0} \left(\frac{Me^2}{r_0} + \frac{6C}{r_0^6} \right) + \phi_0 \quad (13)$$

Analogous expressions derived from eq. 4 and 9 yield results similar to eq. 13. For the alkali superoxides, the parenthetical factor in the repulsion term does not differ by more than 8% for the three calculations. The repulsion term in (13) consists of a sum of terms each of which is one of the attractive energy components Kr^{-n} multiplied by a factor $-n/r$. Now for these salts ρ/r takes on values between $1/9$ and $1/11$. This is in the same range as ρ/r for the alkali halides, cuprous halides, and silver halides. In general, most salts that have been reported in the literature have ρ/r values in the $1/6$ to $1/12$ range. This means that potentials varying between r^{-6} and r^{-12} are largely cancelled in the empirical repulsion term. The general principle can be stated: the lattice energy becomes insensitive to a small energy term, $E(r)$, as

$$\frac{E(r)}{dE(r)} \rightarrow \frac{B(r)}{dB(r)}$$

In the usual case of $E(r)$ varying as r^{-n} and $B(r)$ as $\exp(-r/\rho)$, the lattice energy becomes insensitive to the minor term $E(r)$ as $n \rightarrow r/\rho$. Since ρ is somewhat constant, this criterion can be used *a priori* to determine the effect of a proposed potential term on the resulting lattice energy. For example, in the superoxide case with ρ/r having values between $1/9$ and $1/11$, we may completely neglect the London r^{-8} and r^{-10} terms. This is a fortunate aspect of the lattice energy calculation since those potentials varying with high negative powers of the distance are generally very difficult to determine and contain large uncertainties. This criterion also shows why the lattice energies of the superoxides (and in general any complex system) are considerably more sensitive to the higher pole interaction energy than the London energy. The superoxide ion is a quadrupole and gives rise to a quadrupole-point charge interaction varying as r^{-3} and a quadrupole-quadrupole interaction varying as r^{-5} .

The repulsion energies and repulsion exponents (ρ) for eq. 5 are given in Table IV. Equations 2 and 8 yielded energies which were within 0.3 kcal./mole of the reported values and repulsion exponents which differed by less than 5%. The negligible differences be-

tween the Ladd and Lee method (eq. 6) and the Born-Mayer method (eq. 4) are to be expected for crystals which are not very asymmetric and for which like-ion repulsion is small.

The situation concerning the dependency of the lattice energy on the compressibility is not so favorable. The effects of the compressibility can be seen by expanding the Ladd-Lee repulsion term

$$B(r_0) = \frac{\left[\frac{M_\delta e^2}{r_0} + \frac{6C}{r_0^6} \right]^2}{\frac{2M_\delta e^2}{r_0} + \frac{42C}{r_0^6} + \frac{9V}{N\beta}} \quad (14)$$

The analogous expressions from eq. 4 and 9 yield results which are within 1% of eq. 14. For the superoxides the term $9V/N\beta$ amounts to approximately 75% of the denominator in eq. 14. This means that approximately 75% of the uncertainty in β will be carried into the repulsion energy. This is surely the major uncertainty in this work and contributes an uncertainty of 2 kcal./mole to the lattice energy and electron affinity. That this is a general case for all lattice energy calculations can be shown by observing that the ratio, $(9V/N\beta)/\sigma$, will be sizeable for most salt systems. It is 0.7–0.8 for the alkali superoxides, 0.6–0.8 for the alkali halides, and 0.3–0.5 for the alkaline earth chalcogenides. In fact, if the lattice energy of a system increases, its compressibility decreases. This ensures that the ratio will never become small and that accurate lattice energy calculations by the usual techniques will always require reasonably good compressibility data.

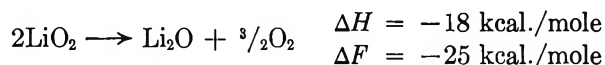
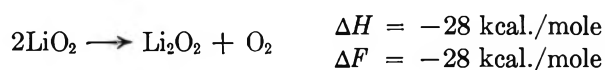
In summation then, this investigation indicates several factors that stand out in applying the classical treatment of lattice energies to complex systems. First, although the Coulomb interaction presents no problem in that the lattice sums can be quickly and accurately determined on modern electronic computing equipment, the charge distribution of the system can become critical, especially in the cases of the larger complex ions and the asymmetric ions. Here the higher pole interactions become important and can seriously affect the lattice energy. Second, the availability of accurate compressibility data has been shown to be of paramount importance. This holds even for simple inorganic systems. Since there is a paucity of accurate compressibility data, this appears to be the weakest link in the calculation. Third, a more simplified expression of the repulsion energy is apparently suitable for crystals that approach cubic symmetry and do not have large like-ion repulsion. This reduces the labor of calculation.

In calculating the electron affinity of oxygen from the superoxides the approximate contributions to the total

error are 1 kcal./mole from the total uncertainties in the Born-Haber cycle, 2 kcal./mole from the uncertainty in the compressibility, and 3 kcal./mole from the uncertainty in the model itself. Accordingly, the electron affinity of molecular oxygen is 15 kcal./mole with an estimated uncertainty of 5 kcal./mole (0.65 ± 0.22 e.v.). This value is in reasonably good agreement with those previously calculated by the thermochemical technique.^{31,33,34} They range from 0.65 to 0.96 e.v., the present value, 0.65, being the most carefully determined. Physical techniques for measuring this quantity (*e.g.*, photodetachment experiments) have indicated a lower value of 0.15 e.v.³⁵ Mulliken³⁶ has attempted to resolve this situation by a semitheoretical argument. He contends that the lower value, 0.15 e.v., is slightly more consistent with his estimate of the superoxide bond dissociation energy. This being established, he then adopts the lower value on the grounds that considerable errors are possible in the thermochemical value. The present work results in a lower electron affinity than previous thermochemical values. However, the value 0.15 derived from photodetachment experiments is still well outside the estimated limits of error. The X-ray data for potassium superoxide have been re-examined by Halverson.³⁷ He interprets the data in terms of a crystal in which the oxygen atoms are revolving around the *c* axis in a circle of 0.15 to 0.34 Å. radius with a resulting coupling of nuclear and electronic motions. Since the higher pole energy term is only of the order of 5 kcal./mole, it is unlikely that the change in electrostatic energy due to the distortion could be large enough to account for the 0.5-e.v. discrepancy between the thermochemical and the photochemical values of the electron affinity. It is also

doubtful that coupling between the nuclear and electronic energies would be large enough to account for the difference. In conclusion, this work confirms the inconsistency between the thermochemical and photodetachment values of the electron affinity of molecular oxygen.

Finally, the lattice energy of LiO₂ can be estimated from a plot of lattice energy *vs.* alkali metal for the superoxide family. This type of plot performed for various alkali metal salts (*e.g.*, halides, cyanides, sulfides, azides, etc.) yields a family of curves of similar slope. The estimate from the extrapolation is $U(\text{LiO}_2) = 210 \pm 10$ kcal./mole. From this value the heat of formation is calculated to be $\Delta H_f^\circ(\text{LiO}_2) = -62 \pm 10$ kcal./mole. This value indicates that LiO₂ is unstable with respect to decomposition to Li₂O₂ and Li₂O. The following properties can be estimated from available data³⁸



This explains the great difficulty that has confronted the attempted preparation of LiO₂.

Acknowledgments. The authors wish to thank Messrs. Ronald W. Smith and Henry L. Anderson for assistance with the calorimetric measurements.

(35) D. S. Burch, S. J. Smith, and L. M. Branscomb, *Phys. Rev.*, **112**, 171 (1958).

(36) R. S. Mulliken, *ibid.*, **115**, 1225 (1959).

(37) F. Halverson, *J. Phys. Chem. Solids*, **23**, 207 (1962).

(38) L. Brewer, *Chem. Rev.*, **52**, 1 (1953).

Thermodynamics of the Higher Oxides. II. Lattice Energies of the Alkali and Alkaline Earth Peroxides and the Double Electron Affinity of the Oxygen Molecule¹

by R. H. Wood and L. A. D'Orazio

Department of Chemistry, University of Delaware, Newark, Delaware (Received January 12, 1965)

The Madelung constants for the alkali metal peroxides and the van der Waals sums for both the alkali and alkaline earth peroxides have been calculated. The results are used to evaluate the lattice energies of the peroxides and the double electron affinity of the oxygen molecule, $E(\text{O}_2 \rightarrow \text{O}_2^{-2}) = -145 \pm 15$ kcal./mole. The covalent bond energy in the peroxide ion ($D = -95$ kcal./mole) is discussed.

During the past 15 years there have been four separate calculations of the double electron affinity of molecular oxygen. Evans and Uri^{2a} using an approximate Madelung constant for the alkaline earth peroxides, found the value $E(\text{O}_2 \rightarrow \text{O}_2^{-2}) = -112 \pm 8$ kcal./mole. Vedenev, *et al.*,^{2b} using an accurate Madelung constant for the alkaline earth peroxides, found $E(\text{O}_2 \rightarrow \text{O}_2^{-2}) = -175 \pm 15$ kcal./mole. More recently, Yatsimirskii³ applied the Kapustinskii approximation to the alkali metal peroxides and obtained $E(\text{O}_2 \rightarrow \text{O}_2^{-2}) = -120$ kcal./mole. Tuck⁴ applied the Kapustinskii approximation to barium peroxide and found $E(\text{O}_2 \rightarrow \text{O}_2^{-2}) = -121$ kcal./mole. He pointed out that the recent determinations of the crystal structures of the alkali metal peroxides⁵⁻⁷ would allow rigorous calculations of the lattice energies of these salts.

All of the previous workers have failed to assess the importance of higher pole interactions and their conclusions rest on the assumption that the peroxide ion can be adequately represented by a point charge. This paper reports the results of a more rigorous calculation of the lattice energies of the alkali metal and alkaline earth peroxides and the double electron affinity of molecular oxygen. As in the first paper in this series⁸ (hereafter referred to as part I) the van der Waals interactions and the effects of the charge distribution in the anion are assessed.

Calculations of Madelung Constants

The Madelung constants of the alkali metal peroxides were calculated by the method of Wood,^{9,10} which involves the direct calculation of the interaction of a molecule with successive shells composed of unit cells. The results are given in Table I for two different charge distributions; case I, a -1 charge on each oxygen atom, and case II, a -2 charge at the center of the peroxide ion (the "point charge approximation"). Case I was used in the calculation of the lattice energy. This case should be closer to the actual charge distribution since molecular oxygen has a very low quadrupole moment^{11,12} and two antibonding electrons are added

(1) This study was supported by Air Force Office of Scientific Research Grant No. AF-AFOSR-325-63.

(2) (a) M. G. Evans and N. Uri, *Trans. Faraday Soc.*, **45**, 224 (1949); (b) A. V. Vedenev, L. I. Kazarnovskaya, and I. A. Kazarnovskii, *Zh. Fiz. Khim.*, **26**, 1808 (1952).

(3) K. B. Yatsimirskii, *Khim. i. Khim. Teknol.*, **4**, 480 (1959).

(4) D. G. Tuck, *J. Inorg. Nucl. Chem.*, **26**, 1525 (1964).

(5) H. Foppl, *Z. anorg. allgem. Chem.*, **291**, 12 (1957).

(6) R. Tallman, J. L. Margrave, and S. W. Bailey, *J. Am. Chem. Soc.*, **79**, 2979 (1957).

(7) F. Feher, I. V. Wilucki, and G. Dost, *Chem. Ber.*, **86**, 1429 (1953).

(8) L. A. D'Orazio and R. H. Wood, *J. Phys. Chem.*, **69**, 2550 (1965).

(9) R. H. Wood, *J. Chem. Phys.*, **32**, 1690 (1960).

(10) A Fortran listing and a set of directions can be obtained by writing to R. H. Wood.

Table I: Madelung Constants of the Alkali Metal Peroxides

Compound	Structure ^a	Madelung constant ^b			$V^{1/3}$ × 10 ⁸ cm.
		$M_{\delta}(M_2O_2)$	$M_{\delta}(M_2[O_2])$	$M_{\delta}(M_2(O_2))$ point charge	
Li ₂ O ₂	P $\bar{6}$ (C _{3h} ¹), $a = 3.142$, $c = 7.650$ Li-a, Li-d, Li-i ($z = 1/4$) O-g ($z = 0.401$), O-h ($z = 0.099$)	5.0057 ± < 0.006%	7.1169 ± < 0.005%	7.4017 ± < 0.1%	3.1978
Na ₂ O ₂	C $\bar{6}2m$ (C _{3h} ³), $a = 6.208$, $c = 4.469$ Na-f ($x = 0.295$), Na-g ($x = 0.632$) O-e ($z = 0.332$), Na-H ($z = 0.168$)	4.6382 ± < 0.02%	7.0870 ± < 0.02%	7.2763 ± < 0.06%	3.6770
K ₂ O ₂	Cmca (D _{2h} ¹⁸), $a = 6.736$, $b = 7.001$, $c = 6.479$ K-e ($y = 0.160$) O-f ($y = 0.088$, $z = 0.934$)	4.5297 ± < 0.02%	7.3221 ± < 0.01%	7.6640 ± < 0.01%	4.2429
Rb ₂ O ₂	Immm (D _{2h} ²⁶), $a = 4.201$, $b = 7.075$, $c = 5.983$ Rb-g ($y = 1/4$) O-i ($z = 0.374$)	4.3360 ± < 0.2%	7.2963 ± < 0.1%	7.4313 ± < 0.07%	4.4633
Cs ₂ O ₂	Immm (D _{2h} ²⁶), $a = 4.322$, $b = 7.517$, $c = 6.430$ Cs-g ($y = 1/4$) O-i ($z = 0.38$)	4.2500 ± < 0.2%	7.3020 ± < 0.1%	7.4472 ± < 0.07%	4.7094

^a The structure is listed as follows: space group, unit cell dimensions, chemical symbols, and Wyckoff symmetry numbers as described in the "International Tables,"¹³ x , y , and z parameters of the Wyckoff symmetries. ^b The Madelung constant is given using the cube root of the molecular volume ($V^{1/3}$ or δ) as the characteristic distance. $M_{\delta}(M_2O_2)$ denotes the Madelung constant for the process $M_2O_2(c) \rightarrow 2M^+(g) + 2O^-(g)$ while $M_{\delta}(M_2[O_2])$ denotes the Madelung constant for the process $M_2O_2(c) \rightarrow 2M^+(g) + O_2^{-2}(g)$ (see ref. 9). The Madelung constants are calculated for a -1 charge on each oxygen atom except for the "point charge" Madelung constant which is for a -2 charge at the center of the peroxide ion.

to get the peroxide ion. Four shells of unit cells were used in each calculation and the contribution of the fourth shell was used as an estimate of the maximum error. The designations of the space groups and Wyckoff symmetries are described in the "International Tables."¹³ The structures of all of the alkali metal peroxides have been taken from Foppl.⁵

In the calculation for Li₂O₂, the unit cell and the "molecule" both had an appreciable net dipole moment so that a correction for the electrostatic energy of the molecule in the field caused by the dipole moment in the cell was necessary.¹⁴ For a unit cell with a dipole moment μ_c along the x direction and a molecular dipole moment μ_m , the correction is equal to

$$U_{d-d} = \frac{2\mu_c\mu_m}{abc} \left(\sin^{-1} 1 - \sin^{-1} \left[\frac{1 + (b/a)^2 + (c/a)^2 - (b/a)^2(c/a)^2}{1 + (b/a)^2 + (c/a)^2 + (b/a)^2(c/a)^2} \right] \right)$$

where a , b , and c are the unit cell lengths along the x , y , and z directions. This equation can be derived by calculating the energy of the molecular dipole in the field of a rectangle $(2n + 1)b$ by $(2n + 1)c$ that is $(n + 1/2)a$ units from the molecule and carries a surface charge of density μ_c/abc . The result is inde-

pendent of the number of shells which are calculated. As a check, the calculation was performed for a unit cell without a dipole moment. The results differed by 0.005% with the correction amounting to 1.4%. This is within the experimental error.

The Madelung constants for the alkaline earth peroxides have been interpolated from the values reported by Wood¹⁴ and are given in Table II. Where necessary for accuracy, Newton's method of interpolation has been used.

The magnesium peroxide structure is taken from Vannerberg,¹⁵ who reports that MgO₂ has a pyrite structure with an oxygen-oxygen distance of 1.498 ± 0.014 Å. The peroxides of barium, strontium, and calcium all have the calcium carbide structure. The z parameter for barium peroxide was taken from Abrahams and Kalnajs,¹⁶ who found $z = 0.1089$ and an

(11) W. V. Smith and R. H. Howard, *Phys. Rev.*, **79**, 132 (1950).

(12) R. S. Anderson, W. V. Smith, and W. Gordy, *ibid.*, **82**, 264 (1951).

(13) "International Tables for X-Ray Crystallography," Vol. I, N. F. M. Henry and K. Lonsdale, Ed., The Kynoch Press, Birmingham, England, 1952, pp. 153, 163, 281, 296.

(14) R. H. Wood, *J. Chem. Phys.*, **37**, 598 (1962).

(15) N. G. Vannerberg, *Arkiv Kemi*, **14**, 99 (1959).

(16) S. C. Abrahams and J. Kalnajs, *Acta Cryst.*, **7**, 838 (1954).

Table II: Madelung Constants of the Alkaline Earth Peroxides

Com- pound	Struc- ture type	Structure	Madelung constant		
			M_{δ} ($M[O_2]$)	M_{δ} ($M[O_2]$) point charge	$\gamma^{1/3}$ $\times 10^3$ cm.
MgO ₂	FeS ₂	Pa3 (T _h ⁶) $a = 4.839$ Mg-b O-c ($x = 0.0894$)	2.19604	2.20177	3.0484
CaO ₂	CaC ₂	I4/mmm (D _{4h} ¹⁷) $a = 3.543, c = 5.92$ Ca-b O-e ($z = 0.1260$)	2.1691	2.2303	3.337
SrO ₂	CaC ₂	I4/mmm (D _{4h} ¹⁷) $a = 3.567, c = 6.616$ Sr-b O-e ($z = 0.1128$)	2.1706	2.2728	3.479
BaO ₂	CaC ₂	I4/mmm (D _{4h} ¹⁷) $a = 3.815, c = 6.851$ Ba-b O-e ($z = 0.1089$)	2.1765	2.2581	3.681

oxygen-oxygen distance of 1.492 ± 0.04 Å. The z parameters for calcium and strontium peroxide were calculated assuming the oxygen-oxygen distance remains constant at 1.492 Å. The lattice constants for barium and strontium peroxides were taken from Swanson, Gilfrich, and Cook.¹⁷ The lattice constants of calcium peroxide were taken from Kotov and Raikhshtein.¹⁸

The heats of formation of the alkali metal peroxides have been taken from Rossini, *et al.*,¹⁹ except for the value for sodium peroxide which was taken from Gilles and Margrave.²⁰ The value of Rossini, *et al.*, for cesium peroxide has been corrected for Friedman and Kahlweit's²¹ heat of formation of the aqueous cesium ion.

The heats of formation of the peroxides of calcium, strontium, and barium were taken from Vedenev, Kazarnovskaya, and Kazarnovskii,^{2b} who measured the heats of solution of the peroxides in excess hydrochloric acid. The heat of formation of MgO₂ was taken from Rossini, *et al.*¹⁹

The van der Waals interaction constants were calculated by the method given in part I⁸ using $\alpha = 2.12 \times 10^{-24}$ cm.³ for the polarizability of each oxygen atom of the peroxide ion²² and an effective number of electrons ($N = 1.61$) the same as for the fluoride ion. Each oxygen atom is assumed to act independently. The results are given in Table III.

The van der Waals sums are also given in Table III. They were calculated using the computer program previously described.⁸

Table III: van der Waals Constants and Sums

	$C_{+-} \times 10^{80}$ erg cm. ⁶	$C_{++} \times 10^{60}$ erg cm. ⁶	S_{+-}	S_{++}	S_{--}
Li ₂ O ₂	1.18	0.073	196.6	30.77	19.16
Na ₂ O ₂	6.89	1.68	183.1	30.85	18.83
K ₂ O ₂	29.4	24.3	201.6	32.52	17.55
Rb ₂ O ₂	47.7	59.4	198.0	31.94	17.55
Cs ₂ O ₂	79.0	152	199.5	31.66	17.80
MgO ₂	3.84	0.7	73	3.61	9.94
CaO ₂	18.2	12	64	3.66	9.97
SrO ₂	32.4	34	59	3.76	9.59
BaO ₂	56.9	97	60	3.72	9.37
$C_{--} = 49.3$ for all compounds					

Results and Discussion

The Ladd and Lee equation (see eq. 13 of ref. 8) was used to calculate the repulsion energies and lattice energies. The electron affinity was calculated from the cycle

$$-E(O_2 \rightarrow O_2^{-2}) = U + \Delta H_f^{\circ}{}_{\text{salt}} - \Delta H_{\text{sub, metal}} - IP - \int_0^{298} C_{\text{P salt}} dT - \int_{298}^0 [C_{\text{P O}_2, g} + C_{\text{P metal, g}}] dT$$

The results are given in Table IV.

Table IV: Results of the Calculations (kcal./mole)

	Coulomb energy	Higher pole interaction energy	van der Waals energy	Repulsion energy ^a	Lattice energy ^b	Electron affinity
Li ₂ O ₂	+768.6	-29.5	+15.9	-133.6	+619.4	-143.3
Na ₂ O ₂	+657.1	-17.1	+13.1	-99.3	+551.8	-142.2
K ₂ O ₂	+599.8	-26.7	+18.7	-84.5	+505.3	-145.4
Rb ₂ O ₂	+552.9	-10.1	+22.2	-79.0	+484.0	-149.8
Cs ₂ O ₂	+525.1	-10.2	+28.3	-75.7	+465.5	-153.3
MgO ₂	+959.4	-2.5	+13.8	-166.5	+802.2	(-94.1) ^c
CaO ₂	+887.8	-24.4	+17.7	-127.6	+751.5	-134.7
SrO ₂	+867.8	-39.0	+20.4	-121.4	+725.8	-149.9
BaO ₂	+814.9	-29.5	+24.5	-111.7	+696.2	-137.4
$\text{Av. } E(O_2 \rightarrow O_2^{-2}) = -144.5$						

^a Calculated from eq. 5 of ref. 8 using $\rho = 0.333 \times 10^{-8}$ cm.

^b The zero point energy is taken as 2 kcal./mole for each compound. ^c The value of EA for MgO₂ (-94.1) was not used in calculating the average EA.

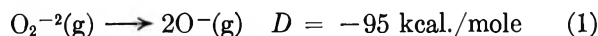
(17) H. E. Swanson, N. T. Gilfrich, and M. I. Cook, National Bureau of Standards Circular 539, Vol. 6, U. S. Government Printing Office, Washington, D. C., 1956, pp. 18, 32.

(18) V. P. Kotov and S. Raikhshtein, *Chem. Abstr.*, **36**, 50734 (1942); see also C. Brosset and N. G. Vannerberg, *Nature*, **177**, 238 (1956).

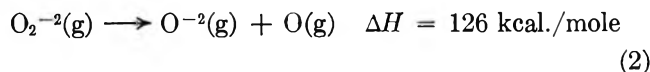
(19) F. D. Rossini, D. D. Wagman, W. H. Evans, S. Levine, and I. Jaffe, "Selected Values of Chemical Thermodynamic Properties," National Bureau of Standards Circular 500, U. S. Government Printing Office, Washington, 1952.

The higher pole interactions are quite large and, therefore, contribute significantly to the uncertainty in U and EA . The repulsion energy contains an uncertainty which is associated with the choice of the repulsion exponent, ρ . The value 0.333 \AA . was chosen on the basis of data on the alkali halides. An estimate of the resulting combined errors which is applied to the lattice energies and electron affinity is 15 kcal./mole . It is concluded that the double electron affinity of molecular oxygen is $-145 \pm 15 \text{ kcal./mole}$. This is less than the values reported by Evans and Uri ($-112 \pm 8 \text{ kcal./mole}$), Tuck (-121 kcal./mole), Yatsimirskii (-120 kcal./mole), and greater than the value reported by Vedenev, *et al.* ($-175 \pm 15 \text{ kcal./mole}$).

This value for the double electron affinity of the oxygen molecule allows the calculation of the energy for the processes



and



These values are calculated from a simple thermochemical cycle using the electron affinities of oxygen atoms $E(\text{O} \rightarrow \text{O}^{-}) = 33.8 \text{ kcal./mole}^{23}$ and $E(\text{O} \rightarrow \text{O}^{-2}) = -154 \text{ kcal./mole}^{24}$.

The negative value for ΔH in eq. 1 is undoubtedly due to the repulsive energy of the two electrons. For two electrons at the nuclei ($R = 1.50 \text{ \AA}$.), the electrostatic energy is 220 kcal./mole .

Acknowledgment. The authors thank the Computing Center of the University of Delaware for the use of their facilities.

(20) P. W. Gilles and J. L. Margrave, *J. Phys. Chem.*, **60**, 1333 (1956).

(21) H. L. Friedman and M. Kahlweit, *J. Am. Chem. Soc.*, **78**, 4243 (1956).

(22) I. A. Kazarnovskii and S. I. Raikhshein, *Russ. J. Phys. Chem.*, **21**, 245 (1947).

(23) L. M. Branscomb, D. S. Burch, S. J. Smith, and S. Geltman, *Phys. Rev.*, **111**, 504 (1958).

(24) For $\Delta H_f^\circ(\text{O}^{-2})$ see M. L. Huggins and Y. Sakamoto, *J. Phys. Soc. Japan*, **12**, 241 (1957), and D. F. C. Morris, *Proc. Roy. Soc. (London)*, **A242**, 116 (1957).

Thermodynamics of the Higher Oxides. III. The Lattice Energy of Potassium Ozonide and the Electron Affinity of Ozone¹

by R. H. Wood and L. A. D'Orazio

Department of Chemistry, University of Delaware, Newark, Delaware (Received January 12, 1965)

The Madelung constant, van der Waals sums, and lattice energy of the potassium ozonide structure have been calculated. The results were used to evaluate the electron affinity of ozone $EA(O_3) = 44 \pm 10$ kcal./mole and the heat of formation of the gaseous ozonide ion $\Delta H_f^\circ(O_3^-)_g = -11 \pm 10$ kcal./mole. The heat of formation of the hypothetical lithium ozonide is estimated ($\Delta H_f^\circ = -63$ kcal./mole) and the energy of its decomposition evaluated

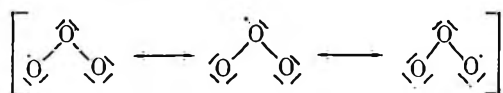
Introduction

This paper is the third in a series on the thermodynamics of the higher oxides.² The lattice energy of potassium ozonide has been calculated by Nikol'skii, Kazarnovskaya, Bagdasar'yan, and Kazarnovskii,³ who neglected the unsymmetrical charge distribution on the ozonide ion, used an estimated Madelung constant, estimated the repulsion on the basis of the Born exponent (n) of the nearest rare gas, and neglected the van der Waals forces. This paper presents a recalculation of the lattice energy using better estimates of these interactions and more recent crystallographic data.

Calculation of Madelung Constant

The Madelung constant was calculated by the method of Wood^{4,5} for the crystal structure of Azaroff and Corvin.⁶ The symmetry is $I4/mcm$ with $a = 8.597$, $c = 7.080$, and with K_I in a , K_{II} in b , O_I in h ($x = 0.287$), and O_{II} in k ($x = 0.075$, $y = 0.275$).⁷

Assuming a uniform charge distribution of $-1/3$ electronic unit on each oxygen (case I) the Madelung constant is calculated to be $M_s(K[O_3]) = 2.1012 \pm 0.03\%$ for the process $KO_3(c) \rightarrow K^+(g) + O_3^-(g)$. The Madelung constant is based on the cube root of the molecular volume ($\delta = 4.02908 \text{ \AA}$). The error was estimated from the contribution of the last (third) shell (0.03%). An alternate charge distribution of $O^{-2/3}O^{+1/3}O^{-2/3}$ (case II) results from assuming an equal contribution from the three Lewis structures



The Madelung constant for this charge distribution is $M_s(K[O_3]) = 2.2554 \pm <0.008\%$. The unit cells in both cases did not have dipole moments so that no correction was necessary.

van der Waals Energy

The van der Waals energy was calculated by the method given in part I.^{2a} The polarizability of an oxygen atom in an ozonide ion ($\alpha = 1.28$) has been estimated from a consideration of the polarizability of ozone⁸ and the variation in polarizability with effective nuclear charge in the oxygen, superoxide, peroxide series. The number of effective electrons, $N = 2.08$, was estimated by assuming a linear change of $N^{1/2}$ vs. charge in the series fluoride ($N^{1/2} = 1.27$), oxygen in ozonide ($N^{1/2} = 1.44$), sodium ($N^{1/2} = 1.77$). The potassium-potassium interaction constant C_{KK} is taken from Mayer⁹ and the potassium-oxygen interaction

(1) This study was supported by the Air Force Office of Scientific Research Grant No. AF-AFOSR-325-63.

(2) (a) L. A. D'Orazio and R. H. Wood, *J. Phys. Chem.*, **69**, 2550 (1965); (b) R. H. Wood and L. A. D'Orazio, *ibid.*, **69**, 2558 (1965).

(3) G. P. Nikol'skii, L. I. Kazarnovskaya, Z. A. Bagdasar'yan, and I. A. Kazarnovskii, *Dokl. Akad. Nauk SSSR*, **72**, 713 (1950).

(4) R. H. Wood, *J. Chem. Phys.*, **32**, 1690 (1960).

(5) The authors thank the Computing Center of the University of Delaware for the use of their facilities.

(6) L. I. Azaroff and I. Corvin, *Proc. Natl. Acad. Sci. U. S.*, **49**, 1 (1963).

(7) "International Tables for X-Ray Crystallography," Vol. I, N. F. M. Henry and K. Lansdale, Ed., The Kynoch Press, Birmingham, England, 1952.

(8) E. A. Moelwyn-Hughes, "Physical Chemistry," 2nd Ed., Pergamon Press, New York, N. Y., 1961, p. 383.

(9) J. E. Mayer, *J. Chem. Phys.*, **1**, 270 (1933).

constant is calculated from the other two. The calculation of the van der Waals energy is not very accurate ($\pm 50\%$) but its contribution to the error in the electron affinity of ozone is small (± 3 kcal./mole).

The van der Waals sums were computed by the method outlined in part I.^{2a} The results are given in Table I.

Table I: van der Waals Sums and Constants for KO_3

$S_{+-} = 96.08$	$C_{+-} = 23.4 \times 10^{-60}$ erg cm. ⁶
$S_{--} = 46.37$	$C_{--} = 26.2 \times 10^{-60}$ erg cm. ⁶
$S_{++} = 4.723$	$C_{++} = 24.3 \times 10^{-60}$ erg cm. ⁶

Results and Discussion

The Ladd and Lee equation was used to calculate the lattice energy (see eq. 13 of ref. 2a). Again, the value $\rho = 0.333 \text{ \AA.}$ was chosen on the basis of data on the alkali halides. The results are given in Table II. The electron affinity of ozone was calculated from the equation

$$-EA(\text{O}_3) = \Delta H_f^\circ(\text{KO}_3, \text{c}) + U - \Delta H_{\text{sub}, \text{K}} - IP - \Delta H_f^\circ(\text{O}_3, \text{g}) - \int_{298}^0 C_{\text{PK}, \text{g}} dT - \int_{298}^0 C_{\text{PO}_3, \text{g}} dT - \int_0^{298} C_{\text{PKO}_3, \text{c}} dT$$

The standard heat of formation of the gaseous ozonide ion was calculated from the equation

$$\Delta H_f^\circ(\text{O}_3^-, \text{g}) = \Delta H_f^\circ(\text{O}_3) - EA(\text{O}_3) + \int_{298}^0 C_{\text{Pe}^-, \text{g}} dT$$

The heat of formation of solid potassium ozonide, -62.1 kcal./mole, was taken from the work of Nikol'skii, *et al.*³ Omitting the heat capacity terms, C_{PO_3} and C_{PKO_3} (these terms partially cancel one another) and averaging the two cases of differing charge distributions, the electron affinity and heat of formation are found to be 44 ± 10 and -11 ± 10 kcal./mole, respectively. This value for the electron affinity is considerably lower than the value of Nikol'skii, *et al.*³

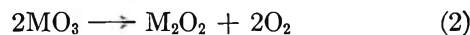
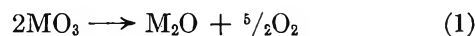
The above data allow the calculation of thermodynamic quantities which demonstrate the difficulty confronting the attempted preparation of LiO_3 . The lattice energy of LiO_3 can be estimated by the extrapolation method of part I to be 215 kcal./mole. The error in this estimate is probably not more than 10 kcal./mole. The heat of formation of LiO_3 calculated

Table II: Results of Calculations^a

Charge distribution	Case I	Case II
Coulomb energy, kcal./mole	174.9	187.7
van der Waals energy	12.8	12.8
Repulsion energy	-21.0	-22.1
Lattice energy	166.7	178.4
Electron affinity	49.9	38.2
$\Delta H_f^\circ(\text{O}_3^-, \text{gas})$	-16.9	-5.2

^a These calculations were made on the hypothetical lattice at 0°K. A 1% decrease in the room temperature lattice parameter was assumed.

from this value is -63 ± 15 kcal./mole. If we further estimate the absolute entropy of LiO_3 to be 20 cal./mole deg., we calculate the entropy and free energy of formation to be -60 cal./mole deg. and -45 kcal./mole, respectively. From the same data the enthalpy, entropy, and free energies for the following reactions may be calculated.



The results are given in Table III.

Table III: Thermodynamic Properties Calculated for Reactions 1, 2, and 3

	Reaction 1		Reaction 2		Reaction 3	
	Li	K	Li	K	Li	K
ΔH , kcal./mole	-16	38	-26	5	2	-12
ΔS , cal./mole deg.	92	96 ^a	68	71 ^a	69	55
ΔF , kcal./mole	-44	9	-46	-13	-19	-28

^a An estimate of $S^\circ(\text{KO}_3) = 25$ cal./deg. mole used in the calculation was taken from ref. 3.

It is seen, then, that although free energy favors the formation of lithium superoxide from the elements, this compound is quite unstable with respect to decomposition to a lower oxide.¹⁰ This behavior is contrasted with potassium ozonide which has been shown to decompose slowly to the superoxide.¹¹

(10) A. J. Kacmarek, J. M. McDonough, and I. J. Solomon, *Inorg. Chem.*, **1**, 659 (1962).

(11) I. A. Kazarnovskii, G. P. Nikol'skii, and T. A. Abletsova, *Dokl. Akad. Nauk SSSR*, **64**, 69 (1949).

Nuclear Magnetic Resonance Dilution Shifts for Carboxylic Acids in Rigorously Dried Solvents. I. Acetic Acid in Acetic Anhydride, Acetone, and 1,4-Dioxane¹

by Norbert Muller and Philip I. Rose

Department of Chemistry, Purdue University, Lafayette, Indiana (Received January 18, 1965)

The chemical shift of the hydroxyl protons of acetic acid has been studied as a function of concentration in the basic solvents, acetic anhydride, acetone, and 1,4-dioxane. The results obtained after taking great care to remove traces of water differ greatly from those reported earlier for similar solutions. The dilution curves were found to be nearly linear at low concentrations, and they could readily be extrapolated to infinite dilution. Association constants estimated from the data indicate that the base strengths of the solvents increase in the order acetic anhydride < acetone < dioxane. The hydroxyl proton chemical shifts for the hydrogen-bonded species acetic acid-acetic anhydride, acetic acid-acetone, and acetic acid-dioxane do not fall in the same order; they are -7.2 , -8.5 , and -8.0 p.p.m., respectively, measured from the methyl resonance of the acid. Results obtained with heated samples support the view that these chemical shift values are not independent of the temperature.

Introduction

Although nuclear magnetic resonance has been recognized for some years as potentially a very powerful method of studying hydrogen bonding,^{2,3} attempts to use n.m.r. data to determine accurately the concentrations of the various hydrogen-bonded species in solutions have often encountered serious difficulties. The present study supports the hypothesis put forward in a preliminary communication⁴ that for carboxylic acids in electron-donating solvents a major source of trouble has been the unsuspected presence of small amounts of water in the experimental materials. Some quite disturbing anomalies associated with the earlier results on such systems disappeared when the observations were repeated using more effective drying techniques.

Three n.m.r. investigations on solutions of acetic acid (AcOH) in acetone have yielded "dilution shift" curves which, though they do not agree precisely with one another, may be taken as typical of the earlier studies.⁵⁻⁷ It was found that the chemical shift, δ_{OH} , of the hydroxyl protons changed very rapidly

with dilution in the concentration range of 1 to 5 mole % acid. This apparently implies that a substantial fraction of the acid is dimerized even in the most dilute solutions and that the degree of dimerization quickly increases as the concentration is raised. However, an impressive accumulation of evidence supports the radically different conclusion that little or no dimer is present in such solutions because of the preferential formation of hydrogen-bonded complexes between monomeric acid molecules and the solvent.⁸⁻¹⁰

(1) This study was supported partially by grant NSF G-17421 from the National Science Foundation and by a David Ross Grant from the Purdue Research Foundation. A portion of this work was presented at the 145th National Meeting of the American Chemical Society, New York, N. Y., Sept. 9, 1963.

(2) G. C. Pimentel and A. L. McClellan, "The Hydrogen Bond," W. H. Freeman and Co., San Francisco, Calif., 1960, p. 143 ff.

(3) E. Lippert, *Ber. Bunsenges. physik. Chem.*, **67**, 267 (1963).

(4) N. Muller and P. I. Rose, *J. Am. Chem. Soc.*, **85**, 2173 (1963).

(5) C. M. Huggins, G. C. Pimentel, and J. N. Shoolery, *J. Phys. Chem.*, **60**, 1311 (1956).

(6) B. N. Bhar, *Arkiv Fysik*, **12**, 171 (1957).

(7) L. W. Reeves, *Trans. Faraday Soc.*, **55**, 1684 (1959).

(8) H. N. Brocklesby, *Can. J. Res.*, **14B**, 222 (1936).

A second anomaly emerges when the earlier data are examined together with the empirical rule^{2,3} that formation of a strong hydrogen bond causes a large downfield shift of the resonance of the participating proton. At high dilution in acetone, for example, AcOH is expected^{9,10} to exist predominantly in the form of the complex, acetic acid-acetone. Since this species must involve at least a moderately strong hydrogen bond, it is expected to produce a hydroxyl resonance lying almost as far downfield as that of the AcOH dimer. Instead it appeared⁵ that the signal for acetic acid-acetone occurs at least 10 p.p.m. to higher field than that of the dimer.

This work was begun because it seemed possible to rationalize these contradictions as results of large systematic errors caused by traces of moisture in the solvents. To show that this was at least plausible, we calculated the effect upon the "dilution shift" of using, as the solvent, acetone containing 0.2% water by weight.¹¹ The mole fraction of water, X_{H_2O} , is then 0.0064. If AcOH is added to this mixture and rapid exchange of protons between water and AcOH is taken into account, the observed "acid" chemical shift will be

$$\delta_{\text{obsd}} = (X_{\text{AcOH}}\delta_{\text{AcOH}} + 2X_{\text{H}_2\text{O}}\delta_{\text{H}_2\text{O}})/(X_{\text{AcOH}} + 2X_{\text{H}_2\text{O}}) \quad (1)$$

It is shown below that δ_{AcOH} , the average hydroxyl chemical shift for the AcOH species present in such a solution, is about -10.3 p.p.m. from tetramethylsilane, and we have found that $\delta_{\text{H}_2\text{O}}$, the shift for water in dilute solutions in acetone, is about -2.3 p.p.m. Taking $X_{\text{AcOH}} = 0.01$, which is about the smallest concentration that will allow the hydroxyl resonance to be observed, eq. 1 then yields a value of -5.8 p.p.m. for δ_{obsd} ; this is more than 4 p.p.m. upfield from the true acid shift. The difference between δ_{obsd} and δ_{AcOH} will decrease rapidly if the concentration of AcOH is made larger while keeping the mole fraction of water constant, and we believe that this is primarily responsible for the shapes of the dilution curves reported in the literature.

We present here new chemical shift data for solutions of AcOH in rigorously dried acetic anhydride, acetone, and 1,4-dioxane. The results are indeed very different from those found previously. Although we have learned to be very cautious in applying the word "anhydrous" to any chemical system, analysis of our data supports the opinion that our samples were sufficiently dry to allow us to observe for the first time the true dilution shifts for AcOH in these basic solvents.

Experimental

Baker C.P. grade *acetic acid* was distilled from a large excess of boron triacetate after several hours of refluxing, under an atmosphere of dry nitrogen.¹² The middle fraction, boiling at 116.5° (747 mm.), was transferred into one leg of an H-tube attached to the vacuum line and further purified by a single fractional crystallization. After decanting the liquid *in vacuo* into the other leg of the H-tube, the connecting tube between the two legs was fused shut, and the solid material was retained and stored on the line for eventual use.

Technical grade *acetic anhydride* was distilled from sodium metal at 32 mm. after refluxing at this pressure for 72 hr.¹³ The middle cut, boiling at 56° (32 mm.), was stored in a tightly stoppered bottle in a drybox. The proton resonance spectrum showed only two impurity signals, attributed to AcOH. Comparison of the methyl peak of the AcOH with the C¹³ satellite peaks of the acetic anhydride showed that the mole fraction of AcOH was 0.008 ± 0.001 .

Matheson Coleman and Bell Chromatoquality *acetone* contained no impurities, other than water, that could be detected by n.m.r. spectroscopy. To dry this material, it was degassed on the vacuum line and transferred onto about one-third its weight of Linde 5A molecular sieve 0.16-cm. pellets. After standing for more than 24 hr., the water content is reduced to less than 0.001 wt. %, ¹⁴ but we found that during this time a small amount of diacetone alcohol is formed, presumably as a result of catalysis by the sieves. This was removed by distilling the acetone from a bath maintained at -22°, through a trap held at the same temperature, into a bulb in which it was then stored until needed.

Technical grade *1,4-dioxane* was purified by standard methods¹⁵ and dried by distilling it from sodium after refluxing for 24 hr. The middle fraction, boiling at 100.4° (751 mm.) and collected under dry nitrogen, was degassed on the vacuum line and distilled onto

(9) F. A. Landee and I. B. Johns, *J. Am. Chem. Soc.*, **63**, 2891, 2895 (1941).

(10) G. Allen and E. F. Caldin, *Quart. Rev. (London)*, **7**, 278 (1953).

(11) P. J. Luchesi found this amount of water in "purified" acetone, using infrared spectroscopic analysis: *J. Am. Chem. Soc.*, **78**, 4229 (1956).

(12) K. B. Wiberg, "Laboratory Techniques in Organic Chemistry," McGraw-Hill Book Co., Inc., New York, N. Y., 1960, p. 249.

(13) A. Weissberger and E. Proskauer, "Organic Solvents," Oxford University Press, New York, N. Y., 1935, p. 149.

(14) R. L. Meeker, F. E. Critchfield, and E. T. Bishop, *Anal. Chem.*, **34**, 1510 (1962).

(15) A. I. Vogel, "Practical Organic Chemistry," Longmans, Green and Co., Ltd., London, 1951, p. 175.

powdered lithium aluminum hydride. After 24 hr., the solvent was transferred to a storage bulb protected from the light, in which it was kept until needed.

The system acetic acid-acetic anhydride is unique in that essentially complete removal of water is possible with quite unsophisticated techniques since water is destroyed by the reaction



Indeed, the *n.m.r. samples* were prepared by adding known quantities of water volumetrically to portions of the anhydride, using a drybox to prevent the solutions from picking up additional moisture from the atmosphere. Samples of the solutions were transferred to *n.m.r.* tubes with a syringe, and the tubes were then sealed and stored until reaction 2 was essentially complete. This process was quite slow and could be followed by observing the *n.m.r.* spectra over a period of several hours (or, for the most dilute solutions, days). In each case, the OH signal was quite broad at first and moved gradually to lower fields. Eventually the chemical shift reached a constant value, and, still later, the signal became sharp. The concentrations of these solutions were corrected for the small amounts of AcOH present initially in the purified acetic anhydride.

N.m.r. samples of AcOH in acetone or dioxane, prepared volumetrically in a drybox, produced such broad hydroxyl signals that we felt forced to conclude that they were not sufficiently dry. Therefore, we eventually abandoned efforts to improve the drybox in favor of a gravimetric procedure in which all filling and weighing operations were done with the materials under vacuum. Portions of AcOH were distilled into tubes equipped with break-off seals, which were then sealed and weighed. The acid was then distilled, through the break-off, into a weighed *n.m.r.* tube, together with an appropriate amount of solvent. Further weighings of the break-off tube and also of the filled and sealed *n.m.r.* tube allow the weights of AcOH and of solvent to be calculated, each to within ± 0.2 mg. For the most dilute samples, the weight of AcOH was about 6 mg., so that the error in the concentration may be several per cent, but we eventually found that the acid chemical shift varied so slowly with increasing dilution that it was not necessary to know the concentrations with greater precision.

A few samples were made by trapping a known volume of AcOH at a known pressure on the vacuum line, condensing the trapped gas in a weighed *n.m.r.* tube, and adding solvent as before. The pressure of the trapped vapor was near 10 mm., low enough to allow its mass to be computed using the ideal gas law.¹⁶

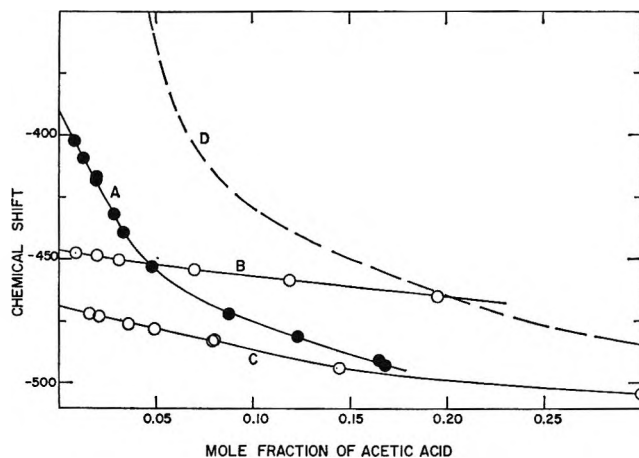


Figure 1. Effect of dilution on the hydroxyl proton chemical shift of acetic acid in donor solvents. Shifts are in c.p.s. at 56.4 Mc.p.s. from the methyl signal of AcOH: curve A, acetic anhydride; B, dioxane; C, acetone; D, results reported in ref. 7 for acetic acid-acetone.

The *n.m.r.* measurements were made with a Varian V-4311 spectrometer using a basic frequency of 56.4 Mc.p.s. Chemical shifts of the hydroxyl peaks were measured by the side-band technique, using the methyl peak from the AcOH as an internal reference.¹⁷ The temperature in the spectrometer probe was 30° during most of the measurements. A number of the samples was also studied at elevated temperatures using variable-temperature accessories purchased from Varian Associates.

Tables I to III show the chemical shifts found for the hydroxyl peaks of AcOH in the three solvents as a function of the mole fraction of acid. Each value is an average of at least five determinations, with average deviations usually near ± 1 c.p.s. except for the most dilute samples, for which the deviations were sometimes as large as ± 2 c.p.s. The room-temperature data are also presented graphically in Figure 1, together with a curve representing the results of ref. 7 for AcOH in acetone.

Discussion

Effect of Residual Moisture. Our results differ strikingly from those of earlier studies, especially for the very dilute solutions. For the first time, we have obtained curves which are readily extrapolated to infinite dilution. The chemical shifts and the slopes of the

(16) For further details see P. I. Rose, Ph.D. Thesis, Purdue University, 1965.

(17) The chemical shift difference between the methyl signal from AcOH and the signal from a trace of added tetramethylsilane depends somewhat on the choice of solvent and concentrations. In very dilute solutions it is 1.99 p.p.m. with acetone as the solvent, 1.95 p.p.m. with dioxane, and 2.03 p.p.m. with acetic anhydride.

Table I: Hydroxyl Proton Chemical Shift as a Function of Concentration for Acetic Acid in Acetic Anhydride at 30°^a

X_{AcOH}	$-\delta_{\text{OH}}$
0.008	402.4
0.013	409.4
0.018	418.4
0.018	417.0
0.028	431.9
0.033	439.4
0.048	453.0
0.088	472.0
0.123	481.4
0.165	490.5
0.168	492.6

^a The shifts are in c.p.s. at 56.4 Mc.p.s. from the methyl peak of AcOH.

Table II: Hydroxyl Proton Chemical Shifts as a Function of Concentration for Acetic Acid in Acetone at Several Temperatures^a

X_{AcOH}	$-\delta_{\text{OH}}$			
	30°	39°	50°	70°
0.016	472	467
0.021	473	468
0.036	476	472	467	...
0.049	478	473	468	...
0.079	483	478	472	463
0.080	482	477	472	462
0.144	494	485	480	471
0.300	504
1.0	544	516

^a The shifts are in c.p.s. at 56.4 Mc.p.s. from the methyl peak of AcOH.

Table III: Hydroxyl Proton Chemical Shifts as a Function of Concentration for Acetic Acid in 1,4-Dioxane at Several Temperatures^a

X_{AcOH}	$-\delta_{\text{OH}}$			
	31°	39°	50°	70°
0.0089	447.6	445
0.0195	448.2	446.7
0.0314	450.6	447.6	444	438
0.0702	454.1	452	448	442
0.119	458.2	457	453	447
0.195	465	464	461	454

^a The shifts are in c.p.s. at 56.4 Mc.p.s. from the methyl peak of AcOH.

Table IV: N.m.r. Parameters and Association Constants for Acetic Acid in Donor Solvents^a

Solvent	$-\delta^0$	p.p.m./m.f.	$-\left(\frac{d\delta}{dX}\right)^0$		
			K_D	K_c	$-\delta_{\text{MS}}$
Acetic anhydride	6.92	0.3 × 10 ²	0.8 × 10 ²	0.14 × 10 ²	7.2 ± 0.2
Acetone	8.31	0.04 × 10 ²	0.8 × 10 ³	0.54 × 10 ²	8.5 ± 0.1
Dioxane	7.91	0.02 ₃ × 10 ²	4. × 10 ³	1.0 × 10 ²	8.0 ± 0.1

^a The chemical shifts are in p.p.m. from the methyl signal of the acid, and the K values are in m.f.⁻¹.

principal solute species in each solvent is a complex stabilized by a fairly strong hydrogen bond.

We feel certain that the difference between this investigation and the earlier ones results from our use of more nearly anhydrous materials. It is therefore important to ask whether or not our samples were indeed dry enough to yield the true acid chemical shifts. Although we did not establish quantitatively how much water still remained in our samples, observations made during this study support the belief that the dilution curves obtained would not have been further displaced by still more rigorous drying of the materials. In this regard, the behavior of the solutions in acetic anhydride is especially significant.

As described above these samples were prepared by adding small portions of water to acetic anhydride and allowing AcOH to be formed by solvolysis. When this reaction is about 80% complete, one has what may be thought of as a "very wet" solution of AcOH in the anhydride. For such solutions, the OH peak moves rapidly as the water concentration drops, and it is so broad that there may be some difficulty in locating it. As the water concentration decreases further, the OH peak approaches a constant, limiting position, but it remains rather broad. Only after the water is almost completely used up and the OH peak has stopped shifting, one begins to observe a progressive sharpening of the peak, which eventually becomes nearly as sharp as the methyl signals. It seems certain that if still more complete removal of water were possible, this would lead only to a further narrowing of the OH peak, not to a change in its chemical shift.

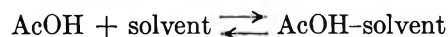
These observations suggest that for the other solvents also, the amount of water required to produce a shift of the OH signal is larger than that required to cause rather severe broadening of the peak. (This applies at least in solutions dilute with respect to both AcOH and water; in fairly concentrated acid solutions proton exchange is fast enough to produce sharp OH peaks even though a large amount of water is present.)

dilution curves, each at zero concentration, are reported in Table IV. The values of the extrapolated shifts are now consistent with the supposition that the

This conclusion is supported by observations made during the course of this research on acetic acid-acetone samples made in the drybox rather than on the vacuum line, and samples found later to have been improperly sealed. These samples were *slightly* contaminated with water and produced broadened OH peaks, but these peaks were found at the same fields as the much sharper ones obtained from comparable samples containing little or no water.

We finally retained only data points obtained with samples that yielded OH peaks with widths of a few cycles per second at most, and we are confident that such peaks would not have occurred in the presence of sufficient residual water to introduce appreciable errors in the chemical shifts.

Interpretation of the Dilution Curves. To understand the data quantitatively, it is necessary to consider in each solvent the simultaneous equilibria



$$K_c = [\text{MS}]/[\text{M}][\text{S}] \quad (4)$$

The abbreviations, D for the acid dimer, M for the free acid monomer, and MS for the monomer-solvent complex have been introduced, and the brackets denote concentrations in mole fraction units. The over-all acid concentration is

$$X = [\text{M}] + 2[\text{D}] + [\text{MS}] \quad (5)$$

and the exchange-averaged hydroxyl chemical shift is

$$\delta = \{2[\text{D}]\delta_D + [\text{M}]\delta_M + [\text{MS}]\delta_{\text{MS}}\}/X \quad (6)$$

where the significance of the symbols δ_D , δ_M , and δ_{MS} is the obvious one. From these, one may readily derive equations for the chemical shift at infinite dilution and the limiting slope. They are¹⁸

$$\delta^0 = \lim_{x \rightarrow 0} \delta = \delta_{\text{MS}} + (\delta_M - \delta_{\text{MS}})/(1 + K_c) \quad (7)$$

$$\left(\frac{d\delta}{dX}\right)^0 = \lim_{x \rightarrow 0} \left(\frac{d\delta}{dX}\right) = \frac{1}{(1 + K_c)^2} \times \left[2K_D\delta_D^* - K_c \left(1 + \frac{2K_D}{1 + K_c} \right) \delta_{\text{MS}}^* \right] \quad (8)$$

The asterisks indicate that the chemical shifts so marked have been redefined using a new scale which has δ_M as its origin.

The behavior of these systems is evidently governed by the five parameters, δ_M , δ_D , δ_{MS} , K_D , and K_c . These quantities cannot be determined uniquely using only the data presented here, but it is now possible at least to select for them a set of plausible, approximate values

which do not conflict with any of the available information.

A starting point for the selection of K_D values is the dimerization constant of 4×10^3 m.f.⁻¹ calculated from data¹⁹ for AcOH in carbon tetrachloride by interpolating to 30°. Since dioxane has almost exactly the same dielectric constant as carbon tetrachloride, K_D in dioxane should have very nearly the same value. Acetic anhydride and acetone have almost the same dielectric constant, about ten times larger than that of dioxane. To estimate K_D in these solvents, we used the formula²⁰ $\Delta F = (-\mu^2/r^3)(D - 1)/(2D + 1)$, for the change in free energy which results when a molecule with permanent dipole moment μ is transferred from a vacuum to a spherical cavity of radius r in a medium whose dielectric constant is D . With reasonable choices of the parameters, this yields $K_D = 0.8 \times 10^3$ m.f.⁻¹ for AcOH in acetic anhydride or acetone.

Returning now to eq. 8, it is obvious that a considerable simplification would result if one could assume that K_c and $2K_D/K_c$ are each large compared to unity. The low apparent degree of dimerization of AcOH in donor solvents⁹ suggests that indeed K_c is perhaps close to 50, so that the error introduced by this assumption should not be too severe. Equation 8 then becomes

$$\left(\frac{d\delta}{dX}\right)^0 \cong \frac{2K_D}{K_c^2} (\delta_D - \delta_{\text{MS}}) \quad (9)$$

where it is no longer necessary to write asterisks because the difference $\delta_D - \delta_{\text{MS}}$ does not depend on the origin chosen for the chemical shift scale. Further, eq. 7 shows that $\delta^0 \cong \delta_{\text{MS}}$, to about the same degree of approximation that is involved in (9), so that

$$\left(\frac{d\delta}{dX}\right)^0 \cong \frac{2K_D}{K_c^2} (\delta_D - \delta^0) \quad (10)$$

Equation 10 can be used with the data in Table IV to evaluate K_c only if a value for δ_D can be obtained from other sources. On the basis of data for AcOH in carbon tetrachloride, Reeves⁷ suggests a value of -12.2 p.p.m. from tetramethylsilane, which becomes -10.1 p.p.m. with the methyl signal of AcOH as the reference. Other measurements,^{16,21} on benzene solu-

(18) C. Lussan, *J. chim. phys.*, **60**, 1100 (1963).

(19) M. Davies, P. Jones, D. Patnaik, and E. A. Moelwyn-Hughes, *J. Chem. Soc.*, 1249 (1951).

(20) A. A. Frost and R. G. Pearson, "Kinetics and Mechanism," 2nd Ed., John Wiley and Sons, Inc., New York, N. Y., 1961, p. 140.

(21) J. C. Davis, Jr., and K. S. Pitzer, *J. Phys. Chem.*, **64**, 886 (1960).

tions, support a value near -11.1 p.p.m. The exact value is no doubt somewhat solvent dependent and not too greatly different from the average of these, -10.6 p.p.m. K_c values calculated with $\delta_D = -10.6$ p.p.m. are given in the fourth column of Table IV. Because K_c appears squared in eq. 10, rather large uncertainties in K_D and δ_D produce relatively small uncertainties in K_c . Hence, although limits of error are difficult to estimate with confidence, it seems unlikely that the K_c values will be off by more than 20%. Thus, the values in Table IV provide a means of specifying the relative concentrations of the species present in these solutions, with moderate accuracy.

The K_c values may be used with eq. 7 to find values of δ_{MS} which are better than those resulting from the crude approximation $\delta_{MS} \cong \delta^0$. Although this requires a knowledge of δ_M , this parameter enters into the equation in such a way that a very large error in δ_M is required to produce even a small error in δ_{MS} . We chose to use $\delta_M = -3.0$ p.p.m. and obtained the δ_{MS} values given in the last column of Table IV. The limits of error are those which result if the main source of error is assumed to be an uncertainty of ± 2 p.p.m. in δ_M .

It is noteworthy that the K_c values show that the base strengths of the solvents increase in the order acetic anhydride < acetone < dioxane but that the hydrogen-bond shifts, $\delta_M - \delta_{MS}$, do not increase in the same order. Since dioxane appears to form stronger hydrogen bonds with methanol or chloroform than acetone does,²² it seems that the K_c values are the more reliable guide to solvent basicity. Approximate calculations¹⁶ show that the magnetic anisotropy of the carbonyl bond could easily contribute as much as 1.2 p.p.m. to the hydrogen-bond shift of the acetic acid-acetone complex. If such an effect is essentially absent in acetic acid-dioxane, the order of the hydrogen-bond shifts could be explained on this basis.

Temperature Dependence of the Chemical Shifts. From the data in Tables II and III one finds that the extrapolated shifts, δ^0 , increase linearly as the temperature is raised, with $\Delta\delta^0/\Delta T = 0.9 \times 10^{-2}$ p.p.m./deg. for the acetone solutions and 0.55×10^{-2} p.p.m./deg. for the dioxane solutions. No measurable temperature dependence is found for the limiting slopes, $(d\delta/dX)^0$.

One may attempt to rationalize the observed $\Delta\delta^0/\Delta T$ by assuming that both δ_M and δ_{MS} are independent of temperature. Then eq. 7 implies that δ^0 is a function

of temperature only because of the temperature dependence of K_c , which in turn is governed by the van't Hoff equation. It is possible to fit the data approximately in this way if it is assumed that the heat of dissociation of the acetic acid-acetone complex is 6 kcal./mole and that of the acetic acid-dioxane complex is 8 kcal./mole. These values are uncomfortably large, and furthermore the variation of δ^0 with T predicted on this basis is noticeably nonlinear.

The more plausible assumption²³ that the heat of dissociation is about 4 kcal./mole for both complexes yields $\Delta\delta^0/\Delta T = 0.5 \times 10^{-2}$ p.p.m./deg. for AcOH in acetone and 0.15×10^{-2} p.p.m./deg. for AcOH in dioxane. In each case, this is about 0.4×10^{-2} p.p.m./deg. less than the observed temperature coefficient. It is probable that, as suggested in a recent publication²⁴ from this laboratory, δ_{MS} is not independent of the temperature since the hydrogen-bond shift is expected to vary with increasing excitation of the hydrogen-bond stretching vibrational mode. This effect could easily produce,²⁴ for each complex, a value of $\Delta\delta_{MS}/\Delta T$ of about 0.4×10^{-2} p.p.m./deg. and thus account for the difference between the observed temperature coefficients and those calculated using the van't Hoff equation and constant δ_{MS} values. To clarify this aspect of hydrogen bonding, it is very desirable to extend the measurements over a larger temperature range.

Conclusions

It has been shown that the dilution curves for AcOH in carefully dried solvents differ drastically from those reported earlier. The new results are consistent with plausible values of dimerization and association constants, reported in Table IV. The data make possible a fairly accurate determination of the chemical shifts for the acidic protons in the respective AcOH-solvent complexes, with results also presented in Table IV. The hydrogen-bond shift in itself appears not to be a reliable index of the base strength of the solvent molecules, unless corrections are made for possible magnetic anisotropy effects. The data obtained at elevated temperatures suggest that the hydroxyl-proton chemical shifts of the AcOH-solvent complexes are not temperature independent.

(22) E. M. Arnett, *Progr. Phys. Org. Chem.*, **1**, 362, 374 (1963).

(23) See ref. 2, p. 218.

(24) N. Muller and R. C. Reiter, *J. Chem. Phys.*, in press.

Hindered Rotation and Carbon-13-Hydrogen Coupling Constants in Amides, Thioamides, and Amidines¹

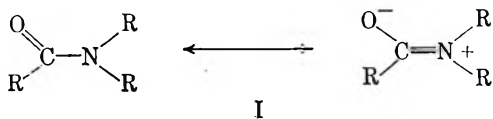
by Robert C. Neuman, Jr.,² and L. Brewster Young

Department of Chemistry, University of California, Riverside, California 92502 (Received January 18, 1966)

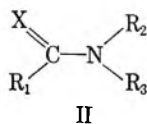
A study of the barriers to rotation about the central carbon–nitrogen bond in *N,N*-dimethyl derivatives of two thioamides, two amides, an amidinium ion, and an amidine has been performed in the solvent formamide by the n.m.r. intensity ratio method. Our results indicate that the rotational barriers decrease in the order thioamides > amides \approx amidinium ion > amidine in this solvent. Values of $J^{13\text{C}\text{H}}$ for the N-CH₃ protons in these compounds have been measured and it appears that there is a direct correlation between the magnitudes of the rotational barriers and the ¹³C–H coupling constants.

Introduction

Electron delocalization in an amide (I) imparts substantial double bond character to the central carbon–nitrogen bond. This is reflected in the relatively



large energy barriers which have been observed for rotation about this bond in various amides.³ One might expect a similar situation in compounds such as thioamides, amidinium ions, and amidines (II, X = S, NH₂⁺, and NH) and, in fact, Hammond and Neuman⁴



demonstrated such rotational restriction in several amidinium ions. An attempt was made to determine the magnitude of the rotational energy barrier in acetamidinium chloride (II, X = NH₂⁺; R₂ = R₃ = H) in the solvent dimethyl sulfoxide; however, temperature-dependent quadrupole coupling between ¹⁴N and its bonded hydrogen atoms prevented a reasonable analysis.⁴ No studies have been reported dealing with thioamides and amidines.

The effect of the group X in II on the magnitudes of rotational barriers seemed to us to be a potentially use-

ful and interesting addition to the understanding of molecular structure and we have initiated a program to obtain rotational barriers for compounds of the general type II. The first results of our studies on representative members of this series are reported here.

In addition to the rotational barriers, we have measured values of $J^{13\text{C}\text{H}}$ for methyl groups (R₂ and R₃ in II) bonded to nitrogen in the various compounds studied. The relationship between these values of $J^{13\text{C}\text{H}}$ and the rotational barriers is discussed below.

Results and Discussion

The solvent formamide was chosen for these n.m.r. studies because of its lack of interfering protons and the fact that it would dissolve the amidinium salt. The barriers to rotation were determined by the intensity ratio method^{3b} using a Varian A-60 n.m.r. spectrometer. All compounds studied were *N,N*-dimethyl (R₂, R₃ = CH₃) derivatives of II. The raw

(1) Presented in part at the Pacific Southwest Regional Meeting of the American Chemical Society, Costa Mesa, Calif., Dec. 5, 1964, and before the Division of Organic Chemistry at the 149th National Meeting of the American Chemical Society, Detroit, Mich., April 1965.

(2) To whom inquiries should be addressed.

(3) (a) H. S. Gutowsky and C. H. Holm, *J. Chem. Phys.*, **25**, 1228 (1956); (b) M. T. Rogers and J. C. Woodbrey, *J. Phys. Chem.*, **66**, 540 (1962); (c) J. C. Woodbrey and M. T. Rogers, *J. Am. Chem. Soc.*, **84**, 13 (1962); (d) A. Allerhand and H. S. Gutowsky, *J. Chem. Phys.*, **41**, 2115 (1964).

(4) G. S. Hammond and R. C. Neuman, Jr., *J. Phys. Chem.*, **67**, 1655 (1963).

n.m.r. data were corrected for overlap and asymmetry of the two components of the N-CH_3 chemical shift doublet using the general line-shape equations of Rogers and Woodbrey^{3b} (see Experimental). These equations were programmed in Fortran II and the data were analyzed using an IBM 1620 computer.⁵ The values of the rotational barriers and frequency factors which we have obtained are reported in Table I.⁶ The data from which the barriers and frequency factors were calculated are reproduced in Figure 1. The error ranges reported in Table I were determined by a least-squares analysis of the data. Sources of error will be discussed more fully both in the Experimental section and below.

Table I: Rotational Barriers and Frequency Factors for Compounds II in Formamide^a

Compd.	X ^b	Mole %	E_a , kcal./mole ^c	Log A ^c
Dimethylthioacetamide	S	9.0	43.7 ± 5.6	23.1 ± 3.1
Dimethylacetamide	O	10.0	24.7 ± 0.8	16.4 ± 0.4
Dimethylformamide	O	12.0	26.3 ± 2.6	15.5 ± 1.5
		100.0 ^d	18.7 ± 0.9 ^e	11.8 ± 0.6 ^e
Dimethylacetamidinium chloride	NH_2^+	5.0	19.6 ± 1.0	12.7 ± 0.5
Dimethylacetamide	NH	...	<i>f</i>	<i>f</i>

^a Measurements were made using a Varian A-60 n.m.r. spectrometer with a variable-temperature probe. ^b Atom X in structure II. ^c Random errors determined by the method of least squares. ^d No solvent. ^e The values 18.3 ± 0.7 kcal./mole (E_a) and 10.8 ± 0.4 (log A) were determined by Rogers and Woodbrey for neat dimethylformamide.^{3b} ^f Not measurable; see text.

Since the work reported here was completed, Allerhand and Gutowsky have discussed the various n.m.r. methods for determining rotational barriers in amides.^{3d} They have suggested that the n.m.r. pulse method gives more accurate barriers to rotation about the central carbon-nitrogen bond for two amides which they have studied (*N,N*-dimethylcarbonyl chloride and *N,N*-dimethyltrichloroacetamide) than does the intensity ratio method^{3b} due to systematic errors in the latter method. Unfortunately, it is more difficult to make use of the pulse method because special n.m.r. apparatus is required, and all of the "nonexchanging protons" (*e.g.*, those in R_1 in II) must be replaced by deuterium.^{3d}

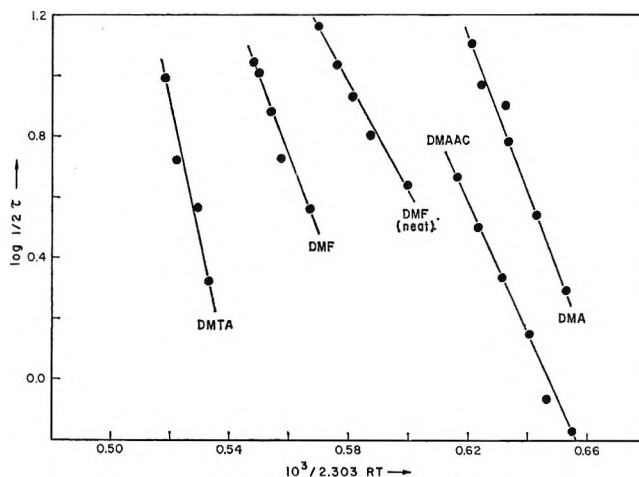


Figure 1. Arrhenius plots of the rotational kinetic data for the compounds II.

Previous studies³ using n.m.r. to determine rotational barriers in amides have demonstrated the hazards of placing a great degree of confidence in the absolute values of these quantities until they have been checked by several of the available methods. Thus, we will confine our discussion to the major trends which we have observed and indicate some of the possible conclusions which the data suggest.

In order to compare our technique with that of other workers who have used the intensity ratio method, we redetermined the rotational barrier for neat *N,N*-dimethylformamide which had been previously measured by Rogers and Woodbrey.^{3b} We consider the agreement (see Table I) between our value and theirs to be satisfactory.

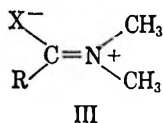
General Trends. The data in Table I suggest that rotational barriers for thioamides may be significantly larger than those for amides. We attempted to measure a rotational barrier for dimethylthioformamide (DMTF); however, the coalescence temperature region was so high that it was not possible to obtain sufficient data to make the calculations meaningful. While the $\text{N}(\text{CH}_3)_2$ doublets for all of the other compounds had completely coalesced below 160° , the $\text{N}(\text{CH}_3)_2$ doublet of DMTF was *just beginning* to show measurable coalescence at 162° . This was not due to an abnormal "nonexchanging" chemical shift as can be seen by an inspection of the data given in the Experimental section in Table III.

(5) The authors wish to thank Miss Marsha Dougall of the University of California, Riverside, Computer Center for assistance in programming and operation of the computer.

(6) The n.m.r. spectral data have been previously reported: R. C. Neuman, Jr., and L. B. Young, *J. Phys. Chem.*, **69**, 1777 (1965). The values of $\delta_{\text{N-CH}_3}$ are given in Table III.

It was not possible to measure a rotational barrier in N,N-dimethylacetamide (DMA) (II, X = NH) because the N-CH₃ protons gave rise to only a single resonance signal in neat solution and in the solvents formamide or chloroform. The signal was not resolved into two components on lowering the temperature to -40° in the solvent chloroform. We suggest that the lack of a chemical shift doublet in this amidine is due to rapid rotation about the central C-N bond. *A priori* one would expect the C=NH group to render the two conformationally different positions for the N-CH₃ groups magnetically nonequivalent and, barring other complications, hindered rotation should give rise to two N-CH₃ proton signals. However, there are several types of specific hydrogen-bonding interactions which might be possible in these amidine-solvent systems due to the proton in the X group, which would not be present in the other systems studied (*vide infra*). These may be responsible for the observed N-CH₃ singlet. A definitive answer must wait until further work has been done, although it should be mentioned here that the ¹³CH coupling constant data (*vide infra*) tends to support rapid rotation.

If the rotational barrier for the amidine is small, the apparent relative order of the rotational barriers (thioamides > amides > amidines) is reasonable. Calculated values of overlap integrals between the atoms in the C=X group are in the same relative order.^{7,8} The relative electrical moments for amides and thioamides⁹ and ultraviolet spectroscopic studies by Janssen¹⁰ on thioamides and other thione-containing compounds also support this order. Thus, the contribution of the dipolar canonical form III to the ground



states of these compounds appears to increase in the order N < O < S.

Frequency Factors. The rotational frequency factors for dimethylthioacetamide (DMTA), dimethylacetamide (DMA), and dimethylformamide (DMF) are higher than the often quoted^{3b,d} range of "expected values" (10¹³-10¹⁴ sec.⁻¹). It is not clear to us, however, why the frequency factors for these internal rotations *in solution* need conform to the 10¹³-10¹⁴-sec.⁻¹ range predicted¹¹ for unimolecular reactions under "ideal" conditions (*e.g.*, reactions in the gas phase). Indeed, a number of unimolecular gas phase reactions show frequency factors which are in the range of those observed for DMF and DMA in formamide.¹¹ High values of frequency factors for unimolecular reactions

in solution may simply be a reflection of desolvation of the transition state, a process which would be characterized by an increase in entropy. In the next section we will show that this may well occur in some of these systems.

The value of log *A* for DMTA seems exceptionally high, however, even on the basis of the previous discussion. The random experimental error was rather high in this case and the value of log *A* may simply reflect this inaccuracy. However, the possibility of systematic error cannot be excluded. An inspection of Figure 1 will show that the temperature region which had to be used to obtain data for this compound was relatively high. Temperature fluctuations at the sample and deviations of the actual temperature from those measured may be more pronounced at these higher temperatures and this could produce errors in the data.¹²

Solvent Effects. Although much of the previous work on amides has been performed using DMA and DMF, we redetermined their rotational barriers because they had not been previously measured in formamide. Gutowsky and Holm obtained the values 12 ± 2 kcal./mole and 10⁷ to 10¹⁰ sec.⁻¹, respectively, for the rotational barrier and frequency factor, for DMA in the neat liquid. Rogers and Woodbrey^{3b} obtained the values 11.6 ± 0.8 kcal./mole and 10⁸ to 10⁹ sec.⁻¹ for neat DMA. The activation parameters for neat DMF are given in Table I. Our data suggest that the solvent formamide may stabilize the ground state of these amides. A specific solvent interaction which would be expected to increase rotational barriers in amides is shown in structure IV. Sunners, Piette, and Schneider¹³ have proposed hydrogen-bonding

(7) (a) The overlap integrals were calculated in the normal manner^{7b} based on the Slater orbitals (μ values)^{7b} for neutral nitrogen, oxygen, and sulfur using the data of Mulliken^{7c} and Jaffé.^{7d} The bond lengths chosen for the C=X bond were: C=N, 1.31 Å.; C=O, 1.21 Å.; and C=S, 1.70 Å. (b) See K. Wiberg, "Physical Organic Chemistry," John Wiley and Sons, Inc., New York, N. Y., 1964, pp. 65, 469; (c) R. S. Mulliken, C. A. Rieke, D. Orloff, and H. Orloff, *J. Chem. Phys.*, **17**, 1248 (1949); (d) H. H. Jaffé, *ibid.*, **21**, 258 (1953).

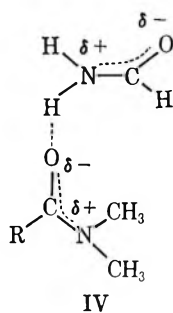
(8) Similar calculations indicated no significant 3d π -2p π overlap of sulfur across space with nitrogen.

(9) (a) G. K. Estok and S. P. Sood, *J. Phys. Chem.*, **66**, 1372 (1962); (b) M. H. Krachov, C. M. Lee, and H. G. Mautner, *J. Am. Chem. Soc.*, **87**, 892 (1965).

(10) (a) M. J. Janssen, *Rec. trav. chim.*, **79**, 454 (1960); (b) *ibid.*, **79**, 464 (1960); (c) *ibid.*, **79**, 1066 (1960); (d) *ibid.*, **81**, 650 (1962); (e) M. J. Janssen, *Spectrochim. Acta*, **17**, 475 (1961).

(11) S. Benson, "The Foundations of Chemical Kinetics," McGraw-Hill Book Co., Inc., New York, N. Y., 1960, pp. 250-266.

(12) If one wishes to assume that the true frequency factors for all of these rotations are 10¹³-10¹⁴ sec.⁻¹, then the relative temperature regions over which measurable coalescence occurred strongly suggest in themselves that the rotational barriers for the thioamides are greater than those for the corresponding amides.



interactions of formamide with itself and with water and acetone in order to explain their observations in rotational barrier studies on formamide. We have observed that the magnitude of spin-spin coupling between the $\text{N}(\text{CH}_3)_2$ protons and the CH_3 -CO protons and H-CO proton in dimethylacetamide and dimethylformamide, respectively, increases on going from the neat amide to formamide as solvent.⁶ In general, bulk properties of solvents do not affect spin-spin splitting interactions, however, a specific solvent effect such as that shown in structure IV might be expected to increase the coupling constants mentioned above since the amount of partial double bond character in the central C-N bond should be increased.

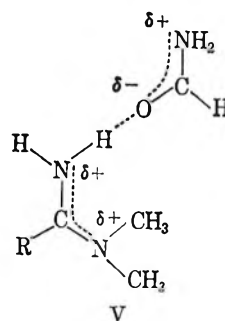
It has been previously observed that transfer of an N,N-dimethylamide from neat solution to many different types of nonaromatic solvents ranging in properties from water to cyclohexane does not significantly alter the mean position of the N,N-dimethyl doublet resonance (when bulk susceptibility effects are compensated for by an internal standard).¹⁴ However, the chemical shift between the doublet components is reduced by several cycles per second.¹⁴ This has been attributed to the disruption of dimeric dipolar interaction between amide molecules which occurs in the neat liquid. It is interesting that the same general lowering of $\delta\nu_{\text{N}-\text{CH}_3}$ has been observed by us in going from the neat amides to formamide as solvent.⁶ Due to the similarity of solute and solvent we would expect dipolar interactions between molecules of a dimethylamide and formamide to be as energetically favorable as those in the neat amides themselves and to give rise to similar values of $\delta\nu_{\text{N}-\text{CH}_3}$. The fact that the values of $\delta\nu_{\text{N}-\text{CH}_3}$ are lower in formamide, as observed for most other nonaromatic solvents (including water), suggests that these interactions are broken up by a more favorable type of solvation such as that shown in structure IV.

If an interaction such as that shown in structure IV is important in these systems, we would expect that formation of the transition state would proceed with desolvation because of partial neutralization of the excess negative charge on the oxygen atom in the dimethyl-

amide. This would lead to an increase in entropy for the total system thus supporting the higher than expected frequency factors for DMA and DMF.

It is not possible to make such an analysis for thioamides because of insufficient data. It might be mentioned, however, that the basicity of amides appears to be greater than that of thioamides.^{9b,10d,15} Protonation occurs on the oxygen¹⁶ or sulfur^{10e} atoms in these systems and, if basicity may be used as a criterion for hydrogen bond strength, it must be concluded that such interactions may be less favorable with the thioamides.

Specific solvation between formamide and the N,N-dimethylacetamidinium ion (DMAAC) is probably different than that shown in structure IV and may be reasonably pictured as shown in structure V. Such



hydrogen bonding should be more favorable in the rotational transition state because the NH_2^+ group of the amidinium ion will then possess a full positive charge. Such a picture would suggest that the rotational entropy of activation may be somewhat lower in the solvent formamide than under hypothetical ideal conditions. The presence of an associated anion of course complicates an analysis of this system. We hope to investigate the effects of anionic variations in future studies.

The possible presence of these specific solvent interactions raises the question of their temperature dependence and its subsequent effect on the determination of the rotational barriers. All temperature-variation kinetic studies on systems involving specific ground-state solvation (such as hydrogen bonding) are characterized by one of the uncertainties which may be present here. One realizes that the extent of hydrogen bonding will be affected by temperature, but it is difficult to correct for this effect. It is generally

(13) B. Sunners, L. H. Piette, and W. G. Schneider, *Can. J. Chem.*, **38**, 681 (1960).

(14) (a) J. V. Hatton and R. E. Richards, *Mol. Phys.*, **3**, 253 (1960); (b) *ibid.*, **5**, 139 (1962); (c) D. G. de Kowalewski and V. J. Kowalewski, *Arkiv Kemi*, **16**, 373 (1961).

(15) R. Huisgen and H. Brade, *Chem. Ber.*, **90**, 1432 (1957).

(16) G. Fraenkel, A. Lowenstein, and S. Meiboom, *J. Phys. Chem.*, **65**, 700 (1961).

ignored. A more serious problem arises in kinetic studies of exchange using n.m.r. techniques such as the peak-separation, intensity-ratio, and line-narrowing methods. In order to determine the specific rate constants for exchange at each temperature it is necessary to know the value of the nonexchanging chemical shift between the protons at the two sites being considered. This quantity is in general slightly temperature dependent^{3d} and its temperature dependence is not easily determined. In systems involving possible temperature-dependent solvation effects a temperature variation in the nonexchanging chemical shift may be more pronounced. We have attempted to ascertain whether this latter factor is important in these studies. An examination of the n.m.r. spectra for each kinetic run showed no apparent change in the value of $\delta\nu_{N-CH_3}$ between ambient temperature and the lowest temperature at which coalescence began to occur. In some cases (thioamides) this temperature range was quite large ($\sim 90^\circ$), but it was lower ($30-50^\circ$) for the amides and the amidinium ion. We feel that the data suggest that temperature-dependent solvation, if present, does not alter the nonexchanging chemical shift significantly. It is, of course, impossible to analyze the region of coalescence, but if large changes were occurring in this region, we would have expected to see them begin at lower temperatures.

The nonexchanging chemical shifts which were used in this study were corrected for overlap and asymmetry of the doublet components. However, the necessary corrections were very small. The corrected and uncorrected values of $\delta\nu_{N-CH_3}$ are given in the Experimental section in Table III.

¹³C-H Coupling Constants. Haake has recently shown that values of J_{13CH} for methyl groups bound to a nitrogen atom are related to the amount of positive charge on the nitrogen atom.¹⁷ For example, values of J_{13CH} for trimethylamine, tetramethylammonium ion, and N,N-dimethylacetamide are 131, 145, and 138 c.p.s., respectively. Although further studies¹⁸ suggest that trimethylamine and tetramethylammonium ion may not be a good basis set for comparison with compounds containing sp² nitrogen (e.g., N,N-dimethylacetamide), a comparison of values of J_{13CH} for the N-CH₃ groups in the general series II would seem to be valid. The data are given in Table II. Since the contribution of the dipolar canonical form III to the ground states of these various compounds largely determines the magnitudes of the rotational barriers, those compounds with high barriers would be expected to have larger values of J_{13CH} than those with low barriers. The data in Table II qualitatively agree with this prediction. The coupling

constant for the amidinium ion is the only obvious deviation. It is suggested that this may be due to the difference in solvent interaction with this compound as discussed above or possibly due to some effect of the associated anion.

The low value of J_{13CH} for N,N-dimethylacetamide seems to offer support for the proposal that the barrier to rotation is very low in this compound.

Table II: ¹³C-H Coupling Constants for the N-CH₃ Protons in Compounds II^a

Compd.	X ^b	Solvent ^c	J_{13CH} , c.p.s. ^d
Dimethylthioacetamide	S	Formamide	140
Dimethylthioformamide	S	Formamide	140
		Neat	140
Dimethylacetamide	O	Formamide	138
		Neat	137 ^e
Dimethylformamide	O	Formamide	138
		Neat	138
Dimethylacetamidinium chloride	NH ₂ ⁺	Formamide	141
Dimethylacetamide	NH	Neat	135

^a All measurements were made using a Varian A-60 n.m.r. spectrometer. ^b Atom X in structure II. ^c Concentrations in formamide were 25-35% by weight. ^d Obtained using a side-band oscillator and frequency counter; values good to ± 0.5 c.p.s. ^e Haake obtained a value of 138 c.p.s.¹⁷

Experimental

Materials. Formamide (Matheson Coleman and Bell, 99%) was purified according to the method of Verhoek¹⁹ and stored over molecular sieves. N,N-Dimethylacetamide and N,N-dimethylformamide (reagent grade) were obtained from Matheson Coleman and Bell and used without further purification. N,N-Dimethylthioacetamide was prepared by the method of Kindler²⁰ and recrystallized several times from benzene, m.p. 72.0-73.5°. N,N-Dimethylthioformamide was prepared in an analogous manner,²⁰ b.p. 87-88° (7 mm.). N,N-Dimethylacetamidinium chloride was prepared by the method of Pinner²¹ from ethyl acetoimidate hydrochloride and dimethylamine in

(17) P. Haake, W. B. Miller, and D. A. Tysee, *J. Am. Chem. Soc.*, **86**, 3577 (1964).

(18) P. Haake, private communication.

(19) F. H. Verhoek, *J. Am. Chem. Soc.*, **58**, 2577 (1936).

(20) K. Kindler, *Ann. Chem.*, **431**, 209 (1923).

(21) See, for example, A. W. Dox in "Organic Syntheses," Coll. Vol. I, John Wiley and Sons, Inc., New York, N. Y., 1941, p. 5.

ethanol, recrystallized from ethanol, and carefully dried over phosphorus pentoxide, m.p. 158.5–160.5°. N,N-Dimethylacetamidine was prepared by neutralization of N,N-dimethylacetamidinium chloride with an equivalent amount of *n*-butyllithium (in hexane) in ether. The solution was filtered and the ether layer was evaporated yielding only a trace of residue. Extraction of the mushy solid remaining after filtration with chloroform and subsequent evaporation of the chloroform yielded an orange liquid. Distillation of this material yielded a clear liquid; apparent b.p. 55–60° (10 mm.) (microdistillation apparatus). This compound showed the following peaks in its n.m.r. spectrum (solvent formamide, internal reference trimethylsilylpropanesulfonic acid sodium salt): τ 7.90 and 7.05 (relative areas 1:2) assigned as C-CH₃, and N-CH₃, respectively. On dissolving the compound in excess dilute hydrochloric acid the following peaks were observed in the n.m.r. spectrum (internal reference trimethylsilylpropanesulfonic acid sodium salt): τ 7.69, 6.88, and 6.75 (relative areas 1:1:1) assigned as C-CH₃, N-CN₃, and N-CH₃, respectively. These latter spectral results were identical with those obtained with a solution of authentic N,N-dimethylacetamidinium chloride in water.

Variable-Temperature N.m.r. Measurements. All spectra were recorded using a Varian A-60 n.m.r. spectrometer equipped with a variable-temperature probe. Sweep widths were calibrated before each experiment using the known separation between tetramethylsilane and chloroform-*d*. Temperatures were determined before and after each series at a given temperature setting by measuring the chemical shift between the methylene and hydroxyl protons in ethylene glycol. The Varian manual states that the temperatures are good to $\pm 2^\circ$. However, we feel that this range may be larger than that actually encountered in our studies. Our agreement with the data of Rogers and Woodbrey^{5b} for neat dimethylformamide (Table I) suggests that this is the case. Also, we would expect a larger amount of scatter in our experimental points with a $\pm 2^\circ$ range. It should be noted that scatter does increase in the higher temperature ranges in which some of the data were collected (Figure 1). This is probably a reflection of the increased difficulty of maintaining a constant temperature at these high temperatures. It might be mentioned that the ethylene glycol calibration method (using an A-60 spectrometer) has been used previously for determining temperatures in rotational studies and apparently gave no particular difficulty.^{3d}

Care was taken to maximize resolution at each temperature. Sweep widths of 50 c.p.s. and sweep times

of 500 sec. were employed. All spectra recorded during a given variable-temperature experiment were taken at fixed values of the filter band width, spectrum amplitude, and radiofrequency field. The last was maintained at a low value, to avoid saturation. Several spectra were recorded at each temperature. A value of the intensity ratio (r) was calculated from each spectrum by taking the ratio of the average signal maximum for the two components of the N-CH₃ doublet to the central minimum between the components. The values of r thus obtained for each temperature were combined to yield an average value of r which was subsequently used in the barrier calculation. The deviation of all of the values at each temperature from the average was in most cases less than 2%.

Analysis of Rotation Experimental Data. The apparent nonexchanging chemical shift value for the two components of the N-CH₃ doublet of each compound was measured at ambient temperature ($\sim 40^\circ$) and corrected for overlap and asymmetry by the use of eq. A-2 of Rogers and Woodbrey.^{5b} The uncorrected and corrected values of $\delta\nu_\infty$ are given in Table III. The general line-shape equations (A-1 and A-2) derived by Rogers and Woodbrey^{5b} were then used in conjunction with the measured values of the transverse relaxation times for the component signals and the corrected value $\delta\nu_\infty$ to obtain a set of values of $\log 1/2\tau$ corresponding to a set of values of the intensity ratio (r) (2τ is defined as the mean lifetime of one of the N-CH₃ groups in one of the nonequivalent sites of the planar conformation). The values of $\log 1/2\tau$ corresponding to the experimentally determined values r were then obtained from these plots and plotted *vs.* the quantities $10^3/2.303RT$. The experimental Arrhenius plots are shown in Figure 1.

Equations A-1 and A-2 were programmed in Fortran

Table III: Corrected Nonexchanging Chemical Shifts for the N-CH₃ Proton Signals^a

Compd. ^b	$T_2(\text{A})^{\text{c,d}}$	$T_2(\text{B})^{\text{c,d}}$	$\delta\nu_\infty$	
			Found ^d	Calcd. ^e
Dimethylacetamide	1.22	0.63	7.36	7.36
Dimethylformamide	1.29	1.09	7.75	7.76
Dimethylthioacetamide	1.39	2.49	7.24	7.29
Dimethylthioformamide	1.34	1.19	5.19	5.20
Dimethylacetamidinium chloride	1.72	0.92	3.77	3.79

^a All values in cycles per second. ^b In formamide as solvent.

^c (A) represents the higher field and (B) the lower field resonance line. ^d Determined from spectra at ambient temperature.

^e Corrected for overlap and asymmetry. See text.

II⁵ and the programs were checked using data given by Rogers and Woodbrey in their paper.^{3b} The calculations were performed using an IBM 1620 computer.

The errors in the rotational barriers and frequency factors were determined by least-squares analysis of the data shown in Figure 1.

Determination of ¹³C-H Coupling Constants. The values of $J^{13\text{C-H}}$ were determined using a Varian A-60 n.m.r. spectrometer at ambient temperature in conjunction with an audiooscillator and frequency counter. The values of $J^{13\text{C-H}}$ are good to ± 0.5 c.p.s.²²

Acknowledgments. This work was supported by a Frederick Gardner Cottrell Grant from the Research Corporation and an Intramural Research Grant from the University of California, Riverside. The assistance of Mr. Ronald Mason and Mr. David Roark, and helpful discussions with Professor Paul Haake are gratefully acknowledged.

(22) NOTE ADDED IN PROOF. W. Walter and B. Maerten, *Ann. Chem.*, **669**, 66 (1963), have suggested on the basis of ambient temperature n.m.r. spectra that thioamides possess hindered rotation about the C-N bond and that these rotational barriers may be higher than those in amides. The authors wish to thank Dr. Albrecht Mannschreck for referring us to this article.

Electrolyte-Solvent Interaction. XVI. Quaternary Salts in

Cyanoethylsucrose-Acetonitrile Mixtures¹

by Claude Treiner² and Raymond M. Fuoss

Contribution No. 1769 from the Sterling Chemistry Laboratory, Yale University, New Haven, Connecticut (Received January 18, 1966)

The products of limiting equivalent conductance and macroscopic viscosity for tetrabutylammonium bromide, tetrabutylammonium tetraphenylboride, and tetramethylammonium bromide in mixtures of acetonitrile and octacyanoethylsucrose increase rapidly in mixtures containing more than about 50% of the latter, where the viscosity is greater than about 0.1 poise. The coefficient of the linear term in the conductance function simultaneously becomes negative and increases rapidly with increasing viscosity. Both of these results show that the resistance to ionic motion in the mixed solvents is much smaller than that calculated from the viscosity, using Stokes hydrodynamics and the sphere-in-continuum model.

In earlier papers of this series, we have shown that the Walden product for a given electrolyte in a mixed solvent usually varies with the composition of the solvent. Much of this variation is due to long-range electrostatic interaction between moving ions and solvent dipoles.³ The range of viscosity covered in the earlier work was about one order of magnitude (0.003 to 0.02). Stokes and Stokes⁴ report some striking deviations of the product from constancy

for a variety of electrolytes in aqueous solutions of sucrose and mannose of high viscosity. The recent

(1) Grateful acknowledgment is made to the donors of the Petroleum Research Fund, administered by the American Chemical Society, for partial support of this work.

(2) Du Pont Postdoctoral Research Fellow, 1963-1964; on leave of absence from the University of Paris.

(3) R. M. Fuoss, *Proc. Natl. Acad. Sci. U. S.*, **45**, 807 (1959).

(4) J. M. Stokes and R. H. Stokes, *J. Phys. Chem.*, **62**, 497 (1958).

availability of octacyanoethylsucrose^{5,6} ("cyanoethylsucrose," CES) made it possible to explore highly viscous nonaqueous systems in a range of dielectric constant where ionic association presumably would not be enough to make difficult the determination of limiting conductances. Cyanoethylsucrose has a dielectric constant about the same as that of acetonitrile (for which $D = 36.01$) and is completely miscible with it. However, it has a viscosity of about 600 poises at 50° and 40 poises at 80°, compared to 0.00345 poise for acetonitrile at 25°.

We present here the conductances of tetrabutylammonium bromide and tetraphenylboride and of tetramethylammonium bromide in mixtures of acetonitrile and cyanoethylsucrose, which cover the viscosity range up to $\eta = 0.3$, about two orders of magnitude higher than that of acetonitrile. The mixtures are essentially isodielectric ($D = 36.0-38.7$), so the observed effects must be hydrodynamic in origin rather than electrostatic. Briefly summarized, the electrolytes behave in a predictable fashion up to about 50-60 weight % cyanoethylsucrose; beyond this, the dependence of conductance on concentration and the parameters of the conductance function change markedly. Also, the empirical relation

$$\Lambda_0 \eta^{0.7} \approx \text{constant} \quad (1)$$

found by Stokes for the aqueous systems is obeyed, showing that the unusual behavior is a consequence of high viscosity *per se* and not merely another peculiarity of aqueous systems.

Experimental

Cyanoethylsucrose (CES) was used as received. Mixtures with purified⁷ acetonitrile (MeCN) were prepared by heating the CES to 60-80° and pouring MeCN into it with constant stirring. For more than about 50 weight % CES, at least 1 hr. of mixing was necessary to achieve uniformity. For these mixtures, the salts were dissolved in a portion of MeCN before adding to the CES; the solution was weighed after cooling to room temperature in order to determine the concentration of the initial solution. A batch of CES-MeCN of the same composition was used for dilution in the conductance determinations. The salts were from previously prepared stock. The solvent conductances were in the range $0.36-0.04 \times 10^{-6}$ mho; the product of solvent conductance and solvent viscosity was approximately proportional to the CES weight per cent ($10^{10} \kappa_0 \eta / w \approx 2$), showing that the CES contained a small amount of electrolytic impurity. The maximum solvent correction was, however, only 0.5%. The con-

ductance of purified MeCN is less than 0.03×10^{-6} mho.

The electrical equipment and thermostat ($25 \pm 0.002^\circ$) have been described.⁸ The cell⁹ consisted of a 20-ml. electrode chamber, containing bright platinum electrodes, attached by two 6-mm. i.d. tubes (4 cm. long) to a 250-ml. dilution chamber. Tungsten wires¹⁰ through the Pyrex connected the platinum electrode posts to the external leads. The cell constant (0.15630) was determined by comparison with a cell whose constant had been determined using aqueous solutions of potassium chloride.¹¹ The cell constant, once the electrode capsule and its attaching tubes were filled and enough solution (10 ml.) was in the dilution chamber to connect their contents electrically, was independent of the total amount of solution in the cell. This cell was designed so that conductance runs could be made using considerably less solution than is needed for our 1-l. erlenmeyer cells.

The properties of the solvents are summarized in Table I, where w is weight per cent of CES in the mixture, ρ is density, η is viscosity, and D dielectric constant. Ubbelohde viscometers were used; capillary diameters were chosen to give flow times of several hundred seconds at least. (If too narrow a capillary is used with the very viscous solutions, the second flow time with the same filling is always longer than the first, because the capillary is dry the first time, but does not drain dry for the second and subsequent flow times; it then has effectively a smaller diameter.) Dielectric constants were measured at 1 Mc.; they were linear in w over the range 0-70% CES in MeCN and extrapolate to about 39.5 for 100% CES. This is higher even than the 60-cycle value⁶ of 38.0 reported for CES; in pure CES, of course, the dielectric constant at bridge frequencies of 60 cycles to 1 Mc. is lower than the static dielectric constant due to the enormous viscosity. Wide-mouth pycnometers were used for the mixtures of higher viscosity; care was taken not to wet the ground areas with solution which only partially filled the pycnometer. After weighing, the pycnometer

(5) We are grateful to Eastman Chemical Products, Inc., for the sample of cyanoethylsucrose with which the exploratory measurements were made.

(6) Technical Data Bulletin, TDS-X-132, Eastman Chemical Products, Inc., Kingsport, Tenn.

(7) M. A. Coplan and R. M. Fuoss, *J. Phys. Chem.*, **68**, 1181 (1964).

(8) J. E. Lind, Jr., and R. M. Fuoss, *ibid.*, **65**, 999 (1961).

(9) M. A. Coplan, Thesis, Yale University, 1963, p. 25.

(10) K. N. Marsh and R. H. Stokes, *Australian J. Chem.*, **17**, 740 (1964).

(11) J. E. Lind, Jr., J. J. Zwolenik, and R. M. Fuoss, *J. Am. Chem. Soc.*, **81**, 1557 (1959).

was then filled with a liquid (heptane) of low viscosity and known density and reweighed.

Table I: Properties of Mixtures of Cyanoethylsucrose-Acetonitrile

<i>w</i>	ρ	$10^2\eta$	<i>D</i>
Solvents for Bu ₄ NBr			
18.6	0.8383	0.573	36.90
29.0	0.8767	0.859	37.24
45.3	0.9457	2.167	37.74
48.3	0.9568	2.756	37.88
51.2	0.9687	3.414	37.97
55.0	0.9881	4.94	38.04
66.4	1.0444	18.14	38.46
70.2	1.0503	32.0	38.68
71.1	1.0549	39.1	38.60
Solvents for Bu ₄ NBPh ₄			
22.6	0.8540	0.683	37.03
30.4	0.8814	0.945	37.28
46.7	0.9493	2.361	37.84
51.8	0.9730	3.69	37.94
55.5	0.9902	5.08	38.11
61.5	1.0177	9.70	38.32
Solvents for Me ₄ NBr			
5.6	0.7944	0.391	36.48
13.3	0.8197	0.478	36.72
19.2	0.8407	0.589	36.90
32.5	0.8875	1.012	37.36
42.7	0.9314	1.793	37.75
48.0	0.9578	2.785	37.96

Table II: Conductance of Tetrabutylammonium Bromide in Cyanoethylsucrose-Acetonitrile Mixtures

10 ^c	Λ	10 ^c	Λ	10 ^c	Λ
18.6%		48.3%		66.1%	
35.214	70.40	32.750	18.77	26.723	4.451
25.973	71.58	25.506	19.00	19.152	4.537
17.885	72.84	17.346	19.30	13.722	4.612
12.127	74.01	11.530	19.54	8.572	4.697
7.338	75.25	8.278	19.74		
29.0%		51.2%		70.2%	
33.881	47.99	32.580	15.052	55.511	2.350
26.324	48.59	22.180	15.331	41.888	2.518
18.161	49.41	14.741	15.561	29.540	2.681
12.308	50.18	9.313	15.774		
8.185	50.87				
45.3%		55.0%		71.1%	
31.193	21.89	35.536	11.590	28.962	1.847
25.976	22.08	28.179	11.718	19.285	2.130
20.370	22.29	19.665	11.923	14.125	2.316
13.459	22.67	12.589	12.135	8.654	2.496
		7.172	12.339		

Conductance data for tetrabutylammonium bromide, tetrabutylammonium tetraphenylboride, and tetramethylammonium bromide in CES-MeCN mixtures are summarized in Tables II and III.

Table III: Conductance of Tetrabutylammonium Tetraphenylboride and of Tetramethylammonium Bromide in Cyanoethylsucrose-Acetonitrile Mixtures

10 ^c	Λ	10 ^c	Λ	10 ^c	Λ
—Bu ₄ N·BPh ₄ —					
22.6%		55.5%		19.2%	
22.728	61.12	33.658	11.366	41.235	84.19
15.978	62.13	23.346	11.598	27.582	87.05
10.506	63.34	16.715	11.758	18.378	89.49
7.255	64.10	10.851	11.933	11.884	91.66
4.450	65.00			7.008	93.75
30.4%		61.5%		32.5%	
26.371	46.38	44.812	6.634	18.511	56.32
19.033	47.13	30.734	6.789	14.031	57.31
13.122	47.92	20.857	6.920	9.432	58.32
8.644	48.66	13.275	7.035	7.003	58.95
5.436	49.33	8.192	7.129	5.252	59.47
46.7%		Me ₄ NBr		42.7%	
25.233		5.6%		30.909	
17.376	21.81	21.426	136.7	20.228	35.69
11.621	22.12	14.876	140.3	14.215	36.25
7.866	22.38	10.454	143.2	9.367	36.82
4.398	22.70	7.503	145.4	6.657	37.19
		4.849	147.9		
51.8%		13.3%		48.0%	
28.957	15.17	31.635	103.9	20.966	33.48
21.285	15.38	20.068	107.6	13.934	34.23
14.867	15.60	13.431	110.3	9.280	34.84
10.129	15.79	9.178	112.4	6.713	35.22
6.223	15.99	6.458	114.0	4.435	35.62

Discussion

In order to obtain limiting conductances, the function Λ' was extrapolated to zero concentration. This quantity includes the observed conductance and the theoretically known square root and transcendental terms as well as part of the linear term. We define Λ' by the equation

$$\Lambda' = \Lambda_{\text{obsd}} + Sc^{1/2} - Ec \log (6E_1'c) \quad (2)$$

where S is the Onsager coefficient and E and E_1' are the Fuoss-Onsager coefficients; note that the former¹² $c \log c$ term has been replaced by the term in $c \log (6E_1'c)$. The present Λ' thus differs from the former function by the linear term $Ec \log 6E_1'$ and now ab-

(12) R. M. Fuoss and F. Accascina, "Electrolytic Conductance," Interscience Publications, Inc., New York, N. Y., 1959, Table 15.1.

sorbs into Λ' this large known linear term. Theoretically, we also have

$$\Lambda' = \Lambda_0 + Lc \quad (3)$$

(where the coefficient L of the linear term differs from the formerly used J by the amount $E \log 6E_1'$). When ionic association is negligible (or slight, so that the ion-pair term $K_{AC}\gamma f^2\Lambda$ in the conductance equation approximates linearity, $\gamma f^2\Lambda \approx \Lambda_0$), the function Λ' defined by eq. 1 is always linear. For all the conductance data given in Tables II and III, linear Λ' - c plots were found; the extrapolated values of Λ_0 are summarized in Table IV.

Table IV: Derived Constants for Electrolytes in MeCN-CES Mixtures

w	Λ_0	Δ_{07}	L	L/Λ_0	\bar{a}
Bu ₄ NBr					
18.6	80.35	0.460	810	10.1	5.13
29.0	54.39	0.467	570	10.5	5.42
45.4	24.50	0.531	220	9.0	5.01
48.3	20.93	0.577	185	8.8	5.06
51.2	16.80	0.574	145	8.6	4.97
55.0	13.01	0.643	70	5.45	3.57
66.4	4.964	0.900	-19	-3.82	...
70.2	3.225	1.030	-103	-32	...
71.1	2.852	1.115	-261	-91	...
Bu ₄ NBPh ₄					
22.6	68.45	0.465	550	8.0	4.22
30.4	52.10	0.492	405	7.8	4.25
46.7	23.73	0.560	200	8.5	4.84
51.8	16.81	0.621	120	7.3	4.40
55.5	12.75	0.648	65	5.0	(3.39)
61.5	7.53	0.730	30	3.9	(3.00)
Me ₄ NBr					
5.6	156.51	0.612	400	2.6	(2.29)
13.3	121.66	0.582	470	3.9	(2.73)
19.2	100.12	0.590	510	5.1	(3.23)
32.5	62.63	0.634	280	4.5	(3.09)
42.7	39.19	0.703	45	1.1	(1.84)
48.0	37.09	1.033	(70)	(2.0)	(2.40)

The corresponding Walden products are shown in Figure 1 as a function of composition. The Walden products in MeCN for Bu₄NBr, Bu₄NBPh₄, and Me₄NBr are 0.555, 0.422, and 0.668, respectively. Up to about 40–50% CES, the curves resemble many others reported in this series for electrolytes in mixed solvents, but beyond this range a drastic change in the dependence of $\Lambda_0\eta$ on composition appears. The product begins to increase very rapidly; that is, the mobility decreases much less than corresponds to the increase in viscosity with increasing CES content. Assuming

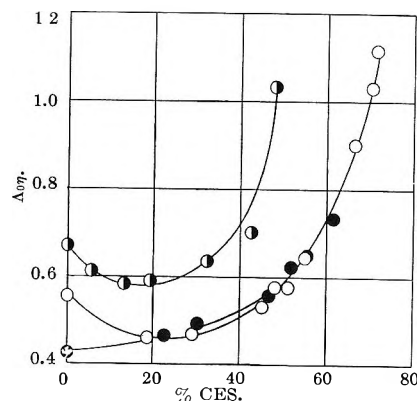


Figure 1. Walden products in cyanoethylsucrose-acetonitrile mixtures: O, tetrabutylammonium bromide; ◐, tetramethylammonium bromide; ●, tetrabutylammonium tetraphenylboride.

that the Λ' - c extrapolations give the correct limiting conductances for infinite dilution, Figure 1 shows that the mobility of the ions in the CES-rich mixtures is much larger than one would calculate from the observed macroscopic viscosity, using the Stokes coefficient of friction $(6\pi\eta R)^{-1}$. The result can be rationalized by arguing that the local resistance to motion experienced by the ions on a molecular scale of distances is much less than the resistance of the bulk solvent to macroscopic laminar flow; that is, the bulky CES molecules ($C_{36}H_{46}N_8O_{11}$, mol. wt. 776.8) impart a high macroscopic viscosity to the mixed solvent, but the ions are able to move through the tangle of solvent molecules by displacing only segments of the cyanoethylated disaccharide. This point of view seems reasonable when one considers a model of the CES molecule. The situation is reminiscent of the high conductance observed for electrolytes in plasticized polymers,¹³ despite the extremely high macroscopic viscosity of these systems.

The three different salts show specific behavior in the acetonitrile-rich ends of the curves, but in the CES-rich end, a common pattern seems to appear, as shown in Figure 2, where the logarithms of the Walden products are plotted against the logarithms of the macroscopic viscosity. The curves for Bu₄NBr and Bu₄NBPh₄ practically coalesce and approach linearity with a slope of about 0.26. The points for Me₄NBr scatter rather badly, but the increase is at about the same rate. Empirically, the data in the CES-rich solvents can be represented by

$$\Lambda_0\eta^{0.74} \approx \text{constant} \quad (4)$$

which is very near to the function found by Stokes⁴

(13) D. J. Mead and R. M. Fuoss, *J. Am. Chem. Soc.*, **67**, 1566 (1945).

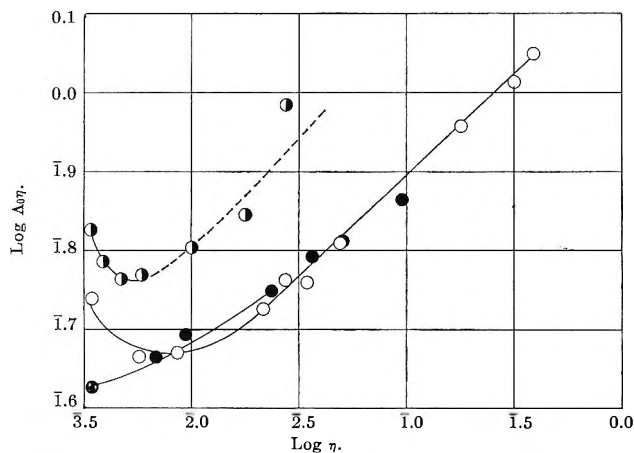


Figure 2. Dependence of Walden products on viscosity; same code as Figure 1.

to describe the Walden products for potassium chloride and other electrolytes in sucrose-water mixtures, which are also (approximately) isodielectric solvents of very high viscosity. It is clear that the model of spheres in a continuum, the latter having the macroscopic properties of the real solvent, fails completely to describe the hydrodynamics of the systems under discussion.

Another, and even more striking, qualitative difference between the low and high viscosity ranges appears when the concentration dependence of the solutions is considered. Since the Λ' - c curves are all linear, the data were analyzed by the 7094 IBM computer to find the constants Λ_0 and L of the equation

$$\Lambda = \Lambda_0 - Sc^{1/2} + E'c \ln(6E_1'c) + Lc \quad (5)$$

The constants are summarized in Table IV. The constant L theoretically¹⁴ should be of the form (for the sphere-in-continuum model)

$$L = A_1\Lambda_0 + A_2(a)/\eta \quad (6)$$

where A_1 depends only on the DT product and A_2 depends on the contact distance a as well as on DT . For a given salt, the ratio L/Λ_0 should therefore be a constant if the Walden product is constant. In Table IV, it is seen that L/Λ_0 is, in fact, approximately constant in the MeCN-rich mixtures, but it abruptly decreases and goes to *negative* values in the CES-rich systems. The change is best shown in Figure 3, where Λ'/Λ_0 is plotted against c for the Bu_4NBr solutions. On the basis of present theory, one would expect the points to lie on straight lines

$$\Lambda'/\Lambda_0 = 1 + (L/\Lambda_0)c \quad (7)$$

all with the same slope. Between 18.6 and 61.3%, this expectation is fulfilled; then with increasing CES

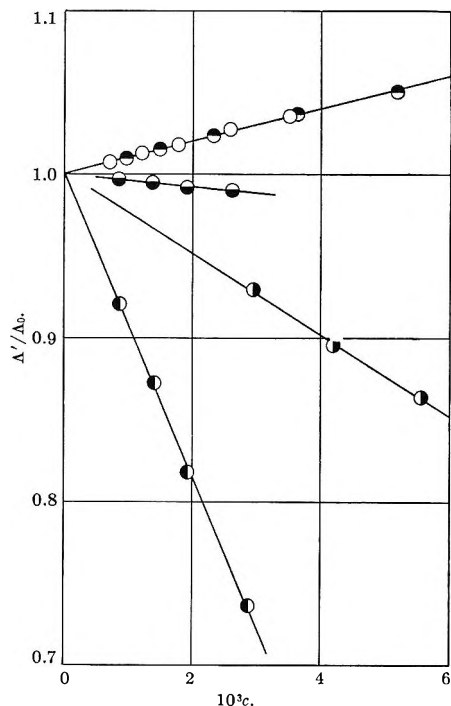


Figure 3. Change of conductance function with composition (tetrabutylammonium bromide): ○, 18.6%; ●, 61.3%; ◐, 66.4%; ◑, 70.2%; and ◒, 71.1% cyanoethylsucrose.

content, the plots (still remaining linear) swing down to increasingly more negative slopes. Ordinarily, one ascribes a negative slope¹⁵ of Λ' - c plots at high dilutions to ionic association, when the negative association term $K_{AC}\gamma f^2\Lambda$ in the conductance function approximates linearity but numerically exceeds the theoretically positive linear term Lc . Ionic association to any great extent for the tetrabutylammonium salts in these solvents, however, is most unlikely: the dielectric constant is too high. For a contact distance of, say, 5 Å., the Bjerrum parameter b is about 3, which is where the ion-pair association constant has its minimum value.¹⁶ Furthermore, if one tries to force fit the data to the conductance function for associated electrolytes, the deviations between calculated and observed values are large and systematic for Bu_4NBr and for Bu_4NBPh_4 , and the uncertainty in the "association constants" is large. Worse still for an association hypothesis, if the data for the tetraphenylboride are force fitted to the equation for associated electrolytes, the "association constant" comes out negative for the 55.5 and 61.5% CES systems. Finally, in the case of

(14) R. M. Fuoss and L. Onsager, *J. Phys. Chem.*, **66**, 1722 (1962); **67**, 621, 628 (1963); **68**, 1 (1964); and unpublished continuation of this work.

(15) R. W. Kunze and R. M. Fuoss, *ibid.*, **67**, 911 (1963); Figure 1.

(16) R. M. Fuoss, *J. Am. Chem. Soc.*, **80**, 5059 (1958).

Me_4NBr , which is known to be associated in acetonitrile,¹⁷ the coefficient of the linear term which is found is too small, as shown by the absurdly small a values (Table IV) calculated from the experimental values of L . There is no doubt that eq. 5 empirically represents the data. There is likewise certainty that the theoretical L coefficient based on the sphere-in-continuum model does not give even the right sign for the observed linear coefficient in the systems of high vis-

cosity. The experimental results therefore show that the hydrodynamic term $A_2(a)/\eta$ of eq. 6 must be large and negative for solvents of high macroscopic viscosities and clearly the quantity in the denominator must be smaller than the bulk viscosity. The theoretical problem to be considered is the motion of ions around segments of much larger molecules.

(17) A. D'Aprano and R. M. Fuoss, *J. Phys. Chem.*, **67**, 1722 (1963).

The Conductance of Symmetrical Electrolytes. V. The Conductance Equation^{1,2}

by Raymond M. Fuoss, Lars Onsager, and James F. Skinner

Contribution No. 1771 from the Sterling Chemistry Laboratory, Yale University, New Haven, Connecticut
(Received April 19, 1965)

Using the potential of total directed force on charged spheres moving in a continuum under an external field and correcting for electrophoresis, the conductance equation $\Lambda = \Lambda_0 - Sc^{3/2} + E'c \ln(6E_1'c) + Lc - Acf^2\Lambda_0$ is derived. Here $S = \alpha\Lambda_0 + \beta_0$, $\alpha = 0.8204 + 10^6/(DT)^{3/2}$, $\beta_0 = 82.50/\eta(DT)^{1/2}$, $E' = E_1'\Lambda_0 - E_2'$, $E_1' = 2.942 \times 10^{12}/(DT)^3$, $E_2' = 0.4333 \times 10^8/\eta(DT)^2$, $L = L_1 + L_2(b)$, $L_1 = 3.202E_1'\Lambda_0 - 3.420E_2' + \alpha\beta_0$, $ab = 16.708 \times 10^{-4}/DT$, $L_2(b) = 2E_1'\Lambda_0h(b) + 44E_2'/3b - 2E' \ln b$, $h(b) = (2b^2 + 2b - 1)/b^3$, $f^2 = \exp[-8.405 \times 10^6 c^{1/2} \gamma^{1/2}/(DT)^{3/2}]$, and $A = K_A = (4\pi Na^3/3000)e^b$. This equation can be generalized to $\Lambda = \Lambda_0 - Sc^{1/2}\gamma^{1/2} + E'c\gamma \ln(6E_1'c\gamma) + Lc\gamma - K_A c\gamma f^2\Lambda$, where $(1 - \gamma) = K_A c\gamma^2 f^2$. The first equation reproduces conductance data for 1-1 electrolytes in solvents of higher dielectric constant. The second is required when the dielectric constant is small enough to stabilize ion pairs in contact. This result confirms our earlier (1957) conductance function and establishes the functional form directly from the equation of continuity, the equations of motion, and Poisson's equation. Values of the contact distance calculated from the parameter b for a given electrolyte in a series of mixed solvents usually increase with decreasing dielectric constant. The source of this variation lies in inadequacy of the sphere-in-continuum model and not in mathematical approximations made in solving the differential equations.

In preceding papers of this series,³ the conductance of symmetrical electrolytes has been investigated theoretically, using the model of rigid charged spheres in a hydrodynamic and electrostatic continuum. This model was the basis of an earlier treatment of the problem^{4,5} which led to the conductance equation

$$\Lambda = \Lambda_0 - Sc^{1/2} + Ec \log c + J(a)c \quad (1)$$

Equation 1 finally gave the theoretical explanation for the observation that, in the usual working range of

(1) Grateful appreciation is expressed to the donors of the Petroleum Research Fund, administered by the American Chemical Society, for partial support of this research.

(2) Several sections of this paper were presented at the Symposium on Electrolytes during the 145th National Meeting of the American Chemical Society, New York, N. Y., Sept. 10, 1963.

concentrations, conductance curves for solutions in solvents of high dielectric constant usually lie above the limiting tangent. Furthermore, the transcendental term required by the theory explained why empirical algebraic extrapolation functions never quite fitted precision data. Use of the auxiliary function

$$\Lambda' \equiv \Lambda(\text{obsd.}) + Sc^{1/2} - Ec \log c \quad (2)$$

$$\Lambda' = \Lambda_0 + Jc \quad (3)$$

gave a function which permitted extrapolation to zero concentration on a linear scale. (Since S and E are theoretically known, given an approximate value of Λ_0 , the right-hand side of (2) is determined. The approximation quickly converges on iteration.) Comparison with a wide variety of experimental data⁶ in solvents of high dielectric constant fully confirmed the functional form of (1).

For solvents of lower dielectric constant (say less than about 30 for the alkali halides in dioxane-water mixtures, for example), the experimental Λ' - c plot become curved, showing that the function (1) no longer reproduces the observed conductances. The *ad hoc* hypothesis that pairs of oppositely charged ions in contact, in concentrations determined by the dielectric constant⁷ and the stoichiometric concentration, would not contribute to (d.c.) transport of charge led to the function^{8,9}

$$\Lambda = \Lambda_0 - Sc^{1/2}\gamma^{1/2} + Ec\gamma \log c\gamma + Jc\gamma - K_{AC}\gamma^2\Lambda \quad (4)$$

(This function obviously reduces to (1) as K_A approaches zero and/or γ approaches unity.) It was found that (4) reproduced experimental data for solutions in both aqueous and nonaqueous mixtures of solvents for all the 1-1 electrolytes for which precision data at low concentrations ($\kappa a < 0.2$) were available.

Reinvestigation³ of the problem was prompted by two motives: (a) dissatisfaction with the arbitrary insertion of the mass action hypothesis into the argument which produced (4) from (1) and (b) the observation that the a values calculated from the linear coefficients $J(a)$ systematically increased for a given electrolyte as the dielectric constant of the solvent mixture decreased. The first point is simply this: if ion association is the consequence⁷ of Coulomb forces only, then the corresponding decrease of conductance with increasing concentration should be predictable directly from the equation of continuity, the equations of motion, and the Poisson equations.¹⁰ In effect, (4) was derived by the following sequence of arguments. First, assume that (1) gives the conductance of free ions, ignoring the possible presence and effects of ion

pairs. Second, assume that the concentration of ion pairs is given by the mass action equation

$$1 - \gamma = K_{AC}\gamma^2f^2 \quad (5)$$

Third, use the Arrhenius hypothesis that

$$\gamma = \Lambda/\Lambda_i \quad (6)$$

where Λ_i , the conductance of the free ions, is given by (1) when c is everywhere replaced by $c\gamma$; and, finally, combine these three equations. Regarding the second point, the dependence of a on D , at least two possible explanations suggest themselves: either the dependence is an artifact, a consequence of mathematical approximations made in deriving (1) from the fundamental differential equations, or else the model is an inadequate physical approximation to the real systems under observation. The results of our present calculations confirm our earlier more approximate treatment. We therefore conclude that a more realistic model, specifically one which includes short-range ion-solvent interactions, must be considered. Also, other sources of linear terms cannot be excluded.

Two kinds of mathematical approximations were made in deriving (1); all terms in the development which would eventually lead to terms of the order $c^{3/2}$ in $\Lambda(c)$ were systematically dropped, and the Boltzmann factor e^{ξ} was approximated in the equation of continuity by the first three terms of its power series. Both in principle and in practice, the effect of the first kind of approximation can be eliminated by restricting the range of application of (1) to sufficiently low concentrations, the latter being practically defined as concentrations from which the deviations between observed and calculated conductances are random and such that their root-mean-square value is within the estimated experimental error. The effect of the approximation by the truncated series, on the other hand, is built into the end result at the very outset of the calculation and can never be removed once it is in.

A new statement of the problem in terms of the po-

(3) Equations from these papers will be cited as III(61), etc. I, *J. Phys. Chem.*, **66**, 1722 (1962); II, *ibid.*, **67**, 621 (1963); III, *ibid.*, **67**, 628 (1963); IV, *ibid.*, **68**, 1 (1964). Footnote 1 of IV lists corrections to I-III.

(4) R. M. Fuoss and L. Onsager, *Proc. Natl. Acad. Sci. U. S. A.*, **41**, 274, 1010 (1955).

(5) R. M. Fuoss and L. Onsager, *J. Phys. Chem.*, **61**, 668 (1957).

(6) R. L. Kay, *J. Am. Chem. Soc.*, **82**, 2099 (1960).

(7) R. M. Fuoss, *ibid.*, **80**, 5059 (1958).

(8) R. M. Fuoss, *ibid.*, **79**, 3301 (1957).

(9) R. M. Fuoss and C. A. Kraus, *ibid.*, **79**, 3304 (1957).

(10) R. M. Fuoss and F. Accascina, "Electrolytic Conductance," Interscience Publishers, New York, N. Y., 1959, Chapters VIII-XIII.

tential of the total directed force (part I) transforms the equation of continuity into a form I(2.5) which can be integrated with retention of the Boltzmann factor explicitly in its exponential form. We can therefore now consider the consequences of the earlier series approximation. When the relaxation field (part II) is computed from the new equation, significant differences as contrasted with the earlier result⁵ appears. The relaxation field ΔX_e calculates to

$$\Delta X_e/X = 1 - \alpha c^{1/2} + E_1 c \log c + A_1 c - A_2 c f^2 \quad (7)$$

The square root and transcendental terms are exactly as before, but, where a linear term appeared before, two terms $A_1 c$ and $A_2 c f^2$ now emerge. Of course, at low concentrations in solvents of high dielectric constant, the activity coefficient is nearly unity, and the last two terms of (7) therefore closely approximate a linear term

$$A_1 c - A_2 c f^2 \approx A_3 c \quad (8)$$

which is the result previously obtained when the Boltzmann factor was replaced by the initial terms of its series; in other words, (7) approaches our earlier result when the Boltzmann exponent ζ is small, which is precisely where the series approximation is valid. The first of the two significant details in (7) is the appearance of the multiplier f^2 in the last term; such a multiplier would appear if an equation of the form (5) were involved in computing ionic concentrations from stoichiometric. Second, and even more revealing, is the form of the coefficient A_2 ; it can be written

$$A_2 = A_4 [E_p(b) - (e^b/b)(1 + 1/b)] \quad (9)$$

where

$$b = \epsilon^2/aDkT \quad (10)$$

The quantity in brackets in (9) is the functional part of the Bjerrum approximation¹¹ to the association constant K_A . When this result is combined with the electrophoresis correction (part III) and the other higher terms (part IV), the conductance equation which results is

$$\Lambda = \Lambda_0 - Sc^{1/2} + E'c \ln \tau^2 + Lc - A\Lambda_0 c f^2 \quad (11)$$

where L and A are constants, which will be discussed later, and $\tau^2 = 6E_1'c$ is proportional to concentration. For solutions of low concentrations in solvents of high dielectric constant, it is clear that (11) reduces immediately to (1), with

$$J = E' \ln (6E_1') + L - A\Lambda_0 \quad (12)$$

On the other hand, (11) is the limit of (4) as γ approaches unity if J has the value given by (12) and A

is identified with K_A . The constant L separates into two terms, one of which is independent of the contact distance a ; as will be shown later, a large part of J is independent of a , so a is much less precisely determined from the data than is the former total linear coefficient J .

The purpose of this paper is to combine the relevant equations of parts I–IV in order to derive (11) and to compare the results with experiments and with the earlier conductance functions. Briefly summarized, we find that numerically the value of the contact distance calculated from J and from L is about the same, and it still shows a systematic dependence on dielectric constant. However, the contribution of the part of the linear term which depends on a to the total conductance is in general small, and any additional small linear term could easily account for the variation of a . On the other hand, the coefficient A closely approximates the former⁷ K_A and eq. 4 in the form

$$\Lambda = \Lambda_0 - Sc^{1/2}\gamma^{1/2} + E'c\gamma \ln (6E_1'c\gamma) + Lc\gamma - K_A c\gamma f^2 \Lambda \quad (4a)$$

can be considered to be theoretically established. The principal contribution of this series³ of calculations is in fact to establish that retention of the Boltzmann factor without approximation leads directly to a term in $c f^2$ into the conductance equation, which in turn heuristically justifies the use of (4a) as the more general function of which (11) is the limit. We shall refer to (4a) as the 1965 equation in order to distinguish it from earlier equations and shall use it in the analysis of conductance data.

1. The Conductance Function

It is convenient to introduce at this stage the dimensionless variable¹²

$$\tau = (6E_1'c)^{1/2} = 816.11c^{1/2}/(D_{25})^{3/2} \quad (1.1)$$

which is the ratio of the Bjerrum distance $\beta/2$, near which most ion-pair distribution functions have a minimum,^{13–17} to the Debye–Hückel distance $(1/\kappa)$. This variable is a rational reduced variable for the description of electrolytic solutions; two solutions at different concentrations at different temperatures in solvents of different dielectric constant have identical

(11) See ref. 10, Chapter XVI.

(12) R. M. Fuoss and L. Onsager, *Proc. Natl. Acad. Sci. U. S.*, **47**, 818 (1961).

(13) N. Bjerrum, *Kgl. Danske Videnskab. Selskab*, **7**, No. 9 (1926).

(14) R. M. Fuoss, *Trans. Faraday Soc.*, **30**, 967 (1934).

(15) R. M. Fuoss, *J. Am. Chem. Soc.*, **57**, 2604 (1935).

(16) H. Reiss, *J. Chem. Phys.*, **25**, 400 (1956).

(17) J. C. Poirier and J. H. de Lap, *ibid.*, **35**, 213 (1961).

electrical properties at the same value of τ . For example, the coefficient of the leading term in the relaxation effect simply becomes a numerical constant

$$\alpha c^{1/2} = \tau/3(1 + q) \quad (1.2)$$

for all symmetrical electrolytes, and the limiting activity coefficient is given by

$$f = e^{-\tau} \quad (1.3)$$

Alternatively, τ is the electrostatic part of the chemical potential, expressed in units kT .

The discussion which follows will be limited to the case of 1-1 electrolytes although the equations are valid for all symmetrical electrolytes. For numerical work, computer programs for 1-1 electrolytes can be easily adapted to z - z electrolytes by replacing the dielectric constant D by D/z^2 and the viscosity η by η/z . This is because charge-square always appears in the numerator when D appears in a denominator in electrostatic terms, while charge appears to the first power in the numerator of hydrodynamic terms, which always have viscosity in the denominator.

The electrostatic part of the relaxation field is given by

$$\Delta X_e/X = F(a) + \Delta X_a/X \quad (1.4)$$

where¹⁸

$$F(a) = -\tau/3(1 + q) - (\tau^2/3)E_n(s\kappa a) - \tau^2 e^{-2\tau} K(b) + (\tau^2/3)(\ln b + \Gamma - 1) + (\tau^2/3)f(b, \kappa a) \quad (1.5)$$

$$(1 - T_1)f(b, \kappa a) = (T_1/2)[E_n(p\kappa a) - E_n(s\kappa a)] - q/(2 + q) + T_1(q - 1/2) \quad (1.6)$$

$$T_1 = e^{-b}(1 + b + b^2/2) \quad (1.7)$$

and¹⁹

$$\Delta X_a/X = -(\tau^2/3)(2 - 8q/3) = -0.1144\tau^2 \quad (1.8)$$

The first term of $F(a)$ in (1.5) is the classical leading term $\alpha c^{1/2}$ due to the relaxation field. The other terms are of higher order in concentration; some have their origin in the retention of the Boltzmann factor e^{ξ} in explicit form in the integration of the equation of continuity. The negative exponential integral $E_n(s\kappa a)$ contributes to the $c \log c$ term when it is expanded in the approximate form²⁰

$$E_n(x) = -\Gamma - \ln x + x + O(x^2) \quad (1.9)$$

but the logarithmic parts of the exponential integrals in $f(b, \kappa a)$ cancel except for a constant, $\ln [(1 + q)/(2 + q)]$. Expanding the integrals, we have

$$(1 - T_1)f(b\kappa a) = (T_1/2)[\ln(s/p) + 2q - 1 - \kappa a] - q/(2 + q) + O(\kappa^2 a^2) \quad (1.10)$$

and on inserting numerical values for p , s , and q

$$(1 - T_1)f(b, \kappa a) = 0.4377T_1 - 0.2612 - T_1\kappa a/2 \quad (1.11)$$

The relaxation field is clearly a function of b ; for b larger than 3 or 4, the main dependence is through the term in $K(b)$, the remaining terms not being very sensitive to b , while $K(b)$ is essentially exponential in b . It will be more convenient to postpone further discussion of the dependence on b until the final equation is assembled.

The expansion of $E_n(s\kappa a)$ in (1.5) gives, to terms of order $\kappa^2 a^2$

$$E_n(s\kappa a) = -\Gamma - \ln(2 + q) - \ln 2 - \ln \tau + \ln b + s\kappa a \quad (1.12)$$

where the identity

$$\ln \kappa a = \ln(2\tau/b) \quad (1.13)$$

has been used to replace κa by τ ; this step yields a negative $\ln b$ which cancels the positive one appearing in (1.5). Combining the various terms above, we obtain

$$\Delta X_e/X = -\tau/3(1 + q) + (\tau^2/3) \ln \tau - \tau^2 e^{-2\tau} K(b) + (\tau^2/3)N'(b) \quad (1.14)$$

where

$$N'(b) = (1.4681 - 1.2916T_1)/(1 - T_1) - [2 + q + T_1/2(1 - T_1)]\kappa a \quad (1.15)$$

The last term in (1.15) leads to a small term in $c^{3/2}$; $(2 + q) = 2.7071$, and the second term in the brackets varies from 1.05 at $b = 2$ to 0.157 at $b = 4$ and thereafter decreases rapidly to zero. To simplify calculations, we shall therefore approximate the last term of (1.15) by $3\kappa a$

$$N'(b) = (1.4681 - 1.2916T_1)/(1 - T_1) - 3\kappa a \quad (1.16)$$

Next, the hydrodynamic and kinetic terms²¹ will be considered. Denoting their sum by $\Delta X_{v,k}$, we have

$$\Delta X_{v,k}/X = [\kappa^2\beta/12\pi\eta(\omega_1 + \omega_2)][P_2(b) + 3e^{-2\tau}K(b)/2] + \beta^2\kappa^2/24(1 - T_1) \quad (1.17)$$

where

(18) See II(A27).

(19) See II(70).

(20) See ref. 10, Figure 13.1.

(21) See IV(3.1) and (3.2).

$$2P_2(b) = 2E_n(2\kappa a) - E_n(\kappa a) - \ln b - \Gamma + 3/2 - 1/3b^2 \quad (1.18)$$

Expanding the exponential integrals as before, we find

$$2P_2(b) = -\ln \tau - 1/3b^2 - 2\Gamma + 3/2 - 3 \ln 2 + 3\kappa a \quad (1.19)$$

$$= -\ln \tau - 1/3b^2 - 1.7338 + 6\tau/b$$

Next, the coefficient of the first term of $\Delta X_{v,k}$ is converted into practical units. The reciprocal friction coefficients ω_j are defined by

$$v^0_j = X \epsilon_j \omega_j \quad (1.20)$$

where the field X is measured in electrostatic units. Single-ion conductances λ^0_j are related to the mobility v^0_j through the Faraday constant F

$$\lambda^0_j = F v^0_j \quad (1.21)$$

The factor 10^{-8} times C , the velocity of light, converts electrostatic units into volts; by combining these definitions, we find

$$\omega_1 + \omega_2 = 10^{-8} C \Lambda_0 / F \epsilon \quad (1.22)$$

and for the denominator of the coefficient in (1.17)

$$\pi \eta (\omega_1 + \omega_2) = \Lambda_0 \kappa / 3 \beta_0 c^{1/2} \quad (1.23)$$

where

$$\beta_0 = F \epsilon \kappa / 3 \pi \eta (10^{-8} C) c^{1/2} \quad (1.24)$$

In order to express the results in terms of a coefficient which also appears in the electrophoresis term, we define E_2' by

$$E_2' = \beta \kappa \beta_0 / 16 c^{1/2} = \tau \beta_0 / 8 c^{1/2} \quad (1.25)$$

(The E terms will carry primes when they multiply natural logarithms; $E = 2.3030E'$ will multiply logarithms to base 10.) Substituting in the coefficients, we finally obtain

$$\beta \kappa^2 / 12 \pi \eta (\omega_1 + \omega_2) = 4E_2' c / \Lambda_0 \quad (1.26)$$

The second term of $\Delta X_{v,k}$ is converted to practical units by defining E_1' so that

$$E_1' = \beta^2 \kappa^2 / 24 c = \tau^2 / 6 c \quad (1.27)$$

For later use, we introduce here a combination of E_1 and E_2 which recurs

$$E = E_1 \Lambda_0 - E_2 \quad (1.28)$$

Using the coefficients

$$\Delta X_{v,k} / X = (4E_2' c / \Lambda_0) [P_2 + 3e^{-2\tau} K / 2] + E_1' c / (1 - T_1) \quad (1.29)$$

The entire relaxation field is now obtained by taking the sum of (1.14) and (1.29); denoting the sum simply by ΔX , we have

$$\Delta X / X = -\alpha c^{1/2} + 2(E' / \Lambda_0) c \ln \tau - 6(E' / \Lambda_0) K(b) e^{-2\tau} c + 2E_1' N'(b) c - 3.4677 E_2' c / \Lambda_0 + E_1' c / (1 - T_1) - 2E_2' c / 3\Lambda_0 b^2 + [(3 - 2b) / b^2] \tau^3 \quad (1.30)$$

Note that the transcendental term is $c \ln \tau$ rather than $c \ln c$; we have now transferred to this term part of the former Jc term. Also, the $c^{3/2}$ term (which, it will be recalled, arises from numerical approximation of the exponential integrals) is most simply computed in terms of τ . Note also that this term increases very rapidly with decreasing dielectric constant: $\tau^3/b^2 \sim D^{-13/2}$.

Next, we consider the electrophoretic correction to the velocity.²² The velocity v_j of an ion of species j in the presence of the other ions is less than the limiting velocity v^0_j , as shown below

$$v_j = v^0_j - \epsilon_j X' / 6 \pi \eta + (\epsilon_j X' \tau^2 / 6 \pi \eta \beta) F(b) \quad (1.31)$$

where $F(b)$ is a rather complicated but not very sensitive function of b , which is tabulated in part III. Here X' denotes the actual field

$$X' = X + \Delta X \quad (1.32)$$

where ΔX represents the total relaxation field plus the kinetic term. In order to make our equations more compact, we shall temporarily use the symbol λ_j' to denote actual conductance divided by $(1 + \Delta X / X)$. Using (1.20), (1.21), and (1.24) to convert to practical units, we obtain

$$\lambda_j' = \lambda^0_j - (F \epsilon_j \kappa / 6 \pi \eta \sigma) [1 - (\tau/2) F(b)] \quad (1.33)$$

$$= \lambda^0_j - \beta_0 c^{1/2} / 2 + 2E_2' c F(b) \quad (1.34)$$

For the equivalent conductance

$$\Lambda = \lambda_1 + \lambda_2 \quad (1.35)$$

we find

$$\Lambda = [\Lambda_0 - \beta_0 c^{1/2} + 4E_2' F(b) c] [1 + \Delta X / X] \quad (1.36)$$

where $\Delta X / X$ is given by (1.30). The product (1.36) is now expanded, and terms of order $c^{3/2}$ are dropped. The cross-product term

$$\alpha \beta_0 = 8E_2' / 3(1 + q) = 1.5621 E_2' \quad (1.37)$$

is retained and combined with the E_2' term (1.30). The final result is

(22) See III(61).

$$\Lambda = \Lambda_0 - S c^{1/2} + E' c \ln \tau^2 - 6E'K(b)ce^{-2\tau} + [E_1'\Lambda_0H(b) - E_2'G(b)]c - [(2b - 3)/b^2]\Lambda_0\tau^3 \quad (1.38)$$

where

$$H(b) = 2N'(b) + 1/(1 - T_1) \quad (1.39)$$

and

$$G(b) = 1.9055 + 2/3b^2 - 4F(b) \quad (1.40)$$

To a sufficient approximation, the functions H and G may be computed in the range $15 > b > 2$ by the empirical formulas

$$H(b) = 3.936 + 329.5 \exp(-3.344b^{1/2}) \quad (1.41)$$

and

$$G(b) = 10.583 - 21.10b^{1/2} \quad (1.42)$$

These functions are shown in Figure 1; for $b > 3$, H changes only slowly with b and asymptotically approaches a value of about 4 for large b (*i.e.*, becomes insensitive to the contact distance a). In general, the quantity $E_1'\Lambda_0H$ is much larger than $E_2'G$. These facts are of practical importance in numerical calculations, as will be shown later.

For b greater than about 4, the $K(b)$ term begins to dominate the linear terms. (To give a feeling for the magnitude of b , we mention that $b \approx 140/D$ for a contact distance $\hat{a} = 4$.) The logarithm of the function

$$K(b) = [E_p(b) - (e/b)(1 + 1/b)]/3 \quad (1.43)$$

multiplied by $(1 - 3/2b)$ is shown in Figure 2. (The multiplier is an estimate for the coefficient $(1 - E_2/E_1\Lambda_0)$ which implicitly is contained in the ion-pair term of (1.38); see eq. 2.10 in the next section.) Plotted on the same scale is the logarithm of the function

$$K'(b) = 2e^b/3b^3 \quad (1.44)$$

which is the first term of the asymptotic expansion of $K(b)$ and also the function of b which appears in the direct theoretical derivation of the association constant.⁷ It will be seen that $(1 - 3/2b)K(b)$ and $K'(b)$ approach each other as b increases. The curves cross at $b \approx 4$. $K'(b)$ has a minimum at $b = 3$ while $K(b)$ goes through zero at 2.35. From the experimentally determined association constants, a value of b is computed, and then b determines the contact distance a through the definition (10). Also in Figure 2 (ordinate scale to the right) is shown the ratio b'/b , plotted against b' for pairs of values obtained by solving $K'(b)$ and $(1 - 3/2b)K(b)$ for b for equal values of the functions. The greatest difference occurs around b

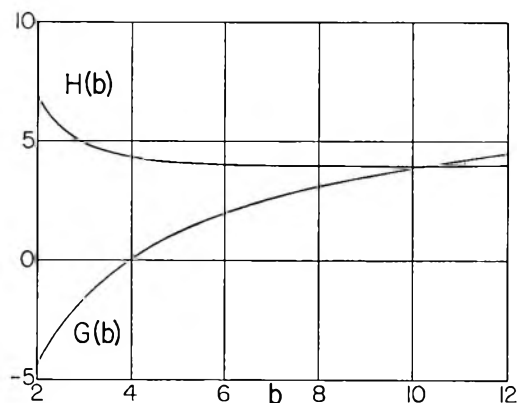


Figure 1. Dependence of $H(b)$ and $G(b)$ on b . (Note location of zero ordinate.)

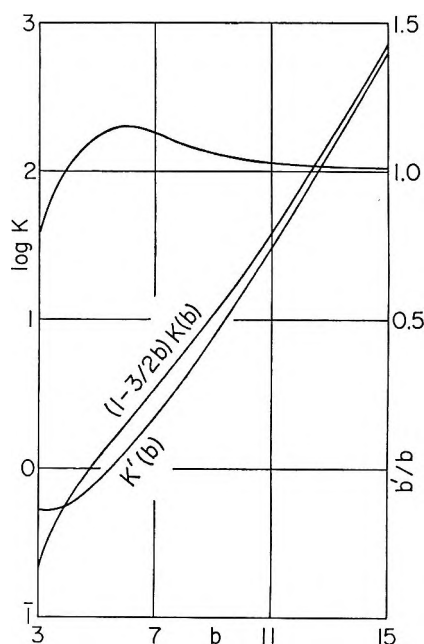


Figure 2. Comparison of approximate and explicit association functions and of b parameters derived therefrom.

≈ 6 , where b' is about 15% larger than b for the same (experimental) value of the association constant. Either function would of course give a self-consistent set of a values if used for data for a given set of electrolytes. Naturally, K cannot be interpreted as a factor in an association constant for b less than 2.35, where it goes through zero to negative values. It will be noted that $K(b)$ has the same dependence on b as the Bjerrum function $Q(b)$. It appears that our derivation of $K(b)$ from the differential equations and its interpretation as a factor in the association constant imply that association ceases from $b < 2.35$. Since such a critical value of b is physically unrealistic, we prefer to conclude that the derivation leads to a function which

for larger values of b is a good approximation to the directly derivable function $K'(b)$.

For numerical calculation of $K(b)$, the following development is convenient. We have

$$E_p(b) = E_p(1) + \int_1^b (e^u - 1)du/u + \ln b \quad (1.45)$$

by writing the definition of the positive exponential as the integral from minus infinity to unity plus the integral from 1 to b and adding and subtracting 1 in the latter integral. The integral in (1.45) converges and can be expanded in an absolutely convergent series

$$\int_1^b (e^u - 1)du/u = \sum_{n=1}^{\infty} b^n/n \cdot n! - \sum_{n=1}^{\infty} 1/n \cdot n! \quad (1.46)$$

where the second sum equals 1.31790. By series expansion and grouping terms

$$(e^b/b)(1 + 1/b) = 3/2 + 2/b + 1/b^2 + \Sigma_1 + \Sigma_2 \quad (1.47)$$

where

$$\Sigma_1 = \sum_{n=1}^{\infty} b^n/(n + 1)! \quad (1.48)$$

and

$$\Sigma_2 = \sum_{n=1}^{\infty} b^n/(n - 2)! \quad (1.49)$$

Substituting (1.45) and (1.47) in (1.43), inserting $E_p(1) = 1.8951$, and collecting terms, we obtain the rapidly convergent series

$$3K(b) = -0.9228 - 2/b - 1/b^2 + \ln b + 2b \sum_{n=1}^{\infty} b^n/(n + 1)[(n + 3)!] \quad (1.50)$$

To simplify the equations in the following discussion, we shall temporarily neglect the τ^3 term in (1.38) and abbreviate the coefficient of the linear term by L . Then the conductance equation becomes

$$\Lambda = \Lambda_0 - Sc^{1/2} + E'c \ln \tau^2 + Lc - 6E'K(b)ce^{-2\tau} \quad (1.51)$$

If we neglect E_2' (which is relatively small) compared to E_1' in E' , and replace $K(b)$ by the leading term of its asymptotic expansion, the last term of (1.51) becomes

$$6E'K(b)ce^{-2\tau} \sim (4\pi\eta Na^3/3000)e^b \Lambda_0 ce^{-2\tau} \quad (1.52)$$

which gives precisely the limiting form of eq. 4 obtained when K_A is small and γ approaches 1. As already stated, (4) is the equation which results by assuming that (1) gives the conductance of the free ions and that nonconducting ion pairs are in equilibrium

with free ions, relative concentrations being given by (5).

We now see that, for the limiting case of small association constants, at least, the hypothesis of ion-pair equilibrium no longer is needed as a special *ad hoc* assumption; retention of the explicit Boltzmann factor e^{ϵ} in the distribution function automatically leads to a decrease in conductance (for $b > 4$) which arises from pairs in contact because it is a function of e^b , which is the value of e^{ϵ} when $r = a$. It is unnecessary to consider how the two ions approach to contact or how long they remain in contact; the equation simply states that a decrease in conductance is an inevitable consequence of Coulomb interaction when b exceeds about 4. It will, of course, be convenient to retain the vocabulary of the ion-pair model. Furthermore, we propose a stochastic extension of (1.38) to lower dielectric constants (where $K(b)$ exceeds unity) by writing

$$\Lambda = \Lambda_0 - Sc^{1/2}\gamma^{1/2} + E'c\gamma \ln \tau^2\gamma + Lc\gamma - Ac\gamma\Lambda \exp(-2\tau\gamma^{1/2}) \quad (1.53)$$

where

$$L = E_1'\Lambda_0H(b) - E_2'G(b) \quad (1.54)$$

and

$$A = 6E'K(\bar{v})/\Lambda_0 = 6E_1'(1 - E_2'/E_1'\Lambda_0)K(b) \quad (1.55a)$$

As stated in part II, since an equation of the functional form (4) reproduces experimental data over a wide range of variables and since, in the limiting case of high dielectric constant, it reduces to (1.51) which is the approximate solution of a rigorous formulation of the conductance problem, we suggest that (1.53), which has the same dependence on c as does (4), is a close approximation to the exact solution of the problem.

2. Comparison with Experiment

For convenience, we list below four versions, (1), (4), (11), and (1.53), of the conductance equation to which frequent reference will be made in this section

$$\Lambda = \Lambda_0 - Sc^{1/2} + Ec \log c + J(a)c \quad (2.1)$$

$$\Lambda = \Lambda_0 - Sc^{1/2}\gamma^{1/2} + Ec\gamma \log c\gamma + Jc\gamma - K_Ac\gamma f^2\Lambda \quad (2.2)$$

$$\Lambda = \Lambda_0 - Sc^{1/2} + E'c \ln \tau^2 + Lc - A\Lambda_0c f^2 \quad (2.3)$$

$$\Lambda = \Lambda_0 - Sc^{1/2}\gamma^{1/2} + E'c\gamma \ln \tau^2\gamma + Lc\gamma - Ac\gamma f^2\Lambda \quad (2.4)$$

Considered as functions of concentration, (2.2) and (2.4) are identical; for γ near unity, both approach (2.3), which for $f^2 \approx 1$ (or $K_A \approx 0$) in turn approaches (2.1).

We shall first consider (2.1) and (2.3), using data for potassium chloride²³ and for cesium iodide²⁴ in dioxane-water mixtures in the higher range of dielectric constants and for some quaternary ammonium salts in acetonitrile.²⁵ The results are summarized in Table I, where two entries are given for each value of D . The first one gives the constants obtained when (2.3), the three-parameter equation, was fitted to the data. The quantity $\delta\Lambda$ is the mean deviation between calculated and observed values for the five points of the run. The contact distances were computed by solving

$$L - A\Lambda_0 = E_1'\Lambda_0H(b) - E_2'G(b) - 6E'K(b) \quad (2.5)$$

for b , whence

$$a = \epsilon^2/bDKT = 560.4 \times 10^{-8}/bD_{25} \quad (2.6)$$

The pattern is the same for all the examples of Table I (as well as for many other sets of data which have been examined): a good fit of the function to the data (small $\delta\Lambda$) but a large uncertainty in L and practically no certainty in the value of A . This simply means that f^2 is so near unity that, if we insist on three parameters, the mean-square computation gives us a wide band of L and A values because the two terms cannot be sharply separated. A large L paired with a large A (for positive A) will fit the data just as well as with both constants small. It would require data of at least 0.001% precision in this range of concentration to resolve the two terms; such data simply do not exist. Also, it is clear that a calculated from $L(a)$ by (1.54) will have a large uncertainty, while, with $\pm 100\%$ uncertainty in $A(a)$, no meaningful value whatsoever can be obtained by solving (1.55) for a . In this range of dielectric constants, the L term dominates the A term. The only way to obtain a value of a is to lump the parameters as was done in (2.5). If, however, we approximate f^2 by unity in (2.3), we obtain the results shown in the second entries for a given dielectric constant when the two-parameter equation (2.7) is fitted to the data.

$$\Lambda = \Lambda_0 - Sc^{1/2} + E'c \ln \tau^2 + (L - A\Lambda_0)c \quad (2.7a)$$

$$\Lambda = \Lambda_0 - Sc^{1/2} + E'c \ln \tau^2 + J'c \quad (2.7b)$$

The coefficient J' is given in the L column, and the contact distances were obtained by solving

$$J' = E_1'\Lambda_0H(b) - E_2'G(b) - 6E'K(b) \quad (2.8)$$

for b and then calculating a by (2.6). It will be immediately noted that the lumped linear coefficient J'

Table I: Constants of Conductance Equation

D	Λ_0	L	A	$\delta\Lambda$	a
KCl in $C_4H_8O_2-H_2O$					
78.54	149.895 \pm 0.005	173.0 \pm 8.1	-0.20 \pm 0.08	0.002	2.85
78.54	149.907 \pm 0.003	193.9 \pm 0.5	...	0.003	2.80
60.16	100.73 \pm 0.05	176 \pm 91	-0.4 \pm 1.4	0.017	3.27
60.16	100.74 \pm 0.02	202.4 \pm 2.9	...	0.012	3.19
41.46	69.13 \pm 0.04	234 \pm 48	1.2 \pm 1.3	0.011	3.78
41.46	69.09 \pm 0.01	193.7 \pm 3.0	...	0.011	3.90
CsI in $C_4H_8O_2-H_2O$					
78.54	154.20 \pm 0.05	217 \pm 90	0.50 \pm 0.82	0.018	2.41
78.54	154.17 \pm 0.02	163.4 \pm 2.6	...	0.016	2.56
60.18	99.44 \pm 0.05	192 \pm 83	-0.6 \pm 1.3	0.017	3.49
60.18	99.46 \pm 0.02	230 \pm 3	...	0.015	3.37
40.57	66.88 \pm 0.01	261 \pm 22	-0.79 \pm 0.61	0.005	4.36
40.57	66.90 \pm 0.01	289.8 \pm 1.6	...	0.005	4.28
29.79	56.46 \pm 0.03	315 \pm 27	1.9 \pm 1.2	0.007	5.09
29.79	56.42 \pm 0.01	276 \pm 3	...	0.008	5.21
Am ₃ NBuBPh ₄ in MeCN					
36.01	116.33 \pm 0.19	686 \pm 530	-7.3 \pm 8.6	0.066	5.80
36.01	116.48 \pm 0.07	1138 \pm 33	...	0.063	5.08
Am ₃ NBuBr in MeCN					
36.01	159.75 \pm 0.05	1084 \pm 201	2.9 \pm 2.2	0.018	4.20
36.01	159.67 \pm 0.02	836 \pm 13	...	0.020	4.42
Pr ₃ NMeI in MeCN					
36.01	178.30 \pm 0.07	310 \pm 278	1.9 \pm 2.7	0.016	3.72
36.01	178.25 \pm 0.02	130 \pm 11	...	0.014	3.82

is very much more precisely determined than was L ; also $\delta\Lambda_0$ and $\delta\Lambda$ in general decrease significantly. These smaller variations simply mean that the two-parameter equation (2.7b) fits the data for systems with small b values (less than about 4) better than the three-parameter equation (2.3). In other words, for high dielectric constants and/or large ions, the 1957 equation (2.1) and the 1965 equation (2.3) in its approximate form (2.7) are *indistinguishable*. The reason is obvious; for systems described by small b values, the series expansion on which (2.1) was based is a valid approximation. In principle, (2.3) is theoretically more sound, but precision of present conductometric technique is inadequate to separate the constants L and $A\Lambda_0$. (For the reason just given, our computer program contains an "IF" instruction; the data are first fitted to eq. 2.4. Then if $A < 10$, the computation is repeated, fitting the data to eq. 2.7b.)

The practical difficulty in separating the terms of the theoretical equation is clearly shown if their relative numerical values are examined. The values shown in Table II for tetrapropylammonium tetraphenylboride

(23) J. E. Lind, Jr., and R. M. Fuoss, *J. Phys. Chem.*, **65**, 999 (1961).

(24) J. E. Lind, Jr., and R. M. Fuoss, *ibid.*, **65**, 1414 (1961).

(25) C. Treiner and R. M. Fuoss, *Z. physik. Chem.*, Falkenhagen Festband, in press.

in acetonitrile²⁶ are typical. For this system, $\Lambda_0 = 128.38 \pm 0.01$, $L = 861 \pm 179$, $A = -5.0 \pm 2.0$, and $\delta\Lambda = 0.004$. Computed by (2.7b), the parameters are $\Lambda_0 = 128.41 \pm 0.01$ and $J' = 1304 \pm 11$. It will be seen that the square root term accounts for most of the change of conductance with concentration.

Table II: Conductance of Pr_4NBPh_4 in MeCN

10 ⁴ c	Λ	S term	E term	L term	A term	$\delta\Lambda$
9.449	118.83	-10.01	-0.80	0.81	0.44	0.002
7.297	119.91	-8.79	-0.65	0.63	0.35	-0.003
5.548	120.94	-7.67	-0.53	0.48	0.28	0.000
3.766	122.20	-6.32	-0.39	0.32	0.20	0.004
2.096	123.72	-4.71	-0.24	0.18	0.12	-0.002

The approximate cancellation of the E and L terms is typical for systems with small b (here equal to 2.81 with $\hat{a} = 5.54$ for the three-parameter equation and $b = 2.98$ and $\hat{a} = 5.22$ for the two-parameter). The latter characteristic, incidentally, explains why earlier purely empirical attempts to determine E , the coefficient of the $c \log c$ term, gave such uncertain results. The A term amounts at most to less than 0.5% of the total observed conductance. It is obvious, from inspection of the L and A columns, that it is very easy to rob Peter to pay Paul here because the A column also is almost linear in c .

Before considering systems in the lower range of dielectric constants where (2.1) and (2.7) no longer fit the data, we shall compare the linear coefficients of the two equations, J and J' . It will be recalled that the former appears in the 1955-1957 derivation where the series approximation for e^x was made, while the latter appears in the present development in which e^x was retained explicitly. These coefficients depend on dielectric constant in two ways: explicitly through the coefficients E_1 and E_2 and implicitly through the appearance of functions of b , which in turn varies inversely as D . In order to separate these two kinds of dependence, we shall consider the special case of equal mobilities ($\omega_1 = \omega$) and further assume Stokes' value $(6\pi\eta a)^{-1}$ for ω . The general case will not differ greatly from this special case which, of course, is much simpler to treat. Substituting $6\pi\eta\omega a = 1$ in (1.26) and using (10) to eliminate a gives

$$\beta^2\kappa^2/4b = 4E_2'/\Lambda_0 \tag{2.9}$$

Then substitution of (1.27) gives a relation between the coefficients in E

$$E_2'/E_1'\Lambda_0 = 3/2b \tag{2.10}$$

for our special case. The coefficient J' , defined in (2.7), is identified in (1.38) as

$$J' = E_1'\Lambda_0H(b) - E_2'G(b) - 6E'K(b) \tag{2.11}$$

Using (1.28) and (2.10), this becomes

$$J' = E_1'\Lambda_0[H(b) - 3G(b)/2b - 6(1 - 3/2b)K(b)] \tag{2.12}$$

$$J' \equiv E_1'\Lambda_0F_{65}(b) \tag{2.13}$$

The coefficient $J(a)$ of (2.1) is given²⁷ by

$$J(a) = 2E_1'[h(b) + 0.9074 + \ln \kappa ac^{-1/2}]\Lambda_0 + \alpha\beta_0 + 11\beta_0\alpha\kappa/12c^{1/2} - 2E_2'(1.0170 + \ln \kappa ac^{-1/2}) \tag{2.14}$$

Substituting

$$\ln \kappa ac^{-1/2} = 0.5 \ln 24E_1' - \ln b \tag{2.15}$$

which follows directly from the definitions (10) and (1.27) of b and E_1' , and combining terms, (2.14) becomes

$$J(a) = E' \ln 6E_1' + E_1'\Lambda_0F_{57}(b) \tag{2.16}$$

where

$$F_{57}(b) \equiv 3.202 + 1.213/b + 26/b^2 - 2/b^3 - 2(1 - 3/2b) \ln b \tag{2.17}$$

The term $E' \ln 6E_1'$ in (2.16) is simply the quantity which converts the transcendental term in (2.1) from the c -scale to the τ -scale and numerically makes up a large part of J which is independent of b . The consequence is that an illusory precision has been ascribed to the values of a derived from J ; actually, the percentage uncertainty in a is considerably larger than that for J . Some numerical examples will be given later; here we shall continue the discussion of functional dependence. If both the 1957 and 1965 equations are written with the transcendental term in the τ -scale, (2.1) and (2.7) become, respectively

$$\Lambda = \Lambda_0 - Sc^{1/2} + E'c \ln \tau^2 + E_1'\Lambda_0F_{57}(b) \cdot c \tag{2.18}$$

and

$$\Lambda = \Lambda_0 - Sc^{1/2} + E'c \ln \tau^2 + E_1'\Lambda_0F_{65}(b) \cdot c \tag{2.19}$$

The two equations now are identical except for the coefficients of the linear terms. The direct dependence of the latter on dielectric constant is immediately obvious: both go inversely as D^3 , as seen by inspection of the definition of E_1' (1.27). The behavior of the b -

(26) D. S. Berns and R. M. Fuoss, *J. Am. Chem. Soc.*, **82**, 5585 (1960).

(27) See ref. 10, XV(34), (35), (36), and (38).

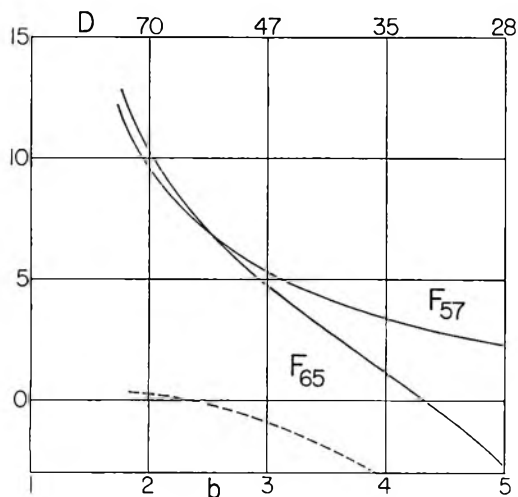


Figure 3. Comparison of 1957 and 1965 functions in the linear coefficient of the conductance equation. (Note location of zero ordinate.)

dependent part is shown in Figure 3, where F_{65} and F_{57} are plotted against b . The D scale shown at the top of the figure is for $\bar{a} = 4.00$. For the approximate range $80 > D > 40$, the 1957 function is a very good approximation for the explicit 1965 function; presumably, the agreement is good also for $D > 80$ because the series approximation of the Boltzmann factor improves as D increases. But for $D < 40$, the two functions diverge rapidly as the exponential-like function $K(b)$ in F_{65} takes control. Since F_{57} is much simpler than F_{65} , we shall eventually replace F_{65} by F_{57} as an adequate approximation.

This study of the two equations suggests the method of analyzing conductance data for solvents of lower dielectric constant where ion association cannot be neglected. The explicit equation (2.3), of which (2.7) is a limiting form, fits the data over a somewhat wider range toward lower dielectric constants than (2.1), but, below $D \approx 25$, it too starts to show systematic deviations. In the range where the two functions of Figure 3 closely approximate each other, the contribution of the $K(b)$ term, shown by the dotted line, is *practically negligible*. (It is therefore not surprising that the A values for the three-parameter equation in Table I were so uncertain.) In other words, the linear coefficients of the 1957 and of the 1965 equations are nearly identical if the terms deriving from the negative exponential integrals are expressed as $Ec \log \tau^2$, in the range where the concentration of ion pairs is negligible. The significant difference between the two derivations is the appearance of the $A\Lambda_0 c f^2$ term of (2.3), which, as has already been emphasized, is a term obtained by setting $r = a$ in an integral,

i.e., a quantity clearly deriving from contact pairs. The logical extension of (2.3) to solvents of lower dielectric constants therefore is (2.4), where A is now to be identified with an association constant K_A , preferably in the explicit form⁷

$$K_A = (4\pi Na^3/3000)e^b = 2.523 \times 10^{-3} \bar{a}^3 e^b \quad (2.20)$$

$$= 2.523 \times 10^{21} \beta^3 (e^b/b^3)$$

rather than in the approximate Bjerrum form which is proportional to the function $K(b)$ defined in (1.43). The coefficient L of (2.4) is, as we have just seen, closely approximated by a much simpler function similar to the special function F_{57} . After considering some examples at lower dielectric constant by the explicit functions $H(b)$, $G(b)$, and $K(b)$ which appear implicitly in (2.4), we shall derive a general formula to replace F_{65} .

As the dielectric constant is decreased, the coefficient A increases, both theoretically and experimentally. For a short range, (2.3) instead of (2.7b) may be used; the A and L terms can be separated. However, much above b values of about 4, the deviations between calculated and observed values of conductance become systematic and steadily greater as b increases. The A term now describes a loss in conductance due to ions in contact, *i.e.*, in nonconducting pairs; it is evident that other higher order effects of ion pairs must also be considered in the range of lower dielectric constants. Contact pairs should not be counted as atmosphere ions in calculating the relaxation field nor the electrophoresis, nor in any of the other long-range effects. By writing $c\gamma$ for the fraction of solute present as free ions, (2.3) is transformed into (2.4), which has the same functional form as (2.2). In Table III are summarized the results of the calculations for potassium chloride²³ and for cesium iodide²⁴ in the mixtures of lower dielectric constant and for tetramethylammonium tetraphenylboride in acetonitrile-carbon tetrachloride mixtures.²⁶ Since $\delta\Lambda$ is uniformly small and of the order of the experimental error, we conclude that (2.4) reproduces the data as far as concentration dependence of Λ is concerned and that it may be used to extrapolate for Λ_0 .

Now consider the constants A and L . Recall that, for small b , they could not both be determined with precision; in fact, for b around 2, A is completely uncertain. However, as seen in Table III, as b increases (D decreases), the constants become separable in the intermediate range, and, considering their contributions to total conductance (see Table IV later), are fixed with fair precision by the data. Then as b increases further, the A term becomes so large that the L

Table III: Constants of Conductance Equation

D	Λ_0	L	A	$\delta\Lambda$	\hat{a}
KCl in $C_4H_9O_2-H_2O$					
30.26	56.45 ± 0.03	370 ± 33	16.6 ± 1.4	0.007	4.00
25.84	52.32 ± 0.02	379 ± 23	32.4 ± 1.3	0.005	4.38
19.32	46.27 ± 0.04	373 ± 42	159 ± 4	0.009	4.86
15.37	42.51 ± 0.08	220 ± 61	460 ± 12	0.010	5.47
12.74	39.55 ± 0.11	-433 ± 108	1702 ± 32	0.017	5.61
CsI in $C_4H_9O_2-H_2O$					
24.44	52.26 ± 0.03	430 ± 37	19.6 ± 2.2	0.009	5.28
18.68	48.22 ± 0.07	349 ± 67	88 ± 7	0.017	5.89
15.29	45.47 ± 0.11	44 ± 85	313 ± 14	0.021	6.10
12.81	41.82 ± 0.03	-869 ± 22	788 ± 6	0.005	6.59
Me_4NBPh_4 in $MeCN-CCl_4$					
36.01	152.32 ± 0.07	1645 ± 1018	3.6 ± 9.6	0.026	4.74
22.32	114.85 ± 0.07	2886 ± 596	25.8 ± 10.0	0.021	6.15
17.45	99.32 ± 0.04	2698 ± 259	58 ± 6	0.010	7.26
13.06	83.63 ± 0.05	1997 ± 108	365 ± 7	0.009	7.71
10.68	74.46 ± 0.10	483 ± 271	1431 ± 27	0.016	7.81

term becomes relatively invisible, as shown by the increasing value of $\delta L/L$. The precision in A increases as b increases. We note that L goes through a maximum and eventually becomes *negative*. According to theory, L should asymptotically approach $4E_1\Lambda_0$ for large b which is always positive. We shall comment later on this discrepancy between theory and experiment. Finally, a systematically increases as D decreases, both for the aqueous and the nonaqueous systems, just as it did in the earlier analysis. We shall also return to this point later.

In order to demonstrate the shift in significance of the various terms in the conductance equation as dielectric constant is decreased, the data of Table IV are presented. They give the conductance of tetramethylammonium tetraphenylboride in acetonitrile and in acetonitrile-carbon tetrachloride mixtures of dielectric constants 17.45 and 10.68. The parameters are: acetonitrile, $\Lambda_0 = 152.32 \pm 0.07$, $L = 1645 \pm 1018$, $A = 3.6 \pm 9.6$, $b = 3.28$, $\hat{a} = 4.74$; mixture 1, $D = 17.45$, $\Lambda_0 = 99.32 \pm 0.04$, $L = 2698 \pm 259$, $A = 58.4 \pm 6.3$, $b = 4.42$, $\hat{a} = 7.26$; mixture 2, $D = 10.68$, $\Lambda_0 = 74.46 \pm 0.10$, $L = 483 \pm 271$, $A = 1431 \pm 27$, $b = 6.72$, $\hat{a} = 7.81$. The square root term is always a large one, and the E term is never negligible. The interesting detail is the relative values of the L and A terms as b increases: the shift from L dominant to A dominant as the dielectric constant decreases is evident. The pattern shown by the specific examples of Table IV is general and leads to a significant conclusion (which is intuitively correct, of course): no useful information can be obtained from the ion-pair term at high dielectric constants nor from the linear term at low.

Table IV: Conductance of Me_4NBPh_4

10^4c	Λ	S term	E term	L term	A term	$\delta\Lambda$
Acetonitrile						
10.308	141.51	-11.00	-1.10	1.69	-0.41	0.006
8.198	142.59	-9.81	-0.92	1.35	-0.34	-0.006
7.094	143.85	-8.46	-0.73	1.00	-0.26	-0.019
4.129	145.34	-6.97	-0.54	0.68	-0.19	0.028
2.083	147.30	-4.95	-0.31	0.34	-0.10	-0.010
Mixture 1						
6.812	84.87	-11.19	-2.91	1.80	-1.85	0.002
5.268	86.53	-10.12	-2.49	1.40	-1.57	-0.006
3.910	88.30	-8.74	-2.05	1.04	-1.28	0.010
2.511	90.53	-7.01	-1.51	0.67	-0.92	-0.007
1.532	92.56	-5.49	-1.06	0.41	-0.62	0.002
Mixture 2						
6.017	46.57	-12.69	-3.92	0.23	-11.51	-0.009
4.764	48.77	-11.41	-3.67	0.19	-10.81	0.012
3.797	50.90	-10.29	-3.38	0.15	-10.04	0.005
2.680	54.10	-8.78	-2.91	0.11	-8.77	-0.016
1.530	58.90	-6.77	-2.17	0.07	-6.69	0.005

So far, the $B\tau^3$ term ($\sim c^{3/2}$) of (1.38) has been neglected. Here, B is defined by the equation

$$B = (2b - 3)\Lambda_0/b^2$$

Its origin is in the next term after $\ln(n\kappa a)$ in the expansion of the negative exponential functions which appear in the relaxation and velocity fields. Its effect was investigated for a number of systems, by the following method. First, the data were analyzed by means of eq. 2.7 for $A < 10$ and by (2.4) for $A > 10$. Using the values of b so obtained, we calculated

$$\Delta\Lambda_{3/2} = (2b - 3)\Lambda_0\tau^3\gamma^{3/2}/b^2 \tag{2.21}$$

and

$$\Lambda(\text{cor.}) = \Lambda(\text{obsd.}) + \Delta\Lambda_{3/2} \tag{2.22}$$

Then the values of $\Lambda(\text{cor.})$, which are the observed conductances corrected to first approximation for the $c^{3/2}$ term, were fed back into the computer, along with the original concentrations, and the values of Λ_0 , L , and A which would reproduce $\Lambda(\text{cor.})$ as a function of concentration were obtained. The net effects were as follows: (1) $\delta\Lambda$ was slightly decreased, indicating a better fit to the data; (2) L became a monotone-increasing function of D^{-1} (instead of going through a maximum) but did not increase as fast as the theoretical $4E_1'\Lambda_0$; (3) the values of A were increased by about 50% for the systems with dielectric constant below about 20; and (4) the spread of \hat{a} values for a given system was decreased, as shown in Table V for some tetraphenylborides in acetonitrile-carbon tetra-

chloride mixtures.²⁶ The columns headed \bar{a} correspond to values obtained neglecting $B\tau^3$; the values obtained by using (2.22) are in the columns headed $\bar{a}_{3/2}$.

Table V: Effect of $B\tau^3$ Term on a Values

D	\bar{a}	$\bar{a}_{3/2}$	D	\bar{a}	$\bar{a}_{3/2}$
Me ₄ NBPh ₄			Pr ₄ NBPh ₄		
36.01	4.74	5.83	36.01	5.54	5.51
22.32	6.15	6.05	19.46	8.67	8.41
17.45	7.26	7.08	16.13	9.16	8.36
13.06	7.71	7.18	12.31	10.36	8.90
10.68	7.81	7.37	9.80	10.11	8.61
Et ₄ NBPh ₄			Bu ₄ NBPh ₄		
36.01	5.78	5.76	36.01	6.30	6.27
20.60	7.30	7.07	19.87	8.57	8.28
17.05	8.02	7.52	17.18	9.09	8.65
14.21	7.78	7.27	13.92	9.66	8.97
12.14	8.89	7.87	11.16	10.43	9.38

While inclusion of the $c^{3/2}$ term is indeed an improvement, the benefits are marginal. Considering the extra work involved in retaining it (usually much more than double the computation time, due to iteration until b converges to a constant value), we propose to neglect it in the analysis of conductance data and allow A and L to absorb the errors. There already has been neglected a multitude of $c^{3/2}$ terms of unknown magnitude and sign; in order to be consistent, it now seems preferable to discard them all and restrict the range of application of the equations to concentrations where the unknown $c^{3/2}$ terms are negligible. The criterion is $\delta\Lambda$, the mean deviation between calculated and observed conductances. When this becomes significantly greater than the known experimental error, the functional form of (2.7) or of (2.4) no longer fits the data. The presumption is that higher terms than those retained have become significant.

We return to a consideration of the coefficient of the linear term. According to (1.54), it should approach approximately $4E_1'\Lambda_0$ as b increases because $H(b)$ levels off at about 4, while $E_2'G(b)$ becomes very small compared to $E_1'\Lambda_0$. Experimentally, as was shown in Table III, L goes through a maximum and becomes negative for small dielectric constants. Possibly part of the terms which we have collected in L should be in A , or perhaps the approximations that resulted in $K(b)$ instead of $K'(b)$ also affect L . In any case, the linear coefficient derived from $J(a)$ for the case of unassociated electrolytes does show the right behavior qualitatively. Instead of the special case treated by

eq. 2.17, consider the general case (2.14). Again substituting the identity (2.15), we find

$$J(a) = E' \ln 6E_1' + L_1 + L_2(b) \quad (2.23)$$

where

$$L_1 = 3.202E_1'\Lambda_0 - 3.420E_2' + \alpha\beta_0 \quad (2.24)$$

and

$$L_2(b) = 2E_1'\Lambda_0 h(b) + 44E_2'/3b - 2E' \ln b \quad (2.25)$$

with

$$h(b) = (2b^2 + 2b - 1)/b^3 \quad (2.26)$$

Both L_1 and L_2 depend on dielectric constant through E_1' and E_2' ; the only part of J , however, which depends on b is the term $L_2(b)$. It is from this part of the coefficient of the linear term that ion size (a_j) is determined. It is easy to see that

$$L' = L_1 + L_2(b) \quad (2.27)$$

will go through a maximum and become negative. For lower dielectric constants, the terms in E_2' become small and $h(b) \sim 2/b$; the dominant part of L' is given by

$$L' \sim 2E_1'\Lambda_0(1.601 - \ln b) \quad (2.28)$$

which goes through zero at $b = 4.96$ and is negative for larger values. In Figure 4, the solid curves are L' for the dioxane-water mixtures which were used as solvents in the work on potassium chloride,²³ calculated for $\bar{a} = 3, 4,$ and 5 . The curve through the circles shows the experimental L values of Tables I and III for potassium chloride. The general patterns of the calculated L' curves and of the observed L curve are the same: flat over the range of high dielectric constants, a maximum, and then a rapid drop (E_1' varies

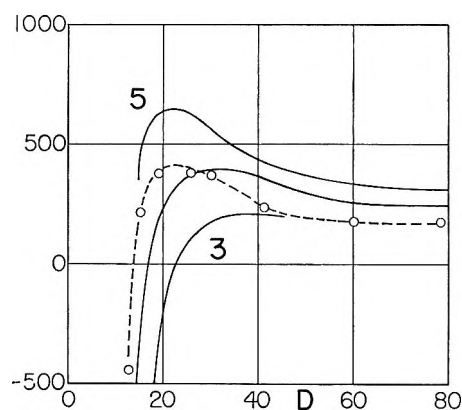


Figure 4. Comparison of empirical and theoretical linear coefficients for various contact distances.

as D^{-3}) to negative values at low dielectric constants. The value $\hat{a} = 3$ fits the data quite well in the high range of D ; then as D decreases, larger and larger values of \hat{a} are needed to match the experimental L values.

The conductance equation is a two-parameter equation because both L and K_A depend on b ; *i.e.*, $\Lambda = \Lambda(c; \Lambda_0, b)$. A program was set up to solve it for these two parameters, but the standard deviation for $\delta\Lambda$, the difference between calculated and observed values, was usually significantly greater than the standard deviation for results calculated by the three-parameter equation $\Lambda = \Lambda(c; \Lambda_0, L, K_A)$. This means that different values of b (or \hat{a} , of course) may be required to give the coefficients of the c term and of the cf^2 term which will best fit the data. Over the intermediate range of D , the agreement was good, as shown by Table VI, where $\hat{a}(L)$ is the value derived from the linear coefficient and $\hat{a}(K_A)$ is the value from the ion-pair term. The last column gives the percentage contribution to the total conductance of the linear term Lc (or $Lc\gamma$) at the highest concentration of the corresponding run; it is obvious that data of very high precision would be needed in order to determine L . (At the higher dielectric constants, the data permit determination of only Λ_0 and L , of course.)

Table VI: Variation of Contact Distance

D	$\hat{a}(L)$	$\hat{a}(K_A)$	%(L)
KCl in $C_4H_8O_2-H_2O$			
78.54	3.20	...	1.37
60.16	3.24	...	1.54
41.46	2.91	...	1.71
30.26	3.94	3.99	2.72
25.84	3.98	4.22	2.73
19.32	4.41	4.41	2.30
15.37	4.70	5.01	1.24
12.74	5.21	5.18	-2.08
CsI in $C_4H_8O_2-H_2O$			
78.54	3.49	...	1.40
60.18	3.65	...	1.83
40.57	3.73	...	2.36
29.79	3.46	...	2.34
24.44	4.18	...	2.94
18.68	4.45	5.78	2.19
15.29	4.76	5.58	0.25
12.81	4.84	6.02	-4.50

The increase of a with decreasing D can be interpreted in several ways. One obvious way is to assume increasing solvation of the ions as the fraction of non-polar component in the mixed solvent is increased.

Alternatively, one could postulate^{28,29} that the more polar component concentrates in the volume around the ions, so that the effective dielectric constant to be used in computing interionic forces is larger than the macroscopic value. In this way, one could retain a fixed ion size for a given system. Enough specific ion-solvent interactions have been observed to suggest that both solvation and local dielectric disproportionation could be involved. Certainly, the next problem for theoretical study is the effects of short-range forces. Finally, we realize that there are other sources of linear terms in the conductance equation besides those summarized by (2.23) and the short-range effects just mentioned. The solution viscosity contains a term proportional to concentration which carries over into the conductance. The volume of the ions, as suggested by Stokes,³⁰ decreases the space available in the solution for ionic motion and so decreases conductance. The Debye-Falkenhagen $c^{1/2}$ term in the dielectric constant will produce a term linear in c in the conductance through the appearance of D in the coefficient S . The fact that an ion pair tends to orient parallel to the field means that it will be struck more often by an ion of the sign which will increase conductance when the resulting three-ion cluster dissociates; the triple-ion clusters themselves give an increase in conductance proportional in first approximation to concentration. There undoubtedly are other effects which are also absorbed in the experimental coefficient. All of these will cause the calculated a to vary. It must, of course, be kept in mind that the real solution is not made up of charged spheres in a continuum; the most theory can achieve is to predict a one to one correspondence between the physical system which is too complex to be treated and a simplified model which is amenable to mathematical description. Including the effects of short-range forces and so on is in last analysis a refinement of the model.

3. Conclusion and Summary

The conductance equation (2.3) which was derived from the consideration of the potential of total directed force is an improvement over the earlier equation (2.1) as far as functional form is concerned. In attempting to include the effects of both long- and short-range interionic forces in one comprehensive treatment, however, comparison with experiment shows that precision in detail in the coefficients has been lost. The coef-

(28) J. B. Hyne, *J. Am. Chem. Soc.*, **85**, 304 (1963).

(29) Y. H. Inami, H. K. Bcdenseh, and J. B. Ramsey, *ibid.*, **83**, 4745 (1961).

(30) B. J. Steel, J. M. Stokes, and R. H. Stokes, *J. Phys. Chem.*, **62**, 1514 (1958).

ficients L and A are both approximations, the first valid for high dielectric constants and the second for low, to the quantities $(J - E \log 6E_1')$ and K_A , both of which can best be computed separately.^{5,7} The long-range interactions between ions not in contact are best described by (2.1); over the range of dielectric constant where the approximations made in its derivation ($e^\xi \approx 1 + \xi + \xi^2/2$), both (2.1) and (2.3) agree numerically, as shown in Figure 3. The short-range interactions which create ion pairs are best described by (2.20); for smaller values of dielectric constant, the coefficient $6E_1'K(b)$ approaches K_A , and the values of a obtained from equating the experimental value of the coefficient of the c^2 term to either differ at most by about 15% in the range where ion pairs might be expected to have physical stability, *i.e.*, where their potential energy ϵ^2/aD is significantly greater than kT . To summarize, observed conductance curves can be described by the equation

$$\Lambda = \Lambda_0 - Sc^{1/2}\gamma^{1/2} + Ec\gamma \log(6E_1'c\gamma) + Lc\gamma - K_A c\gamma^2 \Lambda \quad (3.1)$$

where L is given by

$$L = L_1 + L_2(b) \quad (3.2)$$

and K_A by (2.20). The two terms of L are given by (2.24) and (2.25).

In order to obtain the constants Λ_0 , L , and K_A from the data, the following sequence is convenient for programming. A preliminary value of Λ_0 is obtained by graphical extrapolation, and estimates (which need not be at all accurate) of L and K_A are made. As zeroth approximation, γ is set equal to the conductance ratio Λ/Λ_0 in the square root term, giving as a first approximation

$$\gamma_1 = \Lambda/[\Lambda_0 - S(c\Lambda/\Lambda_0)^{1/2}] \quad (3.3)$$

Since the linear and logarithmic terms usually just about cancel each other, (3.3) is already a fair approximation. (If the estimated Λ_0 is too small, the denominator of 3.3 can become negative, and then (3.4), which calls for the square root of $c\gamma_1$, would set

the computer off on an infinite loop. To avoid this trap, an IF instruction terminates the computation, should γ_1 come out negative.) Then as next approximation

$$\gamma_2 = \Lambda/[\Lambda_0 - Sc^{1/2}\gamma_1^{1/2} + Ec\gamma_1 \log(6E_1'c\gamma_1) + Lc\gamma_1] \quad (3.4)$$

This process is iterated until the condition

$$|\gamma_n - \gamma_{n-1}| < 0.00005 \quad (3.5)$$

is satisfied. Then, if the converged value of γ is less than unity, the data are treated by the conventional least-squares program to obtain Λ_0 , L , and K_A . From both L and K_A , values of b are obtained by solving (2.28) and (2.20). To avoid possible loops (and wasted machine time), the solution of $L_2(b)$ for b is terminated if b becomes less than 1 (which would correspond to absurdly large d values). The function e^b/b^3 has a minimum at $b = 3$; to avoid presenting the machine with the dilemma of a double-valued function and the probable attempt to divide by zero, the calculation of b from K_A is stopped if b becomes less than 3.05. The value at the minimum of e^b/b^3 is $e^3/27 \approx 0.75$. If the corresponding experimental value from K_A is less than 0.75, the machine is instructed not to attempt a solution. Finally, the calculation is terminated if b exceeds 25 (which would correspond to absurdly small d values). For the range of dielectric constants where both L and K_A can be determined with relatively good precision, the values of d from L_2 and from K_A agree within about 10%; for high dielectric constants, the value from K_A becomes unreliable, while for low dielectric constants, the value from L_2 becomes uncertain, as might be expected. If (3.4) converges to a value greater than unity, γ is set equal to 1, and the solution of the three-parameter equation is continued. Then the data are automatically processed by the two-parameter equation

$$\Lambda = \Lambda_0 - Sc^{1/2} + Ec \log(6E_1'c) + Lc \quad (3.6)$$

Also, if K_A from the three-parameter equation (3.1) is less than 10, the data are analyzed by means of (3.6).

The Effect of Pressure on the Dissociation of Manganese Sulfate

Ion Pairs in Water*

by F. H. Fisher and D. F. Davis

University of California, San Diego Marine Physical Laboratory of the Scripps Institution of Oceanography, San Diego 52, California (Received February 1, 1965)

Conductivity at 25° of aqueous solutions of MnSO_4 and MnCl_2 has been measured as a function of pressure up to 2000 atm. for concentrations from 0.0005 to 0.02 *M*. The effect of pressure on the molal dissociation constant of MnSO_4 was calculated with the conductance equation used by Davies, Otter, and Prue. Based on a two-state dissociation model, the difference of partial molal volumes between products and reactants, $\Delta \bar{V}^0$, was found to be in agreement with the value calculated on the basis of theory by Fuoss, namely -7.4 cc./mole. Although MnSO_4 and MgSO_4 solutions show reasonable agreement in $\Delta \bar{V}^0$ at atmospheric pressure at the lower concentrations, small differences in the pressure dependence of the equilibrium constant are observed which may be related to the marked differences in acoustic absorption exhibited by these salts.

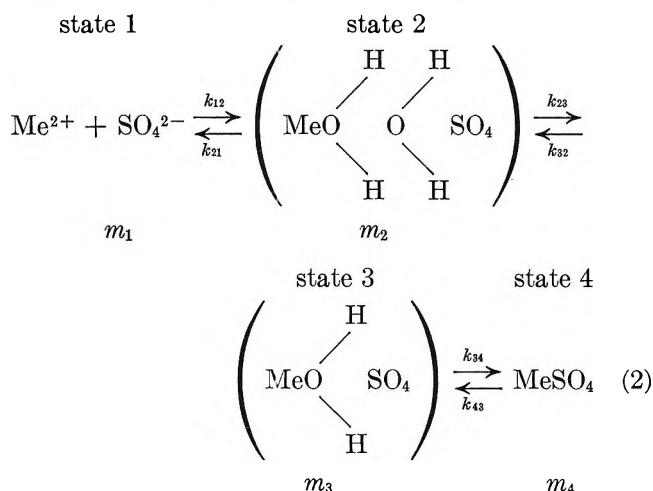
The marked differences in the acoustic absorption exhibited by aqueous solutions of MgSO_4 and MnSO_4 ¹ are in sharp contrast to the general similarities between the thermodynamic properties such as equilibrium constants and activity coefficients.

Eigen and Tamm² have proposed a four-state dissociation model to explain the acoustic absorption observed in MgSO_4 aqueous solutions at atmospheric pressure as a function of frequency and concentration. They assign partial molal volume changes and equilibrium constants which lead to a prediction of the pressure dependence of the acoustic absorption as well as electrical conductivity. The predicted behavior as a function of pressure from the four-state model is consistent with acoustic³ as well as conductivity data.⁴ Measurements of conductivity as a function of pressure for MgSO_4 are also in agreement with the theory of Fuoss for the formation of ion pairs as was pointed out by Hamann, Pearce, and Strauss.⁵ The same behavior should be observed for any other 2-2 sulfate on the basis of theory by Fuoss, that is, in the equation

$$\left(\frac{\partial \ln K_m}{\partial p}\right)_{T,m} = -\frac{\Delta \bar{V}^0}{RT} \quad (1)$$

where K_m is the molal equilibrium constant, $\Delta \bar{V}^0$ should be the same for all salts of a given class.

The relation of K_m to the four-state model is seen from eq. 2 where the free hydrated ions in state 1 associate and approach each other more closely as successive water molecules are removed from between the ions until they are in contact with one another. Only state 1 contributes to electrical conduction.



* This paper represents results of research sponsored by the Office of Naval Research.

(1) G. Kurtze and K. Tamm, *Acoustica*, **3**, 33 (1953).

(2) (a) M. Eigen and K. Tamm, *Z. Elektrochem.*, **66**, 93 (1962); (b) K. Tamm, "Handbuch der Physik," Vol. XI, Springer-Verlag,

The conventional molal equilibrium constant is

$$K_m = \frac{m_1^2 \pi^f}{m_2 + m_3 + m_4} = \frac{m \gamma_{\pm}^2}{1 - \alpha} \quad (3)$$

where m is the molality of the salt, m_i is the molal concentration of the respective states, α is the degree of dissociation, and $\gamma_{\pm}^2 = \alpha^2 f_{\pm}^2 = \alpha^2 \pi^f$.

Eigen and Tamm² proposed two sets of parameters for the four-state model within which they can account for the acoustic effects at atmospheric pressure. The accuracy of their values of equilibrium constants for the steps in eq. 2 are claimed to be within $\pm 50\%$ and the partial molal volumes to be within $\pm 20\%$. Work on the effect of pressure on sound absorption and electrical conductivity in MgSO_4 solutions favors one of the sets of parameters

$$K_{12} = 0.04 = \frac{m_1^2 \pi^f}{m_2} = \frac{k_{21}}{k_{12}}, \Delta V_{12}^0 = 0 \quad (4)$$

$$K_{23} = 1 = \frac{m_2}{m_3} = \frac{k_{32}}{k_{23}}, \Delta V_{23} = -18 \text{ cc./mole} \quad (5)$$

$$K_{34} = 9 = \frac{m_3}{m_4} = \frac{k_{43}}{k_{34}}, \Delta V_{34} = -3 \text{ cc./mole} \quad (6)$$

From these equations it is seen that

$$K_m = \frac{K_{12} K_{23} K_{34}}{1 + K_{34} + K_{23} K_{34}} \quad (7)$$

Decided differences between MgSO_4 and MnSO_4 multistate models exist; Atkinson and Kor⁶ have published values for the equilibrium constants but have assigned no values for the partial molal volume differences. Their values are $K_{12} = 0.0192$, $K_{23} = 2.8$, and $K_{34} = 0.29$. Until ΔV_{ij} values are assigned, a prediction of the pressure dependence of electrical conductivity cannot be made.

The observed acoustic effects are attributed by Eigen and Tamm to transitions between different sorts of intermediate hydrate complexes or ion pairs. Hamann, Pearce, and Strauss point out that the small value of $-\Delta \bar{V}^0$ (less than half the partial molal volume of water) suggests that the ions are almost fully hydrated in the ion-pair state and that an ion pair contains at least one water molecule between the ions. For MgSO_4 there appears to be no conflict between the multistate theory of Eigen and Tamm and the Fuoss theory, for both lead to essentially the same value of $\Delta \bar{V}^0$ although the interpretation of $\Delta \bar{V}^0$ in the Fuoss theory does not consider different species of ion pairs. In the multistate theory $\Delta \bar{V}^0$ is a composite of the volume changes and the equilibrium constants associated with the different species of ion pairs.⁴

Any differences in multistate models to explain sound absorption for MnSO_4 and MgSO_4 solutions might show up in the pressure dependence of the equilibrium constant of these salts.

Experimental

Measurements of electrical conductivity of aqueous solutions of MnSO_4 were made in essentially the same manner as described for MgSO_4 solutions.⁷ The results were obtained using the same equations as for MgSO_4 .

The ratios of equivalent conductivity Λ_p/Λ_1 for MnSO_4 , K_2SO_4 , MnCl_2 , and KCl as a function of concentration are shown in Table I. The equivalent conductivity Λ_p of MnSO_4 is shown in Table II. The degree of association ($1 - \alpha$) and molal dissociation constant K_m are shown in Tables III and IV.

Table I: Λ_p/Λ_1 for Aqueous Solutions at 25°

	$C \times 10^{4a}$	$P, \text{ atm.}$			
		500	1000	1500	2000
MnSO_4	5	1.021	1.034	1.034	1.028
	10	1.027	1.042	1.047	1.043
	20	1.036	1.057	1.065	1.066
	100	1.059	1.098	1.124	1.136
	200	1.068	1.118	1.150	1.169
K_2SO_4	5	1.010	1.011	1.006	0.995
	20	1.010	1.012	1.008	0.998
	200	1.016	1.025	1.025	1.017
MnCl_2	5	1.015	1.021	1.016	1.004
	20	1.015	1.020	1.015	1.005
	200	1.020	1.030	1.023	1.019
KCl	5	1.012	1.015	1.009	0.996
	10	1.011	1.015	1.008	0.996
	20	1.012	1.015	1.009	0.998
	100	1.012	1.015	1.009	0.998
	200	1.013	1.016	1.010	0.999

^a C is atmospheric pressure concentration in moles/liter.

In contrast to the $\Delta \bar{V}^0$ values for MgSO_4 which were obtained with a straight line to fit to $\log K_m$ vs. pressure, the MnSO_4 data clearly showed a quadratic behavior. Accordingly, $\Delta \bar{V}^0$ is a function of pressure, and values are listed for $\Delta \bar{V}^0$ at atmospheric pressure and 2000 atm. in Table IV.

Berlin, 1961, p. 202; (c) K. Tamm, *Scuola Internazionale di Fisica, Enrico Fermi, XXVII, Corso, 1962, 177-222*, in English.

(3) F. H. Fisher, to be submitted to *J. Acoust. Soc. Am.*

(4) F. H. Fisher, *J. Phys. Chem.*, **69**, 695 (1965).

(5) S. D. Hamann, P. J. Pearce, and W. Strauss, *ibid.*, **68**, 375 (1964).

(6) G. Atkinson and S. K. Kor, *ibid.*, **69**, 128 (1965).

(7) F. H. Fisher, *ibid.*, **66**, 1607 (1962).

Table II: Δ_p for Aqueous $MnSO_4$ Solutions at 25°

$C \times 10^{4a}$	$P, \text{ atm.}$				
	1	500	1000	1500	2000
0	133.2 ^b	135.0	135.3	134.5	133.0
5	116.3 ^b	118.7	120.3	120.3	119.6
10	108.7 ^b	111.6	113.3	113.8	113.4
20	99.7 ^b	103.3	105.4	106.2	106.3
100	75.2 ^c	79.6	82.6	84.5	85.4
200	65.9 ^c	70.4	73.7	75.8	77.0

^a C is atmospheric pressure concentration in moles/liter.^b C. J. Hallada and G. Atkinson, *J. Am. Chem. Soc.*, **83**, 3759 (1961). ^c Measured this experiment.**Table III:** Degree of Association ($1 - \alpha$) for Aqueous $MnSO_4$ at 25°

$C \times 10^{4a}$	$P, \text{ atm.}$				
	1	500	1000	1500	2000
5	0.070	0.065	0.055	0.050	0.046
10	0.115	0.105	0.094	0.085	0.079
20	0.172	0.155	0.140	0.129	0.119
100	0.345	0.316	0.292	0.271	0.255
200	0.415	0.383	0.355	0.332	0.314

^a C is atmospheric pressure concentration in moles/liter.**Table IV:** Molal Dissociation Constant (K_m) and $\Delta \bar{V}^0$ for Aqueous $MnSO_4$ at 25°

$P, \text{ atm.}$	$C, \text{ atm. press. concn., } M$				
	0.0005	0.001	0.002	0.01	0.02
1	0.0044	0.0044	0.0046	0.0052	0.0060
500	0.0048	0.0050	0.0053	0.0063	0.0073
1000	0.0059	0.0057	0.0062	0.0073	0.0086
1500	0.0066	0.0065	0.0069	0.0084	0.0099
2000	0.0073	0.0072	0.0077	0.0094	0.0111

$P, \text{ atm.}$	$\Delta \bar{V}^0, \text{ cc./mole}^a$				
	1	500	1000	1500	2000
1	-7.4	-7.1	-8.0	-9.3	-10.0
2000	-5.3	-5.0	-4.8	-5.0	-5.0

^a $\Delta \bar{V}^0$ was calculated by a least-squares fit of $\log K$ to a quadratic curve.**Table V:** Comparison of $K_m(P = 2000)/K_m(P = 1)$ for $MgSO_4$ and $MnSO_4$ Aqueous Solutions at 25°

C, M	$MgSO_4$	$MnSO_4$
0.0005	1.9	1.7
0.001	1.8	1.6
0.002	1.7	1.7
0.01	1.8	1.8
0.02	1.7	1.9

It is seen that at atmospheric pressure the value of $\Delta \bar{V}^0$, as concentration decreases, approaches that predicted from the Fuoss theory, namely, -7.4 cc./mole. There appears to be a concentration dependence of $\Delta \bar{V}^0$ at atmospheric pressure but not at 2000 atm.

A comparison in Table V of the ratios of the equilibrium constants at 2000 and 1 atm. indicates that a

Table VI: Comparison of $\Delta \bar{V}^0$ for $MgSO_4$ and $MnSO_4$ Aqueous Solutions at 25° and 1 Atm.

C, M	$\Delta \bar{V}^0, \text{ cc./mole}$	
	$MgSO_4$	$MnSO_4$
0.0005	-8.5	-7.4
0.001	-7.0	-7.1
0.002	-7.0	-8.0
0.01	-7.3	-9.3
0.02	-6.9	-10.0

Table VII: Cell Constants^a

Cell constants at atm. press.		Press. dependence of cell constant	
Concn., M	L_1	$P, \text{ atm.}$	L^*_p
0.0005	0.808	500	0.991
0.001	0.811	1000	0.986
0.002	0.812	1500	0.982
0.01	0.824	2000	0.979
0.02	0.829		

^a To find cell constant L_p at pressure P multiply atmospheric pressure value L_1 by L^*_p .**Table VIII:** Copy of Original Conductivity Data Measured for Electrolytes at 25° in Aqueous Solutions (Teflon Cell without Glass Bar)

	$P, \text{ atm.}$					
	1	500	1000	1500	2000	1 ^a
0.02 M KCl, mmhos	3.338	3.484	3.582	3.639	3.670	3.322
$MnSO_4$	3.118	3.436	3.681	3.868	4.008	3.104
K_2SO_4	5.769	6.046	6.245	6.381	6.456	5.742
$MnCl_2$	4.941	5.197	5.374	5.482	5.539	4.934
0.01 M KCl, mmhos	1.715	1.790	1.840	1.871	1.886	1.709
$MnSO_4$	1.812	1.977	2.101	2.196	2.264	1.802
0.002 M KCl, μ mhos	359.7	375.0	385.4	391.6	394.8	358.7
$MnSO_4$	486.7	519.9	543.8	560.3	571.5	484.5
K_2SO_4	684.4	712.6	732.3	744.6	751.4	681.2
$MnCl_2$	575.6	602.6	620.3	631.5	637.1	573.2
0.001 M KCl, μ mhos	181.8	189.9	195.0	198.2	199.9	181.3
$MnSO_4$	267.5	283.4	295.0	302.6	307.6	266.5
0.0005 M KCl, μ mhos	92.0	96.1	99.0	100.4	101.4	91.3
$MnSO_4$	144.2	152.0	157.9	161.5	163.8	144.0
K_2SO_4	181.8	189.5	194.5	197.8	199.6	181.3
$MnCl_2$	153.4	160.7	165.7	168.8	170.3	152.9
Water, μ mhos	0.5	0.7	0.9	1.1	1.3	0.8
Series lead resistance, ohms	0.134	0.134	0.134	0.134	0.134	

^a The readings in this column were obtained the day after the pressure run was made.

different trend as a function of concentration exists between MgSO_4 and MnSO_4 solutions.

At atmospheric pressure and at the lower concentrations the values of $\Delta \bar{V}^0$ for both MnSO_4 and MgSO_4 agree with the value predicted by the Fuoss theory. For MnSO_4 there appears to be a dependence of $\Delta \bar{V}^0$ on pressure which was not observed for MgSO_4 . Furthermore, there is a more noticeable concentration dependence of $\Delta \bar{V}^0$ at atmospheric pressure for MnSO_4 and in the opposite direction to that exhibited by Mg -

SO_4 , as shown in Table VI. The change in $\Delta \bar{V}^0$ is greater than would be accounted for assuming errors in Λ_p/Λ_1 to be as great as $\pm 0.5\%$.

The differences in the pressure behavior of these two salts may, in fact, be due to differences in the various ion-pair species which can be related to the differences in acoustic behavior. However, a multistate model cannot be deduced from conductivity data; these results can only provide a check for consistency of any multistate models which may be proposed.

Adsorption of Nonylphenoxyacetic Acid by Metals

by Jerry E. Berger

Shell Oil Company, Research Laboratory, Wood River, Illinois (Received February 2, 1965)

Nonylphenoxyacetic acid was adsorbed from dilute hydrocarbon solutions onto several different metal powders, silica gel, and a magnesium silicate. Adsorption was rapid and tenacious in experiments with metal powders. Contact angle measurements and ellipsometry were used to support the view that adsorption on metals was monomolecular and close-packed. The molecular area of nonylphenoxyacetic acid, determined from film-balance measurements, was used to calculate the specific areas of the various metal powders. Agreement between the calculated values and specific areas determined by gas adsorption methods was good in the case of metal powders. The rapidity of adsorption and the convenience in analysis suggest the use of nonylphenoxyacetic acid as a reference compound for the determination of specific areas of metal powders. Porous solids, such as silica gel, are not amenable to this method of specific area determination; the solution adsorption method provides results which are far below the values obtained from nitrogen adsorption.

Introduction

Adsorption phenomena involving reactions at the hydrocarbon-metal interface are of great practical interest. The prevention of wear and protection against rust are but two examples of the beneficial action of small quantities of polar additives which are incorporated in functional fluids for a specific purpose. Many of these polar materials are acids, and their effectiveness is due to the speed, tenacity, and extent of their adsorption.

The problem of determining specific areas of finely

divided solids by adsorbing reference compounds from solution has received attention from several investigators who have used a variety of techniques. Reference compounds have included dyes,¹ soaps,² quaternary ammonium halides,^{3,4} nitrophenol,⁵ and acids.⁶

- (1) J. J. Kipling and R. B. Wilson, *J. Appl. Chem.*, **10**, 109 (1960).
- (2) S. H. Maron, E. G. Bobalek, and S. M. Fok, *J. Colloid Sci.*, **11**, 21 (1956).
- (3) J. Kivel, F. C. Albers, D. A. Olson, and R. E. Johnson, *J. Phys. Chem.*, **67**, 1235 (1963).
- (4) P. J. Greenland and J. P. Quirk, *ibid.*, **67**, 2886 (1963).

Several authors⁷⁻⁹ have emphasized the pitfalls of using adsorption from solution to calculate specific areas of solids. Conner,¹⁰ in reviewing the subject of surface area measurement, has suggested that surface area is not an unequivocal term but an experimental concept. It may be advantageous, therefore, to estimate specific area by a technique which resembles the particular application at hand. For adsorption at the hydrocarbon-metal interface, nonylphenoxyacetic acid (NPA) appears to be a useful reference compound for appraising surface areas. Adsorption of NPA from several solvents onto several metals was studied in this work; contact angles, metal powder adsorption, and ellipsometric experiments are reported.

Nonylphenoxyacetic acid has a combination of properties which suggest its use as a model compound in studying adsorption at the hydrocarbon-metal interface. This acid is amenable to film balance techniques, and it exhibits a conveniently high molar absorptivity in the ultraviolet region.

Experimental

Materials. *p*-Nonylphenoxyacetic acid (NPA) from the Geigy Chemical Co. was refined by repeated water washings of a hexane solution of the acid. The extracted organic layer was dried, stripped of solvent, and subjected to two vacuum distillations. A single vacuum distillation was used for purifying ω -phenylundecanoic acid (PUA) (Eastman White Label). Solvents were reagent grade materials; each solvent was percolated through a column of silica gel immediately prior to the preparation of solutions.

All metal powders were subjected to Soxhlet extraction with anhydrous benzene for a period of several days. The metals then were freed of benzene in a vacuum desiccator containing silica gel. Samples of 20-30 g. were weighed into glass ampoules and evacuated to 10^{-5} mm. The ampoules were heated gradually to 200° in a silicone oil bath, and pumping was continued until the pressure again dropped to 10^{-5} mm. or lower. The stems of the ampoules were sealed with a torch while the system was under vacuum. Silica gel and Florisil (a synthetic magnesium silicate) were handled in the same way except that they were not subjected to Soxhlet extraction. Approximately 1-g. samples of these materials were used.

Specimens used in contact angle determinations and in ellipsometry were metal disks of chromium, nickel, and type 304 stainless steel. These disks had a diameter of 4 cm. and a thickness of 0.8 cm. and were polished immediately before each adsorption experiment using conventional metallurgical procedures. Levigated alumina abrasives having nominal particle

diameters of 0.3 and 0.1 μ were used on Buehler Red Felt and Microcloth laps, respectively. Final removal of residual alumina from the polished metal surface was accomplished by polishing on clean Microcloth under flowing distilled water. The mirror-like, hydrophilic specimens were dried in a current of air and immersed immediately in the appropriate solution. Attempts to obtain reproducibly clean metal surfaces using solvent-washing techniques were not successful.

Surface roughness of polished metal disks was estimated with a Taylor Hobson Talysurf, Model 3. This instrument expresses roughness in terms of center line averages (CLA), and several traverses were made on nickel and steel disks to compare the finish on the two metals. Values of roughness are given in Table I.

Table I: Surface Roughness of Polished Metals

Metal	CLA, in. $\times 10^{-6}$
Nickel	1.5, 1.3, 1.1
304 stainless steel	1.5, 1.8, 1.3

Apparatus. Film-balance measurements were made using a heavily waxed brass trough fitted with a hanging glass slide attached to a torsion wire. Aqueous substrates of 0.1 *N* HCl were prepared from deionized and distilled water; silica gel treated petroleum ether (b.p. 30-60°) was used as the spreading solvent. Film-pressure determinations were made 2 min. after each compression; films were manipulated manually with waxed brass barriers.

Compressed monolayers were transferred from aqueous substrates by the Langmuir-Blodgett technique.^{11,12} Step wedges of barium stearate were prepared on evaporated chromium substrates for use in calibration of the ellipsometer. Films of NPA were transferred from dilute aqueous HCl to polished chromium disks. Oleic acid and castor oil served as piston oils for stearic acid and NPA, respectively; metal specimens were withdrawn at a rate of 1.5 in./min. in all Langmuir-Blodgett experiments.

- (5) C. H. Giles and S. N. Nakhwa, *J. Appl. Chem.*, **12**, 266 (1962).
- (6) W. D. Harkins and D. M. Gans, *J. Am. Chem. Soc.*, **53**, 2805 (1931).
- (7) Y. Fu, R. S. Hansen, and F. E. Bartell, *J. Phys. Colloid Chem.*, **52**, 374 (1948); **53**, 769, 1141 (1949).
- (8) J. J. Kipling, *Quart. Rev.* (London), **5**, 60 (1951).
- (9) J. J. Kipling and E. H. M. Wright, *J. Chem. Soc.*, 855 (1962).
- (10) P. Conner, *Ind. Chemist*, **37**, 224 (1961).
- (11) K. B. Blodgett, *J. Am. Chem. Soc.*, **57**, 1007 (1935).
- (12) K. B. Blodgett and I. Langmuir, *Phys. Rev.*, **51**, 964 (1937).

Film thickness determinations were performed with a Rudolph Model 437/200E photoelectric ellipsometer. Use of instruments of this type has been described in detail previously.^{13,14} Both quarter-waveplate and polarizer were rotated, and the net change in the polarizer was related to film thickness by reference to working curves constructed from data obtained with barium stearate films.

Metal powder adsorption experiments were performed by crushing an ampoule of metal below the surface of a measured volume of NPA solution of known concentration. Concentrations of NPA ranged from 0.2 to 2 mM in metal powder adsorption experiments; experiments with silica gel and Florisil required concentrations up to 40 mM. Adsorption flasks were stoppered with grease-free standard-taper stoppers of polyethylene. The flasks were shaken mechanically, and samples were withdrawn with a pipet; centrifuging the aliquots removed any entrained metal powder. Concentrations were determined with a Cary recording spectrophotometer; molar absorptivities for solutions of NPA and PUA in isooctane (2,2,4-trimethylpentane) were found to be 1506 l. mole⁻¹ cm.⁻¹ (2750 Å.) and 205 l. mole⁻¹ cm.⁻¹ (2590 Å.), respectively. Both systems obey Beer's law.

Contact angles were measured with a low-power microscope fitted with a goniometer eyepiece. Freshly polished and dried metal specimens were subjected to adsorption from the appropriate solution and then were rinsed briefly in silica gel treated petroleum ether; steel and chromium disks could be withdrawn dry from solutions of NPA or PUA in nitromethane, and measurements were made before and after rinsing in these instances. Water droplets of 25 μ l. provided reproducible contact angles; each datum presented is an average of four values which did not deviate more than 2° from the average.

Electron microscopy was performed with an RCA instrument; specific areas were determined by the B.E.T. gas adsorption method with nitrogen or krypton. All measurements were made at 25 \pm 1°.

Results and Discussion

Molecular Areas. Force-area isotherms for NPA and PUA spread on 0.1 *N* aqueous HCl are presented in Figure 1. Both acids exhibit well-defined collapse pressures. A minimum molecular area of 33 Å.² is observed for NPA; PUA occupies 28 Å.²/molecule just prior to collapse. The molecular area for NPA seems rather high unless it is assumed that the ether oxygen also participates in adsorption at the water-air interface. Adam,¹⁵ for example, found that *p*-alkylphenols occupy 23 to 24 Å.²/molecule; isostearic acid exhibits a

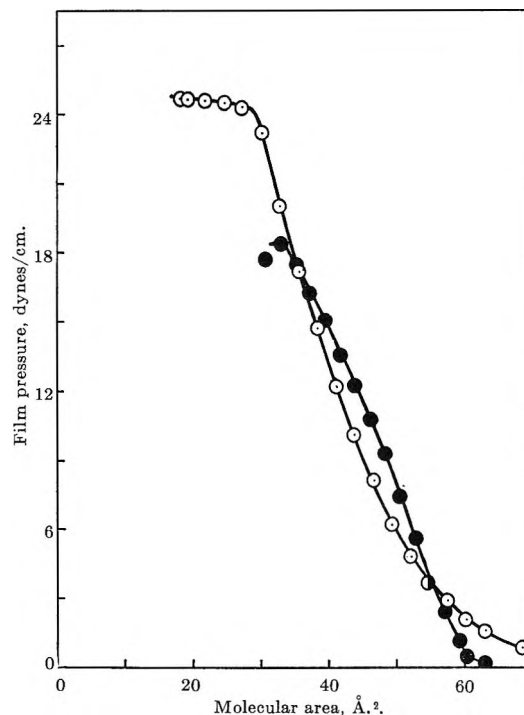


Figure 1. Force-area isotherms on dilute, aqueous HCl at 25°: open circles, PUA; shaded circles, NPA.

minimum molecular area of 28 Å.². Calculations of film thickness, assuming that the monomolecular films have a density identical with that of the bulk liquids, yield approximations of 14 and 16 Å. for NPA and PUA, respectively.

Speed of Adsorption. Experiments designed to assess the speed with which NPA is adsorbed from isooctane by outgassed metal powders reveal that adsorption is essentially complete within a very few minutes. Figure 2 contains data relevant to the adsorption of NPA by two iron powders and an aluminum powder; other metal powders gave similar adsorption *vs.* time plots. These experiments show that the first few minutes are sufficient to account for nearly all of the total, ultimate adsorption.

Although the adsorption *vs.* time isotherms reveal that the "plateau" values are attained very quickly, a continued gradual rise in the quantity of surface-active agent adsorbed is observed for periods of many hours. Several metal-acid systems exhibit this behavior. Companion experiments involving systems which were not shaken but which were occasionally stirred gently also showed a gradual increase in the ad-

(13) A. Rothen, *Rev. Sci. Instr.*, **28**, 283 (1957).

(14) F. L. McCrackin, E. Passaglia, R. R. Stromberg, and H. L. Steinberg, *J. Res. Natl. Bur. Std.*, **67A**, 363 (1963).

(15) N. K. Adam, *Proc. Roy. Soc. (London)*, **103**, 676 (1923).

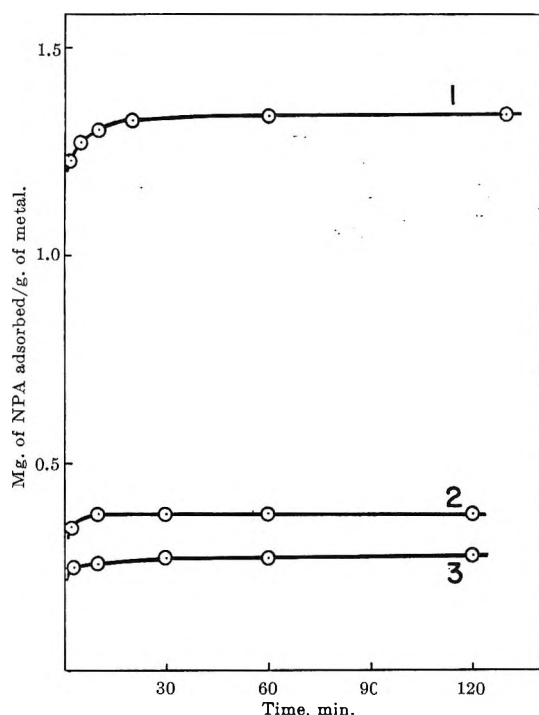


Figure 2. Adsorption of NPA from isooctane solutions by metals at 25°. Curve 1, iron B with initial NPA concentration 1.898 mM; curve 2, iron A with initial NPA concentration 1.999 mM; curve 3, aluminum with initial NPA concentration 0.896 mM.

sorption of NPA. This indicates that the increase in adsorption is not due to increasing the area of the metal powder due to attrition which might occur during the mechanical shaking of the adsorption flasks. The apparent slow increase in adsorption probably is related to a roughening or corrosion mechanism and has little significance in this research. Copper powder presented some experimental difficulties due to formation and subsequent dissolution of copper carboxylate. In one experiment, 100 ml. of 2.6 mM NPA in isooctane was placed in contact with 21.5 g. of copper powder. After 24 hr. at 25°, the supernatant liquid contained 27 p.p.m. of copper. Other metal carboxylates were sufficiently insoluble in isooctane so as to present no problems. For example, a system with iron powder instead of copper produced less than 1 p.p.m. of soluble iron in 24 hr. at 25°. In reporting work with *n*-hexadecane solutions of radiolabeled stearic acid, Walker and Ries¹⁶ also indicate that soluble copper salts are formed; iron did not exhibit this property.

The rapidity of carboxylic acid adsorption at the hydrocarbon-metal interface is illustrated also by contact angle measurements summarized in Table II. Contact angles of water droplets on NPA-steel surfaces are essentially constant following adsorption intervals

from 15 min. to 2 hr. Stearic acid, at a concentration of 1 mM, exhibits a small increase in contact angle as the adsorption time is increased from 15 to 30 min. Bartell and Ruch¹⁷ have shown, however, that contact angles can be approximately constant for coverages above 50%. These contact angles, taken by themselves, therefore do not provide firm evidence for monolayer formation.

Table II: Contact Angles of Water on Film-Covered Metals as a Function of Adsorption Time^a

Solute	Concn., mM	Adsorption time, min.	Contact angle, deg.
NPA	0.99	15	83
NPA	0.99	30	85
NPA	0.99	120	84
NPA	0.99	120	80 ^b
Stearic acid	0.96	15	79
Stearic acid	0.96	30	87
Stearic acid	0.96	120	86
Stearic acid	2.0	15	87
Stearic acid	2.0	120	90
Stearic acid	2.0	120	88 ^c
Stearic acid	2.0	120	76 ^d

^a Solvent is isooctane; metal is stainless steel 304. ^b Following an acetone rinse. ^c 30-min. soak in isooctane. ^d 30-min. soak in acetone.

Adsorbed films of NPA on steel and on nickel exhibited identical water drop contact angles as shown in Table III. Both nitromethane and isooctane were used as solvents. PUA films on steel produced contact angles of 79° with both solvents; a contact angle of 66–69° was observed on a nickel specimen after adsorption of PUA from isooctane, however. Disks could be withdrawn dry from nitromethane solutions of NPA; contact angles were unaffected by brief petroleum ether rinses. Data for dodecylsuccinic acid and stearic acid are included in Table III for comparison. Ellipsometric measurements also indicate rapid adsorption; Table IV shows that only slight increases in film thickness are observed as adsorption time is lengthened to 2 hr. The steel-NPA-nitromethane system, for example, produces films which vary from about 10 to about 11 Å. in 15- and 150-min. experiments. Rapidity of adsorption of acids on metals has been reported previously by Greenhill¹⁸ and by Smith and Fuzek.¹⁹

(16) D. C. Walker and H. E. Ries, Jr., *J. Colloid Sci.*, **17**, 789 (1962).

(17) L. S. Bartell and R. J. Ruch, *J. Phys. Chem.*, **60**, 1231 (1956).

(18) E. B. Greenhill, *Trans. Faraday Soc.*, **45**, 625 (1949).

(19) H. A. Smith and J. F. Fuzek, *J. Am. Chem. Soc.*, **68**, 229 (1946).

Table III: Contact Angles of Water on Different Film-Covered Metals^a

Solute	Solvent	Concn., mM	Metal	Contact angle, deg.
NPA	<i>i</i> -C ₈	1.02	SS 304	84
NPA	<i>i</i> -C ₈	2.24	SS 304	83
NPA	<i>i</i> -C ₈	1.02	Nickel	84
NPA	CH ₃ NO ₂	1.01	SS 304	84
NPA	CH ₃ NO ₂	2.02	SS 304	84
NPA	CH ₃ NO ₂	1.01	Nickel	84
NPA	CH ₃ NO ₂	2.02	Nickel	84
PUA	<i>i</i> -C ₈	0.95	SS 304	79
PUA	<i>i</i> -C ₈	1.99	SS 304	79
PUA	<i>i</i> -C ₈	1.12	Nickel	66
PUA	<i>i</i> -C ₈	1.99	Nickel	69
C ₁₂ H ₂₅ -CHCOOH CH ₂ COOH	<i>i</i> -C ₈	1.00	SS 304	77
Stearic acid	<i>i</i> -C ₈	2.0	SS 304	90
PUA	CH ₃ NO ₂	1.12	SS 304	79

^a Adsorption was carried out at 25° for 2 hr. When isooctane (*i*-C₈) was the solvent, specimens were rinsed in petroleum ether.

Table IV: Adsorbed Film Thickness as Determined by Ellipsometry^a

Solute	Concn., mM	Solvent	Rinse	Adsorption time, min.	Film thickness, Å.
PUA	1.06	Nitromethane	None	15	9.3
PUA	1.06	Nitromethane	Pet. ether	15	8.6
PUA	1.06	Nitromethane	None	60	9.3
PUA	1.06	Nitromethane	None	150	11.0
NPA	0.98	<i>i</i> -C ₈	Pet. ether	30	10.9
NPA	0.98	<i>i</i> -C ₈	Pet. ether	180	11.9, 12.7, 10.7
NPA	0.98	<i>i</i> -C ₈	Pet. ether	240	13.4
NPA	0.98	<i>i</i> -C ₈	Pet. ether	300	13.0, 10.9
NPA	2.24	<i>i</i> -C ₈	Pet. ether	60	10.5
NPA	2.56	<i>i</i> -C ₈	Pet. ether	20	10.9
NPA	2.56	<i>i</i> -C ₈	Pet. ether	180	12.4
NPA	2.08	Squalane	Pet. ether	60	11.0
NPA	2.08	Squalane	<i>n</i> -Heptane	1000	11.9
NPA	1.40	Nitromethane	None	15	10.7
NPA	1.40	Nitromethane	Pet. ether	15	10.0
NPA	1.40	Nitromethane	None	60	10.8
NPA	1.40	Nitromethane	Pet. ether	60	9.6
NPA	1.40	Nitromethane	None	150	11.1
NPA	37.4	Nitromethane	None	15	10.3
NPA	37.4	Nitromethane	None	150	11.7
NPA	36.0	Nitroethane	None	100	12.6, 11.4
NPA	36.0	Nitroethane	Pet. ether	100	12.6, 11.4
Stearic acid	0.98	Nitromethane	None	60	23.2
Stearic acid	0.98	Nitromethane	Pet. ether	60	17.0
<i>n</i> -C ₁₂ NH ₂	0.80	Nitromethane	None	15	25.4

^a Metal is freshly polished 304 stainless steel; temperature 25°.

Tenacity. The adsorption of carboxylic acids on metals is tenacious. For example, iron powder which had been exposed to isooctane solutions of NPA for an interval of 20 hr. exhibited negligible desorption with the addition of fresh solvent at 25°. Tenacity of adsorption also was reflected in the other techniques used. Table II, for example, shows only a slight dependence of contact angle on rinsing technique. Only relatively severe washing procedures, such as prolonged hydrocarbon soaks or acetone rinses, result in reduction of the contact angle of water drops on the adsorbed film. Film thickness measurements listed in Table IV indicate only slight removal of the adsorbed layer by solvent rinsing. Stainless steel disks can be withdrawn dry from many nitromethane solutions, and this fact permits a direct measure of the efficacy of washing techniques. Dilute NPA solutions in nitromethane produced adsorbed films on steel which were determined to vary from 10.7 to 11.1 Å. in thickness; petroleum ether rinses resulted in the removal of about one-tenth of the film material. When relatively concentrated solutions of NPA in nitroethane were employed in the adsorption step, no loss due to rinsing was observed.

Adsorption of NPA by silica gel and Florisil requires a much longer time to attain maximum surface cover-

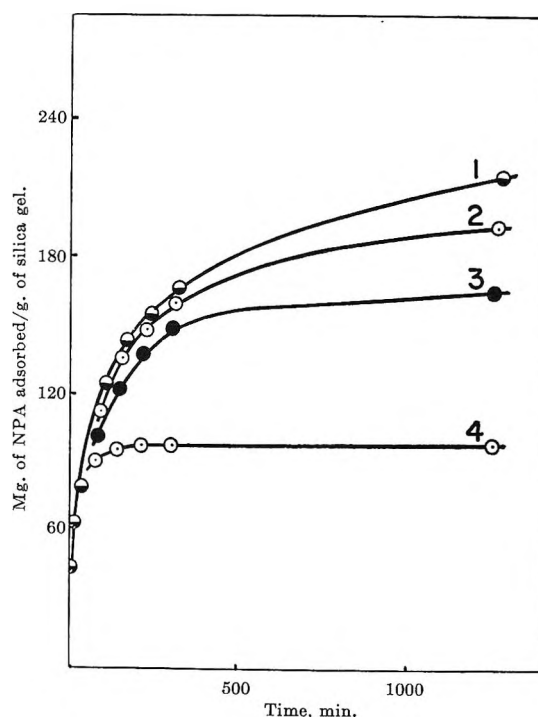


Figure 3. Adsorption of NPA from isooctane by silica gel at 25°. Initial concentrations in millimoles/liter: curve 1, 8.96; curve 2, 5.94; curve 3, 4.50; curve 4, 2.96.

age, as illustrated by data relevant to silica gel in Figure 3. The porosity of these high surface area solids presumably makes rapid and complete coverage impossible. Solvent adsorption also may be occurring. In the case of these high area solids, it was assumed that adsorption was complete after an interval of 1 week.

Each adsorbent was subjected to experiments defining the speed of adsorption; conventional adsorption-concentration plots then were constructed for each system. With solution concentration as the independent variable, it was found that maximum coverage of NPA on metals is attained even when adsorption occurs from relatively dilute solutions. Typical results for several metal powders are contained in Figure 4; data for Florisil-NPA systems are presented in Figure 5. Adsorption experiments with silica gel failed to exhibit a plateau.

Area Determinations. The rapidity and tenacity of NPA adsorption on metals and the convenience of quantitative spectroscopic analysis for this acid suggest the use of NPA as a reference compound for determining surface areas of metal powders. Surface areas were calculated for each adsorbent using the observed "plateau level" of adsorption and the assumption that each adsorbed molecule of NPA occupies 33 \AA^2 . Table V contains surface areas determined by this method; specific areas determined by other tech-

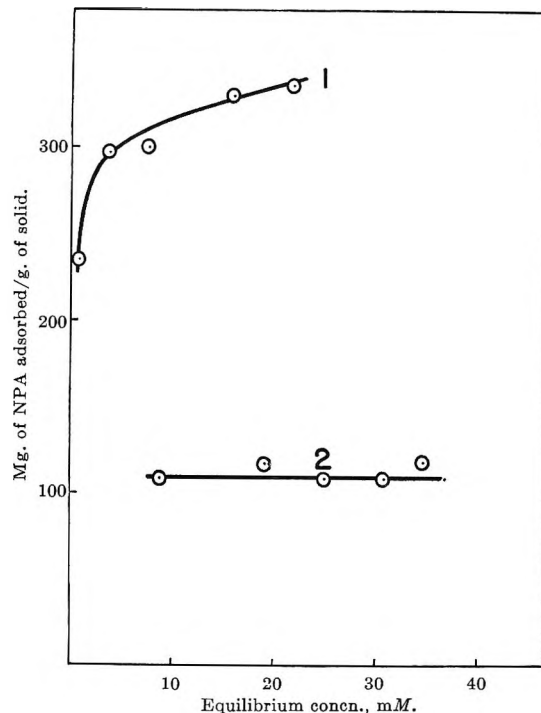


Figure 5. Adsorption of NPA from isooctane at 25°: curve 1, silica gel; curve 2, Florisil.

Table V: Surface Areas Determined by Adsorption from Solution

Adsorbent	Surface areas, m. ² /g.	
	NPA method	Other methods
Iron C (Mallinckrodt No. 5316)	0.18	0.18 ^a
Iron B (Mallinckrodt No. 5321)	0.94	1.08 ^a
Iron A (General Aniline and Film, Carbonyl HP)	0.21	0.24 ^a
Iron A (not outgassed)	0.17	
Chromium (Taylor Chemical)	0.28	0.38 ^a
Aluminum (Matheson Coleman and Bell)	0.19	0.22, 0.24 ^a
310 Stainless Steel (Hoeganaes Corp.)	0.08	...
410 Stainless Steel (Hoeganaes Corp.)	0.05	...
Nickel NF 1M (Sherritt Gordon Mines)	1.07	...
Nickel SF (Sherritt Gordon Mines)	0.28	...
Copper NF 1M (Sherritt Gordon Mines)	0.69	...
Florisil (Floridin Corp.)	77	175 ^b
Silica Gel (Davison Chemical Co.)	204	874 ^b

^a B.E.T. method using krypton. ^b B.E.T. method using nitrogen.

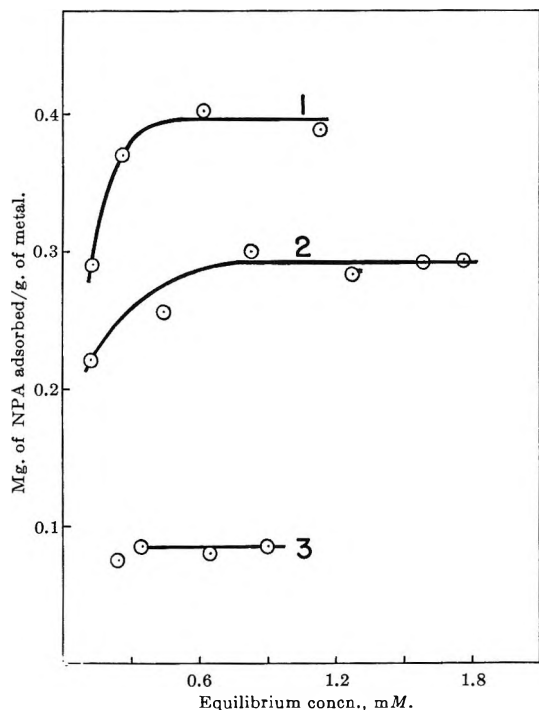


Figure 4. Adsorption of NPA from isooctane at 25° by metal powders: curve 1, nickel SF 530; curve 2, iron A; curve 3, stainless steel 310.

niques are included for comparison. Electron micrographs of iron powder B revealed the existence of an aggregated structure; although the primary particles were relatively uniform in size and roughly spherical, most of these primary particles were associated into

small clumps. The average diameter of the primary particle was estimated to be 0.2–0.3 μ ; assuming perfect spheres and no aggregation, an area of 3 m.²/g. can be calculated for the powder.

Data of Table V show good agreement between gas methods and the NPA method for determining surface areas of metal powders; relatively poor agreement between the two methods occurs when porous solids are measured. This finding is consistent with measurements dealing with unsupported cobalt catalysts and some porous solids; stearic acid and nitrogen methods agreed well when applied to the metal, but discrepancies were observed with porous solids.²⁰

The adsorption of PUA on metal powders appears similar to that of NPA; only a few adsorption determinations were performed with this material because its low molar absorptivity made analysis by ultraviolet spectroscopy relatively inconvenient and inaccurate.

The application of NPA adsorption data to the problem of estimating specific areas of metal powders is open to the same criticisms which have been presented with regard to other techniques involving adsorption from solution.⁸ Fu, Hansen, and Bartell,⁷ for example, have explored in detail the adsorption of some carboxylic acids from aqueous solution. In their work involving butyric acid on graphite, they observed that the adsorbed layer probably is more than one molecule thick and consists of both solvent and solute. The adsorption of formic acid and acetic acid from organic solvents onto Spheron and Graphon has been reported by Kipling and Wright.²¹ They observed that acetic acid adsorbs in the form of a double layer from cyclohexane but a single layer from carbon tetrachloride. The same authors have studied the adsorption of caprylic, lauric, palmitic, and stearic acids by Spheron and Graphon from organic solvents.²² Complete monolayers were formed on Graphon but not on Spheron. Stearic acid could be desorbed from both adsorbents by washing with cold cyclohexane. Some of the individual isotherms are typical of competitive adsorption between two compounds, one of which is adsorbed more strongly than the other.

Adsorption of polar solutes from nonpolar solvents by metals appears to favor strongly the deposition of solute layers. Data presented by Daniel²³ relevant to the adsorption of stearic acid from several hydrocarbons are similar in many respects to the results of this investigation. Several metal powders were employed, and most gave comparable isotherms. Freshly machined metal surfaces, when exposed to cyclohexane solutions of *n*-nonadecanoic acid, exhibit limiting adsorption levels of one monolayer.²⁴ Irreversible monolayer formation involving fatty acids on nickel or

platinum catalysts has been observed by Smith and Fuzek.¹⁹

Mixed adsorbed films of nonpolar solvent and polar solute on metals have been observed in some instances. Levine and Zisman²⁵ demonstrated clearly that such mixed monolayers are capable of existence under certain sets of conditions. These authors encountered mixed films only when the polar solute contained a paraffinic moiety which was similar to the solvent molecule. Hexadecane solutions of stearic acid or of octadecylamine are examples of such systems. It was concluded by Zisman that mixed films represent a transient or metastable state in metal–hydrocarbon–polar solute systems. Mixed films were never encountered when nitromethane was used as solvent; this was cited as evidence that mixed-film formation results from van der Waals attractions involving the hydrocarbon moiety of solutes and paraffinic solvents. Ries and co-workers^{20,26} have reached similar conclusions from experiments in comparable systems.

Ellipsometry provides additional evidence to support the conclusion that the conditions for realizing monomolecular coverage, reasonably free of solvent molecules, are not difficult to achieve. NPA monolayers were deposited on several metal substrates and measured ellipsometrically; some data relevant to stainless steel are contained in Table IV. Solvents employed included squalane, isooctane, nitromethane, and nitroethane. Small differences in film thickness frequently could be attributed to concentration or time variables. Adsorbed films of NPA from solvents as diverse as isooctane and squalane were essentially the same thickness. Nitromethane- or nitroethane-deposited layers also were similar in thickness; rinsing with hydrocarbons caused no increase in apparent thickness, indicating that the rinse species was not incorporated in the film.

Perhaps the most significant ellipsometric measurements were made with films deposited from the vapor phase. Previously, we have observed that capric acid is sufficiently volatile to deposit a monomolecular layer on a chromium specimen suspended in a closed vessel which contains capric acid vapor at 25°. The same type of experiment was employed to deposit monolayers of NPA on stainless steel. In one pro-

(20) H. E. Ries, M. F. L. Johnson, and J. S. Melik, *J. Phys. Chem.*, **53**, 639 (1949).

(21) J. J. Kipling and E. H. M. Wright, *ibid.*, **67**, 1789 (1963).

(22) J. J. Kipling and E. H. M. Wright, *J. Chem. Soc.*, 3382 (1963).

(23) S. G. Daniel, *Trans. Faraday Soc.*, **47**, 1345 (1951).

(24) H. A. Smith and T. Fort, Jr., *J. Phys. Chem.*, **62**, 519 (1958).

(25) O. Levine and W. A. Zisman, *ibid.*, **61**, 1188 (1957).

(26) H. D. Cook and H. E. Ries, *ibid.*, **63**, 226 (1957).

cedure, a 3-l. flask was flushed with clean, dry nitrogen prior to the introduction of a drop of NPA; a polished metal mirror then was suspended in the vapor space. The flask was evacuated to about 0.1 mm., isolated from the pump, and allowed to stand at room temperature for 3 hr. Clean, dry nitrogen then was admitted to the flask, and the metal disk was placed on the stage of the ellipsometer. Immediately after removal from the flask, a thickness of 15.2 Å. was observed; this value decreased steadily for 10 min. to a value of 12.8 Å. This thickness remained constant for an interval of 30 min.; the contact angle of a water drop on this film was 80°.

In a companion experiment, a drop of NPA was placed in a relatively small vessel filled with clean, dry nitrogen at atmospheric pressure. A polished disk of stainless steel was suspended in this vapor space at 25°. Film deposition required much longer under these conditions; values obtained were 8.9 Å. (20 hr.), 10.0 Å. (24 hr.), and 12.3 Å. (90 hr.). The thickness of this film, which was allowed to stand in ordinary laboratory air, remained relatively constant: after a 7-hr. exposure the observed thickness was 13.0 Å.

A Langmuir-Blodgett monolayer of NPA, compressed to 18 dynes/cm. and transferred to chromium, was found to be 13.7 Å. in thickness. Using the adsorption level of NPA on iron B, for example, along with its specific area, it is possible to estimate the thickness of the adsorbed layer if one assumes the density of the NPA monolayer is the same as the bulk density. From the specific area determined by nitrogen adsorption, the estimated thickness is 12.4 Å. This value is in reasonable agreement with the Langmuir-Blodgett thickness.

Metal Preparation. Metal preparation was found to have a pronounced influence on the adsorption of NPA. Note in Table V that the quantity of NPA adsorbed on carbonyl iron is reduced by one-fifth when the powder is not subjected to heating to 200° with concomitant evacuation to 10⁻⁵ mm. The procedure used in preparing metal disks for ellipsometry was especially important. It was not possible to obtain reproducible results using solvent-washed disks; it was necessary to repolish the metal surfaces prior to each experiment and to avoid touching the surface. Prolonged storage of disks between the polishing and the adsorption steps also resulted in lower levels of ad-

sorption and increased scatter of data in repetitive experiments. In one instance, disks which were aged for 2 hr. in ordinary laboratory distilled water before use exhibited negligible adsorption of NPA from iso-octane. Prolonged exposure to air also passivated specimens with respect to NPA adsorption.

With freshly polished nickel specimens, it was possible to measure the changes which occur during aging in air. After exposure to air for 30 min., a fresh nickel mirror exhibited a layer of contaminants 3 Å. in thickness. After a 6-hr. residence in laboratory air, this value had increased to 12 Å. Presumably, this layer of contaminants was composed of water, polar gases, and metal oxide; ellipsometry furnishes no information about the identity of the adsorbed phase. The change in metal specimens from hydrophilic to hydrophobic character due to exposure to air is well known to those accustomed to measuring contact angles. Metal mirrors with adsorbed monolayers generally did not show significant changes in apparent film thickness as a function of time in air.

Conclusions

These data can be interpreted as evidence for the deposition of reasonably "perfect" monolayers of NPA and similar carboxylic acids from hydrocarbon solution onto metals. This interpretation, coupled with a large molar adsorptivity in the ultraviolet region, suggests the use of NPA for a rapid and convenient method for determining the areas of metal powders. The data of Table V reveal a satisfactory check with the B.E.T. areas of metal powders; the method is inapplicable to porous, high area solids such as silica gel and Florisil. In addition to this limitation, the use of NPA adsorption for the determination of specific areas of copper powders presents experimental difficulties. Adsorption of NPA on copper, as with other metals, is rapid, and estimation of specific areas of copper powders is possible provided that all measurements are made within 30 min. before appreciable quantities of copper salts enter solution.

Acknowledgment. The author is grateful to Mr. R. E. Dodc̄ for assistance with some of the experimental work, to Mr. C. F. Zimpel for electron micrographs, and to Mr. M. O. Baker for determinations of specific areas using gas adsorption techniques.

Surface Tension of Liquid Alkali Halide Binary Systems

by G. Bertozzi

*Chemistry Department, High Temperature Chemistry, Euratom, C.C.R., Ispra, Italy
(Received February 2, 1965)*

Surface tension measurements are reported for twelve alkali halide binary systems, having either a common anion or a common cation. Experimental results are shown to be well described by introducing the "Tobolsky parameter" $[(d_1 - d_2)/(d_1 + d_2)]^2$, *i.e.*, a function of interionic distances of the respective pure salts only.

Introduction

In a previous paper¹ the results of measurements of surface tension of alkali nitrate binary systems were reported. Although, in general, this property is not a linear function of composition (not even in thermodynamically "ideal" mixtures), nevertheless we were led to consider as theoretically significant the deviations from linearity since contributions to negative deviations arising from variations of the surface composition are, in comparison with the observed effect, negligible, provided that surface tensions of the pure components are not widely different.²

Then, the maximum values of the deviations of the surface tension isotherms from linearity were found to be proportional to the "Tobolsky parameter" $[(d_1 - d_2)/(d_1 + d_2)]^2$, d_1 and d_2 being the interionic distances of salts 1 and 2, respectively. This parameter was previously used by Kleppa and co-workers in their studies on heats of mixing in liquid nitrate systems.³

In the present paper, the investigation on the surface tension in molten salt binary systems is extended to alkali halide mixtures; the usefulness of the Tobolsky parameter is again verified.

Experimental and Results

The Wilhelmy slide method previously described¹ was again used; the results were always reproducible within 0.5% up to 850–900°.

The surface tension of the following pure salts and binary systems was investigated in the temperature range from the melting point up to 900°: (A) pure salts: NaCl, KCl, RbCl, CsCl, NaBr, KBr, RbBr, CsBr; (B) chloride systems: (Na–K)Cl, (Na–Rb)Cl, (Na–Cs)Cl; (C) bromide systems: (Na–K)Br, (Na–Rb)Br, (Na–Cs)Br, (K–Rb)Br, (K–Cs)Br; (D)

common cation systems: Na(Cl–Br), K(Cl–Br), Rb(Cl–Br), Cs(Cl–Br).

The surface tension of all pure salts, as well as that of the mixtures, showed always a linear dependence on temperature $j = A - Bt$, with a temperature coefficient of the order of 0.07 dyne/cm. deg.

For each system we draw the surface tension isotherm as a function of the molar composition, at 800° (Figures 1 and 2). The isotherms for the systems with common cation are not reported because they are nearly indistinguishable from a straight line.

Discussion

(1) *Systems with Common Anion.* In Figure 3 the maximum deviations from linearity Δj of the surface tension isotherms are plotted as a function of the Tobolsky parameter $[(d_1 - d_2)/(d_1 + d_2)]^2$, which for the sake of brevity will be henceforth termed D .

As well as in the case of the alkali nitrate systems,¹ we can see, from Figure 3 that a linear relationship holds between Δj and the Tobolsky parameter: $-\Delta j/D = K$, where K is a function of the anion. From the plot of Figure 3 the values of the ratio $-\Delta j/D$ for chloride ($K = 980$ dynes/cm.) and bromide ($K = 720$ dynes/cm.) systems are obtained.

These values can be roughly estimated by recalling that, ϵ_1 being the coulombic energy of an ion triplet $A+B-A^+$ (pure salt AB), and ϵ_2 the coulombic energy of a triplet $C+B-C^+$ (pure salt CB), the coulombic energy of the new "mixed" triplet $A+B-C^+$ is not a

(1) G. Bertozzi and G. Sternheim, *J. Phys. Chem.*, **68**, 2908 (1964).

(2) E. A. Guggenheim, "Mixtures," Oxford University Press, London, 1952.

(3) O. J. Kleppa and L. S. Hersch, *J. Chem. Phys.*, **34**, 351 (1961).

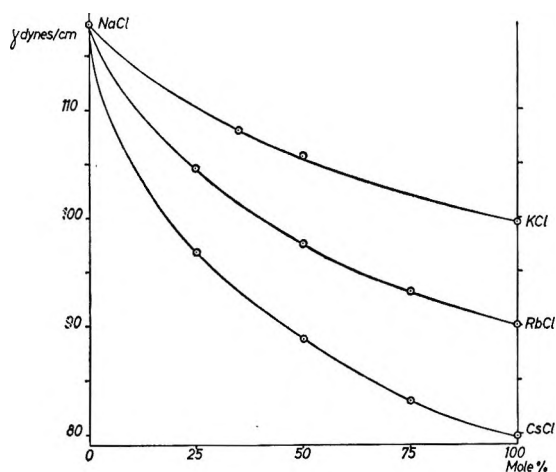


Figure 1. Surface tension isotherms at 800° for chloride systems.

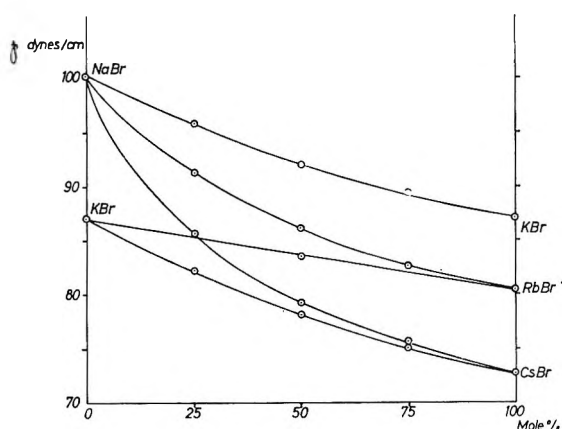


Figure 2. Surface tension isotherms at 800° for bromide systems.

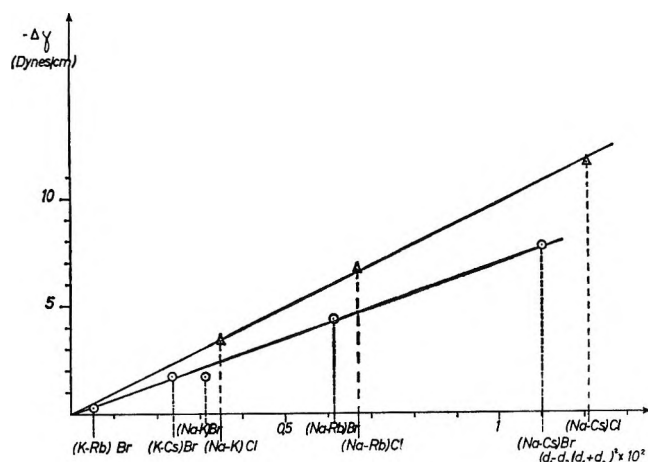


Figure 3. Maximum deviations of surface tension isotherms from linearity as a function of the Tobolsky parameter: \triangle — \triangle , chloride systems; \circ — \circ , bromide systems.

linear function of ϵ_1 and ϵ_2 but rather deviates negatively; this deviation was shown by Förland⁴ to be

$$\Delta\epsilon = -e^2(1/d_1 + 1/d_2)D \quad (1)$$

This energy change, multiplied by $1/a$ (number of molecules per cm^2 , a being the average area per molecule) and by the number of times a mixed triplet is formed ($1/2x_1x_2$) yields a change of a free energy per unit area and hence a surface tension variation

$$\Delta j = -x_1x_2 \frac{e^2}{2a}(1/d_1 + 1/d_2)D \quad (2)$$

x_1 and x_2 are the molar fractions of the components; in the case of an equimolar mixture, eq. 2 becomes

$$\Delta j = -\frac{e^2}{8a}(1/d_1 + 1/d_2)D$$

and hence

$$-\Delta j/D = \frac{e^2}{8a}(1/d_1 + 1/d_2) \quad (3)$$

From eq. 3 we calculated for $-\Delta j/D$ an average value of ~ 1.050 dynes/cm. for chlorides and ~ 820 dynes/cm. for bromides; the agreement with the experimental values is satisfactory.

(2) *Systems with Common Cation.* In the case of alkali halide systems with common cation, the numerical values of the Tobolsky parameter are very small, because of the small difference between the ionic radii of chlorine and bromide, so that values of Δj of 0.3–0.5 dyne/cm. should be expected; this prediction is fully in accord with our experiments.

In Table I the experimental data of the surface tension at 800° for equimolar mixtures of these systems are compared with the average values $1/2(j_1 + j_2)$.

Table I

System	Exptl. j	$1/2(j_1 + j_2)$
NaCl + NaBr	107.7	109
KCl + KBr	93.1	93.4
RbCl + RbBr	85.0	85.3
CsCl + CsBr	76.0	76.2

It is apparent that only the sodium salts deviate slightly from linearity, whereas for the other cations the isotherms are practically linear; the behavior of the sodium salts can be ascribed to the smallness of the cation, the electrical field of which can polarize the anions.

(4) T. Förland, *J. Phys. Chem.*, 59, 152 (1955).

Solubilities of Argon and Nitrogen in Sea Water

by Everett Douglas

Scripps Institution of Oceanography, La Jolla, California^{1,2} (Received February 3, 1965)

The solubility coefficients of argon and nitrogen have been determined in sea water at three chlorinities from 2 to 30‰ with an estimated accuracy of $\pm 0.25\%$ for argon and $\pm 0.5\%$ for nitrogen. These values have been compared with those of previous workers showing the argon values of König to be inconsistent with the present values while those of Rakestraw and Emmel exhibit good agreement at the higher chlorinities. The nitrogen values of Rakestraw and Emmel are higher than those reported here.

Introduction

With the recent interest in the inert gases in sea water,³⁻⁶ it has become necessary to establish accurately their saturation values in sea water. Using a microgasometric method, the solubility coefficients of nitrogen and argon have been determined. The values of Rakestraw and Emmel⁷ for nitrogen have generally been accepted as the standards over those of Fox,⁸ his values being higher than those of Rakestraw and Emmel. Remarkably good results for argon were achieved by Rakestraw and Emmel using atmospheric

air while the solubility of the pure gas was first investigated by König⁹ in 1963.

Experimental

The method employed has been described earlier.¹⁰ The absorption apparatus has been enlarged to accommodate approximately 8 ml. of water in order to maintain the same level of accuracy as obtained with distilled water.¹¹

Gas-free sea water, millipore filtered and stored at 4°, was obtained by vacuum extracting it over mercury.^{12,13} The determination of chlorinity was

Table I: Experimental Solubility Coefficients of Argon

Cl ‰ = 15.376							
Temperature, °C.							
	15.0	6.46	10.00	14.80	19.99	25.01	29.83
	0.04246	0.03780	0.03493	0.03180	0.02891	0.02668	0.02487
	0.04246	0.03797	0.03487	0.03162	0.02894	0.02666	0.02473
	0.04252	0.03775	0.03499	0.03170	0.02889	0.02662	0.02483
Av.	0.04248	0.03784	0.03493	0.03171	0.02891	0.02665	0.02481
Cl ‰ = 18.604							
Temperature, °C.							
	2.17	6.80	10.25	14.71	20.46	25.27	29.72
	0.04019	0.03601	0.03342	0.03066	0.02770	0.02567	0.02413
	0.04020	0.03626	0.03346	0.03065	0.02772	0.02567	0.02412
	0.04023	0.03619	0.03343	0.03060	0.02769	0.02563	0.02405
Av.	0.04021	0.03615	0.03344	0.03064	0.02770	0.02566	0.02410
Cl ‰ = 20.985							
Temperature, °C.							
	2.10	5.92	10.15	15.05	20.50	24.88	29.99
	0.03919	0.03583	0.03267	0.02970	0.02702	0.02512	0.02342
	0.03910	0.03574	0.03273	0.02963	0.02701	0.02514	0.02344
	0.03906	0.03582	0.03266	0.02968	0.02702	0.02517	0.02343
Av.	0.03912	0.03580	0.03269	0.02967	0.02702	0.02514	0.02343

(1) Contribution from the Scripps Institution of Oceanography, University of California, San Diego, Calif.

(2) This investigation was supported by Public Health Service Research Grant No. GM 10521 from the National Institutes of Health.

(3) R. Bieri, M. Koide, and E. D. Goldberg, *Science*, **146**, 1035 (1964).

(4) B. B. Benson and P. D. M. Parker, *Deep-Sea Res.*, **7**, 237 (1961).

(5) T. Enns, P. F. Scholander, and E. D. Bradstreet, *J. Phys. Chem.*, **69**, 389 (1965).

(6) E. Mazer, G. I. Wasserburg, and H. Craig, *Deep-Sea Res.*, **11**, 929 (1964).

(7) N. W. Rakestraw and V. M. Emmel, *J. Phys. Chem.*, **42**, 1211 (1938).

(8) C. J. J. Fox, *Trans. Faraday Soc.*, **5**, 68 (1909).

(9) H. Von König, *Z. Naturforsch.*, **18a**, 363 (1963).

(10) E. Douglas, *J. Phys. Chem.*, **68**, 169 (1964).

(11) Due to an oxidation occurring using pure oxygen with sea water over mercury, the determination of O₂ values could not be undertaken.

(12) As this does not remove all of the CO₂, a possible maximum uncertainty of 0.2% for argon and 0.4% for nitrogen could be introduced if the CO₂ in the sea water reaches equilibrium with the pure gas during equilibration. Analysis of the gas with a Scholander 0.5-cc. gas analyzer,¹³ however, showed the CO₂ concentration to be less than 0.03%.

(13) P. F. Scholander, *J. Biol. Chem.*, **167**, 235 (1947).

Table II: Argon Solubility in Sea Water^a

Temp., °C.	Chlorinity						
	15	16	17	18	19	20	21
0	0.04443	0.04387	0.04331	0.04276	0.04220	0.04165	0.04110
1	0.04326	0.04274	0.04222	0.04170	0.04118	0.04066	0.04014
2	0.04212	0.04164	0.04115	0.04066	0.04017	0.03968	0.03920
3	0.04117	0.04069	0.04021	0.03974	0.03926	0.03878	0.03830
4	0.04022	0.03974	0.03928	0.03882	0.03836	0.03789	0.03742
5	0.03931	0.03885	0.03840	0.03794	0.03748	0.03703	0.03657
6	0.03840	0.03795	0.03751	0.03707	0.03663	0.03618	0.03574
7	0.03752	0.03709	0.03666	0.03623	0.03580	0.03536	0.03494
8	0.03665	0.03624	0.03582	0.03540	0.03500	0.03458	0.03416
9	0.03581	0.03541	0.03502	0.03462	0.03423	0.03383	0.03344
10	0.03504	0.03465	0.03427	0.03389	0.03350	0.03312	0.03273
11	0.03430	0.03393	0.03355	0.03318	0.03281	0.03243	0.03206
12	0.03362	0.03325	0.03288	0.03252	0.03215	0.03178	0.03141
13	0.03295	0.03259	0.03223	0.03187	0.03151	0.03116	0.03080
14	0.03230	0.03195	0.03160	0.03126	0.03092	0.03058	0.03023
15	0.03169	0.03135	0.03102	0.03068	0.03035	0.03002	0.02969
16	0.03112	0.03079	0.03046	0.03013	0.02980	0.02948	0.02915
17	0.03059	0.03025	0.02991	0.02958	0.02924	0.02890	0.02856
18	0.03001	0.02970	0.02938	0.02908	0.02876	0.02846	0.02815
19	0.02949	0.02919	0.02889	0.02858	0.02828	0.02799	0.02768
20	0.02900	0.02870	0.02840	0.02811	0.02782	0.02751	0.02722
21	0.02851	0.02822	0.02793	0.02763	0.02734	0.02706	0.02677
22	0.02806	0.02776	0.02748	0.02718	0.02690	0.02661	0.02632
23	0.02760	0.02732	0.02703	0.02674	0.02645	0.02617	0.02589
24	0.02717	0.02689	0.02661	0.02633	0.02605	0.02576	0.02549
25	0.02675	0.02648	0.02620	0.02593	0.02566	0.02538	0.02511
26	0.02636	0.02608	0.02582	0.02554	0.02527	0.02500	0.02474
27	0.02597	0.02570	0.02544	0.02518	0.02492	0.02466	0.02440
28	0.02560	0.02534	0.02509	0.02483	0.02458	0.02432	0.02407
29	0.02521	0.02496	0.02472	0.02447	0.02422	0.02398	0.02373
30	0.02485	0.02461	0.02437	0.02414	0.02390	0.02366	0.02343

^a It should be noted that chlorinity is expressed in terms of grams of chlorine per kilogram of sea water, while α is given as volume of gas (STPD) absorbed by a unit volume of water when the pressure of the gas is 760 mm.

Table III: Experimental Solubility Coefficients of Nitrogen

Cl ‰ = 15.376							
	Temperature, °C.						
	1.50	6.46	10.00	14.81	19.99	25.08	29.83
	0.01857	0.01661	0.01544	0.01416	0.01299	0.01209	0.01137
	0.01858	0.01667	0.01550	0.01422	0.01303	0.01210	0.01144
	0.01852	0.01670	0.01551	0.01417	0.01304	0.01203	0.01139
Av.	0.01856	0.01666	0.01546	0.01418	0.01302	0.01207	0.01140
Cl ‰ = 18.604							
	Temperature, °C.						
	2.17	6.80	10.25	14.51	19.41	25.27	29.72
	0.01746	0.01588	0.01485	0.01373	0.01264	0.01161	0.01109
	0.01748	0.01589	0.01476	0.01367	0.01269	0.01168	0.01111
	0.01746	0.01592	0.01485	0.01370	0.01268	0.01165	0.01107
Av.	0.01747	0.01590	0.01482	0.01370	0.01267	0.01165	0.01109
Cl ‰ = 20.985							
	Temperature, °C.						
	2.10	5.92	10.15	15.05	19.41	24.88	29.99
	0.01689	0.01566	0.01442	0.01319	0.01227	0.01140	0.01076
	0.01692	0.01563	0.01436	0.01320	0.01222	0.01139	0.01078
	0.01698	0.01567	0.01442	0.01320	0.01231	0.01139	0.01071
Av.	0.01693	0.01565	0.01440	0.01320	0.01227	0.01139	0.01075

Table IV: Nitrogen Solubility in Sea Water

Temp., °C.	α -Nitrogen						
	Chlorinity						
	15	16	17	18	19	20	21
0	0.01931	0.01904	0.01877	0.01850	0.01824	0.01797	0.01770
1	0.01886	0.01860	0.01835	0.01809	0.01783	0.01758	0.01732
2	0.01845	0.01820	0.01795	0.01770	0.01745	0.01720	0.01696
3	0.01804	0.01780	0.01756	0.01732	0.01708	0.01684	0.01660
4	0.01766	0.01742	0.01719	0.01696	0.01673	0.01650	0.01626
5	0.01727	0.01705	0.01683	0.01661	0.01639	0.01616	0.01594
6	0.01691	0.01669	0.01648	0.01627	0.01606	0.01584	0.01563
7	0.01656	0.01635	0.01615	0.01595	0.01574	0.01554	0.01533
8	0.01622	0.01602	0.01582	0.01562	0.01542	0.01522	0.01502
9	0.01587	0.01568	0.01549	0.01530	0.01511	0.01492	0.01473
10	0.01554	0.01536	0.01518	0.01500	0.01481	0.01463	0.01445
11	0.01523	0.01506	0.01488	0.01471	0.01453	0.01436	0.01418
12	0.01496	0.01478	0.01461	0.01444	0.01426	0.01409	0.01392
13	0.01469	0.01452	0.01435	0.01418	0.01401	0.01384	0.01367
14	0.01440	0.01424	0.01408	0.01392	0.01376	0.01360	0.01344
15	0.01419	0.01403	0.01386	0.01370	0.01354	0.01338	0.01321
16	0.01396	0.01380	0.01363	0.01346	0.01329	0.01312	0.01295
17	0.01373	0.01357	0.01341	0.01325	0.01309	0.01293	0.01277
18	0.01351	0.01335	0.01319	0.01303	0.01287	0.01271	0.01255
19	0.01329	0.01314	0.01298	0.01282	0.01266	0.01250	0.01235
20	0.01309	0.01293	0.01278	0.01263	0.01248	0.01232	0.01217
21	0.01288	0.01273	0.01259	0.01244	0.01229	0.01214	0.01199
22	0.01268	0.01254	0.01240	0.01226	0.01211	0.01197	0.01183
23	0.01249	0.01235	0.01222	0.01208	0.01194	0.01180	0.01166
24	0.01231	0.01218	0.01205	0.01192	0.01179	0.01165	0.01152
25	0.01214	0.01202	0.01189	0.01176	0.01164	0.01151	0.01138
26	0.01199	0.01187	0.01174	0.01162	0.01150	0.01137	0.01125
27	0.01185	0.01173	0.01160	0.01148	0.01136	0.01124	0.01112
28	0.01173	0.01160	0.01148	0.01136	0.01124	0.01112	0.01100
29	0.01159	0.01147	0.01135	0.01124	0.01112	0.01101	0.01089
30	0.01146	0.01134	0.01123	0.01111	0.01100	0.01088	0.01077

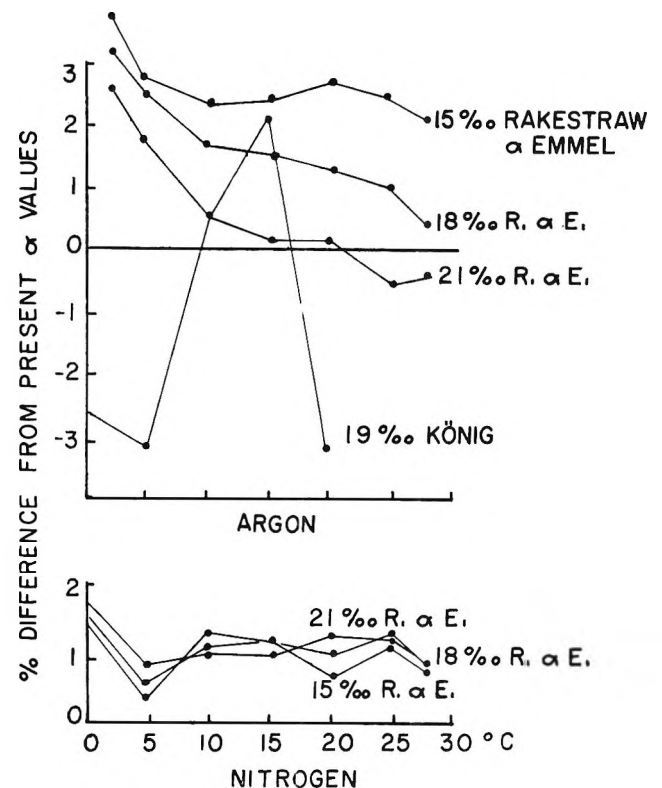


Figure 1. Values of Rakestraw and Emmel (top) were recalculated to 1 atm. of pure argon from atmospheric air values. Values of König were obtained using pure argon.

accomplished by a scaled-down version of the Mohr method. Approximately 1 ml. of sea water with dichromate indicator added plus 2 ml. of double-distilled water was titrated with a silver nitrate solution by means of a syringe microburet¹⁴ for precise delivery. These were all titrated against Copenhagen water. Accuracy at this level was $\pm 0.05\%$.

The purity of the nitrogen and argon used was determined on a mass spectrometer, showing the nitrogen to contain 0.04% oxygen and less than 0.03% argon. The argon contained less than 0.1% nitrogen and less than 0.01% CO₂.

Results and Discussion

Argon. The results obtained for argon in three different chlorinities are shown in Table I. Smooth curves were fitted on these points from which the α -values from 0 to 30° were taken. From these values the linear relations between solubility and chlorinity were plotted and the solubility values from 0 to 30° in

chlorinities ranging from 15 to 21‰ were obtained. These values are tabulated in Table II.

Figure 1 (top) illustrates the per cent difference of previous argon values from the present at the indicated chlorinities.

Nitrogen. The experimental results for nitrogen are given in Table III with the interpolated values shown in Table IV. A comparison with Rakestraw and Emmel in Figure 1 (bottom) shows their values to be somewhat higher.

Acknowledgments. The author wishes to acknowledge numerous helpful discussions with Dr. P. F. Scholander during the course of this work. The author also is indebted to Dr. G. V. Pickwell for some earlier chloride titrations and to J. M. Wells and J. Wright for collection of the sea water. Thanks are due to Dr. Scholander and Dr. T. Enns for their critical readings of the manuscript.

(14) Syringe Microburet Model No. SB2, Micro-Metric Instrument Co., Cleveland, Ohio.

Thermodynamic Properties of Nonaqueous Solutions. I. Heats of Solution of Selected Alkali Metal Halides in Anhydrous N-Methylformamide¹

by Robert P. Held² and Cecil M. Criss

Department of Chemistry, University of Vermont, Burlington, Vermont (Received February 3, 1965)

A precision submarine solution calorimeter has been constructed and used to measure the heats of solution of LiCl, NaCl, KCl, CsCl, NaBr, and NaI in anhydrous N-methylformamide at 25° in the concentration range of 7×10^{-5} to 10^{-2} *m*. These data have been extrapolated to infinite dilution to obtain the standard heats of solution of the corresponding salts. With the exception of CsCl and KCl, the limiting slopes of the heat data vary from 7 to 280 times the value predicted by the Debye-Hückel theory. On the basis of the present results and conductance data in the literature, it is suggested that there is ionic association for some electrolytes in solutions of this high dielectric constant solvent.

Introduction

Although heats of solution at 25° have been measured for several electrolytes in numerous anhydrous solvents,³⁻¹² only a few have been reported for electrolytes in very dilute solutions^{5,6,11,12} and even fewer in solvents with a dielectric constant greater than that of water.^{7,8} The few thermal data which do exist for very dilute solutions are, without exception, for solutions having relatively low dielectric constants. In these solutions it is not unusual for the experimental limiting slopes for heats not to be in agreement with the Debye-Hückel theory.^{4,6,13} Because of the uncertainties in the limiting slopes and corresponding uncertainties in extrapolation of heat data from more concentrated solutions, the standard heats of solution of electrolytes in these solvents reported in the literature may be in serious error.

In view of the fact that N-methylformamide has a very high dielectric constant ($D = 182.4$ at 25°)¹⁴ and conductance measurements have shown it to be a powerful dissociating solvent,¹⁵ it appeared that this solvent would be of particular theoretical interest as a medium for examining the heats of solution of selected electrolytes. Because of its high dielectric constant one would expect very little ionic association and the limiting slopes for heats of solution would be expected to be in agreement with the Debye-Hückel theory. Additionally, one would expect that deviations from the Debye-Hückel theory at higher concentrations

would be less than the deviations in an aqueous solution of corresponding concentration. From a practical view of obtaining thermodynamic data, extrapolations to infinite dilution in this solvent should be considerably more accurate, making possible more accurate standard heats of solution.

In order to minimize extrapolation errors, it is ad-

(1) This paper represents part of the work submitted by R. Held to the Graduate School of the University of Vermont in partial fulfillment of the requirements for the degree of Doctor of Philosophy.

(2) NASA Fellow, 1963-1965.

(3) S. U. Pickering, *J. Chem. Soc.*, **53**, 865 (1888).

(4) F. A. Askew, E. Bullock, H. T. Smith, R. K. Tinkler, O. Gatty, and J. H. Wolfenden, *ibid.*, 1368 (1934).

(5) C. M. Slansky, *J. Am. Chem. Soc.*, **62**, 2430 (1940).

(6) S. R. Gunn and L. G. Green, *J. Phys. Chem.*, **64**, 1066 (1960).

(7) T. L. Higgins and E. F. Westrum, Jr., *ibid.*, **65**, 830 (1961).

(8) K. P. Mishchenko and A. M. Sukhotin, *Dokl. Akad. Nauk SSSR*, **98**, 103 (1954).

(9) K. P. Mishchenko and V. V. Sokolov, *Zh. Strukt. Khim.*, **4**, 184 (1963).

(10) G. P. Katlyarova and E. F. Ivanova, *Zh. Fiz. Khim.*, **38**, 423 (1964).

(11) B. Jakuszewski and S. Taniewska-Osinska, *Bull. Acad. Polon. Sci., Ser. Sci. Chim.*, **9**, 133 (1931).

(12) B. Jakuszewski and S. Taniewska-Osinska, *Lodz. Towarz. Nauk. Wydział III, Acta Chim.*, **8**, 11 (1962).

(13) N. S. Jackson, A. E. C. Smith, O. Gatty, and J. H. Wolfenden, *J. Chem. Soc.*, 1376 (1934).

(14) G. R. Leader and J. F. Gormley, *J. Am. Chem. Soc.*, **73**, 5731 (1951).

(15) C. M. French and K. H. Glover, *Trans. Faraday Soc.*, **51**, 1418 (1955).

vantageous to measure heats of solution in as dilute solutions as possible. In the present study heats of solution of LiCl, NaCl, KCl, CsCl, NaBr, and NaI have been measured in the range of 7×10^{-5} to 10^{-2} *m* and the data extrapolated to infinite dilution to obtain standard heats of solution at 25° for the corresponding salts. The present study represents heat measurements for solutions more dilute than any previously reported for nonaqueous solutions.

Experimental

Materials. N-Methylformamide was treated with NaOH pellets and BaO for at least 4 hr. (generally overnight). (Initially CaH₂ was used, but BaO was found to be adequate.) The solvent was decanted into a distillation flask containing BaO and vacuum distilled through a 35-cm. Vigreux column at about 1 mm. pressure (b.p. 44° at 0.4 mm., 47° at 0.6 mm., and 55° at 1.5 mm.). The reported boiling point is 51° at about 1 mm.¹⁵ After a second distillation from BaO, the product generally had a specific conductance of $3-5 \times 10^{-6}$ ohm⁻¹ cm.⁻¹ at 23°. Values reported in the literature range from 10^{-3} to 4×10^{-7} ohm⁻¹ cm.⁻¹.¹⁴⁻¹⁸ As other authors have found,^{14,15} the conductivity of the solvent increased slightly with time. The solvent was not used if the specific conductance exceeded 8×10^{-6} ohm⁻¹ cm.⁻¹. Karl Fischer titrations on the solvent showed that the water content was less than 0.003%. Automatically recorded warming curves, analyzed by the usual extrapolation methods, showed an average melting range of -3.52 to -2.99°.

NaCl, KCl, CsCl. Reagent grade KCl was further purified by double recrystallization from conductivity water. Reagent grade NaCl was dissolved in conductivity water, treated with chlorine, and reprecipitated according to the method described by Ives and Janz.¹⁹ CsCl was furnished by Henley and Co., and the accompanying analysis showed a 99.95% purity. The salt was used without further purification, except for the removal of water by drying in an air oven with the temperature being gradually raised to about 600° over a period of 24 hr. All three salts were stored at 400° until ready for use.

NaBr. Since reagent grade NaBr contains traces of chloride ion, pure NaBr was synthesized from primary standard Na₂CO₃ and fuming HBr. The solid NaBr was recrystallized from conductivity water, dried in a vacuum desiccator for 24 hr., and heated at 200°, then at 400°.

NaI. Reagent grade NaI was recrystallized from conductivity water, dried in a vacuum desiccator for 24 hr., and heated at 200°, then at 400°.

LiCl. Reagent grade Li₂CO₃ was further purified according to the method of Coley and Ehring²⁰ and then treated with reagent grade concentrated HCl solution. The LiCl formed was dried in a vacuum desiccator, heated at about 350 to 400° under a dry HCl atmosphere. The anhydrous product was stored in closed vials over P₂O₅. Phenolphthalein solution indicated the absence of hydrolysis in all salt samples.

Apparatus. The submarine solution calorimeter (Figure 1) consisted of a silver-plated brass outer jacket

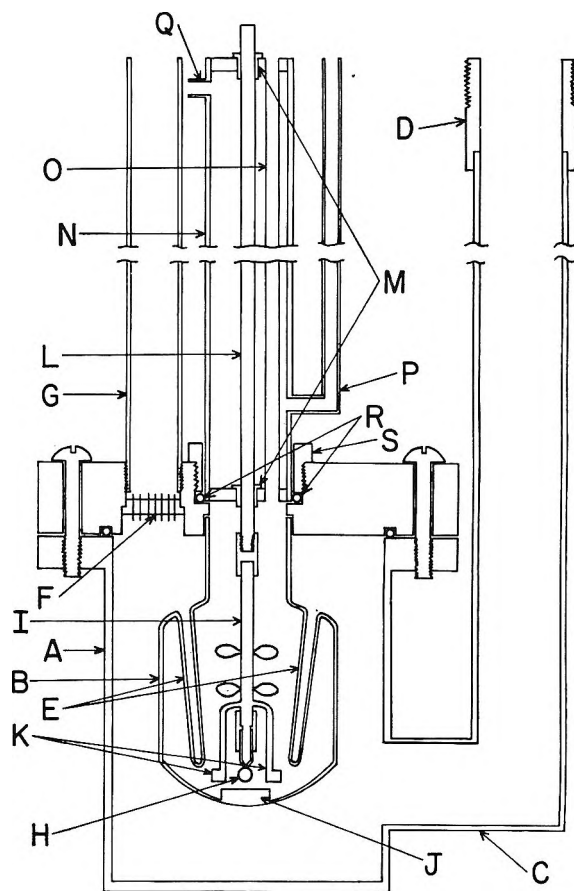


Figure 1. Submarine solution calorimeter: A, brass jacket; B, reaction vessel; C, evacuating tube; D, threaded coupling; E, thermistor and heater wells; F, hermetic electrical seal; G, conduit; H, sample bulb; I, stirring shaft; J, anvil; K, forked paddle; L, steel shaft; M, Teflon bearings; N, shaft housing; O, filling tube; P and Q, tubes for purging with nitrogen; R, "O" ring; S, threaded nut.

(16) Yu. M. Povarov, A. I. Gorbanev, Yu. M. Kessler, and I. V. Safonva, *Dokl. Akad. Nauk SSSR*, **142**, 1128 (1962).

(17) Yu. I. Sinyakov, A. I. Gorbanev, Yu. M. Povarov, and Yu. M. Kessler, *Izv. Akad. Nauk SSSR, Otd. Khim. Nauk*, 1514 (1961).

(18) G. A. Strack, S. K. Swanda, and L. W. Bahe, *J. Chem. Eng. Data*, **9**, 416 (1964).

(19) D. J. G. Ives and G. J. Janz, "Reference Electrodes—Theory and Practice," Academic Press, Inc., New York, N. Y., 1961.

(20) E. R. Coley and P. J. Ehring, *Inorg. Syn.*, **1**, 1 (1939).

(A) 11 cm. high and 9 cm. in diameter and an 80-ml. silvered glass reaction vessel (B). The neck of the inner vessel was cemented to the lid of the submarine with G.E. silicone rubber cement (RTV-60) to make a vacuum-tight seal. The space between the two vessels was evacuated through a 2.8-cm. diameter tube (C), which was connected to an all-metal vacuum system through a threaded coupling (D).

The reaction vessel was fitted with three wells (E) (only two are shown). One contained the calibration heater, another a thermistor, and the third a rough heater for adjusting the temperature of the calorimeter to the approximate operating range. All electrical connections were made through a ceramic hermetic seal (F) and brought to the bath surface through a conduit (G).

The calibration heater was made from No. 36 manganin wire wrapped noninductively around 4-mm. Pyrex tubing. This was painted with Glyptal and baked for several hours. The heater resistance was approximately 25 ohms. High vacuum silicone grease was used to increase thermal contact between the heater and the wall of the well. Two No. 30 copper lead wires were used to carry the current to the heater. These were wrapped two or three times around the outside of the reaction vessel to ensure temperature equilibration between the leads and the vessel, thus eliminating the need for a heat loss correction through the leads. Two other No. 40 copper wires, used for potential leads, were attached to the No. 30 wires at approximately two-thirds the distance from the hermetic seal to the reaction vessel, eliminating the need to make corrections for heat generated in the leads. The instrumentation for the heater circuit was similar to that previously used.²¹

Evacuated thin-walled sample bulbs (H) were fitted to the bottom of the glass stirring shaft (I) with rubber tubing. The entire stirring mechanism could be pushed down, smashing the bulb on the anvil (J) fused into the bottom of the reaction vessel, thus introducing the sample into the solvent. The lower part of the stirrer was equipped with a fork-shaped paddle (K) to increase stirring near the bottom of the reaction vessel.

The upper part of the stirring shaft (L) was fabricated from stainless steel. It passed through well-greased Teflon bearings (M) mounted at the top and bottom of the shaft housing (N). A filling tube (O) also passed through the shaft housing and parallel to the shaft. The shaft housing was fitted with inlet and outlet tubes (P and Q) for purging with dry nitrogen. The top of the stirring shaft was fitted with a pulley which was connected to a constant speed motor (125 r.p.m.).

The shaft housing was fitted to the top of the submarine to make a water-tight seal by means of an "O" ring (R) and threaded nut (S).

Except for a few minor modifications the temperature-sensing circuitry was identical with the apparatus used previously for investigations in aqueous solutions.²² The over-all temperature sensitivity was approximately 10^{-5}° , as indicated by the reproducibility of ΔT for small heat inputs introduced over short intervals of time.

The calorimeter was suspended in a thermostated bath controlled to about $3 \times 10^{-4}^{\circ}$. The bath temperature control unit was identical with that used previously²² except that a Model 151 Keithley microvoltmeter was used as the bridge amplifier. Water circulated through the cooling coils was controlled to $\pm 0.02^{\circ}$ by means of an auxiliary thermostat.

Procedure. Previously weighed thin-walled sample bulbs having a diameter of about 0.6 cm. and a stem 0.5 cm. long, made from 5-mm. Pyrex tubing, were filled with sample, weighed, placed in an oven for at least 8 hr., and then sealed under vacuum according to the method used previously.^{21,23} Phenolphthalein solution indicated that hydrolysis had not occurred on any of the salt samples from this treatment. Samples ranged in size from 0.66 mg. (for LiCl) to 71 mg. (for KCl). The smaller samples were weighed on a Mettler Model M5 microbalance.

When the calorimeter was not being used, the interior of the reaction vessel was kept under vacuum to minimize the water adsorbed on the glass surface. This was done by placing a one-holed stopper in the opening of the reaction vessel and connecting it to the vacuum line by heavy-walled rubber tubing.

In preparation for a measurement, a sample bulb was first attached to the bottom of the stirring shaft. The vacuum was then released from the reaction vessel and the stirring assembly, with the sample, joined to the top of the submarine. A specially designed delivery pipet with a long stem was inserted through the filling tube mounted in the shaft housing. By means of a two-way Teflon stopcock located at the base of the solvent reservoir of the pipet, dry nitrogen was passed through the stem of the pipet until the interior of the reaction vessel was thoroughly purged of air. The stopcock was then turned, permitting the anhydrous solvent to drain into the calorimeter. Dry nitrogen was again passed through the pipet stem as

(21) C. M. Criss and J. W. Cobble, *J. Am. Chem. Soc.*, **83**, 3223 (1961).

(22) E. C. Jekel, C. M. Criss, and J. W. Cobble, *ibid.*, **86**, 5404 (1964).

(23) C. M. Criss, Ph.D. Thesis, Purdue University, Jan. 1961.

it was removed from the filling tube, and a stopper was placed in the opening of the filling tube to ensure that no moisture could get into the anhydrous solvent in the calorimeter. Several analyses on the solution after the calorimetric measurements indicated that the maximum water content was always less than 0.01%.

Procedures used in calibrating the calorimeter, balancing the bridge, and interpolating between unit resistances on the time-temperature drift lines have been previously described.^{21,23} The only major change involved a choice of the time at which the difference between the before and after time-temperature drift lines was determined. Because of the relatively long solution times (5 to 90 min.), this choice is critical. An analysis of the curves using the matched-area method of Dickinson²⁴ indicated that a 0.23 rise time should be used instead of the usual 0.6 rise time used in combustion calorimetry. This same rise time was used as well for the electrical calibrations.

Heat of bulb-breaking measurements indicated that the average exothermic heat effect was 0.0044 cal. This value was either added to or subtracted from the measured heats of solution, depending upon whether the solution process was endothermic or exothermic. Because of the nonreproducibility of this value (in a few instances as much as twice the average) the heats in the more dilute solutions have considerable uncertainties for some salts.

In order to test the electrical calibrating system of the apparatus, the calorimeter was also calibrated by measuring the heat of reaction of Tris (tris(hydroxymethyl)aminomethane) with 0.1 M HCl. Five samples of primary standard Tris (Fisher), dried according to the method of Irving and Wadsö²⁵ and ranging in size from approximately 0.25 to 0.076 mmole, were treated with 80 ml. of the acid solution. These gave an average value of -7113 ± 29 cal./mole, which agrees favorably with the value of -7104 cal./mole reported by Irving and Wadsö.²⁵ Within the limits of experimental error, no concentration dependence could be detected.

Calculations and Results

The measured heats of solution were extrapolated to infinite dilution both by the simple Debye-Hückel method of plotting the measured heats of solution against \sqrt{m} and by the extended Debye-Hückel treatment which has been recently employed for aqueous solutions of electrolytes.^{21,22} The merits of the latter method of extrapolation have been discussed previously.²¹ The extended Debye-Hückel equation can be written as

$$\rho = \Delta H_s^\circ - 2.303RT^2 \left(\frac{dB}{dT} \right)_{\nu+\nu-m}$$

where

$$\rho \equiv \Delta H_s^\circ - \frac{\nu}{2} |Z_+ Z_-| \delta_H I^{1/2} \alpha$$

and

$$\alpha \equiv \left| (1 + I^{1/2})^{-1} - \frac{\sigma(I^{1/2})}{3} \right|$$

The symbols have been defined previously.²¹ If one plots ρ vs. m , a linear relationship results which can be extrapolated to infinite dilution where $\rho = \Delta H_s^\circ$. The theoretical Debye-Hückel limiting slope, δ_H , used for calculating ρ , was calculated with the density data of Sinyakov, *et al.*,¹⁷ and the dielectric constant data of Leader and Gormley.¹⁴ This slope is 927 cal./mole^{-1/2} kg.^{1/2}.^{26,27} The value of $I^{1/2} \alpha$ was obtained from a previously prepared plot of I vs. $I^{1/2} \alpha$.²⁸

Results of the measurements are summarized in Table I. The first, second, and third columns list the molality, \sqrt{m} , and the measured integral heats of solution, respectively. The fourth column lists the theoretical values which are subtracted from the measured heats to obtain the ρ values which are listed in column five.

A comparison of the limiting slopes of the various salts and the theoretical limiting slope is made in Figure 2. Error bars indicate the estimated limits of error for each individual point. Where error bars are missing, the estimated error is less than 30 cal./mole.

The extrapolations do not necessarily represent the best lines that could be drawn through the centers of the points, but in all cases they are drawn consistent with the estimated reliability of the individual points. Within the limits of experimental error both types of extrapolation were linear and gave identical values for the standard heats of solution, except for sodium and lithium chlorides. The standard heat for sodium chloride was obtained by using the average of the two

(24) H. C. Dickinson, National Bureau of Standards Bulletin, No. 11, U. S. Government Printing Office, Washington, D. C., 1914, p. 189.

(25) R. J. Irving and I. Wadsö, *Acta Chem. Scand.*, 18, 195 (1964).

(26) The dielectric constant data of Bass, Nathan, Meighan, and Cole²⁷ gave a theoretical limiting slope of 1092 cal. mole^{-1/2} kg.^{1/2}. However, in the opinion of the authors, the data of Leader and Gormley are to be preferred. In any event, the difference in the values for the limiting slopes has no significant affect on the extrapolation of the present heat data.

(27) S. J. Bass, W. I. Nathan, R. M. Meighan, and R. H. Cole, *J. Phys. Chem.*, 68, 509 (1964).

(28) E. C. Jekel, Ph.D. Thesis, Purdue University, 1964.

Table I: Integral Heats of Solution and ρ -Values of Electrolytes in N-Methylformamide at 25°

$m \times 10^4$, moles/kg. of NMF	\sqrt{m}	ΔH_s^a , kcal./mole	$\delta_H^{1/2\alpha}$, kcal./mole	ρ , kcal./mole	$m \times 10^4$, moles/kg. of NMF	\sqrt{m}	ΔH_s^a , kcal./mole	$\delta_H^{1/2\alpha}$, kcal./mole	ρ , kcal./mole
CsCl					KCl				
4.24	0.0206	0.940	0.013	0.927	14.1	0.0375	0.344	0.023	0.321
5.36	0.0232	0.863	0.014	0.849	21.8	0.0467	0.342	0.028	0.314
8.28	0.0287	0.842	0.017	0.825	34.4 ^b	0.0587	0.304	0.035	0.269
15.3	0.0391	0.926	0.021	0.903	40.4 ^b	0.0635	0.326	0.038	0.288
30.0	0.0548	0.912	0.033	0.879	51.5	0.0715	0.337	0.042	0.295
NaCl					LiCl				
2.27	0.0151	-1.329	0.009	-1.338	1.94	0.0139	-12.5	0.009	-12.5
6.28	0.0251	-1.108	0.015	-1.123	2.73	0.0165	-11.6	0.009	-11.6
17.5	0.0418	-1.168	0.025	-1.193	2.76	0.0166	-11.5	0.010	-11.5
21.6	0.0465	-1.050	0.028	-1.078	4.69	0.0217	-10.62	0.013	-10.63
39.0	0.0556	-0.966	0.037	-1.003	6.42	0.0253	-10.18	0.015	-10.20
41.3	0.0643	-1.009	0.038	-1.047	8.66	0.0294	-10.21	0.018	-10.23
56.3	0.0750	-0.888	0.044	-0.932	10.9	0.0330	-9.83	0.020	-9.85
62.9	0.0793	-0.902	0.046	-0.948	15.2	0.0390	-10.23	0.023	-10.25
76.1	0.0873	-0.900	0.051	-0.951	16.3	0.0404	-9.79	0.024	-9.81
NaBr					NaI				
0.904	0.00951	-4.52	0.006	-4.53	24.8	0.0498	-9.95	0.030	-9.98
1.18	0.0109	-4.21	0.006	-4.22	36.0	0.0600	-10.06	0.036	-10.10
1.24	0.0111	-4.12	0.006	-4.12	0.735	0.00857	-8.26	0.005	-8.27
2.27	0.0151	-4.41	0.009	-4.42	1.03	0.0101	-8.17	0.006	-8.18
2.83	0.0168	-4.41	0.010	-4.42	1.57	0.0125	-8.17	0.007	-8.18
9.20	0.0303	-4.26	0.018	-4.28	5.04	0.0224	-8.23	0.013	-8.24
12.9	0.0359	-4.07	0.022	-4.09	7.74	0.0278	-8.28	0.017	-8.30
16.2	0.0402	-4.19	0.024	-4.21	12.7	0.0356	-7.99	0.021	-8.01
21.4	0.0463	-4.17	0.028	-4.20	13.7	0.0370	-8.17	0.022	-8.19
26.4	0.0514	-4.17	0.031	-4.20	24.0	0.0490	-8.10	0.029	-8.13
28.8	0.0537	-4.02	0.032	-4.05	27.8	0.0527	-7.93	0.031	-7.99

^a No attempt has been made to assign numerical values to the errors of the individual heat measurements. Approximate estimates of the errors are indicated by the error bars shown in Figure 2. ^b These are an average of two or more measurements.

extrapolations. The estimated standard heat for lithium chloride was obtained from an extrapolation of the ρ vs. m plot.

Although the data are not precise enough to determine decisively accurate values of the experimental slopes, certain trends are clear. Cesium and potassium chlorides have slopes that, within experimental error, are consistent with the theoretical limiting slope for heats of solution given by²⁹

$$\lim_{m \rightarrow 0} \frac{d\Delta H_s}{d\sqrt{m}} = \frac{2}{3}\delta_H$$

Sodium chloride, bromide, and iodide have slopes between 7 and 10 times the theoretical limiting slope. Most significantly, lithium chloride shows a sharp break in very dilute solutions and approaches infinite dilution with an estimated slope in the order of 280

times the slope predicted by the Debye-Hückel theory, making accurate extrapolation to infinite dilution impossible. The most dilute thermal data previously reported in a high dielectric constant solvent are for formamide ($D = 109$) in the range of 0.03 to 0.12 m , approximately 100 times more concentrated than the present measurements.⁸ A plot of ΔH_s vs. \sqrt{m} shows a slope that is opposite in sign from that observed in the present work. For the low dielectric constant solvent, liquid ammonia ($D = 16.9$), Gunn⁶ has measured heats of solution of electrolytes down to slightly less than $10^{-3} m$ and has found the limiting slope to be about 12 times more positive than the theoretical slope. Calorimetric measurements in methanol ($D = 32.6$) down to concentrations of about

(29) Since densities of the solutions were used in the calculation of δ_H , the variable is \sqrt{m} instead of the usual \sqrt{c} .

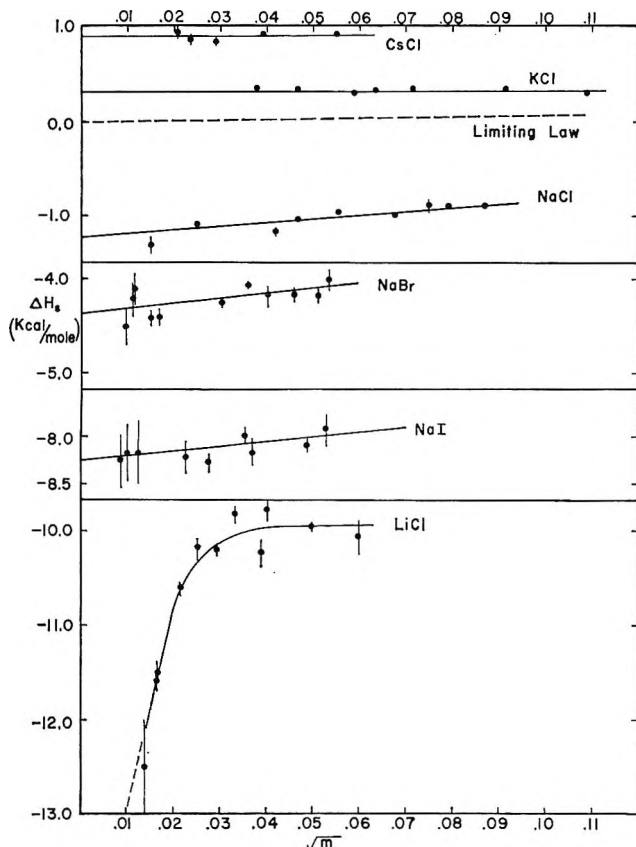


Figure 2. Integral heats of solution (kcal./mole) at 25° in N-methylformamide as a function of \sqrt{m} .

$3 \times 10^{-3} m$ show slopes considerably exceeding the theoretical.¹³ On the other hand, Wallace, Mason, and Robinson³⁰ measured the heat of dilution of sodium chloride in ethylene glycol ($D = 37.7$) down to $10^{-4} m$ and obtained a slope in agreement with the theoretical limiting slope. Even in the relatively high dielectric constant solvent water ($D = 78.5$), slopes considerably exceeding the theoretically predicted slopes are observed for electrolytes of higher valence type.³¹ In general, these positive slopes have been explained in terms of incomplete dissociation of ion pairs.^{6, 31}

In a high dielectric constant solvent such as N-methylformamide, one would anticipate complete dissociation of electrolytes. However, ionic association in high dielectric constant solvents is not unknown. The conductance measurements by Coates and Taylor³² on several electrolytes in liquid HCN show that certain lithium salts, including lithium chloride, are associated. French and Glover¹⁵ measured the conductance of several inorganic electrolytes in N-methylformamide and generally found deviations from the theoretical Debye-Hückel-Onsager slopes to be positive, but

small, possibly indicating a small amount of ionic association. They also found the conductance *vs.* \sqrt{c} curves to be slightly concave to the concentration axis, an effect similar to that found by Coates and Taylor³² for lithium salts in liquid HCN. However, because of the high dielectric constant of this solvent, French and Glover discard the possibility that the concavity is caused by ionic association. Unfortunately, no conductance data are available for LiCl in N-methylformamide. On the basis of these and the present results, it appears to the authors that there probably is ionic association in this solvent for some electrolytes in spite of its high dielectric constant. This is an unexpected result and one that should be investigated further.

Table II lists the standard heats of solution, obtained by extrapolating the measured integral heats to infinite dilution. The indicated errors are the standard deviations of the points from the extrapolated lines. Because of the extremely positive limiting slope for LiCl, the standard heat of solution for this salt is only an estimate. Also listed in Table II are heats reported by Strack, Swanda, and Bahe,¹⁸ calculated from solubility data. The directly measured calorimetric values and those calculated from solubility data agree remarkably well for sodium and potassium chlorides, in spite of the questionable assumption that the activity coefficient does not vary with temperature. The fact that values for sodium bromide do not agree may be caused by the much higher solubility of sodium bromide, making invalid the assumption that the activity coefficient is independent of temperature.

Table II: Standard Heats of Solution of Electrolytes in N-Methylformamide at 25°

Solute	ΔH_s° , kcal./mole ^a	ΔH_s° , kcal./mole
CsCl	0.890 ± 0.042	
KCl	0.308 ± 0.018	0.0
NaCl	-1.244 ± 0.046	-1.197
LiCl	$(-13.1)^c$	
NaBr	-4.393 ± 0.105	-1.539
NaI	-8.258 ± 0.085	

^a This work. ^b See ref. 18. ^c Estimated from the extrapolation of ρ in the ρ *vs.* m plot.

(30) W. E. Wallace, L. S. Mason, and A. L. Robinson, *J. Am. Chem. Soc.*, **66**, 362 (1944).

(31) H. S. Harned and B. B. Owen, "The Physical Chemistry of Electrolytic Solutions," 3rd. Ed., Reinhold Publishing Corp., New York, N. Y., 1958, pp. 335, 336, 577, 578.

(32) J. E. Coates and E. G. Taylor, *J. Chem. Soc.*, 1245 (1936).

Heats of solution in N-methylformamide at 25° are much more negative than those in water. Data from the literature and unpublished data in this laboratory on other nonaqueous solvents indicate that, in general, heats of solution in nonaqueous solvents are more negative than those in water. This

phenomenon is being investigated further and will be reported in a future communication.

Acknowledgment. The authors are indebted to the United States Atomic Energy Commission, which supported this work through Contract AT-(30-1)-3019.

Calculation of the Hall Effect in Ionic Solutions^{1a}

by Harold L. Friedman^{1b}

IBM Watson Research Center, Yorktown Heights, N. Y. (Received February 4, 1965)

The theory of electrical conductance in ionic solutions recently reported by the author has been extended to apply to the transport in combined electric and magnetic fields. Calculations are made with the "brownian" model, essentially the model used in the Debye-Hückel-Onsager conductance theory. General expressions and numerical results are obtained for the ideal and limiting-law terms of the Hall conductance. The calculations indicate that the effect is large enough to be measurable, at least for solutions of the more mobile ions. For symmetrical electrolytes the limiting-law term opposes the ideal term in the Hall conductance, while for unsymmetrical electrolytes it may either aid or oppose the ideal term.

1. Introduction

When an electric field in the x direction and a magnetic field in the y direction of a Cartesian coordinate system act on a conducting body, the electric current that flows tends to have a component in the z direction.^{1c} Depending on the external electrical connections to the body, one may observe this current component, the Hall current, or one may determine the electric field in the z direction required to reduce this current to zero, the Hall field.^{2,3} This phenomenon is most easily observed in materials in which the carriers of electric charge have relatively high mobility. If the carriers are all of one species and if their concentration is low, then the measurement of the Hall effect can be used quite simply to determine the carrier concentration.⁴ For example, this is true in silicon crystals in which the carrier concentration may be as low as $10^{-10} M$ and the mobilities of the carriers (electrons or

holes, depending on the impurities in the silicon) as high as $3000 \text{ cm}^2/\text{v. sec}^5$

The Hall effect due to ionic carriers is difficult to ob-

(1) (a) Paper presented at the 148th National Meeting of the American Chemical Society, Chicago, Ill., Sept. 1964; (b) Department of Chemistry, State University of New York, Stony Brook, N. Y.; (c) throughout this paper we shall assume that the electric field defines the x axis and the magnetic field the y axis of a Cartesian coordinate system.

(2) The latter is the usual arrangement. For example, see A. G. Redfield, *Phys. Rev.*, **94**, 526 (1954). However, in the statistical calculations it seems easier to assume that the Hall current flows unimpeded by any external electric field in the z direction.

(3) See S. R. de Groot and F. Mazur, "Non-Equilibrium Thermodynamics," North-Holland Publishing Co., Amsterdam, 1962, for an account of some of the phenomenological aspects.

(4) R. E. Peierls, "Quantum Theory of Solids," Oxford University Press, Oxford, 1955.

(5) In some circumstances one can observe components of the Hall current due to particular species, depending on the use of electrodes at which only these species act reversibly [J. Swanson, *IBM J. Res. Develop.*, **1**, 39 (1957)]. This can be avoided by using electrodes of the same composition as the solution.

serve in solids⁶ and does not seem to have been observed at all in liquid solutions. The reason for this difficulty is that, for given electric and magnetic fields, the Hall field is proportional to the mobility of the carriers. The mobility of ionic carriers in condensed phases is less than one-millionth of the highest mobility of electrons or holes in semiconductors.

In an ordinary conductance experiment cations and anions are, on the average, moving in opposite directions. The Hall current, by contrast, comes from a flow of cations and anions in the same direction along the z axis. Since the same parameters (ionic friction coefficients, charges, collision radii, ...) needed for a model theory of electric conduction also enter into the theory of the Hall effect and since they must enter in different combinations, because of the difference in relative ionic flows that we have just noted, one can hope to separate these parameters to a certain degree by combining conductance and Hall effect data. In this application, Hall effect measurements may supplement the determination of transference numbers. This was the initial motivation for the work reported here.

The calculations described here consist of applying a rather general theory⁷ to a particular model for electrolyte solutions. This is the so-called brownon model, which is closely related to the model used in the classical Debye-Hückel-Onsager theory of conductance in ionic solutions. The model specifies the laws of interaction among the ions as well as the way each ion, when separated from the others, moves through the solvent at equilibrium. In particular, it is assumed that this motion is Brownian motion, which is certainly not accurately the case for simple ions in ordinary ionic solutions. Nevertheless, the limiting law for conductance that is derived on the basis of this model seems to be in good agreement with experiment in a variety of systems. The work reported here provides a basis for further tests of the model by measuring the ideal and limiting-law terms of the Hall conductance and comparing them with the results of these calculations.

The present theory is based on an adaptation⁷ of Kubo's theory of transport coefficients to the calculation of the electrical conductance of ionic solutions. This adaptation is, in turn, easily extended to calculate the Hall effect as described in section 2. The only new function required, in addition to those appearing in the conductance theory, is the propagator that represents the Brownian motion of a charged body in a magnetic field. The first-order calculation of this propagator, given in section 3, is adequate for our purpose.

Recently the propagator for Brownian motion in a magnetic field has been calculated under very general conditions by Kursanoglu and Polcyn.⁸ However, the simpler function obtained here is adequate for our purpose. We also note that Falkenhagen and Ebeling have recently reported a theory for the Hall effect in plasmas which is applicable to ionic solutions,⁹ although not yet worked out to the degree of the present theory.

The specific conductance σ of an ionic solution of total ion concentration c has the form

$$\sigma = Ac + Sc^{3/2} + Ec^2 \ln c + Jc^2 + \dots \quad (1.1)$$

where the notation for the coefficients is chosen to conform roughly⁷ to that used by Fuoss¹⁰ in the corresponding expansion of the equivalent conductance. The Hall effect may be reduced to an analogous "conductance" σ' which, by the methods of this paper, is found to have the form

$$\sigma' = A'c + S'c^{3/2} + E'c^2 \ln c + J'c^2 + \dots \quad (1.2)$$

The calculation of the coefficient A' of the ideal term is given in section 4, and that of the coefficient S' of the limiting law term is outlined in section 5. These calculations are very similar to those of A and S by the cluster theory. In all cases the only calculations that have been made so far are rigorously applicable only to the brownon model.⁷

Numerical results for a number of cases of interest are given in section 7. The calculations in section 8 lead to the expectation that the Hall effect in ionic solutions is measurable although, probably, not without a considerable effort.

2. General Theory

The ohmic current $\langle \mathbf{J} \rangle$ through a solution due to an electric field \mathbf{E} has the cluster expansion^{7,11}

$$\langle \mathbf{J} \rangle = [\Sigma_a \langle A_0, a \rangle + \Sigma_{ab} \langle J_0, ab \rangle + \langle A_1, ab \rangle + \langle J_1, ab \rangle + \dots] + \Sigma_{abc} \langle J_1, abc \rangle + \dots] \cdot \mathbf{E}V \quad (2.1)$$

where the symbols $\langle \dots \rangle$ represent cluster integrals, and the sums are over solute species. Those cluster

(6) P. L. Read and E. Katz, *Phys. Rev. Letters*, **5**, 466 (1960).

(7) For an introductory account see H. L. Friedman in "Chemical Physics of Ionic Solutions" (a selection of invited papers presented at a symposium on electrolyte solutions sponsored by the Electrochemical Society), B. E. Conway and R. G. Barrades, Ed., John Wiley and Sons, Inc., New York, N. Y., 1965.

(8) R. F. Polcyn, *Phys. Fluids*, **7**, 1719 (1964). The author is grateful to Prof. Kursanoglu for a copy of this in advance of publication.

(9) H. Falkenhagen and W. Ebeling, *Ann. Physik*, **10**, 347 (1963).

(10) See, for example, R. M. Fuoss and F. Accascina, "Electrolytic Conductance," Interscience Publishers, Inc., New York, N. Y., 1959.

(11) H. L. Friedman, *Physica*, **30**, 537 (1964).

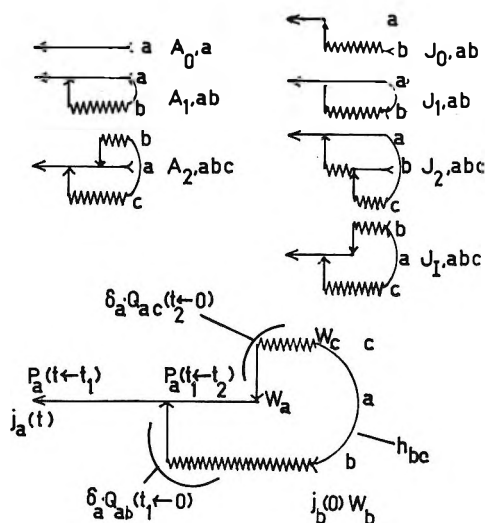


Figure 1. Some graphs corresponding to terms of the cluster expansion of the conductance. The larger graph, which is also a part of the J_I term, is a key to the various bond symbols. Note that $t > t_1 > t_2 > 0$. Each horizontal line, straight or wiggly, has a W function at its early end which is not represented graphically but is shown on the key. The functions that appear may be summarized as follows: $P_a(\{a\}_t \leftarrow \{a\}_0)$ is the conditional probability density or propagator for a solute particle of species a to go to phase $\{a\}_t$ from another phase $\{a\}_0$ in the time t , all in the pure solvent. $F_{ab}(\{a\}\{b\})$ is the solvent-averaged vector force acting on a at phase $\{a\}$ due to b at phase $\{b\}$, all in the pure solvent. $j_a(\{a\}) \equiv p_a e_a / m_a$ is the element of current due to a in the phase $\{a\}$, p_a being the vector momentum in the phase, e_a the charge on a , and m_a the mass of a . $\delta_a \equiv \mathbf{1}_x \partial / \partial (p_a)_x + \mathbf{1}_y \partial / \partial (p_a)_y + \mathbf{1}_z \partial / \partial (p_a)_z$ is the gradient operator in the momentum space of a . $W_a \equiv \exp(-\beta p_a^2 / 2m_a) / [2\pi m_a / \beta]^{3/2}$ is the normalized equilibrium momentum distribution function for a . ($\beta \equiv 1/kT$.) h_{ab} is the equilibrium configuration correlation function, defined by the equation $h_{ab} \equiv \exp(-w_{ab}\beta) - 1$ where w_{ab} is the equilibrium potential of average force for the interaction of a and b in the solution whose conductance is being calculated. c_a is the particle number density of solute species a in the solution. $Q_{ab}(\{a\}_t \leftarrow \{b\}_0)$ is the sum of chains

$$F_{a1} P_1(t_a \leftarrow t_1) [-c_1] \delta_1 \cdot F_{12} W_1 P_2(t_2 \leftarrow t_1) \times [-c_2] \delta_2 \dots \delta_n \cdot F_{nb} W_n P_b(t_n \leftarrow 0)$$

of all lengths and all compositions of the intermediate vertices, and integrated over all the intermediate phases and times. (Note that we have contracted the notation for the propagators here.) Q_{ab} is a vector, but the vector notation for it is suppressed. A cluster term is formed from any graph by multiplying it by

$$[\beta/V] e^{i\omega t} [-]^\nu \Pi_{s=1}^n c_s n_s$$

and integrating over all the phase and time variables. Here n_s is the number of molecules of species s explicitly appearing in the graph (i.e., not counting those in the interior of chain sums), ν is the number of explicit $\delta \cdot F$ or $\delta \cdot Q$ bonds in the graph, and $\omega/2\pi$ is the chosen frequency of the electric field. As an example, we have the cluster term

$$(A_{11}, ab) \equiv -c_a c_b \beta V^{-1} \int_0^\infty dt e^{i\omega t} \int_0^t dt_1 \times \int d\{a\}_t j_a P_a(t \leftarrow t_1) d\{a\}_1 \delta_a \cdot Q_{ab}(t_1 \leftarrow 0) W_b \times P_a(t_1 \leftarrow 0) j_b W_a h_{ab} d\{ab\}_0$$

where the third integral sign specifies a multiple integration over the phases $\{a\}_t$, $\{a\}_1$, and $\{ab\}_0$. The calculations of the present paper are for $\omega = 0$.

integrals appearing in this expression are specified, via a certain code, by the graphs in Figure 1. The code is summarized in the caption of the figure, but for further details the reader should consult the earlier work,^{7,11} especially pp. 538 and 539 of ref. 11.

In our earlier applications of (2.1) it was assumed that E was the only field acting on the system. However, the equation is equally valid for the current in the presence of additional external fields provided that none of them, acting by itself, can keep the system from reaching thermodynamic equilibrium. In particular, this is true for a magnetic field. We now take eq. 2.1 for the current due to an electric field alone, and we write

$$\langle J \rangle^H = [\sum_a (A_{0,a})^H + \sum_{at} \{ (J_{0,ab})^H + \dots \} + \dots] \cdot E V \quad (2.2)$$

for the current due to the combined action of electric field E and magnetic field H .

Now in each cluster integral $\langle \dots \rangle$ the functions W_a , h_{ab} , F_{ab} , and P_a ¹² that appear pertain to the system at equilibrium in the absence of external fields. In the corresponding cluster integral $\langle \dots \rangle^H$ the same functions appear, but now they pertain to the system at equilibrium in the presence of the magnetic field H . We write $P_a^H(t \leftarrow 0)$ for the propagator that is the conditional probability density for a solute particle of species a to go to a specified phase $\{a\}_t$ at time t from a specified phase $\{a\}_0$ at time zero when the system is at equilibrium in the presence of the magnetic field H . The remaining functions W_a , h_{ab} , and F_{ab} are unchanged when a magnetic field is applied to the system at equilibrium. The cluster integrals $\langle \dots \rangle^H$ are then the same as the cluster integrals $\langle \dots \rangle$ except that P_a^H in the former replaces P_a everywhere in the latter.

The perturbation of the propagator due to the field may be expressed by an equation of the Feynman type.^{7,13}

(12) Here we mean $W_a, W_b, \dots; h_{aa}, h_{ab}, h_{bb}, \dots$; etc., where the indices a, b, \dots represent the species of the solute molecules in the system. Thus, W_a may mean either the generic Maxwell-Boltzmann distribution function for a solute particle or the specific Maxwell-Boltzmann distribution function for a particle of species a , depending on the context.

$$P_a^H(t' \leftarrow t) = P_a(t' \leftarrow t) - \int_t^{t'} ds \int P_a(t' \leftarrow s) d\{a\}_s L_a^H P_a^H(s \leftarrow t) \quad (2.3)$$

where L_a^H is the term in the Liouville operator for the system due to the action of the magnetic field on molecule a . It is

$$L_a^H = \hat{c}^{-1} \mathbf{j}_a \wedge \mathbf{H} \cdot \delta_a \quad (2.4)$$

where \hat{c} is the velocity of light and the symbol \wedge indicates the vector cross product. The other symbols have been defined above.

We shall calculate only the part of the Hall effect that is linear in the magnetic field. To this approximation eq. 2.3 becomes

$$P_a^H(t' \leftarrow t) = P_a(t' \leftarrow t) + P_a'(t' \leftarrow t) \quad (2.5)$$

where we define

$$P_a'(t' \leftarrow t) \equiv - \int_t^{t'} ds \int P_a(t' \leftarrow s) d\{a\}_s L_a^H P_a(s \leftarrow t) \quad (2.6)$$

The \mathbf{H} -dependent cluster integrals may be calculated on the basis of (2.5). That is, we make the substitution (2.5) for each \mathbf{H} -dependent propagator that appears in each \mathbf{H} -dependent cluster integral. For an \mathbf{H} -dependent cluster integral in which there are n propagators P_a^H this generates 2^n new cluster integrals. Some examples of this are represented graphically in Figure 2. Fortunately, in each case only a few of the 2^n new cluster integrals need be evaluated; the one with no P_a' propagators contributes to $\langle \mathbf{J} \rangle$, the current in the absence of a magnetic field. Those with more than one P_a' propagator contribute to the dependence of $\langle \mathbf{J} \rangle^H$ on the second or higher power of \mathbf{H} and may be neglected here. Those with exactly one P_a' propagator contribute to $\langle \mathbf{J} \rangle'$, the term in the current that is proportional to \mathbf{H}

$$\langle \mathbf{J} \rangle' = \Sigma_a \langle A_{0,a} \rangle' + \Sigma_{ab} [\langle J_{0,ab} \rangle' + \langle A_{1,ab} \rangle' + \langle J_{1,ab} \rangle' + \dots] + \dots \cdot \mathbf{E}V \quad (2.7)$$

where by $\langle \dots \rangle'$ we designate the sum of distinct cluster integrals obtainable by replacing just one of the propagators P_a in the corresponding cluster integral $\langle \dots \rangle$ by a propagator P_a' . (A number of examples may be found in section 5.) Thus, neglecting quadratic and higher-order terms in \mathbf{H} , we have

$$\langle \mathbf{J} \rangle^H = \langle \mathbf{J} \rangle + \langle \mathbf{J} \rangle' \quad (2.8)$$

Of course, $\langle \mathbf{J} \rangle$ is in the same direction as \mathbf{E} , and in the conductance theory¹¹ we took advantage of this to simplify the equations by replacing the tensor

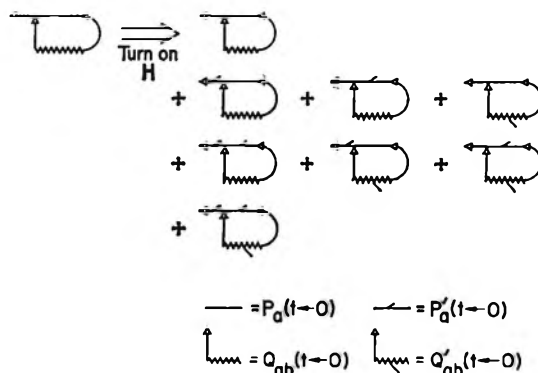


Figure 2. Expansion of A_1 graph in a magnetic field according to eq. 2.5. The chain sum Q' is defined in section 5.

$\langle \dots \rangle$ by one of its diagonal elements $\mathbf{1}_x \cdot \langle \dots \rangle \cdot \mathbf{1}_x$. Now the Hall current is by definition the current component in the direction $\mathbf{E} \wedge \mathbf{H}$. In view of the convention we have made about the direction of these fields¹ we may simplify the equations which follow by defining a scalar Hall conductance σ' by the equation

$$\sigma' = \mathbf{1}_x \cdot \langle \mathbf{J} \rangle' \cdot \mathbf{1}_x / V |\mathbf{E}| \quad (2.9)$$

Finally, in place of (2.7) we have the equivalent equation

$$\sigma' = \Sigma_a \mathbf{1}_x \cdot \langle A_{0,a} \rangle' \cdot \mathbf{1}_x + \Sigma_{ab} \mathbf{1}_x \cdot \langle J_{0,ab} \rangle' \cdot \mathbf{1}_x + \dots \quad (2.10)$$

For additional simplicity of notation in the following equations we shall suppress the $\mathbf{1}_x$ and $\mathbf{1}_x$ unit vectors whenever this can be done without leading to ambiguity.

3. The One-Brownion Propagator in a Magnetic Field

The general expression (2.6) for the linearly \mathbf{H} -dependent term of the one-particle propagator may be written

$$P_a'(t \leftarrow 0) = - \int_0^t ds \int P_a(t \leftarrow s) d\{a\}_s [\mathbf{P}_a \wedge \boldsymbol{\Omega}] \cdot \delta_a P_a(s \leftarrow 0) \quad (3.1)$$

$$\boldsymbol{\Omega}_a \equiv e_a \mathbf{H} / m_a \hat{c} \quad (3.2)$$

where $|\boldsymbol{\Omega}_a|/2$ is the Larmor frequency of a body of species a as a free body in a circular orbit in the field \mathbf{H} . Now to find P_a' in the case that a is a brownion, i.e., a body that moves according to the law of Brownian motion,^{7,11} we need only introduce the form of P_a appropriate for Brownian motion into (3.1). The resulting expression is rather complicated, and for the

(13) R. P. Feynman, *Phys. Rev.*, 76, 749 (1949).

purposes of this paper we need only certain integrals on P_a' which, fortunately, can be simply expressed. These integrals are collected in the Appendix.

It is interesting to note that, at least as far as the ideal and limiting-law terms of σ' are concerned, we get the correct result for any particular $\langle \dots \rangle'$ when we use the approximation

$$P_a'(t \leftarrow 0) = [e_a \mathbf{H} / \hat{c} \zeta_a] P_a(t \leftarrow 0) \quad (3.3)$$

provided that both $\langle \dots \rangle'$ and the corresponding $\langle \dots \rangle$ are nonzero. Here ζ_a is the friction coefficient of a molecule of species a . In the following equations it often appears in the combination $\zeta_a / m_a \equiv \omega_a$.

4. The Ideal Term in the Hall Conductance

This is the $A'c$ term in eq. 1.2 and is the relevant term for a solution of infinitesimal carrier concentration. It is readily evaluated as follows. Note that propagators $P'_{imn(a)}$ are integrals on P_a' as defined in the Appendix.

$$\begin{aligned} A'c &= \Sigma_a \mathbf{1}_z \cdot \langle A_0, a \rangle' \cdot \mathbf{1}_x \\ &= \Sigma_a [c_a e_a^2 \beta / V m_a^2] \times \\ &\quad \int_0^\infty dt \int d\{a\} \mathbf{1}_z \cdot \mathbf{p}_a P_a'(t \leftarrow 0) \mathbf{p}_a \cdot \mathbf{1}_x W_a d\{a\}_0 \\ &= \beta \Sigma_a [c_a e_a^2 / m_a^2] \times \\ &\quad \int_0^\infty dt \int d^3 p \mathbf{1}_z \cdot P'_{212(a)}(t \leftarrow 0) \cdot \mathbf{1}_x d^3 p \\ &= \beta \Sigma_a [c_a e_a^2 / m_a^2] |\Omega_a| m_a / \beta \omega_a^2 \mathbf{1}_y \cdot [\mathbf{1}_z \wedge \mathbf{1}_x] \\ &= |\mathbf{H}| \hat{c}^{-1} \Sigma_a c_a e_a^3 / \zeta_a^2 \quad (4.1) \end{aligned}$$

This may be compared with the ohmic conductance for an ideal solution

$$Ac = \Sigma_a c_a e_a^2 / \zeta_a \quad (4.2)$$

In the case that only one ionic species in the solution, say a , has appreciable mobility we find the ratio of these terms to be

$$\begin{aligned} A'/A &= e_a |\mathbf{H}| / \hat{c} \zeta_a \\ &= 0.9666 \times 10^{-13} z_a \lambda_a^0 |\mathbf{H}| / \text{gauss} \quad (4.3) \end{aligned}$$

where z_a is the ionic charge in protonic units and λ_a^0 is the limiting ionic conductance. The relevance of this small ratio for experiments is discussed in section 8.

The result (4.3) is equivalent to what has been obtained for semiconducting solids on the basis of band theory and the Boltzmann equation.⁴ It seems to depend on the assumed Brownian motion of the carriers but to be otherwise quite independent of the mechanism of transport. It also depends on the assumed Max-

wellian momentum distribution of the carriers at equilibrium, and for metals a slightly different result is obtained.⁴

5. Limiting-Law Terms

There are many graphs that contribute to the limiting-law term $S'c^{3/2}$, many more than contribute to $Sc^{3/2}$. Here it seems adequate to describe the selection and evaluation of the graphs for only a few illustrative cases and then to summarize all of the results that have been obtained.

In Figure 3 we show all the graphs that contribute to the term $J_{1,ab}$ which was defined following eq. 2.7. Although all of these are, in a sense, derived from $J_{1,ab}$ of Figure 1, each corresponds to an integral which may be evaluated separately. Thus, a magnetic field decomposes the cluster integral $J_{1,ab}$ into three cluster integrals corresponding to the three graphs in Figure 3.

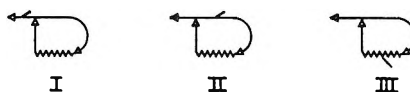


Figure 3. Graphs contributing to $\langle J_{1,ab} \rangle'$.

The first of these, which we may designate as $\langle J_{1,ab} \rangle^I$, has the analytical form

$$\begin{aligned} \langle J_{1,ab} \rangle^I &= -c_a c_b \beta V^{-1} \int_0^\infty dt \int_0^t d\tau \int d\{a\} \mathbf{1}_z \times \\ &\quad j_a P'_a(t \leftarrow \tau) d\{a\}_\tau \left[\frac{P_a(\tau \leftarrow 0) W_a d\{a\}_0}{\delta_a \cdot Q_{ab}(\tau \leftarrow 0) j_b W_b d\{b\}_0} \right] h_{ab} \quad (5.1) \end{aligned}$$

$$= -c_a c_b \beta \int_0^\infty dt \int d\{a\} \mathbf{1}_z j_a P'_a(t \leftarrow 0) d^3 p f(p) \quad (5.2)$$

$$f(p) \equiv \int_0^\infty d\tau \left[\frac{P_a(\tau \leftarrow 0) W_a d\{a\}_0}{\delta_a \cdot Q_{ab}(\tau \leftarrow 0) j_b W_b d\{b\}_0} \right] h_{ab} \quad (5.3)$$

The expression for $J_{1,ab}$ is the same as the expression in (5.2) if P_a' is replaced by P_a . The ratio of the two cluster integrals is

$$\begin{aligned} \frac{\mathbf{1}_z \cdot \langle J_{1,ab} \rangle^I \cdot \mathbf{1}_x}{\mathbf{1}_z \cdot \langle J_{1,ab} \rangle \cdot \mathbf{1}_x} &= \frac{\int_0^\infty dt \int \mathbf{1}_z \cdot P_{112}{}^{(a)}(t, p) f(p) d^3 p}{\int_0^\infty dt \int \mathbf{1}_z \cdot P_{112}{}^{(a)}(t, p) f(p) d^3 p} \\ &= \frac{|\Omega_a / \omega_a^2| \int \mathbf{1}_z \cdot \mathbf{p} f(p) d^3 p}{[1 / \omega_a] \int \mathbf{1}_z \cdot \mathbf{p} f(p) d^3 p} \\ &= |\mathbf{H}| e_a / \hat{c} \zeta_a \quad (5.4) \end{aligned}$$

The propagators $P'_{imn(a)}$ are integrals on the Brownian motion propagator as defined in the Appendix.

Now turning to the term derived from graph II in Figure 3 we have

$$\langle J_{1,ab} \rangle^{\text{II}} \sim \int d\{a\}_1 \left\{ \begin{array}{l} P_a'(t_1 \leftarrow 0) W_a d\{a\}_0 \\ Q_{ab}(t_1 \leftarrow 0) j_b d\{b\}_0 \end{array} \right\} h_{ab} \quad (5.5)$$

where we have omitted factors derived by integrating $P_a(t \leftarrow t_1)$ and then applying Green's theorem (cf. ref. 11, p. 547). According to the brownian model, \mathbf{F}_{ab} is independent of \mathbf{P}_a (except for higher order terms in the hydrodynamic part of the force¹⁴ which may be neglected here), and therefore the same is true of Q_{ab} . It follows that the integral in (5.3) is proportional to

$$\int d^3 p_i P_a'(t \leftarrow 0) W_a d^3 p_0 = P_{200}'^{(a)} = 0 \quad (5.6)$$

From another point of view one sees that in this term the magnetic field, acting on a through $\mathbf{j}_a \wedge \mathbf{H}$ (see eq. 2.4), is as likely to find a going in one direction as another and so on the average has no effect. This is to be contrasted with the case in the other cluster integrals we have evaluated (eq. 4.1 and 5.2) in which P_a' is integrated with a momentum factor giving a preferred direction to the motion of a .

To find the contribution of graph III of Figure 3 we need an explicit expression for the linear response of the chain sum Q_{ab} to a magnetic field. We may begin with the expression for the chain sum given in eq. 6.15 of an earlier paper¹⁵

$$Q_{ab} = [\mathbf{U} + \mathbf{R}]^{-1} Q_{ab}^0 \quad (5.7)$$

in which Q_{ab} , \mathbf{R} , and Q_{ab}^0 are the matrices of the Fourier components of the chain sum Q_{ab} , the repeating element in the chain sum, and the zeroth term of the chain of the chain sum, respectively. \mathbf{U} is the unit matrix. These matrices may equally well be regarded as tensors, and we find it convenient to do so here. Specifically, we have

$$Q_{ab}^0(t \leftarrow 0) = \int \mathbf{F}_{ab} d\{b\} P_b(t \leftarrow 0) \quad (5.8)$$

$$R(t \leftarrow 0) = -\beta \sum_{a=1}^{se} [c_a/m_a] \int Q_{aa}^0(t \leftarrow 0) \mathbf{p}_a W_a d^3 p_a \quad (5.9)$$

The Fourier transforms referred to here are space-time transforms

$$\int_0^\infty e^{i\omega t} dt \int d^3 r e^{i\mathbf{k}\cdot\mathbf{r}} f(\mathbf{r}, t)$$

the momentum variables not being transformed. For example, in applying the transforming operation to $Q_{ab}^0(t \leftarrow 0)$, \mathbf{r} is the vector from the location of body b at time zero to the location of body a at time t . The Fourier transform operation does not change the rank of a tensor, but, following the earlier work,¹⁵ we use

tensor notation for the transforms in (5.7) but not for the direct functions Q_{ab} , Q_{ab}^0 , and R .

Now (5.7) is applicable in the presence of a magnetic field, provided that we use the appropriate propagators in (5.8) and (5.9). Therefore, in view of (2.5), we see that Q_{ab}^{H} , the transform of the chain sum in a magnetic field, has an expansion

$$Q_{ab}^{\text{H}} = Q_{ab} + Q_{ab}' + \dots \quad (5.10)$$

in which Q_{ab} is given by (5.7) with propagators appropriate for zero magnetic field, and the term linear in the field is Q_{ab}' . We find

$$Q_{ab}' = [\mathbf{U} + \mathbf{R}]^{-1} Q_{ab}'^0 - [\mathbf{U} + \mathbf{R}]^{-1} \mathbf{R}' Q_{ab} \quad (5.11)$$

$$Q_{ab}'^0 \equiv \int \mathbf{F}_{ab} d\{b\} P_b'(t \leftarrow 0) \quad (5.12)$$

$$R'(t \leftarrow 0) \equiv -\beta \sum_{s=1}^{se} [c_s/m_s] \int Q_{ss}'^0(t \leftarrow 0) \mathbf{p}_s W_s d^3 p_s \quad (5.13)$$

When we have chain sums the expansion (5.11) is entirely equivalent to making the expansion (2.5) in every term of the chain sum and then collecting terms that are of order zero or unity in \mathbf{H} .

Now we may find the contribution to $S'c^{3/2}$ due to graph III of Figure 3. This is not so simply described as in the case of graph I in this figure because Q_{ab} separates into terms depending on the force,¹¹ and, in the case of the Stokes (hydrodynamic) force, the effective propagator is $P'_{203}^{(b)}$ which is not simply proportional to $P_{203}^{(b)}$ (see Appendix). Nevertheless, the final result is as simple as for graph I, namely

$$\frac{\mathbf{1}_z \cdot \langle J_{1,ab} \rangle^{\text{III}} \cdot \mathbf{1}_z}{\mathbf{1}_z \cdot \langle J_{1,ab} \rangle \cdot \mathbf{1}_z} = \frac{|\mathbf{H}| e_b}{\hat{c} \xi_b} \quad (5.14)$$

for both Coulomb and Stokes forces. In this case and in all of the others that have been investigated, it is found that the second term of Q_{ab}' , the one with R' , does not contribute to the limiting-law term $S'c^{3/2}$. Its contribution vanishes because of symmetry in the case of chains of Coulomb forces and because of electro-neutrality in the case of chains of Stokes forces.

All of the graphs that have been found to contribute to the $S'c^{3/2}$ term of the Hall conductance are listed in Figure 4. In some cases, as in the first row of the figure, two graphs are combined because this simplifies the evaluation of their contributions to σ' . The ratio $\langle \dots \rangle / \langle \dots \rangle$ is given in those cases in which the integral on the given graph is a factor $|\Omega_i|/\omega_i$ times the integral on the corresponding graph in the expansion of σ . The graphs in row 8 + 9 yield a two-term cluster integral. One term, desig-

(14) H. L. Friedman, *J. Chem. Phys.*, **42**, 450 (1965).

(15) H. L. Friedman, *Physica*, **30**, 509 (1964).

nated term 8, is just $|\Omega_b|/\omega_b$ times the cluster integral obtained if the magnetic field perturbations are deleted from the graphs. The other term, designated 9, corresponds to a vanishing term of σ .

In the theory of the ohmic conductance there is no contribution from chains of force-propagator interactions in which some of the forces are Coulomb forces and some are Stokes forces.¹¹ However, such mixed chains, when perturbed by a magnetic field, do contribute to the Hall conductance in the terms derivable from graphs 12 and 13 of Figure 4.

The evaluation of the cluster integrals derived from all of these graphs is readily carried out by the methods of the earlier papers. The results are given in a compact form in the following section.

6. Limiting-Law Results in Practical Form

Following a procedure used in the cluster theory of the limiting law of the ohmic conductance of electrolyte mixtures,¹⁶ we express the Hall conductance as a sum of contributions σ_s' of the ionic species

$$\sigma' = \sum_{s=1}^{se} \sigma_s' \quad (6.1)$$

Each term σ_s' may be calculated as a sum of all cluster diagrams in which the late element of current is carried by an ion of species s . The limiting-law term of σ' can also be expressed as a sum of ionic contributions; for this purpose the following form is particularly convenient

$$S'c^{3/2} = K'\Gamma^{1/2} \sum_{s=1}^{se} S_s' c_s e_s^3 / \zeta_s^2 \quad (6.2)$$

where, if $H \equiv |\mathbf{H}|$

$$K' \equiv [H/c]K$$

$$K \equiv 1.981 \times 10^{-6} [\epsilon T]^{-3/2} \quad (6.3)$$

$1/2\Gamma$ is the molar ionic strength, ϵ the dielectric constant of the solvent, and T the temperature. The new coefficient S_s' is given by the equation

$$S_s' = \lim_{c \rightarrow 0} \left(\frac{\sigma_s'}{[c_s e_s^3 / \zeta_s^2][H/c]} - 1 \right) \frac{3\epsilon}{\beta \kappa e_{ei}^2} \quad (6.4)$$

where e_{ei} is the electronic charge and κ is the reciprocal ion atmosphere radius of the Debye-Hückel theory.

Now S_s' may be expressed as a sum of contributions derived from various cluster diagrams

$$S_s' = \sum_{M=1}^{13} S_s'(M) \quad (6.5)$$

where the numbers M are the designations of the graphs in Figure 4. The variables in the following expressions are: $z_s = e_s/|e_{ei}|$, the signed ionic charge;

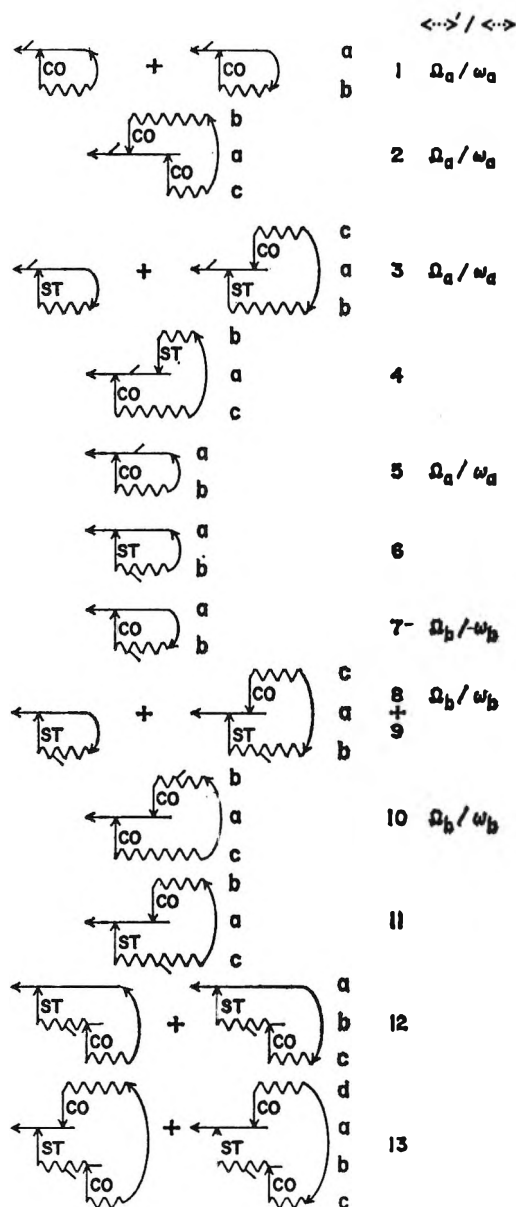


Figure 4. Graphs which contribute to the limiting-law term of the Hall conductance. The numbers are the indices by which the graphs are referred to in the text. The last column indicates the cases in which the integral on the graph is simply proportional to the integral on the graph without the perturbation by a magnetic field.

$u_s = 1/\zeta_s$, the ionic mobility; $\mu_s = 4\pi\beta c_s e_s^2 / \epsilon \kappa^2$, the fraction of κ^2 due to species s ; $u_{ei} = \epsilon / 4\pi\eta\beta e_{ei}^2$, a characteristic mobility, about the same magnitude as the ionic mobilities in many systems. η is the viscosity of the solvent. $\hat{q}_a = [\sum_s \mu_s u_s / (u_a + u_s)]^{1/2}$; I_{abc} and J_{abcd} are algebraic combinations of the variables listed above; see Appendix.

(16) H. L. Friedman, *J. Chem. Phys.*, **42**, 462 (1965).

Here we list the expressions for the $S_a(M)$. Other indices b, c, \dots appearing in the equations are to be summed over all of the species in the solution.

$$S_a(1) = -z_a \mu_b [z_a u_c - z_b u_b] / [u_a + u_b] [1 + \hat{q}_a]$$

$$S_a(2) = z_a \mu_b z_b \mu_c I_{abc}$$

$$S_a(3) = -2u_{ei} / u_a$$

$$S_a(4) = -u_{ei} \mu_b / [u_a + u_b] \hat{q}_a [1 + \hat{q}_a]$$

$$S_a(5) = -z_a^2 u_a \mu_b / [u_a + u_b] [1 + \hat{q}_a]$$

$$S_a(6) = -u_{ei} \hat{q}_a^2 / u_a$$

$$S_a(7) = \mu_b z_b^2 u_b^2 / u_a [1 + \hat{q}_a] [u_a + u_b]$$

$$S_a(8) = -2u_{ei} \mu_b u_b z_b / z_a u_a^2$$

$$S_a(9) = -u_{ei} \mu_b z_b u_b^2 / [u_a + u_b] [1 + \hat{q}_b] u_a^2 z_a$$

$$S_a(10) = \mu_b u_b z_b^2 \mu_c I_{c b c} / u_a$$

$$S_a(11) = u_{ei} z_b u_b \mu_b \mu_c u_c / [u_a + u_c] [u_b + u_c] \hat{q}_c [1 + \hat{q}_c] z_a u_a$$

$$S_a(12) = u_{ei} \mu_b u_b [1 + u_b / [u_a + u_b]] \mu_c [z_c u_c - z_a u_a] / u_a^2 z_a \hat{q}_a [1 + \hat{q}_a] [u_a + u_c]$$

$$S_a(13) = u_{ei} \mu_b u_b \mu_c \mu_d [z_c u_c - z_d u_d] [u_d - u_c] J_{abcd} / 2z_a u_a$$

The terms $S_a'(1)$ and $S_a'(2)$ are identical, respectively, with the terms $S_a(1)$ and $S_a(12) + S_a(13)$ of the ohmic conductance theory.¹⁶ The terms with a u_{ei} factor collectively correspond to the electrophoretic term of the limiting law for the ohmic conductance; the others, to the relaxation term.

7. Numerical Results

The expressions for the $S_a'(M)$ were programmed in Fortran and evaluated, together with the sums in eq. 4.1 and 6.2, for a number of systems of interest by means of an IBM 7090 computer.

In these calculations it is convenient to employ $\lambda_i / |z_i|$ in place of u_i wherever the latter appears (λ_i is the equivalent ionic conductance at infinite dilution). Likewise, $\lambda_{ei} \equiv 1.546 \times 10^{-7} u_{ei}$ is used in place of u_{ei} . This is possible because the expressions for the $S_a'(M)$ are all homogeneous and of order zero in the set $u_1, \dots, u_{se}, u_{ei}$ and because $\lambda_i / |z_i| u_i = 1.546 \times 10^{-7}$ for any ion i . (We note that the electrophoretic term of the limiting law for the ohmic *equivalent* conductance of a solution of a simple electrolyte, commonly written

$$-1.546 \times 10^{-7} \kappa [z_+ - z_-] / 6\pi\eta$$

may also be written

$$-2K\sqrt{\Gamma} [z_+ - z_-] \lambda_{ei}$$

which shows that the combination of functions in λ_{ei} really plays the role of an equivalent conductance.

For aqueous solutions at 25°, $\lambda_{ei} = 19.22$ equivalent conductance units.)

The values of $S_a'(M)$ for some typical systems are given in Table I. It is interesting that the terms for $M = 2, 10,$ and $13,$ which are always small compared to S_a' , are those in which I_{abc} and J_{abcd} appear. These are the only terms that are troublesome to evaluate, both in performing the integrations to get expressions for I_{abc} and J_{abcd} and in getting numerical results from these complicated expressions.

Table I: Cluster-Expansion Terms for Several Systems^a

M	System						
	I		II ^a		III ^b		
	Li ⁺	Cl ⁻	Gd ³⁺	Br ⁻	Li ⁺	Cu ²⁺	SO ₄ ²⁻
				λ_i			
	38.69	76.34	67.35	78.14	38.68	53.6	80.02
1	-284	-304	-618	-704	-486	-1371	-890
2	-9	11	-59	27	-7	-14	15
3	-994	-503	-1712	-492	-993	-1434	-961
4	154	138	278	209	219	230	217
5	-237	-353	-2210	-459	-306	-973	-1246
6	-289	-105	-487	-72	-240	-411	-228
7	513	204	2309	362	941	1553	897
8	483	-124	-788	195	689	718	-322
9	127	-26	-58	0	116	140	-53
10	9	5	9	4	5	6	4
11	-20	7	100	-43	-62	-53	30
12	-442	-128	-208	-205	-488	-698	-210
13	-27	11	-37	22	-17	-13	-8
$\Sigma S_a'(M)$	-1013	-1169	-3480	-1156	-630	-2320	-2739

^a $10^3 S_a'(M)$ for aqueous solutions at 25°. ^b Ionic strength fraction of copper sulfate equals $1/2$.

The fact that some of the $S_a'(M)$ are positive shows that some sequences of ionic interactions tend to promote the motion of ions in the Hall current rather than restrict it. However, the sum S_a' is negative in all cases just like S_a , the corresponding coefficient in the ohmic conductance.

The S_a' are, in principle, measurable just as the S_a are.¹⁶

The ideal and limiting-law terms of the Hall conductances of several systems are given in Table II. The ratio A'/A is, for dilute solutions, close to the ratio σ'/σ so it is clear that the Hall current is less than one-millionth of the ohmic current in each of these systems. Under these circumstances, it would seem that efforts to observe the Hall effect in ionic solutions for the first time ought to be made only in the most favorable systems, those for which A'/A is the largest.

An interesting feature of the results in Table II is that the ratio $S'a^{3/2}/A'c$ is, in most cases, similar in sign and magnitude to the corresponding ratio $Sc^{3/2}/Ac$

Table II: Calculated Hall Effect Terms for Several Systems^a

	Solute									
	Aqueous, 25°, λ _{el} = 19.22							Liquid ammonia, -34°, λ _{el} = 15.55		
	HCl	KCl	LiCl	CuSO ₄	Li ₂ SO ₄	YbBr ₃	Gd-(ClO ₄) ₃	La-(picrate) ₃	Na ⁺ , e ⁻	NaI
λ ₊	349.8	73.52	38.68	53.6	38.69	65.61	67.35	69.51	140.	140.
λ ₋	76.34	76.34	76.34	80.02	80.02	78.14	67.35	30.39	880.	169.
10 ⁹ A'/A	283.	-2.92	-39.0	-27.4	-42.9	-13.0	0	40.6	-768.	-30.1
10 ² S' <i>c</i> ^{3/2} /A' <i>c</i>	-1.87	-2.66	-2.95	-8.50	-7.80	11.0	(-2.20) ^b	-13.2	-14.5	-17.5
10 ² S <i>c</i> ^{3/2} /A <i>c</i>	-1.17	-1.99	-2.38	-5.74	-3.86	-4.31	-4.55	-5.86	-7.94	-11.1

^a H = 10⁴ gauss; ionic strength = 10⁻³ M. ^b The proper entry here would be ± ∞. The entry given is 10⁹S'*c*^{3/2}/A*c*.

of the terms of the ohmic conductance. However, for an unsymmetrical electrolyte S' does not vanish if λ₊/λ₋ = 1, while, of course, A' is positive if λ₊/λ₋ > 1 and negative if λ₊/λ₋ < 1. As a result one may find (e.g., YbBr₃) the limiting-law term of σ' aiding the flow of the Hall current. This happens when the ionic contribution S_a' of the less mobile ion is much more negative than S_a' of the more mobile ion: the slower ion is slowed more, and the net Hall current increases in magnitude.

For a symmetrical electrolyte, on the other hand, if λ₊ = λ₋, both A' and S' vanish, and the leading term in the Hall conductance must then be of still higher order in c.

The calculated dependence of the terms of σ' on the composition of a YbCl₃-LiCl mixture is shown in Figure 5. In this case, the limiting-law term S'*c*^{3/2} tends to increase the magnitude of the Hall conductance in mixtures rich in YbCl₃ while in mixtures rich in LiCl it tends to decrease the magnitude of σ' by just a few per cent.

8. Some Experimental Aspects

For the purpose of this section, to find whether the calculated effects are large enough to be measurable, a number of simplifying approximations may be made. For example, we may replace σ and σ' by their ideal parts, A*c* and A'*c*, respectively.

We assume that the Hall current flows between plane parallel electrodes, each a rectangle of dimensions l_x × l_y, separated by l_z. The lengths l_x, l_y, and l_z are, respectively, parallel to the 1_x, 1_y, and 1_z directions.¹⁷ Then the Hall current is

$$I_H = \langle J^H \rangle / l_z \tag{8.1}$$

$$= \sigma' E l_x l_y$$

If the instrument used to measure I_H has input resistance R_i, then the signal power is

$$P_s = I_H^2 R_i \tag{8.2}$$

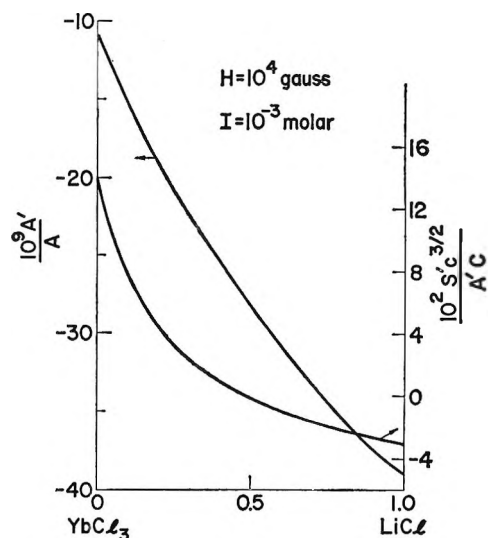


Figure 5. Calculated ideal and limiting-law terms of the Hall conductance for YbCl₃-LiCl mixtures in water at 25°. The abscissa is the fraction of the ionic strength of the mixture due to LiCl.

In our calculation of σ' it has been assumed that the electric field in the l_z direction is negligible; hence, that R_i is much smaller than the resistance

$$R_s = l_z / \sigma l_x l_y \tag{8.3}$$

between the Hall electrodes. However, the maximum signal power is obtained if R_i = R_s. It may be shown that Thevenin's theorem applies and that the maximum signal power is

$$P_s = E^2 V \sigma [\sigma' / \sigma]^2 / 4 \tag{8.4}$$

where V = l_xl_yl_z. Now E²Vσ is seen to be the power that raises the temperature of the solution by Joule heating. Since σ'/σ is so small, this power is enormous compared to P_s and must be held to a value that does

(17) The effect of the Hall electrodes in shorting the driving electric field is neglected here. See I. Isenberg, B. R. Russel, and R. F. Greene, *Rev. Sci. Instr.*, 19, 685 (1948).

not cause an unacceptable temperature rise during the experiment.

We have, neglecting the flow of heat to the surroundings

$$E^2\sigma = C\dot{T} \quad (8.5)$$

where C is the heat capacity per unit volume and \dot{T} the rate of temperature increase.

The sensitivity with which P_s may be detected by the measuring instrument is limited by electrical noise in the instrument and the circuit to which it is connected. The irreducible minimum noise is that due to the thermal motion of the charge carriers

$$P_n = kT\Delta f \quad (8.6)$$

where k is Boltzmann's constant, T is the absolute temperature, and Δf is the band width of the measuring instrument. In the optimum case, $1/\Delta f$ is the duration of the observation. The ratio of signal power to noise power in the measuring instrument is obtained by combining these equations to get

$$P_s/P_n = C\dot{T}V[\sigma'/\sigma]^2/4kT\Delta f \quad (8.7)$$

As an example, for HCl(aq), $H = 10^4$ gauss, $T = 298^\circ\text{K}$., and $V = 10$ cm.³, we find $P_s/P_n = 6 \times 10^7$ if $\dot{T}/\Delta f$, the temperature rise during the experiment, is limited to 10^{-3}° .

To achieve such a favorable signal-to-noise ratio it is probably necessary to modulate both the E and the H fields and to look for I_H at a combination frequency. Unless this is done, the thermal noise can be expected to be small compared to interfering electrical signals from electrode processes, from convection in the liquid,¹⁸ and from imperfect alignment of the Hall electrodes. On the other hand, by observing the Hall current for periods separated by longer intervals to allow the temperature to relax to its initial value and then by combining the observations in an appropriate way, it should be possible to improve on the signal-to-noise ratio given by (8.7).

Under the conditions used to derive (8.7) the voltage across the measuring instrument is

$$\begin{aligned} v_s &= [P_s R_s]^{1/2} \\ &= \frac{1}{2} l_z [\sigma'/\sigma] [C\dot{T}/\sigma]^{1/2} \end{aligned} \quad (8.8)$$

As an example, for $10^{-2} M$ HCl(aq), $H = 10^4$ gauss, $l_z = 5$ cm., and $\dot{T} = 10^{-4}$ deg./sec., we obtain $v_s = 3 \times 10^{-7}$ v.¹⁹

The observed voltage will coincide with the voltage calculated in this way only if the electrodes respond to differences in the electrical potential of the solution

rather than to differences in the electrochemical potential of particular ionic species. The former is the case for certain electrodes with salt bridges, as is well known, but the latter obtains for simple reversible electrodes. Simple calculations of the principal effect of using reversible electrodes in Hall effect measurements have been given by Swanson⁵ and Evseev.¹⁹

Acknowledgment. The author is grateful for the benefit of several discussions of this work with D. W. Jepsen, R. W. Landauer, and A. G. Redfield.

Appendix

The Brownian Motion Propagator in a Magnetic Field. Here we designate the propagator defined in eq. 3.1 as $P_{000}'(t \leftarrow 0)$. The subscript specifies the unmodified propagator; species designations are suppressed in this section. Just as in the Appendix of ref. 11, of which this is an extension, the equations given may be obtained by elementary calculations from the definitions and Chandrasekhar's equation for $P_{000}(t \leftarrow 0)$, the unmodified propagator in the absence of a magnetic field, which is written $P_a(t \leftarrow 0)$ in the body of this paper. Other notations for this Appendix follow: \mathbf{X} and \mathbf{Y} represent arbitrary fixed vectors; $\mathbf{r} \equiv \mathbf{r}_t - \mathbf{r}_0$; $\theta = \exp(-t\zeta/m)$; $\bar{P}_{lmn}' \equiv \int_0^\infty dt e^{i\zeta t} \int d^3r \exp(i\mathbf{k} \cdot \mathbf{r}) \times P_{lmn}'(t \leftarrow 0)$ and similarly for the relation of \bar{P}_{lmn} to P_{lmn} .

$$P_{200}(t \leftarrow 0) \equiv \int d^3p_t P_{000}(t \leftarrow 0) W d^3p_0$$

$$P_{201}(t \leftarrow 0) \cdot \mathbf{Y} \equiv \int d^3p_t P_{000}(t \leftarrow 0) \mathbf{p}_0 \cdot \mathbf{Y} W d^3p_0$$

$$\mathbf{X} \cdot P_{202}(t \leftarrow 0) \equiv \int d^3p_t \mathbf{X} \cdot \mathbf{p}_t P_{000}(t \leftarrow 0) W d^3p_0$$

$$P_{250}(t \leftarrow 0) \equiv [1 - \theta]^2 P_{200}(t \leftarrow 0)$$

$$P_{270}(t \leftarrow 0) \equiv t\theta P_{200}(t \leftarrow 0)$$

Explicit evaluations for \bar{P}_{200} , \bar{P}_{201} , and \bar{P}_{202} for the Brownian motion case are given in ref. 11. We also find, in this case

(18) This effect has been discussed by J. M. Ziman, *Phil. Mag.*, **7**, 865 (1962). Recent measurements on liquid metals, both with modulated fields [A. J. Greenfield, *Phys. Rev. Letters*, **3**, 121, 200 (1962)] and with constant fields [J. E. Enderby, *Proc. Phys. Soc. (London)*, **81**, 772 (1963)], indicate that it need not limit the accuracy of the determination.

(19) A. M. Evseev, *Zh. Fiz. Khim.*, **36**, 1610 (1962), has reported readily measurable electromagnetic effects in a CuSO₄ solution. He also gives a simple, approximate theory of the effect which is in agreement with the result of the present theory for the ideal term. However, this gives a Hall voltage about 10⁶-fold smaller than he reports as a measured value. The latter is apparently not a Hall effect; the experiment is not completely enough described for it to be clear that other sources of voltage between the Hall probes have been eliminated. Evseev's theory does provide a simple way to treat the electrode effects⁶ which have been neglected in this paper.

$$\begin{aligned} \bar{P}_{250}(k, z) &= \bar{P}_{200}(k, z) - \\ & 2\bar{P}_{200}(k, z + i\zeta/m) + \bar{P}_{200}(k, z + 2i\zeta/m) \end{aligned}$$

$$\bar{P}_{270}(k, z) = \Sigma_i$$

$$\frac{[k^2/\beta\zeta]^l}{\Pi_{n=0}^l [k^2/\beta\zeta - iz + n\zeta/m][k^2/\beta\zeta - iz + (n+1)\zeta/m]}$$

Some of the P_{lmn}' and P_{lmn} are scalars, some are vectors, and some are tensors of the second degree. The same font for P is used in any case. Now we readily derive

$$\begin{aligned} \mathbf{Y} \cdot P_{112}'(t \leftarrow 0) &\equiv \int d^3p_t d^3r \mathbf{Y} \cdot p_t P_{000}'(t \leftarrow 0) \\ &= t\theta \mathbf{\Omega} \cdot \mathbf{Y} \wedge \mathbf{p}_0 \end{aligned}$$

$$\begin{aligned} \mathbf{Y} \cdot P_{212}'(t \leftarrow 0) \cdot \mathbf{X} &\equiv \int P_{112}'(t \leftarrow 0) \mathbf{p}_0 \cdot \mathbf{X} W d^3p_0 \\ &= t\theta [m/\beta] \mathbf{\Omega} \cdot \mathbf{Y} \wedge \mathbf{X} \end{aligned}$$

$$P_{200}'(t \leftarrow 0) \equiv \int d^3p_t P_{000}'(t \leftarrow 0) W d^3p_0 = 0$$

$$P_{201}'(t \leftarrow 0) \cdot \mathbf{X} \equiv \int d^3p_t P_{000}'(t \leftarrow 0) \mathbf{p}_0 \cdot \mathbf{X} W d^3p_0$$

$$\bar{P}_{201}' = [m/\zeta][\mathbf{X} \wedge \mathbf{\Omega} \cdot \bar{P}_{201} - [i/\beta]\mathbf{X} \cdot \mathbf{\Omega} \wedge \mathbf{k} \bar{P}_{270}]$$

$$\mathbf{Y} \cdot P_{202}'(t \leftarrow 0) \equiv \int d^3p_t \mathbf{Y} \cdot \mathbf{p}_t P_{000}' W d^3p_0$$

$$\mathbf{Y} \cdot \bar{P}_{202}' = [m/\zeta][\mathbf{\Omega} \wedge \mathbf{Y} \cdot \bar{P}_{202} + [i/\beta]\mathbf{Y} \cdot \mathbf{\Omega} \wedge \mathbf{k} \bar{P}_{270}]$$

$$\mathbf{Y} \cdot P_{203}'(t \leftarrow 0) \cdot \mathbf{X} \equiv \int d^3p_t \mathbf{Y} \cdot \mathbf{p}_t P_{000}' \mathbf{p}_0 \cdot \mathbf{X} W d^3p_0$$

$$\begin{aligned} \mathbf{Y} \cdot \bar{P}_{203}' \cdot \mathbf{X} &= [m/\beta\zeta]^2 \mathbf{X} \cdot [\mathbf{k} \mathbf{k} \wedge \mathbf{\Omega} + \mathbf{k} \wedge \mathbf{\Omega} \mathbf{k}] \cdot \mathbf{Y} [m \bar{P}_{250}/\zeta - \\ & \bar{P}_{270}] + [m/\beta] \mathbf{\Omega} \cdot \mathbf{Y} \wedge \mathbf{X} \bar{P}_{270} \end{aligned}$$

Cluster Integrals Involving More Than Two Ions, aside from Chain Sums. The function I_{abc} appearing in this paper is

$$I_{abc} \equiv \frac{\kappa^5}{\beta^2 \pi^2} \int_0^\infty \frac{k^2 dk}{k^2 + \kappa^2} [i_{abc} - i_{acb}]$$

where

$$i_{abc} \equiv \int_{-\infty}^\infty \frac{dz}{[H_c + iz][H_b - iz][H_a - iz] \phi(z) \phi(-z)}$$

$$H_s \equiv k^2/\beta\zeta_s$$

$$\phi(z) \equiv 1 + \Sigma_s 4\pi c_s e_s^2 / \epsilon \zeta_s [H_s + iz]$$

It has been evaluated in the case $se = 2$ and $se = 3$. In the latter case it is

$$I_{abc} = F \times \left\{ \frac{[1 - \delta_{ab} - \delta_{ac}] \langle \kappa \rangle_1 / \langle \kappa \rangle_3 + \delta_{ab} [g_2(a, c) Z_2(a) + g_0(a, c) Z_0(a)] + \delta_{ac} [g_2(a, b) Z_2(a) + g_0(a, b) Z_0(a)]}{\Pi_{n=1}^3 [u_n + u_a][\kappa_{n-1} + \kappa_a]} \right\}$$

$$F \equiv \kappa^5 / [\langle u \rangle_1 \langle u \rangle_2 - \langle u \rangle_3] [\langle \kappa \rangle_1 \langle \kappa \rangle_2 - \langle \kappa \rangle_3]$$

$$Z_2(a) = \langle A \rangle_1$$

$$Z_0(a) = [\langle A \rangle_1 \langle A \rangle_2 - \langle A \rangle_3] / \langle A \rangle_4$$

where δ_{ab} is the Kronecker delta function, g_2 and g_0 have been defined earlier,¹⁶ and $\langle \dots \rangle_n$ represents the elementary symmetric polynomial¹⁶ (ESP) in the following basis sets

$$\langle u \rangle_n \text{ in } u_1, u_2, u_3$$

$$\langle \kappa \rangle_n \text{ in } \kappa, \kappa_1, \kappa_2$$

$$\langle A \rangle_n \text{ in } \kappa, \kappa_1, \kappa_2, \kappa_a$$

Here κ has its usual meaning, κ_1 and κ_2 have been defined,¹⁶ and $\kappa_a \equiv \kappa \hat{q}_a$.

The function J_{abcd} is defined as

$$J_{abcd} \equiv u_b [u_a - u_b] \Psi_{abcd} - I_{adc}$$

$$\begin{aligned} \Psi_{abcd} &\equiv \frac{\kappa^5}{\pi^2 \beta^5} \int_0^\infty \frac{k^6 dk}{k^2 + \kappa^2} \times \\ & \int_{-\infty}^\infty \frac{z^2 dz}{[H_a^2 + z^2][H_b^2 + z^2][H_c^2 + z^2][H_d^2 + z^2] \phi(z) \phi(-z)} \end{aligned}$$

By using the methods of the earlier work¹⁶ we find

$$\begin{aligned} \Psi_{abcd} &= \frac{F}{\Pi_{n=1}^3 [u_n + u_a][\kappa_{n-1} + \kappa_a]} \times \\ & \{ [\delta_{ac} + \delta_{ad}] \psi_a + [\delta_{bc} + \delta_{bd}] \psi_b + \\ & [\delta_{ac} \delta_{bd} + \delta_{ad} \delta_{bc}] [\psi_{ab} - \psi_a - \psi_b] \} \\ \psi_a &\equiv [u_a + \langle u \rangle_1] Z_2(a) + \bar{u} Z_0(a) \\ \bar{u}^n &= \Sigma \mu_s u_s^n \quad \bar{u}^1 \equiv \bar{u} \end{aligned}$$

$$N_5(a, b) W_5(a, b) +$$

$$\psi_{ab} \equiv \frac{N_3(a, b) W_3(a, b) + N_1(a, b) W_1(a, b)}{[u_a + u_b][\kappa_a + \kappa_b] \Pi_{n=1}^3 [u_n + u_b][\kappa_{n-1} + \kappa_b]}$$

$$W_5(a, b) = \begin{pmatrix} \langle AB \rangle_4 & \langle AB \rangle_5 \\ 1 & \langle AB \rangle_1 \end{pmatrix},$$

$$W_3(a, b) = \begin{pmatrix} \langle AB \rangle_2 & \langle AB \rangle_3 \\ 1 & \langle AB \rangle_1 \end{pmatrix}$$

$$W_1(a, b) = \begin{pmatrix} \langle AB \rangle_3 & \langle AB \rangle_4 & \langle AB \rangle_5 \\ \langle AB \rangle_1 & \langle AB \rangle_2 & \langle AB \rangle_3 \\ 0 & 1 & \langle AB \rangle_1 \end{pmatrix} / \langle AB \rangle_5$$

Here (\dots) represents the determinant and $\langle AB \rangle_n$ is the ESP in the basis set, $\kappa, \kappa_1, \kappa_2, \kappa_a, \kappa_b$. Finally

$$N_5(a, b) = u_c^2 [\alpha_1 \alpha_2 - \alpha_3] + \alpha_1 \alpha_4 - \alpha_5$$

$$N_3(a, b) = u_c^2 [\alpha_2 \beta_1 - \alpha_1 \beta_2 - \beta_3] + \alpha_1 \beta_4 + \alpha_4 \beta_1 - \beta_5$$

$$N_1(a, b) = u_c^2 \beta_1 \beta_2 + \beta_1 \beta_4$$

In these expressions each α_n is $\alpha_n(a,b)$, and each β_n is $\beta_n(a,b)$. They are given by

$$\alpha_1(a,b) = u_a + u_b + \langle u \rangle$$

$$\alpha_2(a,b) = [u_a + u_b]^2 + 2\langle u \rangle_2$$

$$\alpha_3(a,b) = u_a u_b \langle u \rangle + [u_a + u_b] \langle u \rangle_2 + \langle u \rangle_3$$

$$\alpha_4(a,b) = u_a u_b \langle u \rangle_2 + [u_a + u_b] \langle u \rangle_3$$

$$\alpha_5(a,b) = u_a u_b \langle u \rangle_3$$

$$\beta_1(a,b) = \bar{u}$$

$$\beta_2(a,b) = \bar{u} \alpha_1 - \bar{u}^2$$

$$\beta_3(a,b) = \bar{u} \alpha_2 - \bar{u}^2 \alpha_1 + \bar{u}^3$$

$$\beta_4(a,b) = \bar{u} [\alpha_3 - \langle u \rangle_3] - \bar{u}^2 [\alpha_2 - \langle u \rangle_2] + \bar{u}^3 [u_a + u_b]$$

$$\beta_5(a,b) = u_a u_b [\bar{u} \langle u \rangle_2 - \bar{u}^2 \langle u \rangle + \bar{u}^3]$$

Radiolysis of Heavy Water in the pD Range 0-14

by E. Hayon

Service de Chimie physique, C. E. N. Saclay (S. & O.), France (Received February 4, 1965)

Radical and molecular yields from various systems irradiated with ^{60}Co γ -rays in heavy water in the pD range 0-14 were determined and are compared with data obtained in light water. Radical yields were found to increase in acid and alkaline solutions as compared to neutral solutions. This is interpreted as due to scavenging in the "spurs" of the radicals (D_2O) $^-$ and OD by D^+ and OD^- ions, respectively. This is similar to the conclusions reached regarding H_2O . At all pH values, the values of G_{D} , and $G_{\text{D}_2\text{O}}$, are lower in D_2O than those of G_{H} , and $G_{\text{H}_2\text{O}}$, in H_2O , while the yields of G_{Red} and G_{OD} are only slightly lower in D_2O than the corresponding yields in H_2O .

Few detailed studies have been made of the yields of radicals and "molecular" products in the radiolysis of heavy water. Results extrapolated to zero scavenger concentration are available mainly in 0.8 *N* sulfuric acid solutions,¹⁻⁷ a few in neutral solutions,^{2,3,6,8-11} and none in alkaline solutions. In view of the importance possible differences in the primary yield from irradiated H_2O and D_2O may bear on theories of the nature and diffusion of the primary radiation-chemical species, an attempt was made to determine the yields of radicals and "molecular" products in D_2O as a function of pD in the range 0 to 14. The results obtained are presented below.

Experimental

A 200-curie ^{60}Co γ -source was used, and the dose rate was 7.7×10^{16} e.v./ml. min. based on the ferrous sulfate

dosimeter in light water, taking $G(\text{Fe}^{3+}) = 15.5$. In order to minimize the consumption of heavy water,

- (1) H. A. Mahlman and J. W. Boyle, *J. Am. Chem. Soc.*, **80**, 773 (1958).
- (2) J. H. Baxendale and G. Hughes, *Z. physik. Chem.*, **14**, 323 (1958).
- (3) T. J. Hardwick, *J. Chem. Phys.*, **31**, 226 (1959).
- (4) C. N. Trumbore, *J. Phys. Chem.*, **64**, 1087 (1960).
- (5) K. Coatsworth, E. Collinson, and F. S. Dainton, *Trans. Faraday Soc.*, **56**, 1008 (1960).
- (6) F. S. Dainton and D. B. Peterson, *Proc. Roy. Soc. (London)*, **A267**, 443 (1962).
- (7) L. M. Dorfman and I. A. Taub, *J. Am. Chem. Soc.*, **85**, 2370 (1963).
- (8) E. J. Hart, W. R. McDonnell, and S. Gordon, *Proc. Intern. Conf. Peaceful Uses At. Energy Geneva*, **7**, 593 (1955).
- (9) H. A. Mahlman, *J. Chem. Phys.*, **32**, 601 (1960).
- (10) P. J. Dyne, J. W. Fletcher, W. M. Jenkinson, and L. P. Roy, *Can. J. Chem.*, **39**, 933 (1961).
- (11) P. Riesz and B. E. Burr, *Radiation Res.*, **16**, 661 (1962).

5-ml. samples of solution were used throughout; otherwise, the procedures described elsewhere^{12,13} were strictly followed. Each G value given is the result of six measurements on the yield-dose curve.

The deuterium oxide was refluxed in alkaline permanganate for 24 hr. and then doubly distilled. It was further purified by radiolysis and then photolyzed at 2537 Å. to destroy the radiation-produced hydrogen peroxide. On infrared analysis, this final product was found to contain 99.72 ± 0.02 mole % deuterium oxide. The acidity and alkalinity of the solution were normally adjusted using H_2SO_4 and NaOH. At pD values below 1.0 and above 13.0 the results were checked using reagent grade D_2SO_4 and NaOD (supplied by Merck Sharp and Dohme) to adjust the pD. In all cases the G values obtained were within $\pm 3\%$ of those determined using H_2SO_4 and NaOH. The actual pD was obtained using the correction term found by Glasoe and Long¹⁴ to hold over the whole pH range: pD = pH meter reading + 0.40.

The gaseous products were measured by gas chromatography.¹³ Calibration was carried out using H_2 , D_2 , and an equilibrated mixture of H_2 , D_2 , and HD. In this way it was possible to show that the response of the instrument to H_2 , HD, and D_2 was in the ratio of 1.0:0.92:0.70, respectively. All other methods of estimation and extinction coefficients were identical with those used previously.^{12,13} All of the chemicals used were analytical research grade.

Results

The systems used in this work to determine the yields of radicals $(D_2O)^{\cdot-}$, D, and OD, and of "molecular" products D_2 and D_2O_2 , have all been employed in radiolytic studies of light water. It is because the reaction mechanism in each of the systems is thought to be understood, and is expected to be the same in D_2O as in H_2O , that they have been used here. The various systems studied will be referred to below.

Molecular Hydrogen Yields. The production of hydrogen in a dilute degassed KBr solution is taken to be equal to the yield of "molecular" hydrogen. G_{D_2} was found to be equal to 0.36 ± 0.01 in neutral solutions of $10^{-3} M$ KBr, and 0.34 ± 0.01 and 0.32 ± 0.01 at pD 1.0 and 0.5, respectively (Table I). This small but significant decrease of the D_2 yields in acid solutions is of the same order as that observed in light water.¹⁵

As a further check, the values of G_{D_2} were measured in neutral solutions of potassium nitrate; see Table I. Plotting these yields against the cube root of the KNO_3 concentration gives on extrapolation to "infinite dilution" a value of $G_{D_2} = 0.36$. This value compares well

Table I: Hydrogen Yields Obtained on Irradiation of Various Air-Free Deuterium Oxide Solutions

Solute	pD	$G(\text{hydrogen})$
$10^{-3} M$ KBr	Neutral	0.36
$10^{-3} M$ KBr	1.0	0.335
$10^{-3} M$ KBr	0.5	0.32
$5 \times 10^{-4} M$ KNO_3^a	Neutral	0.32
$2 \times 10^{-3} M$ KNO_3^a	Neutral	0.30
$1 \times 10^{-2} M$ KNO_3^a	Neutral	0.24
$3 \times 10^{-2} M$ KNO_3^a	Neutral	0.193
$10^{-1} M$ ethanol + $5 \times 10^{-4} M$ KNO_3	Neutral	0.79
$10^{-1} M$ ethanol	0.8 N H_2SO_4	3.88

^a In presence of $10^{-3} M$ KBr.

with the value of 0.37 obtained by Mahlman⁹ using $NaNO_3$ in D_2O .

In alkaline solutions, the formation of "molecular" hydrogen remains essentially unchanged up to pD 13.5 (see Table II, column ϵ), when it decreases slightly at pD 14.0 to $G_{D_2} = 0.34$. This behavior is similar to that observed in light water.¹³

Table II: Irradiation of Air-Free $10^{-3} M$ KNO_3 and $5 \times 10^{-3} M$ Formate Ions

pD	$G(\text{hydrogen})_T$	$G(NO_2^-)$	$G_{D_2}^a$	G_{Red}^b
6.0	0.77	2.32	0.31	2.78
12.1	0.63	2.52	...	2.84
12.9	0.47	2.89	0.31	3.05
13.3	0.41	3.04	...	3.14
13.5	0.38	3.13	0.31	3.20
14.0	0.29	3.30	0.29	3.30

^a In absence of $5 \times 10^{-3} M$ formate. ^b $G_{Red} = G(NO_2^-) + G(\text{hydrogen})_T - G_{D_2}$.

Hydrogen Peroxide Yields. Aerated solutions of potassium bromide have been used¹⁶ to determine the yield of "molecular" hydrogen peroxide. From the mechanism postulated,¹⁶ the net peroxide production is given by

$$G(\text{peroxide})_T = G(D_2O_2) + \frac{1}{2}(G_{Red} - G_{OD}) \quad (A)$$

where $G(\text{peroxide})_T$ is the total measured yield of per-

(12) E. Hayon, *Trans. Faraday Soc.*, **61**, 723 (1965).

(13) E. Hayon, *ibid.*, **61**, 734 (1965).

(14) P. K. Glasoe and F. A. Long, *J. Phys. Chem.*, **64**, 188 (1960).

(15) E. Hayon, *ibid.*, **65**, 1502 (1961); C. H. Cheek, V. J. Linrenbom, and J. W. Swinnerton, *Radiation Res.*, **19**, 636 (1963).

(16) T. J. Sworski, *J. Am. Chem. Soc.*, **76**, 4687 (1954); A. O. Allen and R. A. Holroyd, *ibid.*, **77**, 5852 (1955).

Table III: Yields of Radicals and Molecular Products on γ -Irradiation of Water

pD/pH	D_2O^a					H_2O^b				
	G_{Red}	G_{OD}	G_{D_2}	$G_{D_2O_2}$	$G(-D_2O)$	G_{Red}	G_{OH}	G_{H_2}	$G_{H_2O_2}$	$G(-H_2O)$
0.50	3.60	2.86	0.32	0.60	4.15	3.66	2.97	0.40	0.78	4.50
0.85	3.55	2.81	4.10	3.61	2.94	4.46
1.25	3.43	2.69	0.34	...	3.99	3.51	2.86	0.41	...	4.36
2.05	3.26	2.52	3.81	3.31	2.69	0.42	...	4.16
2.85	3.07	2.33	3.62	3.07	2.50	3.92
3.30	2.94	2.20	3.49	2.90	2.40	3.80
6.00	2.83	2.12	0.36	0.56	3.40	2.85	2.25	0.45	0.71	3.70
12.10	2.84	2.21	3.42	2.93	2.43	0.43	0.65	3.76
12.90	3.05	2.52	0.36	0.49	3.64	3.12	2.72	0.43	0.60	3.95
13.30	3.14	2.73	3.73	3.23	2.90	...	0.56	4.05
13.50	3.20	...	0.36	0.41	...	3.27	3.04	0.43	0.53	4.12
14.00	3.30	2.99	0.34	0.37	3.86	3.41	3.31	0.37	0.45	4.18

^a This work. ^b See ref. 13.

oxide, $G(D_2O_2)$ is the yield of molecular peroxide at any KBr concentration, and $G_{Red} = G_{(D_2O)^-} + G_D$. Using the stoichiometric relationship

$$G(-D_2O) = 2G_{D_2} + G_{Red} = 2G_{D_2O_2} + G_{OD} \quad (B)$$

eq. A can be converted to

$$G(\text{peroxide})_T = 2G(D_2O_2) - G_D$$

Taking $G_{D_2} = 0.36$, one can calculate $G(D_2O_2)$ at different bromide ion concentrations. In all KBr solutions irradiated in the presence of air, $G(\text{peroxide})_T$ was produced linearly with dose ($0-5 \times 10^8$ e.v./ml.) but with a positive intercept on the peroxide axis of $4-6 \mu M$, thought to be due to the presence of organic impurities in the water.¹⁶ From the plot of $G(D_2O_2)$ against $[KBr]^{1/3}$ one can draw a straight line to give a value of $G_{D_2O_2} = 0.56$ on extrapolation to infinite dilution.

The peroxide yield in alkaline solutions was derived by measuring the yield of oxygen formed on irradiation of deaerated solutions of ferricyanide in the presence of $40 \mu M$ ferrocyanide, as described elsewhere.¹³ In this system, $Fe(CN)_6^{3-}$ reacts with peroxide to yield equivalent quantities of O_2 . The results obtained are given in Table III. On plotting $G_{D_2O_2}$ against $[OD^-]^{1/3}$ one obtains a straight line to give a value of $G_{D_2O_2} = 0.56$ on extrapolation to infinite dilution. The decrease of $G_{D_2O_2}$ with increase in $[OD^-]$ is interpreted, as was done for light water,¹³ to the reaction $OD + OD^- \rightarrow O^- + D_2O$ occurring in the spurs, with the rate constant for combination of OD radicals being significantly greater than that for combination of O^- radicals to give D_2O_2 .

The "molecular" peroxide formed in $0.8 N$ sulfuric acid solution was determined by measuring the yield of O_2 produced on irradiation of an $800 \mu M$ $Ce(SO_4)_2$ solution. $G_{D_2O_2} = G(O_2) = 0.60 \pm 0.02$ was found. The

slight increase of $G_{D_2O_2}$ in acid compared to neutral D_2O solutions is similar to that found in H_2O .¹⁶

Radical Yields. On irradiation of light water hydrogen atoms as well as electrons $(H_2O)^-$ are formed. Similarly, one would expect the yield of total reducing species in D_2O to be

$$G_{Red} = G_D + G_{(D_2O)^-} \quad (C)$$

The deuterium atom yield was obtained on irradiation of neutral solutions of a two-solute system¹⁷: $10^{-1} M$ ethanol to react with the D atoms to form HD by abstraction from the alcohol, and $5 \times 10^{-4} M$ KNO_3 to react with $(D_2O)^-$. In this system $G(\text{hydrogen})_T = G_D + G(D_2) = 0.79$, where $G(D_2) = 0.32$ is the yield of molecular D_2 in the presence of $5 \times 10^{-4} M$ KNO_3 . One obtains, therefore, $G_D = 0.47 \pm 0.02$. A similar run made in light water gave a value of $G_H = 0.55 \pm 0.02$. It would appear, therefore, that G_H is about 15% greater than G_D .

G_{Red} at pD 0.5 ($0.8 N$ H_2SO_4) was obtained on irradiation of an air-free solution of $10^{-1} M$ ethanol. In this system, $G(\text{hydrogen})_T = G_{Red} + G_{D_2}$. The total hydrogen yield was found equal to 3.88, from which one can calculate $G_{Red} = 3.56$. Dorfman and Taub⁷ found $G(\text{hydrogen})_T = 3.87$ on irradiation of $0.5 M$ C_2H_5OD in $0.8 N$ D_2SO_4 , and 3.81 in $0.8 N$ H_2SO_4 , both in D_2O solutions.

Supposing G_D to be independent of pD as is G_H in light water,¹⁸ the variation of G_{Red} with pD—and therefore of $G_{(D_2O)^-}$ —was determined by measuring the hydrogen peroxide formed on irradiation of aerated $5 \times 10^{-3} M$ ethanol solutions, as was done with light

(17) J. T. Allan and G. Scholes, *Nature*, **187**, 218 (1960); J. Rabani, *J. Am. Chem. Soc.*, **84**, 868 (1962).

(18) E. Hayon, *J. Phys. Chem.*, **68**, 1242 (1964).

water.¹² From the mechanism postulated by Jayson, *et al.*,¹⁹ we have

$$G(\text{peroxide})_T = G_{D_2O_2} + \frac{1}{2}(G_{\text{Red}} + G_{\text{OD}}) \quad (\text{D})$$

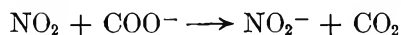
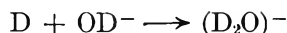
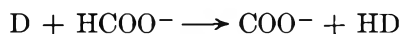
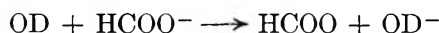
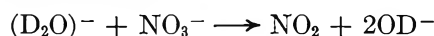
The nature of the reducing species formed on irradiation and of the HO₂ or DO₂ species is not important in this system; neither is the deuteration of C₂H₅OH in D₂O. From eq. D one can calculate ($G_{\text{Red}} + G_{\text{OD}}$), taking the values for $G_{D_2O_2}$ given above. These results are given in Table IV.

Table IV: Irradiation of Aerated Solutions of $5 \times 10^{-3} M$ Ethanol in D₂O

pD	$G(D_2O_2)$	$G_{D_2O_2}$	$G_{\text{Red}} + G_{\text{OD}}$	G_{Red}^a	G_{OD}^a
0.50	3.83	0.60	6.46	3.60 ^b	2.86
0.85	3.78	...	6.38	3.55	2.81
1.25	3.64	...	6.12	3.43	2.69
2.05	3.46	...	5.78	3.26	2.52
2.85	3.26	...	5.40	3.07	2.33
3.30	3.13	...	5.14	2.94	2.20
6.00	3.02	0.56	4.92	2.83	2.09

^a Calculated yields (see Discussion). ^b Taking $G_{\text{Red}} = 3.60$.

The yields of total reducing species in alkaline solutions were determined from the irradiation of dilute aqueous solutions of KNO₃ and formate ions in the absence of oxygen. The mechanism is similar to that postulated in light water¹³

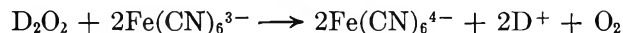
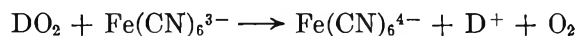
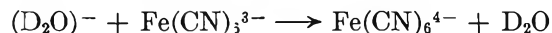
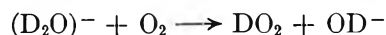
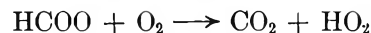
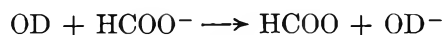


For the purpose of simplicity reactions involving deuterated formate ions were not put down. On the basis of the above reactions.

$$G_{\text{Red}} = G(NO_2^-) + G(\text{hydrogen})_T - G_{D_2}$$

the yields of $G(NO_2^-)$, $G(\text{hydrogen})_T$, and G_{D_2} in this system were determined and are given in Table II.

In order to determine G_{OD} yields in alkaline D₂O solutions, the ferricyanide + formate + O₂ system was used, as was done in light water.¹³ In this system the following reactions are considered to occur in alkaline medium



The above reactions are not dependent on the precise nature of the reducing species, of HO₂ or DO₂, or of O \dot{H} or O⁻ formed in alkaline solutions and give a net reduction yield.

$$G(-Fe^{III}) = G_{\text{Red}} + G_{\text{OD}} + 2G_{D_2O_2} \quad (\text{E})$$

Values of $G(-Fe^{III})$ in 800 μM ferricyanide and $5 \times 10^{-3} M$ formate ions in the pD range 12–14 are given in Table V. Taking the $G_{D_2O_2}$ values given in Table VI and G_{Red} values given in Table II it was possible to calculate G_{OD} from eq. E above.

Table V: Irradiation of Aerated Solutions Containing 800 μM Ferricyanide and $5 \times 10^{-3} M$ Formate Ions

pD	$G(-Fe^{III})$	G_{Red}^a	G_{OD}
12.1	6.11	2.84	2.21
12.65	6.33	2.95	2.38
12.95	6.53	3.05	2.52
13.3	6.71	3.14	2.73
14.0	7.03	3.30	2.99

^a Values taken from Table II.

Table VI: Yields of D₂O₂ in Aerated Bromide Solutions

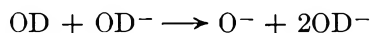
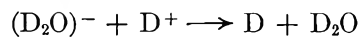
[KBr], M	$G(\text{peroxide})$	$G(D_2O_2)$
5×10^{-4}	0.73	0.50 ₅
2×10^{-3}	0.66	0.47
5×10^{-3}	0.60	0.44
1×10^{-2}	0.51	0.39 ₅

Discussion

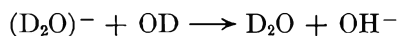
The increase in radical yields in acid and alkaline H₂O solutions was attributed^{12,13} to a scavenging by H⁺ or OH⁻ ions of the radicals (H₂O) \dot{O} and OH produced in the "spurs." Similarly, in D₂O solutions one

(19) G. Jayson, G. Scholes, and J. J. Weiss, *J. Chem. Soc.*, 1358 (1957).

would expect to observe the same scavenging reactions occurring in the spurs



resulting in a decrease of the back reaction to form water



In calculating G_{Red} and G_{OD} values in the aerated ethanol system, it was assumed that scavenging by D^+ ions in the spurs leads to equivalent increases in the yields of oxidizing and reducing species, as this is a requirement for material balance. In this way the change in the yields of G_{Red} and G_{OD} with variation in $[\text{D}^+]$ was calculated on the basis that $G_{\text{Red}} = G_{\text{OD}} = \frac{1}{2}(G_{\text{Red}} + G_{\text{OD}})$. These values of G_{Red} and G_{OD} are given in Table IV, columns 4 and 5. On the basis of the radical diffusion theory and the properties of the medium (the relaxation time and viscosity of D_2O are both larger than in H_2O), it was suggested⁵ that a more extended initial distribution of radicals in D_2O relative to H_2O would give lower molecular product yields and higher radical yields in D_2O compared to H_2O . The radical and molecular yields obtained above have been summarized in Table III and are compared with the respective yields obtained¹³ in H_2O . It can readily be seen that at all pH values the material balance obtained in D_2O is poor compared to that obtained in H_2O . The reason for this inaccuracy is not apparent. Comparison of the yields in D_2O and H_2O solutions, Table III, shows that G_{D_2} and $G_{\text{D}_2\text{O}_2}$ are about 20% lower than the corresponding values in H_2O . The yields of G_{Red} and G_{OD} are, however, about 5–10% lower in D_2O than in H_2O .

Results in the literature on the yields in D_2O solutions vary considerably. Thus, in neutral solutions G_{D_2} values of 0.28,³ 0.30,⁸ 0.36,⁶ 0.37,⁹ and 0.49¹¹ have

been obtained. In 0.8 *N* H_2SO_4 , G_{D_2} values of 0.29,³ 0.38,¹ and 0.44⁶ were obtained. The hydrogen peroxide yield was found to be 0.6⁶ in neutral solutions and 0.65,⁶ 0.77,⁵ and 0.79¹ in 0.8 *N* H_2SO_4 .

Values of G_{Red} of 3.4⁸ and 3.24³ were obtained in neutral $\text{O}_2 + \text{HCOOH}$; $G_{\text{Red}} = 3.7$ in the $\text{H}_2 + \text{D}_2\text{O}$ system¹⁰; and 3.94¹ and 4.1³ in 0.8 *N* H_2SO_4 solutions of $\text{Fe}^{2+} + \text{O}_2$. In 0.8 *N* H_2SO_4 values for G_{OD} of 3.04⁵ and 3.12¹ have been reported.

As a check to the results obtained in this work, aerated solutions of 10^{-3} *M* ferrous ions in 0.8 *N* H_2SO_4 in the presence of 10^{-3} *M* NaCl were irradiated. After making the usual correction for the change in density of D_2O solutions compared to H_2O

$$G(\text{Fe}^{3+}) = 3G_{\text{Red}} + G_{\text{OD}} + 2G_{\text{D}_2\text{O}_2} = 15.0 \pm 0.2$$

was obtained, taking the extinction coefficient for ferric ions at its maximum absorption as 2375 at 25°.²⁰ The yield of $G(\text{Fe}^{3+}) = 15.0 \pm 0.2$ found experimentally is in fairly good agreement with the yields of radicals and molecular products obtained in this work for 0.8 *N* H_2SO_4 solutions and summarized in Table III. This $G(\text{Fe}^{3+})$ value is to be compared with values of 16.22,⁵ 16.72,¹ 16.95,³ and 17.1⁴ previously reported. It does not seem possible to explain these different results. More work is clearly needed to confirm the yields of products formed in the radiolysis of heavy water before one can attempt to interpret them on the basis of the diffusion theory.

Acknowledgments. The author thanks Dr. H. Hering for bringing to his attention the factors inherent in the determination of deuterium gases by gas chromatography, and Miss C. Cery, Service Isotopes Stables, Saclay, for kindly preparing an equilibrated mixture of H_2 , HD, and D_2 .

(20) J. W. Boyle and H. A. Mahlman, *Radiation Res.*, **16**, 416 (1962).

Kinetics of the Ethyl Chlorophyllide Sensitized Photoreduction of Phenosafranine by Hydrazobenzene

by G. R. Seely

Contribution No. 181 from the Charles F. Kettering Research Laboratory, Yellow Springs, Ohio
(Received February 8, 1965)

Ethyl chlorophyllide sensitizes the photoreduction of phenosafranine by hydrazobenzene and other reducing agents. According to the proposed mechanism, the reaction is initiated by transfer of an electron from triplet excited chlorophyllide to the dye, as was proposed earlier for the reduction of methyl red. Although evidently exergonic, because it can be made to occur in the dark, the reaction is subject to strong product retardation. This can be accounted for by the formation of a transient complex of the oxidized chlorophyllide radical with the reductant. This complex may decompose with oxidation of the reducing agent, thus completing the forward reaction, or it may react with leucophenosafranine, reversing the reaction and regenerating chlorophyllide. The direct, nonsensitized photoreduction of phenosafranine is not subject to such strong retardation. E.s.r. measurements of the concentration of phenosafranine semiquinone radicals suggest that these do not play a very important part in the retardation.

Introduction

Photochemical reactions of chlorophyll are of particular interest because of their probable involvement in photosynthesis. We have previously examined the photoreduction of the closely related ethyl chlorophyllide *a* by ascorbic acid in ethanol-pyridine solutions¹ and the chlorophyllide-sensitized reduction of methyl red by ascorbic acid, hydrazobenzene, and mercaptosuccinic acid in ethanol.² The two reactions were found to be quite unrelated: in the second, photoexcited chlorophyllide reacts with methyl red, not with the reductant, as in the first. The reduction of methyl red turned out to be kinetically very complex, apparently because unidentified reaction products affect the efficiency of early steps.

We wanted to examine a chlorophyllide-sensitized reduction in a system in which the dye could be recovered by oxidation, in the hope that side reactions would be less disturbing and the part played by chlorophyllide could be understood more clearly. The chosen oxidant was phenosafranine, a dye of low oxidation potential. Chlorophyll-sensitized reduction of related dyes, such as safranin T, has been reported.³⁻⁷

The reducing agents effective for methyl red reduction

also worked for phenosafranine reduction; hydrazobenzene proved most convenient for detailed study even though the over-all reaction was not strictly reversible.

Experimental

The ethyl chlorophyllide *a* sample was prepared as before.^{1,2} Phenosafranine (Allied Chemical Corp.) was chromatographed on calcium carbonate and precipitated out of ethanol with cyclohexane; its extinction coefficient, in 1:6 ethanol:pyridine mixture, was $60,600 M^{-1} \text{ cm}^{-1}$ at 538 μ . However, the rate of reduction was not sensitive to purification.

Hydrazobenzene (Eastman) was recrystallized under nitrogen from ethanol until colorless. Stock solutions in ethanol were kept in a freezer.

- (1) G. R. Seely and A. Folkmanis, *J. Am. Chem. Soc.*, **86**, 2763 (1964).
- (2) G. R. Seely, *J. Phys. Chem.*, **69**, 821 (1965).
- (3) T. T. Bannister, *Photochem. Photobiol.*, **2**, 519 (1963).
- (4) A. A. Krasnovskii, *Dokl. Akad. Nauk SSSR*, **61**, 91 (1948).
- (5) A. A. Krasnovskii and K. K. Voinovskaya, *ibid.*, **87**, 109 (1952).
- (6) V. B. Evstigneev and V. A. Gavrilova, *ibid.*, **98**, 1017 (1954).
- (7) K. G. Mathai and E. Rabinowitch, *J. Phys. Chem.*, **66**, 954 (1962).

β -Carotene (Eastman) was used as received.

Ethanol was distilled from $Mg(OC_2H_5)_2$, pyridine from BaO or Al_2O_3 . The composition of the solvent, from pure ethanol to pure pyridine, had little influence on the rate of reduction; it was convenient to use a mixture of 1 part ethanol and 6 parts pyridine by volume.

Quantum yields were determined as before,^{1,2} by noting the progress of the reaction at intervals with a Beckman DU spectrophotometer and measuring light intensity with an Eppley thermopile. The reaction could also be followed continuously with a Cary Model 14 spectrophotometer, but quantum yields could not then be measured. Electron spin measurements were made with a Varian Model 4500 e.p.r. spectrometer, radical concentrations being estimated by comparison with known concentrations of diphenylpicrylhydrazyl. Samples were held in flat cells 0.34 mm. thick, which could also be fitted into the Cary spectrophotometer for concentration measurement.

Light absorbed only by chlorophyllide was isolated by a Baird-Atomic 660-m μ interference filter; light absorbed by phenosafranine, with a Spectrolab 530-m μ interference filter.

The quantum yield was essentially independent of absorbed light intensity (usually in the neighborhood of 10^{-6} einstein/1. sec.).

Reactions were conducted under purified nitrogen¹ at 25°.

The following abbreviations are used: Chl is ethyl chlorophyllide *a*; D⁺, D \cdot , and DH are phenosafranine, its semiquinone, and leucophenosafranine, respectively; AH₂, AH \cdot , and A are hydrazobenzene, its hydrazyl radical, and azobenzene, respectively.

Results

Reducing Agents. Sensitized reduction of phenosafranine, with ascorbic acid or mercaptobenzothiazole as reductant, is spontaneously reversible in the dark; regeneration of phenosafranine is complete with a few minutes. In agreement with Bannister's results with safranin T,³ we found that with ascorbic acid a photo-stationary reduction level was established, proportional to the square root of the light intensity. The back reaction was approximately first order.

With cysteine or mercaptosuccinic acid as reductant, the reaction was not reversible in the dark if oxygen was rigorously excluded. The chlorophyllide slowly faded during the reaction, apparently because of attack by mercaptyl radicals. Reduction went almost as fast as with hydrazobenzene. In contrast to the reduction of methyl red, which was about 50 times faster with hydrazobenzene than with mercaptosuccinic acid,²

the reduction of phenosafranine was almost equally rapid with either reductant.

Sensitized reduction with hydrazobenzene is not reversible in the dark when the reductant is pure, and the chlorophyllide does not fade. These features made it the reductant of choice for quantum yield determinations. The reaction between hydrazobenzene and phenosafranine must be exergonic because it can be catalyzed in the dark by a strong base. With one phenosafranine preparation, an adventitious impurity also caused reduction in the dark.

After all of these reactions, phenosafranine could be regenerated immediately and practically quantitatively upon exposure to air.

In the dark, there was often a slow and incomplete recovery of the dye, dependent on the hydrazobenzene concentration. It was probably due to a persistent impurity in the hydrazobenzene. The rate of photo-reduction was insensitive to the rate of the recovery in the dark.

Dependence on Hydrazobenzene Concentration. The most notable difference between the reduction of pheno-

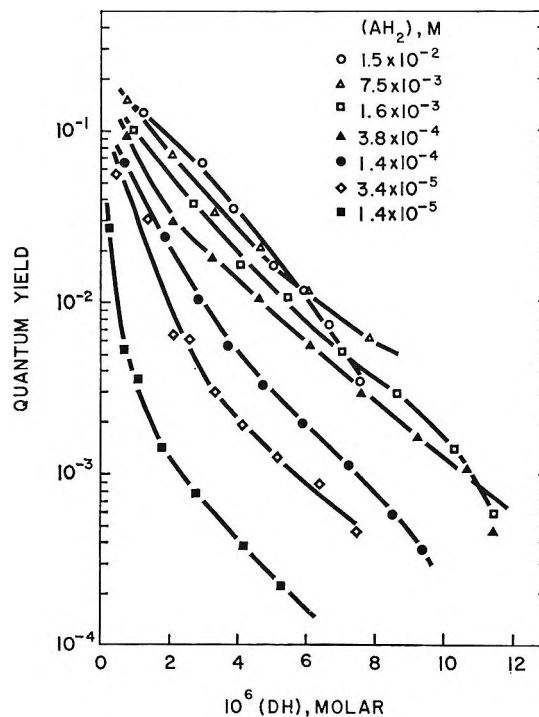


Figure 1. Photoreduction of phenosafranine by hydrazobenzene, sensitized by ethyl chlorophyllide. Semilogarithmic plot of quantum yield against leucophenosafranine concentration ($[DH]$) for runs differing in hydrazobenzene concentration. Approximate initial concentrations: $[D^+]_0 = 1.6 \times 10^{-5} M$, $[Chl] = 2 \times 10^{-6} M$, $I_a = 1.7 \times 10^{-6}$ einstein/1. sec. In the last run there is a deficiency of hydrazobenzene.

safranin and that of methyl red is the occurrence in the former of strong retardation by the reduction product (Figure 1). Although a true photostationary state appears never to be reached, the retardation is so severe that the quantum yield is reduced to $1/10$ or $1/100$ of its initial value before the dye is half-reduced. A similar retardation was found in a run with ethyl pheophorbide *a* as the sensitizer. The retardation can be mitigated, but not overcome, by increasing the concentration of reductant. The initial quantum yield is hard to estimate, but it seems to approach 0.20 at high hydrazobenzene concentration. This is as high a value as any found for the reduction of methyl red.²

If the initial phenosafranin concentration, $[D^+]_0$, is decreased, the initial quantum yield is practically unchanged. The dependence of retardation on $[D^+]_0$ suggests that the quantum yield depends on $[DH]$ (or a quantity proportional to it) rather than on the ratio $[DH]/[D^+]_0$. The curves in Figure 1 have therefore been plotted with $[DH]$ as the abscissa.

Similar strong retardation was found in reduction of phenosafranin by cysteine or mercaptosuccinic acid. It is therefore not peculiar to hydrazobenzene and probably involves reduction products of the dye. Such retardation is rather unexpected for an exergonic reaction, and our experiments were directed partly toward elucidation of its cause.

Nonsensitized Reduction. Unlike methyl red, phenosafranin does not require sensitization for its photo-reduction.⁸ Runs were made in which phenosafranin alone absorbed light; some of the results are shown in Figure 2. The presence or absence of chlorophyllide does not affect the rate of this nonsensitized reduction. The initial quantum yield (ϕ_0) approaches 0.40 at high reductant concentration, distinctly larger than for the sensitized reduction. It obeys the relationship

$$\phi_0 = 0.40 \frac{[AH_2]}{[AH_2] + 1.86 \times 10^{-4}} \quad (1)$$

Retardation is still present but is not nearly so strong and does not prevent nearly complete reduction of the dye within a reasonable time. As shown by varying the initial phenosafranin concentration, the retardation in this case is a function of the ratio $[D^+]/[D^+]_0$. Multiplication of observed quantum yields by $[D^+]_0/[D^+]$ largely compensates for the retardation, except, of course, in the run in which hydrazobenzene was deficient (see dotted curves of Figure 2). The retarder in the sensitized reduction must therefore affect steps involving the chlorophyllide.

The initial quantum yield and the extent of retardation are independent of light intensity. The quantum

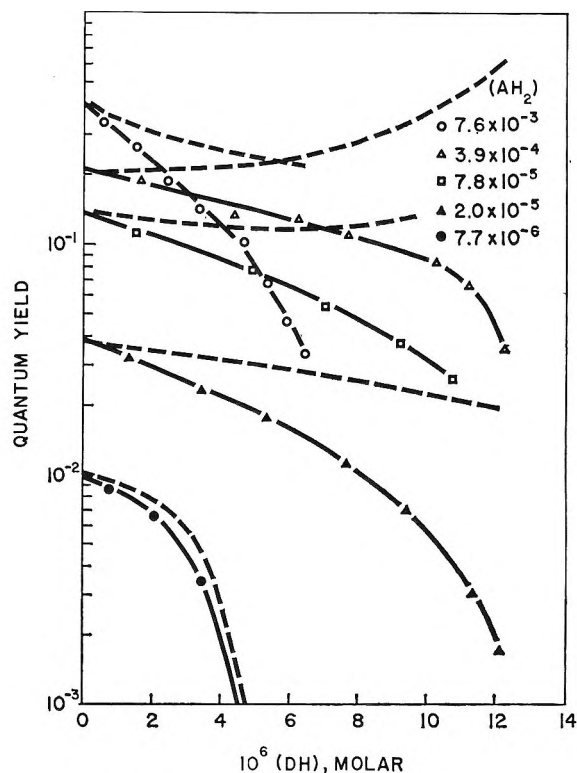


Figure 2. Nonsensitized photoreduction of phenosafranin by hydrazobenzene. Semilogarithmic plot of quantum yield *vs.* leucophenosafranin concentration, $[DH]$. Quantum yields multiplied by $[D^+]_0/[D^+]$ are shown by dashed lines. In the first run (O), $[D^+]_0 = 7.5 \times 10^{-6} M$. In the others, $[D^+]_0 \cong 1.3 \times 10^{-6} M$. In the last run, hydrazobenzene is deficient.

yield is not affected by addition of $FeCl_3$ at $3.5 \times 10^{-6} M$ or of azobenzene at $1.7 \times 10^{-4} M$. It was thought that the retardation might have something to do with the availability of protons, but added acetic acid at 0.023 *M* had no effect. Strong bases (potassium or tetrabutylammonium hydroxide) convert phenosafranin into a form reduced by hydrazobenzene in the dark although the reaction is accelerated by light.

Carotene Inhibition. β -Carotene quenches the triplet state of chlorophyll.^{9,10} From the dependence on carotene concentration of the quantum yield of the sensitized reduction of methyl red by ascorbic acid, it was shown that chlorophyllide in the triplet state reacts with the oxidant rather than with the reductant.² Similarly, the quantum yield of sensitized reduction of phenosafranin by hydrazobenzene depends on the carotene/phenosafranin ratio, rather than on the

(8) G. K. Oster, G. Oster, and C. Dobin, *J. Phys. Chem.*, **66**, 2511 (1962).

(9) E. Fujimori and R. Livingston, *Nature*, **180**, 1036 (1957).

(10) H. Claes, *Z. Naturforsch.*, **16b**, 445 (1961).

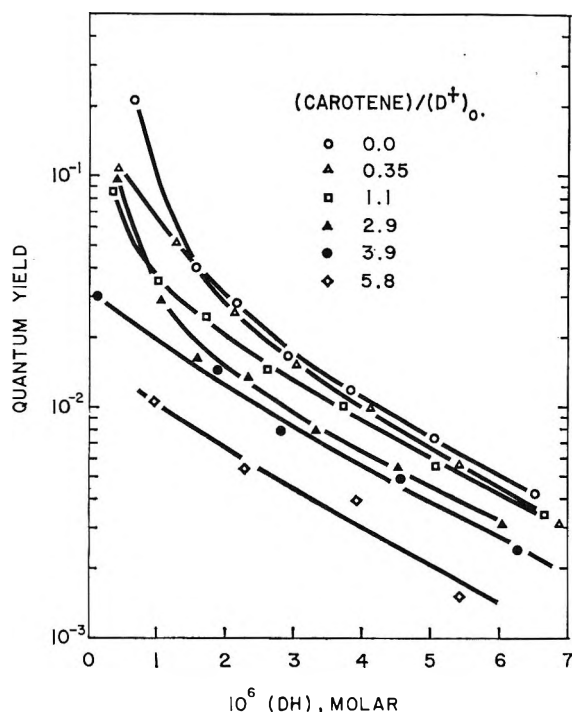


Figure 3. Sensitized photoreduction of phenosafranine by hydrazobenzene in the presence of β -carotene. Initial concentrations: $[D^+]_0 \cong 1.3 \times 10^{-6} M$, $[AH_2] = 4.4 \times 10^{-4} M$, $[Chl] = 2 \times 10^{-6} M$, $I_a = 0.9 \times 10^{-6}$ einstein/l. sec. Compare also with fourth run of Figure 1.

carotene/hydrazobenzene ratio. The quantum yields near the beginning of the runs in Figure 3 indicate that with $4.4 \times 10^{-4} M$ hydrazobenzene, the ratio of the rate constants of the reactions of triplet chlorophyllide with phenosafranine and β -carotene is about 0.7. Similar inhibition was found with $7.6 \times 10^{-3} M$ hydrazobenzene. Since the bimolecular rate constant for the reaction of triplet chlorophyll with β -carotene is about $1.3 \times 10^9 M^{-1} \text{sec.}^{-1}$,^{9,10} the constant for its reaction with phenosafranine must be about $0.9 \times 10^9 M^{-1} \text{sec.}^{-1}$.

The curves in Figure 3 remain nearly parallel during the reaction; *i.e.*, carotene has almost no effect on retardation.

Electron Spin Resonance. We looked for radicals produced during the reduction of phenosafranine and the oxidation of hydrazobenzene that might be present in sufficient concentration to be important retarders.

The e.s.r. spectrum of an acid form of the semiquinone of phenosafranine has been reported.¹¹ We detected a poorly resolved five-banded spectrum, apparently of a "neutral" form of the semiquinone, after chemical (dithionite) or photochemical reduction of phenosafranine in ethanol-pyridine mixtures. At

ca. $10^{-3} M$ phenosafranine and leucophenosafranine, the equilibrium constant for semiquinone formation

$$K_s = [D\cdot]^2/[D^+][DH] \quad (2)$$

had the value $3 (\pm 1) \times 10^{-3}$. However, the equilibrium constant unaccountably depended linearly on the leucophenosafranine concentration

$$K_s = 4.5[DH] \quad (3)$$

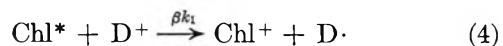
At the phenosafranine concentrations used in the photoreduction experiments ($[D^+]_0 \approx 10^{-6} M$) the semiquinone concentration, according to (3), would not exceed $\sim 2 \times 10^{-9} M$. This low value is supported by our inability to detect intermediates spectrally during air oxidation of leucophenosafranine. The semiquinone concentration is probably too small to account for the retardation, according to the mechanism to be proposed.

No signal could be detected when hydrazobenzene was partially oxidized by I_2 , $FeCl_3$, H_2O_2 , or $CuCl_2$. When as little as 1% of the hydrazobenzene was oxidized with $FeCl_3$, the only product observed spectrally was azobenzene. There is therefore no reason to believe that any product other than azobenzene occurs, except as a transient, during the photochemical oxidation of hydrazobenzene.

Discussion

Primary Reaction. The primary photochemical reaction is between photoexcited chlorophyllide and phenosafranine. This is shown by yields in the presence of carotene and is supported by other considerations. For example, the weak e.s.r. signal detected when a solution of chlorophyllide is illuminated¹² is trebled in the presence of phenosafranine but unaffected by hydrazobenzene. Furthermore, hydrazobenzene is inactive as a reducing agent for chlorophyllide in ethanol-pyridine, unless an acid such as benzoic is added; even then the quantum yield for reduction of chlorophyllide is only about 10^{-4} .

It is reasonable to suppose that the primary photochemical reaction is transfer of an electron from the triplet excited state of chlorophyllide (Chl^*) to phenosafranine



The hypothesis that phenosafranine (or safranin T) has a low-lying triplet state to which it can be excited by energy transfer from chlorophyllide³ is not con-

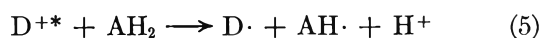
(11) P. B. Ayscough and C. Thomson, *J. Chem. Soc.*, 2055 (1962).

(12) S. S. Brody, G. Newell, and T. Castner, *J. Phys. Chem.*, **64**, 554 (1960).

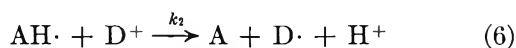
sistent with differences in the degree of retardation of sensitized and nonsensitized reductions and the lack of an effect of carotene on retardation.

Cause of Retardation. Before retardation in the sensitized reduction is explained, it is necessary to account for the much milder retardation of the nonsensitized reduction.

A mechanism consistent with (1) begins with a primary photochemical reaction between photoexcited phenosafranine (D^{+*}) and hydrazobenzene to form radicals.



The radicals $D\cdot$ accumulate to a certain extent and equilibrate with D^+ and DH ,¹³ but the radicals $AH\cdot$ are removed rapidly. The retardation can be adequately accounted for if $AH\cdot$ is removed by the two reactions



and the rate constants k_2 and k_3 are nearly equal. The second reaction is probable because we know from e.s.r. experiments that hydrazobenzene and $D\cdot$ do not react in the dark. As only (6) completes the reduction, a factor

$$k_2[AH\cdot][D^+]/(k_2[AH\cdot][D^+] + k_3[AH\cdot][DH]) \cong [D^+]/[D^+]_0$$

enters the expression for quantum yield.

If this explanation is correct, the same factor should also apply to the sensitized reduction. However, multiplication of the quantum yield curves of Figure 1 by this factor accounts for only a small part of the retardation actually observed.

The retarder does not compete with phenosafranine for Chl^* , for, if it did, the curves of Figure 3 would converge rapidly as the reaction progressed, and the presence of carotene grow less important. The rate constant for the reaction between Chl^* and the retarder would have to have an unreasonably large value $\sim 10^{10} M^{-1} sec^{-1}$, and the retardation would depend on $[DH]/[D^+]$ instead of on $[DH]$ alone.

The retarder does not merely compete with hydrazobenzene for reaction with $Chl\cdot^+$ produced by (4) because retardation is not suppressed by sufficiently large $[AH_2]$. On the other hand, retardation must precede the step by which $AH\cdot$ is formed, for after that the quantum yield is determined by the relative rates of (6) and (7).

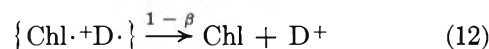
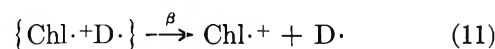
The simplest way of accounting for the retardation

is to assume that reduction of $Chl\cdot^+$ by AH_2 is not immediate upon collision but is preceded by the formation of a relatively long-lived complex $\{Chl\cdot^+ \cdot AH_2\}$. Instead of decomposing to Chl and $AH\cdot$, this complex may react with the retarder, which now may be identified as DH . The radical $D\cdot$ may contribute to the retardation, but, in view of (3), its action would be hard to distinguish kinetically from that of DH .

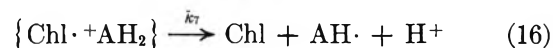
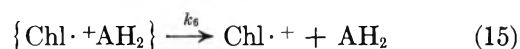
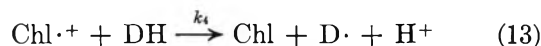
The proposed mechanism of chlorophyllide-sensitized reduction is therefore



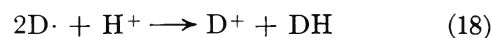
where I_a is the rate of light absorption (einstein/l. sec.) and α is the probability of conversion from excited singlet to triplet state.



where β is the probability that the radicals formed in the reaction "cage" designated by $\{Chl\cdot^+ \cdot D\cdot\}$ will diffuse away from each other.



The reaction is completed by steps 6 and 7 and the disproportionation



Steps similar to (13) and (17) could be included with $D\cdot$ in place of DH . A possible reaction between Chl^* and DH , analogous to the reaction between Chl^* and ascorbic acid¹



and its consequences have been omitted, but they might become important at high $[DH]$.

With the usual steady-state approximations for all transient species the quantum yield becomes

(13) The rate constant for dismutation of the similar semithionine radicals is $2.4 \times 10^9 M^{-1} sec^{-1}$. [C. G. Hatchard and C. A. Parker, *Trans. Faraday Soc.*, 57, 1093 (1961).]

$$\phi = \frac{\alpha\beta k_1 [D^+]}{k_0 + k_1 [D^+]} \times \frac{k_5 k_7 [AH_2]}{(k_6 + k_7 + k_8 [DH])k_4 [DH] + (k_7 + k_8 [DH])k_5 [AH_2]} \times \frac{k_2 [D^+]}{k_2 [D^+] + k_3 [DH]} \quad (20)$$

Since k_0 is about $10^3/\text{sec.}$,^{1,14-16} and k_1 is about $10^9 M^{-1} \text{ sec.}^{-1}$, k_0 can be neglected in comparison with $k_1 [D^+]$ when $[D^+]$ is much above $10^{-6} M$. The first factor on the right side of (20) then reduces to $\alpha\beta$, which is the initial quantum yield, 0.2. The third factor can be approximated by $[D^+]/[D^+]_0$.

As DH builds up and retardation becomes pronounced, k_7 becomes small compared with $k_8 [DH]$. Then, with the approximations of the preceding paragraph, (20) may be rearranged to a form asymptotically valid at high $[DH]$

$$\frac{\alpha\beta [D^+]}{\phi [D^+]_0} \frac{1}{[DH]} = \frac{k_8}{k_7} + \frac{k_4(k_6 + k_7)}{k_5 k_7 [AH_2]} + \frac{k_4 k_8 [DH]}{k_5 k_7 [AH_2]} \quad (21)$$

When the left side of (21) is plotted against $[DH]$, for runs shown in Figure 1 and for other runs also, the points do, in fact, fall on straight lines as $[DH]$ becomes large, with slopes proportional to $1/[AH_2]$. The intercepts at high $[AH_2]$ cluster about the value $k_8/k_7 = 10^8$. The slopes of 11 runs with $[AH_2]$ ranging from 1.6×10^{-3} to $3.4 \times 10^{-5} M$ give the average value $k_4/k_5 = 200 \pm 40$. At higher hydrazobenzene concentrations the slope is quite small, and the left side of (21) becomes practically independent of $[DH]$. Although the intercept tends to increase with decreasing $[AH_2]$, as expected from the second term on the right side of (21), the precision is not sufficient to permit an estimate of k_6/k_7 . Its value, however, is surely less than 1 and perhaps is nearly 0.

It is fairly safe to assume that k_4 and k_8 are less than $10^9 M^{-1} \text{ sec.}^{-1}$. Then $k_7 < 1 \times 10^3 \text{ sec.}^{-1}$ and $k_5 < 5 \times 10^6 M^{-1} \text{ sec.}^{-1}$. The complex $\{\text{Chl}^+ \text{AH}_2\}$ therefore has a natural lifetime of at least 10^{-3} sec.

A complex of a similar sort must evidently be postulated for sensitized reductions with mercaptosuccinic acid and cysteine because these reactions are also retarded by product. It is not clear that such a long-lived complex must exist in reductions with ascorbic acid; the reported³ similarity of quantum yields in the sensitized and unsensitized reactions argues against it. Apparently, that system is kinetically dominated by a rapid back reaction between the phenosafranin semiquinone and dehydroascorbic acid.

An implication of the foregoing is that a long-lived complex is formed between $\text{Chl}^+ \cdot$ and those reducing agents that are not very labile, such as hydrazobenzene and the mercaptans, but not necessarily with ascorbic acid and leucophenosafranin. If such complexes exist as transitory intermediates during photosynthesis, they might be sites of action of inhibitors or stimulators.

Certainly the existence of such complexes makes it easier to accept, if not to explain, the curiously varied effect of reaction products on the quantum yield of methyl red reduction.² Specifically, $\{\text{Chl}^+ \text{AH}_2\}$ must be subject to attack by a transient and a final product, in the product-retarded photosensitized reduction of methyl red by hydrazobenzene.

Acknowledgments. The author is indebted to Mr. D. Stoltz for technical assistance and to Mr. E. Brody for the electron spin resonance measurements, made under the direction of Mr. W. Treharne. The work was supported in part by National Science Foundation Grant No. GB-2089.

(14) P. J. McCartin, *Trans. Faraday Soc.*, **60**, 1694 (1964).

(15) R. Livingston and P. J. McCartin, *J. Am. Chem. Soc.*, **85**, 1571 (1963).

(16) H. Linschitz and K. Sarkanen, *ibid.*, **80**, 4826 (1958).

The Radiation-Induced *cis-trans* Isomerization of Polybutadiene. IV

by Morton A. Golub

Stanford Research Institute, Menlo Park, California (Received February 11, 1965)

Polybutadiene in the solid state undergoes a marked radiation-induced loss of unsaturation in addition to the previously investigated *cis-trans* isomerization. The latter reaction was reinvestigated, and the former reaction studied for the first time, with the help of *cis*-polybutadiene-2,3- d_2 which provided unambiguous spectroscopic evidence for these reactions. Use of the deuterated polymer also revealed that double-bond migration and formation of conjugated triene structures occur to a negligible extent in irradiated polybutadiene. G values for the loss of double bonds in films irradiated with electrons under nitrogen or with γ -rays *in vacuo* are 13.6 and 7.9, respectively, while the initial G value for *cis-trans* isomerization, using either radiation, was redetermined as 7.2. The decrease in unsaturation is attributed to a chain cyclization, but the relative contributions of free radicals and carbonium ions to this process have not yet been established. Other radiation-induced processes in polybutadiene are cross linking and evolution of hydrogen (G values of about 0.9 and 0.45, respectively).

Introduction

Recent studies of the radiation chemistry of squalene¹ and of polyisoprene² have shown that, in addition to *cis-trans* isomerization (as in polybutadiene³) and the usual cross linking and evolution of hydrogen, these isoprenic compounds undergo considerable decrease in unsaturation. In fact, the consumption of double bonds in polyisoprene when irradiated with electrons under nitrogen or with γ -rays *in vacuo* was found to have G values of around 13.4 and 6.7, respectively, in substantial agreement with the findings of Heinze, *et al.*,⁴ Turner,⁵ and Hayden⁶ for comparable systems. Since the loss of double bonds was considered to be only a very minor factor in previous work on the radiation-induced isomerization of polybutadiene,³ it was deemed worthwhile to re-examine the irradiation of this polymer, with both electrons and γ -rays, especially in view of the report⁷ that polybutadiene experiences a very rapid drop in unsaturation, even more so than natural rubber (*cis*-polyisoprene). At the same time, it was desirable to extend preliminary work³ on *cis*-polybutadiene-2,3- d_2 $[(-\text{CH}_2-\text{CD}=\text{CD}-\text{CH}_2-)_n]$ since this polymer should provide direct infrared evidence for any decrease in original unsaturation (through changes in the 4.45- μ band corresponding to the C-D stretching vibration for an olefinic carbon atom) as

well as for any other possible processes, such as double-bond shifts and formation of conjugated double bonds (as might be revealed by new $-\text{CD}=\text{CH}-$ or $-\text{CH}=\text{CH}-$ absorptions, respectively). Moreover, as indicated elsewhere,⁸ because of a required change in the calibrations for the infrared analysis of the *cis* content in polybutadiene from that employed in the previous paper,³ it was necessary to revise the $G(\textit{cis} \rightarrow \textit{trans})$ value and also the value for the radiostationary *cis/trans* ratio. The present paper is concerned, therefore, with assessing the radiation-induced loss of unsaturation in polybutadiene and with re-examining its isomerization yield, *via* a study of *cis*-polybutadiene-2,3- d_2 .

Experimental

The deuterated polybutadiene (initial *cis/trans*

- (1) J. Danon and M. A. Golub, *Can. J. Chem.*, **42**, 1577 (1964).
- (2) M. A. Golub and J. Danon, *ibid.*, in press.
- (3) M. A. Golub, *J. Am. Chem. Soc.*, **82**, 5093 (1960).
- (4) H. D. Heinze, K. Schmieder, G. Schnell, and K. A. Wolf, *Kautschuk Gummi*, **14**, WT 208 (1961); *Rubber Chem. Technol.*, **35**, 776 (1962).
- (5) D. T. Turner, *Polymer*, **1**, 27 (1960).
- (6) P. Hayden, *Intern. J. Appl. Radiation Isotopes*, **8**, 65 (1960).
- (7) A. S. Kuzminsky, T. S. Nikitina, E. V. Zhuravskaya, L. A. Ozentievich, L. I. Sunitsa, and N. I. Vitushkin, *Proc. 2nd Intern. Conf. Peaceful Uses At. Energy, Geneva*, **29**, 258 (1958).
- (8) M. A. Golub, *J. Phys. Chem.*, **66**, 1202 (1962).

ratio $\sim 98/2$; negligible 1,2 units) was specially prepared by the late Dr. David Craig and Mr. Harold Tucker of the B. F. Goodrich Research Center, Brecksville, Ohio, and was kindly donated to us. In addition, a sample of undeuterated polybutadiene, Ameripol CB, with a similar *cis* content,³ was obtained from Goodrich-Gulf Chemicals Inc., Cleveland, Ohio, and used in some supporting experiments.

Thin films were cast from dilute benzene solutions of the purified polybutadienes onto NaCl or KBr plates and irradiated either *in vacuo* at room temperature, using a 1500-c. Co⁶⁰ γ -ray source, or under a stream of cooled nitrogen using 1-Mev. electrons from a G.E. resonant transformer. In the latter case, the polymer films were kept close to room temperature during irradiation by placing the plates in contact with a cooled surface. The films were analyzed before and after irradiation by infrared spectroscopy, using a Perkin-Elmer Model 221 (2–15 μ) or Model 421 (2.5–25 μ) spectrophotometer for the deuterated polybutadiene and the Model 221 for the ordinary polybutadiene.

The *cis* contents of irradiated polybutadiene-2,3-*d*₂ films were calculated from the absorbances *A* of the characteristic bands at 15.6 and 14 μ for *cis* and *trans*—CD=CD— units, respectively,⁹ making use of the fact that the ratio of the *trans* to *cis* extinction coefficients for the deuterated polymer is essentially the same as that for the undeuterated polybutadiene. This ratio is now taken⁸ to be 3.65 instead of the previous value of 1.89. Except for the change in ratio of extinction coefficients, the analysis for *cis* content in the irradiated undeuterated polybutadiene was the same as before,³ involving the characteristic bands at 13.6 and 10.4 μ for *cis* and *trans*—CH=CH— units, respectively. Thus, the per cent *cis*-1,4 double bonds for either polybutadiene was calculated as $100[3.65A_c/(3.65A_c + A_t)]$ where the subscripts, *c* and *t*, refer to the appropriate *cis* and *trans* bands.

The decrease in unsaturation of polybutadiene-2,3-*d*₂ was followed by noting changes both in the absorbance of the 4.45- μ band and in the quantity $3.65A_c + A_t$, relative to the absorbance of the 6.9- μ band (CH₂ bending vibration) as an internal standard. Thus, the per cent residual unsaturation in the deuterated polybutadiene was calculated as $100(A_{4.5}/A_{6.9})_D / (A_{4.5}/A_{6.9})_O$ and as $100[(3.65A_c + A_t)/A_{6.9}]_D / [(3.65A_c + A_t)/A_{6.9}]_O$, where the subscripts D and O refer to the irradiated and unirradiated polymer films, respectively. The values obtained by these two forms were found to agree satisfactorily and, for purposes of constructing Figure 1, only the latter form was used in the case of the deuterated polybutadiene; this form was used also for the undeuterated polymer.

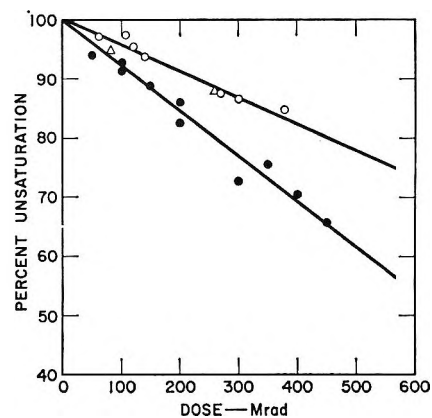


Figure 1. Decrease of original unsaturation in *cis*-polybutadiene (Δ) and in *cis*-polybutadiene-2,3-*d*₂ (O, ●) on exposure to γ -rays (open symbols) or to electrons (closed symbols).

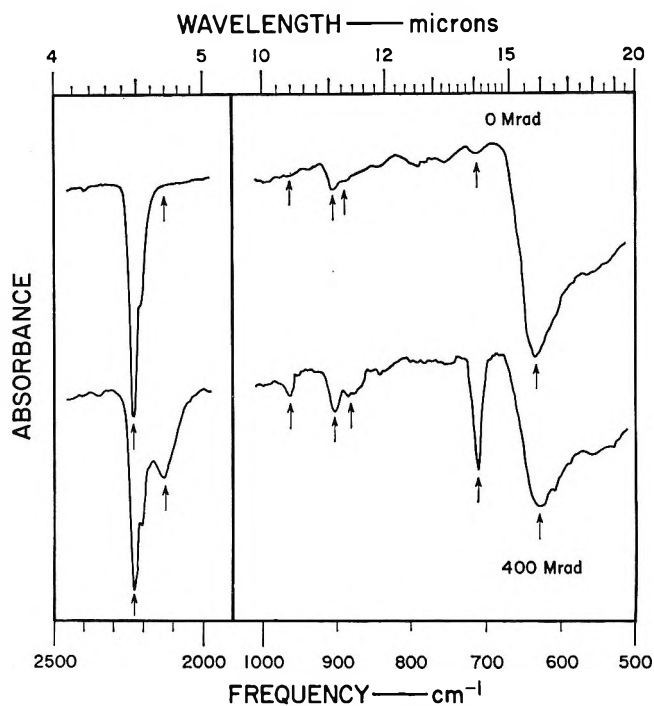


Figure 2. Infrared spectra of *cis*-polybutadiene-2,3-*d*₂ film before and after irradiation with electrons.

Results

From the typical infrared spectrum of irradiated *cis*-polybutadiene-2,3-*d*₂ shown in Figure 2, it is evident that polybutadiene indeed undergoes, in common with polyisoprene, an important radiation-induced loss of original unsaturation, accompanied by considerable *cis*-*trans* isomerization. Thus, the diminu-

(9) M. A. Golub and J. J. Shipman, *Spectrochim. Acta*, **16**, 1165 (1960).

tion of the 4.45- μ band and the development of the 4.65- μ band (C-D stretching vibration for a saturated carbon atom) point unmistakably to the disappearance of double bonds through some saturation process, while the isomerization is demonstrated by the decrease in the 15.6- μ band and the associated growth of the 14.0- μ band. The loss of double bonds in both the deuterated and undeuterated polybutadienes is further indicated by definite decreases observed in the quantity $(3.65A_c + A_t)/A_{6.9}$ for the respective polymers (Figure 1). Although the 6- μ band (C=C stretching vibration of the double bonds) in the spectra of these polymers (not shown here)¹⁰ also dropped in relative intensity, it could not be used to follow the loss of unsaturation since *cis-trans* isomerization itself produces a sharp decrease in this band.

As seen in Figure 1, the consumption of double bonds in polybutadiene films irradiated with electrons under nitrogen was about twice as fast as in those irradiated with γ -rays *in vacuo*. There was no difference in rates between the deuterated and undeuterated polymers. From the straight line plots, G values for the loss of double bonds (-d.b.) in the electron and γ -irradiations were calculated to be 13.6 and 7.9, respectively. These values are practically the same as corresponding ones for polyisoprene² mentioned in the Introduction. The polybutadiene results obtained here, which thus conform to the pattern of polyisoprene, and of squalene ($G(-d.b.) \sim 4-5$),^{1,5} are in marked contrast to the findings of Kuzminsky, *et al.*,⁷ who reported very high values for $G(-d.b.)$ for polybutadiene irradiated with γ -rays *in vacuo* (*e.g.*, 4300 at 0°, and 5000 at 85°). At the same time, the present results serve to correct previous work³ in which the decrease in unsaturation was considered to be negligible.

Figure 3 presents a kinetic plot of the *cis-trans* isomerization of polybutadiene-2,3- d_2 and of the corresponding undeuterated polymer, along with some results from the previous work which have been revised in line with the indicated change in extinction coefficients. Although the isomerization reaction has not been carried to equilibrium in the present work, we can nevertheless consider the radiostationary *cis/trans* ratio to be around 33/67, based on the earlier data which have likewise been recalculated.⁸ As can be seen, there is no significant difference between the deuterated and undeuterated polybutadienes in their rates of isomerization. Also, in contrast to the consumption of double bonds which proceeds at quite different rates in the electron and γ -irradiations, the isomerization is apparently independent of the irradiation conditions, suggesting that the two processes are unrelated mechanistically. From the initial slope

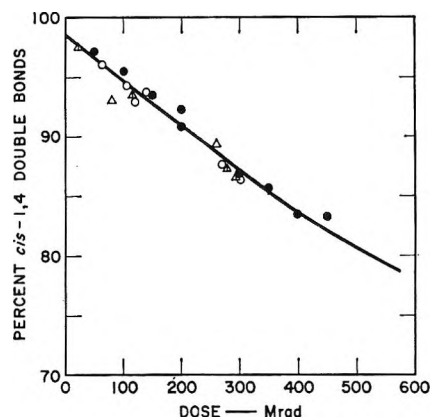


Figure 3. Radiation-induced *cis-trans* isomerization of polybutadiene. Symbols have the same significance as in Figure 1, with the additional symbol, Δ , denoting revised data from the previous paper.³

of the curve in Figure 3, $G_0(cis \rightarrow trans)$ for the deuterated and undeuterated polybutadienes is found to be 7.2. This value thus represents a considerable change from the original one³ of 14.6 and, at the same time, is an improvement over the G value (8.0) given more recently.⁸ The corresponding $G_0(cis \rightarrow trans)$ for polyisoprene^{1,2} has been found to be around 10, which again calls attention to the similarity in radiation chemistry of these diene polymers.

Because of the substantial loss of double bonds, the true percentage of *cis* double bonds isomerized into the *trans* form at any time will, of course, not be given simply by the difference between the initial and final per cent *cis* contents as depicted in Figure 3. Rather, it will be less than this difference by an amount depending upon the decrease in unsaturation. It can be shown, in fact, that the per cent actually isomerized, I , is given by

$$I = \frac{2[(C + T) - L][C - S(C + T)]}{[2(C + T) - L]}$$

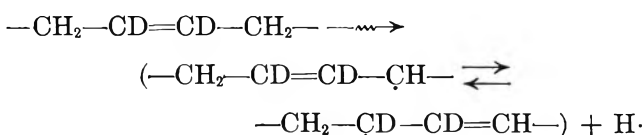
where C and T are the percentages of *cis* and *trans* double bonds present initially, L is the per cent original unsaturation which is lost, and S is the per cent *cis* content from spectroscopic analysis. This relation has been derived on the reasonable assumption that the *cis* and *trans* double bonds are consumed in the course of irradiation in strict accordance with their instantaneous relative amounts. By means of this relation, it is seen, for example, that instead of the (apparent)

(10) Except for a small decrease in the 6- μ band, no other significant spectroscopic changes were observed over the range 5-10 μ , and, so for convenience of presentation, only the abbreviated spectra are given here. However, complete spectra for the *cis* and *trans* forms of polybutadiene-2,3- d_2 are shown elsewhere.⁹

15% *cis* → *trans* isomerization after a dose of 400 Mrads (98.3–83.3%, obtained from Figure 3), the actual percentage of original double bonds isomerized, *I*, using γ -rays ($L = 17.8$, from Figure 1) is 13.5%. This number is confirmed by measurements of the molar concentration of the *trans* —CD=CD— units in the γ -irradiated polybutadiene-2,3-*d*₂, through application of Beer's law to the 14- μ band. Thus, after the indicated dose, the spectrum shows the presence of *trans* —CD=CD— units in the amount of 13.4% of the original unsaturation, or an increase of 13.4 – 1.7 = 11.7% *trans* double bonds. Now, it may be estimated that about 9% of the 17.8% double bonds destroyed or 1.6% were *trans*, so that the over-all formation of *trans* units through direct isomerization of *cis* units would be 11.7 + 1.6, or 13.3%; this, of course, is in very good agreement with the *I* value of 13.5% given above. A similar situation holds for the electron-irradiated films, but, for the same dose of 400 Mrads, the actual isomerization, *I*, is found to be 12.2% while the corresponding value through the Beer's law approach is 12.7%.

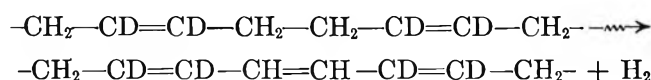
That the number of double bonds actually isomerized in the γ -irradiations is slightly higher than that in the electron irradiations is simply a reflection of the fact that in the former case the energetically rich double bonds have a somewhat lower tendency to undergo the competing saturation process and so have a greater chance to dissipate their energy through isomerization. The net production of *trans* —CD=CD— units in polybutadiene-2,3-*d*₂ (or *trans* —CH=CH— units in ordinary polybutadiene), which follows a nearly linear kinetic plot, has a *G* value of 5.3 in the γ -ray case and 4.5 in the electron case. These values, which are necessarily less than the G_0 (*cis* → *trans*) value of 7.2, can be considered as the polybutadiene counterparts to the *G* values for formation of *trans*-butene-2 ($G \sim 4.0$)¹¹ in the radiolysis of *cis*-butene-2, independent of any isomerization, or the formation of new vinylene units in polyethylene ($G \sim 2.4$),¹² etc.

The spectra of Figure 2, apart from demonstrating radiation-induced *cis*-*trans* isomerization and loss of unsaturation, suggest at first glance the possible occurrence also of double-bond migration and the formation of conjugated triene structures or new vinyl groups. Thus, the slight increase in absorption at 11.2 μ could signify the formation of —CD=CH— units through the process



However, from a comparison of the spectrum of the electron-irradiated *cis*-polybutadiene-2,3-*d*₂ with the spectrum of the conventional *trans* isomerizate of this polymer (see Figure 3, ref. 9), it may be assumed that the very weak 11.2- μ peak in Figure 2 arises solely from isomerization of some of the *cis* —CD=CH— units present as an impurity in the starting polymer. At any rate, as in the radiation chemistry of polyisoprene, there is no firm evidence to indicate that a double-bond shift takes place in the irradiation of polybutadiene.

While the 10.4- μ peak could be due to *trans* —CH=CH— units formed in the process



involving molecular elimination of hydrogen, this assignment cannot be accepted in view of the strong arguments against the formation of a significant amount of conjugated triene structures in irradiated polyisoprene and polyisoprene-3-*d*,² and presumably in polybutadiene as well. A further argument against that assignment is that, if these *trans* —CH=CH— units were indeed responsible for the 10.4- μ peak, its relative intensity (which is about the same for polybutadiene-2,3-*d*₂ and polyisoprene after equal radiation doses) would correspond to a G (—CH=CH—) ~ 0.45 , which is considerably higher than the maximum G (trienes) value of ~ 0.03 obtained by Turner and co-workers¹³ in the γ -irradiation of polyisoprene. The 10.4- μ peak is also too strong to be due to *trans* —CH=CH— units arising from isomerization of corresponding *cis* units since the latter are, at most, a trace impurity in the original polymer. Isotopic substitution of deuterium atoms on the double bonds by radiolytically produced hydrogen atoms can likewise be dismissed since it would presumably bring about a much stronger 11.2- μ absorption (—CD=CH—) in polybutadiene-2,3-*d*₂ than is actually found, and in any case such a process is not observed in polyisoprene-3-*d*.²

The most likely explanation for the 10.4- μ peak in the spectrum of irradiated polybutadiene-2,3-*d*₂ is the one invoked for the appearance of this same absorption in the spectrum of irradiated polyisoprene, *viz.*, that it is due to cyclic structures in the polymer backbone. This interpretation is very reasonable in view of the fact that CH₂ groups in certain substituted cyclohexyl rings have deformation vibrations at around

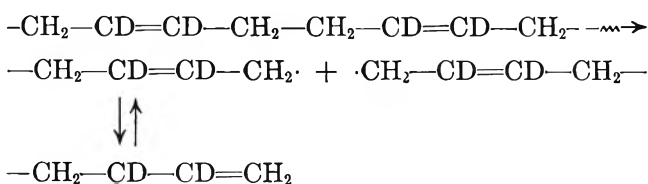
(11) P. C. Kaufman, *J. Phys. Chem.*, **67**, 1671 (1963).

(12) M. B. Fallgatter and M. Dole, *ibid.*, **68**, 1988 (1964).

(13) M. B. Evans, G. M. C. Higgins, and D. T. Turner, *J. Appl. Polymer Sci.*, **2**, 340 (1959).

10.4 μ and also because polybutadiene and polyisoprene have similar, very high G values for consumption of double bonds which in the latter polymer has already been ascribed to cyclization.²

To conclude the examination of Figure 2, it should be noted that the small increase in absorption at 11 μ (also observed in the spectrum of irradiated, undeuterated polybutadiene) is probably due to the formation of some new vinyl groups through occasional chain scission



Such a process appears to take place to an even greater extent in the analogous ultraviolet irradiation of polybutadiene films.¹⁴

Discussion

To sum up the findings of this work, we note that polybutadiene, like polyisoprene, undergoes a marked radiation-induced loss of unsaturation in addition to the *cis-trans* isomerization studied previously and re-examined here. Although the G value for the *trans* \rightarrow *cis* isomerization has not been redetermined, we could nevertheless consider it to be of the order of 3.6, inasmuch as the radiostationary *cis/trans* ratio is 33/67. Adding to the parallelism in the radiation chemistry of polybutadiene and polyisoprene, which is emphasized by the close similarity in G values for the various processes taking place (Table I), is the observation that these polymers display comparable yields for radiolytic production of hydrogen; the G value for the only other process of importance in *cis*-polybutadiene, namely, cross linking, has apparently not yet been determined, but it is probably not far off from the $G(\text{X})$ value of 0.9 for natural rubber (*cis*-polyisoprene).

Since the mechanism for radiation-induced isomerization for polybutadiene and polyisoprene has been discussed in detail elsewhere,^{1-3,15} there is no need to consider it further here. On the other hand, the cyclization mechanism, which has been invoked to explain the sharp drop in unsaturation in polyisoprene² and its low molecular prototype, squalene,¹ and which probably applies also to polybutadiene, requires further comment with regard to this last compound. In contrast to polyisoprene and squalene which undergo facile cyclization by a conventional carbonium ion mechanism,¹⁶ polybutadiene can be made to undergo this reaction only under rigorous conditions.¹⁷ Thus, it would appear that the radiation-induced cyclization of polybutadiene could not involve an ionic process, unless the detailed steps leading to a stable carbonium ion in this polymer just happen to be much more favorable with ionizing radiation than with acid catalysis. If that is the case, we could visualize the following mechanism, involving an ion-molecule reaction and culminating in extensive cyclization of polybutadiene *via* a carbonium ion chain reaction

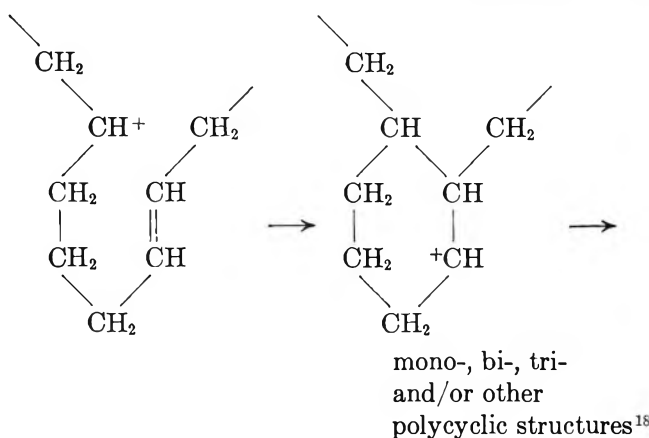
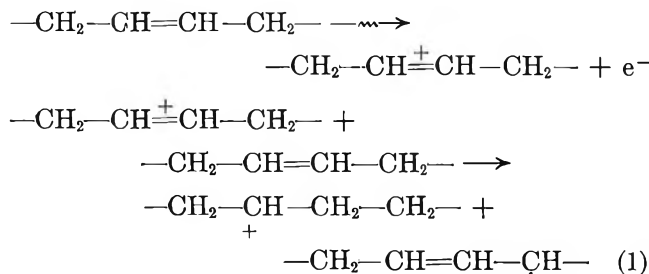


Table I: G Values for Radiation-Induced Effects in Polybutadiene and Polyisoprene

	Polybutadiene	Polyisoprene ^a
$G(-\text{d.b.})$ electrons under nitrogen	13.6	13.4
γ -rays <i>in vacuo</i>	7.9	6.7
$G_0(\text{cis} \rightarrow \text{trans})$	7.2	10
$G_0(\text{trans} \rightarrow \text{cis})$	3.6	10
$G(\text{H}_2)$	0.45 ^b	0.48
$G(\text{X})$	<i>c</i>	0.9

^a See ref. 1 and 2. ^b See ref. 14. ^c Probably also 0.9, by analogy to polyisoprene (see text).

(14) M. A. Golub, unpublished results.

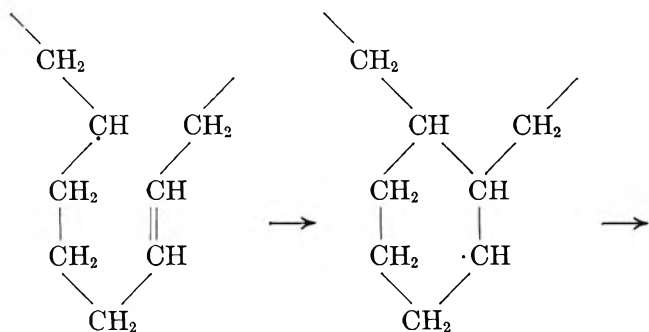
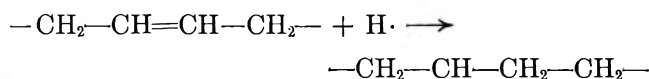
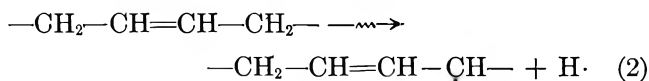
(15) M. A. Golub, *Discussions Faraday Soc.*, **36**, 264, 276 (1963).

(16) M. A. Golub and J. Heller, *Can. J. Chem.*, **41**, 937 (1963).

(17) J. R. Shelton and L. H. Lee, *Rubber Chem. Technol.*, **31**, 415 (1958).

(18) The corresponding *intermolecular* reaction involving carbonium ions (to form cross links) is presumed to be unimportant here since the conventional carbonium ion catalyzed cyclization produces no cross links with polyisoprene¹⁶ and only a very small amount with polybutadiene.¹⁷

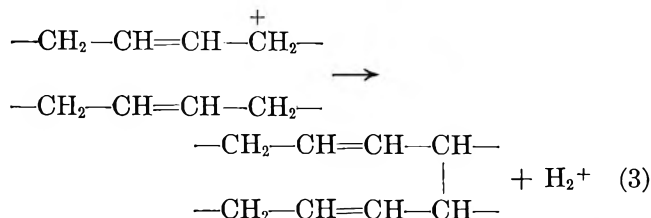
On the other hand, a free-radical mechanism for cyclization is also possible, involving intramolecular addition of an alkyl radical onto a double bond



various
cyclic
structures

At the present time, we cannot say for certain which of the two mechanisms of cyclization is the dominant one, and future work involving additives which can act as radical acceptors should help to resolve this point. However, it may be noted that some preliminary work on polybutadiene films in which small amounts of elemental sulfur are dispersed indicates¹⁴ that the rate of isomerization is somewhat higher in the presence of sulfur than in its absence, while the loss of double bonds (and hence cyclization) is greatly diminished though not eliminated. Since sulfur is believed to act as a free-radical scavenger, the free-radical mechanism may well dominate here, but not necessarily to the exclusion of an ionic component. In fact, some contribution from an ionic process could account for the different rates at which the double bonds of polybutadiene (or polyisoprene) are destroyed when the polymers are irradiated with electrons under nitrogen or γ -rays *in vacuo*. The former irradiation condition might entail the presence of just enough oxygen to intervene in the radiation chemistry by capturing some electrons according to¹⁹ $\text{O}_2 + e^- \rightarrow \text{O}_2^-$, thereby increasing the lifetime of the transitory radical ion $\text{---CH}_2\text{---CH}^+\text{---CH---CH}_2\text{---}$ and hence promoting the carbonium ion mechanism depicted above. Presumably, this oxygen effect would not occur in the γ -irradiation runs.

To conclude the discussion of the radiation-induced effects in polybutadiene, a few remarks concerning energy and material balance are in order. If cross linking arises through the ion-molecule process^{3,20}



(or analogous Stern-Volmer process) and through mutual combination of the $\text{---CH}_2\text{---CH=CH---}\dot{\text{C}}\text{H---}$ radicals formed in (1) and/or (2), we see that

$$G(X) = G(\text{H}_2) + \frac{1}{2}G(\text{---CH}_2\text{---CH=CH---}\dot{\text{C}}\text{H---}) \quad (4)$$

However, for each such radical formed, one new species, $\text{---CH}_2\text{---CH---CH}_2\text{---CH}_2\text{---}$ or $\text{---CH}_2\text{---}\dot{\text{C}}\text{H---CH}_2\text{---CH}_2\text{---}$, is formed capable of initiating a chain cyclization, which appears¹⁴ to have a chain length of about 10. Thus, (4) can be rewritten as

$$G(X) = G(\text{H}_2) + 0.05G(\text{---d.b.}) \quad (5)$$

or, for γ -irradiation runs

$$G(X) = 0.45 + 0.4 = 0.85$$

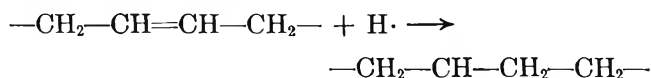
which agrees very well with the $G(X)$ value expected for *cis*-polybutadiene on the basis of its radiation chemical similarity to *cis*-polyisoprene. Since *cis*-*trans* isomerization leads to no net change in amount of unsaturation, and, since other microstructural changes such as double-bond shift, formation of conjugated trienes and new vinyl groups, and intermolecular links involving double bonds are negligible, they can be ignored from the standpoint of the material balance (5).

On the other hand, the isomerization makes the major contribution to the utilization of energy and so must be taken into account in an energy balance. If the isomerization proceeds through the 3.2-e.v. triplet state of the vinylene unit,³ the *minimum* energy utilized in this reaction (per 100 e.v. of energy deposited in the system) would be $[G_0(\text{cis} \rightarrow \text{trans}) + G_0(\text{trans} \rightarrow \text{cis})] \times 3.2$, or 34.6 e.v. The energy required to form a cross link through process 3 is just that required to break one C-H bond (4.2 e.v.) since the subsequent steps leading to the formation of the cross link and the molecule of hydrogen are exothermic, and so no additional energy is needed. Also, the formation of a cross link through combination of two $\text{---CH}_2\text{---CH=CH---}\dot{\text{C}}\text{H---}$ radicals requires, as a precondition, the rupture of two C-H bonds or the consumption of

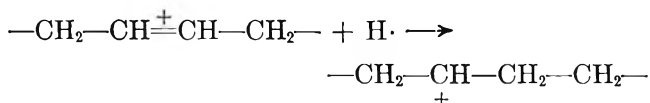
(19) A. Chapiro, "Radiation Chemistry of Polymeric Systems," Interscience Publishers, Inc., New York, N. Y., 1962, p. 43. It should be pointed out that it was not feasible in the electron irradiations to reduce the oxygen partial pressure with nitrogen purging to the extent required ($<10^{-6}$ mm.) to suppress its contribution to the radiation effects, as obtained in the γ -irradiations.

(20) J. Weiss, *J. Polymer Sci.*, **29**, 425 (1958).

8.4 e.v. Thus, for a $G(X)$ given by expression 5 we obtain $(0.45 \times 4.2) + (0.4 \times 8.4) = 5.3$ e.v. Since the cyclization with its associated loss of double bonds requires no additional energy beyond that involved in the formation of the $-\text{CH}_2-\text{CH}=\text{CH}-\dot{\text{C}}\text{H}-$ radicals (the processes



and



being exothermic), we find that the *minimum* energy utilized in bringing about the various radiation chemical effects in polybutadiene is $34.6 + 5.3$, or 39.9 e.v./100 e.v. absorbed by the polymer. This result implies a highly efficient utilization of the energy imparted to the system by ionizing radiation, inasmuch as the energy is not deposited, of course, in quanta of just 3.2 or 4.2 e.v., but instead over a range of 10–15 e.v. on down.

Acknowledgment. The author is indebted to Stanford Research Institute for supporting the present study.

The 300-m μ Band of NO₃⁻

by Eitan Rotlevi and Avner Treinin

Department of Physical Chemistry, The Hebrew University, Jerusalem, Israel (Received February 12, 1965)

The solvent effect on the low intensity ultraviolet band of NO₃⁻ was investigated. In general, the oscillator strength of the band decreases with the polarity of the solvent, but its value for the free ion is not likely to be considerably smaller than $f \sim 7 \times 10^{-5}$. The assignment of the electronic transition is discussed. The forbidden $\sigma^* \leftarrow n$ transition appears to account for the properties of this band.

The weak absorption band of NO₃⁻ at about 300 m μ has been the subject of many papers, and it was usually assigned to the ${}^1A_1'' \leftarrow {}^1A_1'$ ($\pi^* \leftarrow n$) electronic transition. This transition should be extremely weak as it requires the coupling with at least two normal vibrations to make it appear. Since in crystals and solution the oscillator strength f of the band is 10^2 – 10^3 times larger than that calculated, it was suggested that external perturbations lead to a large hyperchromic effect.¹ To support this, it was shown that by varying the solvent from N,N-dimethylformamide to water f changes from 8×10^{-5} to 15×10^{-5} .¹ The few solvents tested were strongly polar, and therefore it was argued that the intensity would further decrease with decrease of polarity.¹ To test this hypothesis we

carried out a detailed investigation of the spectrum of tetraalkylammonium nitrates in various solvents. The choice of the proper cation is decisive in solvents of low polarity at relatively high concentrations (10^{-2} – $10^{-1} M$), where formation of ion pairs may lead to distinct spectroscopic effects. The polarizing effect of the cations is responsible for the blue shifts observed in some previous works² on decreasing the polarity of the solvent. Apart from the work of Strickler and Kasha there is only one early work,³ where this effect

(1) S. J. Strickler and M. Kasha, "Molecular Orbitals in Chemistry, Physics and Biology," Academic Press, New York, N. Y., 1964, p. 241.

(2) (a) H. v. Halban and J. Eisenbrand, *Z. physik. Chem.*, **A132**, 401 (1928); (b) L. I. Katzin, *J. Chem. Phys.*, **18**, 789 (1950).

was eliminated by using tetraethyl- and tetrapropylammonium nitrates. The solvents tested in that work were H_2O , CH_3OH , and CHCl_3 .

Experimental

Materials. Tetraethyl- and tetrabutylammonium nitrates were prepared by accurately neutralizing aqueous solutions of the corresponding hydroxides with nitric acid and then evaporating to dryness under vacuum at 50° . NEt_4NO_3 and NBu_4NO_3 were recrystallized from acetone and ethyl acetate, respectively,⁴ rinsed with acetone, and dried over CaCl_2 . The purity of the salts was checked by measuring their spectra in aqueous solution, which were found to be nearly identical with that of KNO_3 . The solvents used were of purest grade available. Diethylene glycol dimethyl ether (Ansul) and tetrahydrofuran (Fluka) were dried over sodium for several days, then refluxed with LiAlH_4 , and distilled.

Absorption Spectra. The measurements were carried out with a Hilger Uvispek spectrophotometer. Solutions 0.05 – $0.1 M$ were used in 1-cm. silica cells. In the following solvents the spectra of both NEt_4NO_3 and NBu_4NO_3 were measured: water, ethanol, methyl cyanide, *N,N*-dimethylformamide, methanol, 2-propanol, ethylene glycol, dimethyl sulfoxide, and chloroform. No effect of cation was observed. Moreover, in the first four solvents the values obtained for $h\nu_{\text{max}}$ and ϵ_{max} are in good agreement with that obtained for $10^{-2} M$ tetramethylammonium nitrate.¹ For all other solvents the butyl salt was used. Beer's law was also checked in CHCl_3 and CH_3CN , by varying the concentration from 10^{-1} to $10^{-2} M$, and was found to be valid. These results indicate that with these bulky cations ionic association (which may take place in the less polar solvents) has hardly any spectroscopic effect.

Results

Figure 1 shows the absorption spectrum of NO_3^- in all the solvents tested. The position of the peak and its extinction coefficient are recorded in Table I together with some properties of the solvents which reflect their polarity. The general blue shift of the band with increase of polarity is evident. With few deviations the band gains intensity as it shifts to higher energies. The solvent effect appears to be mainly due to hydrogen bonding. (CHCl_3 is known to have some protic properties.⁵) Altogether, on lowering the polarity, the band reaches shape and intensity ($f \sim 7 \times 10^{-5}$) which vary only little with the nature of the solvent. Some vibrational structure is revealed in the aprotic solvents. It is badly resolved; the vibrational spacing appears to be constant at $\sim 700 \text{ cm}^{-1}$.

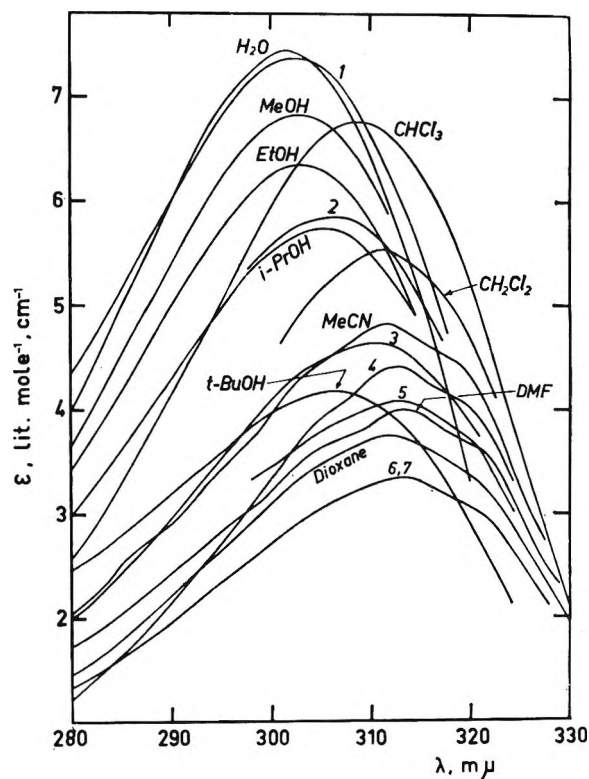


Figure 1. The absorption spectrum of NO_3^- in various solvents. The solvents numbered are (1) $\text{HO}(\text{CH}_2)_2\text{OH}$, (2) $\text{C}_3\text{H}_8\text{O}(\text{CH}_2)_2\text{O}(\text{CH}_2)_2\text{OH}$, (3) $\text{C}_2\text{H}_5\text{CN}$, (4) $(\text{CH}_3)_2\text{SO}$, (5) $\text{CH}_3\text{CO}_2\text{CH}_3$, (6) and (7) tetrahydrofuran and diethylene glycol-dimethyl ether, respectively (in these solvents the spectra are nearly identical).

Figure 2 shows the spectrum of NO_3^- in mixtures of methanol with acetonitrile. There is evidence for an isosbestic point.

Discussion

Our results indicate that the intensity of the $300\text{-m}\mu$ band is not likely to be considerably lower than $f \sim 7 \times 10^{-5}$. This appears to be in discord with the assignment of the $300 \text{ m}\mu$ to ${}^1\text{A}_1'' \leftarrow {}^1\text{A}_1'$ transition; though the intrinsic intensity is low, it is still too large for this type of transition. Sayre carried out a detailed analysis of the vibrational structure displayed by the weak band of crystalline nitrates at 4°K .⁶ It is primarily compounded of vibrational frequencies of about 650 and 260 cm^{-1} .⁷ The $(0-0)$ band was

(3) H. v. Halban and J. Eisenbrand, *Z. physik. Chem.*, **A146**, 294 (1930).

(4) The recrystallization of tetrabutylammonium nitrate is difficult because of its high solubility in many solvents. Benzene should be avoided as it forms a complex with the salt (T. J. Plati and E. G. Taylor, *J. Phys. Chem.*, **68**, 3426 (1964)).

(5) See, e.g., C. M. Huggins, G. C. Pimentel, and J. N. Shoolery, *J. Chem. Phys.*, **23**, 896, 1244 (1955).

(6) E. V. Sayre, *ibid.*, **31**, 73 (1959).

Table I: Effect of Solvent on the Low Energy Band of NO_3^- at 20°

Solvent	λ_{max} , ^a m μ	ϵ_{max} , M^{-1} cm. ⁻¹	Dielec- tric con- stant ^b	Dipole mo- ment ^b	Z value ^c
H ₂ O	301.5	7.44	80	1.8	94.6
HO(CH ₂) ₂ OH	302.5	7.37	39	2.2	85.1
CH ₃ OH	303.0	6.83	33	1.7	83.6
C ₂ H ₅ OH	303.4	6.36	25	1.7	79.6
(CH ₂) ₂ CHOH	305.2	5.75	19	1.7	76.3
(CH ₃) ₃ COH	306.6	4.19	13	1.7	71.3
C ₃ H ₇ O(CH ₂) ₂ O(CH ₂) ₂ OH	306.7	5.85			
CHCl ₃	308.7	6.77	4.8	1.0	63.2
C ₂ H ₅ CN	310.5	4.65	27	4.0	
CH ₂ Cl ₂	311.2	5.55	9.1	1.6	64.2
CH ₃ CN	311.6	4.83	37	3.4 ^d	71.3
CH ₃ CO ₂ CH ₃	311.5	4.09	8.0	1.7	
Dioxane	312.0	3.76	2.3	0	
CH ₃ CO ₂ C ₂ H ₅	312.5	4.01	6.0	1.8	
(CH ₃) ₂ SO	312.6	4.42		4.3 ^d	71.1
Tetrahydrofuran	313.0	3.36	7.6	1.7	
CH ₃ O(CH ₂) ₂ O(CH ₂) ₂ OCH ₃	313.0	3.36			
HCON(CH ₃) ₂	313.2	4.01	37.6	3.8 ^d	68.5

^a λ_{max} was determined by the method of means (G. Scheibe, *Ber.*, **58**, 586 (1925)). In most cases the means were found to lie closely on a straight line. ^b Unless otherwise stated the values of dielectric constant and dipole moment were taken from Landolt-Börnstein, Parts 6I and 3II, respectively. ^c E. M. Kosower, *J. Am. Chem. Soc.*, **80**, 3253 (1958). ^d A. J. Parker, *Quart. Rev.* (London), **16**, 163 (1962).

not observed. All the vibrational bands which appear with relatively strong intensity are polarized in the plane of the ion. The substitution of N¹⁵ for N¹⁴ changes the frequency of the 650 cm.⁻¹ value by about 2.5% whereas the 260 cm.⁻¹ frequency is not affected. A splitting of the vibrational structure is shown by KNO₃ but not by NaNO₃. Sayre pointed out that the combination of E' electronic state with the two e' vibrational modes is consistent with these results. He postulated a large expansion of the ion on excitation in order to explain the relatively large difference in the e' frequencies between the ground and excited states. However, the ¹E' \leftarrow ¹A₁' transitions are allowed and so cannot account for this weak band. The two lowest E' states are (n, σ^*) and (π , π^*) states, in the m.o. treatment. The $\pi^* \leftarrow \pi$ transition should be strong, and actually the 200-m μ band has been assigned to it.^{1,8} The allowed $\sigma^* \leftarrow n$ transition should be rather weak but not as weak as the 300-m μ band, and moreover its intensity should not be much affected by the medium. We are thus led to the conclusion that, although the excited vibronic levels are of E'

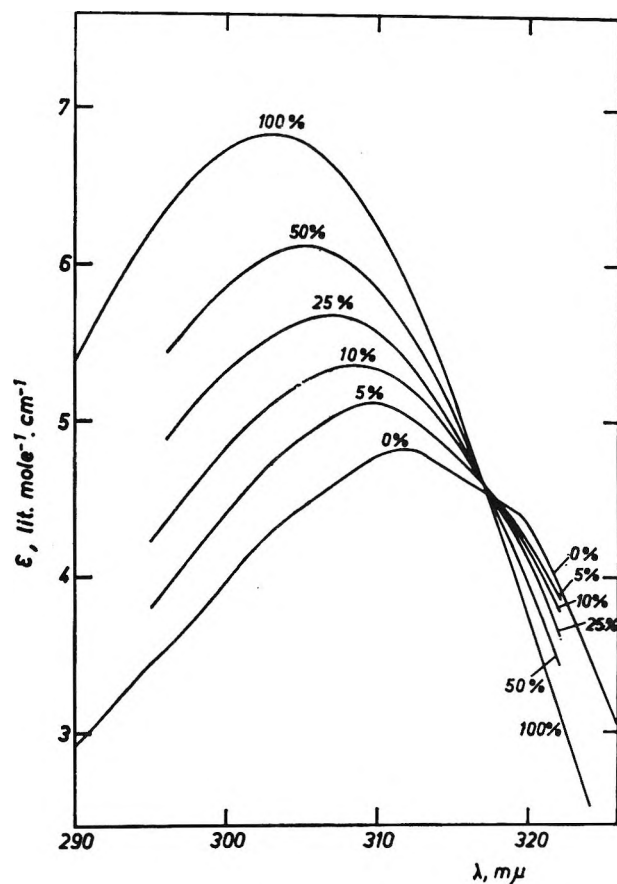


Figure 2. The spectrum of NO_3^- in mixtures of acetonitrile with methanol. (The volume per cent of methanol is recorded.)

symmetry, the corresponding electronic state belongs to another representation.

If we accept Sayre's vibrational analysis, then the appearance of the e' progressions in the spectrum indicates that the ion is planar in its excited state. According to Walsh's correlation diagram⁹ the lowest states that lead to planar configuration (and correspond to forbidden transitions) are (n, σ^*)A₂' and (π , σ^*)E''.

The forbidden $\sigma^* \leftarrow n$ transition can be made to appear by coupling with a vibration of e' symmetry. All the overtones of this vibration belong to reducible representations which contain the e' representation.¹⁰ Thus, all the vibronic levels which belong to the

(7) The latter frequency was completely overlooked by Strickler and Kasha.¹

(8) D. Meyerstein and A. Treinin, *Trans. Faraday Soc.*, **57**, 2104 (1961).

(9) A. D. Walsh, *J. Chem. Soc.*, 2301 (1953).

(10) The symmetries of the overtones of a degenerate vibration are clearly discussed by E. B. Wilson, J. C. Decius, and P. C. Cross, "Molecular Vibrations," McGraw-Hill Book Co., Inc., New York, N. Y., p. 352.

electronic state A_2' and $v' = 1, 2 \dots$ should have the correct symmetry for an allowed transition polarized in the plane of the ion.¹¹ However, the transitions from the ground state to these levels will be weak because the excited electronic state (A_2') does not have the proper symmetry. If this picture is correct, then this case is quite different from that usually encountered when dealing with forbidden transitions which are relaxed by vibrational-electronic interaction (e.g., the 260-m μ band of benzene). In the usual case it is the totally symmetric vibration which appears as a prominent progression, successive quanta of which are excited in combination with one quantum of a nontotally symmetric vibration. In the present case the vibration which appears as a progression has in all its levels ($v > 0$) the proper symmetry to relax the forbidden character of the transition. In both cases the common feature is the absence of the (0-0) band.¹²

The excitation of a nonbonding electron to a highly antibonding orbital (σ^*) is expected to bring about a considerable expansion of the ion, so that the observed reduction in the e' vibration frequencies is not improbable.¹³ McEwen pointed out¹⁴ that the *allowed* $\sigma^* \leftarrow n$ transition in NO_3^- should be 1 or 2 e.v. lower than the corresponding transition in a less symmetrical compound such as nitromethane. The energy of the forbidden $\sigma^* \leftarrow n$ transition is probably even lower since it involves the highest filled n orbital. Thus, this transition may well appear at 4.1 e.v. Leading to a considerable net flow of negative charge from the oxygen atoms to the nitrogen atom,¹⁵ the energy of this transition should be sensitive to environmental effects. However, since the vertical transition does not lead to a change in the dipole moment of the ion, the solvent effect is mainly due to the change in the H-bonding capacity of the ion on excitation. In this respect NO_3^- differs from the pyramidal halate ions which exhibit a linear relation between $h\nu$ and the Z value of the solvent.¹⁶

The pronounced effect of the medium on the intensity of the band is probably due to its effect on the symmetry of the nuclear charge field.¹⁷ Raman and infrared spectra of nitrates in crystals, melts, and solutions¹⁸ have revealed the distortion of the D_{3h} symmetry exerted by polarizing cations. This effect seems to be in parallel with the intensification of the 300-m μ band. In some solvents of low polarity heavy

metal ions were shown to yield a large intensification of this band.^{2b,19} The effects of polar solvent molecules on the symmetry of NO_3^- are probably small. Thus, the splitting of the degenerate $\nu_3(e')$ frequency could not be detected even in water.¹⁸ The largest hyperchromic effects exerted by solvents are due to protic solvents. This is probably due to the formation of definite (weak) compounds between solute and solvent (Figure 2).

A small contribution to the intensification of the band in polar media may result from the decrease in the energy gap between the low and high intensity bands. The intensification results from the "mixing" of the corresponding excited electronic states induced by the proper vibration; the mixing coefficient is inversely proportional to the difference between the energies of the corresponding energy levels. However, the reduction of this gap is relatively small: $\sim 2\%$ when replacing H_2O by CH_3CN ,¹ which may yield a change of about 4% in the intensity.

Finally, we have to consider the $\sigma^* \leftarrow \pi$ (${}^1E'' \leftarrow {}^1A_1'$) transition. By coupling with one quantum of the out-of-plane vibration (a_2'') the excited state gains the E' symmetry. Provided the distortion from planarity is small, this quantum may be excited in combination with successive quanta of e' vibrations. Since the π -orbital is actually a nonbonding orbital,¹ the solvent effects can be readily explained. At present we cannot discard this assignment.

(11) Strickler and Kasha ascribed the vibrational structure to the out-of-plane a_2'' vibration.¹ In the absence of external perturbation only odd quanta of this vibration may appear. This results from their particular assignment of the band to an electronic transition which requires the coupling with a vibration of a_2'' symmetry.

(12) This band may weakly appear in crystals owing to the perturbing effect of the medium.

(13) The C=O stretching vibration in the (n, π^*) state of some carbonyl compounds is 50-70% lower than in the ground state. In the (n, σ^*) state it should be even lower.

(14) K. L. McEwen, *J. Chem. Phys.*, **34**, 547 (1961).

(15) See ref. 1, Figure 2, for a schematic LCAO representation of the molecular orbitals of NO_3^- and a schematic energy level diagram.

(16) A. Treinin and M. Yaacobi, *J. Phys. Chem.*, **68**, 2487 (1964).

(17) C. F. Smith and C. R. Boston, *J. Chem. Phys.*, **34**, 1396 (1961).

(18) For a summary of data and literature on these spectra see: L. I. Katzin, *J. Inorg. Nucl. Chem.*, **24**, 245 (1962); S. C. Wait and G. J. Janz, *Quart. Rev.* (London), **17**, 231 (1963).

(19) C. C. Addison, B. J. Hathaway, N. Logan, and A. Walker, *J. Chem. Soc.*, 4308 (1960).

The Acidity Function, H_0 , of Hydrogen Bromide in Acetic Acid-Water Mixtures

by Walter W. Zajac, Jr., and Robert B. Nowicki¹

Department of Chemistry, Villanova University, Villanova, Pennsylvania (Received February 19, 1965)

The Hammett acidity function, H_0 , for the hydrogen bromide-acetic acid-water system has been determined for solutions between 0.02 and 0.8 M in hydrogen bromide in acetic acid solvent compositions ranging from 39.75 to 95.40% by weight of acetic acid. The indicators used were *o*-nitroaniline and *p*-nitroaniline, with the latter being the reference indicator. It has been established that the hydrogen bromide-acetic acid-water system is quite similar to other systems utilizing solvents of low dielectric constant, insofar as the acidity function, H_0 , is concerned.

Of the many types of organic reactions, those which are catalyzed by acids are both theoretically interesting and synthetically important. One approach to the elucidation of acid catalysis² is a description of the reaction medium in terms of the Hammett H_0 function.³ Although a number of acid-catalyzed reactions utilize a reaction mixture of hydrobromic acid and aqueous acetic acid,⁴ only a few H_0 values for this system have been determined.⁵ Therefore, a study of the hydrogen bromide-acetic acid-water system in terms of the Hammett acidity function, H_0 , was undertaken.

Experimental

Six different solvent compositions were used. Each was prepared by weighing the necessary amount of acetic acid and water. The composition of the acetic acid was determined cryoscopically.⁶ In each solvent, a parent solution of hydrobromic acid was prepared by bubbling anhydrous hydrogen bromide into the solvent until the solution was $\sim 1.5 M$ in hydrobromic acid. The hydrogen bromide concentration of every parent solution in each solvent was determined by the method of Fajans.⁷ The test solutions were prepared by dilution of the parent acid solutions. The final concentrations in the test solutions varied from approximately 0.8 to 0.012 M .

By means of a microburet a certain amount of indicator dissolved in the same solvent was added to each of the test solutions. The concentration of stock indicator solutions varied from 10^{-3} to $10^{-4} M$. The amounts of indicator to be added were determined by comparison with a standard of known absorbance so

that the test solution would have an absorbance in the range of 0.30-0.80.

All absorbances were measured on a Beckman DU spectrophotometer at $25 \pm 0.1^\circ$, using 1-cm. quartz cells. The value of the absorptivity of the unprotonated base was determined by measuring the absorbance of three solutions in every solvent. The value of the absorptivity of each of the test solutions was determined by measuring the absorbance of the test solution. All absorbances were measured at the wave length of maximum absorbance of the unprotonated base in each particular solvent since a slight shift in the maximum⁸ was noted with change of solvent composition. The absorptivity of the protonated form of *p*-nitroaniline

(1) Abstracted in part from the Thesis of Robert B. Nowicki presented to Villanova University in partial fulfillment for the M.S. degree, 1965.

(2) F. A. Long and M. A. Paul, *Chem. Rev.*, **57**, 935 (1957).

(3) M. A. Paul and F. A. Long, *ibid.*, **57**, 1 (1957).

(4) (a) D. M. Biresel, *J. Am. Chem. Soc.*, **52**, 1944 (1930); (b) R. P. Ghaswalla and F. G. Donnan, *J. Chem. Soc.*, 1341 (1936); (c) C. K. Bradsher, *J. Am. Chem. Soc.*, **61**, 3131 (1939); (d) W. S. Johnson and W. E. Heinz, *ibid.*, **71**, 2913 (1949); (e) R. F. W. Ciecuch and F. H. Westheimer, *ibid.*, **85**, 2591 (1963).

(5) (a) T. L. Smith and J. M. Elliot, *ibid.*, **75**, 3566 (1953); (b) R. F. W. Ciecuch, Ph.D. Thesis, Harvard University, 1960; (c) G. Schwarzenbach and P. Stensby, *Helv. Chim. Acta*, **42**, 2342 (1959).

(6) J. S. Fritz and G. S. Hammond, "Quantitative Organic Analysis," John Wiley and Sons, Inc., New York, N. Y., 1957, p. 229.

(7) I. M. Kolthoff and V. A. Stenger, "Volumetric Analysis," Vol. II, 2nd Ed., Interscience Publishers, Inc., New York, N. Y., 1947, pp. 245-248.

(8) The wave length maxima for *o*-nitroaniline and *p*-nitroaniline observed in this work are in excellent agreement with those obtained by (a) J. Roček, *Collection Czech. Chem. Commun.*, **22**, 1 (1957), and by (b) Schwarzenbach and Stensby, ref. 5c.

was taken to be 70. This was established by measuring the absorbances of a number of solutions of *p*-nitroaniline in acetic acid containing enough perchloric acid to completely protonate the base. The absorptivity of the protonated form of *o*-nitroaniline was taken to be zero. The concentration ratios were calculated from the equation

$$\frac{C_{\text{BH}^+}}{C_{\text{B}}} = \frac{E_{\text{B}}^{\lambda} - E^{\lambda}}{E^{\lambda} - E_{\text{BH}^+}^{\lambda}}$$

Results and Discussion

The Hammett acidity function, H_0 , is a measure of the ability of an acid solution to donate a proton to a neutral base and is expressed as

$$H_0 = \text{p}K_{\text{BH}^+} - \log \frac{C_{\text{BH}^+}}{C_{\text{B}}} \quad (1)$$

Even in aqueous systems the establishment of an H_0 scale is dependent on the indicator used. In non-aqueous systems or those of low dielectric constant an establishment of an H_0 scale is even less theoretically sound.⁹ However, judicious choice of indicators and specification of the reference indicator can still lead to a useful acidity function scale.¹⁰

In solvents of low dielectric constant, ion pair association tends to occur. The protonated form of the indicator base may then be a species such as BH^+X^- . Spectrophotometric measurements in this case do not simply yield the concentration ratio ($C_{\text{BH}^+}/C_{\text{B}}$) but a function which is dependent upon the specific indicator base used. The relationship of the resultant "apparent acidity function" to the thermodynamically consistent H_0 scale has been discussed by Bruckenstein.¹¹

Specification of the indicator used as a reference, as pointed out by Roček,^{8a} becomes important. In a solvent system of low dielectric constant, the $\text{p}K$ of a particular indicator as determined from measurements in that system is not generally a thermodynamic one but one that might be termed an auxiliary dissociation constant which is dependent on the medium. The indicator *p*-nitroaniline has in this investigation been chosen as the reference indicator, whose "best value"¹³ is 0.99. In all measurements involving *p*-nitroaniline, this value is used. From measurements in 84.47% acetic acid the $\text{p}K_{\text{BH}^+}$ of *o*-nitroaniline was determined by the stepwise comparison method, by the use of

$$(\text{p}K_{\text{C}})_{\text{B}} = \text{p}K_{\text{B}} + \log \frac{C_{\text{B}}}{C_{\text{BH}^+}} - \log \frac{C_{\text{C}}}{C_{\text{CH}^+}} \quad (2)$$

where C = *o*-nitroaniline, B = *p*-nitroaniline, and $(\text{p}K_{\text{C}})_{\text{B}}$ is the auxiliary dissociation constant of *o*-nitroaniline, referred to *p*-nitroaniline. The difference

in $\text{p}K$ was found to be 1.69. The $\text{p}K_{\text{BH}^+}$ for *o*-nitroaniline with reference to *p*-nitroaniline was then calculated from eq. 2 to be -0.70 .

Table I lists the difference in $\text{p}K$ for *o*- and *p*-nitroaniline as determined by a number of investigators in several acid-water solvents containing various solutes. It can be noted that while there is fair agreement among all of the values, the deviations are slightly greater than those which would be expected solely from experimental error. The solute has an effect upon the activity coefficient ratio of this pair of indicators as reflected by the difference in $\text{p}K$. While comparison of these values may lead to a good first approximation of the $\text{p}K$ difference, it should be recognized that a constant $\text{p}K$ difference should really not be expected as a matter of course for the same solvent system and a wide variety of solutes.

Table I: Difference in $\text{p}K_{\text{BH}^+}$ of *o*- and *p*-Nitroaniline for A Number of Solutes in Various Solvents

$\Delta \text{p}K_{\text{BH}^+}$	Solute	Solvent	Ref.
0.32	Perchloric acid	Water	3
1.56	Perchloric acid	91% acetic acid	<i>a</i>
1.47	Perchloric acid	79.9% acetic acid	5b
1.60	Phosphoric acid	99% acetic acid	8a
1.50	Perchloric acid	90% acetic acid	8a
1.45	Urea-antipyrene	100% acetic acid	<i>b</i>
1.61	Perchloric acid	90% acetic acid	5c
1.69	Hydrobromic acid	84.5% acetic acid	This work

^a K. B. Wiberg and R. J. Evans, *J. Am. Chem. Soc.*, **80**, 3019 (1958). ^b N. F. Hall and F. Meyer, *ibid.*, **62**, 2493 (1940).

A more convenient measure of the deviation from the thermodynamic scale, as suggested by Roček^{8a} is afforded by

$$\Delta H_0 = (H_0)_{\text{C}} = (\text{p}K_{\text{C}})_{\text{B}} - \text{p}K_{\text{C}} \quad (3)$$

in which the H_0 for the same solution with reference to two different indicators is related to the $\text{p}K$ difference between the auxiliary dissociation constant, $(\text{p}K_{\text{C}})_{\text{B}}$, and the thermodynamic dissociation constant, $\text{p}K_{\text{C}}$. From data for hydrogen bromide obtained in this investigation, $\Delta H_0 = 0.45$ as calculated from eq. 3. Roček^{8a} reports a value of $\Delta H_0 = 0.46$ for perchloric acid in 90% acetic acid. The acetic-water system containing either added perchloric or hydrobromic acid

(9) E. M. Arnett, *Progr. Phys. Org. Chem.*, **1**, 223 (1963).

(10) For a recent example, see E. M. Arnett and C. F. Douty, *J. Am. Chem. Soc.*, **86**, 409 (1964).

(11) S. Bruckenstein, *ibid.*, **82**, 307 (1960).

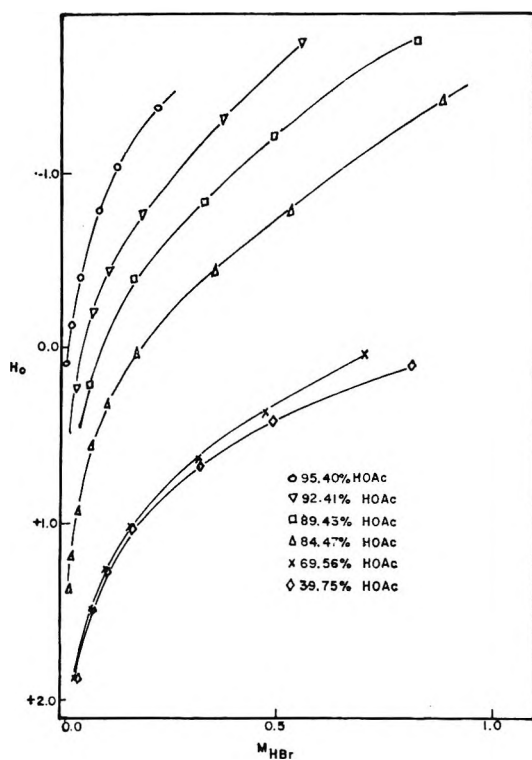


Figure 1. Molarity of HBr as a function of various acetic acid-water mixtures.

shows an appreciable deviation from the "universal" H_0 scale.

The H_0 values for hydrogen bromide in each solvent composition as obtained in this study are listed in Table II.

In Figure 1 the H_0 values from Table II have been plotted against the molarity of hydrogen bromide. Table III shows the variations of the acidity with change in solvent composition for several different concentrations of hydrogen bromide. These values were obtained by interpolation from Figure 1. The values for the aqueous solvent were taken from Vinnik, *et al.*¹² The addition of water produces a rapid decrease in the acidity in those solvents containing large amounts of acetic acid. At lower acetic acid concentrations, the decrease of acidity with addition of water is much less rapid, practically leveling out at about 50% acetic acid. In this respect the data obtained in this investigation are in agreement with the results of Schwarzenbach and Stensby^{5c} for hydrochloric acid in acetic acid and with the study of perchloric acid in acetic acid by Wi-berg and Evans.¹³ The latter, however are not strictly comparable owing to the addition of sodium perchlorate.

A comparison of the acidity function H_0 of 0.3 M perchloric,¹³ sulfuric,^{8a} and hydrobromic acids at varying activities¹⁴ of water in acetic acid-water mixtures¹⁴

Table II: H_0 of HBr in Acetic Acid Solution

[HBr], M	H_0	[HBr], M	H_0
95.40% acetic acid ^a		92.41% acetic acid ^a	
0.810	-2.8 ^b	0.810	-2.4 ^b
0.474	-2.0 ^b	0.558	-1.73
0.218	-1.37	0.372	-1.31
0.131	-1.03	0.186	-0.76
0.087	-0.78	0.112	-0.44
0.044	-0.40	0.074	-0.20
0.026	-0.12	0.037	+0.23
0.017	+0.09	0.022	+0.51
83.43% acetic acid ^a		84.47% acetic acid ^a	
0.820	-1.75	0.880	-1.40
0.492	-1.21	0.528	-0.79
0.328	-0.81	0.352	-0.44
0.164	-0.39	0.176	-0.02
0.098	-0.03	0.106	+0.42
0.066	+0.22		
54.47% acetic acid ^c		69.56% acetic acid ^c	
0.176	+0.03	0.790	+0.02
0.106	+0.33	0.474	+0.36
0.070	+0.55	0.316	+0.61
0.035	+0.93	0.158	+1.01
0.021	+1.20	0.063	+1.49
0.014	+1.38	0.032	+1.87
		0.019	+2.24
		0.013	+2.28

[HBr], M	H_0
39.75% acetic acid ^c	
0.810	+0.09
0.486	+0.40
0.324	+0.68
0.162	+1.02
0.097	+1.26
0.065	+1.49
0.032	+1.84
0.019	+2.17

^a Indicator was *o*-nitroaniline. ^b In this system at these concentrations, it appears that *o*-nitroaniline is at the limits of its usefulness as an indicator. These H_0 values are probably only good to ± 0.5 unit. ^c Indicator was *p*-nitroaniline.

is shown in Figure 2. Bascombe and Bell¹⁵ have suggested that the following relationship should hold

$$-H_0 = \log [H^+] - n \log a_{H_2O} + \log (f_{BH^+} f_{H^+} / f_{BH^+}) \quad (4)$$

(12) M. I. Vinnik, R. N. Kruglow, and N. M. Chirkov, *Zh. Fiz. Khim.*, **30**, 827 (1956).

(13) See footnote a, Table I.

(14) R. S. Hansen, F. A. Miller, and S. D. Christian, *J. Phys. Chem.*, **59**, 391 (1955).

(15) K. N. Bascombe and R. P. Bell, *Discussions Faraday Soc.*, **24**, 159 (1957).

where n is the average hydration number of protons. Strictly speaking, the formal ionic strengths of the various solutions should be maintained constant. However, satisfactory correlation can be obtained even if this condition is not fulfilled.¹⁶

Table III: Acidity Function of HBr in Acetic Acid-Water Mixture

% acetic acid	H_0				
	0.8 M	0.5 M	0.3 M	0.1 M	0.05 M
95.40	-2.5	-2.03	-1.55	-0.90	-0.48
92.41	-2.25	-1.63	-1.10	-0.39	0.00
89.43	-1.75	-1.25	-0.75	-0.05	0.32
84.47	-1.28	-0.72	-0.33	0.33	0.66
69.56	-0.13	0.31	0.60	1.25	1.63
39.75	0.10	0.40	0.73	1.25	1.63
0.00 ¹²	-0.13	0.20	0.52	0.98	1.30

Qualitatively, it appears that perchloric, sulfuric, and hydrobromic acids are behaving similarly and that the activity coefficient behavior of the two indicators and their ions respond similarly to medium changes. In light of the recent work by Arnett and Mach¹⁷ and Robertson and Dunford,¹⁸ it appears that one can no longer attribute differences in acidity to hydration.¹⁹ An alternate explanation is that water is competing with the indicator for protons in the same manner in these three mineral acids. Although the acidity function in solvents of low dielectric constant is open to scrutiny, it still remains a valuable method for

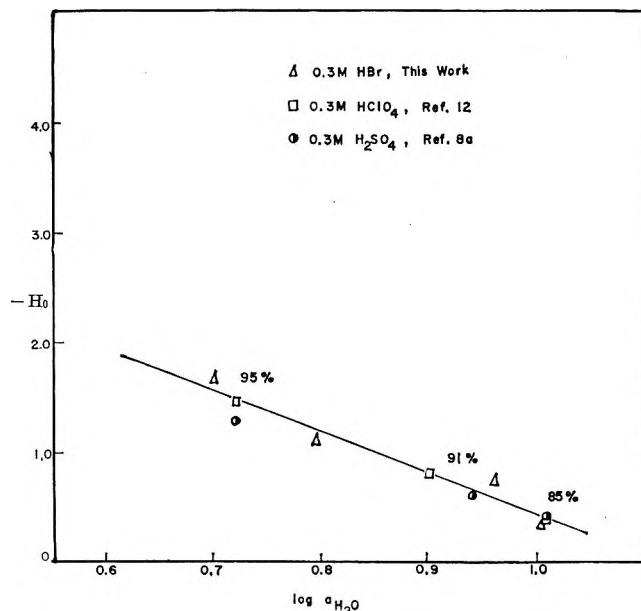


Figure 2. H_0 of 0.3 M HBr, HClO₄, and H₂SO₄ as a function of log activity of water. The values 95, 91, and 85% refer to percentages of HOAc.

evaluating the proton-donating ability of these solutions.

(16) R. P. Bell, "The Proton in Chemistry," Cornell University Press, Ithaca, N. Y., 1959, pp. 81-83.

(17) E. M. Arnett and G. W. Mach, *J. Am. Chem. Soc.*, **86**, 2671 (1964).

(18) E. B. Robertson and H. B. Dunford, *ibid.*, **86**, 5080 (1964).

(19) K. B. Wiberg, "Physical Organic Chemistry," John Wiley and Sons, Inc., New York, N. Y., 1964, pp. 298-302.

A Thermodynamic Study of the Ionization of 3-Amino-4-methylbenzenesulfonic Acid

by Paul J. Conn and D. F. Swinehart

Department of Chemistry, University of Oregon, Eugene, Oregon (Received February 23, 1965)

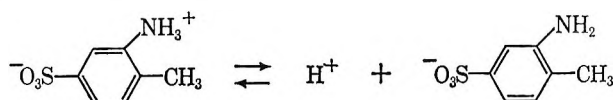
The ionization constant of 3-amino-4-methylbenzenesulfonic acid has been measured from 0 to 50° by use of cells without liquid junction. The equation $-\log K = 1435.05/T + 0.0037197T - 2.2893$ expresses the experimental data as a function of the temperature with a standard deviation of 0.00029 in $-\log K$ for 11 experimental points. The entropy of ionization is small and positive, +0.33 e.u. at 25°. Substitution of a methyl group *ortho* to the amino group in sulfanilic and metanilic acids causes a 28% increase in the ionization constant in each case.

Introduction

The present paper reports experimental results of the measurements of the electromotive forces of cells without liquid junctions which are designed to yield thermodynamic quantities relative to the ionization of 3-amino-4-methylbenzenesulfonic acid, represented by HMaps. Similar results have been reported from this laboratory for the isomer 4-amino-3-methylbenzenesulfonic acid,¹ and the three isomeric unsubstituted acids, sulfanilic,² metanilic,³ and orthanilic.⁴

Ostwald⁵ measured the ionization constant of HMaps by a conductivity method and found a value of 2.36×10^{-4} at 25°.

From the magnitude of the ionization constant and by analogy with the other acids, we assume that HMaps exists in solution as a zwitterion and that the ionization reaction is



The general method of investigation was that developed by Harned and co-workers.⁶ The cells were of the type Pt, H₂|HMaps (m_1°), NaMaps (m_2°), NaCl (m_3°)|AgCl-Ag. Here m_1° , m_2° , and m_3° are molalities. By eliminating $m_{\text{H}^+}\gamma_{\text{H}^+}$ between the cell potential equation

$$E = E^\circ - \frac{2.30259RT}{F} \log m_{\text{H}^+}m_{\text{Cl}^-}\gamma_{\text{H}^+}\gamma_{\text{Cl}^-} \quad (1)$$

and the expression for the thermodynamic ionization constant

$$K = \frac{m_{\text{H}^+}m_{\text{Maps}^-}\gamma_{\text{H}^+}\gamma_{\text{Maps}^-}}{m_{\text{HMaps}}\gamma_{\text{HMaps}}} \quad (2)$$

there results the relation

$$\frac{(E - E^\circ)F}{2.30259RT} + \log \frac{m_{\text{HMaps}}m_{\text{Cl}^-}}{m_{\text{Maps}^-}} = -\log K - \log \frac{\gamma_{\text{HMaps}}\gamma_{\text{Cl}^-}}{\gamma_{\text{Maps}^-}} \quad (3)$$

The magnitude of the ionization constant is such that an appreciable fraction of the acid is dissociated, even in buffered solution, and the molalities must be corrected for the dissociation

$$m_{\text{HMaps}} = m_1^\circ - m_{\text{H}^+}$$

$$m_{\text{Maps}^-} = m_2^\circ + m_{\text{H}^+}$$

(1) S. D. Morrett and D. F. Swinehart, *J. Phys. Chem.*, **67**, 717 (1963).

(2) R. O. MacLaren and D. F. Swinehart, *J. Am. Chem. Soc.*, **73**, 1822 (1951).

(3) R. D. McCoy and D. F. Swinehart, *ibid.*, **76**, 4708 (1954).

(4) R. N. Diebel and D. F. Swinehart, *J. Phys. Chem.*, **61**, 333 (1957).

(5) W. Z. Ostwald, *Z. physik. Chem.*, **3**, 411 (1889).

(6) H. S. Harned and B. B. Owen, "The Physical Chemistry of Electrolytic Solutions," 3rd Ed., Reinhold Publishing Corp., New York, N. Y., 1958.

where m°_1 and m°_2 are stoichiometric molalities obtained from the synthesis of the solutions.

Values of m_{H^+} were obtained from (1) using the Debye-Hückel limiting law for the activity coefficients. Since the ionic strength is a function of m_{H^+} , this calculation required successive approximations. Then, the left-hand side of (3) was plotted *vs.* the ionic strength and extrapolated to zero ionic strength by least squares yielding a first approximation for $-\log K$. Using this value of K , new values of m_{H^+} were calculated from (2) using successive approximations. Again, the left-hand side of (3) was extrapolated to zero ionic strength. A third complete approximation was required to yield values converged to 0.0001 in $-\log K$.

The calculations were so tedious that programs were written for an IBM 1620 computer to carry out all the necessary approximations.

The values of E° used were those of Harned and Ehlers⁷ and were recalculated by Swinehart.⁸

Experimental

Materials and reagents used were purified as described previously by MacLaren and Swinehart² except for the following particulars.

Eastman White Label 3-amino-4-methylbenzenesulfonic acid was recrystallized as the monohydrate in near-total darkness. The acid solutions were colorless under these conditions. Exposed to room lights, solutions turned red in 1 hr. The recrystallized acid was dried for 2 hr. at 110°, rendering the acid anhydrous. The anhydrous acid was stable toward light.

Individual batches of the acid were titrated by weight buret and a pH meter with NaOH solutions, freed of CO₂, and standardized *vs.* N.B.S. potassium acid phthalate and constant-boiling HCl. Extensively dried acid indicated a purity of 99.95%. Any appreciable impurities must be isomeric with HMaps.

The isomeric purity was not known to a high order of precision. The supplier estimated the purity at 97-98% from the method of synthesis and an undisclosed spectroscopic method. The bromination test, used by McCoy and Swinehart³ in establishing the amount of orthanilic and sulfanilic acids in metanilic acid, was insensitive to traces of 4-amino-3-methylbenzenesulfonic and 2-amino-6-methylbenzenesulfonic acids since addition of bromine water to concentrated solutions of HMaps turned solutions a dark red which masked the formation of the white methylbromoanilines from the *o*- and *p*-amino compounds. The visible and ultraviolet spectra of HMaps and its isomers were so nearly identical that they were of no help in estimating the purity of the acid.

Analar analytical grade sodium chloride was further purified by the method recommended by Meites.⁹ The sodium bromide content was estimated to be 0.003 mole % by the method of Bates and Pinching.¹⁰ The purified NaCl was fused in platinum before use.

The cells, electrodes, potentiometer, etc., were the same as described by MacLaren and Swinehart.² The solutions were made up in near-total darkness under hydrogen, and the cells were filled under hydrogen pressure. Measurements were made at 5° intervals from 0 to 50°.

After the cell solutions were prepared and the cells filled under hydrogen, the solutions seemed stable under artificial light.

Results

The data are shown in Table I. E.m.f. values for each cell in absolute volts corrected to 1 atm. hydrogen pressure are the averages of eight measurements from two hydrogen electrodes and four silver-silver chloride electrodes. In general, duplicate measurements in one cell agreed within a range of 0.02 mv., and none showed a range greater than 0.05 mv. Agreement between duplicate cells was poorer by a factor of 2 to 5.

The data were treated as indicated in the Introduction. Representative extrapolations of the left-hand side of eq. 3 to zero ionic strength yielding thermodynamic values of $-\log K$ are shown in Figure 1.

The resulting values of $-\log K$ were fitted to the equation

$$-\log K = A/T + CT - D \quad (4)$$

by least squares yielding the values 1435.05, 0.0037197, and 2.2893 for A , C , and D , respectively. Calculated values of $-\log K$ using these constants together with the experimental values of $-\log K$ and the value of K itself are shown in Table II. The standard deviation of the experimental from the calculated values of $-\log K$ were calculated from the relation

$$\sigma = \text{standard deviation} = \left(\frac{\sum \Delta^2}{n - c} \right)^{1/2}$$

where Δ is the deviation of the experimental point from the calculated curve in the direction of the $-\log K$ axis, n is the number of experimental points, and c is the number of constants in the equation.¹¹

(7) H. S. Harned and R. W. Ehlers, *J. Am. Chem. Soc.*, **55**, 2179 (1933).

(8) D. F. Swinehart, *ibid.*, **74**, 1100 (1952).

(9) L. Meites, *J. Chem. Educ.*, **29**, 74 (1952).

(10) R. G. Bates and G. D. Pinching, *J. Res. Natl. Bur. Std.*, **37**, 311 (1946).

(11) T. B. Crumpler and J. H. Yoe, "Chemical Computations and Errors," John Wiley and Sons, Inc., New York, N. Y., 1940, p. 222.

Table I: Electromotive Force^a of the Cell: Pt, H₂ | HMaps (*m*₁), NaMaps(*m*₂), NaCl(*m*₃) | Ag-AgCl

Approx. μ	0.01		0.011		0.022		0.045		0.059		0.083		0.10	
<i>m</i> ₁	0.004892		0.005251		0.011098		0.020728		0.029297		0.042058		0.050079	
<i>m</i> ₂	0.004963		0.005338		0.010784		0.024113		0.029527		0.041043		0.050486	
<i>m</i> ₃	0.004937		0.008380		0.010812		0.020747		0.029611		0.041048		0.050571	
<i>t</i> , °C.	Cell I	Cell II	Cell I	Cell II	Cell I	Cell II	Cell I	Cell II	Cell I	Cell II	Cell I	Cell II	Cell I	Cell II
0	0.57882	0.57865	0.57679	0.57697	0.55863	0.55855	0.54746	0.54745	0.53546	0.53545	0.52738	0.52738	0.52304	0.52332
5	0.57867	0.57851	0.57666	0.57685	0.55805	0.55798	0.54658	0.54658	0.53439	0.53438	0.52618	0.52617	0.52173	0.52200
10	0.57845	0.57829	0.57639	0.57660	0.55732	0.55726	0.54556	0.54549	0.53305	0.53305	0.52477	0.52477	0.52022	0.52048
15	0.57813	0.57794	0.57597	0.57618	0.55647	0.55639	0.54441	0.54435	0.53166	0.53166	0.52325	0.52324	0.51863	0.51890
20	0.57767	0.57746	0.57546	0.57567	0.55550	0.55543	0.54316	0.54310	0.53033	0.53031	0.52163	0.52162	0.51695	0.51721
25	0.57722	0.57700	0.57480	0.57504	0.55436	0.55428	0.54178	0.54172	0.52875	0.52872	0.51988	0.51986	0.51515	0.51544
30	0.57659	0.57632	0.57416	0.57439	0.55335	0.55317	0.54034	0.54025	0.52702	0.52699	0.51802	0.51800	0.51312	0.51339
35	0.57591	0.57565	0.57334	0.57358	0.55205	0.55192	0.53867	0.53859	0.52516	0.52514	0.51603	0.51603	0.51113	0.51137
40	0.57508	0.57483	0.57259	0.57277	0.55070	0.55057	0.53692	0.53684	0.52322	0.52318	0.51394	0.51389	0.50895	0.50920
45	0.57418	0.57396	0.57167	0.57184	0.54924	0.54911	0.53512	0.53503	0.52122	0.52118	0.51171	0.51165	0.50665	0.50689
50	0.57339	0.57315	0.57064	0.57088	0.54772	0.54758	0.53326	0.53313	0.51904	0.51908	0.50938	0.50931	0.50425	0.50448

^a Absolute volts.

Table II: The Ionization Constant of 3-Amino-4-methylbenzenesulfonic Acid from 0 to 50°

<i>t</i> , °C.	<i>K</i> × 10 ⁴	-Log <i>K</i> (obsd.)	-Log <i>K</i> (calcd.)	Δ × 10 ⁴
0	1.046	3.9802	3.9802	0
5	1.246	3.9043	3.9044	-1
10	1.473	3.8321	3.8319	+2
15	1.728	3.7626	3.7626	0
20	2.013	3.6961	3.6962	-1
25	2.330	3.6323	3.6327	-4
30	2.679	3.5725	3.5720	+5
35	3.063	3.5137	3.5138	-1
40	3.483	3.4581	3.4580	+1
45	3.939	3.4042	3.4046	-4
50	4.432	3.3536	3.3534	+2

Average $\Delta = 2.0 \times 10^{-4}$
 $\sigma = 2.9 \times 10^{-4}$

Discussion

Since programs for the IBM 1620 computer were available, the data from all the previously investigated aminobenzenesulfonic acids¹⁻⁴ were recomputed revealing a few errors in the previous calculations. Shown in Table III is a summary of new values of the constants from eq. 4 for the several cases.

It will be noted that the largest changes occur for sulfanilic acid. The original treatment of this acid only did not use a straight-line extrapolation of the left-hand side of eq. 3 to zero ionic strength. Using a straight-line extrapolation revealed no greater scatter of the experimental points from the line than is true in general for the other acids.

Values of the thermodynamic functions ΔG° , ΔH° , ΔS° , and ΔC_p° for the ionization reactions were calculated from the constants of eq. 4. These values at 25° are shown in Table III. In particular, it should

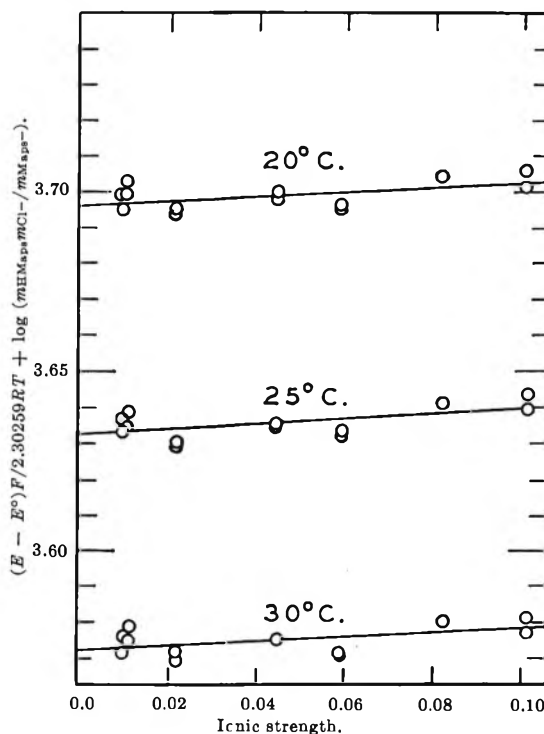


Figure 1.

be noted that some of the values for metanilic acid previously published¹ showed an arithmetical error.

The entropy changes are reported to the nearest 0.01 e.u. An uncertainty of this magnitude represents more than 1% of the value reported in each case. The magnitude of the changes of the e.r.f. over the temperature range and their uncertainties indicate that the slope, dE/dT , has an uncertainty of about 1%.

However, it merits attention that the absolute values reported depend on the assumption of eq. 4 used in fitting the data. Other equations are known to fit the

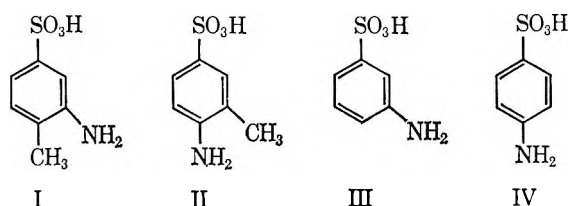
Table III: Comparison of $-\log K$ and Thermodynamic Values for the Dissociation of Aminobenzenesulfonic Acids at 25°^a

Acid	A, deg.	10°C, deg. ⁻¹	D	$-\log K$	ΔG° , cal.	ΔH° , cal.	ΔS° , cal./deg.	ΔC_p° , cal./deg.
Orthanilic	1137.18	6.9543	3.4295	2.4580	3353	2374	-3.28	-19
Metanilic	1306.16	2.5660	1.4074	3.7384	5100	4933	-0.56	-7
Sulfanilic	1075.86	1.6483	0.8682	3.2316	4409	4252	-0.52	-4
3-Amino-4-toluenesulfonic acid (HMAs)	1435.05	3.7197	2.2893	3.6327	4956	5053	+0.33	-10
4-Amino-3-toluenesulfonic acid (HATs)	1361.41	4.2672	2.7144	3.1239	4262	4494	+0.78	-12

^a All results in this table were recalculated from the original data using an IBM 1620 computer.

data as well.⁶ Another equation might yield somewhat different values. Probably ΔC_p° is uncertain to at least 10% from internal consistency and perhaps by a larger amount in absolute value.

3-Amino-4-methyl- (I) and 4-amino-3-methyl- (II) benzenesulfonic acids are structurally similar to metanilic (III) and sulfanilic (IV) acids, respectively, since in both cases a methyl group was substituted for a hydrogen *ortho* to the amino group.



Laidler, *et al.*,¹² have shown from data on ionization constants from the literature¹³ that for anilinium ion dissociation a methyl substituted *ortho* to the amino group caused a decrease in ΔG° and that this change in ΔG° for various methyl-substituted anilines was constant. A similar situation is present in the case of the aminobenzenesulfonic acids since at 25°

$$\Delta G^\circ(\text{I}) - \Delta G^\circ(\text{III}) = -144 \text{ cal./mole}$$

and

$$\Delta G^\circ(\text{II}) - \Delta G^\circ(\text{IV}) = -147 \text{ cal./mole}$$

This constancy of differences in ΔG° predicts that

$$\frac{K(\text{I})}{K(\text{III})} = \frac{K(\text{II})}{K(\text{IV})}$$

These ratios are both equal to 1.278 within less than 0.3%; *i.e.*, adding a methyl group *ortho* to the amino group increases the ionization constant by 28% in both cases.

The entropies and enthalpies are not additive, however, since at 25°

$$\Delta S^\circ(\text{II}) - \Delta S^\circ(\text{IV}) = 1.30 \text{ e.u.}$$

$$\Delta S^\circ(\text{I}) - \Delta S^\circ(\text{III}) = 0.89 \text{ e.u.}$$

$$\Delta H^\circ(\text{II}) - \Delta H^\circ(\text{IV}) = 243 \text{ cal./mole}$$

$$\Delta H^\circ(\text{I}) - \Delta H^\circ(\text{III}) = 120 \text{ cal./mole}$$

The entropy of ionization of HMAs is quite small as is the entropy of ionization for each of the other acids. It is, in fact, positive at 25° and so is that of its isomer 4-amino-3-methylbenzenesulfonic acid. The entropy of HMAs decreases with increasing temperature, being +1.18 e.u. at 0° and -0.53 e.u. at 50°. These values correspond to the zwitterion form of the acid with a large dipole moment. Presumably, the zwitterion binds or "freezes" enough water molecules relative to those "frozen" by the separated ions so that the entropy change due to ordering of water molecules cancels the entropy increase due to creation of two particles on ionization.^{1,14,15}

Millero,¹⁶ *et al.*, have reported entropies of ionization of some pyridinemono-carboxylic acids. They find values in the range -12 to -16 e.u. It is known that the entropy of ionization of benzoic acid¹⁷ is -18.9 e.u., and similar values have been reported for a wide variety of other neutral nonzwitterionic acids⁴ which are approximately constant and average about -20 e.u. It would be reasonable to suppose that, if the pyridinemono-carboxylic acids were zwitterions, their entropies of ionization should be of the order of zero, comparable to those of the aminobenzenesulfonic acids, since both types must have a large dipole moment owing to a large charge separation. It is true

(12) T. W. Zawidzki, H. M. Papeé, W. J. Canady, and K. J. Laidler, *Trans. Faraday Soc.*, **55**, 1738 (1959).

(13) H. C. Brown, D. H. McDaniel, and O. Häfziger, "Determination of Organic Structures by Physical Methods," E. A. Braude and F. C. Nachod, Ed., Academic Press Inc., New York, N. Y., 1955, Chapter 14; F. Kieffer and P. Rumpf, *Compt. rend.*, **230**, 2304 (1950); M. Gillois and P. Rumpf, *Bull. Soc. Chim. France*, **112**, (1954); C. Golumbic and G. Goldbach, *J. Am. Chem. Soc.*, **73**, 3966 (1951).

(14) H. S. Frank and M. W. Evans, *J. Chem. Phys.*, **13**, 507 (1945).

(15) R. E. Powell and W. M. Latimer, *ibid.*, **19**, 1139 (1951).

(16) F. J. Millero, J. C. Ahluwalia, and L. G. Hepler, *J. Phys. Chem.*, **68**, 3435 (1964).

(17) L. P. Fernandez and L. G. Hepler, *ibid.*, **63**, 110 (1959).

that the amino acids are zwitterions and that glycine⁶ has an entropy of ionization of -8.9 e.u., but these acids must have much smaller dipole moments owing to smaller charge separations than the above classes

of acids. Thus, it appears probable that the pyridine-carboxylic acids exist in solutions principally in non-zwitterionic form, contrary to the conclusion of Millero, *et al.*

Thermal Properties of Atactic and Isotactic Polystyrene

by F. E. Karasz, H. E. Bair, and J. M. O'Reilly

General Electric Research Laboratory, Schenectady, New York (Received February 23, 1965)

The heat capacities of atactic polystyrene and of amorphous and partially crystalline isotactic polystyrene have been measured from 300 to 520°K. and, in the case of the atactic sample, in the low-temperature region also. The results show that molecular configuration in itself has only a minor effect on bulk thermodynamic properties, and that the partially crystalline material obeys a two-phase additive model reasonably well. Residual entropies and enthalpies for the amorphous polymer were calculated as a function of temperature and related to current theories of glass formation.

I. Introduction

A fundamental approach to the understanding of the solid state of polymers is through measurements of their heat capacity. Polymers present unusual opportunities in this respect, because in many cases they can be prepared with widely differing degrees of crystallinity, ranging from an amorphous to a highly ordered state. Many of the types of information that can thus be obtained from heat capacity measurements over a wide temperature range have been discussed by Dole.¹

Polystyrene is one of the oldest and most important synthetic polymers. Until recently it was invariably produced in the atactic form, but currently crystallizable isotactic material has been synthesized,² and thus the effect of changes in both molecular configuration and crystallinity on thermal properties may be investigated. Such comparative studies, still relatively rare, have usually revealed that the former factor can have an appreciable effect upon these properties.^{3,4}

One of the continuing problems of all types of

precision polymer measurements is the uncertainty of comparisons in which polymer samples are not completely characterized. Therefore, the fact that atactic polystyrene may now be obtained as a standard sample with known properties from the National Bureau of Standards has added impetus to our study. A further point has been a desire to resolve some discrepancies which are apparent in previous work, particularly in regard to secondary transitions, that is those other than the glass and melting transitions.

Finally, by making measurements of heat capacities over a range which extends from close to absolute zero into the liquid state, it becomes possible to calculate accurately the thermodynamic quantities, entropy and enthalpy, necessary to describe the polymerization equilibria.

(1) M. Dole, *Fortschr. Hochpolymer. Forsch.*, **2**, 221 (1960).

(2) G. Natta, P. Corradini, and I. W. Bassi, *Nuovo Cimento, Suppl.* **1**, 15, 68 (1960).

(3) J. M. O'Reilly, F. E. Karasz, and H. E. Bair, *Bull. Am. Phys. Soc.*, **9**, 285 (1964).

(4) E. Passaglia and H. K. Kevorkian, *J. Appl. Phys.*, **34**, 90 (1963).

Although no single precision measurement has been reported which encompasses both the low-temperature and the liquid-state regions, several authors have determined heat capacities of atactic polystyrene in some part of this range.^{5,6} Unfortunately, other properties of the sample were generally not reported. In addition, Ueberreiter and Otto-Laupenmühlen⁷ have investigated the effect of molecular weight upon the thermal properties. Their fractions extended only up to a molecular weight of 3650, and it is clear from the data that this is not yet in the region where the properties become independent of this parameter. More recently, Dainton, *et al.*,⁸ have made precision low-temperature determinations using a crystalline isotactic polystyrene sample; their investigation did not include the glass or melting transition regions. Finally, after the experimental part of this work had been completed, we learned that Dole and Abu-Isa had made measurements using both atactic and isotactic polystyrene samples between 230 and 550°K.⁹ The relation of these results to our measurements is discussed below.

II. Experimental

A. *Samples.* (i) *Atactic.* The standard N.B.S. broad molecular weight distribution polystyrene sample (N.B.S. No. 706) was used in the atactic series measurement. This has $\bar{M}_w = 2.58 \times 10^5$ (from light scattering) and $\bar{M}_n = 1.36 \times 10^5$ (osmotic pressure). The material was purchased in the form of pellets about 3 mm. in diameter and apart from a vacuum drying treatment (80° for 24 hr.) was used as received. Negligible weight loss was observed during the drying.

(ii) *Isotactic.* An isotactic polystyrene sample was obtained through the courtesy of the Monsanto Co. (sample designation no. 6811). This was stated to be highly tactic with less than 2% solubility in boiling methyl ethyl ketone. The material was received as a crystalline white powder and was not further extracted. As one of the objects of our experiments was to determine the properties of amorphous isotactic polystyrene, a quantity of the powder was molded into sheets about 1.5 mm. thick and quenched from the melt in ice water. (It has previously been determined that the known cooling rates attainable *in situ* in the calorimeter sample container could not produce a totally amorphous sample.) The quenched optically clear sheets were then dried at 70° *in vacuo*, and were broken into small irregularly shaped pieces about 0.5 cm. across for use in the measurements. Viscosity determinations in *o*-dichlorobenzene, using the data of Krigbaum, Carpenter, and Newman,¹⁰ showed that the molecular weight after this treatment

had fallen from 2.2×10^5 to 4.2×10^5 . The fact that this specimen was completely amorphous was established by X-ray and differential scanning calorimeter (Perkin-Elmer DSC-1) measurements, and was verified *a posteriori* from the heat capacity determinations (see below).

For both samples there was some concern regarding the possibility of degradation during measurements, as a result of relatively long residence times at high temperatures. A small quantity of each was therefore heated prior to use in a sealed tube (under helium) and the rate of gas evolution as a function of temperature was determined. From these data, we were able to estimate maximum temperature and residence time combinations which could be employed. The viscosity of both samples after the calorimetric runs was also measured, and confirmed the absence of any further degradation.

B. *Calorimetric.* The calorimetric apparatus was a wide temperature range modification of conventional adiabatic design and will be described elsewhere.¹¹ A modification to the external refrigerant bath since our earlier work¹² permitted the use of liquid hydrogen, and thus extended the useful temperature range down to about 17°K.

The samples, sealed under a few centimeters pressure of helium, were typically heated at between 1 and 15 deg. hr.⁻¹. An intermittent heating technique was used, with intervals ranging from 2 to about 10°. Equilibration times were normally about 20 min., but increased sharply in the vicinity of transitions. The weights of the atactic and isotactic polystyrene samples used were 30.613 and 38.507 g., respectively.

The precision of the apparatus had previously been assessed by a determination of the heat capacity of a standard sample of alumina.¹¹ For the present measurements, we estimate our errors in the heat capacity to average $\pm 0.2\%$ up to about 400°K., with a possible rise to $\pm 0.4\%$ at the highest temperatures used.

(5) F. G. Brickwedde, referred to in "Styrene," R. H. Boundy and R. F. Boyer, Ed., Reinhold Publishing Corp., New York, N. Y., 1952.

(6) I. V. Sochava, *Vestn. Leningr. Univ., Ser. Fiz. i Khim.*, **16**, No. 10, 70 (1961).

(7) K. Ueberreiter and E. Otto-Laupenmühlen, *Z. Naturforsch.*, **8a**, 664 (1953).

(8) F. S. Dainton, D. M. Evans, F. E. Hoare, and T. P. Melia, *Polymer*, **3**, 286 (1962).

(9) I. Abu-Isa and M. Dole, *J. Phys. Chem.*, **69**, 2668 (1965); we thank Prof. Dole for his courtesy in sending us his data prior to publication.

(10) W. R. Krigbaum, D. K. Carpenter, and S. Newman, *ibid.*, **62**, 1586 (1958).

(11) F. E. Karasz and J. M. O'Reilly, to be published.

(12) J. M. O'Reilly, F. E. Karasz, and H. E. Bair, *J. Polymer Sci.*, **C6**, 109 (1964).

C. *Other Properties.* The X-ray diffraction patterns and the densities of several samples with varying thermal histories were also determined.

Diffractions were obtained, in reflection, with a General Electric XRD-5 diffractometer using Ni filter radiation, from molded samples, 0.75–1.5 mm. thick. Air scattering was measured and used to correct the observed traces. In the notation of Hermans and Weidinger,¹³ the value of O_A^*/h_{20}^* was found to be 7.2 (1 cm. = 2°; $h_{20}^* = 3.5$ cm.). Densities were determined by hydrostatic weighing in water and silicone oil at 25°.

In addition, the heats of fusion, ΔQ_t , of the crystalline samples were measured with the Perkin-Elmer differential scanning calorimeter, Model DSC-1, using a heating rate of 40 deg. min.⁻¹.

III. Results

A. *Atactic Polystyrene.* Two series of measurements were made. In the first, the heat capacities of the dried pellets were determined from about 85 to 480°K. The sample was then cooled to 290°K. at about 10 deg. hr.⁻¹ and the measurements were repeated, up to 380°K. The heat capacities for the two series are recorded in Table I, and the over-all results are shown in Figure 1. Specific features are discussed below.

(i) *Glass Temperatures.* Both series of measurements extended through the glass transition region. In the first, the most conspicuous feature is the sharp peak at 367°K. Such a peak is a consequence of previous thermal treatment; it can be generated if the heating rate through the T_g region is greater than the cooling rate.¹⁴ This implies that in practice such peaks will be observed more frequently in d.t.a. or similar rapid heating type of measurements; however, we have on previous occasions also observed maxima of this type in calorimetric determinations with heating rates of only 4–10 deg. hr.⁻¹.³ In this instance it is clear that the drying treatment at 80°, because of its proximity to the glass temperature, created the conditions necessary for the observation of this peak. Thus the second series of measurements through the T_g region using the same sample, but with a different thermal history, delineates more customary behavior, with the glass transition indicated by a straightforward discontinuity in heat capacity ($\Delta C_p = 0.296$ joule deg.⁻¹ g.⁻¹).

It should be pointed out that these variations are due to the fact that the different effective cooling rates through the transition region permitted the glass to attain correspondingly different residual enthalpies.¹⁵ Under these conditions, the observed heat

Table I: Atactic Polystyrene

As received		Annealed	
T_{av}	C_p , joules °K. ⁻¹ g. ⁻¹	T_{av}	C_p , joules °K. ⁻¹ g. ⁻¹
89.431	0.424	293.004	1.185
97.553	0.450	298.087	1.219
104.342	0.469	303.804	1.244
111.921	0.497	309.324	1.268
121.294	0.527	314.698	1.292
131.902	0.567	330.050	1.369
144.529	0.604	346.754	1.429
156.823	0.651	354.178	1.471
167.492	0.691	360.133	1.520
176.628	0.721	364.592	1.629
186.059	0.760	367.985	1.821
198.687	0.807	371.148	1.849
210.230	0.853	374.612	1.843
220.300	0.895	378.610	1.859
230.404	0.942		
240.177	0.984		
250.509	1.017		
259.927	1.056		
268.960	1.096		
279.356	1.140		
289.625	1.185		
299.674	1.233		
309.857	1.291		
320.054	1.321		
327.798	1.356		
336.490	1.397		
344.794	1.433		
350.812	1.463		
355.664	1.528		
360.705	1.673		
364.753	1.852		
367.500	1.988		
370.207	1.869		
372.729	1.819		
376.041	1.836		
381.041	1.842		
386.673	1.836		
393.649	1.898		
402.984	1.931		
413.432	1.961		
422.085	1.990		
430.911	2.035		
444.340	2.072		
459.136	2.114		
474.137	2.158		

capacities, when the samples were subsequently heated, were characteristic of the precise heating regime used, and the relaxation time spectrum associated with this

(13) G. Challa, P. H. Hermans, and A. Weidinger, *Makromol. Chem.*, **56**, 169 (1962).

(14) Y. A. Sharonov and M. V. Volkenstein, *Fiz. Tverd. Tela*, **5**, 590 (1963).

(15) A. J. Kovacs, *Fortschr. Hochpolymer. Forsch.*, **3**, 394 (1963).

regime. In the intermittent heating type of experiment (as used here), the situation is further complicated by the fact that though the heating rates in the two series of measurements were nominally the same, the effective heating rate largely depended on the precise temperature at which each run was terminated and the residence time at that temperature.

The glass transition temperature in this work is defined as the temperature corresponding to the midpoint of the discontinuity in C_p . Alternatively, one may construct enthalpy-temperature curves representing the glass and liquid states and determine the intersection of the extrapolated curves. In the case of a symmetrical C_p vs. T curve, as was that observed for the annealed sample, these definitions are equivalent. The latter procedure is of course thermodynamically analogous to the method often adopted in dilatometric measurements for finding glass temperatures.

We find T_g for the annealed sample to be $362 \pm 1^\circ\text{K}$. This value is somewhat lower than might be expected from earlier reported dilatometric measurements. However, there is clearly some dispersion in reported values. Fox and Flory,¹⁶ using polystyrene fractions, report an extrapolated value for T_g of 373°K . for an infinite molecular weight sample which would be equivalent to a T_g of 372°K . for a sample with our \bar{M}_n ; Beevers¹⁷ found 368.4°K . using a sample with $\bar{M}_n = 7 \times 10^4$ and $\bar{M}_w/\bar{M}_n = 3.0$, while Kovacs^{18,19} has reported values ranging from 360 to 368°K ., depending again on the sample. From Dole's data⁹ we calculate a value of 365°K . if T_g is defined in the manner described above.

It is probable also that the glass transition temperature of our sample is depressed by a few degrees by the 0.8% volatile material stated by the National Bureau of Standards to be present (and apparently not removed by the drying procedure), and differences in heating rates can account for a further variation of 2 or 3°.

(ii) *Liquid*. The heat capacity of the atactic polystyrene above the glass temperature increased linearly with temperature as has been observed with all other polymers.¹ Our values can again be compared with those of Brickwedde⁵ (though these extend only to 400°K .), Dole,⁹ and Ueberreiter.⁷ The latter values have to be extrapolated to essentially infinite molecular weight and this inevitably creates some uncertainties, but even after taking this point into account there are considerable differences between the various measurements. Slightly above T_g , at 380°K ., our results and those of Brickwedde and Ueberreiter agree to within about 0.3%, while Dole's values fall some 2% lower. However, much greater discrepancies

appear in the observed slopes, $dC_p(\text{liquid})/dT$. These are, respectively, 2.5×10^{-3} , 3.4×10^{-3} , 4.7×10^{-3} , and 3.2×10^{-3} , joule deg.⁻² g.⁻¹ for Dole's, Ueberreiter's, Brickwedde's, and the present measurements. It seems improbable, however, that sample differences could account for such a large disagreement and the reason for the divergence remains uncertain. We feel that some indirect support for our value lies in the fact that a linear extrapolation performed on this basis gives excellent agreement with the heat capacity of liquid isotactic polystyrene above 510°K .

(iii) *50° Transition*. A number of mechanical, n.m.r., and other measurements show evidence for a second transition in atactic polystyrene below T_g , centered around 50° .²⁰ This has been interpreted as being due to a freezing-in of the torsional vibrations of the phenyl substituents. Secondary transitions have been observed in a large number of polymers but have not usually been detected by heat capacity measurements. However, Wunderlich and Bodily have recently observed such a transition in atactic polystyrene using high speed d.t.a. measurements (~ 360 deg. hr.⁻¹),²⁰ and Martin and Müller²¹ similarly have reported a broader, less pronounced maximum in runs made at somewhat slower heating rates, 18–36 deg. hr.⁻¹. It was of considerable interest, therefore, to see whether this transition could be detected in the present equilibrium calorimetric studies.

Two runs between 295 and 365°K . were made using the atactic samples with the thermal histories described above. In neither case did we observe any irregularity around 320°K . which could be definitely associated with the reported transition. In the first run one experimental point at 309°K . lay approximately 0.8% above a line joining the remainder (whose average deviation from this line was less than 0.1%), but the second series of measurements failed to confirm this behavior, with all the points falling within about 0.1% of a linear plot.

It is felt, therefore, that as in other systems, equilibrium measurements carried out at relatively low heating rates do not reveal the existence of any dispersion which might be attributable to changes in internal motion.

(iv) *Low Temperature Measurements*. The heat

(16) T. G. Fox and P. J. Flory, *J. Appl. Phys.*, **21**, 581 (1950); *J. Polymer Sci.*, **14**, 315 (1954).

(17) R. B. Beevers, *Trans. Faraday Soc.*, **58**, 1465 (1962).

(18) A. J. Kovacs, *J. Polymer Sci.*, **30**, 131 (1958).

(19) G. Braun and A. J. Kovacs, *Phys. Chem. Glasses*, **4**, 152 (1963).

(20) B. Wunderlich and D. M. Bodily, *J. Appl. Phys.*, **35**, 103 (1964).

(21) H. Martin and F. H. Müller, *Makromol. Chem.*, **75**, 75 (1964).

capacity of the annealed atactic polystyrene was also measured in the range 17 to 80°K. These results will be reported elsewhere.

B. Isotactic Polystyrene. Two series of measurements using the isotactic sample with differing thermal histories were carried out. In the first, the heat capacity of a quenched sample, prepared in the manner previously described, was determined in the range 299 to 524°K. In the second series, C_p of the same sample,

Table II: Isotactic Polystyrene

Amorphous		Annealed	
T_{av}	C_p , joules $^{\circ}\text{K.}^{-1} \text{g.}^{-1}$	T_{av}	C_p , joules $^{\circ}\text{K.}^{-1} \text{g.}^{-1}$
301.911	1.241	304.961	1.251
307.190	1.265	319.047	1.314
312.832	1.291	323.538	1.327
319.651	1.318	330.794	1.369
325.728	1.346	339.396	1.407
332.672	1.384	346.868	1.448
339.272	1.415	352.763	1.487
344.961	1.444	358.168	1.606
350.557	1.493	362.824	1.662
356.318	1.575	367.430	1.702
360.781	1.696	371.820	1.722
364.172	1.807	376.006	1.742
367.677	1.835	381.256	1.762
373.930	1.851	387.749	1.790
383.089	1.883	396.215	1.826
392.887	1.888	403.618	1.842
403.883	1.882	411.150	1.890
414.826	1.796	418.873	1.920
425.205	1.755	426.799	1.967
436.993	1.546	434.166	1.993
449.635	1.563	441.578	2.056
463.059	1.965	450.918	2.081
475.005	1.981	461.135	2.181
482.335	2.076	471.530	2.184
490.236	2.559	478.503	2.162
497.072	3.254	484.224	2.231
500.268	3.988	490.279	2.487
503.498	5.032	495.270	3.066
507.818	4.604	499.273	3.547
512.903	2.290	502.337	4.848
516.947	2.305	505.082	3.962
521.352	2.323	508.383	3.129
		512.194	2.291
		517.829	2.300
		525.850	2.335

this time slowly cooled (~ 15 deg. hr. $^{-1}$) from the melt to 450°K. and annealed for 24 hr. before further cooling to room temperature, was measured. In the lower part of this temperature range the results were found to be in agreement to better than 0.2% with the values obtained by Dainton⁸ and hence no low temperature determinations were made. The calculated

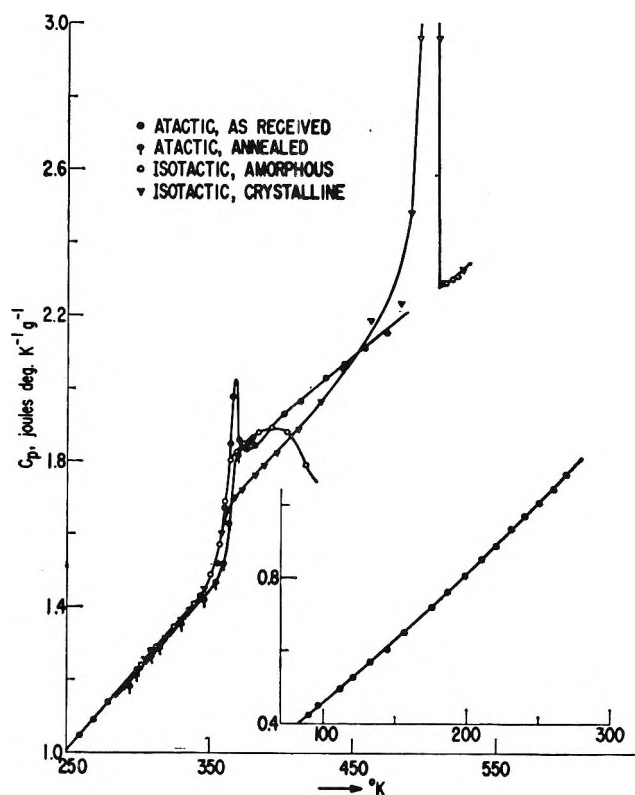


Figure 1. Heat capacity of atactic and isotactic polystyrene.

heat capacities are recorded in Table II and are also plotted as a function of temperature in Figure 1.

(i) *Amorphous Isotactic Polystyrene.* The heat capacity of this material below the glass temperature was some 0.006 joule deg. $^{-1}$ g. $^{-1}$ ($\sim 0.5\%$) greater than the heat capacity of the annealed atactic sample. At about 335°K. this difference started to increase (Figure 2), but still remained somewhat less than 3% up to 355°K.

The center of the glass transition occurs at $360 \pm 2^{\circ}\text{K.}$, while ΔC_p is 0.304 joule deg. $^{-1}$ g. $^{-1}$. These values are practically identical with those found for the annealed atactic polystyrene. At temperatures above T_g , starting at about 380°K., the quenched sample began to crystallize. This was detected by an upward temperature drift in the calorimeter during equilibration periods, and by a depression in the calculated values of C_p in this temperature region. The numerical values, therefore, between 390 and 480°K. are arbitrary in the sense that they depend on the particular time scale in which the data were obtained. Over a period of 24 hr., extensive crystallization occurred, and it is estimated that about 33 joules g. $^{-1}$ was subsequently needed to melt this sample.

The maximum melting point of the material produced in the calorimeter by this heat treatment is 510

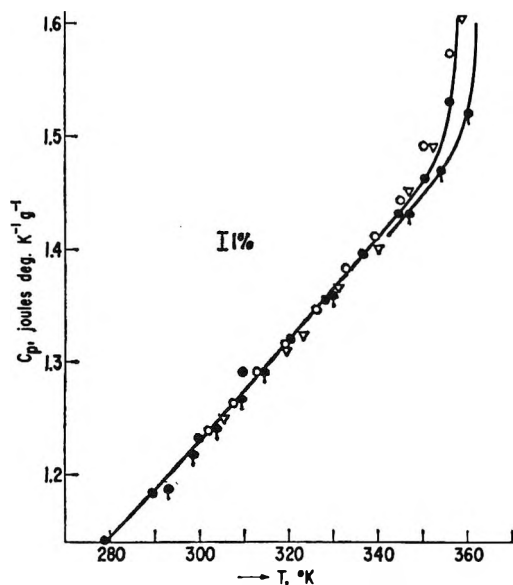


Figure 2. Heat capacity of atactic and isotactic polystyrene below T_g . For key to symbols, see Figure 1.

$\pm 1^\circ\text{K}$. From Figure 1 we note that the heat capacity of this sample, just before crystallization started, is in good agreement with the heat capacity of the atactic material at the same temperature. Furthermore, C_p in this temperature region lies on the line produced by a linear downward extrapolation of C_p of the liquid isotactic polystyrene. These points confirm the initial absence of crystallinity in this sample.

(ii) *Annealed Isotactic Polystyrene*. The molten isotactic sample was cooled as described resulting in the development of considerable crystallinity, and the heat capacity was again determined. It was found that below the glass transition temperature C_p was only marginally lower than that of the amorphous sample. The average difference was about 0.004 joule deg.^{-1} g.^{-1} or 0.3% .

The shape of the heat capacity curve in the T_g region was also very similar to that observed previously, except that ΔC_p was substantially lower, as is to be expected of a partially crystalline polymer, amounting to 0.168 joule deg.^{-1} g.^{-1} . Thus the glass temperature, if it is defined in the manner described in section III.A.(i), is $355 \pm 2^\circ\text{K}$., slightly below that of the amorphous sample. No irregularities in the thermal behavior were encountered above T_g . The heat capacity curve started to turn upward at about 400°K . and a typical polymer melting peak was observed. The maximum melting point was again 510°K . This value is in good agreement with dilatometric data^{10,22,23} and with that observed by Dole,⁹ though it may be noted that, as in the atactic samples, the

latter's heat capacities are consistently lower than ours. This difference amounts to 7% at 520°K .

The area of the melting peak, corresponding to the experimental heat of fusion, ΔQ_f , is 31.4 ± 1.3 joules g.^{-1} . To calculate this quantity it is necessary first to establish the base line which represents the real heat capacity of the quasi-equilibrium mixture of amorphous and crystalline polymer in the melting region. In the present case the following procedure was adopted. It was first assumed that the observed heat capacity curve linearly extrapolated from below T_g to T_m represented the heat capacity of the (hypothetical) totally crystalline polystyrene between these temperatures (see Figure 3). The resultant crystal-

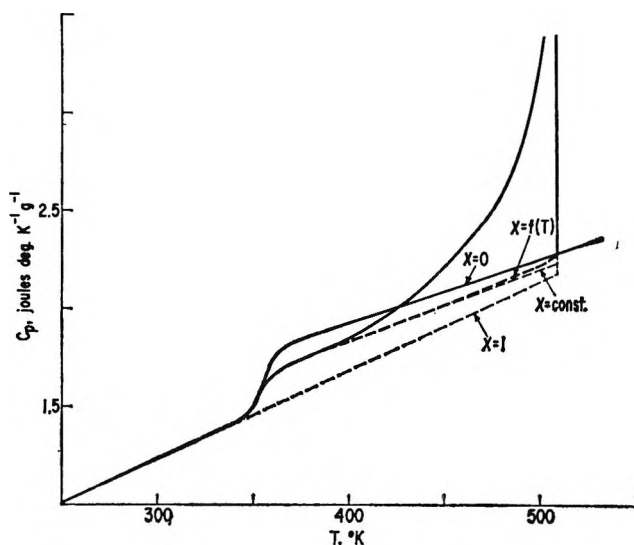


Figure 3. Schematic diagram illustrating the method of obtaining the base line for ΔQ calculation. Continuous lines represent experimental results for amorphous and partially crystalline samples. Heavy dashed line indicates final base line used. For other dashed lines, see text.

liquid discontinuity in C_p at T_m was then divided in the same ratio as was that experimentally observed for the partially crystalline material at T_g . The straight line joining this point of division asymptotically to the semicrystalline curve just above T_g would then constitute the base line if it were assumed that the degree of crystallinity, x , remained constant up to T_m . This, of course, is not the case, and one may make a further minor correction to obtain the true base line by a series of successive approximations, using the fact that

(22) G. Natta, F. Danusso, and G. Moraglio, *Makromol. Chem.*, **28**, 166 (1958).

(23) R. Dedeurwaerder and J. F. M. Oth, *J. chim. phys.*, **56**, 940 (1959).

$x \rightarrow 0$ at T_m . In practice, it is necessary to go through an iteration process only once to define adequately the corrected line, denoted as $x = f(T)$ in Figure 3.

The heat of fusion, ΔQ_f , was then found by summing $\Delta C_p \cdot \Delta T$ increments up to T_m . The quantity ΔC_p is the observed excess heat capacity referred to the base line at the average temperature of the measurement interval ΔT .

This procedure is equivalent to assuming ideal (*i.e.*, additive) two-phase behavior for the amorphous and crystalline components in the sample. As is shown below, for polystyrene this appears to be justifiable. It will also be observed that the shape of the heat capacity curve is such that the first noticeable departure from the base line is about 120° below the maximum melting temperature. Given the assumptions indicated, this point is unambiguously defined.

The heat of fusion of completely crystalline polystyrene, ΔH_f , has been found by Dedeurwaerder and Oth²³ to be 80.3 joules g.⁻¹, in reasonable agreement with a value of 86.3 joules g.⁻¹ reported by Danusso and Moraglio.²⁴ Using the former result we calculate x to be 0.39 for the annealed sample. This is of the same order of magnitude as has been quoted as a representative degree of crystallinity for isotactic polystyrene in other studies,^{8,25} though of course such values depend not only on the thermal history of the material but also on the nature of its synthesis and the method by which the crystallinity had been determined.

A more significant comparison is one in which the internal consistency of this result is checked. As has been pointed out elsewhere,²⁶ in principle, x can be determined not only from ΔQ_f but also from any other thermal property which is significantly crystallinity dependent. We have been particularly interested in comparing ΔC_p (at T_g) for a number of polymers, of varying crystallinities, with the values predicted on the basis of a linearly additive two-phase model. If this model were to be applicable, then

$$x = \frac{\Delta Q_f}{\Delta H_f} = 1 - \frac{\Delta C_p^{\text{obsd}}}{\Delta C_p^{\text{a}}} \quad (1)$$

where ΔC_p^{obsd} refers to the observed quantity for a given crystalline sample with a heat of fusion, ΔQ_f , and ΔC_p^{a} that of a wholly amorphous sample.

In this work, we find $1 - [\Delta C_p^{\text{obsd}}/\Delta C_p^{\text{a}}]$ to be 0.45. While this is somewhat greater than x obtained from the heat of fusion, it should be emphasized that in this respect isotactic polystyrene is a system which adheres much more closely to the two-phase model than any other polymer that has been observed to date.²⁶

C. Other Results. It is informative to compare crystallinities of isotactic polystyrene calculated from different types of physical measurements. Although it was not possible to make these measurements on the crystalline sample discussed above, because the latter was formed in the calorimeter, an approximately equivalent sample (A in Table III) was produced by annealing specimens, mclcd from the original powder, to develop maximum crystallinity. A sample (B) of intermediate crystallinity was also produced, and in addition the quenched material was available. These samples, as well as the atactic material, were then studied by differential scanning calorimetry, X-ray diffraction, and density measurements.

Table III

	X-Ray x	—Density at 25°—		—Calorimetry—	
		ρ , g. ml. ⁻¹	x	ΔQ_f , cal. g. ⁻¹	x
Isotactic					
Amorphous	0	1.053	0	0	0
A	0.26	1.080	0.37	8.7	0.45
B	0.21	1.072	0.26	5.5	0.23
Atactic					
Amorphous	0	1.047	0	0	0

Calorimetric fractional crystallinity was calculated from the ratio $\Delta Q_f/\Delta H_f$ (using, as before, Dedeurwaerder and Oth's value of 86.3 joules g.⁻¹ for ΔH_f), while the volumetric crystallinity was calculated from

$$x = \frac{V_A - V}{V_A - V_C} \quad (2)$$

The measured amorphous specific volume, V_A , of 0.950 ml. g.⁻¹ is in agreement with Newman's result²⁵ but is somewhat lower than that of Kenyon, Gross, and Wurstner.²⁷ The crystal specific volume, V_C , was taken as 0.885 ml. g.⁻¹ from the work of Natta, *et al.*² All specific volume data were obtained at 25°.

Crystallinities were calculated from X-ray diffraction traces using the procedure of Challa, Hermans, and Weidinger.¹³

Results of these measurements for the various samples

(24) F. Danusso and G. Moraglio, *Rend. Accad. Naz. Lincei*, **27**, 351 (1958).

(25) S. Newman and W. P. Cox, *J. Polymer Sci.*, **46**, 29 (1960).

(26) J. M. O'Reilly and F. E. Karasz, presented at 148th National Meeting of the American Chemical Society, Chicago, Ill., Aug. 1964; *Polymer Preprints*, **5**, 351 (1964).

(27) A. S. Kenyon, R. C. Gross, and A. L. Wurstner, *J. Polymer Sci.*, **40**, 159 (1959).

are summarized in Table III. The density and calorimetric methods agree to within the experimental errors if one considers that a limitation in the former is an uncertainty of 1% in V_C which contributes about 10% uncertainty to x . In the calorimetric method we have to rely on values of ΔH_f and these may also be accurate to $\pm 10\%$.

We find that the X-ray crystallinities are lower than those obtained by the other techniques. This in part is due to the fact that these values are based on the Hermans and Weidinger procedure in which the integrated crystalline scattering coefficient is greater than the amorphous scattering coefficient by a factor of 2.16.

Thus crystallinity is calculated from

$$x = \frac{O_C}{O_C + 2.16O_A} \quad (3)$$

where O_C and O_A are the crystalline and amorphous scatterings integrated in the interval $12^\circ \leq 2\theta \leq 30^\circ$. If we were to force agreement between the X-ray crystallinities and those obtained by the other techniques, the factor would be reduced to 1.3.

The above results serve once again to illustrate the complexities of comparing crystallinities of a given polymer sample obtained by different techniques.

IV. Discussion

(i) *Comparison of Isotactic and Atactic Polystyrene.* Some individual points regarding a comparison of the thermal properties have already been brought out above. The most general conclusion that can be drawn is, in fact, that the isomers are markedly similar. The one exception is, of course, the ability of the isotactic form to develop a considerable degree of crystallinity within the experimental time scale of a few hours. Our results show that when this factor is eliminated and attention is confined to the wholly amorphous isomers, the values of the T_g and ΔC_p at T_g , and C_p in the liquid state are very nearly within experimental error. It has already been known from a comparison of earlier data^{5,8} that the heat capacities below T_g are also very similar.

The fact that there is very little difference between the stereoregular and the atactic forms in their thermodynamic properties at T_g is in agreement with other studies, for example Newman's²⁵ observations using mechanical measurements. An analogous conclusion regarding the volumetric properties may also be reached by considering the data obtained in the present and earlier investigations.²² These show, for example, that the densities of amorphous isotactic and atactic

polystyrene both at room temperature and in the melt differ by less than 1%.

A pertinent question which thus arises concerns the possibility that the stereoisomeric distinction between the two forms is not as complete as is currently believed. For example, it could be postulated that conventional atactic polystyrene might consist largely of isotactic sequences interrupted by relatively small numbers of random placements. The latter might effectively hinder the process of crystallization, while having a negligible effect on bulk thermodynamic properties. Such a question, although we believe worth considering, does not appear to be conclusively answerable at present. Evidence from solution measurements hardly supports the hypothesis. The differences between the average unperturbed coil dimensions for the atactic and isotactic polystyrenes¹⁰ are of the same order of magnitude as those displayed, for example, by the corresponding polymethyl methacrylates²⁸ in which considerable differences in the bulk properties are known to occur.

It is interesting to consider further the behavior of polystyrene, particularly with respect to the glass temperature, relative to that of polymethyl methacrylate (PMMA). As is well known, in the latter system stereoregularity has a very large effect on T_g . It may be observed that this difference seems to be closely linked to steric factors and, presumably, to the possibility of rotation about the carbon-carbon bonds in the main chain. Thus we may compare polystyrene and polymethyl acrylate (PMA), on the one hand, with poly- α -methyl styrene (P α MS) and PMMA, on the other. In the latter pair, there is of course a methyl group substituent on the α -carbon in the chain. The glass temperature of the atactic and isotactic forms of each of these four polymers has been measured, and is shown in Table IV.²⁹⁻³¹ First, it may be seen that, as with polystyrene, stereoregularity has little effect in PMA. However, an atactic methyl group substitution raises T_g in both polymers (*i.e.*, P α MS and PMMA) by a substantial margin, 80 to 90°. Finally, it is seen that isotacticity both in P α MS and PMMA lowers T_g , again by roughly the same amount. The symmetry of these relationships is striking, and leads to the prediction that an asymmetric substitution on the α -carbon atom in the main chain will decrease chain flexibility, thereby raising T_g rela-

(28) I. Sakurada, A. Nakajima, O. Yoshizaki, and K. Nakamae, *Kolloid-Z.*, **186**, 41 (1962).

(29) R. F. Boyer, *Rubber Chem. Technol.*, **36**, 1303 (1963).

(30) Y. Sakurada, K. Imai, and M. Matsumoto, *Kobunshi Kagaku*, **20**, 429 (1963).

(31) J. A. Shetter, *J. Polymer Sci.*, **B1**, 209 (1963).

tive to that of the (atactic) reference polymer. Further, the isotactic stereoisomer of the disubstituted polymer will have a lower T_g than that of the atactic form. We would expect these generalizations to become less applicable as the bulk of the substituents increases and the interactions of the latter become dominant.

Table IV

	$T_g, ^\circ\text{C.}$						
	Atactic	Iso-tactic	Δ	Atactic	Iso-tactic	Δ	
P α MS	170 ^a	117 ^b	53	PMMA	103 ^c	42 ^c	61
Poly-styrene	89 ^d	87 ^d	2	PMA	8 (synd.) ^e	10 ^e	-2
Δ	81	30			95	32	

^a See ref. 29. ^b See ref. 30. ^c See ref. 3. ^d This work. ^e See ref. 31.

To conclude this section, we consider the contention that crystallinity can rather strongly affect internal motion in polystyrene, specifically the torsional vibration of the phenyl substituent (see also section III. A. (iii)), and that this is revealed by a comparison of the appropriate heat capacities below T_g .²⁰ We believe that while the suggestion may well be valid, thermal data cannot be used as evidence in its support, for a comparison based on results obtained in the present work shows that the difference C_p (crystal) - C_p (amorphous) is constant and of the order of 0.6 joule deg.⁻¹ mole⁻¹ from about 250 to 350°K. and then rises smoothly at T_g . We see no evidence for a difference of 3 or 4 joules deg.⁻¹ mole⁻¹, for example at 310°K., as is suggested in Figure 1 of ref. 20.

(ii) *Pressure Coefficient of T_g .* If the glass temperature were a reversible thermodynamic transition of second order, uncomplicated by relaxational effects, then $\partial T_g/\partial P$, $TV\Delta\alpha/\Delta C_p$, and $\Delta\beta/\Delta\alpha$ would be identically equal. In these relations, $\Delta\alpha$, $\Delta\beta$, and ΔC_p are the changes in expansivity, compressibility, and specific heat at T_g , respectively. Using our present result for ΔC_p of amorphous, atactic PS and data for the other quantities,³² the three ratios are shown in Table V. It will be seen that, as has been recently discussed by O'Reilly³³

$$\frac{\partial T_g}{\partial P} \cong \frac{TV\Delta\alpha}{\Delta C_p} < \frac{\Delta\beta}{\Delta\alpha}$$

The inequality is dominated by $\Delta\beta$ and is further substantiated by work of Martynyuk, *et al.*^{32c} The agree-

ment of $TV\Delta\alpha/\Delta C_p$ with $\partial T_g/\partial P$ is satisfying and the comparison is limited by the error in $\partial T_g/\partial P$ ($\sim \pm 10\%$) and the uncertainty introduced in ΔC_p , $\Delta\alpha$, T , V_g due to different investigators using different samples. In the absence of measurements of $\partial T_g/\partial P$, $TV\Delta\alpha/\Delta C_p$ can be used as upper limit to $\partial T_g/\partial P$.

Table V

$T_g,$ $^\circ\text{K.}$	$V_g,$ ml. g. ⁻¹	$\Delta\alpha,$ 10 ⁻⁴ $^\circ\text{K.}^{-1}$	$\Delta\beta,$ 10 ⁻⁴ atm. ⁻¹	$\Delta C_p,$ cal. $^\circ\text{K.}^{-1}$ g. ⁻¹	$\partial T_g/\partial P$ $^\circ\text{K. atm.}^{-1}$	$TV\Delta\alpha/\Delta C_p$ $^\circ\text{K. atm.}^{-1}$	$\Delta\beta/\Delta\alpha$
362	0.97 ^a	3.0 ^a	15 ^b	0.075 ^c	0.030 ^d	0.034	0.05
		3.3 ^e	38 ^f		0.031 ^b		0.115

^a See ref. 16. ^b See ref. 32a. ^c This work. ^d See ref. 32b. ^e See ref. 10. ^f See ref. 32c.

(iii) *Thermodynamic Analysis.* One of the principal objects of this experiment has been to measure the residual entropy, $\Delta S_g(T_g)$, of supercooled polystyrene at T_g relative to the crystal and to determine whether the rate of decrease of this quantity with temperature was in accord with the theory of Gibbs and DiMarzio.³⁴ These authors predicted that at a temperature (designated T_2) some tens of degrees below the experimentally observed T_g , the supercooled liquid, if it could be produced, would have negligibly greater entropy than the crystal. One test of the theory, therefore, is to calculate the difference in the entropies of an amorphous isotactic (or atactic) and a partially crystallized polymer as a function of temperature, and to extrapolate the resultant curve to zero $\Delta S_g(T)$. The corresponding temperature is T_2 . Certain ambiguities in this procedure are recognizable, however, though the conditions which would tend to make such a calculation most valid have been summarized by Passaglia and Kevorkian.⁴ These authors themselves carried out an analysis for the atactic-isotactic polypropylene system. We have studied the polymethyl methacrylates from the same point of view, but have concluded that the thermodynamic properties of this system, specifically the widely differing T_g values of the atactic and isotactic forms, make the conclusions from such an analysis more complex.⁵

(32) (a) K. H. Hellwege, W. Knappe, and P. Lehmann, *Kolloid-Z.*, **183**, 110 (1962); (b) S. Matsuoka and B. Maxwell, *J. Polymer Sci.*, **32**, 131 (1958); (c) M. M. Martynyuk, Z. A. Machionis, B. V. Erofeev, and V. K. Semenchenko, *Dokl. Akad. Nauk Belorussk. SSR*, **7**, 170 (1963).

(33) J. M. O'Reilly in "Modern Aspects of the Vitreous State," Vol. 3, J. D. Mackenzie, Ed., Butterworth and Co. Ltd., London, 1964.

(34) J. H. Gibbs and E. A. DiMarzio, *J. Chem. Phys.*, **28**, 373 (1958).

The polystyrene system, however, seems to show promise on several grounds of fulfilling the necessary conditions more completely than either of the above-mentioned cases, and hence should give greater support to any conclusion reached. First, one of the main uncertainties regarding an analysis of this type revolves around the assumption of equal entropies of the atactic and isotactic polymers in the melt. For PMMA this is almost certainly not the case; for polypropylene there is likely to be less doubt though there is evidence of a considerable difference in the enthalpies of the melts.^{26,36} In polystyrene we believe that the very close similarity of the bulk properties, in particular T_g values and the heat capacities in the liquid state, make this assumption least assailable.

Secondly, as has been discussed above, isotactic polystyrene obeys a two-phase model well in regard to its behavior at T_g . It has been shown²⁶ that the lack of such adherence results in the extrapolation to zero entropy difference being very dependent on the degree of crystallinity of the sample used, a result opposite to the anticipated behavior. In addition, the actual values both of ΔS_g and of $T_g - T_2$ are obviously highly sensitive to this point. Thirdly, it is worth noting that in polypropylene there is a small transition, of unknown origin, which is observed in both the atactic and isotactic samples at about 310°K. The calculation is unfortunately again overly sensitive, numerically, to such phenomena, and hence their existence (even apart from any question of origin) must render results less meaningful.

On the basis of the above reasoning, therefore, we calculated $\Delta S_g(T)$ in the expectation that of all systems previously examined, polystyrene was the most appropriate and unambiguous. $\Delta S_g(T)$ was found from the equation

$$\Delta S_g(T) = S_a^{\text{obsd}}(T) - S_i^{\text{obsd}}(T) + k \quad (4)$$

In this expression the terms $S_a^{\text{obsd}}(T)$ and $S_i^{\text{obsd}}(T)$ are obtained by the usual summation of the measured heat capacity functions, divided by the mean absolute temperature, of the amorphous and crystalline isotactic polymer, referred to a convenient zero. The normalization constant k is found by equating the entropies at $T \geq T_m$, the melting point of the crystalline polymer. Thus

$$0 = S_a^{\text{obsd}}(T_m) - S_i^{\text{obsd}}(T_m) + k \quad (5)$$

which yields

$$\Delta S_g(T) = \{S_i^{\text{obsd}}(T_m) - S_i^{\text{obsd}}(T)\} - \{S_a^{\text{obsd}}(T_m) - S_a^{\text{obsd}}(T)\} \quad (6)$$

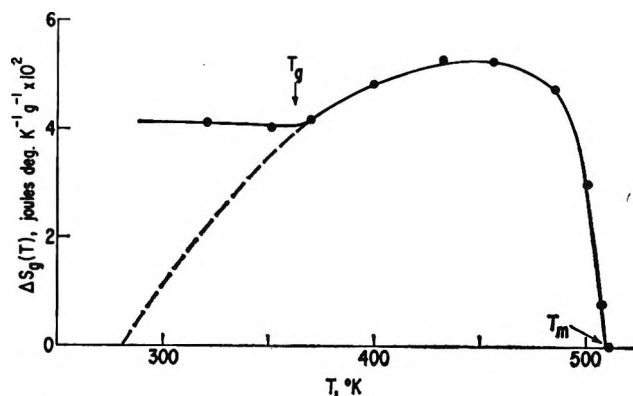


Figure 4. Excess entropy of supercooled liquid and glassy polystyrene relative to the 39% crystalline sample.

As has already been implied, use of the annealed atactic rather than the quenched isotactic polystyrene heat capacities would have negligible effect on $S_a^{\text{obsd}}(T_m) - S_a^{\text{obsd}}(T)$ and hence on $\Delta S_g(T)$. The quantity $\Delta S_g(T)$ as a function of temperature is shown in Figure 4. Unfortunately, it develops that the extrapolation to T_2 is long enough to cast rather considerable uncertainty into the result. To minimize the error, we take into account the significant temperature dependence of ΔC_p by using in the calculation of $\Delta S_g(T)$ for the supercooled liquid below T_g (dashed line in Figure 4) C_p values obtained by linearly extrapolating the heat capacities of the amorphous (liquid-like) and of the semicrystalline samples. On this basis we find $T_g - T_2$ is $81 \pm 15^\circ$. Current approaches to the problem suggest a somewhat lower value, around 50° . Our higher value is a consequence, in part, of the fact that on a mole basis and referred to a wholly crystalline sample, $\Delta S_g(T_g)$ ($= 11.2$ joules deg.⁻¹ mole⁻¹) is seemingly greater than has been observed for other vinyl polymers. [This statement is also true for $\Delta S_g(0)$, because the heat capacities of the amorphous and crystalline samples are virtually identical below T_g .]

The results of an analogous calculation of the residual enthalpy, $\Delta H_g(T)$, are shown in Figure 5. In this case we find that the temperature at which the supercooled liquid and the crystal would have equal enthalpies is 237°K., some 125° below the experimentally observed T_g .

We can compare the above results for polystyrene with those obtained by Passaglia and Kevorkian⁴ for polypropylene. In the latter polymer it was found that the lowering of T_g necessary to obtain a glass of the same entropy and enthalpy as the crystal was 53

(35) E. Z. Fainberg, M. O. Tomareva, S. M. Skuratov, and N. M. Mikhailov, *Vysokomolekul. Soedin.*, **4**, 463 (1962).

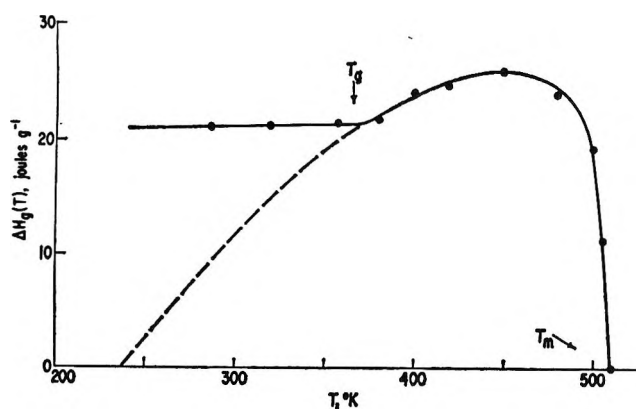


Figure 5. Excess enthalpy of supercooled liquid and glassy polystyrene.

and 150°, respectively. However, as already mentioned, this calculation is highly sensitive to the precise shape of the heat capacity curve of the partially crystalline polymer. In particular, if there had been a discontinuity in C_p at T_g proportional in magnitude to the amorphous content of the polypropylene sample at that temperature, then it can be calculated that the above values would each be increased by at least 40°, the exact amount depending on the further assumptions made. This could bring the values of $T_g - T_2$ (though not the analogous quantities for the enthalpy calculation) for polystyrene and polypropylene into rather better agreement.

Finally, we note that a calculation of the residual volume as a function of temperature carried out by Natta, *et al.*²² (for a different purpose) indicates that the temperature at which the supercooled liquid has the same volume as the crystal is $\sim 195^\circ\text{K}$. The approximations in this estimate are, perhaps, somewhat more doubtful than those employed in the analogous entropy calculation (for example, no correction is made for curvature in the liquid volume *vs.* temperature plot). Nevertheless, it is still possible to assert

that the three first-order residual thermodynamic quantities do not attain a zero value at the same temperature. The inference in this case at least obviously cannot be in support of arguments which postulate that the residual entropy is a function of density alone.³⁶

The results of the above thermodynamic analysis are generally in agreement with the Gibbs and DiMarzio theory, but the confirmation has perhaps been less definitive than might have been anticipated in this "ideal" system.

V. Conclusions

Through the measurement of heat capacities over the appropriate temperature range, it has been demonstrated that it is possible to examine, separately, the effects of both molecular configuration (*i.e.*, tacticity), and crystallinity on thermodynamic properties of polystyrene. The former variable has been shown to have in itself rather negligible effect, and it is believed that this can be related at least semiempirically to features of the chemical structure. Crystallinity, however, affects the bulk properties markedly and in a manner which can be predicted with unexpected precision from the properties of the homogeneous amorphous and crystalline component phases. Whether this finding, which is in contrast to the behavior of many other partially crystalline polymer systems, has a morphological basis and is associated, for example, with relatively perfect crystal domains has not been examined. This clearly is a problem that demands further work.

Polystyrene is useful, also, in that in several respects it forms the ideal polymer with which to test theories of glass formation. To some extent this aspect has been investigated in the present paper, but it has been found that even with precision heat capacity measurements available some difficulties persist.

(36) I. Gutzow, *Z. physik. Chem.*, 221, 153 (1963).

Specific Heat of Synthetic High Polymers. XII. Atactic and Isotactic Polystyrene¹

by Ismat Abu-Isa and Malcolm Dole

Department of Chemistry and Materials Research Center, Northwestern University, Evanston, Illinois
(Received March 4, 1966)

The specific heats of atactic, amorphous isotactic, and annealed semicrystalline isotactic polystyrene have been measured over the temperature range -50 to 280° . The heat of fusion of 100% crystalline isotactic polystyrene was estimated to be 23.0 ± 2.0 cal. g.⁻¹. The data are interpreted in terms of the encratty function which is c_p/T or dS/dT . The increment in encratty at the glass transition temperature is a function only of the fraction of amorphous content and is independent of the tacticity of the sample. In the liquid range above the melting point there is similarly no difference between the atactic and isotactic samples to be seen within the rather large experimental fluctuations of this work. Equations for the encratty and its temperature variation in terms of the Eyring hole theory of the liquid state are developed. The hole contribution to the encratty, theoretically, would pass through a maximum at the low temperature of 175°K . if equilibrium and the liquid state could persist to that temperature. The Ehrenfest relation seems to be valid for the increments in encratty, compressibility, and thermal volume coefficient of expansion.

I. Introduction

After making a specific heat study of atactic and isotactic polypropylene,^{1,2} we became interested in a similar investigation of atactic and isotactic polystyrene. Accordingly, this research was initiated, but on completion of the measurements we learned of a similar investigation by Karasz, Bair, and O'Reilly³ and by mutual agreement decided on simultaneous publication.

II. Experimental

A. Materials. The polystyrene samples were kindly supplied without antioxidants or other additives by Drs. R. F. Boyer and F. L. Saunders of The Dow Chemical Co. The annealed isotactic polystyrene was prepared in this laboratory by heating the amorphous (quenched) isotactic sample to 212° and allowing it to cool slowly to room temperature in a stepwise fashion over a period of 72 hr. The properties of the samples are collected in Table I.

B. Calorimetric Measurements. In the early stages of this research our calorimetric equipment had to be moved from its original location to a laboratory in the

new wing of the Technological Institute. We used this opportunity to rewire much of the equipment and

Table I: Properties of Polystyrene Samples

Polymer type	EP 1340			Styron 690 Atactic
	Quenched	Crystalline	Annealed	
$[\eta]$, toluene at 25° , dl. g. ⁻¹		2.3		0.88
Density, 25°				
Gradient tube	1.056	1.072		1.051
Flotation		1.074	1.077	
Relative crystallinity, %				
X-Ray		40		
Density	8.6	35.6	42	0
Max. melting point, $^\circ\text{C}$.			236	
Molecular weight $[\eta] = 1.10 \times 10^{-4} M^{0.725}$				
Impurities in isotactic sample, p.p.m.		9.0×10^5		2.4×10^5
	Ti 31	Fe <5	Cl <100	

(1) The previous publication of this series: I. Abu-Isa, V. A. Crawford, A. R. Haly, and M. Dole, *J. Polymer Sci.*, C6, 149 (1964).

(2) R. W. Wilkinson and M. Dole, *ibid.*, 58, 1089 (1962).

(3) F. E. Karasz, H. E. Bair, and J. M. O'Reilly, *J. Phys. Chem.*, 69, 2657 (1965).

to install a new higher capacity metal mercury diffusion pump. The watt-hour meter was recalibrated as before⁴ using ice in the calorimeter. In Aug. 1963 the calibration yielded an average value of 12.680 cal./rev. as compared to 12.697 obtained in Nov. 1952. Thus, there is no evidence of any drift with time in the readings of the watt-hour meter. The measurement of the electrical energy input is probably by far the most accurate and reliable part of the experimental procedure. As before, the heat capacity of the empty calorimetric system was determined by measuring the total heat capacity of the calorimeter filled with synthetic sapphire, Al_2O_3 .⁵ A minor modification was introduced of using just enough aluminum oxide so that its total heat capacity was approximately equal to the total heat capacity of the polymer samples to be studied.

III. Results

A. *Specific Heats and the Encraty.* In Table II constants are tabulated of the linear equation

$$c_p = A + Bt \quad (1)$$

where c_p is the specific heat in cal. $\text{g}^{-1} \text{deg}^{-1}$, t is the temperature in $^{\circ}\text{C}$., and A and B are empirical constants. Also listed in the table are the temperature ranges over which the linear equation represents the data within the experimental uncertainty of about $\pm 0.5\%$. Figures 1-3 illustrate the specific heat as a function of temperature of the atactic, amorphous isotactic, and annealed isotactic polystyrene. In Figure 4 the specific heat of a semicrystalline sample of the isotactic polystyrene as received is plotted along with data of Dainton, Evans, Hoare, and Melia.⁶ The agreement between the values obtained in the two different laboratories is excellent; however, our values

Table II: Constants of the Linear Specific Heat Equation for Polystyrene: $c_p = A + Bt$

Polymer	A , cal. deg. ⁻¹ g. ⁻¹	B , cal. deg. ⁻² g. ⁻¹ $\times 10^4$	Temp. range, $^{\circ}\text{C}$.
Below the glass transition			
Atactic	0.2595	1.024	-50 to 65
Amorphous isotactic	0.2599	1.022	-50 to 60
Semicrystalline isotactic	0.2654	1.045	-40 to 70
Annealed isotactic	0.2570	1.082	25 to 75
Above the glass transition and below the melting point			
Atactic	0.3705	0.607	105 to 275
Annealed isotactic	0.2771	1.160	120 to 175
Above the melting point			
Annealed isotactic	0.3506	0.651	245 to 280

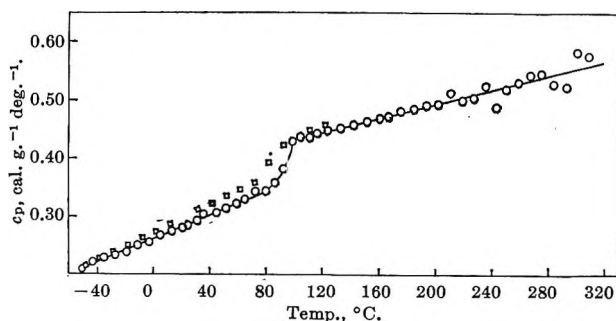


Figure 1. Specific heat of atactic polystyrene: circles, data of this paper; squares, data tabulated by Warfield and Petree.⁷

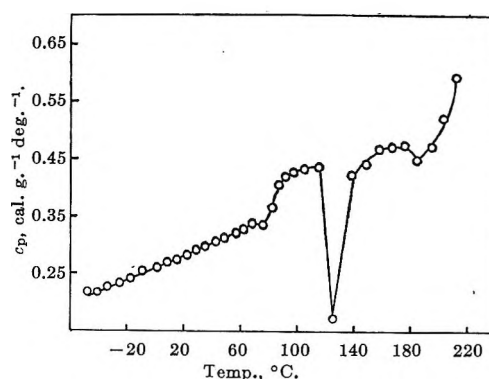


Figure 2. Specific heat of amorphous isotactic polystyrene.

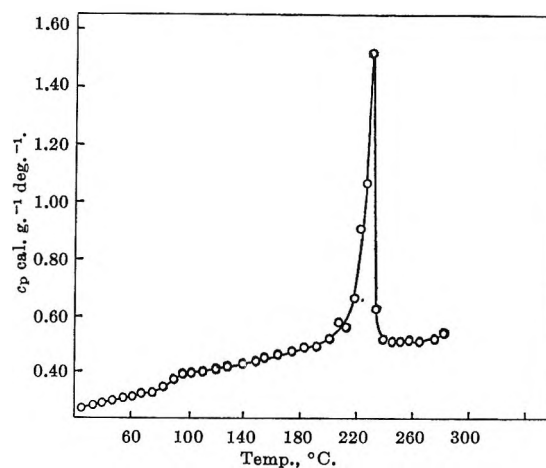


Figure 3. Specific heat of annealed isotactic polystyrene.

of the specific heat of annealed isotactic polystyrene are somewhat lower than those of Dainton, *et al.*

Another way of expressing the results is in terms of the encratty, L . The encratty was defined by Dole,

(4) A. E. Worthington, P. C. Marx, and M. Dole, *Rev. Sci. Instr.*, **26**, 698 (1955).

(5) D. C. Ginnings and G. T. Furukawa, *J. Am. Chem. Soc.*, **75**, 522 (1953).

(6) F. S. Dainton, D. M. Evans, F. E. Hoare, and T. P. Melia, *Polymer*, **3**, 286 (1962).

et al.,¹ as the first derivative of the entropy, S , with respect to temperature or as the negative of the second derivative of the free energy, G , with temperature or simply as c_p/T ; thus (per gram of polymer)

$$L = c_p/T = (dS/dT)_p = -(d^2G/dT^2) \quad (2)$$

For comparison purposes, we have plotted in Figure 5 the encraticity of the atactic and carefully annealed isotactic polystyrene. In Figure 6 the encraticity of the quenched amorphous isotactic polystyrene is plotted along with that of the atactic.

B. The Heat of Fusion. If the total heat required to melt the semicrystalline polymer at the maximum melting temperature T_m , ΔH_f^* , is known, then the true heat of fusion of 100% crystalline polymer at T_m , ΔH_f^m , can be calculated from the equation

$$\Delta H_f^m = \Delta H_f^*/x \quad (3)$$

where x is the fraction of crystallinity. If we let H_m equal the enthalpy per gram of polymer at the maximum melting temperature, T_m , then the true heat of fusion at the temperature T_m , 242°, can be calculated from the equation

$$\Delta H_f^m = \left\{ H_m - H_T + \int_{T_m}^T c_{p,L} dT - x_T \int_{T_m}^T (c_{p,L} - c_{p,C}) dT \right\} / x_T \quad (4)$$

where H_T is the enthalpy per gram at a selected temperature, x_T is the weight fraction of crystallinity at that temperature, and $c_{p,L}$ and $c_{p,C}$ are the estimated specific heats of the liquid and crystalline phases of the semicrystalline polymer, respectively. In this work, all the enthalpies of the isotactic polystyrene were calculated with reference to the enthalpy at the absolute zero of temperature using the data given by Dainton, *et al.*,⁶ up to the lowest temperature at which our work began. Thus, in the case of the annealed isotactic sample, we took the enthalpy at 294.11°K. to be 43.28 cal. g.⁻¹ and added our measured increments in H to this value to obtain enthalpies at higher temperatures. For the heat of fusion calculations only differences of enthalpies appear in the equation; hence, the reference value is immaterial in this case. For the atactic reference enthalpy we adopted the value 24.59 cal. g.⁻¹ at 219.24°K. taken from the tabulation of Warfield and Petree.⁷

In order to calculate ΔH_f^m from eq. 4, it is necessary to know $c_{p,L}$ and $c_{p,C}$ in addition to the measured enthalpy difference $H_m - H_T$ and the degree of crystallinity x_T . This treatment also assumes the validity of the two-phase model of semicrystalline polymers.

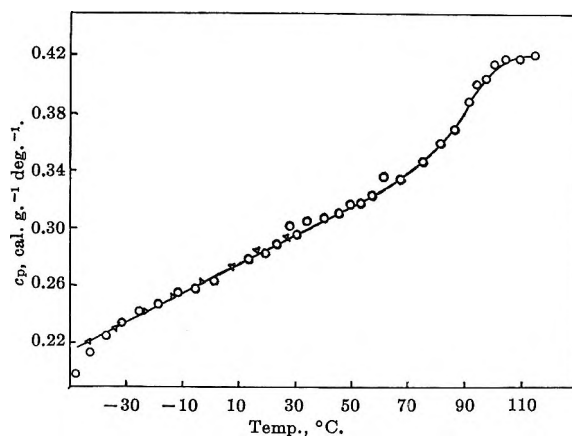


Figure 4. Specific heat of semicrystalline isotactic polystyrene: circles, data of this paper; triangles, data of Dainton, *et al.*⁶

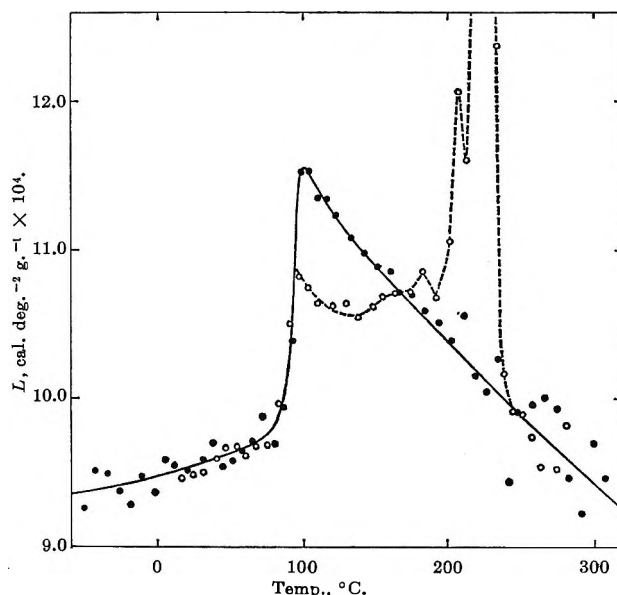


Figure 5. Encraticity of atactic (solid circles) and annealed isotactic (open circles) polystyrene.

For $c_{p,L}$ we used the equation for the atactic non-crystalline sample valid above T_g given in Table II and for $c_{p,C}$ the equation for the carefully annealed isotactic sample valid below T_g . From Table II it can be seen that below T_g all samples have specific heat equations which extrapolate to values at 200° that are within 2% of each other. At 0° the maximum spread is 3%. Thus, we feel that the equation adopted for $c_{p,C}$ is reliable. With respect to the equation for $c_{p,L}$ the specific heat values above the melting point for the atactic and isotactic samples are the same within the rather wide experimental fluctuations

(7) R. W. Warfield and M. E. Petree, *J. Polymer Sci.*, **55**, 497 (1961).

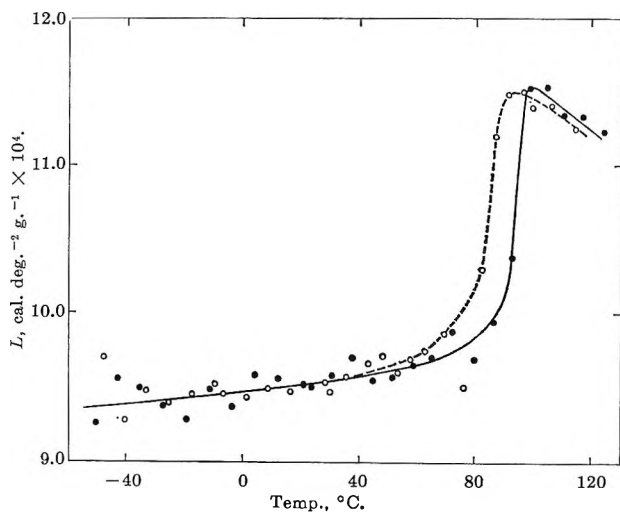


Figure 6. Encratty of atactic (solid circles) and quenched isotactic polystyrene (open circles).

of about 5%. In fact, none of the data reported in this paper demonstrate any difference between the atactic and isotactic samples below T_g or above T_m . Hence, for this reason we believe that our use of the equation for the specific heat of atactic polystyrene above T_g to represent the specific heat of the amorphous component of the semicrystalline solid above T_g is justified.

The validity of eq. 4 can be tested by calculating ΔH_f^m from different values of H_T . This has been done over the temperature range 100 to 210° and the results plotted in Figure 7. A constant value of ΔH_f^m should be obtained, and this can be seen to be the case from about 115 to 160°. Below 115° complications due to the glass transition and above 160° to melting are probably reducing the validity of the equation; certainly the rapid drop from 180° to higher temperatures must be the result of melting. In eq. 4 we assumed x_T to be constant at 0.42 (see Table I) which is obviously incorrect in the temperature range of melting. As a result of this treatment we adopt 23.0 cal. g.⁻¹ as the heat of fusion of 100% crystalline isotactic polystyrene at the maximum melting point. This value is somewhat higher than that obtained by Dedeurwaerder and Oth,⁸ namely 19.20 cal. g.⁻¹, obtained by the melting point depression by diluents method. The heat of fusion calculations depend on the value chosen for x , in this work 0.42 for the carefully annealed polystyrene. The latter was calculated using 0.9515, the specific volume of our atactic sample, for the specific volume of the completely amorphous isotactic polymer and 0.8968 cm.³ g.⁻¹ for the specific volume of the completely crystalline polystyrene.⁸ If we had used

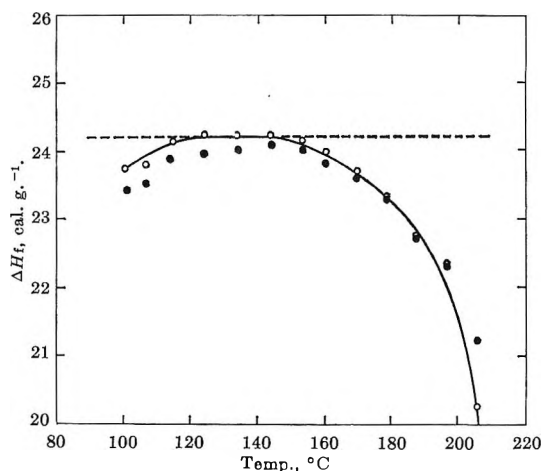


Figure 7. ΔH_f^m calculated from eq. 4.

0.9493 for the amorphous component as estimated from the data of Fox and Flory,⁹ the crystallinity of the highly annealed isotactic sample would have been 0.396 and the estimated heat of fusion 24.4. The Dow Chemical Co. sample of crystalline isotactic polystyrene had a crystallinity of 0.40 on the basis of their X-ray estimates while our density data resulted in the value 0.356. If we correct the heat of fusion by the ratio of 0.356/0.40 or 0.89, the value 20.5 cal. g.⁻¹ results. These different values of ΔH_f illustrate its dependence on the estimated fraction of crystallinity. However, although there is excellent agreement in the case of polyethylene between the calorimetrically determined ΔH_f and that found by the diluent method, there are several examples of discrepancies between these two methods in the case of other polymers, discrepancies which are much higher than that reported here.¹⁰

Knowing ΔH_f^m , the fraction of crystallinity, x , can be calculated at various temperatures above T_g by rearrangement of eq. 4. Of course, this calculation will yield 0.42 over the range of temperatures for which ΔH_f^m was calculated to be 23.0 cal. g.⁻¹, but it is interesting to see how x changes at other temperatures. The results are plotted in Figure 8 where the variation of x with temperature has the expected shape. We are uncertain as to whether the slight decrease in x as the temperature rises from 170 to 200° is real or not. The apparent decrease in x may be due to slightly incorrect coefficients in the empirical equations used

(8) R. Dedeurwaerder and J. F. M. Oth, *Bull. soc. chim. Belges*, **70**, 37 (1961); *J. chim. phys.*, **56**, 940 (1959).

(9) T. G. Fox and P. J. Flory, *J. Polymer Sci.*, **14**, 315 (1954).

(10) See the review by M. Dole, *Fortschr. Hochpolymer. Forsch.*, **2**, 221 (1960).

for the specific heats of the crystalline and amorphous phases.

In concluding this section on the results it should be pointed out that at high temperatures, 200°, our data are about 2% below those of Karasz, *et al.*, with the discrepancy increasing with temperature. This disagreement may result from inaccurate calibration of the empty calorimeter at the high temperature; however, over the range 100 to 200° there is an approximate constant difference of about 2%. Theoretically, there should be no discrepancies because, in the work of Karasz, *et al.*, and this work, synthetic sapphire was the standard substance used for calibration purposes (Karasz, *et al.*, directly measured the heat capacity of the empty calorimeter but checked their calibration with measurements on Al_2O_3). If time permits in the future, we may repeat a few of our measurements using the same N.B.S. standard sample of atactic polystyrene as that used by Karasz, *et al.* Except for the differences in the absolute magnitude of the specific heats, our results agree in general very well with those of Karasz, *et al.*

IV. Discussion

A. The Temperature Range below T_g . By examination of Figure 5 it can be seen that, within the limits of the fluctuations in the data exhibited there, no significant difference can be seen between the specific heats of the atactic or isotactic polystyrene below the glass transition temperature range. This conclusion is different from that of Wunderlich, Jaffe, and Stahl,¹¹ who compared the specific heats of the 43% isotactic polystyrene obtained by Dainton and co-workers⁶ with values for atactic polystyrene tabulated by Warfield and Petree⁷ and found a significant difference in the specific heats beginning at about 220°K. and increasing up to the glass transition temperature. However, these differences are probably due to experimental error inasmuch as the Warfield and Petree⁷ tabulated values for atactic polystyrene do not agree with ours below T_g ; see Figure 1. With rising temperature, specific heat measurements gradually become more difficult to carry out.

From a number of lines of evidence polystyrene undergoes some sort of an intramolecular transition in the neighborhood of 50°. Wunderlich and Bodily¹² observed two small peaks at 53 and 26° in their differential thermal analysis study of atactic polystyrene. A heating rate faster than the cooling rate was required for the observation of these peaks; their heating rates were 3° min.⁻¹ to 9° min.⁻¹, much greater than the heating rate of the experiments of this research. Kilian and Boueke¹³ calculated from an X-

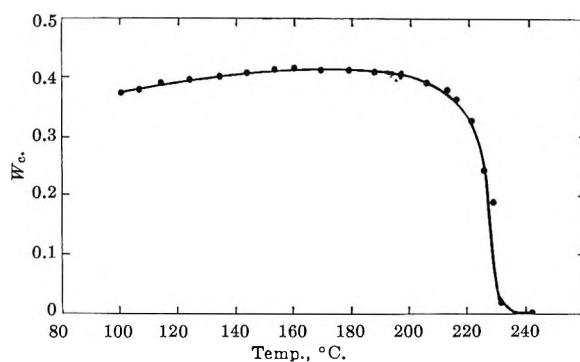


Figure 8. Crystallinity of annealed isotactic polystyrene.

ray analysis of atactic polystyrene that the Bragg intramolecular interference distance, presumably the distance between the phenyl groups, went through a maximum at about 50°. Moraglio, Danusso, Bianchi, Rossi, Liquori, and Quadrifoglio¹⁴ studied the 50° transition in both bulk and molecularly dispersed phases from the standpoint of dilatometric, internal pressure, and optical density measurements. They concluded that the transition was the result of intramolecular motions; hence, the evidence is strong that such an effect exists. We were unable to observe anything abnormal in the specific heat measurements in the 50° temperature range, except perhaps a slight change in the slope of the encrity-temperature plot at 50° for annealed isotactic polystyrene. However, the effect is hardly greater than the experimental error. Probably the transition occurs so gradually over a range of temperature that it cannot be detected in specific heat measurements of the usual type.

B. The Glass Transition Temperature Range. The encrity-temperature plots illustrate rather well the changes in the entropy-temperature coefficient, $(dS/dT)_p$, as the polymer rises slowly in temperature through the glass transition (Figures 5 and 6). We define the glass transition temperature, T_g , as the temperature midway in the rise of the encrity, *i.e.*, the temperature at which ΔL in the glass transition range is equal to one-half of its total magnitude. Somewhat to our surprise we found that T_g for the annealed isotactic polystyrene was identical with that for the highly amorphous atactic sample. Also to our surprise the quenched, amorphous, isotactic polystyrene exhibited a T_g about 9° lower in temperature

(11) B. Wunderlich, M. Jaffe, and M. L. Stahl, *Kolloid-Z.*, **185**, 65 (1962).

(12) B. Wunderlich and D. M. Bodily, *J. Appl. Phys.*, **35**, 103 (1964).

(13) H. G. Kilian and K. Boueke, *J. Polymer Sci.*, **58**, 311 (1962).

(14) G. Moraglio, F. Danusso, U. Bianchi, C. Rossi, A. M. Liquori, and F. Quadrifoglio, *Polymer*, **4**, 445 (1963).

than the atactic sample. The glass transitions and the increments in L at T_g are collected in Table III. Also in Table III are values of x and $\Delta L/(1 - x)$ in order to see if the increment in L is directly proportional to the fraction of amorphous polystyrene. For

$$\frac{\Delta\beta}{\Delta\alpha} = \frac{\Delta\alpha V}{\Delta L} \quad (6)$$

where $\Delta\alpha$, $\Delta\beta$, and ΔL are called the configurational thermal expansion, the configurational compressibility, and (in our language) the configurational encraticity. This relation may also be obtained by combining two equations of Ehrenfest and indeed is called the Ehrenfest equation for a second-order phase change.²⁰ A recent thermodynamic discussion of eq. 6 is that of Goldstein.²¹ It is important to know whether eq. 6 is verified or not. In the case of atactic polystyrene we now have accurate data for ΔL , $\Delta\alpha$, and V ; the chief uncertainty is in the value of $\Delta\beta$. Hellwege, Knappe, and Lehmann²² have published many curves showing the variation of the volume of atactic polystyrene with temperature and pressure. They quote $\Delta\beta$ as being equal to 8.0×10^{-6} cm.²/ktoir (or 2.51×10^{-4} cm.³/cal.) at T_g . However, the compressibility begins to rise rather rapidly as T_g is approached, and if this rise in β is added to the discontinuous rise in β at T_g as Goldstein has done, $\Delta\beta$ becomes equal to 6.2×10^{-4} cm.³/cal. Calculated values for the left- and right-hand side of eq. 6 are given in Table IV. Because of the considerable uncertainty in the value of $\Delta\beta$, it is impossible to come to an exact conclusion regarding eq. 6, but it does seem to be nearly verified.

Table III: Glass Transition Temperatures of Polystyrene and Encraticity Increments at T_g

Polymer	T_g , °C.	ΔL , cal. deg. ⁻² g. ⁻¹ $\times 10^4$	x	$\Delta L/(1 - x)$, cal. deg. ⁻² g. ⁻¹ $\times 10^4$
Atactic	93	1.77	0	1.77
Quenched isotactic	84	1.69	0.086	1.85
Annealed isotactic	92	1.04	0.420	1.79

this table we have computed x in terms of the equation

$$x = (v_a - v)/(v_a - v_c) \quad (5)$$

and as before taken the measured v of the atactic sample, at 25°, 0.9515, for v_a instead of the value 0.9493 cm.³ g.⁻¹ quoted by Dedeurwaerder and Oth⁸ from the work of Fox and Flory.⁹ Considering the uncertainty in estimating ΔL from the data, the constancy of the ratio $\Delta L/(1 - x)$ is rather remarkable. At any rate this study demonstrates that there is no essential difference in this respect between the atactic and amorphous isotactic polystyrenes and also shows that the properties of the amorphous component with respect to ΔL are not affected by the presence of a crystalline phase, at least up to about 40% crystallinity. This conclusion agrees with that recently announced by O'Reilly and Karasz.^{3,15}

However, T_g is different for the amorphous isotactic and atactic samples. T_g for the isotactic is 9° lower than the atactic T_g ; this result is in the same direction as the difference in T_g between the isotactic and atactic polymethacrylates tabulated by Boyer¹⁶ from data of Shetter.¹⁷ As the amorphous isotactic polystyrene becomes partially crystalline, T_g rises so that at 40% crystallinity the T_g values for the atactic and isotactic samples coincide.

The increment in ΔL at T_g from Table III can be taken to be 1.8×10^{-4} cal. deg.⁻² g.⁻¹ at 92°. This is readily converted to a ΔC_p per mole of chain atoms equal to 3.4 cal. deg.⁻¹ mole⁻¹.

Some years ago, Wunderlich¹⁸ tabulated many similar increments for a variety of glass-forming substances and found that ΔC_p values averaged to 2.7 ± 0.5 cal. deg.⁻¹ mole⁻¹. Our value of 3.4 is somewhat higher than this average.

Prigogine and Defay¹⁹ have derived the equation

Table IV: Test of Eq. 6 for Atactic Polystyrene^a

Author of $\Delta\beta$ -value	$\Delta\beta$, cm. ³ /cal.	$\Delta\beta/\Delta\alpha$, deg. cm. ³ /cal.	$V\Delta\alpha/\Delta L$
Hellwege, <i>et al.</i>	2.51×10^{-4}	0.81	1.67
Goldstein	6.20×10^{-4}	1.99	1.67

^a $\Delta\alpha = 3.11 \times 10^{-4}$ deg.⁻¹; $V = 0.966$ cm.³ g.⁻¹; $\Delta L = 1.8 \times 10^{-4}$ cal. deg.⁻² g.⁻¹.

C. The Temperature Range between T_g and T_m .

We now turn to a consideration of the specific heats and encraticities between T_g and the melting range. In the case of the atactic sample, L decreases slowly

(15) J. M. O'Reilly and F. E. Karasz, 148th National Meeting of the American Chemical Society, Chicago, Ill., Sept. 1964.

(16) R. F. Boyer, *Rubber Rev.*, **36**, 1303 (1963).

(17) J. A. Shetter, *J. Polymer Sci.*, **B1**, 209 (1963).

(18) B. Wunderlich, *J. Phys. Chem.*, **64**, 1052 (1960).

(19) I. Prigogine and R. Defay, "Chemical Thermodynamics," translated by D. H. Everett. Longmans, Green and Co., London, 1954, p. 297.

(20) See ref. 19, p. 306.

(21) M. Goldstein, *J. Chem. Phys.*, **39**, 3369 (1963).

(22) K. H. Hellwege, W. Knappe, and P. Lehmann, *Kolloid-Z.*, **183**, 110 (1962).

and nearly linearly from a peak at about 100° up to the highest temperatures studied, but the fluctuations in the data become greater, the higher the temperature. The other polystyrene samples also exhibit a peak in L at about 100° except for the amorphous isotactic sample in which L has a maximum about 10° lower in temperature. The isotactic samples do not exhibit as pronounced a peak as does the atactic, as is to be expected.

In terms of the Einstein specific heat function, the encraticity for a single vibrational mode per molecule (at constant volume) is equal to²³

$$\frac{k^2}{h\nu} \frac{z^3 e^z}{(e^z - 1)^2} \quad (7)$$

where k and h are the Boltzmann and Planck constants, ν is the vibrational frequency, and z is equal to $h\nu/kT$. The variation of L with temperature at constant volume is

$$\left(\frac{dL}{dT}\right)_v = -\frac{L}{T} \left\{ 3 + z - \frac{2ze^z}{e^z - 1} \right\} \quad (8)$$

which goes through a maximum when

$$\frac{ze^z}{e^z - 1} = \frac{3}{2} + \frac{z}{2} \quad (9)$$

For the maximum, z is equal to 2.576. Knowing the latter and the temperature of the peak (100°), we can calculate the frequency that, according to the above equation, would give such a maximum if it were the only frequency operative. The result turns out to be 668 cm.⁻¹. This means that the dominant frequencies determining the specific heat up to this temperature have wave numbers equal to or less than 668. The C-H bending and the C-C stretching frequencies equal to 1000 cm.⁻¹ give L values that peak about 285°. Thus, the dominant frequencies in the glass transition range are the acoustical frequencies and the chain twisting and bending frequencies. The reason that L decreases as T rises above the peak temperature is that the cumulative L for the lower frequencies decreases faster than the L for the high frequencies increases. The peak in L is not to be construed as the peak due to the Einstein function. For the low frequency chain twisting and bending motions the peaks come at a much lower temperature than at 100°, in fact, at 40°K. as demonstrated by the data of Dainton, Evans, Hoare, and Melia.⁶

According to the Eyring hole model of the liquid state as developed by Hirai and Eyring²⁴ for the glass transition, the rise in c_p at T_g results from the requirement of supplying energy to form the greater number

of holes at the higher temperatures. Hirai and Eyring's equation for the hole contribution to the heat capacity per mole of repeating units as expressed in the form given by Wunderlich¹⁸ is

$$\Delta C_p = E_g \frac{\epsilon_h}{RT^2} \exp(-\epsilon_h/RT) \quad (10)$$

where E_g is the internal latent heat of vaporization at T_g , approximately 7320 cal. mole⁻¹ of repeating units as deduced by Wunderlich from molar cohesion energy data, and ϵ_h is the "molar excess energy over the no hole" configuration.

If eq. 10 is divided by T to obtain the hole encraticity, L_h , and if the latter is then differentiated with respect to T to obtain its temperature coefficient, we find

$$\frac{dL_h}{dT} = \frac{E_g \epsilon_h}{RT^4} \left\{ \frac{\epsilon_h}{RT} - 3 \right\} \exp\{-\epsilon_h/RT\} \quad (11)$$

which demonstrates that the hole contribution to the encraticity will go through a maximum at ϵ_h/RT equal to 3. In this work a maximum in the encraticity appeared at about 102°; see Figures 5 and 6. This is not the maximum predicted by eq. 11 because eq. 11 is based on the assumption of equilibrium which does not exist in the glassy state. However, it is possible to calculate the temperature where the maximum in L due to the Eyring hole mechanism would occur provided ϵ_h is known. From the jump in the specific heat at T_g , ϵ_h can be calculated from eq. 10. We found 1044 cal. mole⁻¹ which is slightly less than that estimated by Wunderlich from specific heat data on low molecular weight polystyrenes. Inserting this value for ϵ_h into eq. 11, the value of T necessary to make ϵ_h/RT equal to 3 is only 175°K., far below T_g . This calculation assumes that ϵ_h remains constant with temperature, but a lower value of ϵ_h would make T_{max} still lower. This value of 175°K. is approximately the temperature where the rise in entropy with temperature due to the Eyring hole mechanism would have its greatest value if equilibrium could be attained at all temperatures and if the material were in the liquid state at that temperature. One could conceive of this temperature as being close to that temperature below which the configurational entropy of the liquid due to holes approaches zero.

Our value of ϵ_h is much less than values estimated by Hirai and Eyring who deduced, by assuming a universal value for the fraction of free volume at T_g that ϵ_h/RT_g is approximately equal to 4. In our case this ratio is more nearly equal to 1.5. Wunderlich has

(23) M. Dole and B. Wunderlich, *Makromol. Chem.*, **34**, 29 (1959).

(24) N. Hirai and H. Eyring, *J. Polymer Sci.*, **37**, 51 (1959).

tabulated many values of this ratio ranging all the way from 1.5 for polyvinyl chloride to 4.6 for ethyl alcohol. Most polymers have values around 2.0.

D. The Gibbs-DiMarzio Theory. It is interesting to calculate, as Karasz, *et al.*,³ have done, the temperature, T_2 , to which the glass transition would have to be lowered so that the entropy per gram of the liquid phase becomes equal to that of the crystal. This is the temperature at which the liquid should have a zero configurational entropy according to the theory of Gibbs and DiMarzio.²⁵

Recently, Adam and Gibbs²⁶ have shown how the Gibbs-DiMarzio theory can be adapted to give a theoretical explanation of the Williams, Landel, and Ferry empirical equation by adapting a value of $T_g - T_2$ equal to about 50° .

As stated above, T_2 is to be considered the temperature at which the entropy of the supercooled (but not glassy) liquid becomes equal to that of the 100% crystalline phase. This temperature is readily calculated from the equation

$$\int_{T_2}^{T_m} c_{p,L} \frac{dT}{T} = \Delta S_f^m + \int_{T_2}^{T_m} c_{p,C} \frac{dT}{T} \quad (12)$$

where ΔS_f^m is the entropy of fusion at T_m of the 100% crystalline phase in units of cal. g.⁻¹ deg.⁻¹. The other symbols are the same as those of eq. 4. Using the same values of $c_{p,L}$ and $c_{p,C}$ as used in the calculation of the heat of fusion, we find T_2 to be 261°K , which is 105° below T_g . This value confirms the conclusion of Karasz, *et al.*, that $T_g - T_2$ as estimated from calorimetric data is considerably greater than the 50° average found in the treatment of Adam and Gibbs. The ratio T_g/T_2 is 1.40, which is close to several values

of this ratio²⁷ for other substances tabulated by Adam and Gibbs, hevea rubber, glycerol, and propylene glycol, for example. Bestul and Chang²⁷ have pointed out that if the jump in specific heat per mole of chain beads at T_g is constant¹⁸ and if ΔS_0 , the excess entropy at T_g , is also a universal constant as demonstrated by Bestul and Chang (within a factor of about 2), then T_g/T_2 must be a universal constant (assuming Δc_p to be independent of temperature between T_g and T_2). Thus, our ratio of 1.40 is in line with the observations of Bestul and Chang and of Adam and Gibbs, but the difference, $T_g - T_2$, is too large for agreement with the Adam and Gibbs average value by about a factor of 2. Obviously, if T_g/T_2 is a universal constant, $T_g - T_2$ cannot be because T_g varies widely from substance to substance.

Acknowledgments. We are indebted to Drs. R. A. Boyer and F. L. Saunders of the Dow Chemical Co. for supplying us with the samples of polystyrene and for X-ray crystallinity and other data for the samples. We are grateful to Dr. F. E. Karasz and co-workers of the General Electric Co. for an opportunity of seeing their data in advance of publication and for fruitful discussions with Dr. D. M. Bodily and Dr. F. E. Karasz. This research was supported by the Advanced Research Projects Agency of the Department of Defense through the Northwestern University Materials Research Center.

(25) J. H. Gibbs and E. A. DiMarzio, *J. Chem. Phys.*, **28**, 373, 807 (1958).

(26) G. Adam and J. H. Gibbs, *ibid.*, **43**, 139 (1965). We are indebted to Professor Gibbs for the opportunity of seeing this paper in advance of publication.

(27) A. B. Bestul and S. S. Chang, *ibid.*, **40**, 3731 (1964).

Desorption of Olefins from Silica-Alumina Catalysts

by Yutaka Kubokawa

*Department of Applied Chemistry, University of Osaka Prefecture, Sakai, Osaka, Japan
(Received February 23, 1966)*

The desorption of butene-1 and propylene from silica-alumina catalysts has been studied in order to obtain information on the nature of the adsorbed carbonium ions. The activation energy of desorption of butene-1 is about 10 kcal./mole for physical adsorption and ranges from 13 to 18 kcal./mole for chemisorption. In the case of silica-alumina, the distribution of the desorption products has been determined at various temperatures and has led to the conclusion that paraffin is formed from the olefin by hydrogen transfer. The activation energy for the formation of paraffins decreases from 27 to 17 kcal./mole with increasing carbon number of the products.

Introduction

Although the cracking of hydrocarbons on acidic oxides has been explained by the carbonium ion mechanism, the nature of adsorbed carbonium ions seems to be still uncertain. As a clue to this problem, MacIver, Zabor, and Emmett¹ have investigated the chemisorption of olefins on a silica-alumina catalyst by measuring the extent of chemisorption and also the behavior of chemisorbed olefins when the temperature of the catalyst is increased. The reaction of propylene on a silica-alumina has been investigated by Shephard, Rooney, and Kemball,² who determined the distribution of the products formed during the reaction. However, it seems that the information so far obtained is still of a qualitative nature. Further study is necessary to obtain more information on the nature and the reactivity of adsorbed carbonium ions.

The present author has investigated³ chemisorption on oxide catalysts by measuring the desorption rates and has been able to obtain more complete information on the energy relations for given types of chemisorption than is obtained by the usual methods. In the present work, therefore, similar measurements have been extended to the desorption of olefins from acidic oxides, from which products other than olefins are sometimes desorbed.

Experimental

Materials. The silica-alumina catalyst containing 13% alumina was obtained from Davison Co. The alumina used in the present work was the activated

alumina supplied by The Aluminum Co. of America. The surface areas obtained by the B.E.T. method using nitrogen adsorption were 390 m.²/g. for the silica-alumina and 204 m.²/g. for the alumina catalyst. Butene-1, propylene, and ammonia were obtained from the Matheson Co. and purified by fractional distillation.

Apparatus and Procedure. The adsorbed amount was determined by using a conventional constant volume apparatus. In order to measure the rate of desorption, two U traps were attached to the reaction vessel. By cooling the two traps alternatively, the desorbed amounts were determined as a function of time without interruption; *i.e.*, the rates of desorption were determined. The desorbed products were analyzed gas chromatographically by using a 2-m. dioctyl phthalate column at 92 or 32°. Analyses were made by using standard reference compounds and by measuring peak areas.

Prior to the desorption rate measurements, butene-1 was allowed to adsorb on the catalyst for 1 hr. at -78°, and the butene remaining in the gas phase was condensed by immersing the trap attached to the reaction vessel in liquid nitrogen. Then, the rates of desorption were measured at -45° as described above. During

(1) D. S. MacIver, R. C. Zabor, and P. H. Emmett, *J. Phys. Chem.*, **63**, 484 (1959).

(2) F. E. Shephard, J. J. Rooney, and C. Kemball, *J. Catalysis*, **1**, 379 (1962).

(3) Y. Kubokawa, *Bull. Chem. Soc. Japan*, **33**, 546, 550, 555, 739, 747, 936 (1960); *J. Phys. Chem.*, **67**, 769 (1963); Y. Kubokawa and O. Toyama, *Bull. Chem. Soc. Japan*, **35**, 1407 (1962); Y. Kubokawa, S. Takashima, and O. Toyama, *J. Phys. Chem.*, **68**, 1244 (1964).

the rate measurements the temperature of the catalyst was lowered abruptly.⁴ The rates before the temperature drop were extrapolated to those for the small amount adsorbed when the measurements were carried out after the temperature drop. Thus, the rates at the two temperatures corresponded to the same amount adsorbed, and the activation energy of desorption could be obtained. Afterwards, the temperature of the catalyst was raised in stages, and similar measurements were carried out at each stage.

Before a series of experiments, the catalysts were evacuated at 500° for 12 hr. Regeneration was carried out by passing oxygen through the catalyst at 500° for 12 hr.

Results and Discussion

Activation Energies of Desorption of Butene-1. The results for the desorption of butene-1 from a silica-alumina catalyst are shown in Table I. It is seen that at -30 to -45° the activation energy of desorption is 10-11 kcal./mole and also that isomerization to butene-2 occurs even at -45°.

Table I: Desorption of Butene-1 from 6.72 g. of a Silica-Alumina Catalyst

Temp. of desorption, °C.	Remaining amt. of butene, cc., STP	Butene-1 % in the desorption products	Activation energy of desorption, kcal./mole
Before desorption ^a	233.6	100	
-45	84.5	69-80 ^b	10.4
-30	69.4	9-40 ^b	11.3
0 ^c	65.0		

^a The pressure of butene-1 before desorption was about 1 mm.

^b The remaining part consisted of butene-2 formed by isomerization. ^c In addition to butene, various kinds of hydrocarbons were desorbed.

After a certain amount of ammonia was adsorbed on silica-alumina, similar experiments produced the results shown in Table II. It is seen that the amount of butene desorbed below -45° is almost the same as that with the nontreated catalyst; however, no isomerization occurred at -45° in the case of the ammonia-treated catalyst. This suggests that, since the material can be desorbed below -45° with an activation energy of 10 kcal./mole, the adsorption is probably of a physical type and is not associated with the active sites for the isomerization.

Similar experiments were carried out with an alumina catalyst. Analysis of the desorption products showed that even at 120° the products contained only butene-1

Table II: Effect of Ammonia Adsorption upon Butene Desorption from Silica-Alumina

Temp. of desorption, °C.	Remaining amt. of butene adsorbed, cc., STP	
	37.89 cc. of NH ₃ adsorbed	16.04 cc. of NH ₃ adsorbed
Before desorption	203.9	221.6
-45	67.2	68.9
0	4.4	10.8

and butene-2, suggesting that no polymerization and cracking of butene takes place. Therefore, the activation energy of desorption of butene could be determined over a wide range of coverage. The results are presented in Figure 1. It is seen that the activation energy, determined in the temperature range -30 to -45° is 10 kcal./mole, is similar to that obtained with silica-alumina but increases with decreasing coverage up to 18 kcal./mole. Assuming that the energy of activation of 10 kcal./mole is associated with a physical adsorption, it may be concluded that the strongly chemisorbed species is desorbed with an activation energy of 13-18 kcal./mole. Amenomiya and Cvetanović⁵ have reported similar values of activation energy for the butene-alumina system.

Desorption Products from Silica-Alumina above Room Temperature. In the case of silica-alumina it was found that there were various kinds of hydrocarbon products

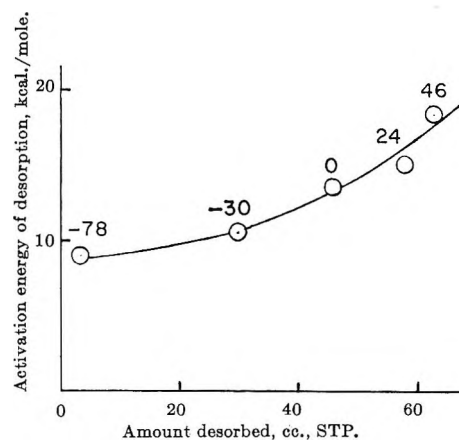


Figure 1. Activation energy of desorption of butene from alumina (6.95 g.). The numbers above the circles indicate the higher temperature in the temperature interval where the activation energy was determined. The amount adsorbed before desorption was 78.1 cc.

(4) In most cases 20-30° lower temperatures were used.

(5) Y. Amenomiya and R. J. Cvetanović, *J. Phys. Chem.*, **67**, 2046 (1963).

in the desorption above room temperature. The product distributions obtained at different temperatures are shown in Table III. It is seen that below 100°

Table III: Product Distributions for Butene-1 from Silica-Alumina^a

	Temp. range, °C.			
	27-81	81-105	122-146	146-197
Total amt. desorbed, cc. STP	0.558	0.587	2.336	3.762
Propane + propylene	0.016	0.017	0.042	0.081
Isobutane	0.016	0.024	0.098	0.206
C ₄ olefins	0.113	0.208	0.184	0.088
Isopentane	0.020	0.030	0.066	0.275
C ₆ olefins	0.018	0.029	0.036	0.044
2-Methylbutane-2	0.111	0.146	0.166	
2-Methylpentane + 2,3-dimethylbutane + 3-methylpentane	0.041	0.060	0.106	0.179
X ₁ (C ₆ or C ₇)	0.075	0.334	0.074	0.024
X ₂ (C ₇)	0.089		0.098	0.058
X ₃ (C ₈)	0.151		0.056	0.020
X ₄ (C ₈)	0.350	0.152	0.074	0.025

^a Fractions of the total amount desorbed at each temperature range.

the relative proportions of C₆ and higher hydrocarbons are much larger than those obtained at higher temperatures. Furthermore, comparison between the distribution below 80° and that at 81-105° shows that there is a reduction in C₈ hydrocarbons and a corresponding increase in the C₄₋₇ hydrocarbons at higher temperatures. In addition, it became apparent that in the consecutive desorption at 80° the amount of C₈ compounds desorbed in the first desorption was much larger than in the second and third desorptions. Such behavior suggests that polymerization of butene to C₈ hydrocarbons occurs readily below room temperature, and above 80° the decomposition to smaller molecules commences.

With regard to the distribution at 122-197°, it is concluded that the paraffin to olefin ratio is less than 1 at 122-146°, but it increases markedly at 146-197°. Furthermore, in the desorption rate measurements at a constant temperature, it was found that with increasing time of desorption the amount of olefin desorbed was decreased markedly, while that of paraffin remained almost constant. Such behavior suggests that olefins are initially formed and then converted to saturated hydrocarbons by hydrogen transfer. Moreover, it appears permissible to conclude that the desorption of olefins is easier than the conversion of olefins to saturated

compounds although the rate of the latter process, of course, depends upon the availability of hydrogen on the surface. In contrast to this, Kemball and his co-workers² found that the opposite situation held in their work; *i.e.*, the hydrogen transfer was easier than the desorption.

In the temperature range of 120-150°, the activation energy of desorption⁶ was determined for individual products with the results shown in Table IV. The values range from 27 kcal./mole for isobutane to 17 kcal./mole for C₈ hydrocarbons. It is interesting that as the carbon number of the products increases, the activation energy decreases. According to Kemball and his co-workers,² the activation energy for the formation of individual products is in the range from 10 to 14 kcal./mole; *i.e.*, it is considerably smaller than found in the present work. Although the reason for the discrepancy is not clear at the moment, it should be mentioned that under conditions used in their work the amounts of reactants adsorbed appear to vary with the reaction temperature, suggesting that their measurements do not give the true values of the activation energies. In the present work, on the other hand, the activation energies were determined in the absence of the gas phase, *i.e.*, from the temperature changes during the desorption rate measurements. It seems, therefore, unlikely that the energies of activation would be affected under such conditions by the heats of adsorption of the reactants.

Table IV: Activation Energy for the Formation of Individual Products

Product	Kcal./mole
Isobutane	27.2
Isopentane	25.1
2-Methylbutene-2	21.0
C ₆ paraffins (branched)	22.4
X ₁ (C ₆ or C ₇)	19.2
X ₃ (C ₈)	17.1

For the ammonia-treated catalyst, no extensive measurements were carried out. Only the product distributions were determined in a similar temperature range. It was found that the amount desorbed above room temperature was decreased by a factor of 5, and the ratio of paraffin to olefin was slightly decreased in the case of the ammonia-treated catalyst.

(6) In this case the activation energy of desorption has the same meaning as the activation energy for the formation.

Similar desorption experiments were carried out for the propylene-silica-alumina system. Above 80°, the activation energies for the formation of individual products, as well as the distribution of the products, were found to be almost the same as those obtained with butene-1. This suggests that above 80° identical chemisorbed layers are formed in both cases.

Acknowledgment. The author wishes to express his sincere thanks to professor P. H. Emmett of Johns Hopkins University for his helpful comments. It is also a pleasure for the author to acknowledge the help of the American Chemical Society in financing this work in the form of a Petroleum Research Fund Grant to Professor P. H. Emmett.

The Effect of Aromatic Solvents on Proton Magnetic Resonance Spectra

by Theodore L. Brown and Kurt Stark

Noyes Chemical Laboratory, University of Illinois, Urbana, Illinois (Received March 1, 1965)

The effect of aromatic solvents on chemical shift in the proton magnetic resonance spectrum has been observed for compounds of the form $(\text{CH}_3)_n\text{MX}_{4-n}$, where M is a group IV element, and X is a halogen, usually chlorine. Chemical shifts relative to tetramethylsilane (TMS) were determined in carbon tetrachloride, benzene, toluene, and mesitylene. The results are not in good accord with the hypothesis that the shifts are due mainly to solvent orientation resulting from hydrogen bonding. They are in better agreement with a model in which dipole-induced dipole interactions are responsible for solvent orientation. The quantity $(\tau_{\text{C}_6\text{H}_6} - \tau_{\text{CCl}_4})$ correlates very well with solute dipole moment for compounds of related geometry. The aromatic solvent shift may have value in certain situations as a method for estimating dipole moments.

The effect of an aromatic solvent on proton magnetic resonance chemical shifts has been discussed by several workers.¹⁻¹¹ Solute protons generally experience a high-field shift, but its magnitude varies widely from one solute to another. It is commonly accepted that the shift arises predominantly from the large diamagnetic anisotropy of aromatic solvent molecules, which in turn owes its origin to the relatively free circulation of π -electrons in the molecular plane.

The magnitude of shift predicted theoretically for complete averaging over the solvent molecule surface is small in comparison with many observed shifts.⁶ Other nonspecific effects may contribute to a larger value for δ ,⁶ but the magnitude of the observed effects for many solutes requires that the time-averaged location of the solute protons relative to the aromatic solvent molecules is preferentially along the sixfold axis normal

to the plane of the ring. Hydrogen bonding of solute protons to the ring has been suggested to account for

- (1) A. A. Bothner-By and R. E. Glick, *J. Chem. Phys.*, **26**, 1651 (1957).
- (2) L. W. Reeves and W. G. Schneider, *Can. J. Chem.*, **35**, 251 (1957).
- (3) T. Schaefer and W. G. Schneider, *J. Chem. Phys.*, **32**, 1224 (1960).
- (4) A. D. Buckingham, T. Schaefer, and W. G. Schneider, *ibid.*, **32**, 1227 (1960).
- (5) A. D. Buckingham, T. Schaefer, and W. G. Schneider, *ibid.*, **34**, 1064 (1961).
- (6) R. J. Abraham, *Mol. Phys.*, **4**, 369 (1961).
- (7) R. J. Abraham, *J. Chem. Phys.*, **34**, 1062 (1961).
- (8) T. Schaefer and W. G. Schneider, *ibid.*, **32**, 1218 (1960).
- (9) J. V. Hatton and W. G. Schneider, *Can. J. Chem.*, **40**, 1285 (1962).
- (10) J. V. Hatton and R. E. Richards, *Mol. Phys.*, **5**, 139 (1962).
- (11) (a) W. G. Schneider, *J. Phys. Chem.*, **66**, 2653 (1962); (b) P. Diehl, *J. chim. phys.*, **61**, 19E (1964).

the solvent shift in many cases.¹⁻⁶ The effect of solute molecular shape⁴ and the orienting influence of solute dipole moment¹¹ have also been mentioned as possible factors.

We have examined the aromatic solvent shift in a series of closely related compounds of the general form $(\text{CH}_3)_n\text{MX}_{4-n}$, where M is a group IV element, and where X is a halogen, usually chlorine. This series of substances is well suited to a test of the hypothesis that hydrogen bonding accounts for extraordinary aromatic solvent shifts; the symmetries are well defined and the compounds are closely similar in over-all shape and geometry. Further, useful proton coupling constant data are readily obtained.

The chemical shifts of all compounds investigated were measured relative to tetramethylsilane (TMS) in carbon tetrachloride, benzene, toluene, and mesitylene as solvents. The use of TMS as an internal standard is particularly apt for the purposes of this work, as effects other than those arising from solute-solvent interactions are all but eliminated in the comparison. All chemical shifts reported are essentially infinite dilution values.

Results and Discussion

Hydrogen bonding has been proposed as an explanation for most large diamagnetic (upfield) shifts of solute proton resonances relative to the shifts exhibited by a nonpolar reference compound such as neopentane, cyclohexane, or TMS. We begin, therefore, by examining the data in Table I in terms of the hydrogen-bonding hypothesis.

The ^{13}C -H coupling constants provide a measure of the acidity of hydrogen bound to carbon. This follows from the relationship between coupling constant and fractional s character in the carbon orbital on the one hand,¹² and the increase in electronegativity of the carbon orbital with increasing s character on the other.¹³ There should be a monotonic relationship between $J_{^{13}\text{C}-\text{H}}$ and the acidity of the proton. If hydrogen-bonding propensity is related to acidity of the proton, as is generally supposed, the degree of hydrogen bonding to aromatic solvents should increase with increase in $J_{^{13}\text{C}-\text{H}}$. Figure 1 shows the chemical shifts of the solute protons in benzene, relative to carbon tetrachloride (all related to TMS) graphed vs. $J_{^{13}\text{C}-\text{H}}$ for the methyl-group protons. A regularity in the relationship is discernable for compounds other than the chlorosilanes. Whatever interpretation is put on the low values of $J_{^{13}\text{C}-\text{H}}$ for the latter compounds, the failure of the relationship between $J_{^{13}\text{C}-\text{H}}$ and $\Delta\tau$ in these instances is not in good accord with the

Table I: Chemical Shift Data for Organomethyl Compounds in Various Solvents

Compd.	CCl_4	$\Delta\tau$			$J_{^{13}\text{C}-\text{H}}$ (neat)	μ , D.
		C_6H_6	$\text{CH}_3\text{C}_6\text{H}_5$	$(\text{CH}_3)_2\text{C}_6\text{H}_3$		
CH_3SnCl_3	8.353	1.432	1.327	1.126	143	3.6
$(\text{CH}_3)_2\text{SnCl}_2$	8.835	0.825	0.763	0.635	137.8	4.2
$(\text{CH}_3)_3\text{SnCl}$	9.368	0.402	0.368	0.312	133	3.5
CH_3SnBr_3	8.148	1.228	1.118	1.042	141.1	3.2
CH_3SnI_3	7.68	1.02	0.90	0.86	140.1	2.6
$(\text{CH}_3)_4\text{Sn}$	9.292	0.091	0.032	0	128	0
CH_3SiCl_3	8.86	0.74	0.67	0.59	126	1.9
$(\text{CH}_3)_2\text{SiCl}_2$	9.249	0.396	0.367	0.311	124.5	2.3
$(\text{CH}_3)_3\text{SiCl}$	9.578	0.244	0.224	0.201	120.5	2.1
CH_3CCl_3	7.257	0.594	0.588	0.502	134.2	1.5
$(\text{CH}_3)_2\text{CCl}_2$	7.828	0.407	0.350	0.290	131.8	2.2
$(\text{CH}_3)_3\text{CCl}$	8.404	0.226	0.224	0.208	127	2.2
$(\text{CH}_3)_4\text{C}$	9.090	0.018	0.018	0	124	0
CH_3HgBr	8.817	1.158	3.1
CH_3HgI	8.750	1.104	2.9
$(\text{CH}_3)_2\text{Hg}$	9.714	0.153	130	0

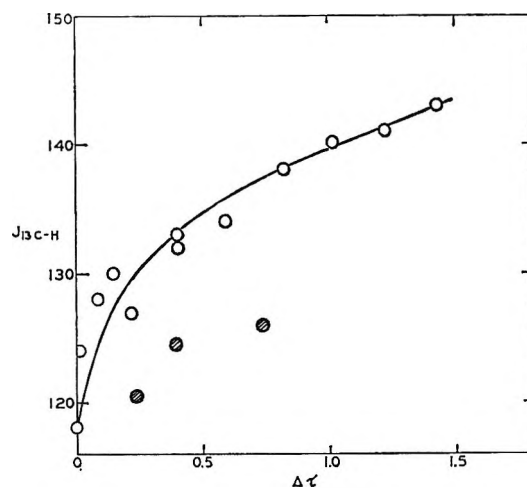


Figure 1. ^{13}C -H coupling constant vs. $\Delta\tau$, the diamagnetic solvent shift in benzene as compared with carbon tetrachloride solution (tetramethylsilane as reference in both solvents). The chlorosilane data are represented by shaded circles.

notion that $\Delta\tau$ is due predominantly to hydrogen bonding.

It is true for every solute in Table I that $\Delta\tau$ decreases in the order benzene > toluene > mesitylene. This is just the reverse of the order of solvent basicity, and therefore of the expected order of enthalpies for hydrogen bonding. The observed $\Delta\tau$ values represent

(12) (a) N. Muller and D. E. Pritchard, *J. Chem. Phys.*, **31**, 768, 1471 (1959); (b) J. N. Schoolery, *ibid.*, **31**, 1427 (1959); (c) C. Juan and H. S. Gutowsky, *ibid.*, **37**, 2198 (1962).

(13) J. Hinze and H. H. Jaffé, *J. Am. Chem. Soc.*, **84**, 540 (1962).

an average value for all solute species. Assuming for simplicity that there is a narrow range of $\Delta\tau$ values, centered at $\Delta\tau_n$, which characterizes nonhydrogen-bonded solute protons, and another narrow range centered at $\Delta\tau_b$ which characterizes the hydrogen-bonded moieties, the observed quantity is $\Delta\tau_0 = F_n\Delta\tau_n + F_b\Delta\tau_b$. Letting $\Delta\tau_b = \Delta\tau_n + \epsilon$, then $\Delta\tau_0 = F_n\Delta\tau_n + F_b(\Delta\tau_n + \epsilon) = \Delta\tau_n + \epsilon F_b$. ϵ is likely to be related to the enthalpy change, whereas F_b is a function of the free energy change. ϵ should increase in the order benzene < toluene < mesitylene. The equilibrium constant for hydrogen-bond formation must therefore decrease in the order benzene > toluene > mesitylene. It is not easy to accept the proposition that steric factors could so affect K_{equil} for hydrogen-bond formation for every solute studied. There is evidence that for many solutes K_{equil} is in the order mesitylene > toluene > benzene.^{14,15} We conclude, therefore, that specific hydrogen bonding is not responsible for a major share of the observed $\Delta\tau$ values in the solutes examined. The magnitudes of many of the $\Delta\tau$ values listed in Table I are as large as any yet reported in the literature (*e.g.*, for chloroform²). The hypothesis that hydrogen bonding (*i.e.*, the formation of specific 1:1 complexes) plays a *major* role in producing large diamagnetic shifts in *any* solute is open to serious question.

It has been reported that group IV halides and related compounds such as the haloforms form charge-transfer complexes with aromatic solvents.¹⁶ This kind of complex formation is possible for the more acidic of the solutes which we have studied, *e.g.*, CH_3SnCl_3 .

We have examined the ^{119}Sn -C-H coupling constants in all the tin compounds to determine whether this quantity shows a dependence on aromatic solvent. On the basis of previous work^{17,18} one expects that if discrete complex formation occurs, with consequent increase in the coordination about tin, $J_{\text{Sn-C-H}}$ should change. There is evidence (Table II) of a small increase in $J_{\text{Sn-C-H}}$ in mesitylene as compared with benzene for CH_3SnCl_3 , but the effect is slight, and is not seen in CH_3SnBr_3 . We conclude that any charge-transfer complex formation which occurs does not significantly affect the coordination about tin, nor in all probability does it affect the chemical shift of the methyl-group protons.

If specific hydrogen-bond formation is excluded as the major cause of the observed $\Delta\tau$ values, there remain solute-solvent interactions of a more general kind. For polar solutes, an orientation of solvent molecules through dipole-induced dipole interactions is the most important effect to be considered. All of

Table II: ^{119}Sn -C-H Coupling Constants^a of Methyltin Compounds in Various Solvents

Compd.	Solvent				
	CCl_4	C_6H_6	$\text{CH}_2\text{C}_6\text{H}_5$	$(\text{CH}_3)_2\text{C}_6\text{H}_3$	Neat
CH_3SnCl_3	99.4	99.5	99.3	101.2	100.0
$(\text{CH}_3)_2\text{SnCl}_2$	69.5	68.8	69.8	72.1	...
$(\text{CH}_3)_3\text{SnCl}$	59.3	58.8	58.6	59.2	60.2
CH_3SnBr_3	88.4	89.1	89.4	88.3	88.6
CH_3SnI_3	74.5	72.7
$(\text{CH}_3)_4\text{Sn}$	54.2	54.7	54.0	54.5	54.0

^a Estimated uncertainty is ± 0.5 c.p.s.

the solutes examined here have an axis of symmetry along which the molecular dipole moment is oriented. The aromatic molecules are more polarizable in the molecular plane than normal to it ($\alpha_{\perp} = 6.35 \text{ \AA}^3$, $\alpha_{\parallel} = 12.3 \text{ \AA}^3$)¹⁹; further, a closer approach to the solute molecules can be made along the sixfold axis than in the molecular plane, because of the hindrance presented by hydrogens or methyl groups. These qualitative considerations suggest that there should be a time-averaged orientation of solvent molecules with the plane of the ring parallel to the solute molecular dipole moment. Protons of the solute methyl groups will, therefore, experience an averaged solvent environment which presents the protons with solvent molecules along the sixfold axes of the latter. The solute protons may not all be simultaneously exposed to the solvent environment. Figure 2 depicts solute molecules containing three, two, or one methyl groups, viewed in each case along the symmetry axis. Solvent molecules, assumed for simplicity to lie parallel to the solute dipole axis, are also shown schematically as oriented normal to the plane of the paper. The purpose of the figure is to show in a crude way how the fractional exposure of protons to solvent molecules varies with the number of methyl groups. The axis of the CH_3 group is, of course, tilted differently with respect to the plane of the paper in the three cases. However, assuming free rotation about the C-M bond, the average angle between a C-H bond and the dipole axis is not greatly different in the three cases. If it is assumed that only solvent orientations parallel

(14) Z. Yoshida and E. Osawa, *J. Am. Chem. Soc.*, **87**, 1467 (1965).

(15) M. R. Basila, E. L. Saier, and L. R. Cousins, *ibid.*, **87**, 1665 (1965).

(16) F. Dörr and G. Buttgerit, *Ber. Bunsenges.*, **67**, 867 (1963). However, see W. B. Person, *J. Am. Chem. Soc.*, **87**, 167 (1965).

(17) J. R. Holmes and H. D. Kaesz, *ibid.*, **83**, 3903 (1961).

(18) N. A. Matwiyoff and R. S. Drago, *Inorg. Chem.*, **3**, 337 (1964).

(19) Landolt-Bornstein, "Zahlenwerte und Functionen," Vol. I, Pt. 3, J. Springer-Verlag, Berlin, 1951, p. 510.

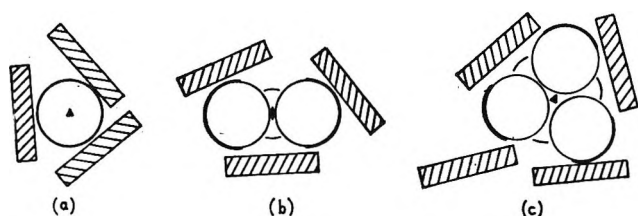


Figure 2. A schematic illustration of the orientation of solvent molecules (viewed along the molecular plane, and shown as rectangles) about solute molecules containing (a) one, (b) two, or (c) three methyl groups. The heavy lines represent the angular segment about each methyl group in which the protons are in contact with the solvent. The solute molecule in each case is viewed along the dipolar (symmetry) axis.

to the solvent molecule axis contribute to $\Delta\tau$, then the relative exposure of solute protons to such oriented solvent molecules is estimated to be: $(\text{CH}_3)_3\text{MX}$, 1.0; $(\text{CH}_3)_2\text{MX}_2$, 1.5; and CH_3MX_3 , 3.0.

The $\Delta\tau$ values observed in benzene for all compounds studied are graphed in Figure 3 vs. the molecular dipole moments.²⁰ For compounds containing equal numbers of methyl groups the relationship is nicely regular, and is adequately approximated as linear. It should be noted that the graph includes the methylchlorosilane data, and that the line for the monomethyl compounds includes compounds other than those in the group IV series. The slopes of the lines are 0.115, 0.188, and 0.384 p.p.m./D. These are in the ratio 1:1.6:3.3, in remarkably good agreement with the estimated relative exposures of protons to solvent environment.

The results shown in Figure 3 are in excellent accord with the hypothesis that dipole-induced dipole orientation of solvent molecules is responsible for the observed $\Delta\tau$ values. The diminished solvent effect in toluene, and still further in mesitylene, is ascribed to steric hindrance which impedes simultaneous packing of solvent molecules about a particular solute. A relationship between $\Delta\tau$ and μ should be observed for any series of suitably related compounds. The relationship shown in Figure 3 for the monomethyl compounds can be expected to hold also for other compounds in which a methyl group is located on the molecular axis, and which have roughly similar shape. Methyl iodide and acetonitrile, for example, with molecular dipole moments of 1.48 and 3.5 D,²⁰ respectively, exhibit corresponding $\Delta\tau$ values in benzene of 0.667 and 1.016. The methyl iodide datum falls close to the line in Figure 3, whereas the acetonitrile point is rather far off. But acetonitrile has a much smaller molecular volume than the other solutes; the packing

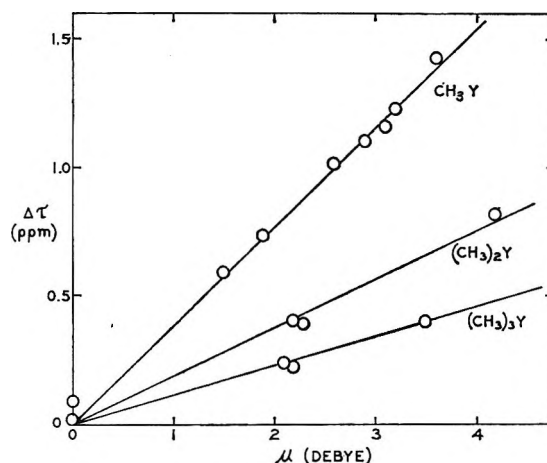


Figure 3. Dipole moment vs. $\Delta\tau$, the diamagnetic shift in benzene as compared with carbon tetrachloride solution.

of solvent molecules about the protons is probably not similar.

The present results, as well as those reported by others,¹¹ suggest that the aromatic solvent shift of proton magnetic resonances could be made the basis of a method for estimating dipole moments. It is obvious that the method would be largely empirical, and that it could not compete in accuracy with the conventional dielectric constant method. It would, on the other hand, possess the singular advantage that it could be applied to the components of mixtures, for estimation of dipole moment, for distinguishing isomers on the basis of polarity, and for other like purposes.

Experimental

Materials. All solutes employed were purified before use. Methyltin tribromide and methyltin triiodide were synthesized; all other solute compounds were obtained from commercial sources. Methyltin tribromide was synthesized by the method described by Krause and Grosse.²¹ The triiodide was prepared by reaction of methyltin trichloride with potassium iodide in liquid SO_2 .

The solvents employed were all reagent grade; benzene, toluene, and mesitylene were dried, distilled and stored over sodium wire. (Solutions of methyltin

(20) All dipole moment data not determined in our laboratory (see Experimental) were taken from "Tables of Experimental Dipole Moments," A. L. McClellan, Ed., W. H. Freeman and Co., San Francisco, 1963. The quality of the data of course varies from one solute to another, but the dipole moments are probably relatively correct to 0.2 D.

(21) (a) CH_3SnBr_3 was prepared from CH_3SnOOH by heating the latter with concentrated aqueous HBr : E. Krause and A. V. Grosse, "Die Chemie der Metallorganische Verbindungen," G. Borntraeger, Berlin, 1937, p. 341; (b) CH_3SnOOH was obtained by reacting SnCl_2 with CH_3I in EtOH and precipitating the acid with CO_2 : P. Pfeiffer and R. Lehnardt, *Chem. Ber.*, 36, 3028 (1903).

trichloride in mesitylene turn a violet color during the course of an hour or so after the solutions are made up. The origin of this color was not fully investigated, but it was ascertained that its appearance is not accompanied by any observable change in the proton magnetic resonance spectrum.)

N.m.r. Spectra. The proton magnetic resonance spectra were obtained for the most part on a Varian Associates Model A-60 spectrometer. Chemical shifts are accurate to ± 0.01 p.p.m.; coupling constants are accurate to within about 0.5%. The reported chemical shifts were obtained from measurements on solutions of varying concentration (2–10%) and extrapolation to infinite dilution. Only small concentration dependences of the J values were noted.

Dipole Moment Determinations. The dipole moments of methyltin tribromide and triiodide, and of methylmercuric bromide and iodide have not been reported heretofore. The dielectric constants of dilute solutions of these compounds in benzene were measured as described previously.²² The relevant results are summarized in Table III. Total polarization is calculated by the method of Halverstadt and Kumler,²³ with slight modification.^{22a} Allowance for atomic and electronic polarization in these compounds presents some difficulties. For nonpolar SnBr_4 and SnI_4 , P_E are 46.8 and 66.0 cm^3 , respectively.^{24,25} For $\text{Sn}(\text{CH}_3)_4$, with d_{25} 1.295, n_D 1.4932, the molar refraction is 40.1 cm^3 , from which the SnC bond refraction is estimated to be 5.0 cm^3 . From these results we obtain P_E for CH_3SnBr_3 and CH_3SnI_3 . We estimate

P_A to be 0.75 of the corresponding values for SnBr_4 and SnI_4 .^{24,25} Proceeding similarly with P_T data for $(\text{CH}_3)_2\text{Hg}$,²⁶ HgI_2 , and HgBr_2 ,²⁵ we obtain the estimates of P_E and P_A shown in Table III.

Table III: Dipole Moments of Methyltin and Methylmercuric Halides in Benzene

Compd.	α^a	β^b	P_T , cm^3	P_E , cm^3	P_A , cm^3	μ (at 25°)
CH_3SnBr_3	3.20	-0.80	262	45.1	6.6	3.20
CH_3SnI_3	1.70	-0.82	212	59.5	10.9	2.64
CH_3HgBr	3.80	-0.9	231	26.0	4.0	3.1
CH_3HgI	3.00	-1.0	210	33.1	6.0	2.9

^a $\alpha = \partial\epsilon/\partial w_2$, where w_2 is weight fraction. ^b $\beta = \partial\nu/\partial w_2$, where ν is specific volume in cubic centimeters per gram.

Acknowledgment. This research was supported by a research grant from the National Science Foundation. K. S. expresses his appreciation for a Fullbright Travel Grant.

(22) (a) T. L. Brown, *J. Am. Chem. Soc.*, **81**, 3232 (1959); (b) T. L. Brown, J. G. Verkade, and T. S. Piper, *J. Phys. Chem.*, **65**, 2051 (1961).

(23) I. F. Halverstadt and W. D. Kumler, *J. Am. Chem. Soc.*, **64**, 2988 (1942).

(24) S. E. Coop and L. E. Sutton, *J. Chem. Soc.*, 1269 (1938).

(25) Reference 19, p. 514.

(26) H. Sawatzky and G. F. Wright, *Can. J. Chem.*, **36**, 1555 (1958).

Vaporization, Thermodynamics, and Dissociation Energy of

Lanthanum Monosulfide¹

by E. David Cater, Thomas E. Lee, Ernest W. Johnson,

Department of Chemistry, University of Iowa, Iowa City, Iowa

Everett G. Rauh,

Argonne National Laboratory, Argonne, Illinois

and Harry A. Eick

Department of Chemistry, Michigan State University, East Lansing, Michigan (Received March 1, 1965)

The congruent vaporization of lanthanum monosulfide has been studied over the temperature range 2012 to 2490°K. by the effusion technique with the aid of vacuum balance and mass spectrometer. The principal vapor species is LaS, and calculation shows that 3 to 10% of the vapor is La + S. The vapor pressure of solid LaS is given by $\log P_{\text{atm}} = 7.365 - 2.873 \times 10^4/T$. The heat and entropy of sublimation at 2240°K. are $\Delta H^\circ_{2240} = 131.5 \pm 1.0$ kcal./mole and $\Delta S^\circ_{2240} = 33.5 \pm 0.6$ e.u. Estimated thermal data yield $\Delta H^\circ_{298} = 141.4 \pm 2.0$ and $\Delta H^\circ_0 = 141.7 \pm 2.0$ kcal./mole. The dissociation energy of gaseous LaS is 137 ± 6 kcal./mole or 5.9 ± 0.2 e.v. The quoted uncertainty for ΔH°_{2240} is the statistical standard deviation; the other uncertainties are estimated limits of accuracy, and the values apply if the ground state of LaS(g) is ⁴Σ. The lattice parameter of LaS at room temperature is 5.854 ± 0.002 Å. The melting point of LaS is at least as high as $2327 \pm 20^\circ$.

Introduction

Recent work on the dissociation energies of gaseous oxides, particularly of metals, has resulted in several summary papers²⁻⁴ in which the periodic behavior and bonding have been discussed. It is of interest to obtain quantitative data on dissociation energies of sulfide molecules for comparison with the oxides to aid in the understanding of the bonding. Lanthanum monoxide, one of the most stable gaseous monoxides, has a dissociation energy of 8.3 e.v.⁵ Thus, by analogy one expects a reasonable stability for a gaseous lanthanum monosulfide molecule. This paper combines the results of two independent investigations of the sublimation of lanthanum monosulfide carried out at the University of Iowa (UI) and Argonne National Laboratory (ANL) to obtain the dissociation energy of gaseous LaS as well as to characterize the thermodynamics of sublimation of solid LaS.

Materials

Previous studies on and the means of preparation of the solid phases in the lanthanum-sulfur system are summarized by Flahaut⁶ and by Samsonov and Radzikovskaya.⁷ The known solid phases are LaS,

(1) Based in part on work performed under the auspices of the U. S. Atomic Energy Commission. Taken in part from the M.S. Thesis of Thomas E. Lee and the Ph.D. Thesis of Ernest W. Johnson, University of Iowa, 1964.

(2) R. J. Ackermann and R. J. Thorn, in "High Temperature Technology," proceedings of a symposium, Stanford Research Institute, 1963.

(3) M. S. Chandrasekharaiah, *J. Phys. Chem.*, **68**, 2020 (1964).

(4) R. J. Ackermann and R. J. Thorn, in *Progr. Ceram. Sci.*, **1**, 39 (1961).

(5) R. J. Ackermann, E. G. Rauh, and R. J. Thorn, *J. Chem. Phys.*, **40**, 883 (1964).

(6) J. Flahaut, *Bull. soc. chim. France*, 1282 (1960).

(7) G. V. Samsonov and S. V. Radzikovskaya, *Russ. Chem. Rev.*, **30**, 28 (1961).

La₃S₄, La₂S₃, LaS₂, and an oxysulfide, La₂O₂S. The phases La₃S₄ and La₂S₃ are probably limiting compositions in a single-phase region.⁸ The monosulfide, LaS, is a refractory, gold-colored, metallic-looking solid with the NaCl-type crystal structure. We have prepared monosulfide samples by a variety of techniques: (1) direct union of stoichiometric amounts of the elements in an initially evacuated fused-silica tube; (2) reaction of excess H₂S with finely divided metal (produced by decomposition of the hydride under vacuum) to give the yellow sesquisulfide, followed by reduction to LaS with La₂O₃ + La at high temperatures; (3) reaction of H₂S with La₂O₃ to produce the oxysulfide or sesquisulfide, followed by reduction to the monosulfide with carbon or lanthanum metal. In all cases the product was homogenized by annealing under high vacuum in tungsten or molybdenum crucibles inductively heated to temperatures from 1800 to 2100°. After the samples had been heated for several hours at elevated temperatures, the background pressure dropped below 10⁻⁶ torr, and the heating was discontinued. Debye-Scherrer patterns of the materials were taken with Norelco cameras of 11.4-cm. diameter and copper radiation of wave length K α_1 1.54050 Å. Only from samples heated to high temperatures were lines of LaS obtained. Those samples chosen for vaporization studies had patterns containing only lines of LaS or LaS with a barely detectable second phase, La₃S₄. Lattice parameters of LaS samples annealed for long periods under high vacuum, and residues from actual vapor pressure studies were constant within the precision of measurement. For example, values of 5.852 to 5.857 Å. and 5.854 to 5.855 Å. were obtained, respectively, from samples coexisting with La₃S₄ and from residues from vaporization measurements which contained only LaS. Presumably, there is essentially no solid solubility of sulfur in LaS. Our "best value" for the lattice parameter is 5.854 ± 0.002 Å., compared to previously reported values of 5.788,⁹ 5.860,⁶ 5.842,^{10a} and 5.84.^{10b} For La₃S₄ our values of 8.722 ± 0.005 and 8.717 ± 0.002 Å. may be compared with the previously reported value of 8.730 Å.¹¹ Diffraction lines of oxide phases were not obtained from samples used in the vaporization studies. The methods of preparation and the purity of the starting materials precluded contamination of the samples with measurable impurities other than oxygen.

During both weight loss and mass spectrometric effusion studies, once a small percentage of the sample had been vaporized so that oxygen contamination was eliminated (see below), it was found that the vaporization behavior became univariant and reproducible with temperature until the sample was essen-

tially completely vaporized. LaS remained the predominant vapor species. We conclude that the sublimation of lanthanum monosulfide is congruent and assume that any deviations from stoichiometry during the measurements at high temperatures may be neglected in calculating the thermodynamic properties reported herein.

To determine the melting point, samples of LaS were inductively heated under vacuum at successively higher temperatures in a sintered tungsten effusion cell, and the residues were observed after each heating. After heatings at 2220 and 2300° no indication of melting was found. On being heated to 2327 ± 20° for 4 min., a 53-mg. sample lost 17 mg. by effusion, 10 mg. was sublimed to the underside of the lid, and 26 mg. disappeared by diffusion into the bottom of the cell, perhaps as a liquid since such diffusion had not occurred at lower temperatures. The melting point of LaS is thus at least 2327 ± 20°, but may be higher. Flahaut reports⁶ that a sample of LaS did not melt at 2200°. Another reported melting point⁹ of 1970° may have been low because of eutectic formation.

Vacuum Balance Measurements

Absolute rate of effusion measurements were performed at UI. An Ainsworth recording vacuum balance Type RV-AU-2 was evacuated through a liquid nitrogen trap by an oil diffusion pump using silicone oil. The effusion cell was suspended from one balance arm by two tungsten wires, 0.1-cm. diameter and approximately 84-cm. length, into a water-jacketed, fused-silica condenser which had a sighting window and prism at its bottom. A 1 × 2-cm. glass plate, rotatable by means of a ball and socket joint, was located between the suspension wires about 23 cm. above the effusion cell to prevent swinging of the cell during heating. The effusion cells were of sintered tungsten¹² of approximately 80% of theoretical density; their design was essentially that of Ackermann and Rauh.¹³ The orifices were of 0.125-cm. nominal diameter and of 0.125-cm. nominal depth. A traveling microscope was used to measure actual orifice diameters. The values were corrected for thermal expansion for calculation of vapor pressures. A radiation shield of strips of tantalum, 1 cm. wide by 10 cm. long,

(8) W. H. Zachariassen, *Acta Cryst.*, **2**, 57 (1949).

(9) M. Picon and M. Patrie, *Compt. rend.*, **242**, 1321 (1956).

(10) As cited in ref. 2: (a) A. Iandelli, *Gazz. chim. ital.*, **85**, 881 (1955); (b) N. P. Zvereva, *Dokl. Akad. Nauk SSSR*, **113**, 333 (1957).

(11) M. Picon and J. Flahaut, *Compt. rend.*, **243**, 2074 (1956).

(12) Obtained from Philips Metalonics.

(13) R. J. Ackermann and E. G. Rauh, *J. Chem. Phys.*, **36**, 448 (1962).

surrounded the cell. Temperatures were measured by means of a Leeds and Northrup disappearing-filament optical pyrometer that had been calibrated by intercomparison with a pyrometer which had been calibrated at ANL by the method of rotating sectors.¹⁴ During weight loss measurements the pyrometer was sighted into a blackbody hole (0.125 cm. in diameter and 0.70 cm. deep) in the bottom of the effusion cell. An intercomparison of temperatures measured in orifice and blackbody hole was made, and the reported experimental temperatures correspond to orifice temperatures. All temperatures were corrected for transmissivity of window and prism. The effusion cell was heated inductively by power generated in a coil of flattened copper tubing by a Ther-monic Model 2500 generator. Background pressure, measured by a cold cathode ionization gauge, was less than 5×10^{-6} torr during all effusion measurements.

Thirty weight loss measurements were made in the temperature range 2066 to 2348°K. Apparent weight losses ranged from 0.03 to 9.43 mg., and heating times were from 30 to 370 min. In all cases the suspension of the previously weighed effusion cell was clamped to preclude swinging, and then power was applied to heat the cell as rapidly as possible to the desired temperature. The temperature was maintained for the desired time (and measured at intervals during this time) after which the power was shut off. The effusion cell suspension was then unclamped and the weight recorded for 3 to 15 min. until constant weight was obtained. Continuous weighing during heating was not possible because of the forces exerted by the high-frequency field on the effusion cell. Occasional manual power adjustment maintained the temperature constant within $\pm 6^\circ$. The time required for the cell to reach temperature (less than 1 min.) was always short relative to the time at temperature. Data were taken in several series of increasing and decreasing temperatures. The effusion cell was maintained under vacuum at all times, except that more sample was added after the third weight loss measurement.

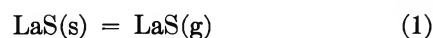
The 12 measurements with weight losses greater than 1.9 mg. were arbitrarily retained for calculation of vapor pressures, and these data are recorded in Table I and plotted in Figure 1. These points were all among the last 18 taken. Analysis of the data from all 30 weight loss measurements showed a very large scatter around a straight line in a plot of $\log p$ vs. $1/T$, particularly among points of least weight loss. However, no trend due to length of heating time, order of temperature, or total elapsed weight loss was apparent. It was felt that static charges on the cell were responsible for the scatter in the data, which for weight losses

Table I: Data from Vacuum Balance Experiments^a

Expt. no.	Time, min.	T, °K.	Wt. loss, mg.	Log 10 ⁷ p, atm.	10 ⁴ /T, °K. ⁻¹	Third-law ΔH° , kcal./mole
19	30	2297	2.00	1.929	4.354	141.0
21	45	2299	2.85	1.907	4.350	141.3
23	60	2289	2.90	1.789	4.369	142.0
25	240	2243	5.64	1.469	4.458	142.6
26	30	2348	3.02	2.113	4.259	141.9
27	60	2321	2.70	1.761	4.308	144.1
29	195	2166	1.95	1.093	4.617	141.8
32	370	2143	5.60	1.271	4.666	138.7
33	120	2210	2.47	1.411	4.525	141.3
34	120	2261	4.52	1.678	4.423	141.1
35	90	2289	4.20	1.774	4.369	142.1
36	90	2347	9.43	2.130	4.261	141.6
Av. (no. 27 and 32 omitted)						141.7

^a Orifice area = 0.01413 cm.² at temperature.

between 0.3 and 1.0 mg. corresponded to up to $\pm 65\%$ of the pressure. Thus, the arbitrary 1.9-mg. cutoff was made. For calculation of pressures it was assumed that the vaporization occurred entirely according to the process



Pressures in Table I were calculated from the Knudsen equation¹⁵

$$P_{\text{atm}} = 0.022557 \frac{w}{at} \sqrt{T/M} \frac{K_s}{K_c} \quad (2)$$

in which w is the weight loss in grams, a the orifice area in cm.², t the time in seconds, T the temperature in degrees Kelvin, and M the molecular weight of LaS, 170.95; $K_c = 0.8013$ is the so-called Clausing factor¹⁶ for an orifice of length equal to its diameter; $K_s = 1.048$ is a correction^{5,13} applied to account for vapor condensing on the suspension wires.

An unweighted least-squares treatment of $\log P$ vs. $1/T$ yields, after rejection of points 27 and 32 which had excessive residuals

$$\log P_{\text{atm}} = (7.47 \pm 0.65) - (28960 \pm 1480)/T \quad (3)$$

The quoted uncertainties are statistical standard deviations. This equation is of the form

(14) See, for example, R. J. Thorn and G. H. Winslow, "Recent Developments in Optical Pyrometry," paper 63-WA-224 presented before the Annual Meeting of the American Society of Mechanical Engineers, Nov. 17-23, 1963.

(15) See, for example, the discussion of S. Dushman and J. M. Lafferty in "Scientific Foundations of Vacuum Technique," 2nd Ed., John Wiley and Sons, Inc., New York, N. Y., 1962.

$$\log P = \frac{\Delta S^\circ}{2.303R} - \frac{\Delta H^\circ}{2.303RT} \quad (4)$$

The slope and intercept yield for the sublimation of LaS at the temperature 2240°K. in the middle of the range $\Delta H^\circ_{2240} = 132.5 \pm 6.8$ kcal./mole and $\Delta S^\circ_{2240} = 34.17 \pm 2.97$ e.u.

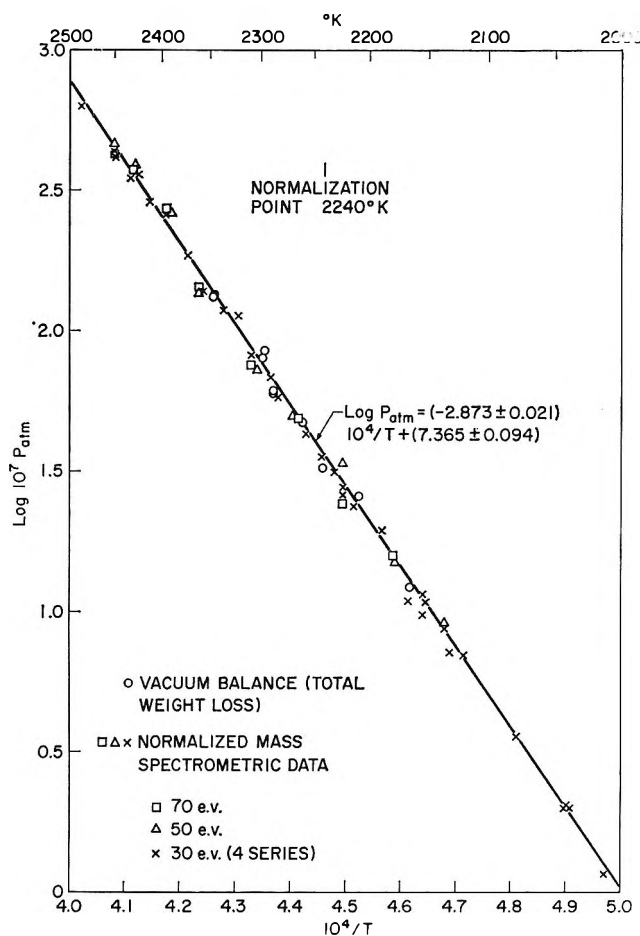


Figure 1. Temperature dependence of vapor pressure of LaS from vacuum balance (total weight loss) and mass spectrometric measurements. Mass spectrometric data normalized at 2240°K.

Mass Spectrometric Studies

The vaporization of LaS from tungsten cells was studied mass spectrometrically both at ANL and UI. In each case the spectrometer employed was a Bendix Model 12-101 time-of-flight instrument operated in the pulsed mode. At UI a standard Bendix Knudsen cell assembly was used; at ANL, the same cell as has been described previously.¹³ In both studies it was found that the principal ion currents observed were due to LaO⁺, LaS⁺, La⁺, and S⁺. No polymers of these

species were detected. The LaO⁺, due to vaporization of LaO(g) from samples containing slight oxygen contamination, eventually disappeared below the limit of detectability.

Rough appearance potential curves obtained at UI are shown in Figure 2. The energy scale was determined by equating the appearance potential of the ion at mass 28 to the ionization potential of N₂, 15.6 v.¹⁶ (The fragmentation behavior indicated the peak to be predominantly N₂ rather than CO.) The appearance potentials of LaO⁺ and LaS⁺, approximately 5 v., indicate these to be primary ions. The appearance potential of La⁺, about 12 v., shows it to be predominantly a fragment since the first ionization potential of La is 5.6 v.¹⁶

At ANL, measurements were made of ion currents of La⁺, LaS⁺, and S⁺ as a function of temperature at electron energies from 20 to 70 v. Temperatures were measured by sighting directly into the orifice of the effusion cell with a Leeds and Northrup optical pyrometer which had been calibrated by the method of rotating sectors.¹⁴ The general apparatus and procedure were essentially the same as described by Ackermann and Rauh.¹³ Four sets of data were obtained from two different samples of LaS at temperatures from 2012 to 2490°K. Slopes were calculated by least-squares treatment of $\log I^+T$ vs. $1/T$. Since the product of ion current and temperature (I^+T) is proportional to the partial pressure of a species, the slopes are presented in Table II as heats of vaporization in units of kcal./mole. It is seen that slopes for La⁺ and S⁺ are the same, within the experimental uncertainty, as those for LaS⁺ at various energies. Furthermore, all are in agreement with the second-law heat of vaporization of LaS obtained from the vacuum balance. This indicates again that LaS⁺ is a primary ion and La⁺ and S⁺ are predominantly fragments. In the final section of the paper calculations are presented which show that the partial pressures of La and S in equilibrium with LaS at 2240°K. are less by a factor of 10 to 20 than that of LaS.

Several other sets of data were obtained but are not reproduced here because the results were identical, within the experimental errors, with those in Table II. For use in the final calculations of thermodynamic properties of LaS we have selected all data taken on LaS⁺ at 30-v. energy and for good measure have included the two sets of data on LaS⁺, respectively, at 70 and 50 g.

(16) F. H. Field and J. L. Franklin, "Electron Impact Phenomena," Academic Press Inc., New York, N. Y., 1957.

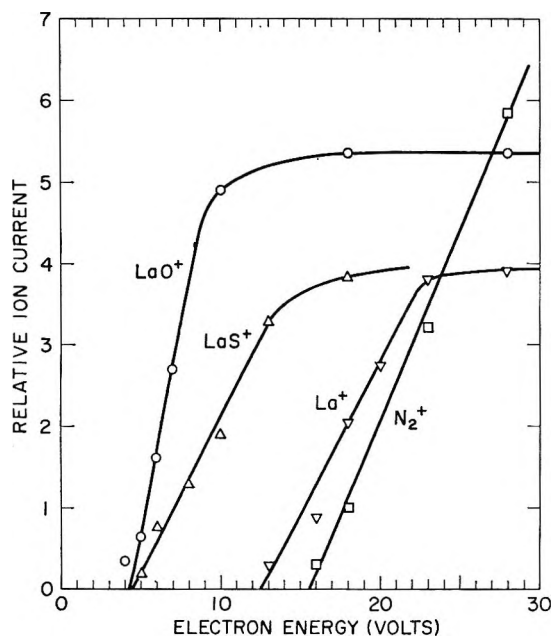


Figure 2. Appearance potential measurements on LaO^+ , LaS^+ , and La^+ from oxygen-contaminated LaS . N_2^+ measurements included to establish energy scale.

Table II: Mass Spectrometric Data on LaS^+ , La^+ , S^+

Expt. no.	Species	Energy, v.	Slope (as $\Delta H^\circ T$), kcal./mole	Temp. range, °K.	No. of points
LaS-7	LaS^+	30	131.3 ± 2.1	2155–2451	7
LaS-8	LaS^+	30	129.4 ± 1.5	2147–2490	6
LaS-9	LaS^+	30	131.7 ± 2.8	2137–2450	9
	LaS^+	50	132.3 ± 3.5	2137–2450	9
	LaS^+	70	133.0 ± 3.5	2137–2450	9
	La^+	30	134.6 ± 3.3	2137–2450	9
	S^+	30	136.0 ± 4.6	2224–2450	7
LaS-10	LaS^+	30	131.3 ± 2.3	2012–2321	15
	La^+	30	133.9 ± 2.2	2012–2321	15
	S^+	30	127.8 ± 2.6	2012–2321	15
Av. for all LaS^+			131.5		

Thermodynamics of LaS

Second-Law Treatment. It is seen that the second-law heats determined by vacuum balance and mass spectrometer are in agreement with each other. In order to get "best" values for the heat and entropy of sublimation, the mass spectrometric values of I^+T for LaS^+ were converted to pressures, and a least-squares treatment of these values combined with the vacuum balance points was made. For this purpose, a constant was added to the intercept of the least-squares line for $\log I^+T$ vs. $1/T$ for each set of data on LaS^+ so that at 2240°K , $\log I^+T = \log P_{\text{LaS}}$ obtained from eq. 3. This same constant was added to each

value of $\log I^+T$ in a given set to convert from $\log I^+T$ to $\log P_{\text{LaS}}$.

In Figure 1 the vacuum balance and mass spectrometric pressures so calculated are plotted as $\log P$ vs. $1/T$. The final second-law heat and entropy of sublimation are obtained from the slope and intercept of the least-squares line through all of these points

$$\log P_{\text{atm}} = (7.365 \pm 0.094) - (28,730 \pm 210)/T \quad (5)$$

The heat of sublimation at temperature is thus $\Delta H^\circ_{2240} = 131.5 \pm 1.0$ kcal./mole, where the uncertainty is the statistical standard deviation. Converted to room temperature and zero degrees by the enthalpy data from Table III, estimated as described below, this becomes $\Delta H^\circ_{298} = 141.4 \pm 2.0$ and $\Delta H^\circ_0 = 141.7 \pm 2.0$ kcal./mole, where the quoted uncertainties are estimated.

Table III: Estimated Thermodynamic Quantities

T , °K.	LaS(g)		LaS(s)	
	$H^\circ T - H^\circ_0$, cal./mole	$S^\circ T$, cal./deg. mole	$H^\circ T - H^\circ_0$, cal./mole	$S^\circ T$, cal./deg. mole
2100	18,120	78.71	27,590	44.65
2200	19,010	79.13	29,000	45.29
2240	19,370	79.29	29,550	45.54
2300	19,900	79.52	30,380	45.91
2400	20,800	79.91	31,780	46.50
298.15	2,219	61.66	2,550	17.50
Estimated error at				
2240°K. ^a	± 290	± 1.06	± 870	± 2.2
		$\pm 3.0^b$		

^a Error estimated for $\pm 20\%$ in r_e , $\pm 50\%$ in ω_e , ± 1 e.u. in $C_p(\text{LaS}_2\text{S})$, ± 1 e.u. in $S^\circ_{298}(\text{LaS}_2\text{S})$, ± 300 cal. in $(H^\circ_{298} - H^\circ_0)$ (LaS_2S). ^b This uncertainty includes the difference between $^4\Sigma$ and $^2\Sigma$ or $^4\pi$ ground states.

The entropy of sublimation is obtained from the intercept of eq. 5 after application of a small correction. The normalization of $\log P$ was made under the assumption that only molecules existed in the vapor. The value from the intercept, 33.70 ± 0.43 e.u., must be decreased by 0.18 e.u. to correct for the presence (see below) of atoms in the vapor. To the standard deviation of the intercept we add an additional uncertainty of ± 0.3 e.u. to account for uncertainties in the experimental pressure determination and the calculation of the proportion of atoms in the vapor. Thus, the entropy of sublimation of LaS is $\Delta S^\circ_{2240} = 33.5 \pm 0.6$ e.u.

Third-Law Treatment. A so-called third-law treatment of the vacuum balance data was performed for

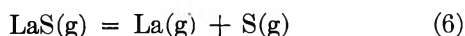
comparison with the second-law heat and entropy. Entropies and enthalpy functions calculated for LaS(s) and (g) are listed in Table III along with estimated limits of accuracy. The third-law value of ΔH°_0 for the vaporization is shown in the last column of Table I for each experimental temperature. Molecular parameters chosen for LaS(g) were $r_e = 2.38 \text{ \AA}$. (20% less than the La-S distance in the solid) and $\omega_e = 490 \text{ cm}^{-1}$ (60% of the value for LaO).¹⁷ The ground state of the LaS molecule was taken to be $^4\Sigma$, the same as deduced by Akerlind¹⁷ for LaO. The entropy of solid LaS at 298°K. was estimated to be 17.5 e.u. by the method of Grønvald and Westrum¹⁸ from the magnetic susceptibility⁹ of 281×10^{-6} c.g.s. unit. The enthalpy ($H^\circ_{298} - H^\circ_0$) for solid LaS was estimated to be 2550 cal./mole by comparison with the values 2590 for CeS¹⁹ and 2667 for US.²⁰ These latter are metallic, refractory compounds, isomorphous with and having physical properties similar to those of LaS. For the extrapolation from 298°K. to the experimental temperatures an average heat capacity of 13.9 cal./mole deg., 2.0 cal./mole deg. higher than the classical $6R$, is reasonable by comparison with the heat capacities of all oxides and sulfides of type AB tabulated by Kelley.²¹

The third-law treatment gives for sublimation of LaS $\Delta H^\circ_0 = 141.7 \pm 7.6$ kcal./mole. There is no trend in ΔH°_0 with temperature of measurement. From $\log P_{\text{LaS}}$ at 2240°K. as calculated from eq. 3 or 5 and the estimated entropy, 33.75 e.u. at 2240°K., one obtains $\Delta H^\circ_{2240} = 132.1 \pm 6$ kcal./mole. These errors are estimated as indicated in Table III. The third-law values are in excellent agreement with the second-law values $\Delta H^\circ_0 = 141.8 \pm 2.0$, $\Delta H^\circ_{2240} = 131.5 \pm 1.0$ kcal./mole, and $\Delta S^\circ_{2240} = 33.5 \pm 0.6$ e.u.

The accord between second- and third-law treatments may be somewhat fortuitous in view of the large uncertainties in the third-law values. The second-law values would seem inherently trustworthy, having been derived from two techniques, using several samples, at two laboratories, by two sets of workers. Alternatively, the excellent agreement may be taken as corroborating the choice of electronic ground state, in which case the uncertainty in the third-law values is overestimated.

Dissociation Energy of LaS

It was originally hoped that the heat of dissociation of LaS might be directly determined from the (hoped for) observable equilibrium



One could then calculate the heat of formation of LaS(s)

and (g) directly. Since the elemental ions appeared to be almost entirely fragments in these studies, we require a heat of formation of LaS(s) to obtain the dissociation energy. It is not available. A reasonable estimate of the heat of formation of LaS(s) from metal and rhombic sulfur is $\Delta H^\circ_{f,298} = -113 \pm 5$ kcal./mole if one compares the known heats of formation of Ce₃S₄, Ce₂S₃, and CeS with those of La₂S₃ and La₃S₄.²² From the thermal data for sulfur,²³ for La(g),²⁴ Ackermann and Rauh's value of 100.0 kcal./mole for the heat of vaporization of La at 298°, the estimated heat of formation and enthalpy functions for LaS(s), and the presently determined heat of vaporization of LaS, one obtains the dissociation energy $D_0(\text{LaS}) = 137 \pm 5$ kcal./mole or 6.0 ± 0.2 e.v. The molecule LaS is thus less stable than the molecule LaO by the amount $D_0(\text{LaS})/D_0(\text{LaO}) = 0.72$.

From the free energy of vaporization at 2240°K. and appropriate other values cited above, one obtains for reaction 6 at 2240°, $\log K = 1.60 \times 10^{-8}$. Since from eq. 3 or 5 $P_{\text{LaS}} = 3.5 \times 10^{-6}$ atm. at 2240°, it follows that in a closed system $P_{\text{La}}/P_{\text{LaS}} = 0.07$. Because of the differences in molecular weight of the species, in an effusion cell $P_{\text{La}}/P_{\text{LaS}} = 0.098$.

The observation that I^+_{La} was due almost entirely to fragmentation is thus corroborated.

Acknowledgment. This work was supported by the United States Atomic Energy Commission at the University of Iowa under Contract No. AT(11-1)-1182. T. E. L. and E. W. J. wish to thank the Commission for research assistantships, and H. A. E. and E. D. C. express their appreciation for temporary appointments as Research Associates at Argonne National Laboratory. The Lunex Co., Pleasant Valley, Iowa, kindly provided some of the samples of lanthanum.

(17) (a) L. Akerlind, *Arkiv Fysik*, 22, 41, 65 (1962); (b) U. Uhlér and L. Akerlind, *ibid.*, 19, 1 (1961).

(18) F. Grønvald and E. F. Westrum, Jr., *Inorg. Chem.*, 1, 36 (1962).

(19) E. G. King and W. W. Weller, U. S. Department of the Interior, Bureau of Mines, Report of Investigations, No. 5485, 1959. We have performed a graphical integration of their data to get $H^\circ_{298} - H^\circ_0 = 2590$ cal./mole.

(20) E. F. Westrum, Jr., and R. R. Walters, reported by E. F. Westrum, Jr., and F. Grønvald in "Thermodynamics of Nuclear Materials," International Atomic Energy Agency, Vienna, 1962, pp. 24-32.

(21) K. K. Kelley, U. S. Bureau of Mines Bulletin 584, U. S. Government Printing Office, Washington, D. C., 1960.

(22) R. L. Montgomery, U. S. Department of the Interior, Bureau of Mines, Report of Investigations, No. 5468, 1959, has recalculated the heats of formation of cerium and lanthanum sulfides on the basis of more recent heats of solution of cerium and lanthanum.

(23) G. N. Lewis and M. Randall, "Thermodynamics," 2nd Ed., revised by K. Pitzer and L. Brewer, McGraw-Hill Book Co., Inc., New York, N. Y., 1961, pp. 671-673.

(24) D. R. Stull and G. C. Sinke, "Thermodynamic Properties of the Elements," American Chemical Society, Washington, D. C., 1956.

A Differential Vapor Pressure Study of the Self-Association of Acids and Bases in 1,2-Dichloroethane and Certain Other Solvents

by J. F. Coetzee¹ and Rose Mei-Shun Lok²

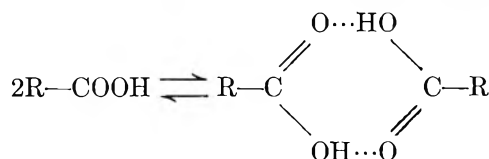
Department of Chemistry, University of Pittsburgh, Pittsburgh, Pennsylvania 15213 (Received March 1, 1966)

A differential vapor pressure technique has been used to study the self-association of certain acids and bases in several nonhydrogen bonding solvents. In 1,2-dichloroethane, the self-association of benzoic acid is markedly decreased by *ortho* substitution with bromine and hydroxy and methoxy groups. *Ortho* substitution in phenol with nitro and methoxy groups has the same effect, which is attributed in part to stabilization of the monomeric form by intramolecular hydrogen bonding. Acetamide appears to form a relatively stable trimer, but amines undergo little association in 1,2-dichloroethane. Benzoic acid shows significant association in nitromethane, but none in acetonitrile which has virtually the same dielectric constant. The lack of association in acetonitrile is attributed to hydrogen bonding between acid and solvent, stabilizing the monomer.

Introduction

The self-association of certain acids and bases is an important manifestation of hydrogen bonding. As early as 1891, Beckmann inferred from cryoscopic and Nernst from distribution studies that carboxylic acids dimerize in certain organic solvents. It now is well known that other classes of compounds, particularly water, alcohols, and phenols, as well as acid amides, also undergo self-association. Primary and secondary amines and imines under certain conditions show self-association, but to a smaller extent.

Carboxylic acids undergo self-association in the solid and vapor states, and also in relatively inert solvents of low dielectric constant. In the vapor state at relatively low pressure, and in dilute solution, association generally does not proceed beyond the dimeric stage



The ring structure has been established in the vapor phase by electron diffraction.³

The equilibrium between the monomeric and dimeric forms of carboxylic acids has been studied by a variety of methods. Vapor phase studies involved infrared

spectroscopy, vapor density determinations with the quartz microbalance, and measurements based on the gas law relationships. Solutions have been studied by cryoscopy, ebullioscopy, absorption spectroscopy, as well as by vapor pressure, distribution, and electric polarization measurements. The results have been reviewed by Allen and Caldin.⁴

In this communication we report the results of a study of the self-association of a number of acids and bases in 1,2-dichloroethane, acetone, acetonitrile, and nitromethane as solvents, by means of a relatively recent differential vapor pressure technique, employing an instrument (Mechrolab vapor pressure osmometer) which measures the net transfer of solvent from a drop of pure solvent to one of the solution held on two thermistor beads. This method has several important advantages. It is rapid and requires only small volumes of sample. It is applicable to solvents such as acetone, acetonitrile, and nitromethane, for which partial or complete miscibility with water rules out distribution experiments. Measurements can be

(1) Address all correspondence to this author.

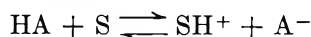
(2) From the M.S. thesis of this author, University of Pittsburgh, 1964.

(3) V. Schomaker and J. M. O'Gorman, *J. Am. Chem. Soc.*, **69**, 2638 (1947).

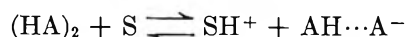
(4) G. Allen and E. F. Caldin, *Quart. Rev. (London)*, **7**, 255 (1953).

carried out at various temperatures, so that enthalpy and entropy values become accessible. However, its use is limited to solutes which have negligible vapor pressures as compared to that of the solvent, and to solvents with appreciable vapor pressures. Recently, Bruckenstein and Saito have used this technique in a detailed study of acid-base reactions in benzene.⁵

The present study is part of a general investigation in this laboratory of acid-base interactions in nonhydrogen bonding solvents. Quantitative interpretation of such interactions requires independent information about any self-association reactions which may occur. Only one illustration will be given here. Whereas the dissociation constant of a weak Brønsted acid in a water-like solvent can be evaluated unambiguously from the concentration dependence of the equivalent conductivity, the same is not true for a nonhydrogen bonding solvent, in which two different over-all dissociation reactions with the same concentration dependence of the equivalent conductivity can occur⁶



and



Clearly, independent information about the possible dimerization of HA is required.

Self-association in the series of solvents listed above also is interesting *per se*, since a fairly broad spectrum of properties that may be expected to influence self-association is covered. Dielectric constants increase in the order 1,2-dichloroethane (10.36), acetone (20.7), nitromethane (35.9), and acetonitrile (36.0). Although extensive studies have been carried out in low dielectric constant solvents, such as benzene ($D = 2.3$), much less is known about self-association in solvents of intermediate dielectric constant. Furthermore, in the series of solvents listed, information about the effect of variations in the specific acid-base properties of the solvent can be obtained.

Experimental

Purification of Solvents. Fisher reagent grade 1,2-dichloroethane was shaken with Brockman Activity 1 basic alumina (1 g./l.) to remove traces of hydrochloric acid. After decantation, the solvent was refluxed for 4 hr. over fresh alumina (1 g./l.) and then fractionally distilled under a reflux ratio of 8:1 (b.p. 83.5° cor.).

Acetone was purified by distillation from phosphorus pentoxide,⁷ acetonitrile by a series of operations culminating in distillation from calcium hydride,⁸ and nitromethane by one vacuum distillation followed by one fractional freezing.⁹

Purification of Solutes. National Bureau of Standards acidimetric grade benzoic acid and Allied Chemical Co. C.P. phenol were used as obtained, after drying *in vacuo* at 100° and at 25° over phosphorus pentoxide, respectively.

The origin of other compounds is indicated in parentheses as follows: Eastman White Label, E; Fisher Certified Reagent, F. The following compounds were recrystallized and then dried *in vacuo*. In each case the solvent and drying temperature also are given in parentheses. *o*-Bromo-, *o*-methoxy-, and *m*-methoxybenzoic acids (E) and salicylic acid (F; from water, at 30, 35, 40, and 85°, respectively); phenylacetic and capric acids (E, ether, 25°); *o*- and *m*-toluic acids (E, ethanol-water, 35°); transcinnamic acid (F, acetone-water, 40°); *o*-nitrophenol (E, methanol, 25°); 2,6-dinitrophenol (K and K Laboratories, water, 40°); picric acid (E, benzene-Skelly B, 40°); 2,6-dimethoxyphenol (E, benzene-Skelly B, 30°); acetamide (F, methanol-ether, 30°); *o*- and *p*-nitroaniline (E, water, 35°); *p*-toluidine and diphenylamine (E, acetone-water, 30°); tribenzylamine (E, ether, 25°); 1,3-diphenylguanidine (E, twice from toluene, 40°); benzil (E, acetonitrile-water, 40°). Finally, dibenzylamine, dicyclohexylamine, and tripropylamine (E) were vacuum distilled from sodium hydroxide pellets.

Apparatus. A Mechrolab Inc. (Mountain View, Calif.) Model 301A vapor pressure osmometer with a 37° thermostat and nonaqueous thermistor probe was used. The instrument was calibrated for each solvent used with benzil as standard. The calibration curve (ΔR vs. molarity) closely approached linearity, and also that obtained with biphenyl as standard. It was found necessary to repeat the calibration approximately every 2 weeks and to replace the solvent and vapor wick in the solvent cup every 4 or 5 weeks. In making measurements, the directions of the manufacturer were followed precisely. Readings were taken after 3-, 4-, and 5-min. intervals to ensure that the instrument functioned properly. In all cases, the 5-min. readings were most stable and were used in the calculations. Generally, five solutions, of concentrations 0.02, 0.04, 0.06, 0.08, and 0.10 *M*, were measured. For each concentration, five different drops were measured and the readings were averaged.

(5) S. Bruckenstein and A. Saito, *J. Am. Chem. Soc.*, **87**, 698 (1965).

(6) W. S. Muney and J. F. Coetzee, *J. Phys. Chem.*, **66**, 89 (1962).

(7) J. F. Coetzee and D. K. McGuire, *ibid.*, **67**, 1810 (1963).

(8) J. F. Coetzee, G. P. Cunningham, D. K. McGuire, and G. R. Padmanabhan, *Anal. Chem.*, **34**, 1139 (1962).

(9) J. F. Coetzee and G. P. Cunningham, *J. Am. Chem. Soc.*, **87**, 2529 (1965).

Table I: Dimerization of Benzoic Acid in 1,2-Dichloroethane as Solvent

Approximate molar concn., as monomer	0.02	0.04	0.06	0.08	0.10
Actual g./l.	2.4432	4.8864	7.3296	9.7728	12.2160
Av. ΔR value at 5 min.	4.88	8.89	12.85	16.69	20.28
Av. molar concn. from calibration curve	0.0148	0.0264	0.0384	0.0496	0.0604
Av. mol. wt., m_x^a	165.1	185.1	190.9	197.0	202.3
Deg. of association, f^b	0.521	0.681	0.721	0.761	0.793
Association const., $K_{f,12}^c$	57	84	78	83	93

^a Molecular weight of monomer, 122.1. ^b See eq. 1a. ^c See eq. 1b.

Table II: Self-Association of Acids and Bases in 1,2-Dichloroethane, Acetone, Acetonitrile, and Nitromethane as Solvents

Solute	$(pK_a)_w$ at 25 ^{ob}	Mol. wt., monomer	—Meas. av. mol. wt. and self-association constants at 37 ^{oa} —					$K_{f,12}$ at 37 ^{oc}
			0.02 M	0.04 M	0.06 M	0.08 M	0.10 M	
A. Solvent: 1,2-Dichloroethane								
Carboxylic acids								
1. Benzoic acid	4.212	122.1	I. 165.1 (57)	185.1 84	190.9 78	197.0 83	202.3 93	
			II. 174.7 97	185.4 85	191.1 79	197.3 84	203.9 102	87
2. <i>o</i> -Bromobenzoic acid	2.854	201.0	I. 256.5 34	276.7 33	284.3 29	298.4 34	306.1 35	
			II. 251.1 28	273.7 30	284.3 29	291.1 27	300.7 29	31
3. <i>o</i> -Hydroxybenzoic acid	2.996	138.1	I. 164.6 (35)	160.7 14	167.2 14	172.8 14	175.4 13	
			II. 168.8 (45)	164.8 18	168.8 15	175.2 16	180.7 15	15
4. <i>o</i> -Methoxybenzoic acid	4.094	152.2	152.1	152.1	154.0	155.2	157.1	Small
5. <i>o</i> -Toluic acid	3.908	136.2	179.2 45	194.5 47	204.3 51	209.5 49	213.9 49	48
6. <i>m</i> -Methoxybenzoic acid	4.088	152.2	205.6 57	220.5 54	235.2 69	237.7 57	243.8 61	60
7. <i>m</i> -Toluic acid	4.272	136.2	189.2 (73)	209.5 94	219.7 118	223.3 101	227.0 101	104
8. Phenylacetic acid	4.312	136.1	170.2 28	183.9 28	193.5 30	200.2 31	202.6 28	29
9. Transcinnamic acid	4.438	148.2	I. 211.9 (95)	224.7 85	231.8 83	239.2 83	243.9 85	
			II. 190.2 (36)	211.9 48	222.5 51	235.5 70	238.5 65	71
10. Capric acid		172.3	215.3 28	234.8 31	246.0 31	253.2 31	260.9 33	31
Phenols								
1. Phenol	9.998	94.1	124.1 45	130.0 34	138.7 42	142.9 43	142.9 34	40
2. <i>o</i> -Nitrophenol	7.234	139.1	151.1 (5.7)	152.8 3.4	154.5 2.6	154.5 2.0	158.0 2.0	2.5
3. 2,6-Dinitrophenol	3.706	184.1	178.8	178.8	184.1	186.8	188.7	Small
4. 2,4,6-Trinitrophenol	0.29	229.1	244.1	231.8	231.1	232.4	233.7	Small
5. 2,6-Dimethoxyphenol		154.2	151.2	152.7	154.2	154.9	154.2	0

Table II (Continued)

Solute	(p <i>K</i> _a) _w at 25° ^b	Mol. wt., monomer	—Measd. av. mol. wt. and self-association constants at 37° ^a —					<i>K</i> _{f,12} at 37° ^c
			0.02 <i>M</i>	0.04 <i>M</i>	0.06 <i>M</i>	0.08 <i>M</i>	0.10 <i>M</i>	
Amines								
1. Dicyclohexylamine		181.3	181.2	181.2	182.6	185.9	187.2	Small
2. Dibenzylamine		197.3	197.2	197.2	197.2	199.2	197.2	0
3. Diphenylamine	0.9	169.2	I. 156.7	162.8	165.9	168.4	169.3	
			II. 166.0	166.8	167.1	166.8	166.7	0
4. 1,3-Diphenylguanidine	10.00	211.3	I. 211.3	232.2	241.9	248.6	256.4	
			(0)	3.4	3.8	3.8	4.2	
			II. 229.6	237.4	245.7	253.0	258.9	
			(5.7)	4.6	4.5	4.6	4.7	4.2
5. Tribenzylamine		287.4	299.5	287.5	285.6	286.1	287.5	0
6. Triamylamine		227.4	227.4	229.7	233.7	233.3	236.2	Small
7. <i>p</i> -Toluidine	5.12	107.2	I. 107.2	112.9	114.9	117.8	122.4	
			(0)	1.6	1.5	1.7	2.2	
			II. 111.6	115.8	119.0	120.4	123.5	
			2.3	2.5	2.6	2.3	2.4	2.1
Amides								
1. Acetamide	-0.5	59.1	92.7	97.0	101.3	106.5	114.1	
			4800	1750	1100	945	1100	1100 ^d
B. Solvent: Acetone								
1. Acetamide	-0.5	59.1	I. 63.0	65.0	67.8	69.5	70.3	
			4.1	3.2	3.9	3.8	3.5	
			II. 68.8	68.0	69.3	71.3	73.2	
			(13.7)	6.1	4.9	4.9	5.2	4.4
C. Solvent: Acetonitrile								
1. Benzoic acid	4.212	122.1	122.8	122.8	122.0	122.2	121.9	0 ^e
2. <i>o</i> -Bromobenzoic acid	2.854	201.0	205.0	205.0	202.3	201.9	202.5	0
3. 1,3-Diphenylguanidine	10.00	211.3	207.3	213.5	212.8	211.4	213.9	0
4. Acetamide	-0.5	59.1	65.6	67.1	69.2	71.6	72.4	
			(7.8)	5.1	5.0	5.1	4.7	5.0
D. Solvent: Nitromethane								
1. Benzoic acid	4.212	122.1	130.1	135.9	140.0	140.6	154.0	
			4.0	4.0	3.9	3.3	6.0	4.2
2. <i>o</i> -Bromobenzoic acid	2.854	201.0	0.018 <i>M</i>	0.030 <i>M</i>	0.048 <i>M</i>	0.060 <i>M</i>	(Solubility limit)	
			196.6	203.7	204.4	206.5		
				0.38	0.36	0.49		0.41
3. <i>p</i> -Nitroaniline	1.02	138.1	144.0	139.6	141.1	141.8	144.0	
			(2.4)	0.29	0.38	0.36	0.48	0.38
4. Acetamide	-0.5	59.1		0.050 <i>M</i>	0.10 <i>M</i>	0.25 <i>M</i>	0.50 <i>M</i>	
				64.2	64.2	65.3	68.0	
				2.2	1.1	0.59	0.49	<i>f</i>

^a For each solute, first line gives molecular weights and second line self-association constants. For certain solutes two independent runs are reported, indicated as I and II. ^b Values mainly from ref. 14; see also A. Albert and E. P. Serjeant, "Ionization Constants of Acids and Bases," John Wiley and Sons, Inc., New York, N. Y., 1962, and G. Kortüm, W. Vogel, and K. Andrüssow, "Dissoziationskonstanten Organischer Säuren in Wasseriger Lösung," Butterworth and Co. Ltd., London, 1961. ^c Weighted arithmetic mean of all self-association constants obtained; often values for 0.02 *M* omitted (indicated by parentheses). ^d Formation constants are those for trimer. See text. At lower concentrations dimerization also may be important. Values should be checked with independent method. ^e Obtained with an aqueous thermistor probe. ^f Not constant. Downward trend also observed in other runs.

Results

If the solute is present as an equilibrium mixture of monomer (*M*) and dimer (*D*) only



and if *f* represents the degree of association of the solute,

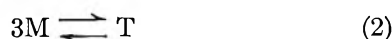
m the molecular weight of the monomer, and *m_x* the average molecular weight measured for the mixture of monomer and dimer, then it follows that

$$f = 2(m_x - m)/m_x \quad (1a)$$

The formation constant of the dimer, *K*_{f,12}, is given by

$$K_{f,12} = \frac{f}{2C(1-f)^2} \quad (1b)$$

where C is the total (analytical) concentration of solute calculated as the monomer. On the other hand, in one case encountered in this study (acetamide in 1,2-dichloroethane), the solute apparently is present largely in the monomeric and trimeric forms



For this system the corresponding equations are

$$f = (m_x - m)/2m \quad (2a)$$

and

$$K_{f,13} = \frac{f(1+2f)^2}{C^2(1-f)^3} \quad (2b)$$

The results of such calculations for a typical case, that of benzoic acid in 1,2-dichloroethane as solvent, are shown in Table I. A list of self-association constants obtained for a variety of solutes in 1,2-dichloroethane, acetone, acetonitrile, and nitromethane as solvents is given in Table II.

Discussion

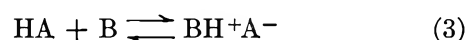
The following conclusions can be drawn from the results presented in Table II.

1. *o*-Bromobenzoic acid and particularly benzoic acid undergo significant self-association in nitromethane, but not in acetonitrile which has virtually the same dielectric constant. The lack of self-association in acetonitrile probably results from hydrogen bonding between acid and solvent, producing species such as $\text{CH}_3\text{CN} \cdots \text{HA}$, thereby stabilizing the monomeric form. Such hydrogen bonding has been observed in n.m.r. studies of carboxylic acids in acetonitrile and also in acetone.¹⁰

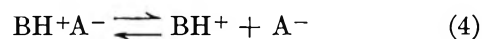
2. Self-association of benzoic acid in 1,2-dichloroethane is decreased markedly by *ortho* substitution with Br, OH, and OCH_3 . This decrease undoubtedly results in part from intramolecular hydrogen bonding (chelation) which stabilizes the monomeric form (also see discussion below). The presence of a strong intramolecular hydrogen bond in *o*-methoxybenzoic acid in benzene as solvent has been indicated by infrared data.¹¹ Self-association of phenols in 1,2-dichloroethane is decreased in the same manner by *ortho* substitution with OCH_3 and NO_2 (Table II). In contrast, *o*-nitrophenol undergoes little or no chelation in aqueous solution,¹² in which hydration competes successfully with chelation.

3. As a first approximation, it may be anticipated that the influence of a given substituent on the dissociation of a dimeric carboxylic acid and on the acid ioni-

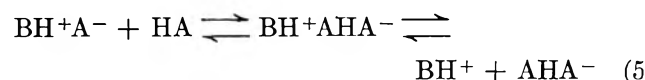
zation of the monomer will be qualitatively similar. No information is available on the ionization of acids in 1,2-dichloroethane. However, on the basis of what is known about acid-base reactions in other low dielectric constant solvents, particularly acetic acid¹³ and benzene, it is to be expected that the primary ionization reaction



where B is a reference base (the solvent, or a stronger added base), rather than the secondary dissociation reaction



will be an index of the "strength" of the acid. On the other hand, the extent of both reaction 4 and of the self-association reaction is influenced by the dielectric constant of the solvent. To complicate matters further, the capacity of the solvent to solvate the anion A^- may exert a dominant effect on reaction 4. In extreme cases, in a nonhydrogen bonding solvent which has little capacity to solvate anions, A^- may resort to stabilization by hydrogen bonding with HA instead



It therefore may be concluded that no simple quantitative correlation can be expected between self-association constants on the one hand, and either ionization or dissociation constants on the other, in solvents of low or intermediate dielectric constant. Likewise, only a rough correlation can be expected between self-association constants in a low dielectric constant solvent and ionization constants in water. Such correlations actually have been found before for limited series of acids in benzene.⁴ In Table III self-association constants for a number of acids in 1,2-dichloroethane (from Table II) and benzene (compiled in ref. 14) are compared with the formation constants of the ion pairs produced with 1,3-diphenylguanidine in benzene,¹⁴ and also with the ionization constants in water. Because of the paucity of data, it is necessary to use data obtained at somewhat different temperatures. However, no serious uncertainties are introduced. For example, for benzoic acid in benzene, the temperature coef-

(10) L. W. Reeves, *Trans. Faraday Soc.*, **55**, 1684 (1959).

(11) M. Davies and D. M. L. Griffiths, *J. Chem. Soc.*, 132 (1955).

(12) L. B. Magnusson, C. Postmus, Jr., and C. A. Craig, *J. Am. Chem. Soc.*, **85**, 1711 (1963); **86**, 3958 (1964).

(13) S. Bruckenstein and I. M. Kolthoff, *ibid.*, **78**, 1, 10, 2974 (1956); **79**, 1 (1957).

(14) M. M. Davis and H. B. Hetzer, *J. Res. Natl. Bur. Std.*, **60**, 569 (1958).

ficient of the self-association constant over the range 25 to 40° amounts to -3% per degree.¹¹ For several other acids for which data are available in benzene,¹⁴ temperature coefficients of -4 to -5% per degree apply. Hence, $\log K_{f,12}$ values in benzene typically should be *ca.* 0.15 unit smaller at 37° than those listed for 30°. The following trends are evident in Table III. First, for all acids, $\log K_{f,12}$ values are smaller in 1,2-dichloroethane than in benzene, as expected on the basis of the higher dielectric constant of the former solvent (10.65, as compared to 2.28, at 20°). Furthermore, for the majority of acids this difference amounts to *ca.* 0.9 unit, or 0.7 to 0.8 unit (*ca.* 1.1 kcal. mole⁻¹) when converted to a common temperature of 37° as described above. The magnitude of this difference is not unreasonable on the basis of a simple electrostatic interpretation.¹⁵ Second, decreasing self-association in 1,2-dichloroethane and benzene correlates very roughly with increasing reaction with 1,3-diphenylguanidine in benzene and increasing ionization in water, but certain marked deviations occur. In particular, the decrease in self-association caused by *ortho* substitution with bromine is less, and with methoxy is greater, than would be predicted from the effect on the "acidity" as shown by the reaction with 1,3-diphenylguanidine in benzene or ionization in water.¹⁶ In the latter case, the deviation undoubtedly is caused by particularly strong intramolecular hydrogen bonding stabilizing the monomer in both nonaqueous solvents, as discussed above. Salicylic acid shows no such deviation. Finally, phenylacetic acid undergoes less self-association than would be predicted from its ionization constant in water. Similar observations have been made in benzene with other acids (*e.g.*, fatty acids) for which no conjugation can occur between the carboxyl group and the rest of the molecule.⁴

4. In principle, imines and primary and secondary amines are capable of self-association. White and Kilpatrick¹⁷ found considerable dimer and trimer formation by 1,3-diphenylguanidine in benzene ($K_{f,12} = 53$, $K_{f,13} = 300$ at 5.5°). In 1,2-dichloroethane, only slight dimerization occurs ($K_{f,12} = 4.2$), and in acetonitrile no self-association was detected. We conclude that in 1,2-dichloroethane and particularly in acetonitrile and nitromethane, self-association of the stronger nitrogen bases probably is relatively unimportant.¹⁸ It is possible that aromatic bases may undergo more extensive self-association. For example, refer to the thorough study of Lady and Whetsel on aniline in cyclohexane.¹⁹

5. Amides present a classical example of self-as-

sociation, which has implications in protein structure.²⁰ In solid acetamide, six planar molecules are arranged in a cyclic structure in a rhombohedral cell; adjacent molecules are held in the ring by N-H...O hydrogen bonds, involving both hydrogen atoms of the -NH₂ group and with two hydrogen bonds to each oxygen atom.²¹ In water at the freezing point, and in aceto-

Table III: Comparison of Self-Association Constants^a of Carboxylic Acids in 1,2-Dichloroethane and Benzene with Acid Strength in Benzene and Water

Acid	Log $K_{f,12}$ for HA + HA → (HA) ₂		Log K_f for HA + B → BH ⁺ A ^{-b}	-Log K_a
	C ₂ H ₄ Cl ₂ (37°)	C ₆ H ₆ (30°)	(C ₆ H ₆ , 25°)	(H ₂ O, 25°)
<i>m</i> -Toluic	2.02	2.75, ^c 2.70 ^d	5.13	4.27
Benzoic	1.94	2.69 ^c	5.26	4.21
Transcinnamic	1.85	2.78 ^d		4.44
<i>m</i> -Methoxybenzoic	1.78		5.38	4.09
<i>o</i> -Toluic	1.68	2.52, ^c 2.62 ^d	4.94	3.91
<i>o</i> -Bromobenzoic	1.49	2.4 ^e	6.17	2.85
Phenylacetic	1.46	2.54 ^d		4.31
Salicylic	1.18	<i>f</i>	7.45	3.00
<i>o</i> -Methoxybenzoic	<1	0.43 ^g	3.67	4.09

^a All constants are on the molar scale. ^b Reference base B: 1,3-diphenylguanidine. ^c F. T. Wall and F. W. Banes, *J. Am. Chem. Soc.*, **67**, 898 (1945): isopiestic measurements. ^d A. A. Maryott, M. E. Hobbs, and P. M. Gross, *ibid.*, **71**, 1671 (1949): electric polarization measurements. ^e Estimated from values given in ref. 14 for *o*-bromo- and *o*-chlorobenzoic acids at 5.5° and that for the latter acid at 30°. ^f Not available for benzene at 30°; however, in cyclohexane, values of 3.14, 2.39, and 1.38 at 24, 36, and 55°, respectively: J. J. Banewicz, C. W. Reed, and M. E. Levitch, *ibid.*, **79**, 2693 (1957): distribution measurements. ^g See ref. 11: distribution measurements at 40°.

(15) M. Davies, P. Jones, D. Patnaik, and E. A. Moelwyn-Hughes, *J. Chem. Soc.*, 1249 (1951).

(16) Differences in "acidity" in benzene and water are not under discussion here. However, the very low acidity of *o*-methoxybenzoic acid in benzene as compared to that in water is striking. It was attributed by Davis and Hetzer¹⁴ to the cumulative effect of two factors: weakening of the acidity in benzene by intramolecular hydrogen bonding, and strengthening of the acidity in water by steric inhibition of resonance caused by hydration of the carboxyl group.

(17) N. E. White and M. Kilpatrick, *J. Phys. Chem.*, **59**, 1044 (1955).

(18) In a previous study in this laboratory,⁶ several amines in acetonitrile gave an unusual concentration dependence of the equivalent conductivity, which could be interpreted on the basis of dimerization of the amines. Evidence obtained in the present work, as well as in a potentiometric study of 35 amines in acetonitrile (to be reported), indicates no dimerization. The unusual conductance behavior must be caused by other factors, such as uncertainties associated with the very weak ionization of amines in acetonitrile.

(19) J. H. Lady and K. B. Whetsel, *J. Phys. Chem.*, **68**, 1001 (1964).

(20) M. Davies and H. E. Hallam, *Trans. Faraday Soc.*, **47**, 1170 (1951).

nitrile at the boiling point, Davies and Hallam²⁰ found no association, but some dimerization ($K_{f,12} = 0.49$) in acetone at the boiling point, and mainly trimerization ($K_{f,13} = 50$ and 34 at 6 and 25° , respectively) in chloroform. We find dimerization in both acetonitrile and acetone, and to approximately the same extent ($K_{f,12} \sim 5$ at 37°). We have found before⁷ that the proton acceptor power of acetone is significantly greater than that of acetonitrile. It is likely that the same will be true of its hydrogen bonding with an acid such as acetamide. Consequently, whereas dimerization of acetamide should be promoted by the lower dielectric constant of acetone, as compared to that of acetonitrile, it should be opposed by increased competition from hydrogen bonding between acetone and acetamide monomer. Apparently these two opposing factors are of comparable influence. In 1,2-

dichloroethane as solvent, our results indicate mainly trimerization at higher concentrations ($K_{f,13} = 1100$). The fact that self-association of acetamide is less extensive in chloroform than in 1,2-dichloroethane, even though the dielectric constant of the former solvent is lower than that of the latter (4.81 , as compared to 10.65 at 20°), may be attributed to stabilization of the monomer by $H \cdots O$ hydrogen bonding in chloroform. Nevertheless, the degree of association found for acetamide (and phenol) in 1,2-dichloroethane is greater than would be expected from that in other solvents,² and should be viewed with some reservation.

Acknowledgment. We gratefully acknowledge financial support by the National Institutes of Health under Grant No. GM-10695.

(21) F. Senti and D. Harker, *J. Am. Chem. Soc.*, **62**, 2008 (1940).

Properties of Organic-Water Mixtures. III. Activity Coefficients of Sodium Chloride by Cation-Sensitive Glass Electrodes¹

by R. D. Lanier

Chemistry Division, Oak Ridge National Laboratory, Oak Ridge, Tennessee (Received March 2, 1965)

Activity coefficients of NaCl in water-organic solvents were measured at 25° with a cation-sensitive glass electrode *vs.* a silver-silver chloride electrode. Results agree fairly well with available literature values for both solutions in water and in mixed solvents. The present study includes as organic components methanol, ethylene glycol, ethylene glycol diacetate, diethylene glycol monomethyl ether, dioxane, urea, and dimethylformamide and for each covers a range of organic fractions. Debye-Hückel behavior is approached at low NaCl concentrations, and reasonably good extrapolations to infinite dilution can be made. The extrapolations are discussed in the light of the Born equation.

Introduction

Renewed interest in the alkaline error of glass electrodes used for pH measurements²⁻⁶ has recently led to a number of studies of the effect of composition of the glass on the cation function of such electrodes.^{7,8} These studies have in turn led to the successful preparation of glass electrodes which respond to monovalent cations such as Na⁺ and K⁺. Such electrodes are now commercially available.⁹

These types of electrodes do not appear as yet to have been used extensively for measurement of activity coefficients of salts of monovalent cations (to which their use is at present restricted) in solvents other than water except for work by Shul'tz and Parfenov.¹⁰ These workers have measured e.m.f. values for sodium chloride-methanol-water solutions with both glass and amalgam electrodes. The response of cation-sensitive electrodes to alkali metal ions in several organic-water mixtures has been investigated by Rechnitz and Zamochnick.¹¹ Crescenzi and co-workers have used a Beckman sodium electrode to measure sodium salt activities in polymethacrylate solutions,¹² but, in this case, the weight fraction of organic material present was small compared to that of methanol in water-methanol mixtures.

The reliability and accuracy of several commercial glass electrodes *vs.* Ag-AgCl have been tested in the two-component system sodium chloride-water. These results were encouraging and e.m.f. measurements

were then made in sodium chloride-organic-water solutions.

Experimental

1. *Apparatus.* (a) *Measurement of Potentials.* A vibrating-reed electrometer, in conjunction with a potentiometer and a Brown recorder, was used for the e.m.f. determinations.¹³ Except for a few measure-

(1) Research sponsored by The Office of Saline Water, U. S. Department of the Interior, under Union Carbide Corporation's contract with the U. S. Atomic Energy Commission. Previous paper in series: C. F. Coleman, *J. Phys. Chem.*, **69**, 1377 (1965).

(2) W. S. Hughes, *J. Am. Chem. Soc.*, **44**, 2860 (1922).

(3) K. Horovitz, *Z. Physik*, **15**, 369 (1923).

(4) H. Schiller, *Ann. Physik*, **74**, 105 (1924).

(5) D. A. MacInnes and M. A. Dole, *J. Am. Chem. Soc.*, **52**, 29 (1930).

(6) B. Lengyel and E. Blum, *Trans. Faraday Soc.*, **30**, 461 (1934).

(7) G. Eisenman, *Biophys. J.*, **2**, Part II, 259-323 (1962).

(8) B. P. Nikol'skii, M. M. Shul'tz, *et al.*, *Vestn. Leningr. Univ., Ser. Fiz. i Khim.*, **18**, No. 4, 73-186 (1963). This series of articles summarizes recent Russian work on the effect of varying the glass composition on electrode properties and chemical stability of a great variety of glasses.

(9) J. E. Leonard, paper presented at the 5th Instrumental Methods of Analysis Symposium of the Instrument Society of America, Houston, Texas, May 1959. Beckman Reprint R-6148.

(10) M. M. Shul'tz and A. E. Parfenov, *Vestn. Leningr. Univ., Ser. Fiz. i Khim.*, **13**, No. 3, 118 (1958).

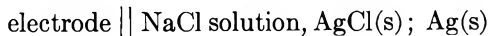
(11) G. A. Rechnitz and S. B. Zamochnick, *Talanta*, **11**, 979 (1964).

(12) V. Crescenzi, V. de Rosa, and D. Malderalla, *Ric. Sci. Suppl.*, **30**, 1680 (1960). Similar studies have been made using an ion-exchange membrane electrode: V. Crescenzi, A. de Chirico, and A. Ripamonti, *ibid.*, **29**, 1424 (1959).

ments carried out with a Rubicon potentiometer, a Leeds and Northrup K-3 was used. Precision is of the order of a few hundredths of a millivolt, more than ample for the electrode system used.

(b) *Electrodes.* The cell was

alkali-sensitive glass



Inside this glass electrode is a 0.1 *m* NaCl solution in water and an Ag–AgCl electrode. The glass electrodes (Beckman Sodium 39278 and Cationic 39137) are described in the Beckman literature.¹⁴ Glass electrodes have been used previously for measurement of activity coefficients of HCl in aqueous solutions in conjunction with Ag–AgCl electrodes, and the precision of the results was satisfactory.¹⁵

The temperature of the measurements was 25°.

These electrodes are not sensitive to divalent ions such as Mg²⁺, Ca²⁺, Sr²⁺, Ba²⁺, etc.,¹⁴ but they are extremely sensitive to monovalent cations. The effects of cations other than Na⁺ on the potential of the glass electrode must be taken into account if an accurate measurement of the activity of a sodium salt is to be made. These effects can be correlated by an equation (for 1–1 electrolytes)

$$E_2 - E_1 = 0.05915 \log$$

$$\frac{([a_{\text{Na}}] + [k_{\text{K}}a_{\text{K}}] + [k_{\text{Ag}}a_{\text{Ag}}] + \dots)_2(a_{\text{Cl}})_2}{([a_{\text{Na}}] + [k_{\text{K}}a_{\text{K}}] + [k_{\text{Ag}}a_{\text{Ag}}] + \dots)_1(a_{\text{Cl}})_1} \quad (1)$$

which follows from a discussion of Scatchard¹⁶ (see also ref. 7 and 8). Equation 1 involves the approximation that $k_{\text{M}} = u_{\text{M}}\gamma_{\text{Na}}/u_{\text{Na}}\gamma_{\text{M}}$ is constant for a given electrode, u being ionic mobility and γ the activity coefficient of the ions in the glass. The monovalent ions which will have the most important effect in these studies are probably Ag⁺, K⁺, and H⁺. Although k_{Ag} is greater than k_{Na} ,¹⁴ all solutions are saturated with AgCl, and, because of this and the low solubility of AgCl, variations in its contribution to the potential should not be important. The potassium impurities in the NaCl used should also not have affected the results appreciably. Spectroscopic analysis (kindly carried out by T. M. Rains, Oak Ridge National Laboratory Analytical Division) showed the mole ratio of Na⁺ to K⁺ to be 10⁵, and, in addition, the mole ratio should be constant in all solutions except perhaps those saturated with NaCl. E.m.f. measurements of solutions containing varying amounts of KCl and NaCl at constant ionic strength indicate that eq. 1 holds; Figure 1 gives an example. It appears however that k_{K} varies among individual glass electrodes. Values of k_{K} for the three electrodes used here were 5.5,

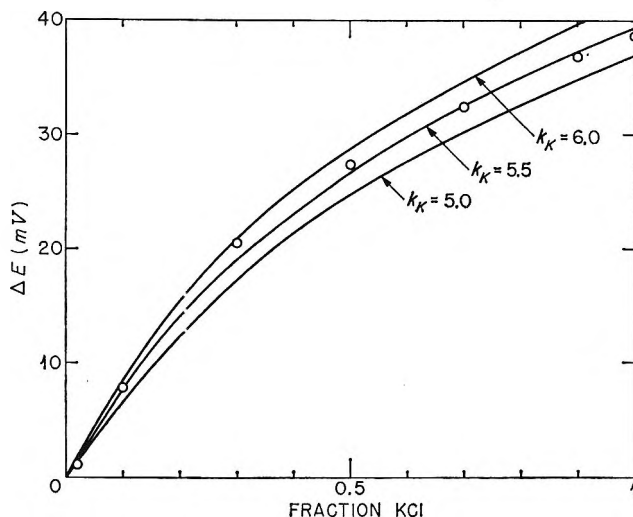


Figure 1. E.m.f. measurements in NaCl–KCl mixtures at 25° (glass electrode $\parallel m_{\text{NaCl}} + m_{\text{KCl}} = 1$, AgCl(s); Ag).

8.8, and 8.9 at 1 *m* total solute; combined with the sodium to potassium concentration ratios, these values indicate negligible interference by potassium.

The effect of acidity was checked by measuring the change of potential of a 0.1 *m* NaCl solution from pH 3 to 12. The Beckman 39278 electrode was found to have a sensitivity of greater than 0.1 mv./pH unit; the response of the 39137 electrodes used was ~ 0.05 mv./pH unit above pH 5, corresponding to $k_{\text{H}} \approx 15$. Consequently, only the 39137 electrode was used in the measurements of NaCl activity coefficients, and the range of acidity in a series, which included a measurement of reference potential, was less than 0.5 pH unit. Errors from this source should therefore not be important.

The potentials of different electrode pairs were somewhat different for a given solution; this is, of course, of no concern since it is the differences in potential for different solutions with a given electrode pair that is of interest. There were also small changes in the potentials measured from time to time with a pair for a given solution. The effect of drift was minimized by referring measurements to saturated solutions, whose potential was measured at intervals.

In principle, if the electrode system is responsive

(13) K. A. Kraus, R. W. Holmberg, and C. J. Borkowski, *Anal. Chem.*, **22**, 341 (1950).

(14) Beckman Instructions 1154-A and 1155-A, Beckman Instruments, Inc., Scientific and Process Instruments Division, Fullerton, Calif., June 1962, 12FW392, 81154.

(15) H. L. Clever and R. M. Reeves, *J. Phys. Chem.*, **66**, 2268 (1962).

(16) G. Scatchard, *J. Am. Chem. Soc.*, **75**, 2883 (1953), and private discussion.

Table I: Observed Differences in Potentials (millivolts) between Saturated NaCl Solutions in Water and Various Media

	glass electrode saturated NaCl solution, AgCl(s); Ag(s)					
	15	25	Wt. % organic			
	$E_{\text{H}_2\text{O}}$		$E_{\text{mixed solvent}}$			
			30	50	75	90
Methanol-water		+1.3	+1.8	+2.1	+2.6	
Glycol-water		+0.6	+0.9	+1.5	+3.3	
DMF-water		± 0	± 0	+0.3	+0.4	
DEGMME-water		+1.5	+1.8	+2.5	+2.7	
Dioxane-water	+0.2		+0.6			

only to NaCl, the potential of a given glass electrode—silver-silver chloride pair should be the same for all solutions saturated with NaCl, whatever the solvent. Some differences, usually small, were observed in the present study (see Table I for typical examples). It is possible that these differences stem from drift of standard potentials or slow attack on Ag-AgCl electrodes at high organic content. By using a saturated solution of NaCl for each organic-water composition as reference, the possible effects of the medium on the electrode system were minimized.

The Ag-AgCl electrodes used in these experiments were of the thermal type.¹⁷ These electrodes were prepared in batches of six to eight at a time, shorted together, then placed in NaCl solution at 80° and allowed to cool overnight.¹⁸

The Ag-AgCl electrodes have proved to be more troublesome in several respects than the glass electrodes in water-organic solutions.

(1) They required for equilibration at least 10 min. and sometimes hours at high organic content, in comparison with 2-5 min. for the glass electrode. The rate of equilibration was established by transferring electrodes from a solution at one NaCl concentration to a solution at a different NaCl concentration and checking the e.m.f. against pre-equilibrated electrodes.

(2) The potential of the Ag-AgCl electrode is often unstable in water-organic solutions at or below 0.1 *m* in NaCl even though solutions are presaturated with AgCl.

(3) The Ag-AgCl electrode reacts with some organic solvents and becomes unstable in a short time (ranging from a few minutes to a few hours).

An observation that may be helpful in some situations is that the Ag-AgCl electrode equilibrates much more rapidly at 40° than at 25°. The reversibility of the cell was demonstrated by an experiment suggested by Harned. The potential of saturated NaCl solution

was measured at 25°. The temperature of the cell was then raised to a higher temperature (40°) and finally allowed to cool to the original temperature of 25° after 1 hr. The potential had returned to within 0.1 mv. of its original value on reaching 25°. The change of potential of saturated NaCl solution with temperature is about 2 mv./deg.

2. *Solutions and Materials.* Activity coefficients of NaCl were determined in solvents of water mixed with methanol, ethylene glycol (EG), ethylene glycol diacetate (EGDA), diethylene glycol monomethyl ether (methyl carbitol or DEGMME), dioxane, urea, and dimethylformamide (DMF). Except for DEGMME (purified), reagent grade chemicals were used without further purification since gas-liquid chromatography and residue checks indicated no significant impurities except water. The DEGMME (principal impurity, ethylene glycol) was purified by vacuum distillation. Peroxide present in dry dioxane presumably decomposed on addition of water and excess AgCl. Laboratory distilled water, which had been deionized by passage through a mixed-bed ion-exchange column, was used for preparation of solutions.

In interpretation of results, literature values of the dielectric constants were used for methanol, dioxane, and ethylene glycol mixtures with water¹⁹; dielectric constants of the other mixtures were measured in this laboratory. (The author is indebted to W. H. Baldwin for purification of DEGMME and for the use of the gas chromatograph, he is also indebted to R. J. Raridon and G. Westmoreland for dielectric constant measurements, solubility measurements, and water titrations.) The values used are given in Figure 2.

3. *Procedure.* For most of the solvents, potentials were measured for sodium chloride-organic-water solutions of 25, 50, 75, and 90% organic by weight; solubility of urea in water limited measurements to ~55% urea solution; for dioxane and EGDA, limited solubility prevented measurements at high organic contents. The organic fraction was constant to $\pm 0.1\%$ in each series. Solid AgCl was added to speed equilibration of the Ag-AgCl electrode with the solutions. Readings were recorded when the drift of potential became negligible. Measurements were at 25°, except some whose objective was to test the reversibility of the cell with changes in temperature.

(17) C. K. Rule and V. K. L. Mer, *J. Am. Chem. Soc.*, **58**, 2339 (1936).

(18) J. H. Ashby, F. M. Croke, and S. P. Datta, *Biochem J.*, **56**, 190 (1954).

(19) H. S. Harned and B. B. Owen, "The Physical Chemistry of Electrolytic Solutions," American Chemical Society Monograph Series, 3rd Ed., Reinhold Publishing Corp., New York, N. Y., 1958.

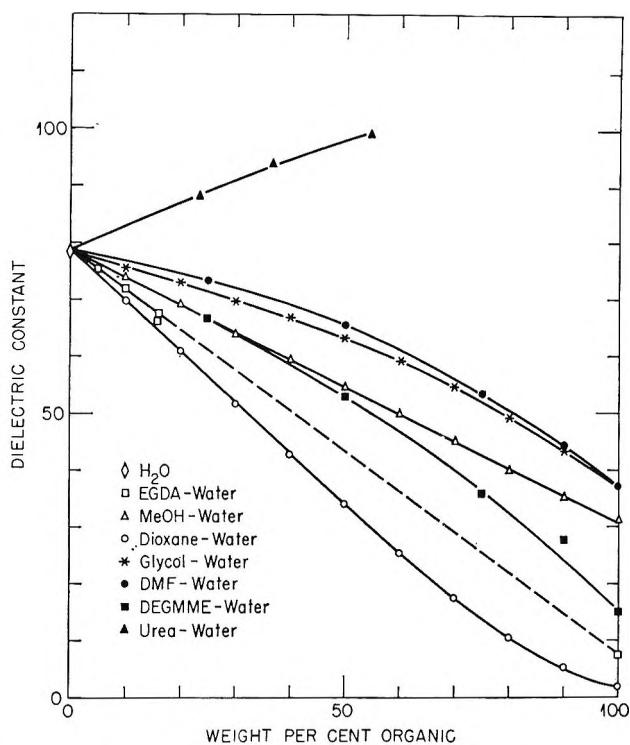


Figure 2. Dielectric constants of water-organic mixtures.

As one would expect, equilibration was faster at higher temperatures.

The procedure of carrying out all measurements for a given solvent composition in close succession, including that of the reference potential, should minimize effects of drifts in cell potential and of possible effects of solvent composition on e.m.f.

Some potentials of NaCl-H₂O solutions were also measured to test electrode performance. The saturation concentration in water was taken to be 6.144 m^{20} and the value of $\gamma_{\pm\text{NaCl sat}}$ to be 1.027, based on 0.7784 at 0.1 m NaCl¹⁹ and the measured difference in e.m.f. between 0.1 m NaCl and saturated aqueous solution.

Results and Discussion

The mean ionic activity coefficients γ_{\pm}^* were calculated from the measured potentials by the Nernst equation

$$E_{\text{ref}} - E = 0.1183 \log (a_{\pm\text{ref}}/m^*\gamma_{\pm}^*) \quad (2)$$

where a_{\pm} is mean ionic activity; the subscript "ref" indicates the reference, usually a solution of the water-organic mixture in question saturated in NaCl; and m^* is the salt concentration in moles per kilogram of water. It should be noted here that starred values of activity coefficients are referred to a value of unity at infinite dilution in water, with the concentration scale expressed in moles per kilogram of water.

The symbol $m = m^*f_w$ (where f_w is the weight fraction of water) refers to concentration in the conventional units, moles of NaCl per kilogram of mixed solvent. (Note that in the first two papers of this series, the symbols $m_{(o)}$ and $\gamma_{\pm(o)}$ were used to represent m^* and γ_{\pm}^* .)

1. *Reliability of Electrode Systems.* (a) *Activity Coefficients of NaCl in Aqueous Solution.* The most definitive test of cell performance with NaCl-H₂O solutions should be comparison of the observed differences of potential between solutions of different concentrations with differences computed from values of activity coefficients obtained by standard techniques. Precision obtained with this electrode system is illustrated in Figure 3 by the deviation of the experimental points, $E_{\text{ref}} - E$, from an average curve drawn through all points by eye. The activity coefficients given by Harned and Nims²¹ (sodium amalgam electrodes) tabulated by Robinson and Stokes,²²

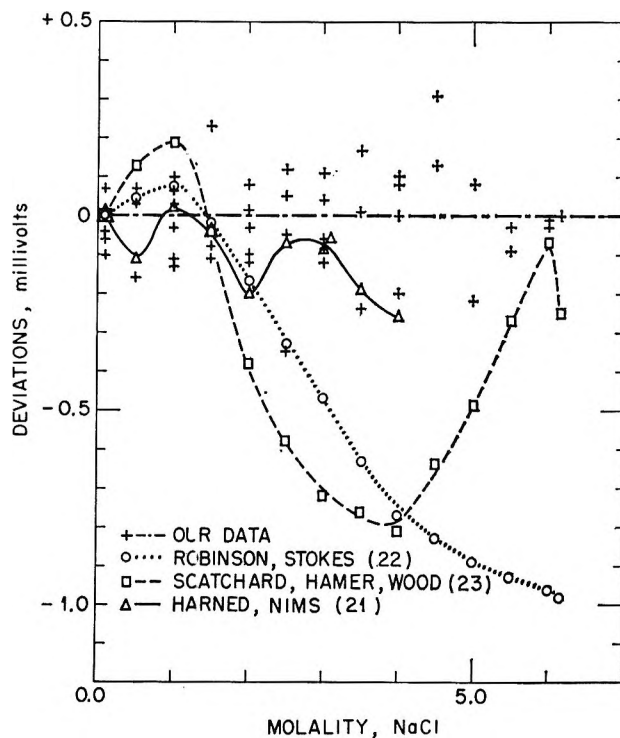


Figure 3. Precision of glass silver-silver chloride cell; comparison with literature activity coefficients of NaCl.

(20) A. Seidell and W. F. Linke, "Solubilities of Inorganic and Metal Organic Compounds," 4th Ed., D. Van Nostrand Co., Inc., New York, N. Y., 1958.

(21) H. S. Harned and L. F. Nims, *J. Am. Chem. Soc.*, **54**, 423 (1932).

(22) R. A. Robinson and R. H. Stokes, "Electrolyte Solutions," 2nd Ed., Butterworth and Co. Ltd., London, 1959.

and listed by Scatchard, *et al.*,²³ are compared with this average curve in Figure 3. The literature values were matched at 0.1 *m* with the present glass electrode results. With respect to precision, most of the present data are within ± 0.2 mv. of the reference curve though a few fall outside these limits. Comparison with literature values is somewhat difficult since the values from different sources disagree with each other by as much as 1 mv. The present results agree best with Harned's over the range he measured, diverge sharply from those given by Robinson and Scatchard at intermediate concentrations, and agree with the values of Scatchard but disagree with those of Robinson near saturation.

The divergence between the sets of values reported by such distinguished sources is disturbing, especially since NaCl is frequently used as a reference solute in isopiestic measurements. There appears to be a need for a resolution of these differences if the accuracy of standards in this widely used technique is to be comparable to the precision with which isopiestic ratios can be measured. The implication for the present study is that the alkali-sensitive glass electrode system data agree with literature results about as well as the literature values agree with one another.

(b) *Reliability of Electrodes in Water-Organic Systems.* Reproducibility of potentials in water-organic media varied with concentration of salt and of organic fraction, being generally better at high water content and high salt concentration. In general, precision was within 0.3 mv., often within 0.1 mv.

There is little in the literature allowing performance checks. Bower and Robinson²⁴ measured activity coefficients of NaCl in water-urea mixtures by the isopiestic method. Probably the best performance check is comparison with Åkerlöf's results²⁵ in methanol-water obtained with sodium amalgam electrodes. Comparison with these two studies will be discussed below. Comparison with the cation-sensitive glass electrode measurements of Shul'tz and Parfenov¹⁰ is more difficult. These workers estimate their reproducibility as *ca.* 1 mv. with glass electrodes. Their measurements of potentials of aqueous solutions do not give the theoretical variation of e.m.f. with activity of NaCl, which the electrodes in this study clearly approximate (Figure 3). They corrected their potentials in water-organic media by a calibration curve of observed e.m.f. in 100% water *vs.* salt activity; corrections amounted to several millivolts. With these corrections, the average deviation from Åkerlöf's differences of potential between water and water-organic solutions for 0.2 and 0.5 *m* NaCl is about 0.3 mv. in the range of 0-80% methanol (better than the accuracy attributed to either set of results by the

respective authors above 50% methanol). Above 80% methanol, deviations are several millivolts. The present measurements were carried out at different weight per cent methanol and cannot be compared directly.

Grunwald and Bacarella have measured activity coefficients of NaCl in 50% water-dioxane by a vapor pressure method.²⁶ Direct comparison with the present results is again not possible, but the two sets of measurements appear consistent with one another.

2. *Activity Coefficients of NaCl in Water-Organic Media. General.* The data ($E_{\text{sat}} - E$) for most water-organic mixtures are presented in Table II. The subscript "sat" indicates a solution saturated in NaCl. When phase splits precluded measurements of E_{sat} for a given solvent composition, measurements were carried out by two slightly different procedures, and the results ($E_{\text{ref}} - E$) are given in Table III. If a succession of solutions of the same solvent composition was measured consecutively, differences in potential are reported between the solutions and one selected as reference, the difference between the reference (m^*_{ref}) and an aqueous solution having $m = m^*_{\text{ref}}$ also being given. If solutions of the same m^* but different organic content were measured successively, differences of potential between the mixed solvent and aqueous solutions are listed.

The values of $\log \gamma_{\pm}^*$ obtained from these data are given in Figures 4-10 along with points for the saturated solutions obtained from solubilities.²⁷ Those values of $\log \gamma_{\pm}^*$ based on the e.m.f. values of Table III, which could not be referred to a saturated NaCl solution of the same water-organic content, may not be as reliable on an absolute basis. The $\Delta \log \gamma_{\pm}^*$ values from Table III for solutions of different NaCl concentration in the same water-organic medium, however, should be about as good as those from Table II. Literature values²² for $\log \gamma_{\pm \text{NaCl}}$ in water are also shown in the figures.

The approach to Debye-Hückel behavior is shown at the low concentration end; the curves are obtained from the equation (γ_{org} is the mean ionic (molal)

(23) G. Scatchard, W. J. Hamer, and S. E. Wood, *J. Am. Chem. Soc.*, **60**, 3061 (1938).

(24) V. E. Bower and R. A. Robinson, *J. Phys. Chem.*, **67**, 1524 (1963).

(25) G. Åkerlöf, *J. Am. Chem. Soc.*, **52**, 2353 (1930).

(26) E. Grunwald and A. L. Bacarella, *ibid.*, **80**, 3840 (1958).

(27) K. A. Kraus, R. J. Raridon, and W. H. Baldwin, *ibid.*, **86**, 2571 (1964). Solubilities in water organic mixtures not given in this reference were measured by R. J. Raridon and G. Westmoreland in this laboratory.

Table II: E.m.f. Measurements for Sodium Chloride-Water-Organic Solutions (wt. % organic: m^* , ΔE^a)

Methanol 25%: 0.00996, 306.2; 0.0389, 240.75; 0.0737, 210.4; 0.0949, 199.3; 0.2888, 147.7; 0.9242, 94.0; 1.005, 89.05; 2.992, 32.5; 3.158, 30.35. 50%: 0.00996, 278.9; 0.0389, 213.65; 0.0737, 183.7; 0.0949, 172.35; 0.2888, 121.5; 0.9242, 69.5; 0.9978, 65.9; 3.011, 12.35; 3.158, 10.3. 75%: 0.00996, 256.0; 0.0389, 191.65; 0.0818, 157.6; 0.0949, 151.05; 0.2888, 101.6; 0.9242, 51.4; 0.9921, 48.0. 90%: 0.00996, 262.2; 0.0389, 196.65; 0.0899, 157.35; 0.0949, 155.6; 0.2888, 106.25; 0.9102, 57.6; 0.9242, 56.65; 2.716, 10.95; 3.158, 3.85.

Ethylene glycol 25%: 0.00996, 326.35; 0.03894, 261.3; 0.0949, 219.5; 0.1149, 210.45; 0.2888, 167.95; 0.9242, 112.6; 0.9970, 108.3; 2.987, 49.35; 3.158, 45.95. 50%: 0.00996, 317.25; 0.0389, 253.15; 0.0949, 211.8; 0.1030, 207.85; 0.2888, 160.4; 0.9242, 106.0; 1.006, 101.85; 2.972, 46.55; 3.158, 40.6. 75%: 0.00996, 319.7; 0.03894, 255.3; 0.0924, 217.85; 0.0949, 214.45; 0.2888, 163.05; 0.9242, 110.2; 1.012, 106.0; 2.959, 55.05; 3.158, 50.35; 6.144, 12.9. 90%: 0.00996, 340.9; 0.3894, 276.7; 0.0884, 238.9; 0.09074, 235.3; 0.2888, 184.1; 0.9242, 131.9; 1.080, 125.4; 2.994, 79.0; 3.158, 76.45; 6.144, 44.5.

Diethylene glycol monomethyl ether 25%: 0.00996, 323.85; 0.03894, 260.05; 0.0949, 217.95; 0.2888, 166.0; 0.9242, 111.2; 3.154, 44.35. 50%: 0.00996, 295.05; 0.03894, 232.6; 0.0949, 191.35; 0.2888, 141.55; 0.9242, 89.7; 3.150, 29.2. 75%: 0.00996, 250.05; 0.03894, 189.0; 0.0949, 151.3; 0.2888, 105.85; 0.9242, 58.6; 3.146, 5.7. 90%: 0.00996, 222.1; 0.03894, 163.05; 0.0949, 128.05; 0.2888, 86.6; 0.9242, 45.35.

Dioxane 15%: 0.01206, 308.7; 0.02695, 272.25; 0.0923, 215.15; 0.0990, 212.85; 0.2717, 165.8; 1.002, 104.8; 1.010, 104.3; 3.002, 45.5; 3.103, 43.55. 30%: 0.01206, 291.6; 0.02695, 254.65; 0.0923, 198.75; 0.1080, 195.85; 0.2717, 150.5; 0.9966, 91.7; 1.010, 91.35; 2.990, 34.85; 3.103, 33.2.

Urea 23% (5 m): 0.00996, 336.05; 0.03894, 276.9; 0.0949, 235.1; 0.2888, 181.35; 0.9242, 122.7; 3.158, 51.85. 37.5% (10 m): 0.00996, 343.55; 0.03894, 279.4; 0.0949, 236.45; 0.2888, 182.6; 0.9242, 123.75; 3.158, 52.95. 54.5% (20 m): 0.00996, 343.6; 0.0389, 283.15; 0.0949, 240.8; 0.2888, 186.6; 0.9242, 127.6; 3.158, 57.8.

Dimethylformamide 25%: 0.01206, 305.45; 0.02695, 266.9; 0.0923, 208.35; 0.1093, 200.85; 0.2717, 157.85; 0.9874, 97.1; 1.010, 95.8; 3.009, 37.6; 3.103, 35.65. 50%: 0.01206, 272.75; 0.02695, 234.0; 0.0923, 176.15; 0.1126, 166.8; 0.2717, 126.70; 0.9624, 70.45; 1.010, 67.6; 2.920, 16.25; 3.103, 12.8. 75%: 0.01206, 230.05; 0.02695, 192.15; 0.0923, 134.8; 0.1125, 126.4; 0.2717, 86.85; 0.9860, 30.65; 1.010, 30.55. 90%: 0.01206, 200.35; 0.02695, 161.65; 0.0923, 104.15; 0.2717, 56.35.

^a $\Delta E = E_{\text{sat}} - E$, in millivolts, measured at same solvent composition.

activity coefficient though the \pm subscript is dropped for convenience)

$$\log \gamma_{\text{org}} = \frac{-S\sqrt{c}}{1 + a'\sqrt{c}} \quad (3)$$

where c is concentration in moles per liter, S is the Debye-Hückel limiting slope for the appropriate dielectric constant, and the parameter a' is taken to be 1.5 for water and adjusted for the dielectric constant of the medium in question (ref. 19, pp. 164-166). Values of the activity coefficients computed with

Table III: E.m.f. Measurements for Sodium Chloride-Water-Organic Solutions. Immiscible Phases when Saturated with NaCl (wt. % organic: m^* , ΔE^a)

Dioxane 60%: 0.01206, 172.6; 0.02695, 138.85; 0.0923, 89.95; 0.2717, 49.45; 1.010, 0 (-67.70)

Ethylene glycol diacetate 5%: 0.00995, -5.6; 0.0296, -4.55; 0.0998, -4.3; 0.9989, -3.35; 3.192, -2.6. 5%: 0.01206, 96.15; 0.0270, 58.2; 0.0923, 0 (-4.3); 0.2717, -50.3; 1.010, -112.3; 3.103, -174.4. 10%: 0.00995, -10.2; 0.0296, -8.3; 0.0998, -8.0; 0.999, -5.9. 10%: 0.01206, 96.05; 0.02695, 58.15; 0.0923, 0 (-8.0); 0.2717, -49.65; 1.010, -111.8. 20%: 0.00995, -16.9; 0.0296, -14.75; 0.0998, -13.55. 20%: 0.01206, 94.00; 0.02695, 56.7; 0.0923, 0 (-13.55)

^a ΔE (millivolts) in Roman type is difference in potential between solution and reference solution (for which $\Delta E = 0$) having same solvent composition. E.m.f. difference between reference and aqueous solution, $m^*_{\text{ref}} = m$, is given in parentheses. ΔE (millivolts) in italics is the difference between solution and aqueous solution, $m^* = m$.

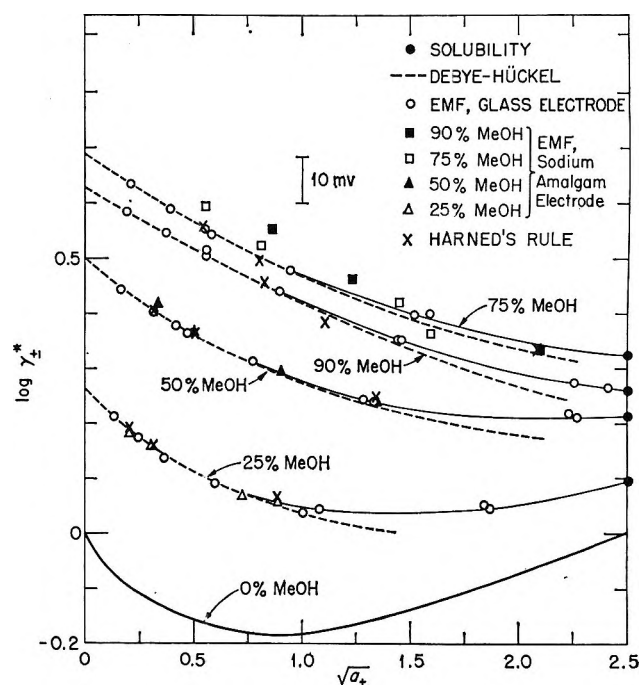


Figure 4. Activity coefficients of NaCl in methanol-water; comparison with Åkerlöf's measurements made with sodium amalgam electrode.

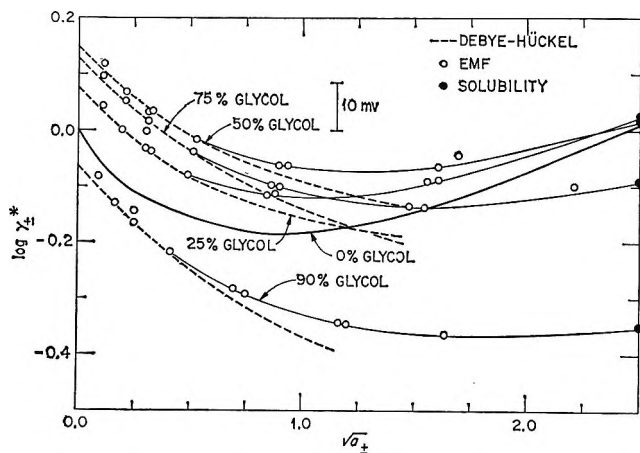


Figure 5. Activity coefficients of NaCl in ethylene glycol-water.

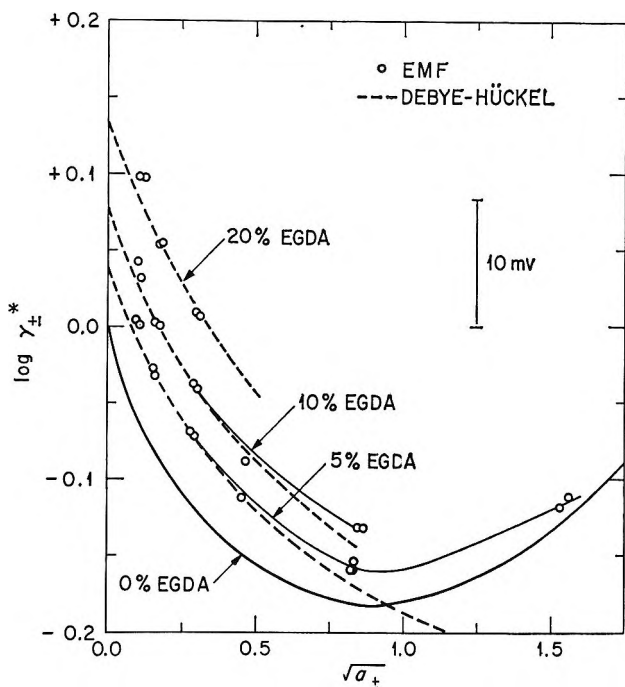


Figure 6. Activity coefficients of NaCl in ethylene glycol diacetate-water.

eq. 3 are of course referred to unity at infinite salt dilution in the medium; they are adjusted to the reference of the figures by matching to the experimental curve at low NaCl concentration. Between any two NaCl concentrations at the same organic fraction

$$\Delta \log \gamma_{\text{ORG}} = \Delta \log \gamma_{\pm}^* \quad (4)$$

It can be seen that in most cases the values of $\log \gamma_{\pm}^*$ approach closely Debye-Hückel behavior at low concentrations. Extrapolation to obtain $\log \gamma_{\pm}^*_{\infty}$,

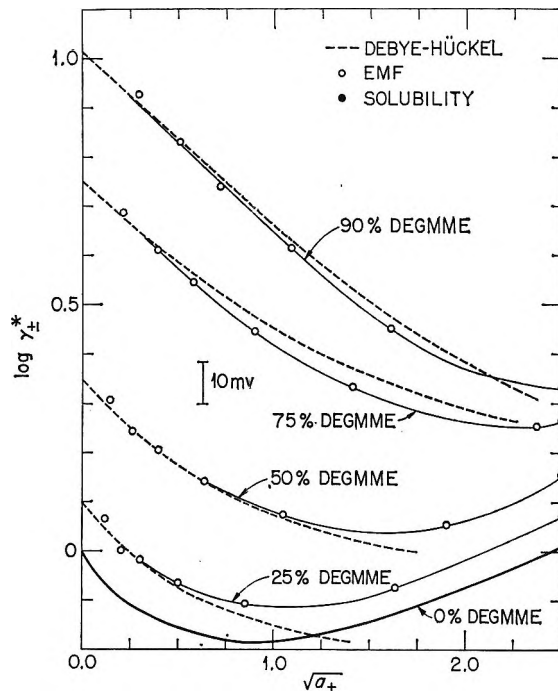


Figure 7. Activity coefficients of NaCl in diethylene glycol monomethyl ether-water.

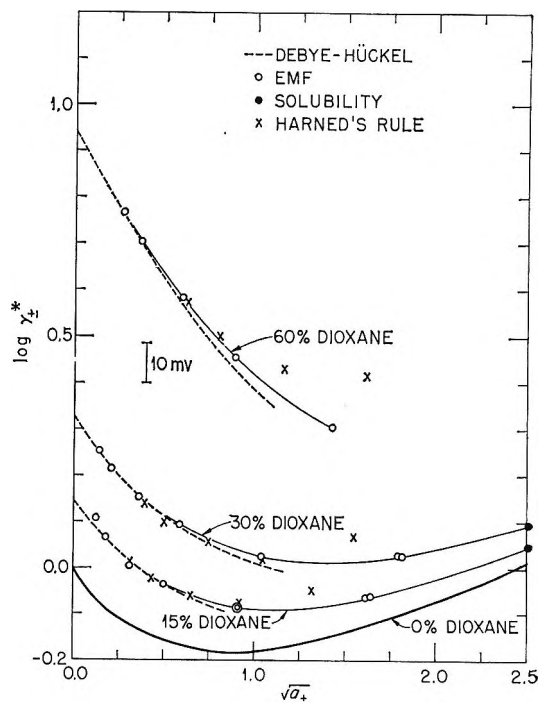


Figure 8. Activity coefficients of NaCl in dioxane-water; comparison with estimates made from activity coefficients of HCl by Harned's rule for mixed solvents.

the value at infinite dilution of salt, can therefore be made with considerable confidence.

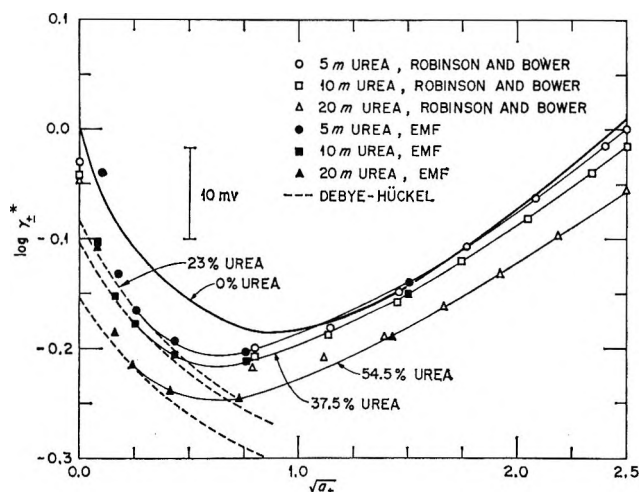


Figure 9. Activity coefficients of NaCl in urea-water; comparison with values of Robinson and Bower.

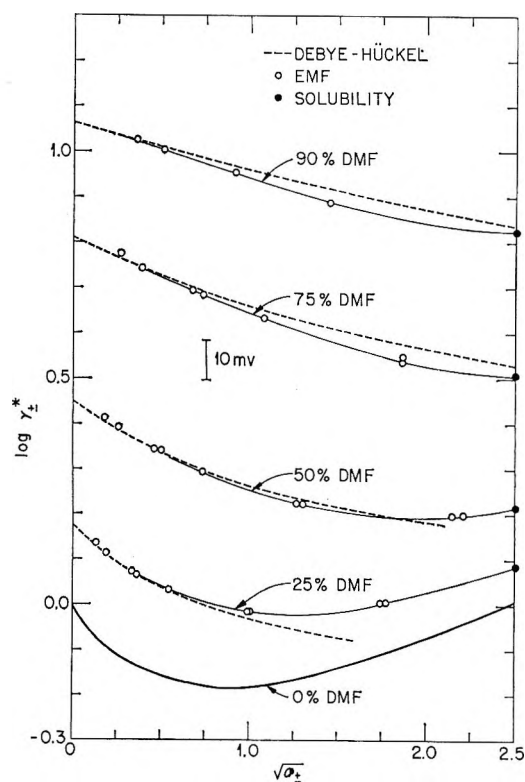


Figure 10. Activity coefficients of NaCl in dimethylformamide-water.

Results for the various systems are discussed individually.

(a) *Methanol-Water*. Values (Figure 4) of $\log \gamma_{\pm}^*$ increase with organic content for 0–75% organic, but the values for 90% are lower than those for 75%. Such a maximum must occur with the definition of starred

activity coefficient; since m^* goes to infinity as water fraction goes to zero, γ_{\pm}^* must go to zero.

In Figure 4 comparison is made with values computed from the data of Åkerlöf,²⁵ obtained with a sodium amalgam electrode (at 25 and 75% organic interpolation of Åkerlöf's data was necessary). Agreement is fairly good at 25 and 50% methanol (mostly within a fraction of 1 mv.), somewhat poorer at 75%, and poor at 90%. Åkerlöf expresses reservations about his accuracy at high organic content; from the consistency of the present results with values obtained for saturated NaCl from solubility measurements, it seems that the glass electrode measurements may be better at high organic content than the amalgam measurements.

(b) *Ethylene Glycol and Its Diacetate*. Values of $\log \gamma_{\pm}^*$ are considerably less for ethylene glycol (Figure 5) than for methanol at a given weight per cent organic. Correlation with solubility values seems satisfactory.

Measurements for EGDA (Figure 6) are on the water-rich side of a phase split, and consequently the reference potential is not measured at the same organic content. The primary interest with this system was to obtain activity coefficients for NaCl in water-rich solutions in order to estimate activity coefficients in equilibrated organic-rich phases from distribution coefficient measurements.²⁸ For a given per cent organic, values of $\log \gamma_{\pm}^*$ are somewhat higher for the diacetate than for ethylene glycol.²⁷

(c) *Diethylene Glycol Monomethyl Ether*. Activity coefficients (Figure 7) for a given per cent organic are higher than for ethylene glycol and are comparable to values with methanol.

The negative deviation from the Debye-Hückel line for 75 and 90% DEGMME may indicate ion-pair formation, but this deviation could also be accounted for by an error in the dielectric constant used to get the Debye-Hückel curve (see Figure 2).

(d) *Dioxane*. Activity coefficients in dioxane-water (Figure 8) were measured only to 60% organic because of phase splitting. The reference concentration at 60% was taken to be $m^* = 1$, and its γ_{\pm}^* was computed from the difference in E measured between this solution and 1 *m* aqueous NaCl.

(e) *Urea*. Activity coefficients in water-urea mixtures (Figure 9) are compared with the isopiestic results of Robinson and Bower.²⁴ Above $\sqrt{a_{\pm}} = 0.2$, agreement appears good (within 1 mv.) in the region of

(28) W. J. Wallace, R. J. Raridon, and K. A. Kraus, unpublished results.

overlap for 23 and 37.5% urea. In 54.5%, deviations are greater.

There is a sharp rise in measured values of γ_{\pm}^* with decreasing concentration at low NaCl concentrations. The data do not appear to fit the Debye-Hückel equation in this case, but systematic errors may account for this. An error at low NaCl concentration seems likely (e.g., the urea may have been contaminated by chloride). The Debye-Hückel curve was therefore matched above $\sqrt{a_{\pm}} = 0.2$. The Robinson-Bower points extrapolated to zero molality of NaCl are also high, however, and the procedure adopted is open to criticism.

In any case, it appears that with this organic compound, the only one studied which increases the mixed solvent dielectric constant, values of γ_{\pm}^* decrease with increasing organic content.

(f) *Dimethylformamide-Water*. Activity coefficients of NaCl in dimethylformamide-water are given in Figure 10. Here, as with DEGMME, experimental values at high organic content fall below the Debye-Hückel curve, but the dielectric constants in this case are not low enough for ion pairing to be expected. The solubility of AgCl appears to be enhanced by the presence of DMF and may account for the discrepancies.

3. *Discussion*. (a) *Correlation of Activity Coefficients with Dielectric Constants*. It is of interest to examine extrapolations of activity coefficients, as $\log \gamma_{\pm}^*_{\infty}$, in the light of the Born equation; a convenient form for NaCl is obtained from eq. 8 of ref. 29 by dropping terms involving concentration of NaCl and distance from interfaces.

$$\log \gamma_{\pm}^*_{\infty} - \log X_1 = \frac{\epsilon^2}{4.606DkT} \left(\frac{1-\rho}{\rho b_{\pm}} \right) \quad (5)$$

where X_1 is the mole fraction of water; ϵ , the charge of the electron; D , dielectric constant of water; D_{org} , dielectric constant of the water-organic phase; $\rho = (D_{org}/D)$; T , absolute temperature; k , the Boltzmann constant; and b , the radius of the ions

$$1/b_{\pm} \equiv \frac{1}{2} \left(\frac{1}{b_+} + \frac{1}{b_-} \right)$$

for NaCl. The left side of (5) plotted vs. $(1-\rho)/\rho$ thus should give a straight line, whose slope is proportional to $1/b_{\pm}$.

In Figure 11, extrapolations of Figures 4-10 are presented in this way. It is apparent that for mixtures of a given organic solvent, the plotted function is roughly linear vs. $(1-\rho)/\rho$ for organic components decreasing the solvent dielectric constant though most systems show a slight concavity downward. An

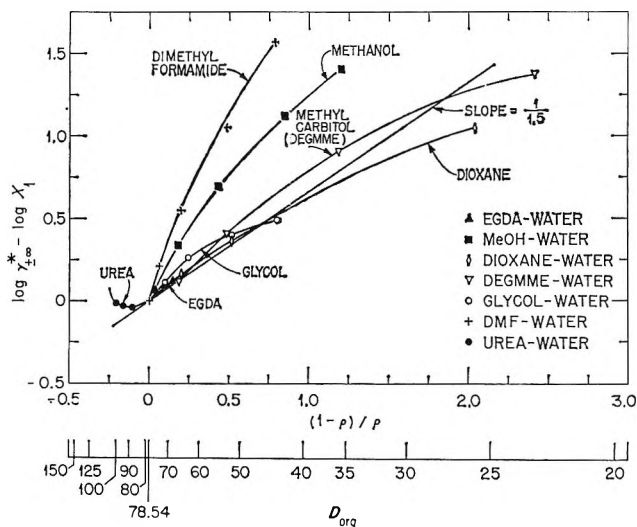


Figure 11. Activity coefficients of NaCl in water-organic mixtures at $m^* = 0$. Theoretical line, slope = $1/1.5$, consistent with the Debye-Hückel "distance of closest approach."

approximate value of activity coefficients at high organic content should be obtainable from data taken in water-rich solutions. It is clear that no single value of ionic radii fits all systems, but this is not surprising for a number of reasons³⁰—concentration of one solvent component preferentially around ions or orientation of organic molecules in the neighborhood of ions, for example. The value of b_{\pm} is thus best considered as an adjustable parameter, similar to the Debye-Hückel distance of closest approach, but smaller in magnitude.

(b) *Harned's Rule for Organic-Water Mixtures*. Harned³¹ has proposed a rule for computation of activity coefficients of single (not mixed) electrolytes in mixed solvents, which can be stated

$$(\gamma_{org})_{NaCl} = (\gamma_{\pm})_{NaCl} \frac{(\gamma_{org})_{HCl}}{(\gamma_{\pm})_{HCl}} \quad (6)$$

where the activity coefficients of NaCl and HCl are taken for the same moles of NaCl per kilogram of total solvent. He has tested this relation with Åkerlöf's sodium chloride-methanol-water data up to 20% methanol. Values for higher weight per cent alcohol solutions are shown in Figure 4 (matched by multiplying by $\gamma_{\pm}^*_{\infty}$). (The HCl activity coefficients were obtained from ref. 25.) A test of eq. 6 with dioxane is also made, and the comparison is shown in Figure 8.

(29) G. Scatchard, *J. Phys. Chem.*, **68**, 1056 (1964).

(30) G. Scatchard, *Trans. Faraday Soc.*, **23**, 454 (1927); *J. Chem. Phys.*, **9**, 34 (1941).

(31) H. S. Harned, *J. Phys. Chem.*, **66**, 589 (1962).

Agreement seems good as long as Debye-Hückel behavior is observed.

(c) *Hyperfiltration Implications.* In the hyperfiltration, or reverse osmosis, desalination process, salt is removed from water by forcing solution through a membrane which tends to reject salt. The performance of a membrane depends both on the kinetics of water and salt transport and on the equilibrium distribution of salt and water between solution and membrane phases. To the extent that water-organic mixtures can serve as models for membranes made of chemically similar groups linked in some way to form an insoluble matrix, activity coefficients of salt in liquid media can give information on the equilibrium properties of membranes. The correlation is especially evident with the starred activity coefficient; the ratio $\gamma_{\pm}/\gamma_{\pm}^*$, compared at the same activity of NaCl in the two media, is equal to the distribution coefficient, m^*/m , between the water and the membrane phase containing the same weight per cent of water as the water-organic mixture if it is assumed that the mixed solvent is a perfect model of the membrane.²⁷

Since the abscissas of Figures 4-10 are in terms of activity of NaCl, the vertical distance between the $\log \gamma_{\pm}^*$ curves for water and for water-organic media are measures of the rejection ability of a membrane for which the water-organic solution is a model. It appears that, in most cases, rejection is expected to increase somewhat with decreasing feed concentration. The argument that a solution of given organic-water content should be a good model for a membrane may be questioned with respect to the significance of the $\log X_1$ term of eq. 5 in application to membranes, but for a given value of X_1 the relative change of rejection with feed concentration should not be affected.

Acknowledgment. The author wishes to acknowledge the very sizable contribution of Dr. J. S. Johnson to this paper. His advice and assistance have greatly improved the final presentation. Thanks are also due to Prof. George Scatchard and to Dr. K. A. Kraus for many helpful discussions during the course of this work.

The Radiation Chemistry of Cyclopentane

by B. Mason Hughes and Robert J. Hanrahan

Chemistry Department, University of Florida, Gainesville, Florida (Received March 3, 1965)

The products of the radiolysis of pure liquid cyclopentane were found to be hydrogen, methane, ethane, propylene, propane, cyclopropane, C_4 's, *n*-pentene, *n*-pentane, cyclopentene, and bicyclopentyl. The *G* value of the major products are: hydrogen, 5.20; ethylene, 0.40; *n*-pentene, 0.62; cyclopentene, 3.10; bicyclopentyl, 1.22. The total *G* value for radical production was determined to be 6.40 using HI as a scavenger. Hydrogen production was shown to be temperature dependent when scavengers were present at concentrations between 1 and 10 mM. The reaction scheme is similar to that of cyclohexane except for the occurrence of greater C-C bond rupture and ring cleavage. The latter effects can be attributed to strain in the C_5 ring.

Introduction

There has been considerable interest in the radiation chemistry of cyclohexane for a number of years. Recently there have been studies of the radiolysis of mixtures of the analogous C_5 compound, cyclopentane, with cyclohexane as well as other substances.^{1,2} However, to date, little effort has been devoted to studies of the radiation chemistry of pure cyclopentane.³ Because of its low freezing point (-93°) there are a number of questions which may be investigated using this compound, such as temperature dependence of various processes and possible measurement of activation energies. This paper includes a report of major and minor product yields in the radiolysis of pure liquid cyclopentane and a discussion comparing its radiation chemistry with that of cyclohexane. A preliminary report of experiments showing temperature dependence of the hydrogen production with scavengers present is also included.

Experimental

Phillips Petroleum Co. pure grade cyclopentane was stirred with fuming sulfuric acid for 2 to 3 hr., washed, and distilled. The first fraction was collected, and the cyclopentane peak was isolated on an Aerograph Autoprep preparative scale gas chromatograph. The first fraction was used since the lower boiling impurities could be separated chromatographically from the cyclopentane fraction more easily than could the higher boiling impurities that would be present in the later fractions. Flame ionization gas chromatography

showed the cyclopentane purified in this manner to be purer than Phillips research grade, with no impurity of cyclopentene. Standards of methane, ethane, propane, propylene, and cyclopropane were obtained at 99% purity from Matheson Co.; ethylene and pentene-1 was obtained at 99% purity and cyclopentene was obtained at 99.89% purity from Phillips Petroleum Co. Iodine was Merck resublimed, methyl iodide was obtained from Eastman Kodak Co., and hydriodic acid was Baker Analyzed Reagent.

Bicyclopentyl was prepared by a Wurtz-type reaction of sodium with cyclopentyl bromide. The fraction that was collected at 184° was further purified by gas chromatography to a purity better than 99%. The collected peak was confirmed to be bicyclopentyl by mass spectral analysis.

Hydrogen iodide was produced by dehydrating hydriodic acid. The hydriodic acid was frozen to liquid nitrogen temperature in a round-bottom flask, and P_2O_5 was added on top of it. The frozen acid was then attached to the vacuum line and degassed. The hydriodic acid was allowed to melt and interact with the P_2O_5 , and the HI gas released was collected in another portion of the vacuum system. This collected hydrogen iodide was degassed again and stored at liquid

(1) J. A. Stone, *Can. J. Chem.*, **42**, 2872 (1964).

(2) G. A. Muccini and R. H. Schuler, *J. Phys. Chem.*, **64**, 1436 (1960).

(3) (a) A. R. Lepley, *Anal. Chem.*, **34**, 322 (1962); (b) A. R. Lepley, Dissertation, University of Chicago, 1957.

nitrogen temperature until used. The amount of hydrogen iodide added to the samples was determined by gas measurements.

Samples were dried over P_2O_5 , degassed and melted three times, and distilled under vacuum to the radiation vessels. For determination of the liquid products, 4-ml. vessels were used. For the hydrocarbon products which were gases at room temperature, 178- μ l. ampoules were prepared using a vacuum-line buret.⁴ Irradiations were performed using a cobalt-60 γ -irradiator which has been described previously.⁵ The dose rate absorbed by cyclopentane in the 4-ml. vessel was determined by the Fricke dosimeter [$G(Fe^{3+}) = 15.6$] to be 4.42×10^{17} e.v./ml. min., and the absorbed dose rate in the 178- μ l. sample was found to be 1.04×10^{18} e.v./ml. min. by using $G(I_2) = 2.11$ for the radiolysis of ethyl iodide. (This value of $G(I_2)$ is the value obtained when ethyl iodide was irradiated in the 4-ml. vessel at the above dose rate.)

The radiolyses of cyclopentane with added iodine or hydrogen iodide were done in 4-ml. vessels with attached optical cells. The optical densities were measured at various time intervals of irradiation with a Beckman DU spectrophotometer obtaining either rates of production or consumption of iodine. The extinction coefficient of iodine in cyclopentane was measured to be 906 l./mole cm. at the absorption maximum of 524 m μ .

The identification of products was done in two independent ways: comparison of retention times of known standards with the irradiation products and direct determination of mass spectroscopic fragmentation patterns of the individual radiolysis products. The mass spectroscopic techniques have previously been described by Fallgatter and Hanrahan.⁶ In their procedure a gas chromatograph is connected with a Bendix time-of-flight mass spectrometer so that a spectrum of each component of the radiation mixture can rapidly be recorded. These spectra are then compared with standard spectra to determine their identity.

For quantitative determinations, liquid standards were diluted with the g.l.c. purified cyclopentane and injected into a laboratory-made gas chromatograph with an Aerograph flame ionization detector. These injections varied from 5 to 35 μ l. Gas standards were injected into the chromatograph using 35 μ l. injections of the pure gas with gas-tight Hamilton syringes.

To determine the yields of the liquid products, the 4-ml. vessels were broken open, and samples of the standard and the irradiated cyclopentane were alternately injected. The peak areas were compared with the standard peak areas using a Photovolt electronic integrator. The yields of the gaseous products

were determined slightly differently. First, an ampoule was placed in the chromatograph within a breaking device; then the gas standards were injected with a gas-tight Hamilton syringe and analyzed. After three or four injections of the various standards, the ampoule was finally broken, and the peak areas of the irradiation products were compared with the average peak area of the standard injections. Using a McLeod gauge, the hydrogen gas yields were determined as the gas volatile at -196° .

Table I: Yields in Cyclopentane Radiolysis (G Values)

Product	This work	Lepley ^a	Other workers		
Hydrogen	5.20	3.79	5.2 ^b	5.25 ^c	4.97 ^d 5.78 ^e
Methane	0.04	1.50			
Ethylene	0.40	1.40			
Ethane	0.08				
Propylene	0.16	0.55			
Propane	0.08	0.16			
Cyclopropane	0.10	0.13			
C ₄	Trace				
n-Pentene	0.62	0.59			
n-Pentane	0.16	0.15			
Cyclopentene	3.10	1.50	3.4 ^b	2.94 ^c	3.0 ^d
Bicyclopentyl	1.22	1.62	1.06 ^b	1.30 ^d	
$G(-I_2)$	3.0 ^f		2.53 ^g	3.6 ^h	
$G(I_2)$ (added HI)	3.20				

^a Lepley's data³ were taken at several doses to 100 Mrads and beyond. Values given here are approximate extrapolations of his data to zero dose. ^b Holroyd.¹⁰ ^c Toma and Hamill.¹¹ ^d Stone.¹ ^e Hardwick.¹² ^f Approximate initial value; after ca. 5×10^4 rads, $\mathcal{F}(-I_2)$ is 2.47, in agreement with the value of Dauphin.¹⁷ ^g Dauphin.¹⁷ ^h Weber, Forsyth, and Schuler.¹⁶

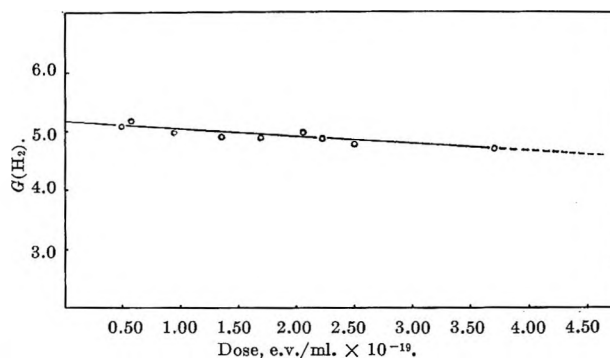


Figure 1. Dependence of hydrogen yield on total dose absorbed.

- (4) R. J. Hanrahan, *J. Chem. Educ.*, **41**, 623 (1964).
 (5) R. J. Hanrahan, *Intern. J. Appl. Radiation Isotopes*, **13**, 254 (1962).
 (6) M. B. Fallgatter and R. J. Hanrahan, *J. Phys. Chem.*, **69**, 2059 (1965).

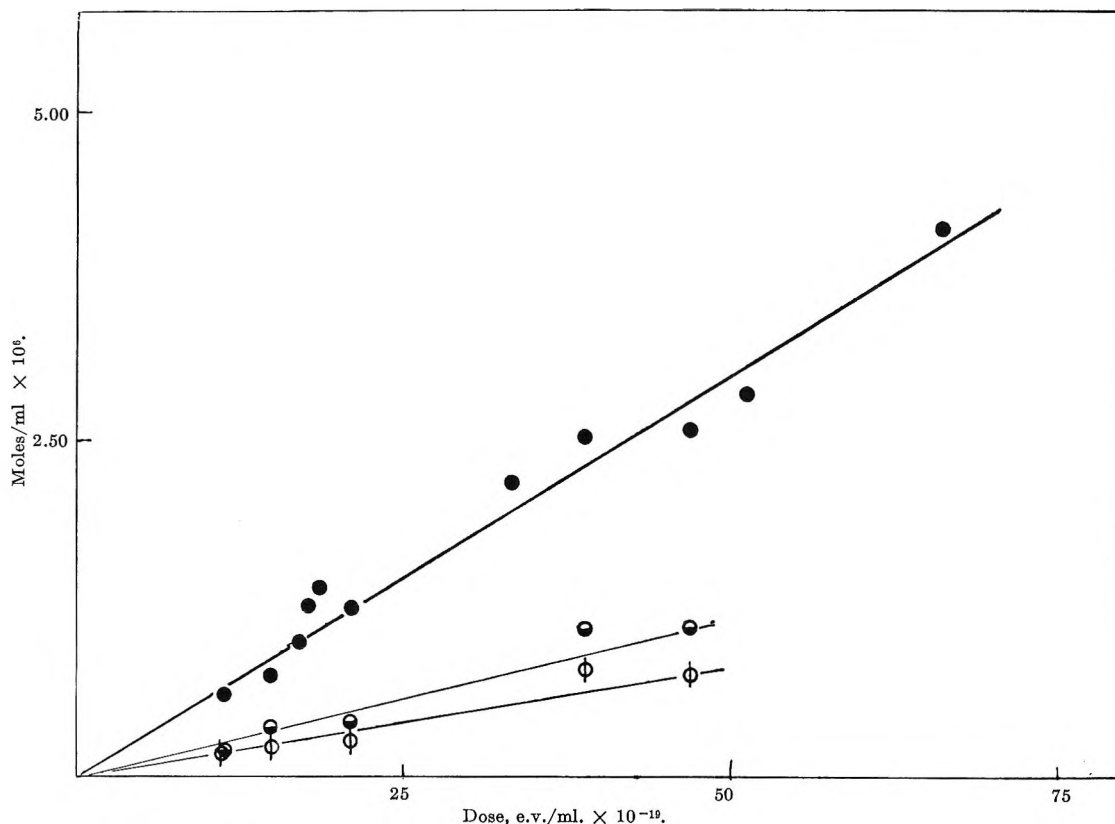


Figure 2. Production of ethylene (●), propylene (◐), and cyclopropane (◑) vs. dose.

Results

Pure Cyclopentane. The main products of the radiolysis of cyclopentane are hydrogen, cyclopentene, and bicyclopentyl with lesser amounts of *n*-pentene and ethylene. A resumé of all of the *G* values is given in Table I.

All of our reported values are extrapolated to zero dose. The *G* value for production of H_2 was found to be 5.20. As can be seen from Figure 1, it is quite dependent upon dose. Of the C_1 - C_4 products, by far the largest product is ethylene with a yield of 0.40. The other low boiling products include all of the possible alkane and alkene hydrocarbons between C_1 and C_3 , including cyclopropane. The rates of production of ethylene, propylene, and cyclopropane are shown in Figure 2. The linearity at these low doses suggests that they are being produced in primary processes. Although the precision of the ethylene determination is not especially good, the absolute error in the *G* value is not more than ± 0.05 .

The C_5 yields are 3.10 for cyclopentene, 0.62 for *n*-pentene, and 0.16 for *n*-pentane, and the yield of bicyclopentyl is 1.22. Figure 3 shows that there is only slight dependence of the yields on dose at these low doses.

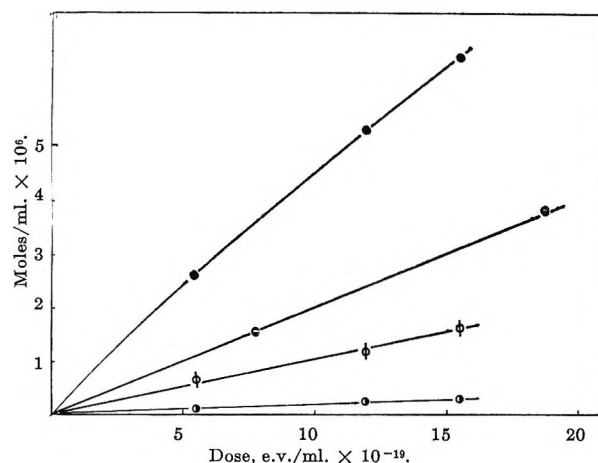


Figure 3. Production of cyclopentene (●), bicyclopentyl (◐), *n*-pentene (◑), and *n*-pentane (◒) vs. dose.

Cyclopentane with Scavengers. The initial *G* value for I_2 production in systems in which HI was added to cyclopentane was determined to be 3.20. As can be seen from Figure 4 the initial slope of a graph of I_2 concentration vs. dose for all of the runs was the same, regardless of the initial concentration of HI. The graphs for more dilute solutions began their curvature earlier, indicating competitive scavenging by the

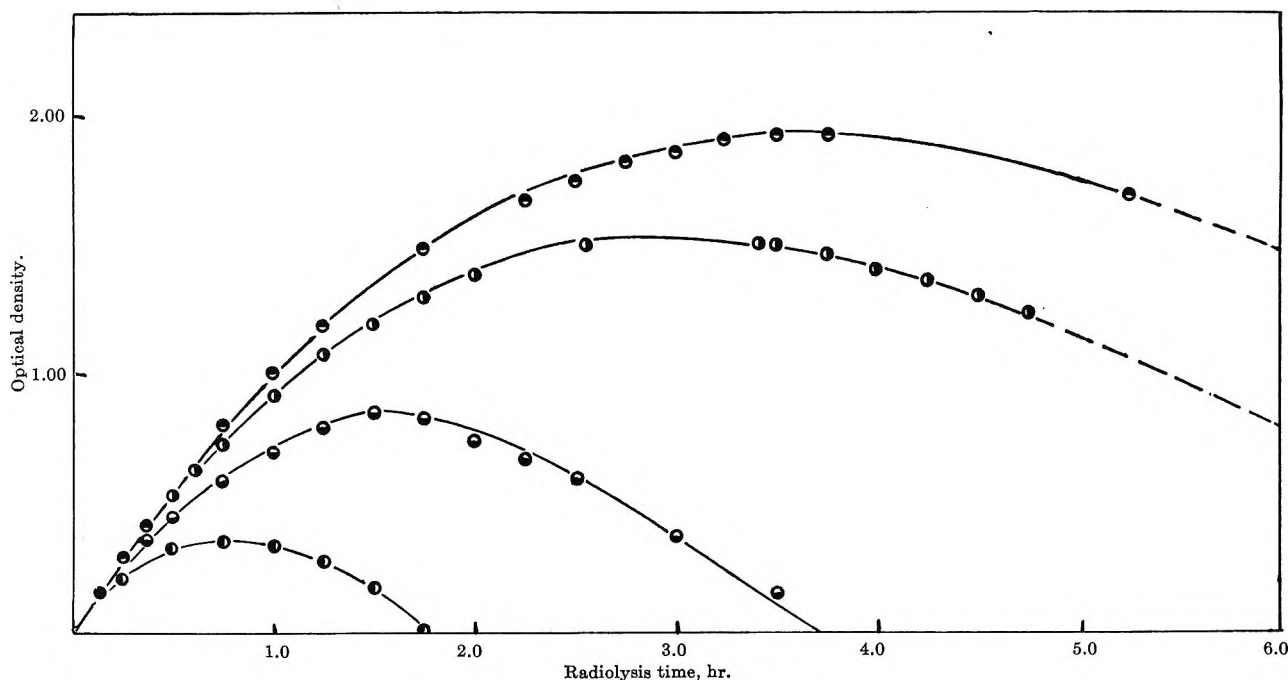


Figure 4. Iodine production in the radiolysis of pure cyclopentane with added HI. The initial molar concentration of HI for each experiment: \bullet , 10.1×10^{-3} ; \circ , 7.66×10^{-3} ; \blacksquare , 4.52×10^{-3} ; \square , 1.92×10^{-3} .

I_2 produced in the reaction. An interesting regularity is found if the approximation is made that, at the maximum of the experimental graphs, the residual HI concentration can be calculated by subtracting from the initial HI concentration the number of equivalents of iodine atoms present as I_2 . With this assumption, it is found that the ratio of the concentration of HI to I_2 at the maximum is a constant, 0.365, with a variation of only 3% in a set of three experiments in which the initial HI concentration varied by a factor of 5.

Results of several experiments with iodine added as a scavenger are shown in Figure 5. It can be seen that these graphs of I_2 concentration vs. dose are curved. After doses of the order of 50,000 rads the G value for iodine consumption in all of the experiments reached a nearly constant value of 2.47, decreasing somewhat at greater doses. Some difficulty was encountered in extrapolating iodine disappearance plots to zero dose because of initial curvature. Our best current value for $G(-I_2)$ is 3.0, which is probably within experimental error of the value of 3.20 for iodine production with added HI.

Variation of Temperature. Temperature dependence was noted in the G value for the production of H_2 with scavengers present. The G value for hydrogen production was found to have the same value, 3.24, at 25 and -78° for solutions in which $[MeI] = 0.02 M$ and $[I_2] = 0.002 M$; presumably, the value obtained at

both temperatures is just the "plateau" value for complete scavenging of the bimolecular hydrogen yield.^{7,8} However, in radiolyses of cyclopentane with 0.001 M MeI and I_2 , there is approximately a 10% decrease in $G(H_2)$ at the lower temperature. Although these measurements are somewhat qualitative, they do show that the production of hydrogen with scavengers present is temperature dependent when the concentration of scavengers is in the region in which only a part of the bimolecular hydrogen yield is being scavenged.

Discussion

Qualitative Identification of Products. Our qualitative results agree, for the most part, with those reported by Lepley.³ The only disagreements are the trace amount of C_4 compounds detected here with the aid of a flame ionization detector but not reported by Lepley and the intermediate products between cyclopentene and bicyclopentyl reported by Lepley but not found in the present work. We believe that these higher boiling substances are secondary radiolysis products which might be expected at the very high doses used in Lepley's investigation.

Hydrogen Yield. As in the radiolysis of cyclohexane,⁹ the hydrogen yield decreases with dose, presumably

(7) R. H. Schuler, *J. Phys. Chem.*, **61**, 1472 (1957).

(8) M. Burton, *et al.*, *Radiation Res.*, **8**, 203 (1958).

(9) W. S. Guentner, T. J. Hardwick, and R. P. Nejak, *J. Chem. Phys.*, **30**, 601 (1959).

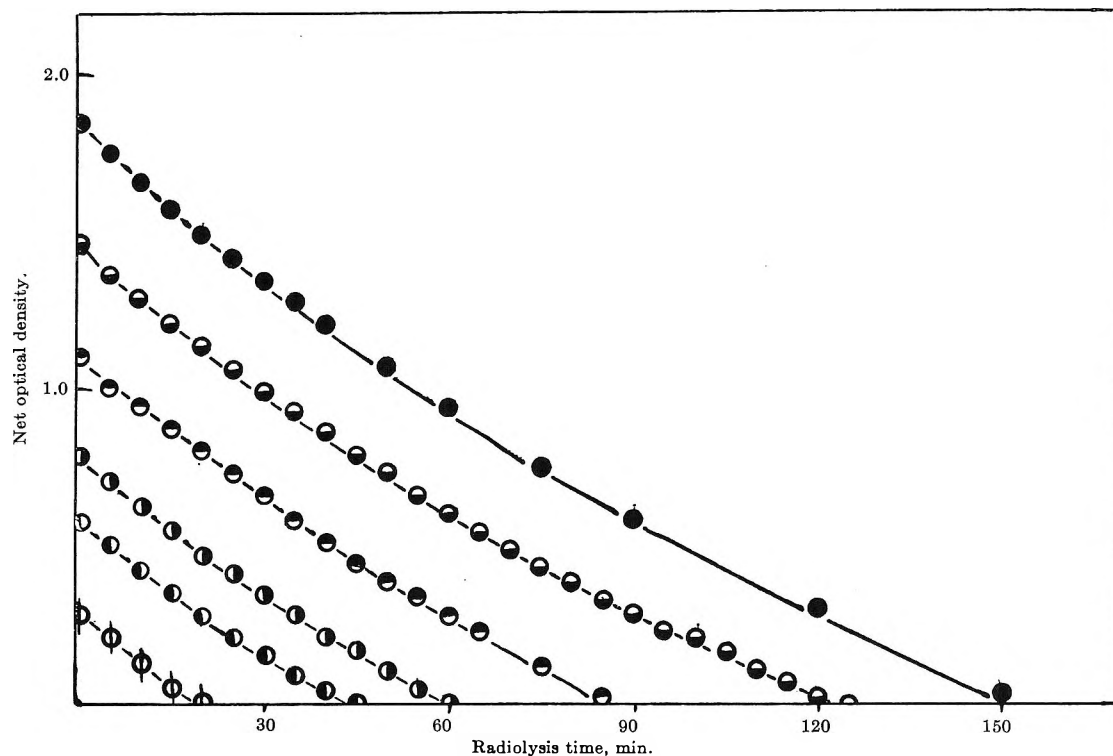


Figure 5. Iodine consumption in the radiolysis of pure cyclopentane with added I_2 .

owing to scavenging by unsaturated products. Our value for the hydrogen yield extrapolated to zero dose is 5.20, which agrees well with results reported earlier by Holroyd¹⁰ and by Toma and Hamill.¹¹ Stone's value¹ of 4.97 is also consistent with our result if a correction is made for the fact that his measurement does not refer to zero dose. The value of 3.79 reported by Lepley was taken at a dose of 30 Mrads, and his data are not sufficient to allow extrapolation of this figure to lower doses. The G value for hydrogen production of 5.78 reported by Hardwick¹² appears to be inconsistent with other values reported to date.

Other Gaseous Products. The only data available for products in the range C_1 through C_4 are those of Lepley and the results reported here. The G values reported by Lepley for methane, C_2 hydrocarbons, and propylene seem unusually large, presumably owing to his very high doses. His value for propane is at least comparable to ours, and his value for cyclopropane agrees with the present work within experimental error. We estimate that our G values for these products are accurate to within approximately 20%. Since the G values for all of these compounds are small, errors of this magnitude have only minor effect on the material balance.

Products Liquid at Room Temperature. The yields of n -pentane, n -pentene, cyclopentene, and bicyclo-

pentene determined from the yield curves in Figure 4 are estimated to be accurate to approximately $\pm 5\%$. Since these are the main radiolysis products, the mass balance depends primarily upon these measurements. In addition to the C_5 products reported, there were also four other chromatograph peaks in the C_5 region which were not identified but corresponded to a combined G value of less than 0.1. Lepley's yields for the liquid products, corrected approximately to zero dose, are also recorded in Table I. His data for n -pentene and n -pentane agree well with ours, and his value for bicyclopentyl is high but reasonable. However, Lepley's value of 1.5 for the yield of cyclopentene cannot be compared with our results because the yield of this compound is strongly dose dependent; an extrapolation from his high doses to zero dose is not possible. Stone¹ and Toma and Hamill¹¹ obtained values near 3.0 for the cyclopentene yield, but their values are probably (according to our results) lower than the initial yields by 0.1 or 0.2 G unit, owing to the dose used. The initial cyclopentene yield must lie in the range 3.1 to 3.4, the latter being the result obtained by Holroyd.¹⁰

(10) R. A. Holroyd, *J. Phys. Chem.*, **66**, 730 (1962).

(11) S. Z. Toma and W. H. Hamill, *J. Am. Chem. Soc.*, **86**, 1478 (1964).

(12) T. J. Hardwick, *J. Phys. Chem.*, **65**, 101 (1961).

It can be seen from Table I that values of the bicyclopentyl yield varying from 1.06 to 1.62 have been reported by four groups; we obtain an intermediate value of 1.22. The average of the reported yields is 1.30.

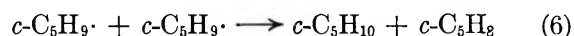
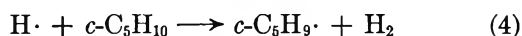
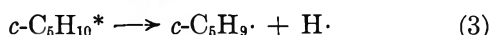
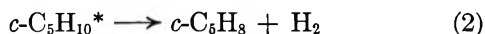
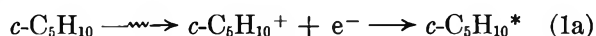
Material Balance. For the hydrogen yield in the cyclopentane system the material balance expression can be written

$$G(\text{H}_2) = G(\text{cyclopentene}) + G(\text{bicyclopentyl}) - \\ G(n\text{-pentane}) - G(\text{methane}) - \\ G(\text{ethane}) - G(\text{propane})$$

If our G values are inserted in the above equation it is found that 1.30 moles of hydrogen are not accounted for. Use of average values from Table I does not improve the situation appreciably. However, Toma and Hamill¹¹ have recently shown that the ultraviolet spectrum of irradiated cyclopentane cannot be accounted for by the known products, particularly cyclopentene. They suggest that cyclopentadiene is produced; a G value for this compound of 0.65 would account for the previously mentioned discrepancy in the hydrogen yield. It seems unlikely that the discrepancy could be due to errors in the experimental results since it corresponds to 25% of the total hydrogen yield.

An examination of the data reveals that rupture of the C_5 ring to give C_1 and C_4 fragments is a very minor process ($G \cong 0.04$), while rupture to give C_2 and C_3 fragments is relatively important ($G \cong 0.4$).

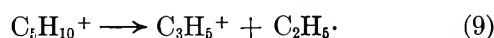
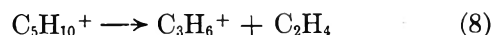
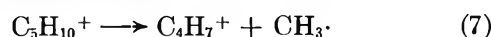
Radiolysis Mechanism. The high yields of hydrogen gas, of olefin derived from the parent cycloalkane, and of dimer suggest that the major portion of the reaction in the radiolysis of cyclopentane is analogous to the case of cyclohexane and that similar mechanistic steps apply



The same difficulty with respect to the actual nature of the bimolecular hydrogen yield, namely, the question whether it is really a simple hydrogen abstraction reaction as shown in step 4 or a more complex energy-transfer process, applies here as in the case of cyclohexane.^{11,13}

The analogy with cyclohexane cannot be extended to the low molecular weight products because there is considerably more fragmentation in the present case than in the case of cyclohexane.¹⁴ It is reasonable to postulate that this difference is due to greater ring strain in cyclopentane, leading to a greater probability of ring opening and fragmentation. It is known that ions of mass 70, 55, 42, and 41 are the most intense in the mass spectral fragmentation pattern of cyclopentane.¹⁵ These correspond to the formulas $\text{C}_5\text{H}_{10}^+$, C_4H_7^+ , C_3H_6^+ , and C_3H_5^+ , respectively. n -Pentane and n -pentene could result from ring rupture either of the parent ion or of the excited species produced on neutralization. However, in the case of n -pentane at least, it seems preferable to assume that ring opening and hydride ion transfer from substrate (followed by hydrogen atom abstraction) occur rather than neutralization since the latter process would necessitate double hydrogen atom abstraction from substrate in order to produce the saturated straight-chain compound. Production of n -pentene could follow from ring rupture of either the ion or the excited molecule.

Production of lower molecular weight fragment ions in the mass spectrometer can be formulated as



It seems likely that similar reactions occur under radiolysis. Reaction 7 is quite important in the mass spectrometer since the ion C_4H_7^+ has a high abundance but apparently is a rather minor process in the liquid phase radiolysis. Reaction 8 must be very important in the mass spectrometer since the ion C_3H_6^+ is the most abundant in the fragmentation pattern and is the base peak. This reaction appears to occur fairly efficiently in the liquid phase radiolysis as well since $G(\text{C}_2\text{H}_4)$ is 0.40. The total G value of C_3 hydrocarbons was found to be 0.32, and the precursors are probably both C_3H_6^+ and C_3H_5^+ ; the latter is also prominent in the mass spectral results. Although it is possible to write a reasonable set of reactions leading to the various observed products from the ions indicated and involving various ion-molecule reactions, neutralization steps, and free-radical reactions, we have chosen not to do so because such a scheme would be speculative and could not be defended in any detail on the basis of present results.

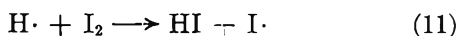
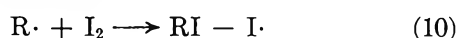
(13) P. J. Dyne, *J. Phys. Chem.*, **66**, 767 (1962).

(14) S. Sato, *et al.*, *J. Chem. Phys.*, **41**, 2216 (1964).

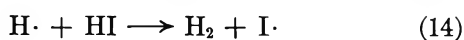
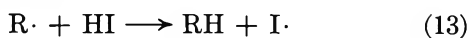
(15) American Petroleum Institute Research Project 44, Serial No. 116.

Scavenger Experiments. Previously reported scavenger measurements of the free-radical yield in cyclopentane include G values for iodine disappearance of 3.6 reported by Weber, Forsyth, and Schuler¹⁶ and 2.53 reported by Dauphin.¹⁷ Our initial G value of 3.0 for iodine disappearance is probably a minimum, owing to marked initial curvature of the yield *vs.* dose curves. The rate of iodine production with added HI can also be taken as an indication of the free-radical yield¹⁸; our value of 3.20 is in reasonable agreement with the results of the iodine experiments.

Although HI and I_2 at concentrations in the region 10^{-2} to 10^{-3} M may interfere with the radiolysis of a hydrocarbon solvent by electron capture or energy transfer,¹⁹ they are certainly capable of participating efficiently in free-radical reactions



and for hydrogen iodide



The nonlinear decrease of iodine concentration in radiolysis mixtures to which iodine has been added can be accounted for by HI formed in reaction 11 and competing with I_2 for radicals as in steps 13 and 14. At very small doses, the ratio of HI to iodine changes very rapidly, changing the rate of iodine consumption. After several minutes of radiolysis the HI/ I_2 ratio becomes approximately constant, and the yield curves are then nearly linear.

In experiments with added hydrogen iodide, during the early stages of the radiolysis, the only efficient free-radical scavenger present is HI, and each thermal free radical should release an iodine atom by reaction 13 or 14. In this case, 1 mole of radicals causes the production of 0.5 mole of I_2 , while with added I_2 1 mole of radicals causes the disappearance of 0.5 mole of I_2 . Thus, $G(I_2)$ with added HI should be equal to $G(-I_2)$ with added I_2 ; this is observed to be true, at least approximately. During the experiments with added HI, as the radiolysis proceeds, I_2 accumulates and begins to compete with HI for free radicals. When the net rate of (10) plus (11) equals the net rate of (13) plus (14), a maximum should be reached in the concentration of I_2 . If a single rate constant can represent reactions of these scavengers with both alkyl radicals and hydrogen atoms, it is possible to write for the condition at the maximum

$$k_{I_2}(R\cdot + H\cdot)(I_2) = k_{HI}(R\cdot + H\cdot)(HI) \quad (15)$$

or

$$[(I_2)/(HI)]_{\max} = k_{HI}/k_{I_2} = \text{constant} \quad (16)$$

As was noted above, such concentration ratios (calculated approximately) were found to be constant experimentally. Further work related to this interpretation is in progress in our laboratory.²⁰

It should be noted that the above considerations are not directly affected by the possibility that varying proportions of thermal hydrogen atoms may be scavenged as the total concentration of scavenger varies. As indicated in eq. 4, when a hydrogen atom abstracts from substrate, it is replaced by an alkyl radical, and the total concentration of alkyl radicals plus hydrogen atoms is unaffected.

A more important question concerns the possibility that substances such as HI and I_2 may have important effects on the radiolysis of hydrocarbons aside from their action as free-radical scavengers. Nash and Hamill¹⁹ have shown that HI can interfere with the radiolysis of *c*- C_6D_{12} , presumably by electron capture, at concentrations as low as 5×10^{-3} M , and that the effect increases with increasing HI concentration. If the resultant yield of H_2 noted by Nash and Hamill is matched by a corresponding yield of I_2 from this process, then solutions of HI in cyclopentane at concentrations from 5×10^{-3} to 10^{-2} M might be expected to show a concentration-dependent excess yield of I_2 compared to the yield for I_2 disappearance using added I_2 . Although we have noted that $G(I_2)$ with added HI is somewhat greater than $G(-I_2)$, the difference is only about 0.2 molecule/100 e.v., and it is not concentration dependent (*cf.* initial slopes, Figure 4). The reason for this disagreement with the implications of the work of Nash and Hamill¹⁹ is not apparent.

In spite of the problem discussed in the preceding paragraph, we believe that the features of graphs of iodine concentration with added HI and I_2 can be accounted for by free-radical competition reactions as indicated in eq. 10-14. Although a given total quantity of electronegative solute may modify radical and molecular yields somewhat as compared with the pure hydrocarbon substrate, this effect should be relatively small when the additive concentration is not much greater than 10^{-3} M . Furthermore, the inter-

(16) E. N. Weber, P. F. Forsyth, and R. H. Schuler, *Radiation Res.*, **3**, 68 (1955).

(17) J. Dauphin, *J. chim. phys.*, **59**, 1207 (1962).

(18) R. H. Schuler, *J. Phys. Chem.*, **62**, 37 (1958).

(19) J. R. Nash and W. H. Hamill, *ibid.*, **66**, 1097 (1962).

(20) I. Mani, this laboratory, unpublished results.

conversion of small amounts of I_2 , HI, and alkyl iodides should have only a small effect on the electron capture yield.

Temperature Effects. In general, temperature changes are expected to have little effect on primary processes in radiation chemical reactions since the fundamental cause of reaction is deposition of energy from a radiation source, rather than collisions of molecules. Temperature changes can affect secondary processes provided that alternate routes exist with differing activation energies. In hydrocarbon radiolysis such a competitive situation may exist with respect to the hydrogen yield if it is assumed that part of the observed yield is due to thermalized hydrogen atoms. On the assumption that a thermalized hydrogen yield does exist, the fully scavenged H_2 yield observed with *ca.* $10^{-2} M$ I_2 would not be temperature dependent, nor would the unscavenged yield (at least near room temperature). However, the hydrogen yield with intermediate concentrations of scavengers might be expected to decrease with temperature.

Unfortunately, investigation of temperature dependence of scavenging by I_2 is prevented by the decrease in its solubility at low temperature. We chose to use methyl iodide as an alternate scavenger²¹ since it should react efficiently with hydrogen atoms according to the equation



It is necessary that iodine be present as well to prevent a chain reaction yielding methane.²² It has been established that the effects of CH_3I and I_2 on the hydrogen yields from cyclohexane at room temperature are very similar.^{21,22}

Using solutions of MeI and I_2 in cyclopentane, we have confirmed that the fully scavenged or "plateau value" of the H_2 yield in cyclopentane is not temperature dependent. The unscavenged hydrogen yield found here is 5.20, and the plateau value is 3.24. A solution which was 1.0 mM in both methyl iodide and iodine gave $G(H_2)$ of 4.17 at room temperature and 3.70 at -78° . The difference between 4.17 and 3.24 represents the residual, unscavenged thermal hydrogen atom yield in the solutions studied, at room temperature; the difference between 3.70 and 3.24 represents the corresponding residual unscavenged thermal hydrogen atom yield at -78° . The decrease of 0.47

G unit is 50% of the thermal hydrogen atom yield of 0.93 unit (that is, $4.17 - 3.24$) which was unscavenged in these solutions at room temperature. This decrease of 50% in the residual hydrogen atom yield for a drop of 103° corresponds to only about 2 kcal./mole for the difference in activation energy between hydrogen atom abstraction and reaction with scavenger. This is much lower than the value of 6 to 8 kcal./mole expected from conventional kinetics¹² and suggests that the hydrogen atoms in question may be "hot" or that other more complex effects such as energy transfer or electron capture are involved. (This conclusion is in agreement with results of several other lines of investigation.^{11,13,23-25})

There appears to be only one previously reported value for the fully scavenged hydrogen yield in cyclopentane, a value of 2.72 published by Hardwick.¹² Although this is in fair agreement with our value of 3.24, Hardwick also found a much higher unscavenged hydrogen yield of 5.78 molecules/100 e.v. Hence, Hardwick's value for the "thermal hydrogen atom yield" is 3.06, approximately 50% greater than ours. Although we cannot fully resolve this discrepancy, it does not affect the qualitative conclusion obtained above concerning the temperature effect. The temperature effect is even smaller on a percentage basis using Hardwick's data, making the apparent activation energy even less than 2 kcal./mole.

The present experimental results do not bear directly on the nature of the unimolecular yield of hydrogen from irradiated hydrocarbons. Although formal recognition of a scavenger-insensitive component of the hydrogen yield was made in steps 1 and 2 of the reaction sequence given above, there is evidence that this portion of the reaction mechanism is more complex and is, in fact, related in some way to the bimolecular hydrogen yield.²³⁻²⁵

Acknowledgment. This work was supported by A.E.C. Contract AT-(40-1)-3106 and by the University of Florida Nuclear Science Program.

(21) L. C. Forrestal and W. H. Hamill, *J. Am. Chem. Soc.*, **83**, 1535 (1961).

(22) R. H. Schuler *J. Phys. Chem.*, **61**, 1472 (1957).

(23) P. Dyne and W. Jenkinson, *Can. J. Chem.*, **39**, 2163 (1961).

(24) P. Dyne, J. Lenhartog, and D. R. Smith, *Discussions Faraday Soc.*, **36**, 521 (1964).

(25) S. Z. Toma and W. H. Hamill, *J. Am. Chem. Soc.*, **86**, 4761 (1964).

An Infrared Study of the Dimerization of Trimethylacetic Acid in Carbon Tetrachloride Solution¹

by T. C. Chiang and R. M. Hammaker

Department of Chemistry, Kansas State University, Manhattan, Kansas 66504 (Received March 4, 1965)

The OH stretching fundamental has been used to determine K , ΔG° , ΔH° , and ΔS° for the dimeric association of trimethylacetic acid in dilute solution in carbon tetrachloride at 11, 21.5, 26.5, 34, and 50°. The results, $\Delta H^\circ = -9.55$ kcal./mole of dimer and $\Delta S^\circ = -11.5$ cal./deg. mole of dimer, are in agreement with literature data for carboxylic acids. The results for K at 26.5° have been checked using the C=O stretching fundamental. The large concentration dependence of K reported by Chang and Morawetz is not observed in the lower concentration range (1.0×10^{-4} to 4×10^{-3} M) studied in this research. It has been shown that the presence of both cyclic and linear dimers may cause the concentration dependence of K reported by Chang and Morawetz. It has been concluded that cyclic dimerization is the major association process at acid concentrations below 4×10^{-3} M but that linear dimerization also occurs to a significant extent especially as acid concentration increases above 10^{-3} M.

Introduction

Although the thermodynamics of hydrogen bonding by carboxylic acids has been investigated, only a few systems have been thoroughly studied.^{2a} Thermodynamic data for the dimerization of trimethylacetic acid are limited. Johnson and Nash^{2b} obtained an equation for the dimerization association constant, K , from 80 to 200° and a dimerization enthalpy of -14 kcal./mole for gaseous trimethylacetic acid from vapor density data. The electric polarization data of Pchl, *et al.*,³ at 30° for dilute trimethylacetic acid solutions in benzene give $K = 680$ l./mole. Infrared data reported by Longworth and Morawetz⁴ for trimethylacetic acid in benzene solution at 25° give $K = 420$ l./mole. Chang and Morawetz⁵ have used the intensity of the carbonyl stretching frequency to obtain $K = 1730$ l./mole and $K = 80$ l./mole at 29.6° for trimethylacetic acid in carbon tetrachloride and 1,1,2,2-tetrachloroethane, respectively. These K values are averages of results obtained by Chang and Morawetz at four concentrations in the 3×10^{-3} to 4×10^{-2} M range since the individual K values showed a systematic decrease with increasing concentration, a result previously reported for acetic acid in carbon tetrachloride and chloroform.⁶

Reeves⁷ has shown that the carboxyl-proton chemical shift for trimethylacetic acid in carbon tetrachloride at 28° decreases with increasing acid concentration up to mole fraction 0.2 and then remains constant from mole fraction 0.2 to 0.9. This type of concentration dependence of the carboxyl-proton chemical shift has also been observed for eight other C₃ to C₁₈ aliphatic carboxylic acids.⁸ For acetic acid and various halogenated acetic acids,⁷⁻⁹ the carboxyl-proton chemical shift decreases to a minimum and then increases as the acid mole fraction in carbon tetrachloride increases from 0.02 to 1.0. Reeves pro-

(1) Abstracted from the M.S. Thesis of T. C. Chiang, Kansas State University, 1964.

(2) (a) G. C. Pimentel and A. L. McClellan, "The Hydrogen Bond," W. H. Freeman and Co., San Francisco, Calif., 1960, Chapter 7; (b) E. W. Johnson and L. K. Nash, *J. Am. Chem. Soc.*, **72**, 547 (1950).

(3) H. A. Pohl, M. E. Hobbs, and P. M. Gross, *J. Chem. Phys.*, **9**, 408 (1941).

(4) R. Longworth and H. Morawetz, *J. Polymer Sci.*, **29**, 307 (1958).

(5) S. Chang and H. Morawetz, *J. Phys. Chem.*, **60**, 782 (1956).

(6) G. M. Barrow and E. A. Yerger, *J. Am. Chem. Soc.*, **76**, 5248 (1954).

(7) L. W. Reeves, *Can. J. Chem.*, **39**, 1711 (1961).

(8) L. W. Reeves, *Trans. Faraday Soc.*, **55**, 1684 (1959).

(9) L. W. Reeves and W. G. Schneider, *ibid.*, **54**, 314 (1958).

poses that this difference is due to the complete dimerization of trimethylacetic acid and the other eight carboxylic acids above a certain concentration as contrasted to a new association in addition to dimerization, probably the formation of chainlike polymers, in concentrated carbon tetrachloride solutions of acetic acid and halogenated acetic acids.

Although a cyclic structure has usually been assigned to the carboxylic acid dimer, Bellamy, *et al.*,¹⁰ have proposed that both linear and cyclic dimers are formed in carbon tetrachloride solution. This proposal is based on the detailed structure of the associated OH stretching mode of acetic acid, phenylacetic acid, and several halogenated acetic acids in carbon tetrachloride solution.

The present paper reports the results of the determination of the dimerization association constant (K) and the thermodynamic properties (ΔG° , ΔH° , and ΔS°) for trimethylacetic acid in carbon tetrachloride using the intensity of the unassociated OH stretching fundamental determined at five temperatures in the 11 to 50° range. A determination of K at one temperature using the intensity of the carbonyl stretching mode was made to check the present result from the OH stretching mode and the result reported previously⁶ from the carbonyl stretching mode. Two purposes of the present work are to further investigate the increase in K with decreasing concentration by going to lower acid concentrations and to investigate the structure of the trimethylacetic acid dimer formed in dilute carbon tetrachloride solution.

Experimental

Carbon tetrachloride (Fisher Scientific Co., Spectro grade) was dried by storage in an open beaker in a desiccator containing P_2O_5 until the spectrum of carbon tetrachloride in a 1-cm. cell *vs.* air had no OH stretching absorption. Trimethylacetic acid (Eastman White Label) was dried by pumping on a sample maintained close to its freezing point until the acid freezing point rose to the literature value (35.4°). All solution-making and cell-filling manipulations were carried out in a drybox under a nitrogen atmosphere which was continuously dried and recirculated using Linde 13X Molecular Sieve and a 08-000-77 Dia-Pump recirculator (Air Controls, Inc., Narbeth, Pa.). The filled cells were transferred from inside the drybox to the spectrophotometer in a desiccator containing P_2O_5 .

All spectra were run on a Perkin-Elmer 221 PG infrared spectrophotometer recording linearly in reciprocal centimeters. The OH stretching spectra were run at 11, 21.5, 26.5, 34, and 50° in a 2.5-cm. cell (Barnes Engineering Co., Type H) with sodium

chloride windows against air in the reference beam. The background was obtained with pure solvent in the cell and air in the reference beam. The C=O stretching spectra were run at 25° using a 5-mm. rock salt cavity cell (Barnes Engineering Co., Type E) in the sample beam and a wedge cavity cell (Barnes Engineering Co., W-2E) in the reference beam. The sample temperatures were controlled to within $\pm 1^\circ$ using a variable temperature chamber (Barnes Engineering Co., VTC-104). Spectra were obtained as soon as possible after the solutions were prepared. Solutions were between 1×10^{-4} and 4×10^{-3} M in trimethylacetic acid. The molarities of solutions at temperature other than those at which solutions were made were calculated by assuming that the solution density change with temperature was the same as that of the solvent.

Results and Discussion

A. Thermodynamic Data. The OH stretching mode absorbance data were treated by the method of Harris and Hobbs¹¹ who have shown that if the only association process is dimerization, and the free OH band is due only to monomer, and the Bouguer-Beer law is obeyed, then

$$d = \frac{\epsilon_M 2l^2 c}{2K d} - \frac{\epsilon_M l}{2K} \quad (1)$$

where d is absorbance for the free OH band, l is cell length (in centimeters), ϵ_M is the monomer absorption coefficient, c is the trimethylacetic acid concentration (molarity), and K is the dimerization association constant. Figure 1 shows plots of d *vs.* c/d whose linearity is consistent with dimerization as the only association process. The slopes and intercepts of these plots were used to calculate ϵ_M and K at the five temperatures. The values of ϵ_M were in the range $147 \pm$

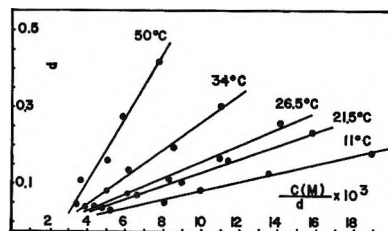


Figure 1. Plot of d *vs.* c/d for the free OH stretching fundamental of trimethylacetic acid in carbon tetrachloride solution where d is absorbance and c is acid concentration (molarity).

(10) L. J. Bellamy, R. F. Lake, and R. J. Pace, *Spectrochim. Acta*, **19**, 443 (1963).

(11) J. T. Harris, Jr., and M. E. Hobbs, *J. Am. Chem. Soc.*, **76**, 1419 (1954).

Table I: Thermodynamic Functions for Dimeric Association of Trimethylacetic Acid in Carbon Tetrachloride Solution

Temp., °K.	$K \times 10^{-3}, M^{-1}$	$K \times 10^{-4}, X^{-1}$	ΔH° , kcal.	$-\Delta G^\circ$, kcal.	$-\Delta S^\circ$, cal.
			Mole of dimer	Mole of dimer	Deg.-mole of dimer
284 ± 1	6.80 ± 0.20	7.13 ± 0.21	-9.55 ± 0.5	6.30 ± 0.04	11.4 ± 1.9
294.5 ± 1	3.52 ± 0.18	3.64 ± 0.19		6.15 ± 0.04	11.5 ± 1.7
299.5 ± 1	2.75 ± 0.15	2.83 ± 0.17		6.12 ± 0.06	11.4 ± 1.9
307 ± 1	2.04 ± 0.15	2.08 ± 0.16		6.07 ± 0.06	11.4 ± 1.8
323 ± 1	0.83 ± 0.15	0.83 ± 0.18		5.80 ± 0.15	11.6 ± 2.0

8 cm.⁻¹ M⁻¹ and any variation of ϵ_M with temperature was indistinguishable from the uncertainties in the ϵ_M values. The values of K which are averages over a range concentrations are listed in Table I using both molarity (M) and mole fraction (X) units. The molar volume of the dilute solution was assumed to be equal to the molar volume of the solvent in converting $K (M^{-1})$ to $K (X^{-1})$. Figure 2 shows a log $K (M^{-1})$ vs. $1/T$ plot whose slope gives $\Delta H^\circ = -9.55$ kcal./mole for dimerization. The ΔG° and ΔS° values for dimerization calculated from $K (X^{-1})$ and ΔH° are listed in Table I. These calculations assume the ideal associated-solution model of Prigogine¹² where the trimethylacetic acid monomer and dimer activities equal their mole fractions.

The C=O stretching mode absorbance data were treated by the method of Chang and Morawetz,⁵ who have shown that if the only association process is dimerization, and the two carbonyl bands are due only to monomer and dimer, respectively, and the Bouguer-Beer law is obeyed, then

$$K = \frac{1}{2c_1} \frac{d_2 \epsilon_2}{d_1 \epsilon_1} \quad (2)$$

and

$$c_1 = \left(c \frac{d_1 \epsilon_2}{d_2 \epsilon_1} \right) / \left(1 + \frac{d_1 \epsilon_2}{d_2 \epsilon_1} \right) \quad (3)$$

where c_1 is monomer concentration, d_1 and d_2 are absorbance for the free and bonded C=O groups, respectively, ϵ_1 and ϵ_2 are molar absorption coefficients for the free and bonded C=O groups, respectively, c is the trimethylacetic acid concentration (molarity), and K is the dimerization association constant. Chang and Morawetz⁵ have also shown that a plot of d_2/c vs. d_1/c is linear with its slope giving ϵ_2/ϵ_1 . Our data were plotted in this way to obtain ϵ_2/ϵ_1 and then eq. 2 and 3 were used to calculate $K (M^{-1})$ at four concentrations as shown in Table II along with the results of Chang and Morawetz. The K values from this research shown in Table II appear to increase as concentration decreases; however, the effect barely exceeds the un-

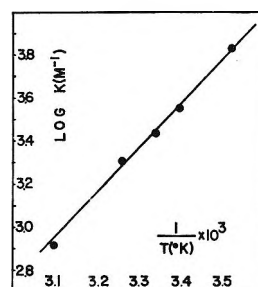


Figure 2. Plot of log $K (M^{-1})$ vs. $1/T$ for trimethylacetic acid in carbon tetrachloride solution.

certainties in the K values and is significantly smaller than the trend in the K values of Chang and Morawetz, whose lowest concentration is almost twice our highest concentration. The average of the four K values from our C=O stretch data at 25° (Table II) is 2835, in good agreement with the K value of 2750 ± 150 from our OH stretch data (Table I) which is an average over the concentration range. Figure 2 predicts $K = 2400 \pm 150$ at 29.6° from our OH stretch data in reasonable agreement with $K = 2130$ at 29.6° from the data of Chang and Morawetz at their lowest concentration. Thus it appears that our K values from both OH and C=O stretching data and those of Chang and Morawetz are in accord where comparisons are valid.

The thermodynamic functions shown in Table I are in good agreement with available literature data for carboxylic acid dimerization in CCl₄ and benzene as measured by a variety of methods.¹³ The result, $\Delta H^\circ = -9.55 \pm 0.5$ kcal./mole of dimer, is in good agreement with the recent measurement of Affspring, *et al.*,¹⁴ for acetic acid in carbon tetrachloride, $\Delta H = -10.7 \pm 1.2$ kcal./mole of dimer. Our ΔH° value is also consistent with the range of values for a single hydrogen bond of -4.0 to -5.5 kcal./mole of bond obtained¹³ for a number of substituted and nonsub-

(12) I. Prigogine, "The Molecular Theory of Solutions," Interscience Publishers, Inc., New York, N. Y., 1957, pp. 305-322.

(13) G. C. Pimentel and A. L. McClellan, *ref. 2a*, pp. 351, 352.

(14) H. E. Affspring, S. D. Christian, and A. M. Melnick, *Spectrochim. Acta*, **20**, 285 (1964).

Table II: Concentration Dependence of K Determined by C=O Stretching Mode

Temp., °C.	Concn., $M \times 10^3$	K, M^{-1}	Source
25 ± 1	0.185	3100 ± 300	This research
25 ± 1	0.463	3000 ± 250	This research
25 ± 1	0.927	2740 ± 150	This research
25 ± 1	1.853	2500 ± 150	This research
29.6	3.16	2130	<i>a</i>
29.6	6.32	1920	<i>a</i>
29.6	12.64	1640	<i>a</i>
29.6	19.0	1230	<i>a</i>

^a Reference 5.

stituted aliphatic and aromatic carboxylic acids in CCl_4 or benzene solution provided the dimer is taken to be cyclic. The result, $-\Delta S^\circ = 11.5 \pm 2$ e.u., is in the range of 9–17 e.u. (based on K in M^{-1} units) reported¹³ for nine aromatic carboxylic acids in benzene solution and in excellent agreement with 11.2 e.u. reported¹³ for benzoic acid in CCl_4 .

B. Dimer Structure. The equilibrium constants and thermodynamic functions obtained from the OH stretch data are based on the assumption that the free OH band is due to the monomer species only. Smith and Creitz¹⁵ found that sterically hindered alcohols in carbon tetrachloride solution have a free OH peak with a low-frequency shoulder such that increasing alcohol concentration causes the lower frequency shoulder to become the dominant absorption with a higher frequency shoulder. This result was assigned to absorption of the free OH group of a linear dimer near the monomer absorption. Kuhn¹⁶ has also concluded from studies of intramolecular hydrogen bonding that an OH group having its oxygen but not its hydrogen participating in hydrogen bonding may absorb near the monomer frequency. The fact that the shape of the free OH band for trimethylacetic acid in carbon tetrachloride is independent of concentration for the concentrations studied here supports the assignment of the free OH band to monomer absorption only. However, a sufficiently low concentration of linear dimers could fail to cause a detectable change in band shape. Also, the frequency for the free OH stretching mode of a linear dimer may be too close to the monomer frequency to cause a concentration dependence of band shape.

Linear dimer contributions to the free OH stretching mode cause the Bouguer-Beer law to become $d = \epsilon_M l C_M + d_L$ where C_M is monomer concentration, d_L is absorbance due to the free OH group of a linear dimer, and the other symbols are as defined previously.

For a mixture of cyclic and linear dimers, the method of Harris and Hobbs¹¹ yields

$$d = \frac{\epsilon_M l^2}{2K} \left[\frac{c}{d} + \frac{2d_L}{\epsilon_M l^2} + \frac{d_L}{\epsilon_M l d} - \frac{d_L^2}{\epsilon_M l^2 d} \right] - \frac{\epsilon_M l}{2K} \quad (4)$$

where $K = K_C + K_L$; K_C and K_L are association constants for cyclic and linear dimers, respectively, and the other symbols are as defined previously. Of the three terms in brackets in eq. 4, in addition to c/d , only $d_L/\epsilon_M l d$ may be significant compared to c/d for the magnitudes of d and c/d in Figure 1. Trial calculations indicate that $d_L/\epsilon_M l d$ may remain at less than 10% of c/d when d_L is a significant fraction (13 to 30% depending on concentration) of d . Consequently, the linearity of the d vs. c/d plot in Figure 1 supports but does not prove that the dimerization of trimethylacetic acid is cyclic since a mixture of cyclic and linear dimers or even linear dimers alone appears to be capable of giving linear d vs. c/d plots under fortuitous circumstances. However, the total dimerization constant, K , and monomer absorption coefficient, ϵ_M , obtained from Figure 1 are expected to be approximately correct even if some linear dimerization occurs.

Trial calculations indicate that even if both cyclic and linear dimerization occurs so that $K = K_L + K_C$ and K_L and K_C have different temperature variations the $\log K$ vs. $1/T$ plot shown in Figure 2 will still be linear if ΔH° is temperature independent and the ΔH° value obtained will be a material-weighted average of ΔH° for cyclic and linear dimerization. The result, $\Delta H^\circ = -9.55$ kcal./mole of dimer, is consistent with cyclic dimerization as the major association process if one accepts the view¹³ that hydrogen bonds of the $\text{OH} \cdots \text{O}=\text{C}$ type in nonpolar solvents have ΔH° values between -4 and -5.5 kcal./mole of bond. However, this range of ΔH° values is also based on the assumption that only cyclic dimerization occurs. An alternative view is that, although only cyclic dimerization occurs in the gas phase, the solvation of the free OH group of the linear dimer causes linear dimerization to occur along with cyclic dimerization in solution. Then the result, $\Delta H^\circ = -7$ kcal./mole of hydrogen bond, from the gas phase work of Johnson and Nash^{2b} represents an upper limit for solution. Here it is assumed that solvation of the monomer lowers its enthalpy more than solvation of the dimer lowers its enthalpy with the result that ΔH° in solution is less negative than ΔH° in the gas phase. If it is arbitrarily assumed that ΔH° per hydrogen bond is identical

(15) F. A. Smith and E. C. Creitz, *J. Res. Natl. Bur. Std.*, **46**, 145 (1951).

(16) L. P. Kuhn, *J. Am. Chem. Soc.*, **76**, 4323 (1954).

in linear and cyclic dimers and that $\Delta H^\circ = -6$ kcal./mole of hydrogen bond for CCl_4 solution, then the result, $\Delta H^\circ = -9.55 \pm 0.5$ kcal./mole of dimer, is caused by dimerization which averages $41 \pm 8\%$ in a linear structure over the temperature range investigated with the remainder in a cyclic structure. This calculated extent of linear dimerization is almost certainly too high for the d vs. c/d plots in Figure 1 to remain linear. However, the result, $\Delta H^\circ = -9.55 \pm 0.5$ kcal./mole of dimer, does not appear to permit a definite choice between only cyclic dimerization and cyclic dimerization accompanied by some linear dimerization.

Linear dimer contributions to the free and bonded C=O stretching modes cause the Bouguer-Beer law to become $d_1 = \epsilon_1(c_1 + c_L)$ and $d_2 = \epsilon_2(2c_C + c_L)$ where c_L is linear dimer concentration, c_C is cyclic dimer concentration, the other symbols are as defined previously, and it is assumed that the free and bonded C=O groups of the linear dimer have the same absorption coefficients ϵ_1 and ϵ_2 as the monomer and cyclic dimer, respectively. The method of Chang and Morawetz⁵ applied to a mixture of cyclic and linear dimers yields eq. 2 for $K = K_C + K_L$ and the result

$$(c_1 + c_L) = \left(c \frac{d_1 \epsilon_2}{d_2 \epsilon_1} \right) / \left(1 + \frac{d_1 \epsilon_2}{d_2 \epsilon_1} \right) \quad (5)$$

It may be easily shown that a plot of d_2/c vs. d_1/c is linear with its slope giving ϵ_2/ϵ_1 regardless of whether only cyclic dimerization, both linear and cyclic dimerization, or only linear dimerization is occurring. Consequently, the linearity of a d_2/c vs. d_1/c plot merely shows that dimerization is the only significant association process and does not specify the structure of the dimer. The calculation of K by eq. 2 will give a correct result if only cyclic dimers are formed or if c_L is small compared to c_1 when linear dimers are present. As shown by eq. 5, the calculation of c_1 from eq. 3 really gives $c_1 + c_L$ when any linear dimers are present so that K calculated from eq. 2 will decrease with increasing acid concentration since c_L increases relative to c_1 as acid concentration increases. Although the decrease in our K values with increasing acid concentration shown in Table II barely exceeds experimental uncertainty, the trend of decreasing K with increasing concentration is definitely established by the results of Chang and Morawetz⁵ shown in Table II. This

trend is just what is expected if linear dimers are present in significant amounts at the higher acid concentrations used by Chang and Morawetz.⁵

The weight of the evidence resulting from the infrared data seems to these authors to indicate that cyclic dimerization is the major association process at acid concentrations below $4 \times 10^{-3} M$ but linear dimerization is also occurring to a significant extent especially as acid concentration increases above $10^{-3} M$. The complete conversion of monomer to a mixture of linear and cyclic dimers above a certain concentration of trimethylacetic acid in CCl_4 is consistent with the n.m.r. data of Reeves and dipole moment measurements in both dilute benzene solution³ and pure liquid acid.¹⁷ Pohl, *et al.*,³ reported dipole moments of 1.70 and 0.92 D. for trimethylacetic acid monomers and dimers, respectively, in $0.4\text{--}93 \times 10^{-3} M$ solution in benzene at 30° . The fact that the dimer dipole moment has a value of 0.92 D. while a planar cyclic dimer is expected to have no dipole moment has been attributed to either high atomic polarization in the cyclic dimer or the existence of linear dimers.¹⁸ Pure liquid dipole moments reported¹⁷ for propionic acid and higher aliphatic carboxylic acids range from 1.12 to 1.22 D. at 25° while the value for acetic acid is 1.90 D. at 20° . The dipole moment results in benzene solution³ are consistent with the implication of our infrared data for trimethylacetic acid in carbon tetrachloride that both linear and cyclic structures occur for aliphatic carboxylic acid dimerization in nonpolar solvents. Reeves conclusion that propionic acid and higher saturated fatty acids only dimerize in various solvents while acetic acid and substituted acetic acids further associate, presumably to linear polymers, is consistent with the pure liquid dipole moment results. Thus, the $\text{C}_3\text{--C}_{18}$ acids presumed to dimerize completely have pure liquid dipole moments¹⁷ nearer to the dimer dipole moments obtained in dilute benzene solution; but acetic acid, which is presumed to associate further to linear polymers, has a pure liquid dipole moment nearer the monomer dipole moment obtained in dilute benzene solution.

(17) R. P. Phadke, *J. Indian Inst. Sci.*, **34**, 189 (1952); *Chem. Abstr.*, **47**, 3060i (1953).

(18) G. C. Pimentel and A. L. McClellan, *ref. 2a*, p. 16.

The Effect of Urea on the Structure of Water and Hydrophobic Bonding¹

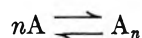
by Mohammad Abu-Hamdiyyah

Department of Chemistry, University of Southern California, Los Angeles, California 90007
(Received March 5, 1965)

Nonpolar solutes, especially hydrocarbons and hydrocarbon moieties, dissolve interstitially in water and in aqueous urea solutions. Physicochemical properties of aqueous urea solutions indicate that urea does not influence the structure of water the way ions do, but actively participates in the formation of clusters. Weakening of hydrophobic bonding upon addition of urea is due to the increased ease of cluster formation. However, since urea and water molecules have different geometries, strengthening of hydrophobic bonding occurs in the case of methane and ethane (and presumably the rare gases) at low temperatures because of the more exacting geometrical requirements for the formation of the interstices that accommodate these molecules.

Introduction

Hydrophobic bonding is the term coined to describe the phenomenon in which nonpolar residues or moieties (usually hydrocarbon) in the presence of water associate together to form intramolecular aggregates, as in the native protein solutions, intermolecular aggregates such as micelles in surfactant solutions, or, in the extreme case, the precipitation of a separate phase, *i.e.*, the limited solubility in water, as is the case for hydrocarbons.²⁻⁵ Schematically the process may be represented by



where A is the nonpolar residue and A_n the aggregate of the residues. This association has been explained in the past by energetic (enthalpic) considerations alone. Nowadays, however, it is believed that entropy plays a dominant role in this process^{3,4,6} especially for not very long chain compounds⁷ and at low temperatures, and furthermore that the process is largely controlled by the water structure. Recently, several authors have called attention to the effect of urea upon various facets of hydrophobic bonding and the purpose of this paper is to arrive at a coherent interpretation of the available evidence.

The structure of water has been discussed by many authors and up-to-date reviews of the present situation of water structure theories exist.⁸⁻¹² All the modern theories are refined versions of the model proposed by Bernal and Fowler,¹³ the main feature of which is the

tetrahedral hydrogen bonding of water molecules to each other in three dimensions, giving rise to an extensive open structure. Whether the hydrogen bonding involves all the molecules in the liquid at a given time (the uniformist approach)¹⁴⁻¹⁶ or whether only part of the molecules are hydrogen bonded, the rest being non-bonded monomers (the mixture approach),¹⁷⁻¹⁹ is im-

(1) Based on a proposition submitted in partial fulfillment of the requirements for the Ph.D. degree at the University of Southern California.

(2) W. Kauzmann, *Advan. Protein Chem.*, **14**, 1 (1959).

(3) G. Némethy and H. A. Scheraga, *J. Chem. Phys.*, **36**, 3401 (1962).

(4) A. Wishnia, *J. Phys. Chem.*, **67**, 2079 (1963).

(5) E. S. Hand and T. Cohen, *J. Am. Chem. Soc.*, **87**, 133 (1965).

(6) E. D. Goddard, C. A. J. Hove, and G. C. Benson, *J. Phys. Chem.*, **61**, 593 (1957).

(7) L. Benjamin, *ibid.*, **68**, 3575 (1964).

(8) F. S. Feates and D. G. Ives, *J. Chem. Soc.*, 2798 (1956).

(9) G. Némethy and H. A. Scheraga, *J. Chem. Phys.*, **36**, 3382 (1962).

(10) O. Ya. Samoilov, *Zh. Strukt. Khim.*, **4**, 459 (1963).

(11) H. S. Frank in "The Proceedings of the Conference on Desalination Research," Publication 942 of National Academy of Sciences, National Research Council, Washington, D. C., 1963, p. 141.

(12) R. P. Marchi and H. Eyring, *J. Phys. Chem.*, **68**, 221 (1964).

(13) J. D. Bernal and R. Fowler, *J. Chem. Phys.*, **1**, 515 (1933).

(14) J. A. Pople, *Froc. Roy. Soc. (London)*, **A205**, 163 (1951).

(15) D. N. Glew, *J. Phys. Chem.*, **66**, 605 (1962).

(16) J. A. Barker, *Ann. Rev. Phys. Chem.*, **14**, 245 (1963).

(17) L. Hall, *Phys. Rev.*, **73**, 775 (1948).

(18) G. Wada, *Bull. Chem. Soc. Japan*, **34**, 955 (1961).

(19) L. Pauling in "Hydrogen Bonding," D. Hadzi, Ed., Pergamon Press Ltd., London 1959, p. 1.

material for our purposes since both approaches agree on the formation of interstices and cavities as a result of the hydrogen-bonded structures which are essential for our treatment. Therefore we may use the language of either approach without any loss.

When nonpolar solutes dissolve in water, they increase the mutual ordering of water molecules around them as shown by thermodynamic studies.^{6,20} Thus the idea of "icebergs" being formed around nonpolar solutes was born,²⁰ and such solutes have been called structure formers.¹¹

The effect of urea on the strength of the hydrophobic bond²¹⁻²³ has recently been investigated and, according to all recent studies,²¹⁻²⁷ the effect of urea is to reduce the strength of the hydrophobic bonding in all cases except for CH₄ and C₂H₆ molecules and hence CH₃ and C₂H₅ moieties at low temperatures where the reverse is true.^{24,25} No explanations were offered for this exceptional strengthening of hydrophobic bonding by urea. The reasons given for the usual weakening of hydrophobic bonding are varied and sometimes clearly confused. It was suggested that the weakening of hydrophobic bonding may be due to the favorable interaction of urea with the "iceberg" region or the formation of urea-hydrocarbon clathrate-like aggregates in solution,²¹ or may be due to the reduction of the cooperative structure of water that is responsible for the solvent structure effects, *i.e.*, to the destruction of the "icebergs" which form around the hydrocarbon moieties.^{22,23} Others²⁴ suggested that the increased solubility of hydrocarbons in aqueous solutions may either be due to the facilitation of hydrocarbon solvation by water in the presence of urea or to the solvation of the hydrocarbon by both urea and water molecules. Recently it was hinted^{25,26} that ordered structures may be formed around the solute by both urea and water molecules. Nevertheless, it was concluded²⁶ that urea behaves as a structure breaker. On the other hand it was concluded²⁸ that urea disrupts the structure of water and solubilizes the hydrocarbons since "the solubility properties of hydrocarbons in water result in large part from an ordering of the solvent." More specifically, the role of urea was likened to that of an ion,^{27,28} *i.e.*, orienting neighboring water molecules, restricting their participation in hydrogen-bonded water clusters and leading to a region of disorder around the solvated solute molecule, thus "ions and urea may modify the iceberg structure around the hydrocarbon chains of the single ions and consequently affect micelle formation of ionic detergents."²⁷

In this paper the mechanism of the dissolution of hydrocarbon solutes in water is first reviewed and then an attempt is made to analyze the way in which urea

affects the structure of water and hence hydrophobic bonding. It will be pointed out (i) that hydrocarbon solutes always dissolve interstitially in pure water as well as in aqueous urea solutions, (ii) that urea is able to participate in cluster formation with water molecules, and (iii) that the formation of interstices to accommodate relatively large hydrocarbon moieties becomes easier in aqueous urea solutions than in pure water, but the converse holds for small interstices that would accommodate short-chain compounds (CH₄ and C₂H₆) at low temperatures.

In order to avoid confusion and because the word "structure forming" is used in discussing the role of ions,²⁹ of nonpolar solutes,²⁹ and of urea (in this paper), it is worthwhile to point out the differences between their effects. The structure-forming ions destroy the hydrogen-bonded structures of water and draw the water molecule to themselves to form a compact structure (of water molecules around the ions).^{11,30} The nonpolar solutes shift the thermodynamic equilibrium between the molecules of liquid water towards the open (icelike) structure components.^{29,31} The structure-forming properties of urea differ from both kinds of solutes just described by the fact that (as will be shown later) it takes active part in the formation of the open structure in the solution (*i.e.*, the formation of clusters). Thus, urea contributes to the open structure in the solution by the same mechanism as water molecules, instead of filling interstices in the open structure like nonpolar solutes, or of substituting for water molecules in the "lattice" sites and drawing the water molecule to itself to form a new different structure at the expense of the original one like a structure-forming ion.

Discussion

The Solubility of Nonpolar Solutes in Strongly Polar Solvents. In the condensed state two extreme types

(20) H. S. Frank and M. W. Evans, *J. Chem. Phys.*, **13**, 507 (1945).

(21) W. Brunning and A. Holtzer, *J. Am. Chem. Soc.*, **83**, 4865 (1961).

(22) P. Mukerjee and A. Ray, *J. Phys. Chem.*, **67**, 190 (1963).

(23) P. Mukerjee and A. K. Ghosh, *ibid.*, **67**, 193 (1963).

(24) D. B. Wetlaufer, S. K. Malik, L. Stoller, and R. L. Coffin, *J. Am. Chem. Soc.*, **86**, 508 (1964).

(25) Y. Nozaki and C. Tanford, *J. Biol. Chem.*, **238**, 4074 (1963).

(26) G. C. Kresheck and L. Benjamin, *J. Phys. Chem.*, **68**, 2476 (1964).

(27) M. J. Schick, *ibid.*, **68**, 3585 (1964).

(28) J. A. Rupley, *ibid.*, **68**, 2002 (1964).

(29) H. S. Frank and W. Y. Wen, *Discussions Faraday Soc.*, **24**, 133 (1957).

(30) I. G. Mikhanilov and Yu. P. Syrnikov, *Zh. Strukt. Khim.*, **1**, 12 (1960).

(31) V. I. Yashkichev and O. Ya. Samoilov, *ibid.*, **3**, 195 (1962).

of solutions are possible: (a) substitutional, where the solute particle occupies a "lattice" site normally occupied by a solvent molecule and thus competes with the solvent molecules for the sites, as in the case of substances whose molecules have comparable sizes and force fields; and (b) interstitial, where the solute particle occupies a cavity in the structure of the solvent and thus does not compete with the solvent molecules for the "lattice" sites, as in the case of nonpolar solutes and strongly polar solvents.³² Ample support for this comes from thermodynamic calculations (*e.g.*, Frank and Evans²⁰ and D'Orazio and Wood³³) and recently from nuclear magnetic relaxation measurements in aqueous and nonaqueous solutions of a large number of substances containing alkyl groups.³⁴ The results of the last reference clearly indicate the change in the type of solution as the polarity of the solvent decreases, showing interstitial solution in water on the one hand and substitutional in acetone on the other.

Therefore, in the case of hydrocarbons (or hydrocarbon residues) and water substitutional solution is not to be expected. This can also be roughly demonstrated using regular solution theory³⁵ taking methane as the hydrocarbon. From the solubility of methane in cyclohexane at 25° and 1 atm.,³⁵ the substitutional solubility of methane in water at the same temperature and pressure has been estimated using the solubility parameters 2.6, 8.2, and 16.8 for methane, cyclohexane, and water, respectively. It has been found that the mole fraction of methane in water expected on this basis is 3.5×10^{-10} which is about one-millionth of the actual solubility (2×10^{-5}).³⁵ In contrast, the interstitial solubility of methane (and other hydrocarbons) has been calculated by Némethy and Scheraga³ and the calculated value is in reasonable agreement with experiment.

The stability of the interstitial solution must depend on the sizes of the solute particles and of the interstices. For example, a small particle in a comparatively large cavity cannot stabilize the structure and thus the system is unstable. However, a large solute particle may draw upon more than one cluster in order to accommodate the nonpolar moiety.³ It is most probably for this reason that no clathrates of helium, neon, or hydrogen by themselves are known,³⁶ whereas hydrates of innumerable complex molecules have been prepared.³⁷

Formation of Urea-Water Clusters. It can be expected on structural grounds that urea enters into cluster formation in aqueous solutions since it was inferred²⁹ that hydrogen-bonded solutes (*e.g.*, NH₃) or groups (*e.g.*, OH or NH₂) "don't alter water structure much, if at all" because these solutes or groups "should be able to enter clusters with only slight distortion and

to transmit both cluster-forming and cluster-disrupting tendencies." Urea falls into this group of solutes and the carbonyl group should modify the structure only slightly.

Evidence to support this point of view comes from two main sources, from the physical properties of pure aqueous urea solutions and from the fact that this is the only structure capable of accounting for the effects of urea upon the "solvent" power of aqueous solutions towards nonpolar solvents including hydrophobic bonding.

(a) *Physical Properties of Aqueous Urea Solutions.*

(1) *Solubility.* It is a well-known fact that urea has an extremely high solubility in water (about 20 *M* at 25°). The ease of mixing of urea with water means that urea is able to compete with water molecules for the hydrogen bonds.

(2) *Heat Capacity.* The partial molal heat capacity of urea at infinite dilution, C_p° urea (which is indicative of the environment of the urea molecule at this dilution)^{2,32} is of the order of +20 cal./mole deg., which is very close to that of the solid.³⁸ This shows that a similar environment exists in the solid state and in aqueous urea solutions. As it is known that in the solid the urea molecule is hydrogen bonded,³⁹ the same must be true in water except that here, at infinite dilution, the molecules surrounding the urea molecules are no longer urea but only water molecules.

Any analogy of urea to ions, whether structure forming or breaking, is ruled out completely by the partial molal specific heats of both structure-breaking and structure-forming ions at infinite dilution which are large and negative²⁹ in contrast to the large and positive value for urea.

(3) *Viscosity.* If the extensive hydrogen bonding indicated in aqueous urea solutions were fundamentally different from that existing in pure water and responsible for its cooperative structure, *i.e.*, if water molecules hydrogen bonded to urea were not able to hydrogen

(32) R. W. Gurney, "Ionic Processes in Solution," McGraw-Hill Book Co., Inc., New York, N. Y., 1953, p. 54.

(33) L. A. D'Orazio and R. H. Wood, *J. Phys. Chem.*, **67**, 1435 (1963).

(34) H. G. Herz and M. D. Zeidler, *Ber. Bunsenges.*, **68**, 821 (1964).

(35) J. H. Hildebrand and R. L. Scott, "The Solubility of Non-Electrolytes," Reinhold Publishing Corp., New York, N. Y., 1950, p. 134.

(36) J. H. van der Waals and J. C. Platteen, *Advan. Chem. Phys.*, **2**, 1 (1959).

(37) G. A. Jeffrey and R. K. McMullan, *J. Chem. Phys.*, **37**, 2231 (1962), and references therein.

(38) E. J. Edsall and J. T. Cohn, "Proteins, Amino Acids and Peptides as Ions and Dipolar Ions," Reinhold Publishing Corp., New York, N. Y., 1943, pp. 163, 169.

(39) A. K. Kitaigorodskii, "Organic Chemical Crystallography," Consultants Bureau, New York, N. Y., 1961, p. 154.

bond with other neighboring molecules, then this would also be reflected in the value of the B coefficient in Dole-Jones viscosity equation.³² In fact, the B coefficient for urea in water is a small positive quantity indicating only a weak structure-forming tendency when compared to the corresponding values of structure-forming ions in water.³² On the other hand, if the urea molecules would tend to destroy the structure of water and produce disorder, then the B coefficient would be a negative quantity.³²

(4) *Dielectric Constant.* Further evidence which points towards the increase of structure in the aqueous urea solution as a result of hydrogen bonding comes from dielectric constant measurements which show that addition of urea to water raises the value of the dielectric constant.⁴⁰ A high dielectric constant is indicative of the existence of strong cooperative structures which give rise to a strong orientation polarization⁴⁰ and flickering clusters.¹¹ That this large positive increment in the dielectric constant of water is not due to the large dipole moment of urea ($\mu = 4.56$ D.^{40,41}) but due to a structural effect as explained above, may be seen from the fact that $\Delta\epsilon/\Delta c$ for urea equals 2.72, whereas for symmetrical dimethylurea, which would not be able to enter into cluster formation and which has a larger dipole moment than urea ($\mu = 4.80$ ^{40,41}), $\Delta\epsilon/\Delta c$ is approximately zero.⁴¹ Furthermore, if urea were to destroy the cooperative structure of the solution, as is the case of structure-forming and -breaking ions,²⁹ then the dielectric constant would decrease and not increase as found by experiment.⁴² Thus again it is clear that urea does not behave like an ion.

(5) Finally, if urea is indeed very similar to water in hydrogen-bonding ability and is thus able to participate in cluster formation as indicated in the previous paragraphs, then aqueous urea solutions should be nearly ideal. The activity of water in urea solutions up to the saturation point (20 M at 25°) has been measured^{43,44} and led to the conclusion that the solutions were indeed "nearly ideal."⁴⁴ This also rules out any association of urea molecules to themselves in the solution, since any significant amount of self-association would produce a large nonideality.

(b) *The Effect of Urea on the Strength of the Hydrophobic Bond.* Recent investigations which have already been cited²¹⁻²⁷ show that addition of urea to aqueous solutions weakens hydrophobic bonding, except^{24,25} for the CH_4 and C_2H_6 molecules which will be discussed separately.

Since, as has already been pointed out, hydrocarbon solutes dissolve interstitially in water on one hand and addition of urea to water does not diminish the polarity of the solvent on the other,²² it is expected that hy-

drocarbon solutes would also dissolve interstitially in aqueous urea solutions. However, in view of the fact that urea is capable of forming clathrates in the solid state, something similar might be taking place in aqueous urea solutions, which would account for the increased solubility of hydrocarbons in the latter solvent. That this does not happen in aqueous urea solutions is indicated by the near ideality of urea-water mixtures and the following: firstly, it has been shown⁴⁵ that the formation of urea clathrates is restricted to the solid state only; secondly, addition of urea to water increases the solubility of substances that have branched-hydrocarbon moieties²⁴ which are incapable of forming urea clathrates in the solid state⁴⁶; and thirdly, if pure urea clathrates were to form in aqueous urea solutions, the increase in the solubility of the hydrocarbon²⁴ or the increase in the c.m.c. of the surface-active agent²² would be a nonlinear function of the urea concentration and the solubility would rise steeply because of the cooperative nature of cage formation as has been pointed out by Tanford, *et al.*²⁵ However, it is found experimentally that the increase in the solubility of the hydrocarbon or the increase in the c.m.c. is almost a linear function of the urea concentration.^{21,22,25}

Since interstitial solution seems, therefore, to be the mechanism by which the hydrocarbon residues stay in solution, their increased solubility in urea solution means that the number of possible interstices which can accommodate the molecularly dispersed nonpolar moieties has increased (or more precisely, that the formation of cavities to accommodate the hydrocarbon molecules has become easier in aqueous urea solutions). It seems that hydrophobic bonding is weakened also in other cases where the three-dimensional hydrogen bonding in solution increases.⁴⁷

Urea, which is a very good hydrogen-bonding agent, actively participates in the formation of "mixed" clusters in aqueous urea solutions. There is evidence^{24,26} that these clusters are less thermally stable

(40) J. T. Edsall and J. Wyman, "Biophysical Chemistry," Academic Press, Inc., New York, N. Y., 1958, p. 323.

(41) J. Wyman, *Chem. Rev.*, 19, 213 (1936).

(42) R. A. Robinson and R. H. Stokes, "Electrolyte Solutions," Academic Press, Inc., New York, N. Y., 1955, p. 18.

(43) G. N. Lewis and G. H. Burrows, *J. Am. Chem. Soc.*, 34, 1515 (1912).

(44) C. Scatchard, W. J. Hamer, and S. E. Wood, *ibid.*, 60, 3061 (1938).

(45) J. A. A. Ketelaar and B. A. Loopstra, *Rec. trav. chim.*, 74, 113 (1955).

(46) J. A. A. Ketelaar, "Chemical Constitution," 2nd Ed., Elsevier Publishing Co., Amsterdam, 1958, p. 367.

(47) M. Abu-Hamdiyyah and K. J. Mysels, *J. Phys. Chem.*, 69, 1466 (1965).

than the pure water clusters. This indicates that the enthalpy is higher in the aqueous urea solutions and therefore the driving force for the spontaneous transfer of nonpolar solutes from pure water to aqueous urea solution is entropic in origin. According to the concepts developed here, the increase in entropy can be attributed to the increase in the number of available cavities or interstices for the solute molecules in aqueous urea solutions (again because their formation becomes easier).

If the above conclusions are correct, then it is possible to predict the effect of alkyl-substituted ureas on the strength of the hydrophobic bond. First, an alkylurea derivative will have a decreased ability to hydrogen bond with water compared to that of the unsubstituted urea, and this tendency will increase with the number of the substituent groups, and, as a result of this, the ability to participate in cluster formation will also be reduced. Secondly, the alkyl (or the nonpolar) substituent groups themselves, when they are introduced in the solution (as part of the urea derivative), can only accommodate themselves in cavities in the aqueous solution with the result that the number of "would be" cavities in the solution decreases. We see that both of these properties of alkylurea derivatives work against the weakening of the hydrophobic bond and it is expected, therefore, that these compounds would have an effect opposite to that of the unsubstituted urea.

There are no experimental data regarding the effect of these derivatives on simple systems involving hydrophobic bonding, but recently a study of the effect of several urea derivatives on the denaturation of serum albumin was reported.⁴⁸ It was found that the alkyl-substituted ureas have an effect opposite to that of urea itself and this action increases with the length and the number of alkyl substituents.

It must be pointed out, however, that denaturing of proteins seems to be a complex process which is incompletely understood and therefore other factors besides hydrophobic bonding may be involved in this process. However, if the point of view that the native structure of globular proteins (of which serum albumin is a member) in aqueous solution is primarily the result of hydrophobic bonding as suggested by Tanford, *et al.*,⁴⁹⁻⁵³ is accepted, then the action of alkylurea derivatives on the native structure of serum albumin is readily understandable.

The results of Schick²⁷ are also similarly explained. The explanation that the increase in the c.m.c. of nonionic surfactants is due to the increased hydration of the ether oxygens because urea destroys the water structure and thus makes water molecules more free

and therefore more available for hydration is very unlikely for the reasons already stated. Again, if urea were to play the same role as an ion that draws the water molecules towards itself and prevents them from participation in hydrogen bonding with other neighboring water molecules as was suggested,²⁷ then the c.m.c. of these nonionic surfactants should decrease, and not increase as found by experiment, on addition of urea.

Since urea is a nonionic solute its addition to a colloidal association electrolyte solution affects mainly the structure of the solution. Thus the finding²⁷ that urea increases the c.m.c. of various dodecyl sulfates in the order $R_4N^+ > Na^+ > Li^+$ seems to be indicative of the effect of these ions on the structure of the solution. Li^+ has the most disturbing effect, by polarizing the neighboring water molecules to itself and preventing them from participation in hydrogen-bonded clusters; Na^+ effect is less than Li^+ and R_4N^+ has the least effect. In addition, the tetraalkylammonium ion has a tendency to leave the surface of the micelle for the bulk solution when urea is added because the formation of clusters (or cavities) to house such a hydrophobic ion²⁹ becomes easier in the presence of urea as has already been pointed out. Therefore, we have two effects which are acting in the same direction in the case of the tetraalkylammonium ion to enhance the increase in the c.m.c. and indeed the effect is much larger when the tetraalkylammonium ions are the counterions than when the counterion is Na^+ or Li^+ .

According to these ideas, urea should increase the c.m.c. of RSO_4M according to their counterions in the following order: $R_4N^+ > Cs^+ > Rb^+ > K^+ > Na^+ > Li^+$. In the absence of urea the effect of these ions is mainly electrostatic as governed by the charge and the effective size of the ion (the structural effect is small compared to the electrostatic) and, therefore, the explanation of Mysels, *et al.*,^{27,54} still holds.

The Anomalous Solubility of Methane and Ethane. Water and urea molecules have different geometries and, since both partake in the formation of clusters, it is expected that these would not be as symmetrical

(48) J. A. Gordon and W. P. Jencks, *Biochemistry*, **2**, 47 (1963).

(49) C. Tanford, P. Z. De, and V. G. Taggart, *J. Am. Chem. Soc.*, **82**, 6028 (1960).

(50) C. Tanford, *ibid.*, **84**, 4240 (1962).

(51) C. Tanford and P. K. De, *J. Biol. Chem.*, **236**, 1711 (1961).

(52) P. L. Whitney and C. Tanford, *ibid.*, **237**, 1735 (1962).

(53) J. F. Brandt, *J. Am. Chem. Soc.*, **86**, 4302 (1964). This paper gives a good discussion of Tanford's views.

(54) K. J. Mysels, Final Report, Project NR 356-254, Office of Naval Research Contract NONR-274 (00).

as those of pure water and that the sizes and symmetries of the interstices would also be different. This is indicated by the solubilities²⁴ of methane (in the temperature range 5–45°) and of ethane (below 20°), which are reduced upon addition of urea. Thus here, in contrast to all previous cases, the molecularly dispersed hydrocarbon is destabilized, *i.e.*, hydrophobic bonding is strengthened.

As was pointed out earlier, two factors govern the solubility of a nonpolar solute in the interstitial solution: the size of the solute molecule and that of the cavity in the solution. Methane is a small molecule and the cavities that accommodate it in aqueous solutions are small. Glew¹⁵ found that the structure of water around the methane molecule is a broken-down methane gas-hydrate type polyhedron and that the size of the interstitial hole occupied by the methane molecule has very nearly the same size as that occupied by the methane molecule in the gas-hydrate lattice, namely the 20-coordinated site. Methane molecules do not occupy the comparatively larger cavities which are approximately equal to the 24-coordinated sites. In other words, methane molecules are incapable of stabilizing a cluster that forms a comparatively large cavity. Since addition of urea to an aqueous methane solution decreases the solubility of methane (in the given temperature range), some of the clusters which originally housed the methane molecules must have been destroyed and it became more difficult to form such small cavities.

The same thing happens in the case of ethane, which occupies in pure water an interstice of approximately the 24-coordinate site size,¹⁵ *viz.*, addition of urea decreases the solubility of ethane in the range of temperature 5–20°. Hence, it may be concluded that urea destroys some of the "polyhedra" or "icebergs" which are formed around methane and ethane molecules, and that the cavities formed by the mixed urea-water clusters are less favorable for housing the small molecules than those of water with the result that a decrease in solubility occurs.

However, as the temperature rises, other factors operate which tend to normalize the solubility of methane (or ethane) in aqueous urea solutions. Firstly, the number of cavities formed by pure water, the polyhedra housing the methane (or ethane) molecules, will tend to decrease with increasing temperature as is evident from the decrease of the solubility of methane (and ethane) in pure water in the temperature range

5–50°. Secondly, although the mixed clusters are less favorable for housing the methane (or ethane) molecules than those of pure water, they tend to persist at higher temperatures, which is related to the fact that the enthalpy of the mixed clusters is higher than that of pure water clusters (the polyhedra). The first, which is the larger, factor tends to decrease the solubility as a whole; the second factor tends to increase the solubility in urea solutions. Moreover, the second factor favors the larger molecule, ethane, more than methane, the smaller molecule, and so the normalizing temperature for the former tends to occur at a lower temperature than that of the latter.

This tendency is very clearly seen in the solubility curves of methane and of ethane²⁴ in aqueous urea and in water. The curves for ethane intersect at 20° and those for methane—the smaller molecule—approach each other in the investigated range and would intersect probably just above 50°.

In this connection it would be very interesting to find out experimentally the effect of urea on the solubility of the rare gases in water. It is expected that the solubility of the rare gases in aqueous urea would be less than their solubility in pure water at low temperatures.

Summary and Conclusions

(1) Nonpolar solutes dissolve interstitially in strongly polar solvents. (2) Addition of urea to water increases the hydrogen bonding in solution. (3) Urea partakes in the formation of urea-water clusters that are responsible for the formation of interstices in the solution which accommodate the nonpolar moieties of the solute and therefore in this sense may be looked upon as a structure former. (4) Likening urea to an ion does not fit the facts and must therefore be rejected. (5) It is easier to form a large cavity in aqueous urea solution than in pure water and the converse is true for small cavities that house methane or ethane molecules and presumably also the rare gases at low temperatures.

Acknowledgments. The author is very grateful to Professor Karol J. Mysels for his help and advice throughout the preparation of this manuscript. This work was supported by a fellowship sponsored by the Continental Oil Company and by Public Health Service Research Grant GM 10961-01 from the Division of General Medical Sciences, Public Health Service.

Electrical Conductances of Aqueous Solutions at High Temperature and

Pressure. II. The Conductances and Ionization Constants of Sulfuric

Acid-Water Solutions from 0 to 800° and at Pressures up to 4000 Bars^{1,2}

by Arvin S. Quist, William L. Marshall, and H. R. Jolley³

Reactor Chemistry Division, Oak Ridge National Laboratory, Oak Ridge, Tennessee (Received March 8, 1965)

The electrical conductances of dilute aqueous sulfuric acid solutions have been measured at temperatures from 0 to 800° at pressures to 4000 bars. Molar conductances were calculated from which, by several methods, limiting equivalent conductances of H₂SO₄ as a function of temperature and density were obtained. The second ionization constant of H₂SO₄ was calculated at temperatures up to 300°, and the first ionization constant was calculated between 400 and 800°. Estimates were made of the standard heat of ionization, ΔH° , for the first ionization process between 400 and 800° at pressures of 1000, 2000, 3000, and 4000 bars.

Introduction

In a continuing study on the properties of aqueous electrolyte solutions at high temperatures and pressures, the electrical conductances of dilute sulfuric acid solutions were measured at temperatures from 0 to 800° and at pressures from 1 to 4000 bars. Earlier papers in this series presented a description of the conductance cell⁴ and the conductance measurements on K₂SO₄ solutions.⁵ From the present measurements on H₂SO₄ solutions, the second ionization constant was calculated at temperatures from 100 to 300° and at densities up to 1.0 g. cm.⁻³. Above 300° this constant became too small to be calculated accurately. The first ionization constant of H₂SO₄ was calculated at densities below 0.8 g. cm.⁻³ at 400°, and up to 800° at all experimentally attainable densities. Other calculations include estimations of the change in hydration numbers for the ionization processes, the heat of ionization (for the first ionization step), and limiting equivalent conductances at temperatures above 400°.

Experimental

Apparatus. The conductance cell and associated equipment described previously^{4,5} were used with some modification. The 0.125-in. o.d. high pressure tubing was replaced by higher strength, 100,000-

p.s.i. tubing. This tubing, in contact with sulfuric acid solution only at 25°, was made from 316 stainless steel, 0.250 in. o.d., 0.030 in. i.d. (Superior Tube Co., Norristown, Pa.). The valves that were exposed to dilute sulfuric acid also were constructed of 316 stainless steel for use to 100,000 p.s.i. (Autoclave Engineers, Erie, Pa., Model 100V-1003), but modified to use 0.25-in. o.d. instead of the designed 0.31-in. o.d. tubing. The normally supplied 18-4-1 valve tips were replaced by tips made of Stellite 6 (Haynes-Stellite Co., Kokomo, Ind.). Although there was no evidence that the solution contained in the separator unit⁵ was contaminated by water leaking around the close-fit floating piston, this piston was modified by the addition of a neoprene "quad" ring (Minnesota Rubber Co., Minneapolis, Minn.). The piston was also electroplated very lightly (approximately 0.0003 in. thick) with chromium to lessen the possibility of galling.

(1) Research sponsored by the U. S. Atomic Energy Commission under contract with the Union Carbide Corporation.

(2) Presented in part at the 146th National Meeting of the American Chemical Society, Denver, Colo., Jan. 1964.

(3) Summer Participant, 1963, Department of Chemistry, Loyola University, New Orleans, La.

(4) E. U. Franck, J. E. Savolainen, and W. L. Marshall, *Rev. Sci. Instr.*, **33**, 115 (1962).

(5) A. S. Quist, E. U. Franck, H. R. Jolley, and W. L. Marshall, *J. Phys. Chem.*, **67**, 2453 (1963).

Materials. The conductivity water was prepared in the manner described previously.⁵ Stock solutions of sulfuric acid were prepared from sulfuric acid collected from a quartz distillation unit. These stock solutions were standardized with a sodium hydroxide solution (Fisher Scientific Co., Fairlawn, N. J.) that had been standardized against potassium acid phthalate (Baker analyzed reagent, primary standard). From the sulfuric acid stock solutions three concentrations (0.002424, 0.004893, and 0.009855 *m*) were prepared for the conductance measurements by using weight burets. A 0.0005 *m* solution was also prepared, but its concentration was too low to give suitably reproducible results.

Cell Constants. Two inner electrode assemblies were used throughout the series of measurements. The cell constants, determined at $25.00 \pm 0.01^\circ$ by using 0.01 Demal KCl solutions, were 0.286 and 0.270 cm.^{-1} , respectively.

Accuracy of Measurements. The earlier measurements on K_2SO_4 were estimated to be precise to within $\pm 1\text{--}2\%$. However, for sulfuric acid solutions, possible corrosion in the tubing and valves increased the maximum uncertainty in the measurements to an estimated $\pm 4\text{--}5\%$. Reproducible measurements were most difficult to obtain in the temperature range 100–300°, where the highest conductances were observed.

Procedure. Because of the corrosive nature of H_2SO_4 solutions, the procedure previously described⁵ was modified. A schematic drawing of the essential high-pressure equipment is shown in Figure 1. Pressures to 1000 bars were generated by a hand-turned pressurizer and measured on a calibrated Heise bourdon tube gauge. Pressures from 1000 to 4000 bars were produced by the air-driven hydraulic pump and the intensifier system and were measured by a calibrated strain gauge. By changing the tubing connections, solution could be added (pressurization) to the conductance cell from either the top or bottom and subsequently removed (depressurization) from the opposite end. Consequently, the cell was now a "flow-through" type, in contrast to the previous design wherein tubing was connected only to the bottom. This new arrangement permitted more effective flushing of the cell at the temperature of the experiment. At temperatures below 400°, the solution usually was introduced through the top connection and removed from the bottom, but at higher temperatures the opposite method was used. Although flushing the cell from the top probably was the most effective method, at the higher temperatures there was greater probability of cracking the alundum tube by thermal shock when room temperature solution was introduced into the

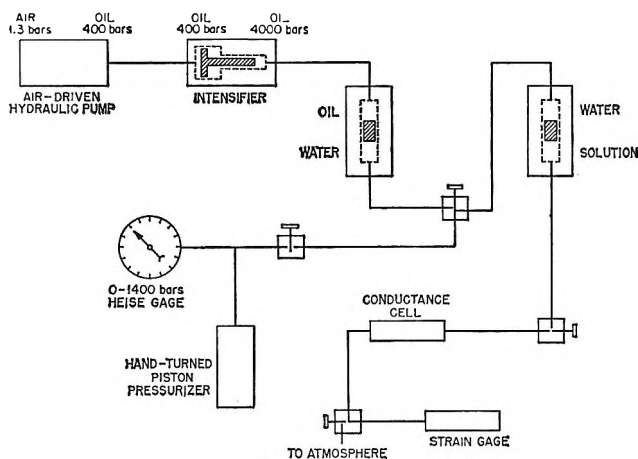


Figure 1. Schematic drawing of equipment for conductance measurements at high pressures.

red-hot cell. (The alundum insulating tube, a part of the inner electrode assembly, enters the top of the cell.)

The conductance cell, high pressure tubing, and separator unit were always rinsed thoroughly with solution before each run. After reaching the desired temperature, the system was again flushed by flowing solution through the cell (by alternate pressurization and depressurization). With the present arrangement, the separator unit containing the solution reservoir could be isolated from the rest of the system by closing the proper valves, and then could be refilled easily with fresh solution for continuing the experiment.

The data taken for each run were temperature, conductance, and pressure in bars (to 1000 bars with bourdon gauge) or millivolts (1000 to 4000 bars with strain gauge). A digital computer (IBM-7090) was used to convert strain gauge readings to bars and to correct resistances both for the effect of frequency and for lead resistance. Solvent conductances at the experimental temperatures and pressures were interpolated by the computer from previously determined solvent conductances. Since all solutions were very dilute, their densities were assumed to be that of pure water and were determined (with the computer) by a nonlinear interpolation of Sharp's⁶ table of specific volumes at integral temperatures and pressures. This compilation, based mainly on the data of Kennedy, *et al.*,^{7–11} gives values at the highest pressures slightly

(6) W. E. Sharp, "The Thermodynamic Functions for Water in the Range -10 to 1000° and 1 to $250,000$ Bars," University of California Radiation Laboratory Report UCRL-7118 (1962).

(7) G. C. Kennedy, *Am. J. Sci.*, **248**, 540 (1950).

(8) G. C. Kennedy, *ibid.*, **255**, 724 (1957).

(9) G. C. Kennedy, W. L. Knight, and W. T. Holser, *ibid.*, **256**, 590 (1958).

(10) W. T. Holser and G. C. Kennedy, *ibid.*, **256**, 744 (1958).

(11) W. T. Holser and G. C. Kennedy, *ibid.*, **257**, 71 (1959).

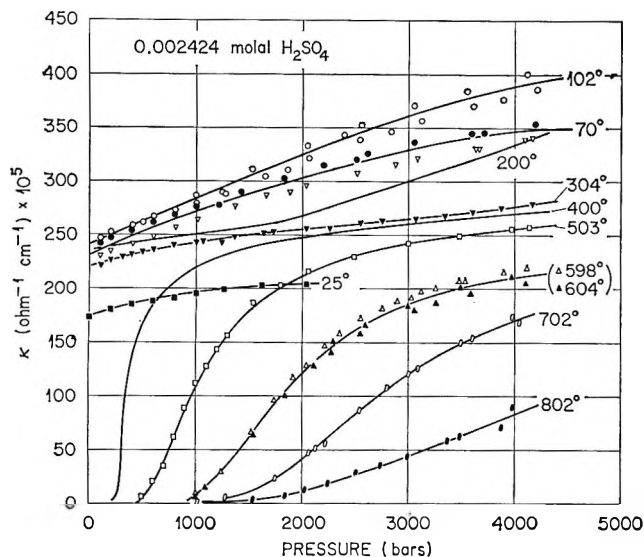


Figure 2. Specific conductances of 0.002424 *m* H₂SO₄ solutions as a function of pressure at several temperatures.

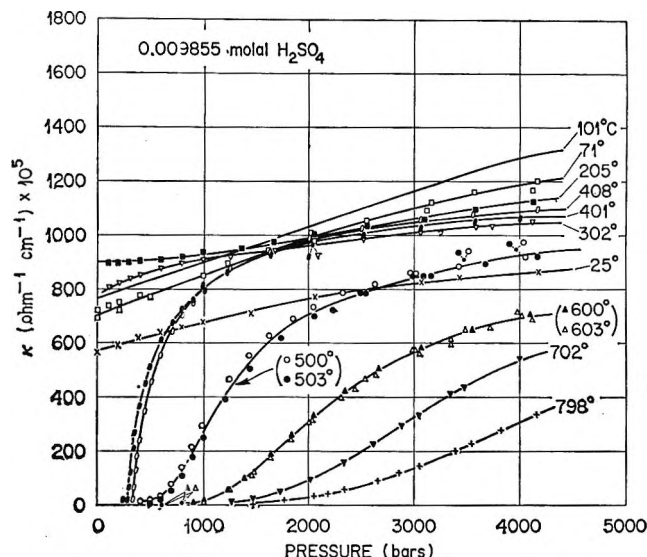


Figure 4. Specific conductances of 0.009855 *m* H₂SO₄ solutions as a function of pressure at several temperatures.

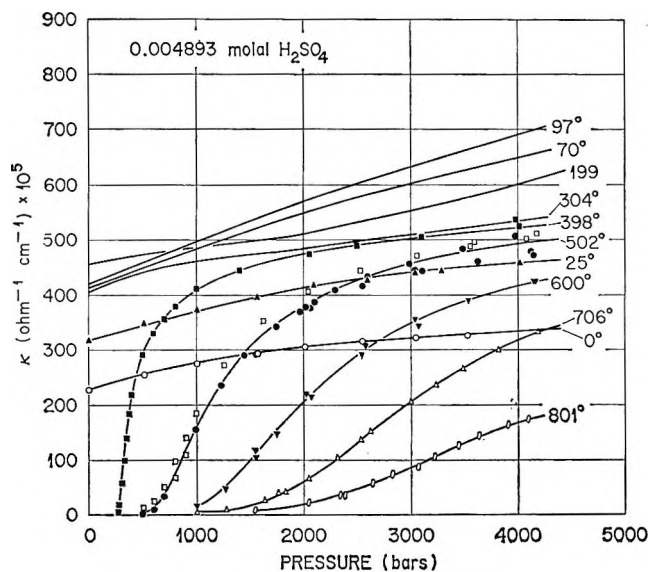


Figure 3. Specific conductances of 0.004893 *m* H₂SO₄ solutions as a function of pressure at several temperatures.

different from those used previously,⁵ based also on Kennedy's data. The output from the computer provided a printed record and also magnetic tape input for an automatic plotter (California Computer Products, Inc., Anaheim, Calif.). This plotter drew graphs of specific and equivalent conductances as a function of both density and pressure for each temperature and solution concentration.

Results and Discussion

Specific conductances of the H₂SO₄ solutions, corrected for solvent conductance, are shown in Figures

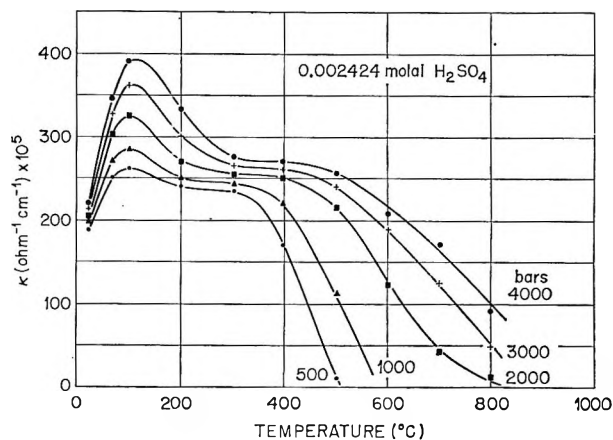


Figure 5. Specific conductances of 0.002424 *m* H₂SO₄ solutions as a function of temperature at several pressures.

2-4 as a function of pressure for each temperature. The curves where individual points are not shown represent averages of two or more different runs at that particular temperature. For clarity of presentation, the individual points were not given. From enlargements of these figures, specific conductances at integral pressures were obtained by interpolation. Isobaric specific conductances plotted against temperature are shown in Figures 5-7. The results for 0.004893 *m* H₂SO₄ at temperatures to 100° are in good agreement (within 1%) with the measurements of Franck and Hartman¹² but are somewhat higher (approximately 7%) than their measurements near 200°. The graphs

(12) D. Hartman, Thesis, Institut für physikalische Chemie und Elektrochemie, Technische Hochschule, Karlsruhe, Germany, 1964.

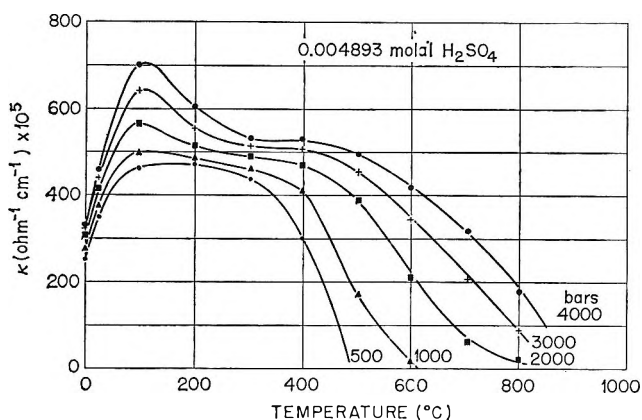


Figure 6. Specific conductances of 0.004893 *m* H₂SO₄ solutions as a function of temperature at several pressures.

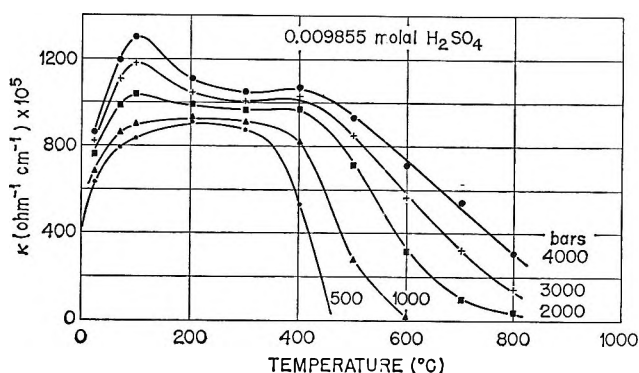


Figure 7. Specific conductances of 0.009855 *m* H₂SO₄ solutions as a function of temperature at several pressures.

for sulfuric acid are considerably different from those obtained previously for K₂SO₄. For K₂SO₄ solutions at temperatures of 200° and below, the isothermal specific conductance is nearly independent of pressure. In contrast, the specific conductances of H₂SO₄ increases markedly with increasing pressure. This behavior of H₂SO₄ is believed to result predominantly from increasing ionization of the bisulfate ion with increasing pressure (see Table I). The increased ionization is presumably due to the enhanced hydration of the ions caused by increasing pressure.^{13,14}

Another striking difference between these graphs (Figures 5-7) and those for K₂SO₄ appears in the position and shape of the maximum of the curves. With K₂SO₄ this maximum lies near 300°, whereas with H₂SO₄ the maximum is close to 100°. The difference is believed to be due also to the behavior of HSO₄⁻ in the H₂SO₄ solutions. As the temperature increases from 0 to 100°, the conductance increases rapidly due to a rapid decrease in the viscosity of water. Therefore, the mobilities of the separate ions increase rapidly.

Table I: Negative Logarithm of the Second Ionization Constant of H₂SO₄, $-\log K_2^\circ$; Standard State Is the Hypothetical 1 *M* Solution

Temp., °C.	Saturation vapor pressure	Density, g. cm. ⁻³					
		0.75	0.80	0.85	0.90	0.95	1.0
100	3.10	2.60
150	2.83
200	4.09	3.85	3.56	3.13
250	3.85	3.65	3.35
300	4.09	4.03	3.91	3.73	3.58

With K₂SO₄ the conductance increases until temperatures near 300° are reached. At higher temperatures, the decreasing dielectric constant of water, caused both by increasing temperature and decreasing density, permits association between ions and begins to offset the effect of decreasing viscosity; therefore, conductance decreases. For H₂SO₄ solutions, the dissociation constant for HSO₄⁻ decreases with increasing temperature. Near 100° its rate of decrease with increasing temperature begins to counteract the increase in conductance of ions due to decreasing viscosity. Although a plateau (conductance *vs.* temperature) occurs between 200 and 400° with H₂SO₄ (where the bisulfate ion dissociation is very small), the conductance begins to decrease more rapidly with increasing temperature at temperatures above 400° (at constant pressure) than is observed for K₂SO₄. This difference appears due to increasing association between H⁺ and HSO₄⁻ ions with increasing temperature which occurs to a greater extent than any association between the ions in K₂SO₄ solutions. A direct comparison of K₂SO₄ and H₂SO₄ solutions of approximately equal molal concentration is shown in Figure 8.

The molar conductances of the H₂SO₄ solutions as a function of density are shown in Figures 9 to 11, and smoothed values are tabulated at integral temperatures and densities in Tables II to IV. At temperatures of 200° and below, the effect of increasing density on increasing the dissociation of the bisulfate ion is readily apparent. At constant density at temperatures above 400°, the decrease in the first ionization constant of H₂SO₄ with increasing temperature can be noted by comparing the graphs with those for K₂SO₄.⁵

(13) S. D. Hamann, "Physico-Chemical Effects of Pressure," Academic Press, New York, N. Y., 1957, pp. 137-159.

(14) S. D. Hamann in "High Pressure Physics and Chemistry," Vol. II, R. S. Bradley, Ed., Academic Press, New York, N. Y., 1963, Chapter 7, ii.

Table II: The Molar Conductances ($\text{cm}^2 \text{ohm}^{-1} \text{mole}^{-1}$) of 0.002424 m H_2SO_4 Solutions at Integral Temperatures and Densities

Temp., °C.	Density, g. cm^{-3}													
	0.4	0.45	0.5	0.55	0.6	0.65	0.7	0.75	0.8	0.85	0.9	0.95	1.0	
0													460	
25													720	
100													1170	
150													1210	
200												1110	1120	1220
250												1150	1160	1210
300								1270	1230	1200	1180	1180	1190	
350							1310	1290	1280	1250	1200	1190		
400	580	800	980	1130	1230	1290	1310	1310	1300	1270	1220	1190		
450	500	680	890	1050	1180	1280	1290	1300	1300	1280				
500	380	540	780	940	1120	1240	1250	1270	1270	1260				
550	280	420	640	810	1030	1160	1200	1220	1220	1250				
600	180	310	500	690	920	1060	1130	1150	1140					
650	130	240	400	580	800	960	1060	1120						
700	100	190	320	490	690	860	1000	1070						
750	90	160	250	380	570	740								
800	80	120	200	300	450	620								

Table III: The Molar Conductances ($\text{cm}^2 \text{ohm}^{-1} \text{mole}^{-1}$) of 0.004893 m H_2SO_4 Solutions at Integral Temperatures and Densities

Temp., °C.	Density, g. cm^{-3}													
	0.4	0.45	0.5	0.55	0.6	0.65	0.7	0.75	0.8	0.85	0.9	0.95	1.0	
0													470	
25													680	
100													1010	
150													1080	
200												1050	1060	1110
250												1100	1090	1120
300								1160	1140	1130	1130	1120	1110	
350							1200	1210	1200	1190	1170	1130		
400	480	650	800	940	1080	1160	1210	1240	1240	1230	1200	1150		
450	350	520	720	870	1020	1140	1200	1240	1240	1240				
500	230	390	600	770	940	1080	1170	1220	1240	1240				
550	150	280	480	660	860	1010	1130	1180	1200	1220				
600	100	200	370	560	760	930	1060	1130	1140					
650	90	170	300	480	680	850	1000	1080						
700	80	150	240	390	590	760	940	1020						
750	70	130	200	310	490	660								
800	60	100	160	260	390	540								

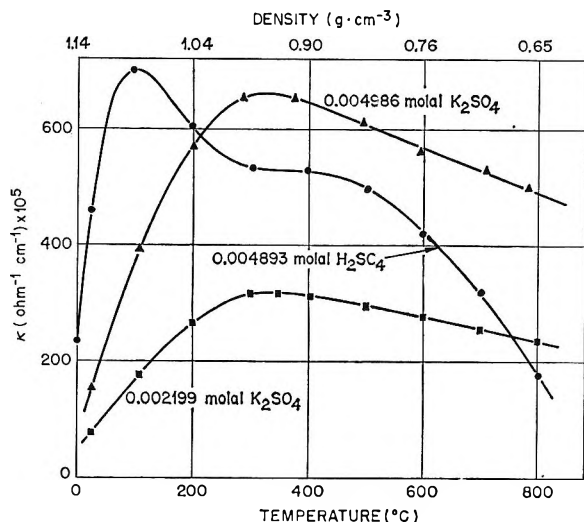
Calculation of Limiting Equivalent Conductances. For evaluating the limiting equivalent conductance of an electrolyte from measured equivalent conductances for H_2SO_4 [$\Lambda(\text{equivalent}) = \Lambda(\text{molar})$ or $1/2\Lambda(\text{molar})$ depending upon treatment either as a 1-1 or 1-2 electrolyte, respectively], all the available procedures depend on extrapolating the conductance (or some function of conductance) *vs.* concentration (or some function of concentration) curves to zero concentration. The several methods used below 300° were unsatisfactory for H_2SO_4 , probably because incomplete ionization of HSO_4^- gave extrapolated limiting con-

ductances too low assuming complete ionization to H^+ and SO_4^{2-} ions, but too high for ionization only to H^+ and HSO_4^- . At 300 and 400° at respective densities of 0.75 and 0.80 (or below) g. cm^{-3} , and at higher temperatures, when the dissociation of HSO_4^- is negligible, sulfuric acid can be considered a uni-univalent electrolyte. Under these conditions, several extrapolation procedures were used with varying degrees of success. The simplest procedure assumes that the Onsager limiting law¹⁵ is obeyed and involves merely

(15) L. Onsager, *Physik. Z.*, 28, 277 (1927).

Table IV: The Molar Conductances ($\text{cm}^2 \text{ohm}^{-1} \text{mole}^{-1}$) of 0.009855 m H_2SO_4 Solutions at Integral Temperatures and Densities

Temp., °C.	Density, g. cm^{-3}													
	0.4	0.45	0.5	0.55	0.6	0.65	0.7	0.75	0.8	0.85	0.9	0.95	1.0	
0														410
25														580
100														910
150														1000
200												1020	1030	1060
250											1060	1060		1080
300								1140	1130	1110	1100	1100		1090
350							1190	1200	1190	1170	1140	1120		
400	340	510	680	820	980	1120	1200	1230	1220	1210	1180	1140		
450	240	390	570	740	900	1050	1150	1190	1190	1200				
500	160	260	440	620	800	960	1070	1120	1130	1150				
550	90	200	340	500	700	850	970	1040	1050	1090				
600	60	140	260	400	600	730	870	950	960					
650	50	120	210	330	520	660	800	860						
700	40	100	170	270	440	580	760	780						
750	40	90	150	220	360	520								
800	40	80	120	200	300	460								


Figure 8. Comparison of the specific conductances of K_2SO_4 and H_2SO_4 solutions as a function of temperature; pressure = 4000 bars.

extrapolating Λ vs. $(\text{molarity})^{1/2}$ to zero concentration. This was successful only when H_2SO_4 behaved as a *strong* uni-univalent electrolyte. Similarly, plots of Λ vs. $(\text{molarity})^{1/2}/(1 + (\text{molarity})^{1/2})$ (an empirical extension to the limiting law, assuming the $B\delta$ parameter in the equation given by Robinson and Stokes¹⁶ was constant at 1.0) gave only slightly larger Λ_0 values. A third procedure (also used in the evaluation of the K_2SO_4 data), suggested originally by Owen,¹⁷ made use of the Fuoss-Onsager conductance equation

$$\Lambda = \Lambda_0 - Sc^{1/2} + Ec \log c + Jc$$

(where in this case E and J are empirical parameters) to solve for Λ_0 , E , and J using Λ -values from three or more concentrations. The limiting Onsager slope, S , was calculated from dielectric constants and viscosities given elsewhere.^{18,19} The Owen method worked better than the first two procedures, and for an unsymmetrical electrolyte (such as K_2SO_4) was better than any other procedure. However, when both E and S can be calculated, the Fuoss-Onsager method of extrapolating the quantity $\Lambda + Sc^{1/2} - Ec \log c$ vs. c to zero concentration gave perhaps the best values for Λ_0 .²⁰

Where H_2SO_4 behaved as a *weak* uni-univalent electrolyte, the best method for obtaining Λ_0 was presumably that of Shedlovsky,^{21,22} in which Λ_0 and the ionization constant are determined simultaneously. At solution densities below 0.6 g. cm^{-3} and temperatures above 550° , H_2SO_4 behaved as a *very weak* electrolyte. Thus conductances were not available at sufficiently low concentrations for reliable use of the previous methods for extrapolation to accurate Λ_0 -values. Estimates of the limiting conductances in

(16) R. A. Robinson and R. H. Stokes, *J. Am. Chem. Soc.*, **76**, 1991 (1954).

(17) B. B. Owen, *ibid.*, **61**, 1393 (1939).

(18) A. S. Quist and W. L. Marshall, *J. Phys. Chem.*, in press.

(19) E. U. Franck, *Z. physik. Chem. (Frankfurt)*, **8**, 107 (1956).

(20) R. M. Fuoss and F. Accascina, "Electrolytic Conductance," Interscience Publishers, Inc., New York, N. Y., 1959.

(21) T. Shedlovsky, *J. Franklin Inst.*, **225**, 739 (1938).

(22) R. M. Fuoss and T. Shedlovsky, *J. Am. Chem. Soc.*, **71**, 1496 (1949).

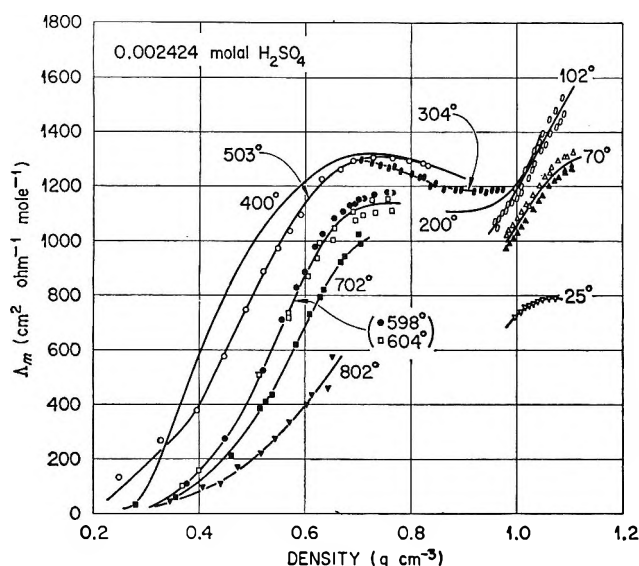


Figure 9. Molar conductances of 0.002424 m H_2SO_4 solutions as a function of the density of the solution at several temperatures.

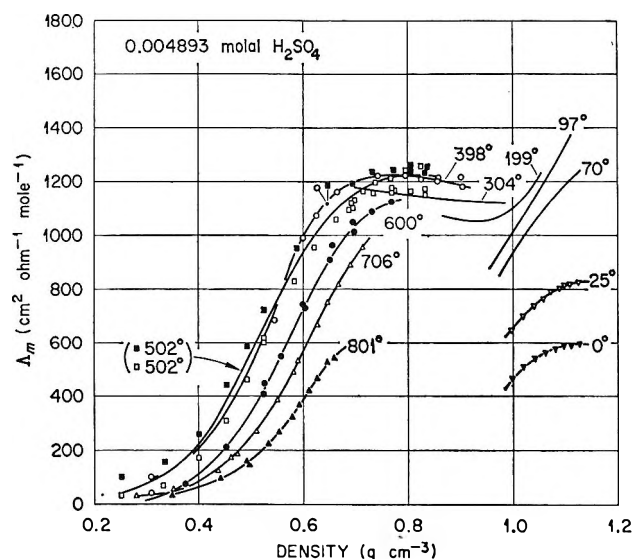


Figure 10. Molar conductances of 0.004893 m H_2SO_4 solutions as a function of the density of the solution at several temperatures.

these regions of uncertainty were therefore obtained by extrapolating the linear relationship of Walden product ($\Lambda_0\eta_0$) vs. density, observed at densities above 0.6 $g. cm^{-3}$ using Λ_0 -values derived from the Fuoss-Onsager and/or Shedlovsky methods, to densities below 0.6 $g. cm^{-3}$. Since there was only a slight variation in this relationship (above $d = 0.6 g. cm^{-3}$) with temperature from 400 to 550°, the Walden product was assumed to be independent of temperature (at

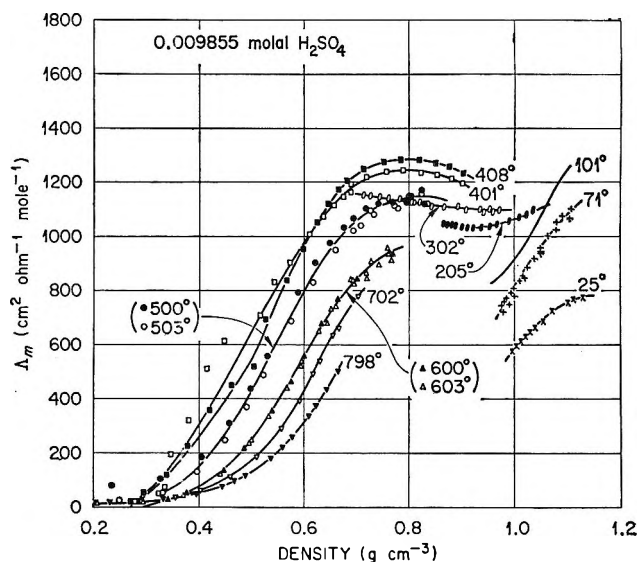


Figure 11. Molar conductances of 0.009855 m H_2SO_4 solutions as a function of the density of the solution at several temperatures.

constant density above 400°). The following empirical equation, obtained from the data at 400 to 550° at high densities, was therefore used to calculate limiting conductances for H_2SO_4 at all densities and temperatures above 550° and at densities below 0.6 $g. cm^{-3}$ at 400–550°

$$\Lambda_0(H_2SO_4) = (0.60 + 0.78d)/\eta_0$$

where d = density ($g. cm^{-3}$) and η_0 = viscosity (poise). Viscosities used were those estimated by Franck to 800° and 1.0 $g. cm^{-3}$.¹⁹

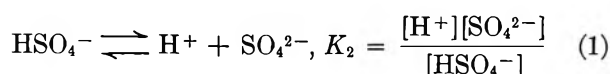
From 0 to 400° at densities to 1.0 $g. cm^{-3}$, values of $\Lambda_0(H_2SO_4)$, treated either as a 1–1 or 1–2 electrolyte, can be obtained from the limiting ionic conductances given elsewhere.²³ The $\Lambda_0(H_2SO_4)$ values at temperatures of 400° and higher calculated by the methods described in the preceding paragraphs are given in Table V. The upper right portion of Table V, separated by a heavy line from the rest of the table, contains $\Lambda_0(H_2SO_4)$ values evaluated by extrapolation of experimental data. This is the region where both the Fuoss-Onsager and Shedlovsky methods gave the same values. The method of least squares was used for the extrapolations, and the standard errors associated with the Λ_0 -values were approximately 1–3%. The other values in the table are those calculated from the equation given in the previous paragraph.

Second Ionization Constant of H_2SO_4 . To calculate equilibrium constants (in molar units) for the dissociation of the bisulfate ion

(23) A. S. Quist and W. L. Marshall, *J. Phys. Chem.*, in press.

Table V: Limiting Equivalent Conductances of H₂SO₄, Calculated as Described in the Text (Where H₂SO₄ Is Treated as a 1-1 Electrolyte)

Temp., °C.	Density, g. cm. ⁻³									
	0.40	0.45	0.50	0.55	0.60	0.65	0.70	0.75	0.80	0.85
400	1720	1640	1595	1560	1505	1460	1380	1370	1360	1325
450	1720	1670	1625	1560	1505	1475	1400	1390	1380	1350
500	1720	1670	1625	1580	1525	1495	1470	1445	1400	1365
550	1690	1670	1625	1580	1525	1515	1490	1465	1425	1400
600	1660	1640	1595	1560	1525	1515	1490	1465	1440	
650	1630	1610	1595	1560	1525	1515	1490	1480		
700	1600	1585	1570	1560	1525	1515	1490	1480		
750	1570	1560	1570	1535	1505	1495				
800	1545	1560	1545	1515	1505	1495				



$$K_2 = \frac{(1 + \theta)C_0}{(1 - \theta)} f_{\text{SO}_4^{2-}} \quad (5b)$$

at temperatures to 400° from the conductance data, the method of Davies²⁴ was used.

In this method, sulfuric acid is considered to be a mixture of two completely dissociated electrolytes, H₂SO₄ and HHSO₄, where H₂SO₄ refers to sulfuric acid that dissociates *only* to 2H⁺ and SO₄²⁻, whereas HHSO₄ is the hypothetical molecule that dissociates only to H⁺ and HSO₄⁻. The fraction of total sulfate that exists in solution as the sulfate ion, θ , is then given by

$$\theta_{\text{T.d.c.}} = \frac{\Lambda - 0.5[\Lambda_0(\text{HHSO}_4) - S(\text{HHSO}_4)I']}{\Lambda_0(\text{H}_2\text{SO}_4) - S(\text{H}_2\text{SO}_4)I' - 0.5[\Lambda_0(\text{HHSO}_4) - S(\text{HHSO}_4)I']} \quad (2)$$

where Λ is the experimentally determined equivalent conductance and I' is given by

$$I' = \frac{I^{1/2}}{1 + I^{1/2}} \quad (3)$$

In eq. 3, I is the ionic strength calculated from

$$I = (1 + 2\theta C_0) \quad (4)$$

where C_0 is the stoichiometric concentration of H₂SO₄ in moles/liter. The limiting equivalent conductances were obtained from limiting ionic conductances given elsewhere.²³ The limiting Onsager slopes were calculated in the usual manner. With a digital computer, eq. 2, 3, and 4 were iterated (θ first approximated as 0.5) until successive values of θ differed by less than 0.1%.

An ionization constant was then calculated for each concentration of H₂SO₄ from eq. 5b.

$$K_2 = \frac{[\text{H}^+][\text{SO}_4^{2-}]}{[\text{HSO}_4^-]} \frac{f_{\text{H}^+} f_{\text{SO}_4^{2-}}}{f_{\text{HSO}_4^-}} \quad (5a)$$

where the activity coefficients of H⁺ and HSO₄⁻ in (5a) were assumed to be equal and the sulfate ion activity coefficient was calculated by

$$\log f_{\text{SO}_4^{2-}} = -4AI' \quad (6)$$

where A is the theoretical Debye-Hückel limiting slope for a 1-1 electrolyte. The thermodynamic ionization constant, K_2° , was obtained by extrapolation to zero ionic strength of $\log K_2$ vs. I .

These determined values for the second ionization constant of sulfuric acid at temperatures to 300°, based on molar concentrations, are given in Table I. The standard errors associated with the $\log K_2^\circ$ values in this table are on the order of 0.03 unit in $\log K_2$, except for the values at 300° at densities of 0.80 and 0.85 g. cm.⁻³ where the standard errors are 0.2 and 0.1 unit, respectively. The same value of $-\log K_2^\circ$ at 100° and saturation pressure was obtained by combining the present results (three concentrations) with those reported earlier by Noyes²⁵ (nine concentrations, 0.00010 to 0.050 m).

Lietzke, Stoughton, and Young²⁶ have calculated K_2° from 25 to 225° at saturation vapor pressure from measurements on the solubility of Ag₂SO₄ in dilute sulfuric acid solutions. Their values for $-\log K_2^\circ$ (molal concentrations) are 3.01 and 4.49 at 100 and 200°, respectively. Our present molal ionization constants, converted to molal units, give $-\log K_2^\circ(m)$

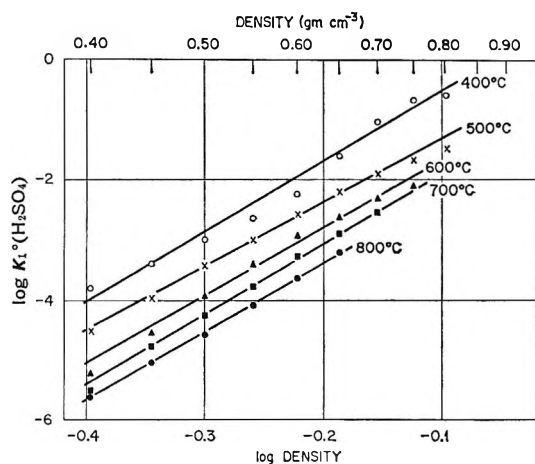
(24) E. C. Righellato and C. W. Davies, *Trans. Faraday Soc.*, **26**, 592 (1930).

(25) A. A. Noyes, *et al.*, "The Electrical Conductivity of Aqueous Solutions," Publication No. 33, Carnegie Institution of Washington, Washington, D. C., 1907.

(26) M. H. Lietzke, R. W. Stoughton, and T. F. Young, *J. Phys. Chem.*, **65**, 2247 (1961).

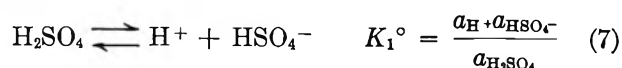
Table VI: Negative Logarithm of the First Ionization Constant of H_2SO_4 , $-\log K_1^\circ$; Standard State Is the Hypothetical 1 M Solution

Temp., °C.	Density, g. cm. ⁻³									
	0.40	0.45	0.50	0.55	0.60	0.65	0.70	0.75	0.80	0.85
400	3.90	3.40	3.00	2.65	2.24	1.61	1.32	0.66	0.37	...
450	4.18	3.67	3.19	2.79	2.39	1.99	1.58	1.28	1.04	0.64
500	4.52	3.99	3.43	3.01	2.58	2.20	1.89	1.66	1.46	1.24
550	4.90	4.25	3.67	3.23	2.76	2.42	2.12	1.90	1.75	1.56
600	5.24	4.53	3.91	3.42	2.94	2.62	2.30	2.08	1.99	...
650	5.39	4.67	4.10	3.60	3.10	2.76	2.43	2.26
700	5.53	4.80	4.29	3.79	3.27	2.92	2.52	2.40
750	5.58	4.90	4.43	3.99	3.46	3.05
800	5.62	5.05	4.61	4.10	3.66	3.22

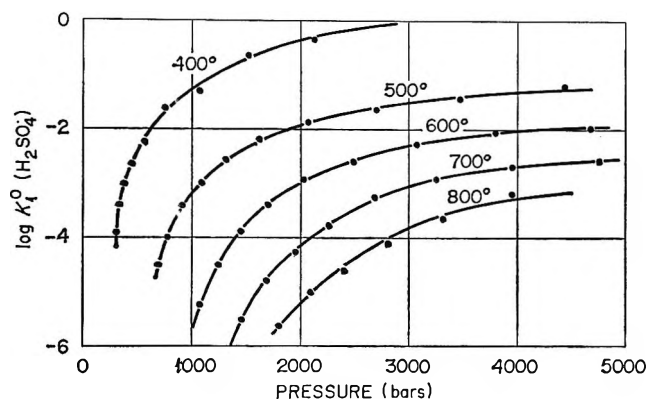
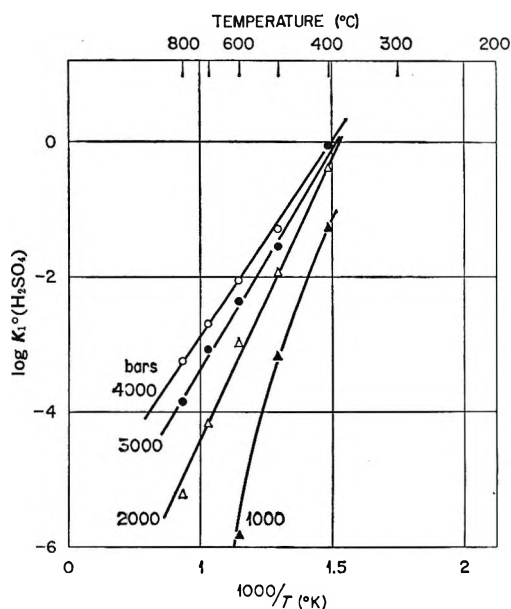
**Figure 12.** $\log K_1^\circ(H_2SO_4)$ vs. \log density at temperatures from 400 to 800°.

at 100 and 200° of 3.08 and 4.03, respectively, which is in good agreement with the results of Lietzke, *et al.*²⁶

First Ionization Constant of H_2SO_4 . The Shedlovsky method is frequently used to calculate ionization constants for weak uni-univalent electrolytes from experimental conductance data. In its usual application, limiting equivalent conductances are calculated simultaneously with the ionization constants. As mentioned in a preceding paragraph, the limiting equivalent conductances of H_2SO_4 obtained by the Shedlovsky method are apparently much too low at high temperatures and low densities. We have used the limiting equivalent conductances in Table V along with the Shedlovsky method to obtain the first ionization constant for H_2SO_4 from 400 to 800°. These values are given in Table VI and are for the equilibrium

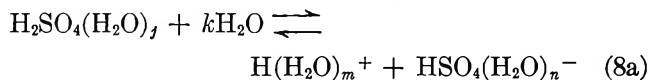


The standard error in the values of $\log K_1^\circ$ as deter-

**Figure 13.** Isothermal variation of $\log K_1^\circ(H_2SO_4)$ with pressure at temperatures from 400 to 800°.**Figure 14.** $\log K_1^\circ(H_2SO_4)$ vs. $1/T$ at several pressures.

mined by this method is approximately 0.02–0.04 unit.

By following the procedure that Franck used in his treatment of the ionization constants of KCl in supercritical aqueous fluids, eq. 7 may be rewritten to include waters of hydration.



$$K_1' = \frac{a_{\text{H}(\text{H}_2\text{O})_m^+} a_{\text{HSO}_4(\text{H}_2\text{O})_n^-}}{a_{\text{H}_2\text{SO}_4(\text{H}_2\text{O})_j} a_{\text{H}_2\text{O}}^k} = \frac{K_1^\circ}{a_{\text{H}_2\text{O}}^k} \quad (8b)$$

$$\log K_1' = \log K_1^\circ - k \log a_{\text{H}_2\text{O}} \quad (9a)$$

Since the activity of a molecular or ionic species is proportional to its concentration, and since the concentration of water is proportional to its density ($C_{\text{H}_2\text{O}} = 55.55 \times d$), eq. 9a may be rewritten

$$\log K_1^\circ = \log K_1' + k \log 5.55 + k \log d \quad (9b)$$

According to eq. 9b if $\log K_1^\circ$ is plotted against density, a straight line would be obtained, with intercept $\log K_1' + k \log 5.55$ and slope k . Figure 12 contains plots

of this type for temperatures of 400 to 800° over the density range 0.4–0.8 g. cm.⁻³. The average slope of the lines in Figure 12 is 11.3 ± 0.2 . If the lines in Figure 12 are extrapolated to density = 1.0 g. cm.⁻³, and if these values for $\log K_1^\circ$ at $d = 1.0$ g. cm.⁻³ are plotted against $1/T$ (for 400–800°) and an extrapolation is made to 25°, the extrapolated value for K_1° at 25°, 1.0 g. cm.⁻³ is 10^5 .

$\log K_1^\circ(\text{H}_2\text{SO}_4)$ was plotted *vs.* pressure at temperatures from 400 to 800° (Figure 13). Interpolations were made to pressures of 1000, 2000, 3000, and 4000 bars. The values for $\log K_1^\circ$ at these pressures were then plotted against $1/T$ as shown in Figure 14. ΔH° for the ionization process was calculated from the average slopes of the lines and was found to be -63, -39, -30, and -27 kcal./mole at pressures of 1000, 2000, 3000, and 4000 bars, respectively.

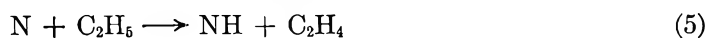
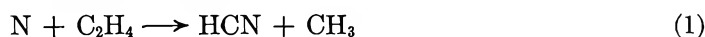
Acknowledgments. The authors wish to thank Ronald White (summer participant, 1963) for writing the initial versions of the computer programs.

Mass Spectrometric Study of the Reaction of Nitrogen Atoms with Ethylene

by John T. Herron

Physical Chemistry Division, Mass Spectrometry Section, National Bureau of Standards, Washington, D. C. 20234 (Received March 10, 1965)

The reaction of nitrogen atoms with ethylene has been studied using a mass spectrometer to follow the partial pressures of reactants and products. From the experimental results the initial steps in the reaction are postulated to be

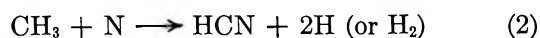


Addition of H atoms greatly increases the yield of HCN and effectively removes the discrepancy between the nitric oxide and the ethylene titration techniques for the measurement of nitrogen atom concentrations. An upper limit to the rate of reaction 1 at 320°K. is found to be $k_1 \leq 7 \times 10^9 \text{ cm}^3 \text{ mole}^{-1} \text{ sec.}^{-1}$.

Introduction

Because of its rapidity and apparent simplicity, the reaction of ethylene with active nitrogen has been extensively used as a means of measuring the nitrogen atom concentration.¹ Since about 95% of the nitrogen in the condensable products is in the form of hydrogen cyanide,² the amount of hydrogen cyanide recovered under conditions of complete consumption of nitrogen atoms is taken to be equivalent to the quantity of nitrogen atoms originally present.

The generally accepted mechanism of the reaction is



However, as was pointed out in an earlier mass spectrometric study of the reaction, the ratio of nitrogen atoms consumed to ethylene consumed is much too large to be accounted for by this simple mechanism.³

In view of these earlier results this reaction has been reinvestigated in considerably greater detail in order to define unambiguously the stoichiometry of the reaction and hence to understand better the mechanism.

Experimental

The apparatus and general procedure have been described previously.⁴ In brief, prepurified grade nitrogen gas, partially dissociated into atoms by means of a 245C-Mc./sec. electrodeless discharge, was flowed into a 24.5-mm. i.d. tubular reactor. A second reactant could be added through a movable central inlet tube which could be located between 1 and 15 cm. from the sampling orifice of a mass spectrometer. Total pressure was varied from about 1 to 3 torr.⁵

The partial pressures of stable reactants and products were followed using an ionizing energy of 44 e.v. while the relative partial pressures of nitrogen and hydrogen atoms were followed using an ionizing energy of 24 e.v.

(1) Extensive references are given by H. G. V. Evans, G. R. Freeman, and C. A. Winkler [*Can. J. Chem.*, **34**, 1271 (1956)] and by A. N. Wright, R. L. Nelson, and C. A. Winkler [*ibid.*, **40**, 1082 (1962)].

(2) Since these reactions are carried out in a great excess of N₂, any N₂ produced in the reaction is undetectable.

(3) J. T. Herron, *J. Chem. Phys.*, **33**, 1275 (1960).

(4) F. S. Klein and J. T. Herron, *ibid.*, **41**, 1285 (1964).

(5) A torr is defined as 1/760 of a standard atmosphere.

The relative nitrogen atom partial pressure was put on an absolute basis by means of the nitric oxide titration technique.⁶ Although this titration technique has been subject to criticism,⁷ the recent e.s.r. measurements of Westenberg and deHaas⁸ and the present work (see below) would seem to settle the question in its favor.

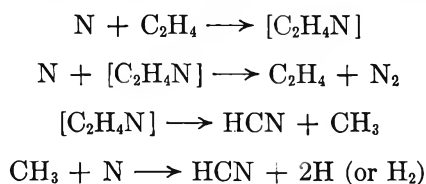
No attempt has been made to put the hydrogen atom partial pressure on an absolute basis. Instead, it has been assumed that hydrogen and nitrogen atoms have the same mass spectrometric sensitivity. Thus the partial pressures of hydrogen atoms given below could be in error by a factor of 2 or more.

Results and Discussion

Figure 1 shows the variation in partial pressure of reactants and products at a fixed reaction time as a function of the initial ethylene partial pressure. The limiting yield of hydrogen cyanide is seen to be considerably less than the initial nitrogen atom partial pressure. Of greater interest is the fact that the ratio of nitrogen atoms consumed to hydrogen cyanide produced is a function of the initial ethylene partial pressure. This is shown in Figure 5 (curve A).

The simple mechanism, consisting of reactions 1 and 2, is inadequate to explain these observations.

In the earlier mass spectrometric study of the reaction, the following mechanism was employed⁹



This mechanism predicts that the ratio of nitrogen atoms consumed to hydrogen cyanide produced should be a function of the initial atom concentration. However, Verbeke and Winkler⁷ measured the ratio of nitric oxide consumed in the nitric oxide reaction to hydrogen cyanide produced in the ethylene reaction over about a tenfold range in initial atom concentration, and found the ratio to be constant. Assuming that the nitric oxide consumed is a measure of the nitrogen atom concentration, their results would rule out the above mechanism.

These observations have been confirmed in the present work. Figure 2 gives the ratio $\Delta\text{N}/\text{HCN}$ as a function of time for two different initial nitrogen atom partial pressures. The curves are seen to be identical within experimental uncertainty.

Since nitrogen atom abstraction reactions from either ethylene or methyl radicals are not energetically feasible, a mechanism involving hydrogen atoms offers

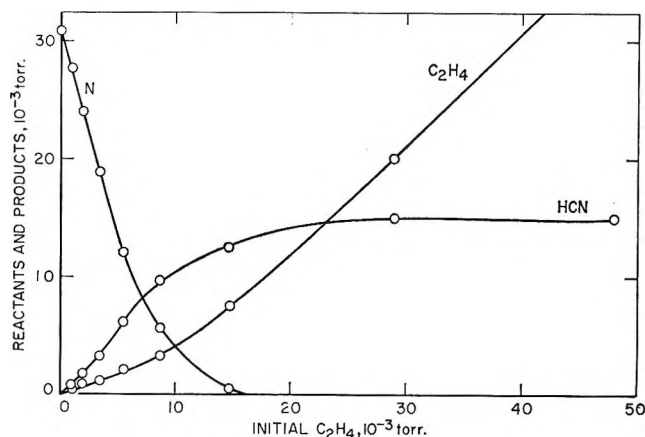


Figure 1. Partial pressure of reactants and products as a function of initial ethylene partial pressure: total pressure, 2.0 torr; reaction time, 0.05 sec.

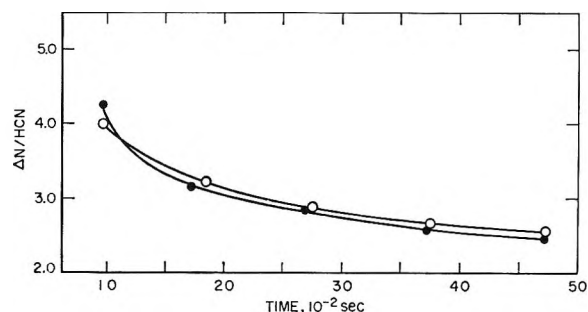


Figure 2. Ratio of nitrogen atoms consumed to hydrogen cyanide produced as a function of time for two different initial nitrogen atom partial pressures and the same initial ethylene partial pressure: open circles, $(\text{N})_0 = 42.4 \times 10^{-3}$ torr; shaded circles, $(\text{N})_0 = 22.3 \times 10^{-3}$ torr; $(\text{C}_2\text{H}_4)_0 = 10.7 \times 10^{-3}$ torr; total pressure, 2.6 torr.

an alternative explanation for the experimental observations. That hydrogen atoms are present at a sufficiently high partial pressure to play some part in the reaction can be seen from Figure 3.

To account for these observations, the following reaction mechanism is proposed

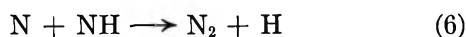
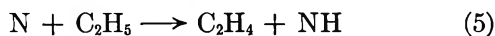


(6) G. B. Kistiakowsky and G. G. Volpi, *J. Chem. Phys.*, **27**, 1141 (1957).

(7) G. J. Verbeke and C. A. Winkler, *J. Phys. Chem.*, **64**, 319 (1960).

(8) A. A. Westenberg and N. deHaas, *J. Chem. Phys.*, **40**, 3037 (1964).

(9) This type of mechanism has been discussed by W. Forst, H. G. Evans, and C. A. Winkler, *J. Phys. Chem.*, **61**, 320 (1957).



followed by the usual atom- and radical-recombination reactions. This list of reactions is not meant to be inclusive. It does not account for the formation of nitrogen-containing products other than hydrogen cyanide or molecular nitrogen, and it takes no account of radical-disproportionation reactions, or of radical-addition reactions to ethylene.¹⁰

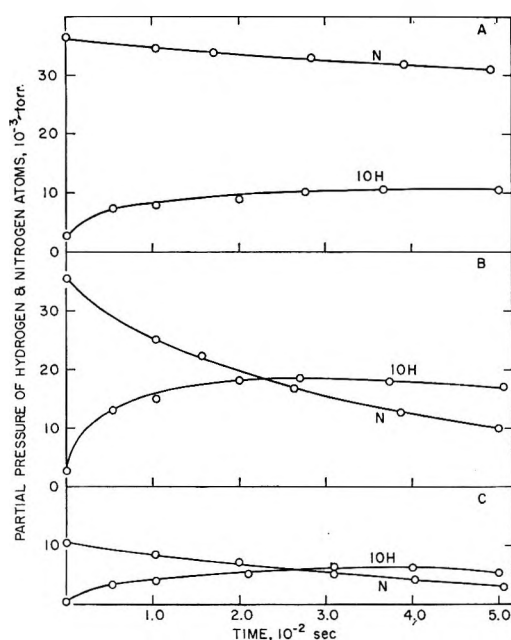


Figure 3. Hydrogen and nitrogen atom partial pressure as a function of time at $(\text{C}_2\text{H}_4)_0/(\text{N})_0$ ratios of: A, 0.066; B, 0.32; and C, 1.0. The data in curve C were taken with a liquid nitrogen cooled trap on the low-pressure nitrogen line ahead of the discharge zone.

The most important feature of the mechanism is the competition between hydrogen and nitrogen atoms for ethyl radicals in steps 4 and 5, respectively. This competition roughly determines whether the nitrogen atom will be detected as hydrogen cyanide (reaction 4 followed by 2) or remain undetected as molecular nitrogen (reaction 5 followed by 6). An increase in the hydrogen atom partial pressure would favor reaction 4 relative to reaction 5 and hence bring about a decrease in the $\Delta\text{N}/\text{HCN}$ ratio.

To introduce hydrogen atoms into the reactor, molecular hydrogen was added to the incoming nitrogen gas ahead of the discharge zone. The molecular hydrogen was partially dissociated into hydrogen atoms,

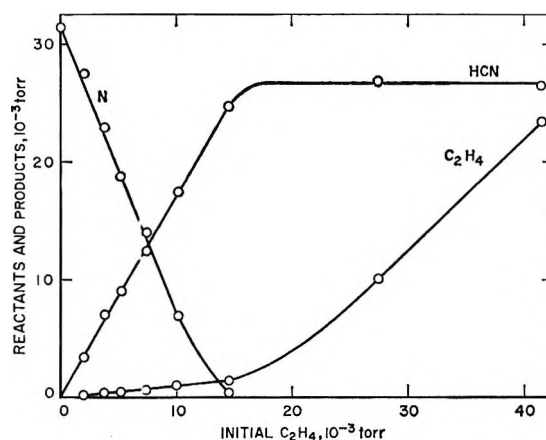


Figure 4. Partial pressure of reactants and products as a function of initial ethylene partial pressure: 2% hydrogen added to the incoming nitrogen gas; total pressure, 2.0 torr; reaction time, 0.05 sec.

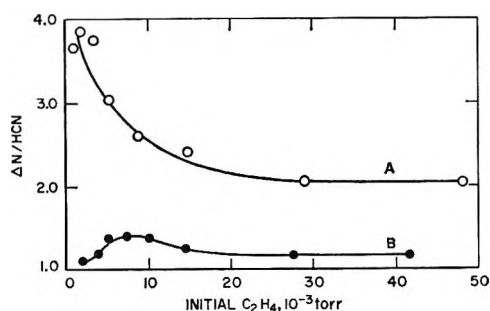


Figure 5. Ratio of nitrogen atoms consumed to hydrogen cyanide produced as a function of the initial ethylene partial pressure; curve A from the data of Figure 1 and curve B from the data of Figure 4.

which entered the reactor along with the nitrogen atoms. The effect of adding about 2% molecular hydrogen is shown in Figure 4. Under these conditions the ratio $\Delta\text{N}/\text{HCN}$, shown as curve B in Figure 5 approaches unity.^{11,12}

These data indicate that the argument as to whether the nitrogen atom concentration is correctly deter-

(10) The reaction of nitrogen atoms with molecular hydrogen or with hydrogen cyanide is immeasurably slow under the conditions of these experiments. The same is true for the reaction of hydrogen atoms with hydrogen cyanide. In studying the reaction of nitrogen atoms with ethylene-*d*₄, a peak was observed in the mass spectrum at m/e 44 which might be due to CD_3CN . Its intensity was about 5% of that of hydrogen cyanide.

(11) Ideally, this experiment should be carried out by premixing ethylene with partially dissociated hydrogen and in turn reacting this with active nitrogen. This would eliminate any question as to whether or not NH compounds, formed when a mixture of N_2 and H_2 are passed through a discharge, play any part in the reaction.

(12) When C_2D_4 was reacted under these conditions, some $\text{C}_2\text{D}_3\text{H}$ was formed. This would appear to confirm the occurrence of reaction 5. However, the possibility of $\text{C}_2\text{D}_3\text{H}$ being formed by means of an exchange reaction cannot be ruled out.

mined by the maximum amount of nitric oxide consumed in the $N + NO$ reaction, or the maximum amount of hydrogen cyanide produced in the $N + C_2H_4$ reaction is based on an erroneous assumption as to the mechanism of the ethylene reaction. The addition of hydrogen atoms brings the two methods into substantial agreement.¹³

As can be seen from Figure 3 there is a residual hydrogen atom partial pressure at zero ethylene flow due to impurities in the nitrogen. If the nitrogen is further purified by trapping out condensable impurities before passing the gas through the discharge, the hydrogen atom partial pressure is reduced almost to zero (curve C of Figure 3). At the same time, however, the nitrogen atom partial pressure drops to about one-third of its original value. The reasons for the latter phenomenon is somewhat uncertain^{14,15} and need not concern us here. The significant point is that the addition of ethylene to purified active nitrogen leads to the same marked increase in the hydrogen atom partial pressure as in the case of the untreated active nitrogen (Figure 3). Thus, there is no reason to expect that the over-all mechanism differs in the two cases.

The Rate of the Reaction

The question as to the rate of reaction 1 is dependent on our knowledge of the over-all mechanism. Since previously reported values for k_1 are based on the assumption that reactions 1 and 2 adequately describe the over-all reaction, it must be concluded that these values are incorrect.

If the mechanism given in the previous section is correct, then k_1 can only be obtained by first making some simplifying assumptions. These are that at low initial ethylene partial pressures, the mechanism can be represented by eq. 1-6, and that a steady-state treatment in terms of C_2H_5 is valid under these conditions. The latter assumption appears to be justified since the partial pressure of C_2H_5 , as indicated by measurements made at reduced electron energies, was vanishingly small.

Solution of the relevant equations leads to the expression

$$k_1 = \frac{2.303 \log (C_2H_4)_0 / (C_2H_4)_t}{\int_0^t (N) dt} - \frac{\int_0^t \frac{k_3 k_4 (H)^2}{k_4 (H) + k_5 (N)} dt}{\int_0^t (N) dt}$$

where the subscripts refer to zero time and time t .

The first term in this expression can be readily found. The numerator is the ratio of the partial pressure of ethylene at time zero to the partial pressure of ethylene at time t . The integral in the denominator is graphically evaluated from measurement of the nitrogen atom partial pressure as a function of time. The second term cannot be readily evaluated. However, it is observed that the first term becomes smaller as the ratio $(C_2H_4)_0 / (N)_0$ is reduced. A plot of the first term, designated as k_1' , vs. $(C_2H_4)_0 / (N)_0$ is shown in Figure 6. Extrapolation of these data to $(C_2H_4)_0 / (N)_0 = 0$ gives a value of k_1' which can be identified with k_1 on the assumption that, as $(C_2H_4)_0 / (N)_0$ approaches zero, the second term becomes negligible with respect to the first.

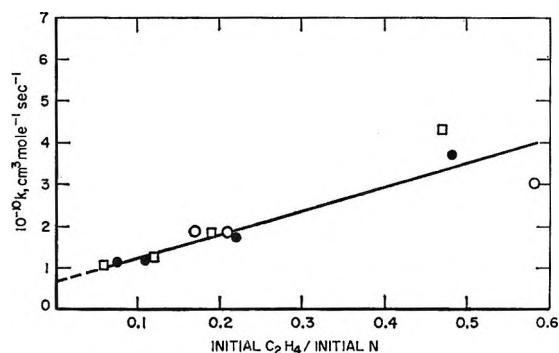


Figure 6. Apparent rate constant of reaction 1 as a function of the ratio of initial ethylene partial pressure to initial nitrogen atom partial pressure: total pressure O, 0.82 torr; ●, 1.63 torr; □, 2.47 torr.

Since normally there is a residual hydrogen atom flow at zero ethylene flow, the second term is never zero, and k_1 is only an upper limit. The value so obtained at 320°K. is $k_1 \leq 7 \times 10^{10} \text{ cm.}^3 \text{ mole}^{-1} \text{ sec.}^{-1}$.

Some previously reported values for k_1 are: k_1 (470-600°K.) = $5.8 \times 10^{10} \text{ cm.}^3 \text{ mole}^{-1} \text{ sec.}^{-1}$,³ k_1 (310°K.) = $9.6 \times 10^{10} \text{ cm.}^3 \text{ mole}^{-1} \text{ sec.}^{-1}$,¹⁶ and k_1 (295°K.) = $1.0 \times 10^{10} \text{ cm.}^3 \text{ mole}^{-1} \text{ sec.}^{-1}$.¹⁷ The range of values is not unexpected in view of the different experimental techniques used and the different reaction mechanisms assumed.

(13) It should be emphasized that these observations on the effect of added hydrogen on the $\Delta N / HCN$ ratio do not involve the nitric oxide titration reaction. The latter was used solely to relate the measured ion current to partial pressure and was carried out only in pure nitrogen.

(14) R. A. Young, R. L. Sharpless, and R. Stringham, *J. Chem. Phys.*, **40**, 117 (1964).

(15) J. T. Herron, *J. Res. Natl. Bur. Std.*, **A69**, 287 (1965).

(16) E. R. V. Milton and H. B. Dunford, *J. Chem. Phys.*, **34**, 51 (1961).

(17) E. M. Levy and C. A. Winkler, *Can. J. Chem.*, **40**, 686 (1962).

The activation energy for reaction 1 has been reported to be less than about 1 kcal./mole.^{3,17} However, in view of the chain mechanism postulated above, it is

possible that it could be greater since reaction 1 could be masked by the much faster atomic hydrogen reaction.

Effect of Adsorbed Polyelectrolytes on the Polarographic Currents. I

by I. R. Miller

Polymer Department, Weizmann Institute of Science, Rehovoth, Israel (Received March 10, 1965)

The diffusion current of an ionic depolarizer through an adsorbed polyelectrolyte layer of equal charge has been calculated. It was assumed that the diffusion coefficient of the depolarizer is considerably smaller in the surface layer than in the solution and that its distribution coefficient between the layer and the aqueous phase is given by the Donnan equilibrium. The experimentally established square root time dependence up to saturation level of the polyelectrolyte surface coverage was applied. Two extreme cases were considered, lateral interaction and no lateral interaction at partly covered surfaces. In the first case, the instantaneous current was assumed to be proportional to the surface coverage. In the second case, the distribution coefficient of the depolarizer and its diffusion coefficient in the surface layer were considered to be linearly dependent on the surface occupancy of the polyelectrolyte. The theory was checked with respect to experimental data obtained on positively charged polyvinylpyridine with Cd^{2+} as depolarizer.

Introduction

The effect of surface-active agents on reversible diffusion currents has not been treated quantitatively although it has been studied experimentally by several authors.¹⁻⁴ There were, however, attempts to elucidate quantitatively the influence of surface-active substances on the electrode reactions and thus on the irreversible polarographic currents. Weber, Koutecky, and Koryta⁵ assumed the over-all rate constant k_{eff} to be linearly dependent on the coverage; Kuta and Weber⁶ further took into account the variation in potential by the adsorbed surface-active substance, which they assumed to be proportional to the coverage. They obtained for the instantaneous current i_a at any mercury drop age t the expression

$$i_a = nFqt^{2/3}C^0 [{}_0k_e(1 - \theta) + {}_1k_e\theta] \times \exp(-z/\alpha n - 1)(\alpha nF/RT)\Delta\psi\theta \quad (1)$$

In this case, ${}_0k_e$ and ${}_1k_e$ are the rate constants for the free and covered surface, respectively, n is the number of electrons involved in the reaction, F is Faradays, q is a constant depending on the flow velocity of mercury, z is the charge of the depolarizer, α is the transfer coefficient, and $\Delta\psi$ is the potential difference between the completely covered and the uncovered surfaces.

The purposes of the present work is to elucidate the effect of adsorbed charged polyelectrolytes which partly or fully cover the surface on the diffusion current.

- (1) P. Delahay and I. Trachtenberg, *J. Am. Chem. Soc.*, **80**, 2094 (1958).
- (2) C. Tanford, *ibid.*, **74**, 211 (1952).
- (3) J. Kuta and I. Smoler, *Z. Elektrochem.*, **64**, 285 (1960).
- (4) C. N. Reilly and W. Stumm, *Progr. Polaro.*, **1**, 81 (1962).
- (5) J. Weber, J. Koutecky, and J. Koryta, *Z. Elektrochem.*, **63**, 583 (1959).
- (6) J. Kuta and J. Weber, *Electrochim. Acta*, **9**, 541 (1964).

It is assumed that the current is determined by diffusion of the depolarizer through the aqueous phase and an adsorbed polyelectrolyte layer of finite thickness.

Theoretical

a. *The Model.* We wish to calculate the instantaneous diffusion current when the depolarizer diffuses to the surface from a concentration C^0 in the aqueous solution (phase I), through a surface layer (phase II) of thickness ξ , its concentration at the surface being maintained at zero. κ is the distribution coefficient of the depolarizer between phase I and phase II. The diffusion coefficient in phase II (D_{II}) differs from that in phase I (D_I). κ and D_{II} may depend on the occupancy θ of surface phase II, which is assumed to be equal to $(t/\vartheta)^{1/2}$, where ϑ is the time required for full surface coverage to be reached. This assumption has been shown to be correct for polyelectrolytes of any composition.⁸⁻¹⁰

In our treatment we shall consider two alternatives, the first consisting of the case in which there is no lateral interaction between the adsorbed polyelectrolyte molecules, which move freely in the surface. In this case D_{II} and κ for any depolarizer entering the surface layer will depend on its chances to hit upon a bare spot or upon an adsorbed polymer molecule. Hence, D_{II} and κ are assumed to be linearly proportional to the surface occupancy by polyelectrolyte molecules θ , that is, to $(t/\vartheta)^{1/2}$.

$$D_{II} = D_I + (D_{sat} - D_I)(t/\vartheta)^{1/2} \quad (2)$$

$$\kappa = 1 + (\kappa_{sat} - 1)(t/\vartheta)^{1/2} \quad (3)$$

D_{sat} and κ_{sat} are the diffusion and distribution coefficient for a fully covered surface; for $t > \vartheta$, $D_{II} = D_{sat}$ and $\kappa = \kappa_{sat}$.

Alternatively, we consider the case in which there is a strong lateral interaction and immediate dimensional phase separation into patches of fully covered and only sparsely occupied surface. In this case the diffusion current is assumed to be a linear function of the surface coverage

$$i_t = i_{o,t} - (i_{o,t} - i_{s,t})(t/\vartheta)^{1/2} \quad (4)$$

In this expression $i_{o,t}$ and $i_{s,t}$ are the currents at time t when the surface is uncovered and when it is fully covered, respectively.

b. *Solution of the Diffusion Equation.* The differential equations in the two phases

$$\frac{\partial C_I}{\partial t} = D_I \frac{\partial^2 C_I}{\partial X^2}$$

and

$$\frac{\partial C_{II}}{\partial t} = D_{II} \frac{\partial^2 C_{II}}{\partial X^2} \quad (5)$$

give, for the initial conditions, at $X = 0$, $C = 0$ for $t \geq 0$, and at $X > 0$, $C = C^0$ for $t = 0$, the following solutions

$$C_I = C^0 - B_I[1 - \text{erf}(X/2\sqrt{D_I t})] \text{ for } \xi < X < \infty \quad (6)$$

$$C_{II} = B_{II} \text{erf}(X/2\sqrt{D_{II} t}) \text{ for } 0 < X < \xi \quad (7)$$

The constants B_I and B_{II} are obtained from the boundary conditions: the number of depolarizer molecules N crossing both sides of the boundary between I and II (at $\xi + 0$ and at $\xi - 0$) in unit time is equal.

$$(\partial N/\partial t)_{X=\xi+0} = (\partial N/\partial t)_{X=\xi-0} \quad (8)$$

or

$$D_I(\partial C_I/\partial X)_{X=\xi} = D_{II}(\partial C_{II}/\partial X)_{X=\xi}$$

and

$$(C_{II})_{\xi} = \kappa(C_I)_{\xi} \quad (9)$$

For simplicity, we consider only the practical case where $\xi \ll (D_I t)^{1/2}$, namely, the adsorbed polyelectrolyte layer is thinner by many orders of magnitude than the diffusion layer.

We obtain for the constants B_I and B_{II}

$$B_I = C^0/[1 + (\xi/\kappa D_{II})(D_I/\pi t)^{1/2}] = C^0/\delta \quad (10)$$

where

$$\delta = 1 + (\xi/\kappa D_{II})(D_I/\pi t)^{1/2}$$

and

$$B_{II} = B_I(D_I/D_{II})^{1/2} \quad (11)$$

For the instantaneous diffusion current we obtain

$$i_t = nFA_t D_{II}(\partial C_{II}/\partial X)_{X=0} = nFm^{2/3} D_I^{1/2} t^{1/6} \pi^{-1/2} B_I \quad (12)$$

Introducing the numerical values together with the Ilkovic¹¹ correction factor

$$i_t = 7.08 \times 10^4 n m^{2/3} t^{1/6} D_I^{1/2} C^0/\delta = i_{o,t}/\delta \quad (13)$$

where m is the rate of flow of mercury in grams per second and A_t is the area of the mercury drop at time t .

(7) J. Koryta, *Collection Czech. Chem. Commun.*, **18**, 206 (1953).

(8) I. R. Miller and D. C. Grahame, *J. Colloid Sci.*, **16**, 23 (1961).

(9) I. R. Miller, *Trans. Faraday Soc.*, **57**, 301 (1961).

(10) I. R. Miller, *J. Mol. Biol.*, **3**, 229 (1961).

(11) D. Ilkovic, *Collection Czech. Chem. Commun.*, **6**, 498 (1934).

Comparison with Experimental Results

Let us consider the two extreme cases of strong lateral interaction taking place and of zero lateral interaction. In the first case for the covered fraction of the surface $\kappa = \kappa_{\text{sat}}$, $D_{\text{II}} = D_{\text{sat}}$, and the instantaneous diffusion current, according to eq. 4 and 13, is given by

$$i_t = i_{t,0} [1 - (1 - 1/\delta_a)(t/\vartheta)^{1/2}] \quad (14)$$

where

$$\delta_a = 1 + (\xi/\kappa_{\text{sat}}D_{\text{sat}})(D_{\text{I}}/\pi t)^{1/2}$$

In the second case D_{II} and κ are expressed by eq. 2 and 3, respectively. For obtaining the complete $i-t$ curves we must evaluate κ_{sat} and D_{sat} , namely, the distribution and diffusion coefficients for the fully covered surface.

The term κ_{sat} and D_{sat} include the steric as well as the electrostatic contribution. κ_{sat} can be expressed by means of the Donnan equilibrium. As the surface concentration of the polymer charges $\nu\Gamma_p/\xi$ is very high, the volume occupied by the polymer $\nu\Gamma_p v$ comprises a large fraction of the surface phase and therefore must be taken into consideration. In the presence of excess supporting electrolyte and taking into account the excluded volume in the surface phase, the Donnan equilibrium, $C_{\text{II}}^{\text{sat}}(C_s^o)^z = C_{\text{I}}(C_s)^z$, gives the following expression for κ_{sat}

$$\kappa_{\text{sat}} = C_{\text{II}}^{\text{sat}}/C_{\text{I}} = (C_s/\phi)^z ((\xi/\nu\Gamma_p) - v)^z \times (1 - (\nu\Gamma_p v/\xi)) \quad (15)$$

In this expression z is the valency of the depolarizer, Γ_p the polymer surface excess at saturation, ν the charge per polymer molecule, ϕ the osmotic factor^{12,13} of the counterions, v the volume per charged residue, and C_s the concentration of the supporting electrolyte. In eq. 15 the effective ion concentration in the surface phase was assumed to be

$$C_s = \phi\nu\Gamma_p/(\xi - \nu\Gamma_p v) \quad (16)$$

The osmotic factor ϕ is a function of the electrostatic potential. As $\nu\Gamma_p$ can be calculated^{6,7} from the polymer adsorption kinetics and v is readily obtainable, determination of κ_{sat} also gives the thickness of the polymer layer. In order to obtain κ_{sat} from the current-time curves, D_{sat} values obtained from independent diffusion experiments in thick polyelectrolytes or gels are required. We can, however, calculate $\xi/\kappa D_{\text{II}}$ from the curve section which represents the fully covered mercury surface. We can then reconstruct the $i-t$ curve section for the partly covered mercury drop either with

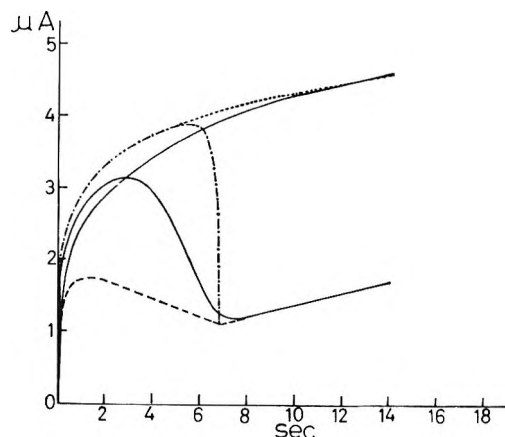


Figure 1. Measured and calculated $i-t$ curves of $0.001 N \text{ Cd}^{2+}$ in the presence of $0.001 N$ 2PVP and in the absence of polyelectrolyte. Supporting electrolyte: $0.05 N \text{ HNO}_3 + 0.15 N \text{ KNO}_3$. The fully drawn curves are measured, the broken lines are calculated: - - -, Cd^{2+} with supporting electrolyte only; according to the Ilkovic equation; — — —, in the presence of $0.001 N$ 2PVP for strong lateral interaction; according to eq. 13 and 14; - · - · -, in the presence of $0.001 N$ 2PVP without lateral interaction; according to eq. 2, 3, and 13.

the aid of eq. 2, 3, and 13 or of eq. 13 and 14. The reconstructed curves depend only slightly on the choice of κ_{sat} and D_{sat} , as long as they fit together into the $\xi/\kappa_{\text{sat}}D_{\text{sat}}$ obtained from experiment.

In Figure 1, we present the reconstructed as well as the measured $i-t$ curves of Cd^{2+} in the presence of $0.001 N$ poly-2-vinylpyridine and of $0.05 N \text{ HNO}_3 + 0.15 N \text{ KNO}_3$ as supporting electrolytes. It is evident from the figure that the experimental curve lies between those calculated for the two extreme cases. Almost no lateral interaction is indicated until about 40–50% surface coverage; with further increase in surface occupancy, lateral interaction and dimensional phase separation seem to become of growing importance.

Equation 15 indicates a strong dependence of κ_{sat} , and thus also of the diffusion current across the saturated polyelectrolyte layer, on the salt concentration. This expectation is experimentally verified,¹⁴ the current increasing with increases in concentration of the supporting electrolyte in accordance with eq. 13 and 15.

Acknowledgment. This study was supported by Research Grant GM-08519-03 from the National Institutes of Health, U. S. Public Health Service.

(12) Z. Alexandrowicz, *J. Polymer Sci.*, **56**, 1115 (1961).

(13) Z. Alexandrowicz and A. Katchalsky, *ibid.*, **A1**, 3231 (1963).

(14) Y. F. Frei and I. R. Miller, *J. Phys. Chem.*, in press.

The Vapor Pressure and Enthalpy of Arsenic Triiodide and Its

Absolute Entropy at 298°K.¹

by Daniel Cubicciotti and Harold Eding

Stanford Research Institute, Menlo Park, California 94025 (Received March 17, 1965)

The vapor pressure of liquid AsI_3 and the enthalpy of the solid and liquid above room temperature have been measured. Thermodynamic functions for the gas were calculated from molecular constant data. These data were combined to calculate the absolute entropy of the crystal at 298°K. and the thermal functions (entropies, enthalpies, and free energy functions) above 298°K. for the condensed and gas phases.

Introduction

The structure and fundamental vibration frequencies are known for the gaseous molecule AsI_3 ; therefore, the thermal functions (entropy, enthalpy, and free energy function) can be calculated for the substance in the standard gaseous state. By measuring the vapor pressure of the liquid, and thus the enthalpy of vaporization, we have obtained the absolute entropy of the liquid. Then by measuring the enthalpy above room temperature for the condensed phases we have been able to calculate the thermal functions for the condensed phases including the absolute entropy for the crystal at room temperature.

Vapor Pressures

The vapor pressure of liquid arsenic triiodide was measured in a fused-quartz cell by the Rodebush quasi-static method that we have used previously in this laboratory.² Arsenic triiodide was prepared from the elements. Some arsenic (99.99% from United Mineral & Chemical Corp., New York, N. Y.) was heated in an N_2 stream in a Pyrex bulb to distil off any oxide impurity, which is volatile and would interfere with the pressure measurements. A somewhat less than stoichiometric amount of iodine (Mallinckrodt, resublimed) contained in an auxiliary bulb was then opened to the arsenic bulb, and the system was sealed off. The bulbs were heated over a period of several days so that the iodine slowly distilled and reacted to form arsenic triiodide with an excess of arsenic. The system was then sealed onto the vapor pressure cell and the arsenic triiodide distilled under a

partial pressure of N_2 . The excess arsenic ensured reducing conditions so that no excess iodine was distilled over with the triiodide. A sample of the distillate was collected in a side arm for analysis. Volumetric determination³ by I_3^- indicated an arsenic content of 16.55%, compared with 16.44% theoretical for AsI_3 . A sample of the material left in the vapor pressure cell after the measurements was also analyzed and found to have the same percentage of As. During the course of the vapor pressure measurements, a small amount of iodine (less than 50 mg.) was observed in the cold leg of the apparatus. This was taken to indicate that there was a finite partial pressure of iodine, owing to decomposition of the sample. Since the arsenic triiodide sample was about 150 g., the small amount of decomposition was considered to have a negligible effect on the vapor pressure measurements. The temperature of the sample was measured with a Pt-10% Rh thermocouple checked against one calibrated by the National Bureau of Standards. The pressures were measured with a mercury manometer (12-mm. i.d.) and a cathetometer. The vapor pressures observed are given in Table I.

The vapor pressures are also shown in Figure 1. The highest pressures obtained by Horiba and Inouye⁴

(1) This work was made possible by support from the Research Division of the Atomic Energy Commission under Contract No. AT(04-3)-106.

(2) For a description see F. J. Keneshea and D. Cubicciotti, *J. Chem. Phys.*, **40**, 199 (1964).

(3) W. F. Hillebrand, G. E. F. Lundell, H. A. Bright, and J. I. Hoffman, "Applied Inorganic Analysis," 2nd Ed., John Wiley and Sons, Inc., New York, N. Y., 1953, p. 268.

Table I: Vapor Pressure Data over Liquid AsI₃

Temp., °C.	Press., mm.	Temp., °C.	Press., mm.
164.0	2.9	255.1	64.6
164.0	2.95	255.7	65.5
164.1	2.95	255.7	65.8
185.8	7.1	277.8	117.0
186.0	7.3	278.2	117.0
186.0	7.3	278.2	117.9
186.7	7.4	278.7	119.3
187.7	7.7	299.2	189.7
208.1	15.4	299.6	195.0
208.6	15.6	301.7	206.1
209.2	16.1	328.0	356.3
209.6	16.3	328.9	368.6
231.1	32.5	329.5	376.4
231.1	32.5		
231.1	32.6		
232.0	33.4		

are also shown in the figure. The pressures they reported fall in the neighborhood of our data and, so, may be said to agree. The present data were analyzed by a Σ -plot treatment.⁵ The heat capacity of the liquid (from the enthalpy data below) is 33.5, and that of the gas⁶ (as calculated from molecular constants) is 19.7 cal./mole deg. Thus with ΔC_p equal to -13.8 the equation for Σ becomes

$$-\Sigma = \log p(\text{mm.}) + 7.0 \log T(^{\circ}\text{K.})$$

The Σ -plot is also shown in Figure 1. The data were well represented by a straight line from which the vapor pressure equation was calculated to be

$$\log p(\text{mm.}) = \left[-\frac{4897}{T} - 7.0 \log T + 30.148 \right] \pm 2\% \quad (450 \text{ to } 600^{\circ}\text{K.})$$

The normal boiling point calculated from the equation is 370.7°. This value is somewhat lower than literature values⁴; however, no precise measurements seem to have been made. Based on the report by Dolique⁴ that the vapor density near the boiling point is within 2% of the theoretical value for the gaseous species AsI₃, we assume that the only important vapor species in the saturated vapor is the monomer AsI₃.

The enthalpy of vaporization as derived from the vapor pressure equation is

$$\Delta H_T = [22,400 - 13.8T] \pm 100 \text{ cal./mole} \quad (450 \text{ to } 600^{\circ}\text{K.})$$

At 500°K. the enthalpy of vaporization is 15,500 cal./

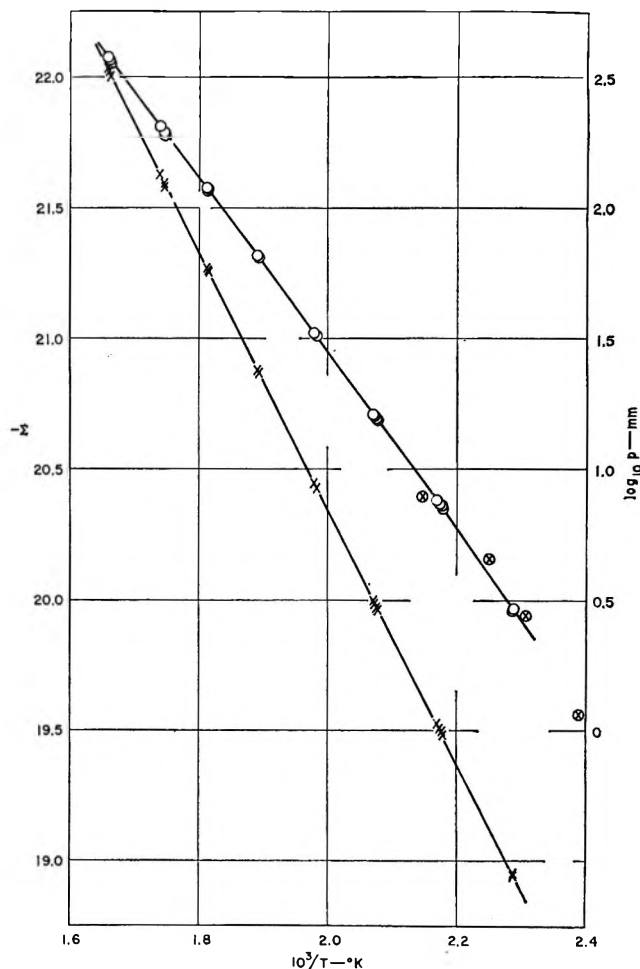


Figure 1. Vapor pressure of liquid AsI₃. Upper curve: measured vapor pressures; circled points are present data; circled crosses, those of Horiba and Inouye. Lower curve: Σ -plot of present data.

mole. From the vapor pressure equation $\log p(\text{mm.})$ is 1.461 and $\log p(\text{atm.})$ is -1.420 at 500°K.; hence, ΔF° is 3250 cal./mole. These give a value of 24.50 e.u. for the standard entropy of evaporation at 500°K. This result will be used below to obtain the absolute entropy of the condensed phases.

The enthalpy increments from 298 to 500°K. are 3.94 for the gas and 11.15 for the condensed phases. Combination of these values with the enthalpy of evaporation at 500°K. gives a value of 22.71 kcal./mole for the enthalpy of sublimation at 298°K.

(4) These data were reported by R. Dolique in "Nouveau Traité de Chimie Mineral," Vol. XI, P. Pascal, Ed., Masson and Co., Paris, 1958, p. 171.

(5) For a discussion, see K. S. Pitzer and L. Brewer, revision of "Thermodynamics," by G. N. Lewis and M. Randall, McGraw-Hill Book Co., Inc., New York, N. Y., 1961, p. 175.

(6) K. K. Kelley, U. S. Bureau of Mines Bulletin 584, U. S. Government Printing Office, Washington, D. C., 1960, p. 20.

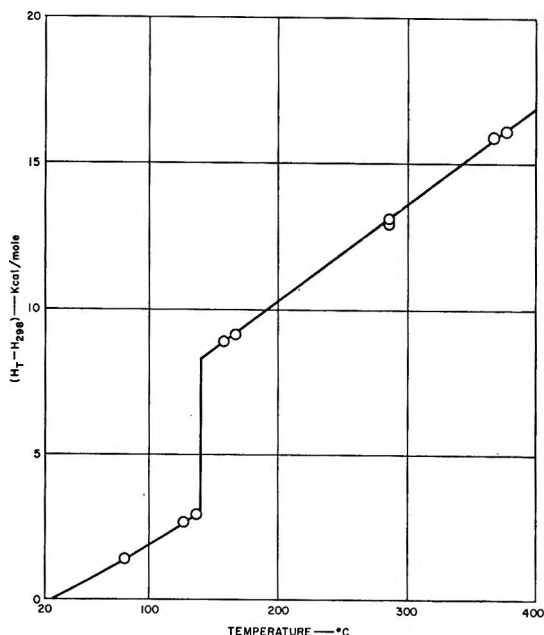


Figure 2. Enthalpy of solid and liquid AsI_3 above 298°K. Points are experimental data; curves are calculated from the derived enthalpy equations given in the text.

At the boiling point the enthalpy of vaporization is 13.51 kcal./mole, and the entropy of vaporization is 21.0 e.u. This entropy is quite close to that estimated by Brewer⁷ (21.5 e.u.) and is essentially the Trouton rule value for molecular liquids. There are no other literature values for comparison.

Thermodynamic Functions of Gas

The absolute entropy, free energy function, and enthalpy above room temperature for gaseous AsI_3 were calculated from molecular constant data.⁸ The molecular constants used were as follows. The fundamental vibration frequencies were those reported by Stammreich, *et al.*⁹ The gaseous molecule is pyramidal with the As-I distance¹⁰ of 2.54 Å. and the IAsI angle of 98.5°. The principal moments of inertia calculated from these data were 172×10^{-39} g. cm.² for the two equal ones and 320×10^{-39} for the third. The molecule has a symmetry number of 3. It was assumed that there was no contribution to the thermodynamic functions at these temperatures from excited electronic states because the lowest electronic state for the gaseous As^{+3} ion is about 76,000 cm.⁻¹ above ground.¹¹ The values calculated for the thermodynamic functions for the gas are given in Table II. The value of the gas constant used in these calculations was 1.987 cal./mole deg. The number of significant figures maintained for these functions is larger than the accuracy of the data warrants; however, it is convenient to

maintain them to obtain differences with temperature. The values are in agreement with those calculated by Kelley⁶ from similar molecular constant data.

Table II: Thermodynamic Functions for AsI_3 in the Standard Ideal Gas State^a

$T, ^\circ\text{K.}$	$H_T - H_{298}$, cal./mole	S_T , cal./(mole deg.)	$-\left(\frac{F_T - H_{298}}{T}\right)$, cal./(mole deg.)
298	0	108.67	108.67
400	1,970	114.43	109.49
500	3,940	118.73	110.85
600	5,910	122.37	112.52
700	7,880	125.34	114.08
800	9,860	128.08	115.75
900	11,840	130.27	117.11
1000	13,820	132.52	118.69

^a $H_{298} - H_0 = 4828$ cal./mole.

Enthalpies of Condensed Phases

A sample of about 20 g. was prepared by sealing stoichiometric amounts of arsenic and iodine into one bulb of a double-bulb Pyrex container and heating slowly until the arsenic and iodine reacted. The AsI_3 was then distilled into the second bulb and sealed off. Appropriate taring procedures allowed calculation of the weights of glass and contents in the bulb. The melting point of the sample was determined visually in an oil bath using a Pt-10% Rh thermocouple. It melted at $140.4 \pm 0.3^\circ$.

The enthalpy above room temperature was determined with a drop calorimeter, which consisted of a tube furnace mounted above a Parr adiabatic calorimeter. A hole was placed in the lid of the calorimeter, and the calorimeter bucket was replaced with a metal block containing two cavities. The samples dropped into one cavity. The other cavity contained a small amount of silicone oil in which the calorimetric thermometer oscillated and registered the temperature rise of the unit. A lid for the block closed automatically after the sample dropped into the tube. The calorimeter equivalent was determined using an

(7) L. Brewer in "The Chemistry and Metallurgy of Miscellaneous Materials," NNES Vol. IV-19B, L. L. Quill, Ed., McGraw-Hill Book Co., Inc., New York, N. Y., 1950, p. 206.

(8) See ref. 5, Chapter 27.

(9) H. Stammreich, R. Fornieris, and Y. Tavares, *J. Chem. Phys.*, 25, 580 (1956).

(10) L. E. Sutton, "Interatomic Distances and Configuration in Molecules and Ions," Special Publication No. 11, The Chemical Society, London, 1958.

(11) C. E. Moore, National Bureau of Standards Circular 467, U. S. Government Printing Office, Washington, D. C., Vol. II, 1952.

N.B.S. sample of sapphire (Al_2O_3) sealed in a platinum tube which approximately matched the arsenic triiodide sample in heat content. A blank tube was also used to correct for the small amount of radiation loss. The furnace temperature was determined with a chromel-alumel thermocouple calibrated at the melting point of zinc.

The enthalpy data obtained are given in Table III. The results can be represented by the following equations, from which the average deviation of the experimental points is slightly less than 1%

$$(H_T - H_{298}) \text{ solid, cal./mole} = 3.5T + 3.2 \times 10^{-2}T^2 - 3880$$

$$(H_T - H_{298}) \text{ liquid, cal./mole} = 33.5T - 5600$$

Table III: Experimental Values of Enthalpy Increments above 298°K. for Solid and Liquid AsI_3

Temp., °C.	Enthalpy above 298°K., cal./g.
81.6	3.02
81.6	3.02
127.3	5.85
137.0	6.42
151.8	19.52
166.8	19.95
285.3	28.34
285.5	28.78
366.3	34.87
377.0	35.38

These equations are represented graphically in Figure 2, which also shows the experimental points. From these equations the following derived quantities were obtained

$$C_p \text{ solid, cal./mole deg.} = 3.5 + 6.4 \times 10^{-2}T$$

$$C_p \text{ liquid, cal./mole deg.} = 33.5$$

$$\Delta H_{\text{fusion}}, \text{ kcal./mole} = 5.21$$

$$\Delta S_{\text{fusion}}, \text{ cal./mole deg.} = 12.6$$

From these results the enthalpies and entropies above room temperature for several temperatures were calculated. They are given in the second and third columns of Table IV.

Table IV: Thermodynamic Functions for Solid and Liquid AsI_3

$T, ^\circ\text{K.}$	$H_T - H_{298},$ cal./mole	$S_T - S_{298},$ cal./mole deg.)	$-\left(\frac{F_T - H_{298}}{T}\right),$ cal./mole deg.)
298	0	0	66.3
400	2,640	6.56	66.3
413.6(c)	3,035	8.54	67.4
413.6(l)	8,250	21.1	67.4
500	11,150	27.9	71.9
600	14,500	34.4	76.5
700	17,800	39.8	80.7
800	21,200	44.5	84.3
900	24,600	48.7	87.7
1000	27,900	52.5	90.9

Absolute Entropy and Free Energy Function of Condensed Phases

The absolute entropy of the solid at 298°K. can be calculated from the information presented above, and from that value and the enthalpies, the free energy function can be obtained. At 500°K. the standard entropy of vaporization was calculated (above) to be 24.50 e.u. The standard absolute entropy of the gas at 500°K. from Table II is 118.73 e.u., and the entropy increment for the condensed phases above 298°K. from Table IV is 27.9 e.u. Therefore, the absolute entropy of the solid at 298°K. is 66.3 ± 0.3 e.u. The uncertainty quoted is an over-all estimate of the reliability of the data.

From the absolute entropy of the crystal at 298°K. and the enthalpy data for the condensed phases, the free energy function for the condensed phases was calculated, and the data are presented in the last column of Table IV.

Acknowledgment. The vapor pressure measurements were performed by Mr. William E. Robbins.

On the Unification of the Thermal and Chain Theories of Explosion Limits

by B. F. Gray and C. H. Yang

Defense Research Corporation, Santa Barbara, California (Received March 17, 1966)

A theory of explosions is developed which contains, as special cases, both the thermal theory and the isothermal chain theory of Semenov. It contains qualitative features not present in either theory but under special circumstances reduces to each. Two illustrative applications are discussed in a general manner. Phase plane analysis, particularly suited to systems with only one important intermediate, is used.

I. Introduction

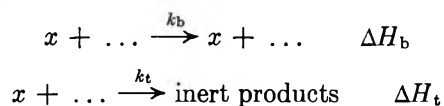
It is well established in the literature that two alternative mechanisms of explosion exist for gaseous systems. In the thermal theories the heat generated in the system by chemical reaction or other means is compared with the heat lost by the system to its surroundings by means of conduction or radiation in a closed system. The explosion limit is given by¹ $\mathcal{R}(T,P) = l(T,P,d)$, where T and P are the temperature and pressure in the gaseous system and d is a parameter connected with the physical size and shape of the system. \mathcal{R} is usually an Arrhenius-like function of temperature. This type of theory does not need detailed knowledge of chemical kinetics. It is *therefore* incapable of yielding any chemical kinetic data or explaining purely chemical effects such as sensitization, inhibition, etc.

On the other hand, the alternative type of theory, the isothermal chemical kinetic or branched-chain theory, originally devised by Semenov,² ignores the energy balance in the system. No account is taken of the fact that the chain branching and termination reactions are not isothermal and must, in fact, raise the temperature of the system above that of its surroundings, which in turn causes losses to the latter. In fact, if the heat produced exceeds the losses before branching exceeds termination, it is conceivable that a branched chain reaction may explode for purely thermal reasons. In the H_2-O_2 reaction it has been noted that the determination of the chain limit is complicated by the tendency of the gases to self-heating,³ thus causing thermal explosion. Purely isothermal theories in the form discussed by Semenov cannot account for the effect of added chain carriers on the explosion limits; *i.e.*, they predict that the explosion limit is inde-

pendent of the initial condition. In fact, the limits are very sensitive to the initial concentration of chain carriers. The present paper presents a unified treatment of the thermal and chain mechanisms of explosion by considering, simultaneously, the kinetic equation of the chain reaction and the energy conservation equation of the system. The explosion phenomenon is analyzed by studying the behavior of the solutions of these equations in the phase plane.

II. The Unified Mathematical Model

To illustrate a unified theory for both the thermal and the chain mechanisms, let us consider a simple reaction scheme with first-order chain branching and termination.



where x represents the concentration of the chain carrier and k_b and k_t are the rate constants for branching and termination, respectively. The initiation of the chain carrier is neglected as only the solutions with finite initial concentration of the chain carrier are considered. The kinetic equation, which completely characterizes the isothermal chain theory, is

$$\frac{dx}{dt} = (k_b - k_t)x \quad (1)$$

(1) C. H. Yang, *Combust. Flame*, **6**, 215 (1962).

(2) N. N. Semenov, "Chemical Kinetics and Chain Reactions," Pergamon Press, Ltd., Oxford, 1953.

(3) G. J. Minkoff and C. F. H. Tipper, "Chemistry of Combustion Reactions," Butterworth, 1962, p. 13.

whereas the energy conservation equation, which completely characterizes the thermal theory, is

$$\frac{dT}{dt} = \frac{x}{c}(k_b \Delta H_b + k_t \Delta H_t) - l \quad (2)$$

where $l(T - T_0)$ is the thermal loss term and c is an average specific heat for the system. We assume fixed pressure throughout this discussion and also spatial homogeneity of the system; *i.e.*, T and x are mean values across the reaction vessel. Now let us put $\Delta H_b/c = h_b$, etc., so we have to deal simultaneously with the two equations

$$\begin{aligned} \frac{dx}{dt} &= (k_b - k_t)x \\ \frac{dT}{dt} &= (k_b h_b + k_t h_t)x - l \end{aligned} \quad (3)$$

As neither of these equations contains the independent variable explicitly on the right-hand side, we can make use of the methods of the phase ($T - x$) plane⁴ in this case. (The present method is particularly suited to systems with only one important intermediate. If more than one has to be considered, the same type of analysis can be used with somewhat greater complication.) Clearly simultaneous integration of eq. 3 to give x and T as explicit functions of time is extremely difficult owing to the temperature dependence of the rate constants ($k \sim e^{-E/RT}$). Although numerical computation of the trajectory is possible when a proper set of initial values is given, these computations usually fail to give an over-all picture of the physical behavior. To study eq. 3 in the phase plane, the first step is to eliminate the independent variable

$$\frac{dT}{dx} = \frac{(k_b h_b + k_t h_t)x - l}{(k_b - k_t)x} \quad (4)$$

The next step is to find the singularities of this equation which are given by solving the simultaneous equations

$$\begin{aligned} x(k_b - k_t) &= 0 \\ x(k_b h_b + k_t h_t) - l &= 0 \end{aligned} \quad (5)$$

We denote the coordinates of the singular points by (x_s^j, T_s^j) , and in this case there are only two so $j = 1, 2$. The third step is to transform to new dependent variables

$$\begin{aligned} x' &= x - x_s^j \\ T' &= T - T_s^j \end{aligned} \quad (6)$$

to enable eq. 4 to be linearized in the neighborhood of each of the singular points. Having done this, we can

then apply the well-known stability theorems of Liapounov to determine the behavior of the integral curves in the ($T - x$) plane near the singularities and possibly the qualitative nature of the integral curves in the whole phase plane.

Retaining only linear terms, the transformed equation is easily shown to be

$$\begin{aligned} \frac{dT'}{dx'} &= \frac{x'R(T_s)^2(k_t h_t + k_b h_b) + T'(x_s k_b E_b h_b - \alpha)}{x'R(T_s)^2(k_b - k_t) + T'(x_s k_b E_b)} \\ &= \frac{Ax' + BT'}{Cx' + DT'} \end{aligned} \quad (7)$$

where $\alpha = RT_s^2(\partial l/\partial T)_{(T=T_s)}$. x_s and T_s are used here without subscript since we have not yet specified which singularity is involved. To derive this equation we have written $k_b = A_b e^{-E_b/RT}$ and $k_t = A_t$ where A_b and A_t are independent of temperature, and we have assumed the activation energy of the recombination reaction to be zero although, in actual practice, it will usually be a small negative number.

The nature of the singularity is found by examining the characteristic equation associated with (7), *i.e.*

$$\lambda^2 - (B + C)\lambda + BC - AD = 0 \quad (8)$$

the roots of which are

$$\lambda_{\pm} = 1/2(B + C) \pm 1/2\sqrt{(B - C)^2 + 4AD} \quad (9)$$

If λ_{\pm} are both real and differing in sign, that particular singularity is a saddle point. The condition for this is $AD > BC$, *i.e.*

$$(k_b h_b + k_t h_t)x_s k_b E_b > (k_b - k_t)(x_s k_b E_b h_b - \alpha) \quad (10)$$

Equation 10 can be rewritten as

$$(k_b h_b + k_t h_t) \left(\frac{\partial k_b}{\partial T} - \frac{\partial k_t}{\partial T} \right) x_s > \left(-\frac{\partial \mathcal{R}}{\partial T} + \frac{\partial l}{\partial T} \right) (k_t - k_b) \quad (11)$$

if all the positive terms in eq. 3 are represented by \mathcal{R} as the total heat release rate. If we assume $\partial k_t/\partial T = 0$, the left-hand side of (11) is always positive. Inequality (11) will be satisfied with either $\partial \mathcal{R}/\partial T \geq \partial l/\partial T$ or $k_t \geq k_b$. The former relationship is the condition for explosion in the thermal theory while the latter one is the condition for explosion in the chain theory. One solution of (5) is obviously $k_b = k_t$ so (11) is satisfied for this singularity, which is therefore a saddle point. T_s^1 is identical with the explosion limit temperature as deduced from Semenov's isothermal

(4) H. T. Davis, "Introduction to Nonlinear Differential and Integral Equations," Dover Publications, New York, N. Y., 1962.

chain theory. The second singularity is obviously $x_s^{(2)} = 0$, $T_s^{(2)} = T_0$, which turns out to be a stable nodal point with no reactive intermediate and the temperature of the system coinciding with the temperature T_0 of the heat bath. As there are only these two singularities in the phase plane we can draw a qualitative diagram of the integral curves; see Figure 1.

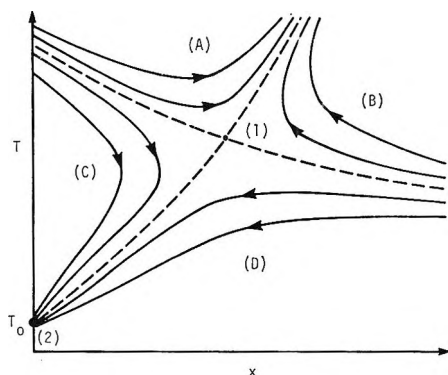


Figure 1.

The saddle point (1) is cut by two dotted curves, the separatrices, which divide the positive quadrant of the phase plane into four regions (A, B, C, and D). The slope of the separatrix which cuts the T axis is negative owing to the presence of the heat loss term in the energy conservation equation.

Obviously, any initial condition in quadrants A or B will result in explosion, while any initial condition in quadrants C or D will result in the system approaching the stable nodal point (2) without any increase in temperature. In the limit, as all the heats of reaction get smaller and smaller, the separatrix gets almost parallel to the x axis, and the result is that the explosive quadrants A and B are separated from C and D by the line $k_t = k_b$; *i.e.*, it reduces to Semenov's isothermal result from the chain theory. Thus, the main qualitative effect of removing the restrictive assumption of isothermal processes is that the explosion limit (separatrix) becomes dependent upon the initial concentration of the chain carrier, as occurs in experimental results. At very low x concentrations it is obvious, from eq. 4, that the slope dT/dx of any integral curve, as well as the separatrix, is largely determined by the heat loss term. The slope dT/dx of the separatrix reflects the sensitivity of the explosion limits to the initial concentration of x . The nonisothermal theory provides a framework for the explanation of the effects of vessel coatings on explosion limits insofar as the coatings are carrier sinks. In view of the negative slope of the separatrix, it can be concluded that the weaker the carrier sink, the lower

the explosion temperature. The detailed application to surface effects in specific reactions will be discussed elsewhere.

Examination of Figure 1 indicates some interesting types of behavior; *e.g.*, in some explosions one should observe an initial spontaneous decrease in temperature just before the large and rapid increase characterizing the explosion itself. However, the chain carrier itself is increasing all through the process. On the other hand, if we have an initial condition over to the right of quadrant B, the temperature will increase very slowly at first, then suddenly increase rapidly (highly nonlinear behavior). However, the near-discontinuity in the temperature variation is well characterized in the carrier concentration behavior since, during the slow temperature rise, it is in fact decreasing and starts to increase rapidly with the temperature.

Similarly, from the phase diagram one can discuss various types of stable behavior in an equally simple manner.

III. Application to a Pure Thermal Explosion: The Reaction $A \rightarrow x \rightarrow B$

We have shown in the previous section that the unified model of explosions reduces to the chain theory when heat release and loss are neglected. Now we will examine the case of a pure thermal explosion. Consider the reaction scheme $A \rightarrow x \rightarrow B$, in which there is no radical chain, although an intermediate radical x is involved. The conservation equations are (in the initial stages)

$$\frac{dx}{dt} = k_1 - k_2x$$

$$\frac{dT}{dt} = k_1h_1 + k_2h_2x - l \quad (12)$$

and the singular points are given by

$$k_1(h_1 + h_2) = l \quad x_s = \frac{k_1}{k_2} \quad (13)$$

Obviously if $l > 0$, the reaction must be exothermic; otherwise (13) would have no solution. The transformed equation is easily shown to be

$$\frac{dT'}{dx'} = \frac{R(T_s)^2k_2h_2x' + (k_1h_1E_1 - \alpha)T'}{-R(T_s)^2k_2x' + k_1E_1T'} \quad (14)$$

From the previous discussion it is obvious that for the system to exhibit explosive behavior it must have at least one saddle point. The necessary and sufficient condition for this is

$$R(T_s)^2k_2h_2k_1E_1 > (k_1h_1E_1 - \alpha)R(T_s)^2k_2$$

i.e.

$$(k_1 h_1 E_1 - \alpha) > h_2 k_1 E_1 \quad (15)$$

or

$$k_1 E_1 (h_1 + h_2) > \alpha$$

i.e., the reaction must be exothermic ($h_1 + h_2 > 0$) and sufficiently so that (15) is satisfied, or the singularity is a stable nodal point, no explosive behavior being possible. Obviously, in an adiabatic system ($l = 0$, $\alpha = 0$) inequality 15 is satisfied, and explosive behavior will be shown. Again the separatrix which cuts the T axis has a nonzero slope (negative in most cases), and the intermediate concentration will determine if the explosion is to occur. Thus, in a nonchain explosion of this type, vessel coating with materials which affect the value of x will alter the explosion limits.

IV. Conclusion

By consideration of the kinetic and energy conservation equations simultaneously, one can deduce a considerable amount of semiquantitative and qualitative information about potentially explosive materials. The restrictive assumptions of both the isothermal chain and purely thermal theories are removed, and the resultant generalized theory naturally explains phenomena not amenable to explanation by either theory separately. For example, vessel coating, addition of chain carriers and intermediates, etc., all affect the explosion limit explicitly within the framework of the theory. Also, as the separatrix is not parallel to the x axis, it may be possible to account for the irreproducibility of results encountered with certain coatings if these coatings produce x concentrations in a region where the slope of the separatrix is large.

Dissociation Constant of Acetic Acid in Deuterium Oxide from 5 to 50°.

Reference Points for a pD Scale

by Robert Gary, Roger G. Bates, and R. A. Robinson

National Bureau of Standards, Washington, D. C. (Received March 19, 1965)

Electromotive force measurements of a cell without liquid junction have been used to determine the dissociation constant of acetic acid in deuterium oxide from 5 to 50°. The enthalpy, entropy, and heat capacity changes on dissociation of acetic acid have been calculated. Values of $-\log(a_{D^+} \gamma_{Cl^-})$ and the conventional p_{aD} values for the equimolar (0.05 *m*) acetic acid-sodium acetate buffer solutions have been determined. These provide a second fixed point for standardizing the pD scale, supplementing data for the equimolar mixture of KD_2PO_4 and Na_2DPO_4 established in an earlier investigation.

Introduction

The measurement of the second dissociation constant of deuteriophosphoric acid in deuterium oxide has been reported recently,¹ along with values of $p(a_{D^+} \gamma_{Cl^-})$ and p_{aD} for equimolar KD_2PO_4 - Na_2DPO_4 buffer solutions.

We have now measured the e.m.f. of the cell

Pt; $D_2(g)$ at 1 atm., CH_3COOD (*m*),
 CH_3COONa (*m*), $NaCl$ (*m'*), $AgCl$; Ag

at 5° intervals from 5 to 50°. The dissociation constant of acetic acid has been derived over this tem-

(1) R. Gary, R. G. Bates, and R. A. Robinson, *J. Phys. Chem.*, **68**, 3806 (1964).

perature range, and from these results the partial molal enthalpy, entropy, and heat capacity changes on dissociation have been obtained. These quantities are compared with the corresponding changes when the dissociation occurs in ordinary water as solvent.

In addition, values of $p(a_D\gamma_{Cl})$ [$\equiv -\log(a_D+\gamma_{Cl-})$] have been calculated for the equimolal (0.05 *m*) acetic acid-sodium acetate buffer solution containing sodium chloride at molalities of 0.05, 0.025, and 0.01. A linear extrapolation then gave the limiting values of $p(a_D\gamma_{Cl})^0$ in the absence of sodium chloride. Values of pa_D [$\equiv -\log a_D$] in deuterium oxide were calculated with the aid of a convention consistent with that on which standard pH values in water are based² but modified to allow for the differences in density and dielectric constant.

Experimental Results

Deuterium gas was taken from commercial cylinders; mass spectrometric analysis³ gave a deuterium content of 99.5 atom %. The deuterium oxide had an isotopic purity of 99.75%; this was reduced to 99.70% on dissolution of the acetic acid and sodium carbonate to produce a solution 0.1 *m* with respect to both acetic acid and sodium acetate. The solutions made by dilution of this stock solution with deuterium oxide were proportionally closer to 99.75% in isotopic purity.

Acetic acid was purified by fractional freezing. Titration with standard base indicated 100.18 mole % CH_3COOH . Sodium carbonate was dried at 250° for 3 hr. Titration with standard acid indicated a purity of 100.01%.

The cells have already been described.⁴ The measured values of the e.m.f., corrected to 1 atm. of the gas used, are given in Table I. Each entry is the mean value given by two cells. The average difference between the e.m.f. of duplicate cells at all 10 temperatures was 0.04 mv.

Discussion

Values of $p(a_D\gamma_{Cl})$ were calculated by means of the equation

$$(E - E^0)/k + \log m_{Cl-} = -\log(a_D+\gamma_{Cl-}) \equiv p(a_D\gamma_{Cl}) \quad (1)$$

where k is written for $(RT \ln 10)/F$. Values of the standard electrode potential, E^0 , have already been tabulated.⁴

The mass law expression for the dissociation constant of acetic acid ($DAc = CH_3COOD$) is

$$K = \frac{m_D+m_{Ac-}}{m_{DAc}} \frac{\gamma_D+\gamma_{Ac-}}{\gamma_{DAc}} \quad (2)$$

and, if this is combined with eq. 1, there results the equation

$$pK' \equiv pK - \log \frac{\gamma_{Cl-}\gamma_{DAc}}{\gamma_{Ac-}} = p(a_D\gamma_{Cl}) + \log \frac{m_{DAc}}{m_{Ac}} \quad (3)$$

Here $m_{Ac-} = m + m_{D+}$ and $m_{DAc} = m - m_{D+}$; for all but the two most dilute solutions it suffices to put $m_{Ac-} = m_{DAc} = m$, and even for these two solutions the introduction of the m_{D+} term affects only the fourth decimal place of pK .

The pK' calculated by eq. 3 proved to be almost independent of concentration, as might be expected since the activity coefficient term in eq. 3, $\log(\gamma_{Cl-}\gamma_{DAc}/\gamma_{Ac-})$, should be small. At each temperature, pK was derived by fitting the values of pK' by the method of least squares to an equation linear in ionic strength; the ionic strength, I , is $(m + m' + m_{D+})$. The values of pK so obtained are given in Table II along with the standard deviations, σ_t .

These values of pK have been fitted, also by the method of least squares, to the equation⁵

$$pK = A_1/T - A_2 + A_3T \quad (4)$$

where T is the temperature in degrees Kelvin. The values of A_1 , A_2 , and A_3 are given at the bottom of Table II, and the values of pK calculated by eq. 4 are found in the fourth column of this table. Values of pK for acetic acid in ordinary water⁶ are given in the fifth column, and the difference, pK in D_2O - pK in H_2O , in the last column. These differences are not quite so large as those found for the second dissociation constant of phosphoric acid,¹ for example, 0.5562 at 25°, compared with 0.5799 for phosphoric acid.

La Mer and Chittum⁷ found $K = 0.55 \times 10^{-6}$ ($pK = 5.260$) for acetic acid in deuterium oxide at 25°. They used conductance measurements and expressed concentrations as molarities. Presumably, therefore, K is in molarity units, so that on the molality scale

(2) R. G. Bates and E. A. Guggenheim, *Pure Appl. Chem.*, **1**, 163 (1960).

(3) Analysis by E. E. Hughes of the Analysis and Purification Section.

(4) R. Gary, R. G. Bates, and R. A. Robinson, *J. Phys. Chem.*, **68**, 1186 (1964).

(5) H. S. Harned and R. A. Robinson, *Trans. Faraday Soc.*, **36**, 973 (1940).

(6) H. S. Harned and R. W. Ehlers, *J. Am. Chem. Soc.*, **55**, 652 (1933).

(7) V. K. La Mer and J. P. Chittum, *ibid.*, **58**, 1642 (1936).

Table I: Electromotive Force of the Cell Pt; D₂(g) at 1 atm., DAc (*m*), NaAc (*m*), NaCl (*m'*), AgCl; Ag (in volts) from 5 to 50°^a

<i>m</i>	<i>m'</i>	5°	10°	15°	20°	25°	30°	35°	40°	45°	50°
0.005	0.005	0.64734	0.65135	0.65521	0.65922	0.66301	0.66687	0.67068	0.67447	0.67823	0.68196
0.01	0.01	0.63071	0.63443	0.63810	0.64168	0.64534	0.64875	0.65224	0.65573	0.65919	0.66275
0.025	0.025	0.60899	0.61229	0.61543	0.61858	0.62186	0.62493	0.62806	0.63117	0.63418	0.63727
0.05	0.05	0.59251	0.59541	0.59835	0.60122	0.60410	0.60688	0.60964	0.61248	0.61517	0.61788
0.10	0.10	0.57604	0.57868	0.58134	0.58388	0.58639	0.58883	0.59132	0.59375	0.59619	0.59856
0.05	0.01	0.63105	0.63476	0.63838	0.64202	0.64558	0.64912	0.65261	0.65609	0.65950	0.66293
0.05	0.025	0.60907	0.61241	0.61559	0.61887	0.62201	0.62514	0.62825	0.63129	0.63434	0.63736

^a Ac = CH₃CO₂.**Table II:** Dissociation Constant of Acetic Acid in Deuterium Oxide from 5 to 50°

<i>t</i> , °C.	p <i>K</i> , obsd.	<i>σ</i> _±	p <i>K</i> , calcd. ^a	p <i>K</i> , in H ₂ O	Δ ^b
5	5.3463	0.0012	5.3468	4.7701	0.5767
10	5.3343	0.0010	5.3338	4.7628	0.5710
15	5.3236	0.0007	5.3238	4.7581	0.5657
20	5.3168	0.0003	5.3166	4.7558	0.5608
25	5.3130	0.0009	5.3120	4.7558	0.5562
30	5.3100	0.0006	5.3099	4.7581	0.5518
35	5.3093	0.0008	5.3100	4.7624	0.5476
40	5.3118	0.0008	5.3125	4.7688	0.5437
45	5.3167	0.0005	5.3171	4.7770	0.5401
50	5.3245	0.0008	5.3237	4.7871	0.5366

^a p*K* (calcd.) = $A_1/T - A_2 + A_3T = 1316.56/T - 3.3181 + 0.0141348T$. ^b Δ = p*K* (calcd.) in D₂O - p*K* in H₂O.

p*K* = 5.303. This result compares reasonably well with our value of 5.313 at 25°. It may be noted that Rule and La Mer⁸ found p*K* = 7.750 for the second stage of the dissociation of phosphoric acid. As they expressed their concentrations in volume units, the value on the molality scale should be 7.793. This compares with p*K* = 7.780 which we obtained recently.¹

Thermodynamic Quantities

From eq. 4 and the numerical values of A_1 , A_2 , and A_3 , standard partial molal enthalpy, entropy, and heat capacity changes on dissociation can be evaluated. A few such values are given in Table III, corresponding values for ordinary water as solvent being given in parentheses. At 25°, $\Delta C_p^\circ = -38.6$ cal. deg.⁻¹ mole⁻¹, as compared with -36.6 cal. deg.⁻¹ mole⁻¹ for ordinary water as solvent. The dissociation constant has a maximum value at 32.0° ($-\log K_{\max} = 5.3096$); when the solvent is ordinary water, the maximum ($-\log K_{\max} = 4.7555$) is found at 22.4°. The above results are expressed in thermochemical calories (1 thermochemical calorie = 4.1840 joules).

Table III: Enthalpy and Entropy Changes for the Dissociation of Acetic Acid

<i>t</i> , °C.	Δ <i>H</i> ^o , cal. mole ⁻¹	Δ <i>S</i> ^o , cal. deg. ⁻¹ mole ⁻¹
0	1192 (781)	-20.2 (-18.8)
25	275 (-98)	-23.4 (-22.1)
50	-730 (-1047)	-26.6 (-25.1)

Value of p*D*

Table IV gives the values of p(*a*_Dγ_{Cl}), calculated from the e.m.f. data (Table I) and eq. 1, for three solutions each 0.05 *m* in acetic acid and sodium acetate but containing different concentrations of sodium chloride. The value of p(*a*_Dγ_{Cl}) varied very slightly with sodium chloride concentration, and extrapolation

Table IV: Standard Reference Values of p*a*_D for the Equimolal Buffer Solution HAc (0.05 *m*), NaAc (0.05 *m*) in Deuterium Oxide

<i>t</i> , °C.	p(<i>a</i> _D γ _{Cl}) ^a				p <i>a</i> _D	p <i>a</i> _D (calcd.)
	0.05 <i>m'</i>	0.025 <i>m'</i>	0.01 <i>m'</i>	0 <i>m'</i>		
5	5.353	5.352	5.353	5.352	5.265	5.265
10	5.339	5.340	5.340	5.341	5.254	5.252
15	5.329	5.330	5.330	5.331	5.243	5.243
20	5.321	5.323	5.324	5.325	5.236	5.235
25	5.316	5.318	5.319	5.319	5.230	5.230
30	5.313	5.316	5.316	5.317	5.227	5.227
35	5.312	5.315	5.316	5.317	5.226	5.225
40	5.315	5.317	5.318	5.319	5.227	5.226
45	5.318	5.321	5.322	5.323	5.230	5.230
50	5.325	5.327	5.328	5.329	5.236	5.235

^a Values in these four columns are for the respective values of *m'* (NaCl).(8) C. K. Rule and V. K. La Mer, *J. Am. Chem. Soc.*, 60, 1974 (1938).

by the method of least squares gave values of $p_{\text{D}}(\gamma_{\text{Cl}^-})^0$ in the absence of sodium chloride.

With the aid of a convention for $-\log \gamma_{\text{Cl}^-}$, similar to that adopted for aqueous solutions,² values of p_{D} have been calculated and are recorded in the sixth column of Table IV. As modified to apply to dilute solutions ($I < 0.1$) in deuterium oxide, this convention may be represented as

$$-\log \gamma_{\text{Cl}^-} = \frac{A(d_0 I)^{1/2}}{1 + B\bar{a}(d_0 I)^{1/2}} \quad (5)$$

where A and B are the Debye-Hückel constants for deuterium oxide (density d_0) as solvent and \bar{a} , the ion-size parameter, is 4.56 Å. The use of this value of the ion-size parameter makes $B\bar{a}d_0^{1/2} = 1.5 \text{ kg.}^{1/2} \text{ mole}^{-1/2}$ for aqueous solutions at 25°. The values of $A\bar{a}d_0^{1/2}$ and $B\bar{a}d_0^{1/2}$ for the solvent deuterium oxide have been summarized elsewhere.⁴

The conventional p_{D} given in Table IV can be represented by the equation

$$p_{\text{D}}(\text{calcd.}) = 5.279 - 0.003072t + 0.000044t^2$$

where t is in degrees centigrade. Following the procedure on which a practical scale of pH has been established, this conventional p_{D} may be regarded as a reference point for the standardization of an operational pD scale.¹ In other words, p_{D} is identified with $p_{\text{D}}(\text{S})$ in the operational definition of pD.

The accuracy of the practical pD scale fixed by this acetate reference solution and the phosphate solution studied in the earlier work¹ depends on the constancy of the potential at the liquid junction between the standard (or test) solution in deuterium oxide and the aqueous potassium chloride of the calomel reference electrode. The internal consistency of the standard pD scale will be the subject of further study.

Excess Properties of Some Aromatic-Alicyclic Systems. I. Measurements of Enthalpies and Volumes of Mixing¹

by A. E. P. Watson,² I. A. McLure,³ J. E. Bennett,⁴ and G. C. Benson

Division of Pure Chemistry, National Research Council, Ottawa, Canada (Received March 19, 1965)

Excess enthalpies and volumes have been measured at 25° for eight binary aromatic-alicyclic systems formed by mixing benzene and toluene with cycloparaffins containing five to eight carbon atoms.

I. Introduction

It has frequently been pointed out that the molecular interaction between an aromatic and an aliphatic molecule is relatively weak compared to the average of the energies of interaction between like pairs of molecules. Rowlinson⁵ noted that values of the excess functions for benzene-cyclohexane mixtures support this view and the second virial coefficients⁶ for the same system also provide corroboration. Other

supporting evidence has been obtained from measure-

- (1) Issued as National Research Council No. 8562.
- (2) National Research Council of Canada Postdoctorate Fellow, 1959-1961.
- (3) National Research Council of Canada Postdoctorate Fellow, 1962-1963.
- (4) National Research Council of Canada Postdoctorate Fellow, 1961-1963.
- (5) J. S. Rowlinson, "Liquids and Liquid Mixtures," Butterworth and Co. Ltd., London, 1959, see p. 338.
- (6) J. S. Rowlinson, *Nature*, **194**, 470 (1962).

ments of solubilities⁷ and of gas-liquid critical temperatures.⁸

In order to investigate further the strength of aromatic-aliphatic interactions the molar excess enthalpy H^E and molar excess volume V^E have been measured for two series of binary systems, benzene with cyclopentane, cyclohexane, cycloheptane, and cyclooctane, and toluene with the same addends. The experimental methods used in the investigation and the results obtained are described in the following sections. The application of various theories of molecular solutions to the data is reported in a second paper.

II. Experimental

Materials. Determinations of (i) excess enthalpies and (ii) excess volumes of mixing were carried out in separate series of measurements and in some cases materials from different sources were used.

(i) In the calorimetric studies, the benzene and toluene were Reagent grade chemicals obtained from the Nichols Chemical Co. Ltd.; the cycloheptane and cyclooctane (98 mole % minimum purity) were purchased from the Aldrich Chemical Co. Before use, all the preceding materials were treated with concentrated sulfuric acid, washed until neutral, dried, and fractionally distilled through a 50-cm. gauze-packed column fitted with a silvered vacuum jacket. Cyclopentane, a Pure grade chemical (99 mole % minimum purity, from Phillips Petroleum Co.), and Spectro grade cyclohexane (Eastman Organic Chemicals) were used without further purification.

(ii) Pure grade toluene and cyclohexane supplied by the Phillips Petroleum Co. were used for the volumetric determinations. The benzene, cyclopentane, cycloheptane, and cyclooctane were the same as described in (i).

Typical values of the refractive indices and densities of the materials at 25.00° are given in Table I along with results taken from the tables compiled by the American Petroleum Institute.⁹ A Bausch and Lomb refractometer was used to measure the refractive indices. Densities were determined in twin-stem pycnometers and corrections were applied for buoyancy, vapor space, and capillary effects. The temperature of the bath used for the density work was controlled to within $\pm 0.002^\circ$ and its absolute value was established with a calibrated platinum resistance thermometer.

The purity of the materials was also examined in a Perkin-Elmer refractometer and was found to exceed 99.7% in all cases with the exception of cyclohexane. The latter material showed traces of an impurity suspected to be methylcyclopentane; this probably

Table I: Properties of Component Liquids

Component	d^{25}_4 , g. cm. ⁻³		Refractive index, μ^{25}_D	
	Exptl.	A.P.I.	Exptl.	A.P.I.
Benzene	0.87345	0.87368	1.4979	1.49792
Toluene	0.86242	0.86228	1.4942	1.49414
Cyclopentane	0.74029	0.74043	1.4038	1.40363
Cyclohexane	0.77320	0.77387	1.4235	1.42354
Cycloheptane	0.80732	0.8066	1.4434	1.4424
Cyclooctane	0.83151	0.8320	1.4560	1.4563

accounts for the poor agreement between the observed density and the A.P.I. value for cyclohexane.

Measurement of H^E . Two different adiabatic calorimeters were used in determining the molar excess enthalpies reported in section III. The essential features of the equipment have been described previously.^{10,11} For the present work the guillotine bulb breaker was removed from the calorimeter vessel and replaced by a Pyrex mixing cell which was supported from the lid of the vessel by a metal framework. The remaining space in the vessel was filled with water to provide good thermal contact with the cell. The shape of the cell was similar to that used by Benjamin and Benson¹² but the design of the Teflon stoppers was modified to facilitate filling and to reduce the vapor volume (generally less than 0.2 cm.³). Initially the two components to be mixed were separated by mercury; the solution was formed by rotating the calorimeter assembly (vessel and adiabatic environment) back and forth through 180°.

The composition of the mixture was derived from weighings made during the filling process. Measurements were made on 0.1-0.2 mole of total material and three cells of varying dimensions were used to cover the whole composition range.

Quantities of heat absorbed during the mixing process varied from 25 to 75 joules. The precision of the results depends mainly on the accuracy in determining changes in thermocouple e.m.f. during the mixing and calibration periods. A reasonable estimate of the error in these voltages is 0.15 μ v. which, in a relatively un-

(7) A. J. Ashworth and D. H. Everett, *Trans. Faraday Soc.*, **56**, 1609 (1960).

(8) E. J. Partington, J. S. Rowlinson, and J. F. Weston, *ibid.*, **56**, 479 (1960).

(9) American Petroleum Institute, Research Project 44, "Selected Values of Properties of Hydrocarbon and Related Compounds," Carnegie Press, Pittsburgh, Pa., 1953.

(10) G. C. Benson and G. W. Benson, *Rev. Sci. Instr.*, **26**, 477 (1955).

(11) G. C. Benson, E. D. Goddard, and C. A. J. Hoeve, *ibid.*, **27**, 725 (1956).

(12) L. Benjamin and G. C. Benson, *J. Phys. Chem.*, **67**, 858 (1963).

favorable case, corresponds to an uncertainty of 5 joules mole⁻¹ in the excess enthalpy. The vapor space was small in all cases and corrections for vaporization and condensation effects¹³ were negligible (generally less than 0.1 joule mole⁻¹). The values of H^E were obtained at temperatures within $\pm 0.1^\circ$ of 25° and correction to 25.00° would not alter the results significantly.

Measurement of V^E . The volume studies were carried out in dilatometers similar to the type described by Desmyter and van der Waals¹⁴ and used recently by McLure and Swinton.¹⁵ With this apparatus it is possible to determine V^E over the full composition range by direct observation of the volume changes occurring as an initially single-component liquid is diluted by successive portions of a second. In order to allow for the larger vapor pressures in systems containing cyclopentane, the original form of the dilatometer was modified slightly by lengthening one of the arms of the U-shaped capillary.

All measurements were made at 25.00° in a water bath, the temperature of which was controlled to $\pm 0.001^\circ$ by a sensitive mercury-toluene regulator and a fast-response solid-state relay circuit. A thermistor bridge connected to a recorder was used to monitor the bath temperature.

Calculations of values of V^E from the primary data were done on an IBM 1620 computer. The accuracy of the measurements is estimated to be about $\pm 2\%$.

III. Results

Excess Enthalpies H^E . The results of the experimental measurement of heats of mixing at 25.00° are summarized for the benzene and toluene series in Tables II and III, respectively. For each system, the data were fitted with equations of the type

$$H^E = x(1-x) \sum_p^n A_p (1-2x)^p \quad (1)$$

in which x indicates the mole fraction of the aromatic component. The sum in eq. 1 consists of $n+1$ terms corresponding to integer values of p from 0 to n . Values of the coefficients A_p were determined by the method of least squares using an IBM 1620 computer and the statistical significance of varying the number of coefficients was examined in terms of Fisher's F-distribution.¹⁶ This analysis indicated that the use of forms with more than four coefficients ($n > 3$) was unjustifiable.

Values of the coefficients A_p for the case $n = 3$ are collected in Table IV. The standard deviations σ_H between the experimental and calculated values of H^E , given in the last column of Table IV, are based on

Table II: Experimental Values of the Molar Excess Enthalpy H^E (joules mole⁻¹) for Systems of the Benzene Series at 25.00° (x = mole fraction of benzene)

$\text{C}_6\text{H}_6\text{-C}_6\text{H}_{10}$ x	H^E	$\text{C}_6\text{H}_6\text{-C}_8\text{H}_{12}$ x	H^E	$\text{C}_6\text{H}_6\text{-C}_7\text{H}_{14}$ x	H^E	$\text{C}_6\text{H}_6\text{-C}_8\text{H}_{16}$ x	H^E
0.1261	269.4	0.1389	364.5	0.1506	354.9	0.1705	402.1
0.1320	269.0	0.1400	358.2	0.2379	525.5	0.3761	722.1
0.2168	421.2	0.2258	546.2	0.4044	717.5	0.4147	760.7
0.2748	485.8	0.3015	678.7	0.5113	752.2	0.4488	777.8
0.3825	589.6	0.3023	665.7	0.5760	751.6	0.5782	795.3
0.4392	612.6	0.3625	730.6	0.5826	749.4	0.6165	773.4
0.5356	630.9	0.4032	772.7	0.6810	681.3	0.6210	770.1
0.5657	624.4	0.4539	798.2	0.7038	662.0	0.7632	626.9
0.5753	615.4	0.4975	797.6	0.7535	596.3	0.8183	523.7
0.6454	582.7	0.5180	804.1	0.8424	437.9	0.9176	273.8
0.7398	499.2	0.5253	795.3	0.9063	280.5		
0.8202	385.3	0.5673	793.3				
0.8918	250.3	0.6347	753.6				
		0.6906	665.3				
		0.8962	310.5				

Table III: Experimental Values of the Molar Excess Enthalpy H^E (joules mole⁻¹) for Systems of the Toluene Series at 25.00° (x = mole fraction of toluene)

$\text{C}_7\text{H}_8\text{-C}_6\text{H}_{10}$ x	H^E	$\text{C}_7\text{H}_8\text{-C}_8\text{H}_{12}$ x	H^E	$\text{C}_7\text{H}_8\text{-C}_7\text{H}_{14}$ x	H^E	$\text{C}_7\text{H}_8\text{-C}_8\text{H}_{16}$ x	H^E
0.1068	146.0	0.1189	273.6	0.1309	277.8	0.1265	251.3
0.2021	245.6	0.2662	508.5	0.2782	482.8	0.2292	436.7
0.3164	325.6	0.3617	590.3	0.4030	565.9	0.2572	456.5
0.4468	365.4	0.4459	624.4	0.4731	593.9	0.4216	600.3
0.5003	362.8	0.4899	624.4	0.5170	584.9	0.5067	619.7
0.6509	320.0	0.5595	605.6	0.5564	581.0	0.5078	611.4
0.7661	250.6	0.6404	560.0	0.5896	564.7	0.5560	602.2
0.8707	150.6	0.7438	460.3	0.6609	517.9	0.6173	581.3
		0.8815	244.2	0.7614	426.6	0.6178	589.5
				0.8928	220.1	0.6929	516.8
						0.7163	500.1
						0.8507	316.8
						0.9115	201.7

the number of degrees of freedom in each instance (*i.e.*, four less than the number of experimental points).

The experimental data for H^E have been plotted in Figures 1 and 2. The curves in these illustrations represent the values calculated from eq. 1 and the coefficients in Table IV.

Excess Volumes V^E . The values of V^E (in cubic centimeters per mole) for each system were derived from the results of two independent determinations, each involving about 17 successive dilutions. In

(13) M. L. McGlashan in "Experimental Thermochemistry," Vol. II, H. A. Skinner, Ed., Interscience Publishers, Inc., New York, N. Y., 1962, Chapter 15.

(14) A. Desmyter and J. H. van der Waals, *Rec. trav. chim.*, **77**, 53 (1958).

(15) I. A. McLure and F. W. Swinton, *Trans. Faraday Soc.*, **61**, 421 (1965).

(16) C. A. Bennett and N. L. Franklin, "Statistical Analysis," John Wiley and Sons, Inc., New York, N. Y., 1961, p. 431.

Table IV: Values of the Coefficients of Eq. 1 Determined by the Method of Least Squares

System	A_0	A_1	A_2	A_3	σ_H , joules mole ⁻¹
C ₆ H ₆ -C ₆ H ₁₀	2519.3	-132.0	-23.1	-3.5	4.8
C ₆ H ₆ -C ₆ H ₁₂	3219.0	-45.1	-99.8	-306.2	6.0
C ₆ H ₆ -C ₇ H ₁₄	3033.0	-306.2	5.3	-75.2	4.5
C ₆ H ₆ -C ₈ H ₁₆	3189.7	-445.1	-16.7	-147.9	4.7
C ₇ H ₈ -C ₆ H ₁₀	1460.2	129.2	-40.9	-7.1	2.3
C ₇ H ₈ -C ₆ H ₁₂	2499.8	224.9	-31.7	-79.9	3.1
C ₇ H ₈ -C ₇ H ₁₄	2353.6	70.6	42.3	38.1	4.5
C ₇ H ₈ -C ₈ H ₁₆	2470.5	43.6	-139.6	-312.5	6.6

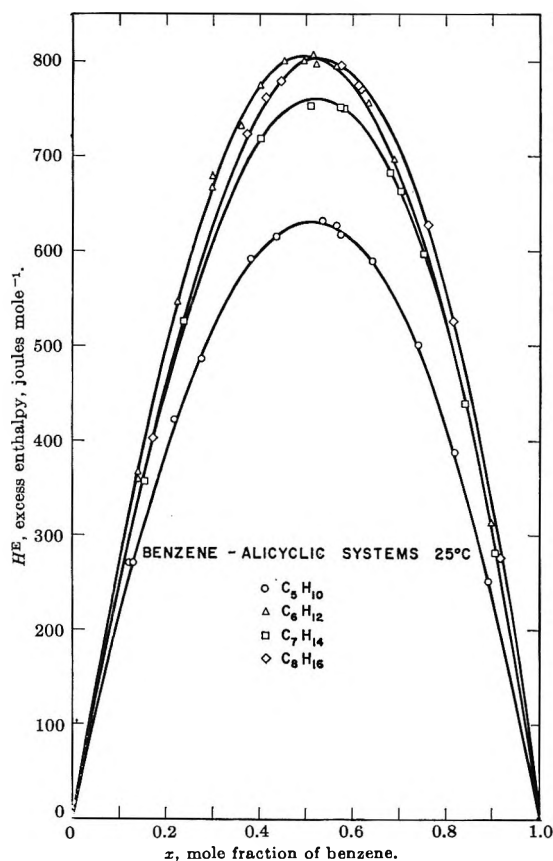


Figure 1. Molar excess enthalpies of benzene-alicyclic systems at 25°.

most cases the initial locations of the two components in the dilatometer were reversed in the two runs, but for systems containing cyclopentane the large vapor pressure of this compound at 25° made such a procedure unworkable, and the data were obtained from two runs performed in the same way.

Smoothing and interpolation of the data was done by fitting the results of each run with an equation of the form

$$V^E = x(1-x) \sum_p 2B_p(1-2x)^p \quad (2)$$

As in the treatment of the calorimetric data, values of the coefficients were calculated by a least-squares procedure. The coefficients, B_p , representing the mean results for each system are collected in Table V; these values were used in plotting the curves of V^E shown in Figures 3 and 4. The last column of Table V gives the standard deviation (σ_V) between the experimental results and values calculated from eq. 2.

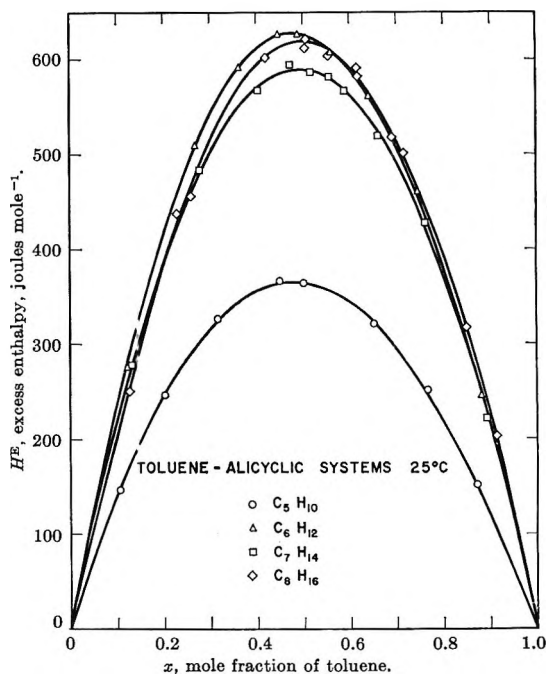


Figure 2. Molar excess enthalpies of toluene-alicyclic systems at 25°.

IV. Discussion

A comparison of the excess enthalpies with data recorded in the literature is only possible for the benzene-cyclohexane and toluene-cyclohexane systems. The former has been investigated repeatedly; the present comparison is restricted to a selection of data¹⁷⁻²⁹

- (17) E. Baud, *Bull. soc. chim. France*, **17**, 329 (1915).
- (18) G. Scatchard, L. B. Ticknor, J. R. Goates, and E. R. McCartney, *J. Am. Chem. Soc.*, **74**, 3715 (1952).
- (19) R. Thacker and J. S. Rowlinson, *Trans. Faraday Soc.*, **50**, 1036 (1954).
- (20) C. P. Brown, A. R. Mathieson, and J. C. J. Thynne, *J. Chem. Soc.*, 4141 (1955).
- (21) W. R. Moore and G. E. Styan, *Trans. Faraday Soc.*, **52**, 1556 (1956).
- (22) R. M. A. Noordtjij, *Helv. Chim. Acta*, **39**, 637 (1956).
- (23) H. W. Schnaible, H. C. van Ness, and J. M. Smith, *A.I.Ch.E. J.*, **3**, 147 (1957).

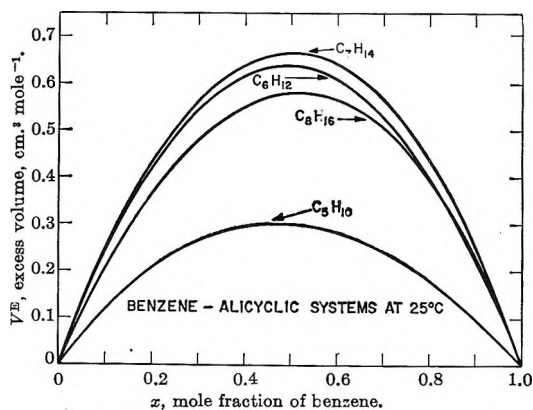


Figure 3. Molar excess volumes of benzene-alicyclic systems at 25°.

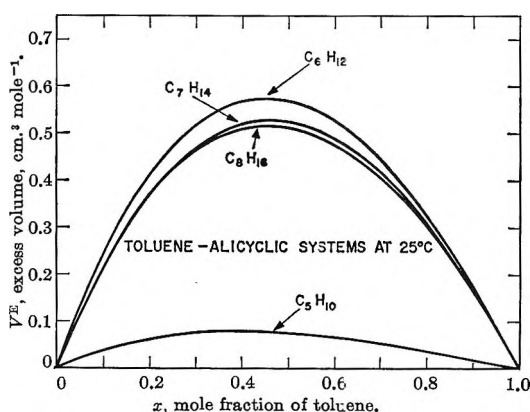


Figure 4. Molar excess volumes of toluene-alicyclic systems at 25°.

derived from measurements made in the range 15–35°. In all cases the curves reported are fairly symmetrical with the maximum of the excess enthalpy occurring generally at mole fractions of benzene from 0.50 to 0.53. There is, however, considerable variation among the values of H^E published by different investigators. This is illustrated in Table VI, where values of H^E for an equimolar solution at 25° are listed along with estimates of their errors (where available). A temperature coefficient³⁰ of -2.85 joules mole⁻¹ deg.⁻¹ was used to obtain values at 25° from data measured at other temperatures.

The value of 805 ± 5 joules mole⁻¹ obtained in the present work differs from the data of Brown, Mathieson, and Thynne,²⁰ of Goates, Sullivan, and Ott,²⁶ of Anderson and Prausnitz,²⁷ and of Ratnam, Rao, and Murti²⁸ by more than the combined estimates of experimental errors, but agrees well with the other values in Table VI. A detailed comparison over the whole concentration range with the recent results of Lundberg²⁹ shows that at concentrations above $x = 0.6$, the data

Table V: Values of the Coefficients of Eq. 2 Determined by the Method of Least Squares

System	B_0	B_1	B_2	σ_{V^E} , cm. ³ mole ⁻¹
C ₆ H ₆ -C ₅ H ₁₀	1.203	0.132	0.017	0.007
C ₆ H ₆ -C ₆ H ₁₂	2.557	0.098	-0.019	0.007
C ₆ H ₆ -C ₇ H ₁₄	2.665	-0.023	0.135	0.015
C ₆ H ₆ -C ₈ H ₁₆	2.324	-0.154	0.110	0.009
C ₇ H ₈ -C ₅ H ₁₀	0.302	0.129	0.025	0.004
C ₇ H ₈ -C ₆ H ₁₂	2.278	0.455	0.070	0.015
C ₇ H ₈ -C ₇ H ₁₄	2.106	0.331	0.034	0.015
C ₇ H ₈ -C ₈ H ₁₆	2.051	0.346	0.135	0.009

in columns 3 and 4 of Table II are consistently smaller; however, the maximum deviation between the two sets of results is only about 8 joules mole⁻¹.

In the case of toluene-cyclohexane mixtures, values of H^E for an equimolar solution estimated from published data are: 650 (Baud¹⁷ at 15 to 20°), 596 (Mathieson and Thynne³¹ at 20°), and 613 joules mole⁻¹ (Amaya³² at 25°). Comparison of the first two of these with the result of the present investigation (625 joules mole⁻¹) is uncertain due to lack of independent knowledge of the temperature coefficient of H^E . However, since this quantity is probably negative, the results of Mathieson and Thynne appear to be low around $x = 0.5$. The data for toluene-cyclohexane in Table III agree with the results of Amaya within the accuracies of the two investigations over the whole concentration range.

Volumes of mixing have been measured previously for benzene with cyclopentane³³ at 22° and with cyclohexane³⁴ at 25°. Agreement with the present data is reasonable in both cases. Excess volumes for the sys-

(24) M. B. Donald and K. Ridgway, *J. Appl. Chem.* (London), 8, 403 (1958).

(25) J. R. Goates, R. J. Sullivan, and J. B. Ott, *J. Phys. Chem.*, 63, 589 (1959).

(26) R. V. Mrazek and H. C. van Ness, *A.I.Ch.E. J.*, 7, 190 (1961).

(27) R. Anderson and J. M. Prausnitz, *Rev. Sci. Instr.*, 32, 1224 (1961).

(28) A. V. Ratnam, C. V. Rao, and P. S. Murti, *Chem. Eng. Sci.*, 17, 392 (1962).

(29) G. W. Lundberg, *J. Chem. Eng. Data*, 9, 193 (1964).

(30) The temperature coefficient is based on the results of Noordtzijs²² at 15 and 30°, and of Mrazek and van Ness²⁶ at 25 and 35°, which are in reasonable agreement. A much higher value published by Goates, Sullivan, and Ott²⁶ was rejected since the excess enthalpies which these authors report for 25° appear to be low (cf. Table VI).

(31) A. R. Mathieson and J. C. J. Thynne, *J. Chem. Soc.*, 37C8 (1956).

(32) K. Amaya, *Bull. Chem. Soc. Japan*, 34, 1278 (1961).

(33) H. Klaproth, *Nova Acta Leopoldina*, 9, 305 (1940).

(34) S. E. Wood and A. E. Austin, *J. Am. Chem. Soc.*, 67, 480 (1945).

Table VI: Values of the Molar Excess Enthalpy in an Equimolar Benzene-Cyclohexane Solution

Investigator	Ref.	Temp. of measurement, °C.	H^E at 25°, joules mole ⁻¹
Baud (1915)	17	15-20	802
Scatchard, Ticknor, Goates, and McCartney (1952)	18	20	808 ± 12
Thacker and Rowlinson (1954)	19	20	826 ± 40
Brown, Mathieson, and Thynne (1955)	20	20	823 ± 6
Moore and Styan (1956)	21	25	824 ± 40
Noordtzi (1956)	22	30	809 ± 24
Schnaible, van Ness, and Smith (1957)	23	25	786 ± 16
Donald and Ridgway (1958)	24	20	802
Goates, Sullivan, and Ott (1959)	25	25	759 ± 8
Mrazek and van Ness (1961)	26	25	810 ± 8
Anderson and Prausnitz (1961)	27	25	842 ± 2
Ratnam, Rao, and Murti (1962)	28	35	935 ± 27
Lundberg (1964)	29	25	799 ± 4
Present authors		25	805 ± 5

tem toluene-cyclohexane at mole fractions 0.416 and 0.571 of the aromatic component reported by Mathieson and Thynne⁸¹ are about 3 and 8% larger, respectively, than the values calculated from the coefficients in Table V.

Comparison of Figures 1 and 2 shows a striking similarity between the heat effects for the benzene and toluene series. The enthalpy changes are larger for the benzene series, but the relative positions of the curves for the different alicyclic addends are very

nearly the same for both series. The curve for cyclopentane lies considerably lower than those of the other three systems, which are closely grouped.

The mole fraction corresponding to the maximum of the enthalpy curve can be calculated from the formula

$$x_{\max} \approx 0.5 + 0.25A_1/(A_2 - A_0) \quad (3)$$

Using the coefficients in Table IV, it is evident that the maxima for the benzene and toluene systems are displaced to mole fractions above and below $x = 0.5$, respectively.

A considerable difference between systems containing cyclopentane and those formed from larger alicyclic compounds can also be seen in the excess volume plots in Figures 3 and 4. In all cases the volume changes for the toluene systems are smaller than for the corresponding systems of the benzene series, but the relative positions of the four curves are different for the two series. The positions of the maxima of the excess volume curves for the benzene series shift from mole fractions below 0.5 to values above 0.5 as the size of the alicyclic component increases. All the maxima for the toluene systems occur at mole fractions below 0.5.

Acknowledgment. The authors wish to thank Mr. P. J. D'Arcy for technical assistance during the calorimetric work and Mr. C. Halpin for performing some of the dilatometric measurements. We are also indebted to Mr. C. Chaffay and Mr. M. Ihnat for carrying out some preliminary density studies.

Excess Properties of Some Aromatic-Alicyclic Systems. II. Analyses of H^E and V^E Data in Terms of Three Different Theories of Molecular Solutions¹

by I. A. McLure,² J. E. Bennett,³ A. E. P. Watson,⁴ and G. C. Benson

Division of Pure Chemistry, National Research Council, Ottawa, Canada (Received April 27, 1965)

The experimental data for the molar excess enthalpies and volumes of aromatic-alicyclic systems, presented in part I, have been examined from three different points of view—the Scatchard-Hildebrand equation, a quasi-lattice treatment, and a form of corresponding states theory. None of these approaches is able to provide satisfactory independent estimates of the excess enthalpy but in most cases it is possible to fit the theoretical forms approximately to the data and to obtain information about the molecular interactions. For the eight systems studied, the energy of interaction between unlike molecules is found to be about 3% less than the arithmetic mean of the interactions of like pairs of molecules.

I. Introduction

In part I⁵ of this series, the results of measurements of the molar excess enthalpy (H^E) and molar excess volume (V^E), both at 25°, were reported for the binary systems of benzene with cyclopentane, cyclohexane, cycloheptane, and cyclooctane, and of toluene with the same alicyclic compounds. The present paper describes attempts to interpret the data in terms of several current theories of molecular solutions. The three different theoretical approaches considered are the Scatchard-Hildebrand equation,⁶ the quasi-lattice theory as developed by Barker,⁷ and the corresponding states average potential model due to Prigogine and co-workers.⁸

The treatment of Scatchard and Hildebrand is essentially an elaboration of that of van Laar and assumes a random distribution of the molecules (both in position and orientation) which is independent of the temperature. This approach should be fairly applicable to nonpolar systems. On the other hand, the quasi-lattice theory was formulated originally to describe the properties of mixtures in which the molecular interactions are strongly directional in character, as in hydrogen-bonded systems. The average potential model is probably best suited for mixtures of small spherically symmetric molecules. The aromatic-alicyclic systems which have been investigated do not fall unambiguously into any of these categories. In the past all three treatments have been applied to the

interpretation of the excess properties of benzene-cyclohexane solutions^{6,8-10} but a comparative study of their application to a fairly extensive series of similar systems has not been carried out previously.

II. Scatchard-Hildebrand Theory

Scatchard¹¹ derived the expression

$$\Delta U^M = (x_1V_1 + x_2V_2)A_{12}\phi_1\phi_2 \quad (1)$$

for the energy change when a mole of binary solution is formed at constant temperature and volume by mixing x_1 and x_2 moles of the pure components, having molar volumes V_1 and V_2 , respectively. In eq. 1, ϕ_i represents

- (1) Issued as National Research Council No. 8563.
- (2) National Research Council of Canada Postdoctorate Fellow, 1962-1963.
- (3) National Research Council of Canada Postdoctorate Fellow, 1961-1963.
- (4) National Research Council of Canada Postdoctorate Fellow, 1959-1961.
- (5) A. E. P. Watson, I. A. McLure, J. E. Bennett, and G. C. Benson, *J. Phys. Chem.*, **69**, 2753 (1965).
- (6) J. E. Hildebrand and R. L. Scott, "Regular Solutions," Prentice-Hall Inc., Englewood Cliffs, N. J., 1962, see Chapter 7.
- (7) J. A. Barker, *J. Chem. Phys.*, **20**, 1526 (1952).
- (8) I. Prigogine, "The Molecular Theory of Solutions," North Holland Publishing Co., Amsterdam, 1957, Chapters 10 and 11.
- (9) G. Scatchard, S. E. Wood, and J. M. Mochele, *J. Phys. Chem.*, **43**, 119 (1939).
- (10) J. B. Ott, J. R. Goates, and R. L. Snow, *ibid.*, **67**, 515 (1963).
- (11) G. Scatchard, *Chem. Rev.*, **8**, 321 (1931).

the volume fraction of component i and is defined with reference to the unmixed state as

$$\phi_i = x_i V_i / (x_1 V_1 + x_2 V_2) \quad (2)$$

The coefficient A_{12} is a constant having the form

$$A_{12} = c_{11} - 2c_{12} + c_{22} \quad (3)$$

in which the quantities c_{ij} characterize the interactions between various pairs of molecules 11, 12, and 22. In particular, c_{ii} is the cohesive energy density of component i and can be calculated from the standard molar heat of vaporization ΔH_i^v (for vaporization to the ideal gas state) using the expression

$$c_{ii} = (\Delta H_i^v - RT) / V_i \quad (4)$$

where R and T are the gas constant and absolute temperature. Energy densities for the aromatic and alicyclic compounds considered in this paper are listed in Table I. The references¹²⁻¹⁸ indicate the source of the heat of vaporization data; molar volumes were based on the experimental densities given in part I.

Table I: Values of Cohesive Energy Densities (c), Thermal Expansion Coefficients (α), and Isothermal Compressibilities (β) of Pure Component Liquids at 25°

Component	c , joules cm. ⁻³	$10^3\alpha$, deg. ⁻¹	$10^6\beta$, atm. ⁻¹
C ₆ H ₆	351 ^a	1.217 ^{a,b}	98.12 ^c
C ₇ H ₈	332 ^a	1.071 ^a	95.0 ^d
C ₈ H ₁₀	276 ^a	1.390 ^a	135.1 ^e
C ₈ H ₁₂	281 ^a	1.261 ^a	155.1 ^e
C ₇ H ₁₄	296 ^f	1.00 ^a	98.0 (estimated)
C ₈ H ₁₆	303 ^f	0.99 ^a	81.2 ^g

^a Reference 12. ^b Reference 14. ^c Reference 15. ^d Reference 16. ^e Reference 17. ^f Reference 13. ^g Reference 18.

In the case of dispersive forces between molecules with approximately equal ionization potentials the Berthelot relation

$$c_{12}^2 = c_{11}c_{22} \quad (5)$$

may be used to eliminate c_{12} from eq. 3, giving

$$A_{12} = (\sqrt{c_{11}} - \sqrt{c_{22}})^2 \quad (6)$$

The term solubility parameter¹⁹ is commonly used to indicate the quantity $\sqrt{c_{ii}}$.

The assumptions involved in the derivation of eq. 1 have been discussed in detail by Hildebrand and Scott.¹⁹ For the present purpose it is important to note that the mixing process considered is one carried out at constant volume. This restriction is frequently ignored

and values of ΔU^M are compared with heats of mixing at constant pressure. In the present work, experimental values of U_v^E , the molar excess energy at constant volume, were obtained from the excess enthalpies and volumes given in part I by using the thermodynamic relation

$$U_v^E = H^E - T(\alpha/\beta)V^E \quad (7)$$

Values of α , the coefficient of thermal expansion, and β , the isothermal compressibility, were estimated for the mixtures at 25° from data for the pure components (summarized in Table I) by assuming additivity on a volume fraction basis. The experimental excess energies for the benzene and toluene systems are plotted in Figures 1 and 2. In order to separate the curves for the different alicyclic compounds, the origin of the ordinate axis has been displaced for each curve.

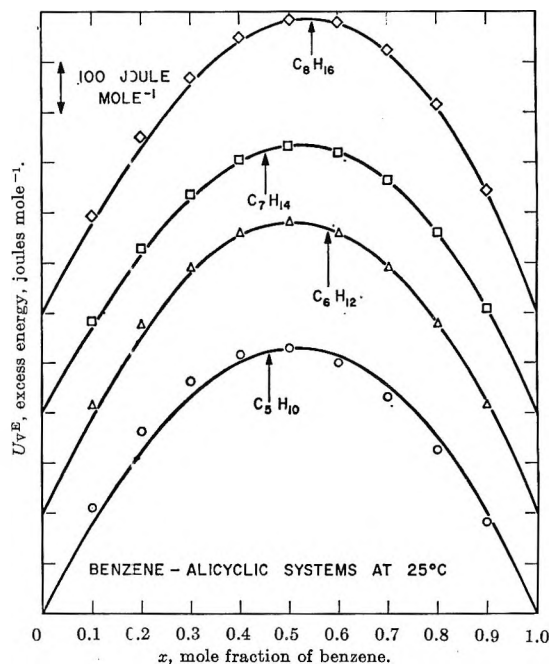


Figure 1. Excess energy at constant volume for benzene-alicyclic systems at 25°: curves experimental, points calculated from quasi-lattice theory.

(12) American Petroleum Institute, Research Project 44, "Selected Values of Properties of Hydrocarbons and Related Compounds," Carnegie Press, Pittsburgh, Pa., 1950, and later revisions.

(13) H. L. Finke, D. W. Scott, M. E. Gross, J. F. Messerly, and G. Waddington, *J. Am. Chem. Soc.*, **78**, 5469 (1956).

(14) S. E. Wood and A. E. Austin, *ibid.*, **67**, 480 (1945).

(15) G. A. Holder and E. Whalley, *Trans. Faraday Soc.*, **58**, 2095 (1962).

(16) B. Jacobson, *Acta Chem. Scand.*, **6**, 1485 (1952).

(17) A. Weissler, *J. Am. Chem. Soc.*, **71**, 419 (1949).

(18) E. Butta, *Ric. Sci.*, **26**, 3643 (1956).

(19) J. H. Hildebrand and R. L. Scott, "Solubility of Nonelectrolytes," 3rd Ed., Reinhold Publishing Corp., New York, N. Y., 1950.

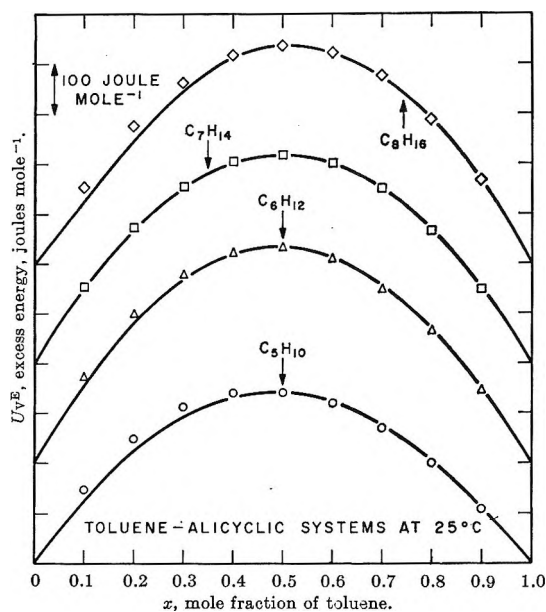


Figure 2. Excess energy at constant volume for toluene-alicyclic systems at 25°: curves experimental, points calculated from quasi-lattice theory.

Representation of the experimental results for U_v^E by two different empirical forms

$$U_v^E = (x_1V_1 + x_2V_2)\phi_1\phi_2 \sum_p C_p (\phi_2 - \phi_1)^{p-1} \quad (8)$$

and

$$U_v^E = x_1x_2 \sum_p C_p' (x_2 - x_1)^{p-1} \quad (9)$$

was investigated. The values of the coefficients C_p and C_p' in these were determined by least-square calculations. For $n = 1$ it was generally possible to obtain a closer fit in terms of the volume fractions; the resulting values of A_{12} (i.e., C_1 for $n = 1$) are summarized in Table II along with σ_U , the standard deviation between the experimental and calculated values of U_v^E . The superiority of eq. 8 over eq. 9 for $n = 1$ appears to indicate that the use of the volume fraction takes account of spatial considerations in these systems more realistically. However, the best fits to the experimental data were obtained by employing three or four constants in eq. 8 and 9. The values of σ_U were then very nearly the same as those given for σ_H in part I and there was no significant difference in the ability of either form to represent the results.

An examination of the differences of $\sqrt{A_{12}}$ shows that eq. 6 is not valid and that the Berthelot relation cannot be applied to the present systems. Optimum values of c_{12} obtained for each system by inserting in

Table II: Summary of Calculations for Scatchard-Hildebrand Theory

System	Least-square fit				Based on eq. 10	
	A_{12} , joules cm. ⁻³	σ_U , joules mole ⁻¹	c_{12} , joules cm. ⁻³	$\sqrt{c_{11}c_{22}}$, joules cm. ⁻³	c_{12} , joules cm. ⁻³	A_{12} , joules cm. ⁻³
C ₆ H ₆ -C ₆ H ₁₀	22.87	7.4	302	312	310	7
C ₆ H ₆ -C ₆ H ₁₂	23.65	9.5	304	314	311	10
C ₆ H ₆ -C ₇ H ₁₄	20.35	7.9	314	323	317	14
C ₆ H ₆ -C ₈ H ₁₆	21.34	8.0	316	326	317	20
C ₇ H ₈ -C ₆ H ₁₀	13.43	2.6	298	330	303	3
C ₇ H ₈ -C ₆ H ₁₂	16.02	6.2	299	306	305	3
C ₇ H ₈ -C ₇ H ₁₄	14.67	8.5	307	314	312	5
C ₇ H ₈ -C ₈ H ₁₆	14.24	8.9	310	317	314	8

eq. 3 the value of A_{12} and of c_{11} and c_{22} for the pure components are given in Table II along with values of $\sqrt{c_{11}c_{22}}$ for comparison.

Kohler²⁰ has described a method of calculating the interaction between unlike molecules which leads to the expression

$$c_{12} = \frac{16\alpha_1\alpha_2}{V_1V_2(V_1^{1/3} + V_2^{1/3})^3} \left(\frac{\mu_1\mu_2}{\mu_1 + \mu_2} \right) \quad (10)$$

where α_i is the molecular polarizability of species i and

$$\mu_i = c_{ii}V_i^3/\alpha_i^2 \quad (11)$$

Equation 10 is based on the London formula for dispersive forces but has the advantage that the ionization potentials of the molecules do not appear explicitly. This approach has been used by Munn²¹ in discussing the relative deviations of the interaction energies between unlike molecules from a geometric mean combining rule in a number of hydrocarbon systems.

In the present work polarizabilities were estimated from the Lorenz-Lorentz equation and the refractive indices of the pure components (μ^{25D}) given in part I. The values of c_{12} calculated from eq. 10 and the corresponding results for A_{12} are given in the last two columns of Table II. The Kohler formula leads to values of c_{12} which are somewhat less than those given by the Berthelot relation, but the values obtained for A_{12} are still much too small for all the systems with the exception of C₆H₆-C₈H₁₆. In deriving eq. 10 the interactions between the molecules are assumed to occur between point centers. The use of this crude approximation for fairly large molecules may be responsible for the failure of eq. 10 to provide a satisfactory estimate of c_{12} .

(20) F. Kohler, *Monatsh.*, **88**, 857 (1957).

(21) R. J. Munn, *Trans. Faraday Soc.*, **57**, 187 (1961).

III. Quasi-Lattice Theory

In the quasi-lattice model, the molecules of a solution are distributed over the sites of a fixed lattice which is usually assumed to have a coordination number of 4. Different molecular sizes are considered by allowing the molecules to occupy different numbers of sites. Various contact areas are recognized on each molecular species and the configurational energy of the mixture is expressed as a sum of contributions from interactions between different areas on molecules occupying nearest-neighbor sites. For details of the theory, reference should be made to Barker's original publication⁷; only the special forms of the equations needed for the present application will be outlined here.

An alicyclic molecule of ring size p is assumed to have $2p$ similar contact areas which will be called type 1. Benzene possesses 12 aromatic (type 2) areas; toluene in addition to 11 type 2 areas also has three areas of a different kind (type 3) around the methyl group. The energy of interaction (per mole) for a contact between areas of types i and j is denoted by U_{ij} and is defined in such a way that $2U_{ij}$ is the increase in energy (per mole) when two i - j contacts are formed from a pair of i - i and j - j contacts.

Due to the restriction imposed by the fixed underlying lattice, the excess energy calculated from the model again refers to a mixing process at constant volume. In the case of the benzene systems, the theoretical expression for the molar excess energy is

$$U_v^E = -2RTX_1X_2\eta_{12} \ln \eta_{12} \quad (12)$$

The quantities X_1 and X_2 are solutions of the pair of equations

$$X_1(X_1 + \eta_{12}X_2) = p(1 - x) \quad (13)$$

and

$$X_2(\eta_{12}X_1 + X_2) = 6x \quad (14)$$

In these expressions R represents the gas constant, T the absolute temperature, x the mole fraction of the aromatic species, and

$$\eta_{ij} = \exp(-U_{ij}/RT) \quad (15)$$

For toluene systems the formula corresponding to eq. 12 is

$$U_v^E = -2RT[X_1X_2\eta_{12} \ln \eta_{12} + X_1X_3\eta_{13} \ln \eta_{13} + (X_2X_3 - xX_2'X_3')\eta_{23} \ln \eta_{23}] \quad (16)$$

where now the quantities X_1 , X_2 , and X_3 must satisfy the conditions

$$X_1(X_1 + \eta_{12}X_2 + \eta_{13}X_3) = p(1 - x) \quad (17)$$

$$X_2(\eta_{12}X_1 + X_2 + \eta_{23}X_3) = 5.5x \quad (18)$$

$$X_3(\eta_{13}X_1 + \eta_{23}X_2 + X_3) = 1.5x \quad (19)$$

In eq. 16 X_2' and X_3' denote the values of X_2 and X_3 obtained from eq. 18 and 19 for the special case $x = 1$.

Since the equations which define U_v^E as a function of the contact energies are quite complicated, a least-square determination of the best values of these parameters was not attempted. Instead, the use of the above equations was essentially empirical and values of the contact energies were adjusted by a trial and error procedure in an attempt to fit the theoretical forms to experimental results. Numerical calculations were done on an IBM 1620 computer using programs developed previously.²²

The values of the aromatic-alicyclic interaction energy for the benzene systems were chosen to fit the experimental U_v^E data around $x = 0.5$. Treatment of the toluene systems was based on the assumption that the difference between methyl (aliphatic) and alicyclic contact areas could be neglected. In this approximation $U_{12} = U_{23}$, $U_{13} = 0$, and the value of U_{12} was again selected to fit the results for an equimolar solution. The interaction energies obtained in this way are summarized in Table III and results for U_v^E calculated from the quasi-lattice theory are plotted as points in Figures 1 and 2. In general, the theoretical values tend to be skewed more to small mole fractions of the aromatic component than is observed experimentally. Values of the standard deviations, σ_U , between the experimental and theoretical results (also included in Table III) show a greater variation in goodness of fit than that found in section II.

Table III: Values of the Contact Energies used in the Quasi-Lattice Theory Calculations (Energies in joules mole⁻¹)

System	U_{12}	σ_U	System	$U_{12} = U_{23}$	σ_U
C ₆ H ₆ -C ₆ H ₁₀	2(2)	25.5	C ₇ H ₈ -C ₆ H ₁₀	200	15.6
C ₆ H ₆ -C ₆ H ₁₂	2(2)	13.5	C ₇ H ₈ -C ₆ H ₁₂	230	9.9
C ₆ H ₆ -C ₇ H ₁₄	171	7.5	C ₇ H ₈ -C ₇ H ₁₄	203	4.6
C ₆ H ₆ -C ₈ H ₁₆	177	3.2	C ₇ H ₈ -C ₈ H ₁₆	198	14.6

It is evident that the data for all the systems cannot be fitted by a single value of U_{12} . An energy of about 200 joules mole⁻¹ gives fairly reasonable representations for five of the systems but a variation of $\pm 14\%$ in this energy is needed to cover the other three systems.

One of the drawbacks of the quasi-lattice theory is the

(22) B. Dacre and G. C. Benson, *Can. J. Chem.*, **41**, 278 (1963).

fact that the assignment of contact energies is often somewhat arbitrary and several different schemes may be found which fit the experimental excess energy equally well. The benzene systems studied here are of some interest since they involve only one kind of contact and hence, within the framework of the treatment outlined above, each system leads to a unique value for the aromatic-alicyclic interaction energy. The average value found for this energy (188 joules mole⁻¹) is only about half the magnitude of the aromatic-aliphatic contact energy obtained by Ott, Goates, and Snow.¹⁰ This difference reflects the different approach used by the latter authors, in particular their neglect of volume changes. In the case of the present systems the volume term in eq. 7 provides a sizable correction and has the general effect of making the values of U_v^E more nearly the same for the various systems of both series than were the original enthalpy results.

Other energy schemes in which the over-all variation of U_{12} is somewhat less than for that shown in Table III can be obtained by assigning U_{23} a small nonzero value. However, the fit between experiment and theory does not appear to be improved sufficiently to warrant the introduction of extra parameters at this time.

It should be noted that the computation of U_v^E does not use the lattice coordination number or require a knowledge of the number of sites occupied by the various species of molecules. Some calculations of the excess free energy and entropy of mixing, which do depend on these geometric factors, were also carried out.²³ The excess entropies obtained are all small and negative; the excess free energies appear to be too large,^{24,25} but the experimental information is meager. If reliable free energy data were available, it might be possible to assign the contact energies in a less arbitrary fashion.

IV. Corresponding States Average Potential Model

The corresponding states approach is based upon the assumption that the potential functions for molecular interaction between the various species of the system can be reduced to a common form by the introduction of suitable scale factors ϵ^* and r^* for the energy and molecular separation. In the average potential model, the average interaction energy of a particular molecule in the solution is set equal to the mean of its interactions with neighboring molecules. These may be either of the same or different species, and their relative numbers are proportional to their mole fractions.

The formulas which have been derived^{8,26} for the molar excess enthalpy and molar excess volume are

$$H^E = x_1x_2 \left[(h_1 - Tc_{p1})(2\theta - 9\rho^2) - \frac{1}{2}T^2 \frac{dc_{p1}}{dT} (\delta^2 - 4\theta\delta x_2 - 4\theta^2x_1x_2) + \frac{1}{2}T^2 \frac{dc_{p1}}{dT} \{\theta(x_1 - x_2) + 0.5\delta\}^2 \right] \quad (20)$$

and

$$V^E = x_1x_2 \left[1.5V_{1\rho}(2.75\rho + \theta(x_1 - x_2) + 0.5\delta) + T \frac{dV_1}{dT} (-2\theta - \delta^2 + 4\theta\delta x_2 + 4\theta^2x_1x_2 + 9\rho^2 + 3\rho\delta - 6\rho\theta x_2) + \frac{1}{2}T^2 \frac{d^2V_1}{dT^2} (-\delta^2 + 4\theta\delta x_2 + 4\theta^2x_1x_2) - \frac{1}{2}T \frac{\partial V_1}{\partial p} \frac{\partial c_{p1}}{\partial V_1} \times \{\theta(x_1 - x_2) + 0.5\delta\}^2 \right] \quad (21)$$

In these equations component 1 (the aromatic compound) is chosen as a reference standard and V_1 , h_1 , and c_{p1} and c_{v1} indicate the molar volume, configurational enthalpy, and configurational heat capacities of this material, respectively, as a pure substance at temperature T . The three parameters δ , θ , and ρ in eq. 20 and 21 are defined by the equations

$$\epsilon_{22}^* = \epsilon_{11}^*(1 + \delta) \quad (22)$$

$$\epsilon_{12}^* = \epsilon_{11}^* \left(1 + \frac{\delta}{2} + \theta \right) \quad (23)$$

$$r_{22}^* = r_{11}^*(1 + \rho) \quad (24)$$

The values of δ , θ , and ρ together with the combining rule

$$r_{12}^* = (r_{11}^* + r_{22}^*)/2 \quad (25)$$

can be used to specify the energy and distance parameters for 12 and 22 interactions in terms of those occurring in the reference compound. It is implicit in the

(23) Formulas for these functions can be found in ref. 7. A lattice coordination number of 4 was used and it was assumed that the number of sites covered by a molecule was equal to the number of carbon atoms contained in it.

(24) J. S. Rowlinson, "Liquids and Liquid Mixtures," Butterworth and Co. Ltd., London, 1959, see Section 4.8.

(25) R. W. Hermesen and J. M. Prausnitz, *Chem. Eng. Sci.*, **18**, 485 (1963).

(26) We believe several typographical errors have occurred in the printing of eq. 10.7.8 in ref. 8. The result given above for V^E was obtained by the methods outlined in Chapter X of Prigogine's treatise.

derivation of eq. 20 and 21 that the magnitudes of δ , θ , and ρ are small.

The contributions of the last terms in eq. 20 and 21 are generally relatively small and, in the present numerical calculations, both were neglected. The data used for the properties of the aromatic compounds are summarized in Table IV. Values of δ and ρ for the

Table IV: Values of Properties of the Reference Compounds at 25°^a

	Compounds	
	C ₆ H ₆	C ₇ H ₈
h_1 , joules mole ⁻¹	-31,370	-35,510
c_{p1} , joules mole ⁻¹ deg. ⁻¹	57.7	63.6
$\frac{dc_{p1}}{dT}$, joule mole ⁻¹ deg. ⁻²	-0.2	≈0
V_1 , cm. ³ mole ⁻¹	89.385	106.857
$\frac{dV_1}{dT}$, cm. ³ mole ⁻¹ deg. ⁻¹	0.1072	0.1114
$10^3 \times \frac{d^2V_1}{dT^2}$, cm. ³ mole ⁻¹ deg. ⁻²	0.285	0.311

^a Most of the data are derived from ref. 12.

alicyclic compounds referred to benzene and toluene were obtained from molar volumes of the pure substances as functions of temperature.^{8,12} For cycloheptane and cyclooctane the data available in the A.P.I. Tables cover only a small temperature range and this was extended by density measurements from 30 to 60°. The values of δ and ρ which lead to a reasonable superposition of the molar volume curves are listed in Table V. As far as the molar volumes are concerned it appears that all six compounds obey the law of corresponding states fairly well; this is evidenced by the fact that the ratios of $1 + \delta$ and $1 + \rho$ for the same alicyclic

Table V: Summary of Values Used for the δ , ρ , and θ Parameters and the Excess Volumes Calculated from Eq. 21

System	δ	ρ	θ	σ_H, V^E at $x_1 = 0.5$, joules cm. ³ mole ⁻¹		
				Calcd.	Found	
C ₆ H ₆ -C ₆ H ₁₀	-0.056	0.0120	-0.0253	9.1	0.41	0.30
C ₆ H ₆ -C ₆ H ₁₂	0.0	0.0680	-0.0124	13.2	0.98	0.64
C ₆ H ₆ -C ₇ H ₁₄	0.085	0.1183	0.0318	21.4	2.10	0.67
C ₆ H ₆ -C ₈ H ₁₆	0.150	0.1645	0.0879	17.4	3.82	0.58
C ₇ H ₈ -C ₆ H ₁₀	-0.144	-0.057	0.0012	10.2	0.70	0.08
C ₇ H ₈ -C ₆ H ₁₂	-0.084	-0.0037	-0.0229	14.5	0.36	0.57
C ₇ H ₈ -C ₇ H ₁₄	-0.001	0.0442	-0.0128	6.8	0.59	0.53
C ₇ H ₈ -C ₈ H ₁₆	0.061	0.0874	0.0117	8.9	1.41	0.51

compound referred to different aromatic components show a variation of only 1.7 and 0.2%, respectively. It should be noted, however, that this behavior is not sufficient to establish the applicability of the corresponding states treatment and that, in fact, other experimental data (*e.g.*, second virial coefficients and critical constants²⁷) indicate that the law of corresponding states does not hold for these compounds.

Calculation of H^E and V^E from eq. 20 and 21 requires a value of θ for each system. Use of the relation

$$\theta = -\delta^2/8 \quad (26)$$

which corresponds to the geometric mean combining rule for ϵ_{12}^* , in general failed to reproduce the experimental results. As an alternative approach, calculations were carried out for a series of θ values and the results were compared with experimental data. For most of the systems it was not possible to fit both H^E and V^E with the same value of θ ; in general, a value of θ which gave agreement with the enthalpy data led to excess volumes which were too large and *vice versa*. A reasonable compromise was possible for several systems but the determination of θ , which is an energy parameter, from enthalpy data should provide a fairer basis for comparison. Values of θ chosen to fit H^E at $x_1 = 0.5$ are given in Table V along with the calculated and experimental results for V^E at this concentration. Column 5 of the table lists standard deviations, σ_H , between the experimental and theoretical excess enthalpies. From these it again appears that there is a wider variation in the goodness of fit than that obtained in section II.

It is interesting to note that sizable deviations between experimental and calculated excess volumes for the benzene series of solutions occur for the two larger alicyclic compounds and that the range of agreement shifts to higher members in the toluene series. These observations can be explained qualitatively in terms of the relative sizes of the component molecules since the range of validity of eq. 20 and 21 is restricted to small values of the parameter ρ (*i.e.*, the molecules must be of nearly equal size.)

V. Conclusion

It has not been possible to establish unambiguously which of the approaches considered above provides the best basis for an analysis of the data. None of the theories leads to satisfactory *a priori* calculations of the excess enthalpies (or energies), but in most cases the theoretical forms can be fitted approximately to the experimental data by assigning to the various param-

(27) J. S. Rowlinson, *Nature*, **194**, 470 (1962).

eters values which are reasonable in magnitude. The corresponding states treatment appears to be of less general utility than the other theories but the requirement of fitting both H^E and V^E separately is more severe than that of fitting U_v^E in the other approaches.

Estimates of the relative weakness of the interaction between aromatic and alicyclic molecules can be obtained from the empirical values of the parameters in all three theories. In the four systems for which the corresponding states treatment leads to consistent results, θ is negative, indicating that the aromatic-alicyclic interaction energy is less than the arithmetic mean of the aromatic-aromatic and alicyclic-alicyclic interactions. It can be shown in the case of the Scatchard-Hildebrand theory that

$$\theta = (2c_{11}V_1)^{-1}[16c_{12}V_1V_2(V_1^{1/2} + V_2^{1/2})^{-2} - c_{11}V_1 - c_{22}V_2] \quad (27)$$

A reasonable definition of θ in the quasi-lattice theory is

$$\theta = -12U_{12}[2(\Delta H_1^v - RT)]^{-1} \quad (28)$$

for the benzene systems, and

$$\theta = -(11U_{12} + 3U_{13})[2(\Delta H_1^v - RT)]^{-1} \quad (29)$$

for those which contain toluene. In both instances ΔH_1^v is the latent heat of vaporization of the aromatic compound. Values of θ calculated from eq. 27-29, using the least-square values of c_{12} in Table II and the contact energies in Table III, are collected in Table VI.

Table VI: Values of θ Estimated According to the Three Theories

System	Scatchard-Hildebrand theory	Quasi-lattice theory	Corresponding states theory
$C_6H_6-C_6H_{10}$	-0.0281	-0.0386	-0.0253
$C_6H_6-C_6H_{12}$	-0.0509	-0.0386	-0.0124
$C_6H_6-C_7H_{14}$	-0.0560	-0.0327	...
$C_6H_6-C_8H_{16}$	-0.0509	-0.0339	...
$C_7H_8-C_6H_{10}$	-0.0240	-0.0313	...
$C_7H_8-C_6H_{12}$	-0.0226	-0.0360	-0.0229
$C_7H_8-C_7H_{14}$	-0.0223	-0.0318	-0.0128
$C_7H_8-C_8H_{16}$	-0.0277	-0.0310	...

Estimates of θ for the eight systems are all roughly similar in magnitude and indicate that the interaction between aromatic and alicyclic molecules is about 3% less than the mean of the interactions between like pairs. Partington, *et al.*,²⁸ reached a similar conclusion from a study of gas-liquid critical temperatures for a number of aromatic-aliphatic (both cyclic and noncyclic) systems. Values of θ calculated by different methods do not show parallel trends and evidently reflect to some degree the various assumptions and approximations inherent in the different approaches. It appears unwise at present to attribute differences in θ entirely to variations in the interaction energies.

(28) E. J. Partington, J. S. Rowlinson, and J. F. Weston, *Trans. Faraday Soc.*, 56, 479 (1960).

Solvent Effects on Charge-Transfer Complexes. II. Complexes of 1,3,5-Trinitrobenzene with Benzene, Mesitylene, Durene, Pentamethylbenzene, or Hexamethylbenzene¹

by C. C. Thompson, Jr.,

Department of Soils and Crops, Rutgers, The State University, New Brunswick, New Jersey

and P. A. D. de Maine

Department of Chemistry, University of California, Santa Barbara, California (Received March 23, 1966)

Formation constants (K), heats of formation (ΔH), and absorptivities (a_c) of 1:1 charge-transfer complexes of 1,3,5-trinitrobenzene with hexamethylbenzene, pentamethylbenzene, durene, mesitylene, or benzene dissolved in CCl_4 , n -hexane, n -heptane, cyclohexane, or CHCl_3 were calculated from spectroscopic data collected at 20 and 45° for a dozen wave lengths between 2800 and 4200 Å. K values for all complexes vary with solvent in the order: cyclohexane > n -heptane \approx n -hexane > CCl_4 > CHCl_3 , with a 10 to 20-fold variation in K in passing from cyclohexane to CHCl_3 at 20°. K is independent of wave length near the band maximum, but in some systems K increases at longer wave lengths, probably because of the simultaneous formation of 1:1 and higher order complexes.

Introduction

Although the effects of the solvent on formation constant, absorptivities, and heat of formation of charge-transfer complexes² have been noted for several systems, few quantitative studies of these effects have been made. Previously,³⁻⁷ reference has been made to recent literature pertaining to charge-transfer, contact charge-transfer, simultaneous complex formation, and solvent-shift theories. Literature concerned with complexes between aromatic nitro compounds and various donors has also been noted.^{3b,4}

As a natural consequence of the valence bond approach, Mulliken² has emphasized the importance of ionic contributions in charge-transfer complexes. Thus for a given complex the formation constant (K), absorptivities (a_c), and heat of formation (ΔH) should all increase if the electrical properties (dipole moment, dielectric constant, etc.) of the solvent are increased. In the Dewar-Lepley⁸ molecular orbital theory of charge-transfer, back coordination can nearly equal the charge transfer, and thus K , a_c , and ΔH can be virtually unaltered by a change in solvent.

In this work, complexes of 1,3,5-trinitrobenzene with each of benzene, mesitylene, durene, pentamethylbenzene, and hexamethylbenzene are studied with carbon tetrachloride, chloroform, n -hexane, n -heptane, and cyclohexane as solvents. Precise analytical treatment of the data was achieved by use of the self-judging method of curve fitting.⁹

(1) Taken from the Ph.D. Thesis of C. C. Thompson, Jr., University of Mississippi, 1964.

(2) R. S. Mulliken, *J. Am. Chem. Soc.*, **74**, 811 (1952); *J. Phys. Chem.*, **56**, 801 (1952).

(3) (a) C. C. Thompson, Jr., Ph.D. Thesis, University of Mississippi, 1964; (b) C. C. Thompson, Jr., and P. A. D. de Maine, *J. Am. Chem. Soc.*, **85**, 3096 (1963).

(4) N. B. Jurinski and P. A. D. de Maine, *ibid.*, **86**, 3217 (1964).

(5) N. B. Jurinski, Ph.D. Thesis, University of Mississippi, 1963.

(6) V. Ramakrishnan and P. A. D. de Maine, *J. Miss. Acad. Sci.*, **10**, 82 (1964).

(7) N. B. Jurinski, C. C. Thompson, Jr., and P. A. D. de Maine, *J. Inorg. Nucl. Chem.*, in press.

(8) M. J. S. Dewar and A. R. Lepley, *J. Am. Chem. Soc.*, **83**, 4560 (1961).

(9) P. A. D. de Maine and R. D. Seawright, "Digital Computer Programs for Physical Chemistry," The Macmillan Co., New York, N. Y.: (a) Vol. I, 1965; (b) Vol. II, 1965.

Table I: Details of the Systems Studied at 20 and 45°

System ^a	Wave length ^b range, Å.	Concn. ^c range, M	No. of samples	System ^a	Wave length ^b range, Å.	Concn. ^c range, M	No. of samples
TNB-CCl ₄	2700-4300	3.80×10^{-4} - 1.90×10^{-3}	9	PMB-TNB-CCl ₄	3400-4000	5.55×10^{-4}	18
TNB- <i>n</i> -C ₇ H ₁₆	2650-4300	1.63×10^{-4} - 8.17×10^{-4}	9	PMB-TNB- <i>n</i> -C ₇ H ₁₆	3400-4000	1.53×10^{-2} -0.230	18
TNB- <i>n</i> -C ₈ H ₁₄	2650-4300	1.71×10^{-4} - 8.55×10^{-4}	9	PMB-TNB- <i>n</i> -C ₈ H ₁₄	3400-4000	5.68×10^{-4}	18
TNB- <i>c</i> -C ₆ H ₁₂	2650-4300	1.75×10^{-4} - 8.75×10^{-4}	9	PMB-TNB- <i>n</i> -C ₆ H ₁₂	3400-4000	1.52×10^{-2} -0.228	18
TNB-CHCl ₃	2750-4200	4.51×10^{-4} - 2.26×10^{-3}	9	PMB-TNB- <i>c</i> -C ₆ H ₁₂	3400-4000	5.67×10^{-4}	18
HMB-CCl ₄	3600-4200	0.138-0.276	3 ^d	PMB-TNB- <i>c</i> -C ₈ H ₁₆	3400-4000	1.44×10^{-2} -0.217	18
HMB- <i>n</i> -C ₇ H ₁₆	3600-4200	0.171-0.342	3 ^d	PMB-TNB- <i>c</i> -C ₈ H ₁₆	3400-4000	5.61×10^{-4}	18
HMB- <i>n</i> -C ₈ H ₁₄	3600-4200	0.185-0.371	3 ^d	PMB-TNB-CHCl ₃	3400-4000	1.47×10^{-2} -0.220	18
HMB- <i>c</i> -C ₆ H ₁₂	3600-4200	0.152-0.305	3 ^d	PMB-TNB-CHCl ₃	3400-4000	1.08×10^{-3}	18
HMB-CHCl ₃	3600-4200	0.131-0.219	3 ^d	Dur-TNB-CCl ₄	3250-3800	2.17×10^{-2} -0.325	18
PMB-CCl ₄	3300-4000	3.96×10^{-2} -0.198	9	Dur-TNB-CCl ₄	3250-3800	5.64×10^{-4}	18
PMB- <i>n</i> -C ₇ H ₁₆	3300-4000	4.22×10^{-2} -0.211	9	Dur-TNB- <i>n</i> -C ₇ H ₁₆	3250-3800	1.61×10^{-2} -0.242	18
PMB- <i>n</i> -C ₈ H ₁₄	3300-4000	4.09×10^{-2} -0.204	9	Dur-TNB- <i>n</i> -C ₇ H ₁₆	3250-3800	5.81×10^{-4}	18
PMB- <i>c</i> -C ₆ H ₁₂	3300-4000	3.95×10^{-2} -0.198	9	Dur-TNB- <i>n</i> -C ₈ H ₁₄	3250-3800	1.68×10^{-3} -0.251	18
PMB-CHCl ₃	3400-4000	4.53×10^{-2} -0.227	9	Dur-TNB- <i>c</i> -C ₆ H ₁₂	3250-3800	5.62×10^{-4}	18
Dur-CCl ₄	3200-3800	5.56×10^{-2} -0.278	9	Dur-TNB-CHCl ₃	3250-3800	1.75×10^{-2} -0.262	18
Dur- <i>n</i> -C ₇ H ₁₆	3200-3800	5.45×10^{-2} -0.273	9	Dur-TNB-CHCl ₃	3250-3800	5.67×10^{-4}	18
Dur- <i>n</i> -C ₈ H ₁₄	3200-3800	5.43×10^{-2} -0.271	9	Dur-TNB-CHCl ₃	3250-3800	1.71×10^{-2} -0.256	18
Dur- <i>c</i> -C ₆ H ₁₂	3200-3800	5.51×10^{-2} -0.275	9	Mes-TNB-CCl ₄	3100-3700	1.17×10^{-3}	18
Dur-CHCl ₃	3250-3800	6.30×10^{-2} -0.315	9	Mes-TNB-CCl ₄	3100-3700	2.13×10^{-2} -0.320	18
Mes-CCl ₄	3100-3700	0.144-0.719	9	Mes-TNB- <i>n</i> -C ₇ H ₁₆	3100-3700	5.66×10^{-4}	18
Mes- <i>n</i> -C ₇ H ₁₆	3100-3700	0.144-0.719	9	Mes-TNB- <i>n</i> -C ₇ H ₁₆	3100-3700	3.59×10^{-2} -0.539	18
Mes- <i>n</i> -C ₈ H ₁₄	3100-3700	0.144-0.719	9	Mes-TNB- <i>n</i> -C ₈ H ₁₄	3100-3700	5.94×10^{-4}	18
Mes- <i>c</i> -C ₆ H ₁₂	3100-3700	0.144-0.719	9	Mes-TNB- <i>n</i> -C ₈ H ₁₄	3100-3700	3.60×10^{-2} -0.540	18
Mes-CHCl ₃	3100-3700	0.145-0.717	9	Mes-TNB- <i>c</i> -C ₆ H ₁₂	3100-3700	5.61×10^{-4}	18
Bz-CCl ₄	2750-3300	0.281-2.81	10	Mes-TNB- <i>c</i> -C ₆ H ₁₂	3100-3700	3.60×10^{-2} -0.539	18
Bz- <i>c</i> -C ₆ H ₁₂	2750-3300	0.281-2.81	10	Mes-TNB-CHCl ₃	3100-3700	5.65×10^{-4}	18
HMB-TNB-CCl ₄	3650-4200	5.75×10^{-4}	18	Mes-TNB-CHCl ₃	3100-3700	3.60×10^{-2} -0.539	18
HMB-TNB- <i>n</i> -C ₇ H ₁₆	3650-4200	1.62×10^{-2} -0.121	18	Bz-TNB-CCl ₄	2750-3300	1.02×10^{-3}	15
HMB-TNB- <i>n</i> -C ₈ H ₁₄	3650-4200	5.58×10^{-4}	18	Bz-TNB- <i>c</i> -C ₆ H ₁₂	2750-3300	7.19×10^{-2} -1.08	15
HMB-TNB- <i>c</i> -C ₆ H ₁₂	3650-4200	1.53×10^{-2} -0.115	18			8.35×10^{-4}	
HMB-TNB-CHCl ₃	3650-4200	5.69×10^{-4}	18			0.113-1.13	
		1.53×10^{-2} -0.115				5.71×10^{-4}	
		5.72×10^{-4}				0.113-1.13	
		7.42×10^{-4} -0.111					
		1.61×10^{-3}					
		9.70×10^{-4} -0.146					

^a Symbols used are: TNB, 1,3,5-trinitrobenzene; HMB, hexamethylbenzene; PMB, pentamethylbenzene; Dur, durene; Mes, mesitylene; Bz, benzene. ^b Measurements were made at 50-Å. intervals over the indicated wave length range. ^c For ternary systems the first concentration refers to TNB and the second to the donor. ^d Measured absorbance below 0.005 absorbance unit.

Experimental

All solid materials were Eastman Kodak reagent grade chemicals. 1,3,5-Trinitrobenzene (m.p. 121-122°) was recrystallized from Fisher Spectrograde methanol. Durene (m.p. 79-80°) and pentamethylbenzene (52-53.5°) were recrystallized from absolute ethanol. Hexamethylbenzene (m.p. 166-167°) was recrystallized from CCl₄.

Fisher Spectrograde benzene (b.p. 79.5-80.0°) and Eastman Kodak reagent mesitylene (b.p. 163.0-163.5°) were distilled through a Vigreux column in a system protected from atmospheric moisture. The distilled liquids were then purged with oxygen-free dry nitrogen (dew point less than -40°). Fisher Spectrograde CCl₄, *n*-hexane, *n*-heptane, and cyclohexane were purged with oxygen-free dry nitrogen immediately before use. Fisher Spectrograde CHCl₃ was purified as described previously^{3b,10} and then was

purged with nitrogen immediately before use. Solvent purity was checked with an Aerograph Hy-Fi Model 600 gas chromatograph.

The techniques of solution preparation and of measurement of the absorption spectra at 20 and 45° for selected wave lengths between 2650 and 4200 Å. have been described elsewhere.^{3b} The calibrated Beckman DU spectrophotometers^{3b} were equipped with photomultiplier tubes, temperature control accessories and four matched 1-cm. stoppered quartz cells. Pure solvent served as the reference. To within the limits of reproducibility, all systems except pentamethylbenzene-trinitrobenzene-chloroform were stable for at least 24 hr. Experimental details for the systems studied are given in Table I.

For each two-solute system, duplicates were pre-

(10) P. A. D. de Maine, *J. Chem. Phys.*, **26**, 1036 (1957).

pared from separate portions of the components for six of the eighteen solutions. On the basis of reproducibility of data and calibration results for the two spectrophotometers, an experimental error of less than 1% is claimed for the data here reported.

Data Processing Method

Data for the trinitrobenzene (TNB)-inert solvent and TNB-donor-inert solvent systems were processed by the self-judgment method^{9,11} as already described.^{3b} In the spectral region considered, donor-solvent solutions show low absorptivities, and values at each temperature and wave length were calculated without use of the self-judgment principle.

The data for the TNB-solvent systems were compatible with the equation

$$a_A = {}_0a_A + a_1[A] \quad (1)$$

where a_A is the absorptivity of the solute, A, whose molar concentration is denoted by $[A]$ and where ${}_0a_A$ and a_1 are constants for each temperature and wave length.

For the reversible reaction, $A + B \xrightleftharpoons{K} C$, the following equations can be derived

$$C_C = [KC_A + KC_B + 1 - \sqrt{(K^2(C_A - C_B)^2 + 2KC_A + 2KC_B + 1)}] / 2K \quad (2)$$

$$A_C = a_C C_C = A_0 - a_A(C_A - C_C) - a_B(C_B - C_C) \quad (3)$$

$$C_A C_B / A_C = 1 / K a_C + (C_A + C_B - C_C) / a_C \quad (4)$$

In these equations, C_A and C_B are initial concentrations of A and B, respectively; C_C is the equilibrium concentration of C; K is the formation constant; a_A , a_B , and a_C are absorptivities of A, B, and C, respectively; and A_C and A_0 are the absorbance due to the complex C and the measured absorbance, respectively. In the derivation of eq. 2, 3, and 4, it is assumed only that the law of mass action is obeyed. The assumptions common to earlier methods ($C_A \gg \gg C_B$; A and B obey Beer's law) are not made. In our calculations we have assumed that the complex, C, obeys Beer's law.

Equations 2, 3, and 4 were solved for K and a_C by an iterative method^{3b} with data at each wave length and temperature. Preselected^{3b,9} limits of experimental error (*i.e.*, $DEVF1 = DEVF2 = 0.01$) were used to compute an *error zone* for eq. 4 and data points outside this zone were discarded. From the error zone and the points within it was calculated the maximum permitted error (MPE) for the computed values of K and a_C .

In this paper the original definition of MPE^{3b,4,9a} has been retained. The more recent definition^{9b} makes the MPE values appreciably larger.

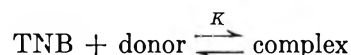
Results

The absorbance data for TNB-solvent systems are compatible with eq. 1 to within $\pm 1\%$. Details of the computer analysis for the TNB-solvent and donor-solvent systems have been given elsewhere.^{3a,12}

Attempts to study benzene-carbon tetrachloride mixtures were not entirely successful. For mixtures containing more than 50% by volume of benzene, oxygen absorbed during even careful handling produced erratic results.¹³ With less than 20% benzene band enhancement due to absorbed oxygen was not observed, even in samples prepared 24 hr. earlier. Thus only data for solutions with less than 20% benzene were used in our calculations.

The absorption for pentamethylbenzene-TNB- CHCl_3 solutions gradually increases with time. This phenomenon is especially pronounced at wave lengths below 3750 Å. but it is not found for the single solute systems. Thus only data from the 3750 to 4000-Å. region are used in calculating values reported in this paper.

New absorption bands with a single maximum in the 2800 to 3950-Å. region were observed in all TNB-donor-solvent systems. At each temperature and wave length the new data are compatible to within 1% with the 1:1 reaction



Mean formation constants (K) are given in Table II. Near the band maxima the values for K are independent of wave length for all donor-acceptor pairs studied. For most systems, K increases slightly at longer wave lengths, especially in paraffin solvents. Detailed numerical results for the ternary systems studied are given elsewhere.^{3a,14} Mean formation constants for the wave length invariant regions are given in Table III. In Table IV are given values for the mean heats of formation computed with the van't Hoff equation from values in Table III.

Plots of a_C , absorptivity of the complex, *vs.* wave length for each temperature and each system yielded a

(11) P. A. D. de Maine and R. D. Seawright, *Ind. Eng. Chem.*, **55**, 29 (1963).

(12) C. C. Thompson, Jr., and P. A. D. de Maine, *J. Miss. Acad. Sci.*, **10**, 123 (1964).

(13) D. F. Evans, *J. Chem. Soc.*, 345 (1953); 1351, 3885 (1957); 2753 (1959).

(14) C. C. Thompson, Jr., and P. A. D. de Maine, *J. Miss. Acad. Sci.*, **10**, 137 (1964).

Table II: Average Formation Constants (in l. mole⁻¹) for All Wave Lengths Studied

Donor ^a	Temp., °C.	CCl ₄	n-C ₇ H ₁₆	n-C ₈ H ₁₄	c-C ₆ H ₁₂	CHCl ₃
HMB	20	4.86 ± 0.18 ^b	14.69 ± 0.20	15.41 ± 0.39	17.50 ± 0.28	0.90 ± 0.15
	45	2.76 ± 0.10	8.70 ± 0.12	9.41 ± 0.10	9.78 ± 0.16	1.01 ± 0.14
PMB	20	3.09 ± 0.07	8.69 ± 0.12	8.91 ± 0.16	10.45 ± 0.10	1.02 ± 0.04
	45	2.28 ± 0.12	5.91 ± 0.08	5.98 ± 0.14	6.48 ± 0.10	0.85 ± 0.03
Dur	20	2.29 ± 0.07	5.77 ± 0.19	5.30 ± 0.10	6.02 ± 0.14	0.97 ± 0.26
	45	1.57 ± 0.13	3.91 ± 0.09	4.10 ± 0.11	4.18 ± 0.15	0.70 ± 0.25
Mes	20	1.36 ± 0.07	3.02 ± 0.12	2.76 ± 0.19	3.51 ± 0.06	0.17 ± 0.04
	45	1.00 ± 0.05	2.18 ± 0.05	2.26 ± 0.06	2.60 ± 0.06	0.12 ± 0.03
Bz	20	0.56 ± 0.06			0.88 ± 0.03	
	45	0.45 ± 0.09			0.77 ± 0.07	

^a Symbols for the donors are given in Table I. ^b Square-root-mean-square deviations.

Table III: Mean Formation Constants (in l. mole⁻¹) for Wave Length Invariant Regions

Donor ^a	Temp., °C.	CCl ₄	n-C ₇ H ₁₆	n-C ₈ H ₁₄	c-C ₆ H ₁₂	CHCl ₃
HMB	20	4.87 ± 0.08 ^b (9/12) ^c	14.82 ± 0.17 (7/12)	15.34 ± 0.18 (6/12)	17.50 ± 0.20 (8/12)	0.92 ± 0.10 (5/12)
	45	2.77 ± 0.08 (8/12)	8.92 ± 0.12 (6/12)	9.19 ± 0.13 (8/12)	9.70 ± 0.12 (6/12)	0.87 ± 0.09 (6/12)
PMB	20	3.08 ± 0.05 (7/13)	8.82 ± 0.11 (5/13)	8.82 ± 0.12 (6/13)	10.39 ± 0.13 (6/13)	0.98 ± 0.07 (5/7)
	45	2.22 ± 0.14 (8/13)	5.84 ± 0.09 (7/13)	5.90 ± 0.09 (7/13)	6.43 ± 0.09 (8/13)	0.85 ± 0.08 (7/7)
Dur	20	2.24 ± 0.09 (8/12)	5.76 ± 0.10 (6/12)	5.33 ± 0.09 (6/12)	5.97 ± 0.09 (7/12)	0.84 ± 0.11 (5/11)
	45	1.66 ± 0.11 (6/12)	3.86 ± 0.07 (7/12)	3.96 ± 0.07 (6/12)	4.13 ± 0.08 (5/12)	0.54 ± 0.11 (5/11)
Mes	20	1.34 ± 0.06 (8/13)	3.06 ± 0.05 (4/13)	2.81 ± 0.05 (5/13)	3.32 ± 0.06 (5/13)	0.13 ± 0.03 (6/13)
	45	0.92 ± 0.04 (5/13)	2.07 ± 0.04 (6/13)	2.21 ± 0.04 (6/13)	2.44 ± 0.05 (7/13)	0.08 ± 0.03 (5/13)
Bz	20	0.47 ± 0.02 (5/12)			0.81 ± 0.02 (5/12)	
	45	0.36 ± 0.03 (5/12)			0.66 ± 0.05 (4/12)	

^a Symbols for donors given in Table I. ^b Mean maximum permitted errors. ^c Number of wave lengths used in calculating K and total number of wave lengths studied.

single broad band with a poorly defined maximum. In Table V are given the maximum value of a_c and the corresponding wave length for each system.

Discussion

For each ternary system, the data near the charge-transfer band maximum are consistent with the existence of a single 1:1 complex. In part I^{3b} it was shown that the variation in the value of the formation con-

stant, K , with wave length for a fixed temperature cannot be attributed to neglect of unsuspected 1:1 interactions between donor and acceptor molecules themselves or with the solvent. Jurinski¹⁵ and Hayman¹⁶ have shown mathematically that the simultaneous formation of higher order complexes and

(15) N. B. Jurinski, *J. Miss. Acad. Sci.*, 10, 74 (1964).

(16) H. J. G. Hayman, *J. Chem. Phys.*, 37, 2290 (1962).

Table IV: Heats of Formation^a (kcal. mole)

Donor ^b	CCl ₄	<i>n</i> -C ₇ H ₁₆	<i>n</i> -C ₈ H ₁₈	<i>c</i> -C ₈ H ₁₈	CHCl ₃
HMB	-4.18 ± 0.18 ^c	-3.77 ± 0.18	-3.80 ± 0.19	-4.37 ± 0.18	-0.44 ± 1.63
PMB	-2.44 ± 0.61	-3.05 ± 0.20	-2.97 ± 0.21	-3.55 ± 0.20	-1.06 ± 1.20
Dur	-2.24 ± 0.80	-2.96 ± 0.27	-2.20 ± 0.26	-2.72 ± 0.25	-3.26 ± 1.95
Mes	-2.81 ± 0.69	-2.90 ± 0.25	-1.78 ± 0.27	-2.30 ± 0.27	-3.14 ± 4.65
Bz	-2.03 ± 0.92			-1.47 ± 0.70	

^a Calculated from mean formation constants at 20 and 45° listed in Table III. ^b Symbols for donors given in Table I. ^c Maximum permitted errors.

Table V: Maximum Molar Absorptivities and Wave Lengths of Band Maxima

Donor ^a	Temp., °C.	CCl ₄		<i>n</i> -C ₇ H ₁₆		<i>n</i> -C ₈ H ₁₈		<i>c</i> -C ₈ H ₁₈		CHCl ₃	
		ϵ_C	$\lambda_{max}, ^b \text{ \AA.}$	ϵ_C	$\lambda_{max}, ^b \text{ \AA.}$	ϵ_C	$\lambda_{max}, ^b \text{ \AA.}$	ϵ_C	$\lambda_{max}, ^b \text{ \AA.}$	ϵ_C	$\lambda_{max}, ^b \text{ \AA.}$
HMB	20	2565 ± 21 ^c	3920	2270 ± 1	3860	2229 ± 8	3880	2391 ± 38	3870	2374 ± 206	3890
	45	2565 ± 57	3920	2175 ± 8	3860	2190 ± 8	3860	2197 ± 24	3870	2089 ± 180	3880
PMB	20	2394 ± 16	3700	2140 ± 1	3620	2169 ± 1	3630	2180 ± 1	3650
	45	2260 ± 92	3690	2041 ± 5	3610	2079 ± 6	3620	2061 ± 4	3640
Dur	20	1966 ± 39	3430	1883 ± 3	3350	1940 ± 3	3350	1977 ± 1	3380	1537 ± 110	3390
	45	1886 ± 67	3430	1860 ± 6	3360	1831 ± 4	3350	1836 ± 5	3380	1899 ± 219	3390
Mes	20	2280 ± 49	3350	2220 ± 3	3300	2296 ± 4	3300	2205 ± 2	3300	6036 ± 955	3350
	45	2398 ± 60	3350	2229 ± 7	3300	2188 ± 8	3300	2082 ± 7	3300	7978 ± 1795	3350
Bz	20	3893 ± 80	2830					3867 ± 6	2800		
	45	4133 ± 152	2800					3775 ± 94	2770		

^a Symbols for donors are given in Table I. ^b Due to the broad absorption bands, the values given here are considered accurate to within ±20 Å. ^c Maximum permitted errors. ^d Time effect at short wave lengths.

1:1 species can account for the variation in value of K with wave length. Although exact computer methods^{9b} have been devised for resolution of data for a system with both 1:1 and 2:1 complexes, limited computer storage capacity prevented the treatment of the present data in this way.

For each donor-acceptor-solvent system, a change of the "inert" solvent effects drastic changes in the computed K values (Tables II and III) which, except for CHCl₃, are not reflected in the values for the heat of formation (Table IV). The absorptivity of the assumed 1:1 complex near the absorption maxima are approximately constant (Table V). Competitive donor-solvent complexes in CHCl₃, and possibly CCl₄, can block either the LN or TN donor orbital and thus reduce the apparent formation constant (K_Q) in these solvents.^{3b} Certainly, the variation in K_Q with solvent cannot be attributed solely to the assumption of ideality, to the neglect of higher complexes, or to changes in the average properties of the solvent environment.^{3b}

Variations in K_Q for hydrocarbon solvents can be explained qualitatively if it is supposed that the "short-range lattice structures" of the solvent, the molecular dimensions and the orbital symmetry of the interacting donor-acceptor pair, and the magnitude of the forces between the solute molecules themselves or with the solvent each play an important role in complex formation.¹⁷

Constants for the naphthalene-trinitrobenzene complex at 20° were found^{3b} to be 5.16 ± 0.07 , 9.15 ± 0.17 , and 1.82 ± 0.08 in CCl₄, cyclohexane, and CHCl₃, respectively. The K_Q for the hexamethylbenzene complex (Table III) is considerably greater than that for the naphthalene complex in cyclohexane (and other hydrocarbons), while for CCl₄ and CHCl₃ the order is reversed. These results indicate that CHCl₃ and CCl₄ are more effective in blocking complex sites of hexamethylbenzene. The importance of considering

(17) P. A. D. de Maine, *J. Chem. Phys.*, **26**, 1042, 1192 (1957); *J. Miss. Acad. Sci.*, **9**, 150 (1963).

solvent effects in comparisons of relative donor strengths is thus demonstrated.

For each solvent, except CHCl_3 , and a fixed temperature the absorptivities of the complex (a_c) (Table V) vary with donor thus: benzene > hexamethylbenzene > pentamethylbenzene > mesitylene > durene. The corresponding order for the formation constants (Table III) and (except for CCl_4 systems) for ΔH , heat of formation, (Table IV) is hexamethylbenzene > pentamethylbenzene > durene > mesitylene > benzene. If the comparatively large uncertainties in ΔH are considered it is possible that this order also applies for CCl_4 systems. Thus except for benzene, and either mesitylene or durene, the relative absorptivities are in the predicted order.² Higher values for a_c with mesitylene and benzene have been cited as evidence of contact charge transfer.¹⁸⁻²⁰ Contact charge-transfer theories predict that a_c should increase with temperature. In only four of the twenty-two systems studied did a_c increase with temperature (Table V) and in the remainder a_c was unchanged or decreased slightly.

The presence of isomeric 1:1 complexes can explain the temperature variations of a_c if it is supposed that back coordination charge-transfer bands⁸ are formed. Arguments to support this suggestion have already been presented.^{3b}

Plots of a_c vs. wave length (not shown) indicate that the durene complex has the broadest charge-transfer band with the lowest maximum absorptivity. Of the donors used in this study durene has the largest difference in energy of the e_{1g} orbitals.²¹ Thus, transitions involving these orbitals should occur at considerably different wave lengths to form a broad absorption band composed of the separate transitions. Several workers^{17,20,22,23} have pointed out that integrated band intensities should be used in comparing the relative absorption for a series of complexes.

For the systems reported here, the wave length of maximum absorption for a given complex varies with solvent thus: heptane \cong hexane < cyclohexane < CHCl_3 < CCl_4 . Foster²⁴ and Bhattacharya²⁵ have re-

ported similar results for various complexes in CCl_4 , CHCl_3 , and cyclohexane or heptane. The results cannot be explained in terms of average solvent properties alone, but they can be interpreted by the supposition that the formation of one isomeric complex is favored by the "structure of the solvent."

Time effects in the pentamethylbenzene-trinitrobenzene-chloroform system are similar to those reported previously for naphthalene-trinitrobenzene^{2b} and iodine-nitromethane²⁸ complexes. For the separate components dissolved in CHCl_3 no changes in the measured absorbance with time are observed. This behavior can be attributed to reactions of the pentamethylbenzene-chloroform complex to yield products which subsequently interact with the trinitrobenzene molecules.

It seems that theories which predict more extensive complexing in polar solvents and which emphasize the importance of nonspecific solvent-solute interactions are incorrect in principle.

In conclusion, it can be said that charge-transfer theories which do not consider the role of the solvent are inadequate.

Acknowledgments. Financial support for this work was provided by the United States Air Force under Grant No. AF-AFOSR 62-19, monitored by the Directorate of Chemical Sciences, Air Force Office of Scientific Research. C. C. T. wishes to thank the National Science Foundation for the award of Cooperative Graduate Fellowships.

(18) L. E. Orgel and R. S. Mulliken, *J. Am. Chem. Soc.*, **79**, 4839 (1957).

(19) S. P. McGlynn, *Chem. Rev.*, **58**, 1113 (1958).

(20) J. N. Murrell, *Quart. Rev. (London)*, **15**, 191 (1961).

(21) L. E. Orgel, *J. Chem. Phys.*, **23**, 1352 (1955).

(22) S. F. Mason, *Quart. Rev. (London)*, **15**, 287 (1961).

(23) R. S. Mulliken and W. B. Person, *Ann. Rev. Phys. Chem.*, **13**, 107 (1962).

(24) R. Foster, *J. Chem. Soc.*, 1075 (1960).

(25) R. Bhattacharya, *J. Chem. Phys.*, **30**, 1367 (1959).

(26) P. A. D. de Maine and W. C. Ahlers, *J. Chem. Soc.*, 211 (1960).

Kinetics of the Reactions of Elemental Fluorine. IV. Fluorination of Graphite

by A. K. Kuriakose and J. L. Margrave

Department of Chemistry, Rice University, Houston, Texas (Received March 25, 1965)

The reaction of graphite with fluorine has been investigated between 315 and 900° at various fluorine partial pressures ranging from 6.5 to 75 torr in helium. Graphite gains weight in fluorine at temperatures between 315 and 530° linearly because of the formation of the solid intercalation compound poly(carbon monofluoride) (C_xF_x), while above 600° it loses weight with the formation of only gaseous fluorides. Between 530 and 600°, there is an overlapping of the two types of reactions. At all the temperatures, the reaction rate is proportional to the fluorine partial pressure. An activation energy of 42.5 kcal./mole is calculated for the reaction forming poly(carbon monofluoride) between 315 and 400°, and the dissociation of fluorine on the graphite surface by chemisorption is believed to be the rate-determining step in this process. From 400 to 900° the Arrhenius plots are discontinuous, and two other regions with activation energies 2 and 2.5 kcal./mole are observed in the temperature ranges 400–493 and 650–900°, respectively. Diffusion mechanisms seem to operate in these temperature ranges.

Amorphous forms of carbon burn in fluorine at room temperature, but graphite and diamond are not attacked by fluorine at ordinary temperatures.¹ Ruff and Bretschneider² seem to be the first to have found that around 420° graphite reacts with fluorine to form a gray solid which they called carbon monofluoride (C_xF_x). From 460 to 700° the reaction is sometimes explosive, and above 700° graphite burns in fluorine with the production of fluorocarbons, mainly CF_4 . Later work by Rüdorff and Rüdorff^{3–5} showed that, depending on the temperature (between 410 to 550°) and the particle size of graphite, various compositions from $CF_{0.68}$ to $CF_{0.988}$ could be obtained and that hydrogen fluoride was a catalyst in the reaction. The same authors^{5,6} also synthesized another solid product of composition approximately C_4F in the presence of fluorine and hydrogen fluoride at temperatures below 75°. Very recently, Watanabe, *et al.*,⁷ have also reported the formation of carbon monofluoride from graphite and fluorine in the temperature range 300–500°. As a continuation of studies on the kinetics of the reactions of elemental fluorine, the fluorination rate of graphite was measured under various conditions of temperature and fluorine pressure. The term poly(carbon monofluoride) will be used for the solid carbon monofluoride in order to distinguish it from the gaseous CF .

Experimental

The apparatus and general experimental procedures have been described earlier.⁸ The only modification was that, for runs below 600°, a small aluminum or nickel cup was attached beneath the graphite samples in order to collect any falling particles from the specimen, and the sample, together with the cup, was suspended from the quartz spring balance. The reaction rates of the aluminum or nickel cups were negligibly small compared to the fluorination rate of graphite at the low temperatures.

The samples were cut from a single spectroscopically pure graphite electrode, about 9 mm. in diameter, manufactured by the National Carbon Co. The circular pieces, about 2 mm. thick, were polished on abrasive

(1) H. Moissan, *Compt. rend.*, **110**, 276 (1890); *Ann. chim. phys.*, [6] **24**, 242 (1891).

(2) O. Ruff and O. Bretschneider, *Z. anorg. allgem. Chem.*, **217**, 1 (1934).

(3) W. Rüdorff and G. Rüdorff, *ibid.*, **253**, 281 (1947).

(4) W. Rüdorff and G. Rüdorff, *Chem. Ber.*, **80**, 413 (1947).

(5) W. Rüdorff, *Advan. Inorg. Chem. Radiochem.*, **1**, 230 (1959).

(6) W. Rüdorff and G. Rüdorff, *Chem. Ber.*, **80**, 417 (1947).

(7) N. Watanabe, Y. Koyama, and S. Yoshizawa, *Denki Kagaku*, **31**, 756 (1963); *J. Electrochem. Soc. Japan*, **31** (4), 187 (1963).

(8) A. K. Kuriakose and J. L. Margrave, *J. Phys. Chem.*, **68**, 290 (1964).

Table I: Kinetic Data on the Graphite-Fluorine Reaction

Temp., °C.	P_{F_2} , torr	k_1 , mg./cm. ² min. of graphite	Remarks	Temp., °C.	P_{F_2} , torr	k_1 , mg./cm. ² min. of graphite	Remarks
315	13.2	0.008	Wt. gain	486	30.6	1.066	Wt. gain
315	52.5	0.020	Wt. gain	486	52.5	1.722	Wt. gain
315	74.7	0.028	Wt. gain	486	74.7	2.456	Wt. gain
333	13.2	0.017	Wt. gain	493	13.2	0.656	Wt. gain
333	52.5	0.045	Wt. gain	493	30.6	1.151	Wt. gain
333	74.7	0.087	Wt. gain	493	52.5	1.829	Wt. gain
360	13.2	0.123	Wt. gain	493	74.7	2.249	Wt. gain
360	13.2	0.136	Wt. gain	530	13.2	0.533	Wt. gain
360	21.2	0.210	Wt. gain	530	30.6	0.810	Wt. gain
360	30.6	0.328	Wt. gain	530	52.5	1.447	Wt. gain
360	52.5	0.476	Wt. gain	530	74.7	1.877	Wt. gain
360	52.5	0.439	Wt. gain	570	13.2	...	Nonlinear
360	74.7	0.820	Wt. gain	570	30.6	...	Nonlinear
396	2.8	0.263	Wt. gain	570	35.5	...	No weight change
396	13.2	0.451	Wt. gain				
396	30.6	0.861	Wt. gain	570	52.5	...	Wt. loss, nonlinear
396	52.5	1.105	Wt. gain	570	74.7	...	Wt. loss, nonlinear
396	74.7	1.658	Wt. gain	600	6.5	0.327	Wt. loss, nonlinear
411	13.2	0.557	Wt. gain	600	6.5	0.286	Wt. loss, nonlinear
411	30.6	0.710	Wt. gain	600	13.2	0.655	Wt. loss, nonlinear
411	52.5	1.579	Wt. gain	600	30.6	1.027	Wt. loss, nonlinear
411	74.7	2.672	Wt. gain	600	52.5	1.917	Wt. loss, nonlinear
422	13.2	0.573	Wt. gain	650	6.5	0.525	Wt. loss, nonlinear
422	30.6	0.932	Wt. gain	650	13.2	1.040	Wt. loss, nonlinear
446	13.2	0.585	Wt. gain	650	30.6	2.400	Wt. loss, nonlinear
446	30.6	1.149	Wt. gain	650	52.5	3.647	Wt. loss, nonlinear
446	52.5	1.666	Wt. gain	700	6.5	0.557	Wt. loss, nonlinear
446	74.7	2.267	Wt. gain	700	13.2	1.093	Wt. loss, nonlinear
464	13.2	0.609	Wt. gain	750	6.5	0.625	Wt. loss, nonlinear
464	30.6	1.081	Wt. gain	750	13.2	1.192	Wt. loss, nonlinear
464	52.5	1.710	Wt. gain	800	6.5	0.652	Wt. loss, nonlinear
464	74.7	2.239	Wt. gain	800	13.2	1.324	Wt. loss, nonlinear
486	13.2	0.567	Wt. gain	900	6.5	0.673	Wt. loss, nonlinear
				900	13.2	1.500	Wt. loss, nonlinear

cloth and finally on ordinary cloth. The surfaces were then cleaned with a blast of air to remove any adhering loose particles. The areas of the specimens were calculated from average micrometer readings of the diameter and thickness.

Results and Discussion

No measurable reaction occurred between graphite and fluorine up to about 300° and 1 atm. fluorine pressure. Detectable reaction started at about 315° at a low fluorine pressure of 13.2 torr, and the kinetic studies were carried out between 315 and 900°.

The reaction rate was linear under all experimental conditions except for an initial fast spurt which might be the reaction of residual graphite dust still within the pores of the graphite. The linear rate constants were calculated only after the fast reaction had subsided. After taking the necessary kinetic readings at

the required fluorine partial pressure, the fluorination was completed by increasing the fluorine pressure to 1 atm. From the weight gain data, up to about 530°, carbon monofluoride with compositions ranging from $CF_{0.65}$ to $CF_{0.8}$ was the product with the higher fluorine content being obtained at the higher temperature. The product was collected in the attached cup and was gray in color. A small quantity of the product was obtained also at 600° which was white in color. An infrared spectrum of the product showed a single absorption band at 1220 cm^{-1} characteristic of the poly(carbon monofluoride).^{5,9}

The kinetic data on the fluorination of graphite from 315 to 900° are presented in Table I. The rate constants are given in terms of the graphite reacted in $mg./cm.^2$ min. Figure 1 is an Arrhenius plot of the

(9) W. Rüdorff and K. Brodersen, *Z. Naturforsch.*, 12b, 595 (1957).

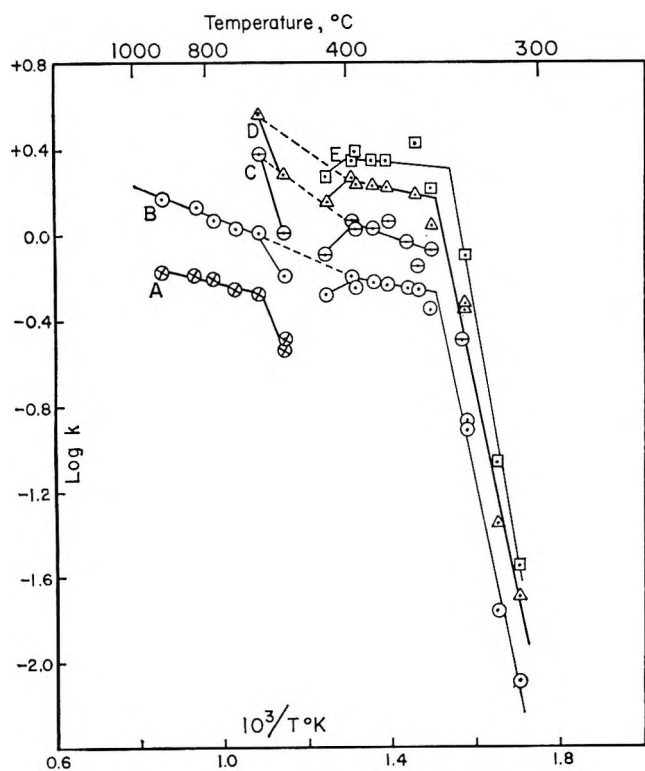


Figure 1. Arrhenius plot for the fluorination of graphite at various fluorine partial pressures with He: A, \otimes , 6.5; B, \circ , 13.2; C, \ominus , 30.6; D, \triangle , 52.5; E, \square , 74.7 torr.

results at various fluorine partial pressures in helium and shows a family of nearly parallel curves with breaks at particular temperatures. Up to 530°, the points represent weight gain, and above 600°, weight loss data. From 315 to about 400°, there is a rapid increase in the reaction rate while the rate between 410 and 493 is rather insensitive to temperature. There is a slight decrease in the rate at about 530° using the weight gain data which indicates that poly(carbon monofluoride) and volatile products are being formed simultaneously at this temperature. Above 650° no solid products are observed, and the reaction rate remains rather insensitive to temperature up to 900°, the highest temperature investigated.

The breaks in the curves may be attributed to changes in the mechanism of the fluorination of graphite. From 315 to 400° the reaction seems to be chemisorption controlled because of the relatively high activation energy, 42.5 kcal./mole, obtained in this temperature range. This also suggests that the activated complex involves dissociation of fluorine on the graphite surface since the dissociation energy of fluorine, 37.7 kcal./mole, is very close to the observed activation energy, as was the case in the fluorination of boron.¹⁰ A mechanism of this type readily explains the formation

of poly(carbon monofluoride). Between 410 and 493° the activation energy is only 2 kcal./mole although the product is still mainly poly(carbon monofluoride). Why the activation energy drops in this temperature range is not quite clear. The diffusion of fluorine through the graphite pores may be the rate-determining step under these conditions, and, also, gas phase diffusion is becoming significant since mass spectrometric studies have shown that the monofluoride decomposes partly in this temperature region. The low activation energy of 2.5 kcal./mole between 650 and 900° definitely means that gas phase diffusion of fluorine to the graphite surface through the CF_4 product gas is the rate-limiting process in the high-temperature range.

Variation of the fluorine partial pressure between 2.8 and 74.7 torr in helium showed that throughout the temperature range studied, the reaction rate was directly proportional to the fluorine pressure. However, the behavior of the reaction at 570° is interesting. Up to a fluorine partial pressure of 30.6 torr the graphite gains weight, although nonlinearly, and above 40.5 torr it loses weight, while in the region of about 35 torr it neither loses nor gains. The reason for this is that under the latter conditions the rate of formation of poly(carbon monofluoride) is equal to the rate of formation of volatile products.

The temperatures corresponding to the breaks in the Arrhenius plots seem to be independent of the fluorine partial pressure. This shows that surface temperature changes during the formation of poly(carbon monofluoride) are not detectable under low fluorine partial pressure conditions. There are no data on the heat of reaction of fluorine with graphite to form C_nF_n , but for $1/n(\text{C}_n\text{F}_n)$ it should be more positive than one-fourth of the heat of formation of CF_4 , i.e., the exothermicity of the reaction would be less than 55 kcal./mole. Table II shows the graphite surface temperature rises for various fluorine partial pressures at a furnace temperature of 790°, as observed with an optical pyrometer, with samples of nearly identical dimensions (surface area $\approx 2 \text{ cm.}^2$; weight $\approx 0.25 \text{ g.}$). The reaction product is mainly $\text{CF}_4(\text{g})$. If the fluorination rates at 400 to 500° are approximately one-third to one-half of the rate at 800°, then the graphite surface temperature increase in the 400 to 500° range should be about one-tenth of the surface temperature increase at 800° for any particular fluorine partial pressure, assuming that the temperature rise is directly proportional to the rate constant. At a partial pressure of 13.2 torr, thus, the surface temperature

(10) A. K. Kuriakose and J. L. Margrave, *J. Phys. Chem.*, **68**, 2671 (1964).

effects would be comparable with the experimental error of temperature measurement ($\pm 1^\circ$). Therefore, no corrections are necessary for the temperatures with $P_{F_2} = 13.2$ torr, and the calculated activation

energies are valid for the fluorination of graphite at this partial pressure. At higher fluorine pressures, there will be correspondingly greater surface effects, and temperature corrections may be significant. However, the lack of thermochemical data on C_nF_n precludes quantitative corrections, and one expects them to be small since the monofluoride detaches itself from the graphite surface as soon as it is formed at the higher temperatures.

Table II: Surface Temperatures of Graphite in Various Fluorine Partial Pressures at a Furnace Temperature of 790°

P_{F_2} , torr	Surface temp., $^\circ\text{C}$.	Temp. rise, $^\circ\text{C}$.
0	790	0
2.8	795	5
6.5	800	10
13.2	810	20
52.5	890	100
74.7	940	150

Acknowledgment. This work was supported by the Aeronautical Research Laboratory, Wright Air Development Division, United States Air Force, in part, under a subcontract with A. D. Little, Inc., administered by Dr. Leslie A. McClaine.

The Reaction of Triphenylphosphine with Alkali Metals in Tetrahydrofuran¹

by A. D. Britt and E. T. Kaiser²

Department of Chemistry, University of Chicago, Chicago 37, Illinois (Received March 29, 1965)

The first reaction of triphenylphosphine with alkali metals which has been detected is a phenyl cleavage rather than formation of the triphenylphosphine negative ion. Radical formation occurs in a second reaction when the metal diphenylphosphine produced by the first reaction is reduced by additional metal. The resultant radical has the formula $(C_6H_5)_2PM^\cdot$, as identified by electron spin resonance and chemical tests.

Introduction

The reaction of triphenylphosphine $((C_6H_5)_3P)$ and alkali metals in tetrahydrofuran (THF) has been reported to produce the mononegative ion $((C_6H_5)_3P^-)$, identified by its electron spin resonance (e.s.r.) spectrum.³ Since the phenyl cleavage of $(C_6H_5)_3P$ by alkali metals in THF is a well-known reaction,⁴⁻⁶ the nature of this reported radical has been reinvestigated.

The reaction was studied as a function of the concentration of $(C_6H_5)_3P$ for each of the following alkali metals: K, Na, and Li. The course of the reaction was determined by chemical tests and e.s.r.

Experimental

Materials. The solvents and metals were purified and the solutions prepared in the usual way.^{7,8} Com-

(1) Grateful acknowledgment is made to the donors of the Petroleum Research Fund for support of this research.

(2) To whom inquiries regarding this article should be made.

(3) M. W. Hanna, *J. Chem. Phys.*, **37**, 685 (1962).

(4) D. Wittenberg and H. Gilman, *J. Org. Chem.*, **23**, 1063 (1958).

(5) K. Issleib and H. O. Frohlich, *Z. Naturforsch.*, **14b**, 349 (1959).

(6) A. M. Aguir, J. Beisler, and A. Mills, *J. Org. Chem.*, **27**, 1001 (1962).

(7) D. E. Paul, D. Lipkin, and S. I. Weissman, *J. Am. Chem. Soc.*, **78**, 116 (1956).

mercial triphenylphosphine was recrystallized from diethyl ether to yield white plates melting at 80° (lit.⁹ m.p. 80°). Diphenylphosphine was prepared from diphenylchlorophosphine ((C₆H₅)₂PCl).¹⁰ The diphenylphosphine was obtained as a colorless oil, b.p. 69–71° at 0.3 mm. Samples were stored in evacuated break-seals.

Determination of Biphenyl Concentration. The possibility that biphenyl might be formed in the reaction of (C₆H₅)₃P with alkali metals was investigated. For the determination of biphenyl, the following procedure was used. The solutions resulting from the reaction of (C₆H₅)₃P with alkali metals were opened to air and transferred to 25-ml. flasks. Five milliliters of 0.1 N HCl was added dropwise to each solution followed by 10 μl. of diphenylmethane. The THF was slowly evaporated at 40° until the volume of the mixture corresponded to approximately 5 ml. The solutions were then extracted with benzene, and the benzene extract was dried over Na₂SO₄ and slowly evaporated to a small volume (1 or 2 drops). Aliquots were then analyzed by vapor phase chromatography.

Two standard samples were also analyzed by this procedure: one consisted of 10.5 mg. of biphenyl and the other was 10.5 mg. of biphenyl which was first reduced *in vacuo* to the biphenyl negative ion (determined by e.s.r.). Results on both samples showed that biphenyl and diphenylmethane are carried through the analysis procedure in the same weight ratio as their initial weight ratio. Therefore, the final ratio of biphenyl to diphenylmethane together with the known initial concentration of diphenylmethane can be used to provide a good estimate for the maximum concentration of biphenyl in the triphenylphosphine-alkali metal reaction mixtures.

Results and Discussion

The reaction of (C₆H₅)₃P with K in THF was first studied as a function of the concentration of (C₆H₅)₃P. Variation of the initial concentration of (C₆H₅)₃P over the range 7×10^{-5} to 2×10^{-1} M established the presence of two distinct reactions. Below 10^{-3} M (C₆H₅)₃P, the reaction yields products which are yellow-green in solution and which give no e.s.r. signal. From 10^{-3} to 10^{-2} M (C₆H₅)₃P, a second reaction occurs, yielding products which are orange-red in solution and which give the e.s.r. spectrum previously reported for (C₆H₅)₃P^{•-}.³ This spectrum was recorded at -20° and is shown in Figure 1.

The concentration range of (C₆H₅)₃P which was found to be most convenient for study was 10^{-2} to 10^{-1} M. Careful treatment with the alkali metal permits the reaction either to be stopped at the first

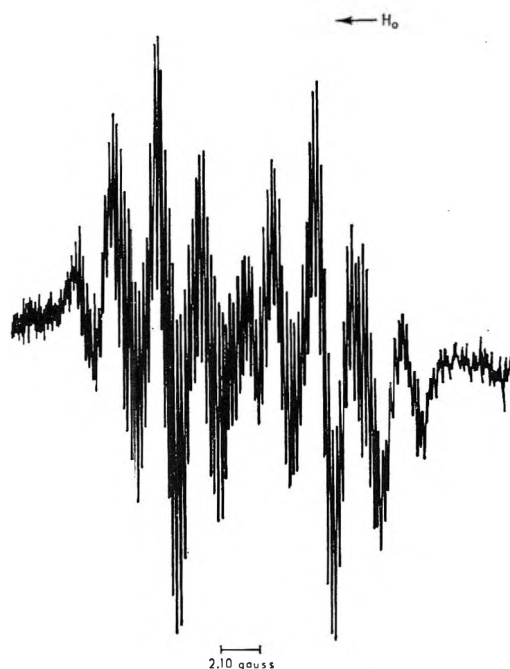


Figure 1. E.s.r. spectrum of (C₆H₅)₂PK⁻ at -20°.

stage or carried further to the second stage. If the reaction is stopped at the first stage and the yellow-green solution is removed from the metal, then the orange-red color cannot be obtained either by concentration of the solution or by addition of unreacted (C₆H₅)₃P. Therefore, the second reaction appears to occur between the metal and the products of the first reaction, rather than with (C₆H₅)₃P directly.

The possibility that a one-step reduction might occur at a lower reaction temperature was investigated. Independent variation of the reaction temperature over the range -60 to 25° showed no change in the two-reaction sequence apart from longer reaction times at lower temperatures. The products of the first reaction did not appear unstable with respect to temperature. The radical obtained in the second stage of K reduction was relatively stable at -20°, but slowly decomposed above that temperature.

Opening the solutions to air caused rapid conversion of the orange-red color back to the yellow-green color, which was thereby intensified. Treatment with aqueous acid and subsequent analysis yielded the types of products described for the phenyl cleavage reaction.⁴⁻⁶ The phenyl cleavage products were obtained regardless

(8) P. Balk, G. J. Hoijtink, and J. W. H. Schreurs, *Rec. trav. chim.*, **76**, 813 (1957).

(9) I. Heilbron, Ed., "Dictionary of Organic Compounds," Oxford University Press, London, 1953.

(10) F. G. Mann and J. T. Millar, *J. Chem. Soc.*, 4453 (1952).

tion level of $(C_6H_5)_3P$ necessary for radical production, and final products were the same with Li, Na, and K. However, the lithium and sodium diphenylphosphine negative ions differed from the potassium diphenylphosphine negative ion in two important respects—temperature stability and e.s.r. spectra. Both $(C_6H_5)_2PLi^-$ and $(C_6H_5)_2PNa^-$ appeared unstable above -50° .

The e.s.r. spectrum of $(C_6H_5)_2PLi^-$ at -65° showed two main groups of three broad lines each. The splitting between the centers of the main groups was about 8 gauss; the splitting between the three broad lines in each group was about 2 gauss. The crude outline of the $(C_6H_5)_2PK^-$ spectrum is therefore seen with $(C_6H_5)_2PLi^-$. Attempts to resolve the spectrum further showed additional unresolved splittings in each of these six lines. To the extent to which these additional splittings could be resolved, great variations in line width were observed (0.2–0.5 gauss).

The e.s.r. spectrum of $(C_6H_5)_2PNa^-$ at -65° showed essentially one broad derivative curve covering the entire spectrum. The peak-to-trough splitting was about 8 gauss. Under high resolution, 8–9 unresolved lines were seen on each side of the spectrum. To the extent to which these 16–18 lines could be resolved, great variations in line width were observed (0.2–1.0 gauss).

The nature of this effect remains to be established. However, we would speculate on the effect in the following way. The K radical derivative is relatively stable at -20° ; simple replacement by Na or Li at the metal-phosphorus bond might alter the temperature stability by a few degrees, but not as drastically as is observed. This might indicate the possibility of intramolecular rearrangement to different configurations with the metal at a different location, for example, one of the *para* positions. With the K derivative, the principal configuration involves a P–K bond; with the smaller Li and Na, other configurations might also be present in appreciable percentages. These other configurations could serve as an avenue for temperature instability. In addition, such intramolecular exchange of the metal atom to positions in the two rings could produce great variations in the proton line widths, as is observed.¹²

Once the e.s.r. spectra of the Li, Na, and K derivatives were obtained, the nature of the radical could be subjected to a third test, direct preparation by means of reaction 2 in the absence of $(C_6H_5)_3P$. For this test, $(C_6H_5)_2PH$ was prepared and treated with Li, Na, and K. The initial reaction of $(C_6H_5)_2PH$ with the alkali metal led to formation of a yellow-green solution which gave no e.s.r. signal.

The solution was outgassed to eliminate H_2 and then concentrated. No orange-red color or e.s.r. signal was obtained. The concentrated solution was then diluted back to its original volume and treated further with the alkali metal. An orange-red solution was obtained which gave an e.s.r. spectrum identical with the e.s.r. spectrum of the corresponding metal derivative of $(C_6H_5)_3P$. These results prove that the radical is produced from $(C_6H_5)_2PM$, not $(C_6H_5)_3P$, and therefore support the two-reaction sequence.

An additional point was investigated concerning the nature of the $(C_6H_5)_2PM^-$ radical. It is known that the metal is closely associated in $(C_6H_5)_2PM$.¹³ One might reasonably assume that the metal is even more strongly associated in the corresponding negative ion $-(C_6H_5)_2PM^-$. Therefore, it should be difficult to dissociate the species and obtain the e.s.r. spectrum of the $(C_6H_5)_2P^\equiv$ ion.

Two experiments were performed to explore this point. In the first experiment, a $K-(C_6H_5)_3P$ reaction was performed in 1,2-dimethoxyethane, and a radical spectrum identical with Figure 1 was obtained at -20° . The second experiment was more extreme, involving a $Na-(C_6H_5)_3P$ reaction in liquid NH_3 . Na was chosen because it was the most effective alkali metal in terms of obscuring the basic spectrum. Correspondingly, the greatest difference should be seen between $(C_6H_5)_2PM^-$ and $(C_6H_5)_2P^\equiv$ if Na is used.

The e.s.r. spectrum of the radical produced in liquid NH_3 was recorded at -65° and was identical with the $(C_6H_5)_2PNa^-$ spectrum in THF at -65° . Use of other alkali metals or different temperatures might disclose appreciable dissociation, but this does not appear likely. We found no alterations in e.s.r. spectra over temperature ranges consistent with the stability of the $(C_6H_5)_2PM^-$ radicals.

Attempts were made to investigate possible intermolecular exchange by measurements of line broadening as a function of temperature. The e.s.r. spectra of the Na and Li derivatives were scanned from -50 to 25° and the e.s.r. spectrum of the K derivative from -20 to 25° . Broadening occurred in all cases, but the intensity of the signal also decreased rapidly with increasing temperature. For this reason, the broadening cannot be attributed solely to some intermolecular exchange process. In any event, the narrow lines in Figure 1 demonstrate that for the $(C_6H_5)_2PK^-$ system at -20° , any intermolecular exchange reaction possesses a half-time longer than the range of half-times which may be observed by e.s.r. line broadening.

(12) E. DeBoer and E. L. Mackor, *J. Am. Chem. Soc.*, **86**, 1513 (1964).

(13) K. Issleib and A. Tzschach, *Chem. Ber.*, **92**, 1118 (1959).

Finally, since the formation of biphenyl from the reaction of $(C_6H_5)_nX_m$ species (where X is a heteroatom) with alkali metals is a fairly common occurrence and can cause complications in the interpretation of e.s.r. spectra, it was considered of interest to analyze several of the radical-containing solutions for biphenyl. An estimate of the maximum concentration of biphenyl which might be present was obtained. It was in the

range $2-5 \times 10^{-6} M$ for the various metal radical solutions. Therefore, the effect of biphenyl was considered to be negligible.

Acknowledgments. We wish to express our appreciation to Professor S. I. Weissman for his help in obtaining several of the spectra. We also thank Mr. T. F. Wulfers and Mr. P. L. Hall for their aid in the vapor phase chromatographic analysis.

NOTES

On the Chlorophyllide-Sensitized Reduction of Azobenzene and Other Compounds

by G. R. Seely

Contribution No. 185 from the Charles F. Kettering Research Laboratory, Yellow Springs, Ohio (Received February 8, 1965)

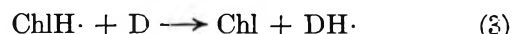
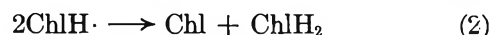
We have found¹ that the reduction of phenosafranine by hydrazobenzene in ethanol-pyridine mixtures, photosensitized by ethyl chlorophyllide *a*, is not retarded by one of its products, azobenzene, at $1.7 \times 10^{-4} M$. This suggested that excited chlorophyllide, Chl^* , reacts much faster with phenosafranine than with azobenzene.

We have now found that azobenzene at the same concentration almost completely prevents the photochemical reduction of ethyl chlorophyllide by ascorbic acid in ethanol-pyridine mixtures.^{2,3} At a lower azobenzene concentration ($4 \times 10^{-6} M$), where the reduction of chlorophyllide is still strongly retarded, the loss of azobenzene can be followed by the decline of absorptivity at 335 $m\mu$. As the azobenzene disappears, the reduction of chlorophyllide is accelerated. Without ascorbic acid there is no loss of azobenzene; there is no reaction in the dark. Livingston and Pariser reported that chlorophyll sensitized the photoreduction of azobenzene by phenylhydrazine, but not by ascorbic acid, in methanol solution.⁴

It seemed likely that azobenzene was reduced to hydrazobenzene in this reaction. To see whether this was so, or whether azobenzene was converted to

some other product, we tried hydrazobenzene as a reductant, in 1:6 ethanol:pyridine containing 0.05 *M* benzoic acid. (Hydrazobenzene is inert as a reductant for Chl^* in ethanol-pyridine mixtures, unless acid is present.) As expected, the absorption at 335 $m\mu$ did not remain constant or decrease but slowly increased by an amount commensurate with the amount of chlorophyllide reduced.

We believe that azobenzene is reduced by the radical $ChlH\cdot$ formed in the reduction of chlorophyllide⁵ for the following reasons. Azobenzene and $ChlH_2$, the stable photoreduction product of chlorophyllide (absorption maximum at 525 $m\mu$),² coexist in the dark without reaction, which rules out $ChlH_2$ as the effective reducing agent. Increasing the ascorbic acid concentration from 2×10^{-3} to $2 \times 10^{-2} M$ accelerates both the reduction of chlorophyllide and the reduction of azobenzene, but the former more than the latter. This is compatible with the mechanism (I)



D and AH_2 represent the oxidant and the reductant, in this case azobenzene and ascorbic acid. The product of step 1 is written $ChlH\cdot$ because transfer of a

(1) G. R. Seely, *J. Phys. Chem.*, **69**, 2633 (1965).

(2) A. A. Krasnovskii, *Dokl. Akad. Nauk SSSR*, **60**, 421 (1948).

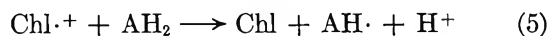
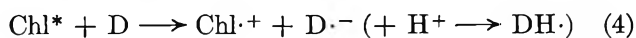
(3) G. R. Seely and A. Folkmanis, *J. Am. Chem. Soc.*, **86**, 2763 (1964).

(4) R. Livingston and R. Pariser, *ibid.*, **78**, 2948 (1956).

(5) V. B. Evstigneev and V. A. Gavrilova, *Dokl. Akad. Nauk SSSR*, **92**, 381 (1953).

proton to chlorophyll appears to be indispensable for its photoreduction by ascorbic acid.³ The quantum yield of reduction of azobenzene is not more than about twice that of reduction of chlorophyllide in the absence of azobenzene. Reduction of azobenzene is slow and incomplete in ethanol without pyridine, as is the reduction of chlorophyllide.³

The ethyl chlorophyllide sensitized reduction of the azo dye, methyl red, by ascorbic acid, hydrazobenzene, and mercaptosuccinic acid in ethanol goes by a different mechanism (II)⁶



Other compounds for which there is evidence of photoreduction by this mechanism are phenosafranine,¹ quinones,⁷⁻⁹ pyocyanine, and phenazine methosulfate.⁹

The existence of different mechanisms for the sensitized reduction of two such apparently similar compounds as azobenzene and methyl red gives rise to the question of which mechanism operates in other cases. They differ in that mechanism I requires conditions under which the sensitizer is reduced. In practice, this means that hydrazobenzene and mercaptans are much less effective than ascorbic acid in (I). Ascorbic acid in ethanol, without base, is active in (II) but not in (I). Hydrazobenzene is active in (I) only in the presence of acid (*e.g.*, pyridinium benzoate).

With ascorbic acid in pyridine-ethanol, the bimolecular rate constant for step 1 is $1.8 \times 10^6 M^{-1} \text{sec}^{-1}$,³ but the rate constant for step 4 is around $10^9 M^{-1} \text{sec}^{-1}$ in those cases studied.^{1,6,10} The disparity is so great that (I) can only be seen when (II) is inoperative. With ascorbic acid, quantum yields by (I) are typically $\sim 10^{-2}$ or less, whereas initial quantum yields by (II) are typically $\sim 10^{-1}$ or more; however, exceptions must be expected.

We now attempt to decide by which mechanism chlorophyll and related compounds perform some of the sensitized reductions reported in the literature.

Livingston and Pariser noted a considerable difference in the kinetics of the sensitized reductions of methyl red¹¹ and butter yellow.¹² We have found that methyl orange (butter yellow sulfonate) is reduced in much the same way as is azobenzene, and we therefore assign (I) to it and to butter yellow. In the reduction of butter yellow, the role of dimethylaminoaniline is probably that of activating base¹³ for the reduction of pheophytin.

The description of the reduction of fast red S (2-hydroxy-1,1'-azonaphthalene-4'-sulfonic acid, sodium

salt) by chlorophyllin in water certainly supports the mechanism (I) assigned to it.¹⁴ However, we have found that fast red S is reduced by hydrazobenzene in ethanol, ethyl chlorophyllide as sensitizer, with a similar quantum yield ($\sim 10^{-3}$). Mechanism I is inoperative under these conditions. It is possible that the mechanism depends on the solvent or the sensitizer or that the dye reacts *via* (II) only in its quinone-hydrazone tautomeric form. (The maximum absorption in water was at $480 m\mu$ ¹⁴; in ethanol, $510 m\mu$.)

Thionine¹⁵ and riboflavin¹⁶ are probably reduced by ascorbic acid *via* (II) because of the high quantum yield. For riboflavin, this conclusion is supported by e.s.r. measurements.¹⁷ Safranin T is reduced *via* (II), analogously to phenosafranine.^{16,18} The bacteriochlorophyll-sensitized reduction of ubiquinone by reduced phenazine methosulfate¹⁹ probably goes *via* (II).

We found that triphenyltetrazolium chloride ($1.6 \times 10^{-4} M$) was reduced rapidly by both ascorbic acid ($4.1 \times 10^{-3} M$) and hydrazobenzene ($3.7 \times 10^{-3} M$) in 15 vol. % aqueous pyridine, with ethyl chlorophyllide as sensitizer. The complications encountered with hydrazine²⁰ were absent in these systems. This salt and probably also tetrazolium blue²¹ are reduced by (II).

The sensitized reduction of pyridine nucleotides²²⁻²⁶

-
- (6) G. R. Seely, *J. Phys. Chem.*, **69**, 821 (1965).
 (7) A. A. Krasnovskii and N. N. Drozdova, *Dokl. Akad. Nauk SSSR*, **150**, 1378 (1963); **158**, 730 (1964).
 (8) G. Tollin and G. Green, *Biochim. Biophys. Acta*, **60**, 524 (1962).
 (9) B. Ke, L. P. Vernon, and E. R. Shaw, *Biochemistry*, **4**, 137 (1965).
 (10) E. Fujimori and R. Livingston, *Nature*, **180**, 1036 (1957).
 (11) R. Livingston and R. Pariser, *J. Am. Chem. Soc.*, **70**, 1510 (1948).
 (12) R. Livingston and R. Pariser, *ibid.*, **78**, 2944 (1956).
 (13) A. A. Krasnovskii, G. P. Brin, and K. K. Voinovskaya, *Dokl. Akad. Nauk SSSR*, **69**, 393 (1949).
 (14) G. Oster, J. S. Bellin, and S. B. Brody, *J. Am. Chem. Soc.*, **86**, 1313 (1964).
 (15) K. G. Mathai and E. Rabinowitch, *J. Phys. Chem.*, **66**, 954 (1962).
 (16) A. A. Krasnovskii, *Dokl. Akad. Nauk SSSR*, **61**, 91 (1948).
 (17) G. Tollin and G. Green, *Biochim. Biophys. Acta*, **66**, 308 (1963).
 (18) T. T. Bannister, *Photochem. Photobiol.*, **2**, 519 (1963).
 (19) W. S. Zaugg, L. P. Vernon, and A. Tirpack, *Proc. Natl. Acad. Sci.*, **51**, 232 (1964).
 (20) E. Fujimori, *J. Am. Chem. Soc.*, **77**, 6495 (1955).
 (21) L. P. Vernon, *Acta Chem. Scand.*, **15**, 1639 (1961).
 (22) A. A. Krasnovskii and G. P. Brin, *Dokl. Akad. Nauk SSSR*, **67**, 325 (1949).
 (23) G. P. Brin and A. A. Krasnovskii, *Biokhimiya*, **24**, 1085 (1959).
 (24) T. T. Bannister and J. E. Bernardini, *Biochim. Biophys. Acta*, **59**, 188 (1962).
 (25) L. P. Vernon, A. San Pietro, and D. A. Limbach, *Arch. Biochem. Biophys.*, **109**, 92 (1965).
 (26) A. A. Krasnovskii, G. P. Brin, and N. N. Drozdova, *Dokl. Akad. Nauk SSSR*, **150**, 1157 (1963).

Table I: Conditions of Chlorophyll-Sensitized Reductions of Various Oxidants, and Mechanisms Assigned. Comparison with Oxidation-Reduction Potentials at pH 7 (E_7) and Polarographic Half-Wave Potentials ($E_{1/2}$), vs. Saturated Calomel Electrode

Oxidant	$E_{1/2}$ (s.c.e.) ^a	E_7^b	Conditions of sensitized reduction			Mechanism	Ref. ^f
			Sensitizer ^c	Reductant ^d	Solvent ^e		
Phenazine methosulfate	-0.07, -0.32 ^g	+0.08	Chl	...	eth	II	9
Pyocyanine	-0.20 ^g	-0.03	Chl	...	eth	II	9
1,4-Benzoquinone ^h	-0.21	(+0.30)	Chl	...	eth-gly, -70°	II	7
1,4-Benzoquinone			Chl	...	EPA, -150°	II	8
Thionine	-0.29	+0.06	Chl	asc	30% aq. pyr	II	15
Methyl red, neutral	-0.32 ⁱ	...	Chld	asc, hzb, msa	eth	II	6
Methyl red, neutral			Chl	phen	meth	II	11
Safranine T	-0.33, -0.59, ^j -0.80, 0.91	-0.29	Chl	asc	aq. pyr	II	16, 18
Ubiquinone 6	-0.35	(+0.13)	Chl	...	eth	II	9
Ubiquinone 6			Chl	...	EPA, -150°	II	8
9,10-Phenanthrenequinone	-0.39	(+0.06)	Chl	...	EPA, -150°	II	8
Trimethylbenzoquinone	-0.42	(+0.11)	Chl	...	eth	II	9
Triphenyltetrazolium chloride	-0.43, -0.80 ^k	...	Chld	asc, hzb	15% aq. pyr	II ^l	0
Triphenyltetrazolium chloride			Chl	hydrazine	meth	II	20
Menadione	-0.52	(+0.01)	Chl	...	eth-gly, -70°	II	7
Riboflavin	-0.55	-0.19	Chl	asc	pyr	II	16
Riboflavin			Pheo2-HCl	...	eth	II	17
Phenosafranine	-0.60	-0.25	Chld	hzb	eth-pyr	II	1
Fast red S	(-0.35), ^m -0.80, -1.04	...	Chln	asc	water	I(?)	14
Fast red S			Chld	hzb	eth	II	0
Azobenzene	-0.91	...	Chld	asc	eth-pyr	I	0
Azobenzene			Chl	phen	meth	I	4
NAD	-1.01, -1.36 ^g	-0.31	Chl	asc	aq. pyr, NH ₃	I	26
NAD			Chld	asc	15% aq. pyr, NH ₃	I	0
Methyl orange, basic	-1.05 ⁿ	...	Chld	asc	eth-pyr	I	0
Butter yellow	-1.09	...	Pheo	asc	meth	I	12
Methyl red, basic	-1.10 ⁱ	...	Chld	hzb	eth	? ^o	6

^a Measured in deaerated 7:2:1 ethanol:water:pyridine, containing 0.1 M LiClO₄ as electrolyte and 0.02% polyvinylpyrrolidone as maximum suppressor; pH 8.2. ^b Taken from W. M. Clark, "Oxidation-Reduction Potentials of Organic Systems," Williams and Wilkins Co., Baltimore, Md., 1960. Quinone potentials are not measurable at pH 7; values listed parenthetically are $E_0 - 0.414$. ^c Chl = chlorophyll, Chld = ethyl chlorophyllide, Chln = chlorophyllin, Pheo = pheophytin. ^d asc = ascorbic acid, hzb = hydrazobenzene, msa = mercaptosuccinic acid, phen = phenylhydrazine. Where no reductant is given, the reversible interaction of sensitizer with oxidant was followed directly by e.s.r. or visible absorption changes. ^e eth = ethanol, gly = glycerol, pyr = pyridine, meth = methanol, EPA = ether:isopentane:ethanol, 8:3:5 (by volume). ^f "0" refers to present paper. ^g Appear to be one-electron reductions, from low relative values of diffusion current. ^h Benzoquinone and other quinones may have reacted with the solvent before polarograms could be made. However, all quinones gave single, two-electron reduction waves. ⁱ The wave ascribed to the neutral form of methyl red is suppressed by addition of KOH, and the wave ascribed to the basic form exalted. ^j Safranine O (K & L Laboratories) gave four small, overlapping waves, all together barely equal to a single, two-electron reduction step. ^k Both appear to be two-electron steps; second probably represents reduction of the formazan. ^l Reduction to the formazan is by mechanism II, but the formazan was not further reduced. ^m The three waves had current ratios of 3:15:10. The first, small wave may be from an impurity or from the quinonehydrazone form. Allied Chemical Corp. sample. ⁿ Starting material was the acidic (zwitterionic) form of methyl orange. This showed, in addition to the wave for the basic form, a wave at -0.55 v., suppressed by added KOH and ascribed to the acidic form. ^o We detected reversible reduction of the basic form of methyl red, even with hydrazobenzene as reductant. It is not clear whether chlorophyllide reacts with the basic form itself or with a small amount of neutral form in equilibrium with it.

is particularly important because it occurs during photosynthesis. The fact that reduction of chlorophyll often accompanies sensitized reduction of nucleotide by ascorbic acid *in vitro*²²⁻²⁴ supports the original assignment of mechanism I to this reaction.²² We found further support for this assignment. NAD

(β -nicotinamide adenine diphosphate, Sigma, 98% assay) at 1.2×10^{-3} M in 15% aqueous pyridine, 0.1 M in ammonia,^{23,26} is reduced smoothly by ascorbic acid, 4×10^{-3} M, in a chlorophyllide-sensitized reaction. The generation of NADH was followed by the growth of its band at 340 m μ , and after precipita-

tion of reaction products²³ the presence of NADH was verified by comparison of the fluorescence spectrum with that of an authentic sample. However, when hydrazobenzene was used in place of ascorbic acid, the rate of formation of NADH, measured at 340 μ , was less than 1% of that found with ascorbic acid. The inability of hydrazobenzene to replace ascorbic acid under these conditions is concordant with (I) but not with (II).

There is a close relation between the mechanism by which an oxidant is reduced and the polarographic half-wave potential of the oxidant. Table I summarizes reported conditions of sensitized reduction of a number of oxidants and lists the oxidation-reduction potential (when known) and the polarographic half-wave potentials determined by us for each oxidant. Those oxidants for which mechanism I had been assigned (yellow azo dyes and NAD) are all reduced at 0.9 v. or more below the s.c.e. Those oxidants for which (II) had been assigned are reduced at potentials 0.6 v. or less below the s.c.e.

All oxidants were polarographed in a 7:2:1 mixture of 95% ethanol:water:pyridine of pH 8.2, containing 0.1 *M* LiClO₄ as electrolyte, with a Sargent Model XXI polarograph, over a 2-v. range below the s.c.e. Good polarograms were obtained for all oxidants except the two safranine dyes, which noticeably adsorbed to surfaces. Oxidant concentrations were around 10⁻³ *M*, or lower for the more surface-active dyes. For riboflavin, phenosafranine, and thionine the difference between E_7 and $E_{1/2}$ (s.c.e.) is about 0.35 v.; this may be regarded tentatively as the difference between $E_{1/2}$ values, measured under the present conditions, and potentials on the hydrogen scale (pH 7).

Acknowledgment. The technical assistance of Mr. D. Stoltz is gratefully acknowledged. The work was supported in part by National Science Foundation Grant No. GB-2089.

Diffusion in Deuterio-Normal Hydrocarbon Mixtures

by J. D. Birkett and P. A. Lyons

Department of Chemistry, Yale University, New Haven, Connecticut
(Received March 31, 1965)

Self-diffusion coefficients for hydrocarbons deriving from fairly precise, absolute measurements might be

useful additions to the literature. In this laboratory, they are needed for the understanding of the details of binary diffusion for simple nonaqueous systems. Encouraged by Longsworth's success with D₂O-H₂O solutions, it was decided to measure tracer diffusion coefficients for a number of hydrocarbons using the Rayleigh interferometric procedure.¹

Experimental

The modified Rayleigh-Philpot-Cook interferometer² used is equivalent to an unfolded Spinco electrophoresis unit. With minor changes we have used the equipment in the manner described by Longsworth.³

The cost of deuterated compounds limited any series of experiments on a given hydrocarbon to the use of a total of 5 ml. of the deuterated species. Therefore a small Pyrocell electrophoresis cell with channel length 6.302 mm. was used for this work. In the particular cell chosen, the optical flats which constitute the faces of the cell extend about 3 mm. beyond the channel. The original purpose for this override was to provide compensation in the reference optical path which passed immediately adjacent to the cell channel through a temperature-controlled bath. By cementing a drilled plate against these overlapping optical flats a small auxiliary chamber was formed which could be filled with a reference liquid (in these experiments the appropriate undeuterated hydrocarbon).

"Non-Aq" was used as a cell lubricant precluding the use of a water thermostat. Fortunately, the experiments were performed in an isolated basement laboratory. Using large circulating fans behind controlled electric heaters, it was possible to maintain the room at 25° for long periods within $\pm 0.1^\circ$ after preliminary equilibration. During the course of a given experiment (about 2 hr.) temperature variations were rarely greater than $\pm 0.05^\circ$.

Since the deuterated compound was to be reused, the sharpening procedure used was a bit unconventional. It was performed by manual operation of a screw linked to the piston of a 10-ml. syringe. Sharpening was interrupted for about 10 min. after the boundary had been brought on axis and about 2 ml. had been removed. The deuterated material from all sources remaining at the end of one experiment was reused in another diffusion run against the pure normal hydrocarbon and this procedure was repeated until the refractive increment became too small for further work.

Viscosities for the final accumulated dilute mixtures

- (1) L. G. Longsworth, *J. Phys. Chem.*, **58**, 771 (1954).
- (2) J. St. J. Philpot and G. H. Cook, *Research*, **1**, 234 (1948).
- (3) L. G. Longsworth, *J. Am. Chem. Soc.*, **74**, 4155 (1952).

were measured in a Cannon-Fenske viscometer. As evident in Table I, the viscosity of the benzene mixture is lower than a value inferred from precise viscosity studies which we assume to be definitive. Viscosities were assumed to vary linearly with concentrations. Relative concentrations were estimated using a Zeiss differential refractometer.

Table I

	x_D^a	η/η^0_H	$D\eta/\eta^0_H$	Average ($\times 10^6$)	Other values ($\times 10^6$)	
Benzene	0.5	1.00 ₅	2.15×10^{-6}			
	0.39 ₉	1.00 ₃	2.14×10^{-6}			
	0.25 ₃	1.00 ₂	2.14×10^{-6}	2.14		
				2.19 ^f	2.15 ^b	2.21 ^c
					2.25 ^d	2.1 ^e
Cyclo- hexane	0.5	1.02	1.42×10^{-6}			
	0.34 ₇	1.02	1.42×10^{-6}			
	0.27 ₁	1.01	1.41×10^{-6}			
	0.21 ₁	1.01	1.42×10^{-6}	1.42	1.4 ^e	
				1.42 ^f	1.43 ^g	
Isooctane	0.5	1.01 ₅	2.26×10^{-6}			
	0.31 ₈	1.01	2.31×10^{-6}			
	0.19 ₀	1.00 ₆	2.27×10^{-6}	2.28		
<i>n</i> -Heptane	0.5	1.03	3.07×10^{-6}			
	0.27 ₈	1.02	3.09×10^{-6}			
	0.21 ₅	1.01	3.15×10^{-6}	3.10	3.1 ^e	

^a Mole fraction deuterated species assuming $x_D = 1$ of original.

^b K. Graupner and E. P. S. Winter, *J. Chem. Soc.*, 1145 (1952).

^c R. E. Rathbun and A. L. Babb, *J. Phys. Chem.*, **65**, 1072 (1961).

^d R. Mills, *ibid.*, **67**, 600 (1963). ^e D. W. McCall, D. C. Douglas, and E. W. Anderson, *J. Chem. Phys.*, **31**, 1555 (1959). ^f Calculated using viscosities given by J. A. Dixon and W. Schiessler, *J. Phys. Chem.*, **58**, 430 (1954). ^g M. V. Kulkarni, G. F. Allen, and P. A. Lyons, *ibid.*, **69**, 2491 (1965).

Materials. The deuterated compounds used, isooctane, benzene, cyclohexane, and *n*-heptane, were obtained from Merck Sharpe and Dohme, Montreal. The only recognized problem was a 0.3% low boiling component in the isooctane sample (as estimated by vapor chromatography); this was assumed to introduce no significant error. The undeuterated *n*-heptane and isooctane were Phillips research grade; Fisher Certified reagent benzene and cyclohexane were used. All compounds were used without further purification.

In Table I are listed the values for the tracer diffusion coefficients at various mean concentrations. They have been corrected for the difference in viscosity relative to pure undeuterated hydrocarbon.

Representative data from other sources are included. It is interesting to note the disparity between the values for benzene. It is evident that the corrected value based on viscosity data of Dixon and Schiessler agrees very well with other measurements. For cyclo-

hexane all data are consistent. For the other hydrocarbons the order of magnitude of the viscosity correction is what would be expected; the value for benzene in this work appears to be incorrect. All of the values (except the benzene value with the suspected viscosity correction) are consistent with precise binary diffusion data obtained in this laboratory.

Within the experimental error, which would appear to be about $\pm 1\%$, the corrected quantities are independent of the concentration of the deuterated species. The invariance of $D\eta/\eta^0_H$ with concentration is what would be expected in the nearly ideal case.⁴ Thus, if

$$D\eta/\eta^0_H = (x_H D_D + x_D D_H)\eta/\eta^0_H$$

(where x_H is the mole fraction of the normal hydrocarbon and D_H is its intrinsic diffusion coefficient at that concentration with corresponding notation for the deuterated species) we may identify the limiting value of D_H with the average of the values of $D\eta/\eta^0_H$ assuming, in keeping with the data, the equality and constancy of D_D and D_H . Viewed in this way, these data illustrate striking explicit examples of ideal diffusion in binary mixtures.

Given a sufficient quantity of a deuterated compound, better precision would be possible (to an optimum of about $\pm 0.2\%$) when a slight variation of $D\eta/\eta^0_H$ with concentration might be apparent. Certainly the availability of a large amount of deuterated hydrocarbon would permit a more rational extrapolation to zero concentration of the normal hydrocarbon (lim $D\eta/\eta^0_H$ is the quantity to be determined).

Acknowledgment. This work was supported by Atomic Energy Commission Contract AT(30-1)-1375.

(4) G. S. Hartley and J. Crank, *Trans. Faraday Soc.*, **45**, 801 (1949).

Diffusion in the System Cyclohexane-Benzene

by L. Rodwin, J. A. Harpst, and P. A. Lyons

Department of Chemistry, Yale University, New Haven, Connecticut (Received March 31, 1965)

For binary nonaqueous solutions showing only a slight deviation from ideality, it has been proposed that diffusion data may be described by the Hartley-Crank relation¹

(1) G. S. Hartley and J. Crank, *Trans. Faraday Soc.*, **45**, 801 (1949).

$$D = \frac{RT}{N\eta} \frac{d \ln f_1 x_1}{d \ln x_1} \left[\frac{x_1}{\sigma_2} + \frac{x_2}{\sigma_1} \right]$$

if the frictional coefficients, σ_i , for each component at given mole fractions, x_i , are evaluated from a straight line joining the measured values at $x_i = 0$ and $x_i = 1$.²

At $x_i = 0$, σ_i may be obtained from the limiting value of the binary diffusion coefficient as $x_i \rightarrow 0$. At $x_i = 1$, σ_i may be obtained from a self-diffusion experiment. This procedure fits the carbon tetrachloride-cyclohexane system very well.³

Whereas a linear approximation for the σ_i terms may be the normal first-order approximation, deviations from this simple rule are to be expected for systems showing larger deviations from ideality. In particular, in systems with large positive deviations from ideality, diffusive mobilities relative to viscosity may be expected to be high with correspondingly abnormally low frictional coefficients.⁴

Data for the system cyclohexane-benzene support this thesis. They are listed in Table I together with auxiliary data of interest in predicting the results.

Table I

Diffusion data		Auxiliary data		
$x_{C_6H_{12}}$	$D \times 10^6$	$x_{C_6H_{12}}$	Density, g./ml.	Viscosity, cp.
0.0100	2.090	0.0407	0.86765	0.5938
0.0501	2.044	0.0977	0.85963	0.5871
0.0911	1.999	0.1489	0.85291	0.5839
0.1101	1.978	0.1991	0.84648	0.5810
0.2000	1.903	0.3011	0.83424	0.5852
0.3017	1.845	0.3991	0.82282	0.5953
0.3658	1.822	0.4987	0.81322	0.6127
0.3961	1.815	0.6017	0.80344	0.6403
0.5205	1.796	0.6986	0.79503	0.6783
0.6418	1.799	0.8006	0.78688	0.7301
0.7795	1.829	0.8959	0.77992	0.7929
0.9299	1.866	0.9313	0.77757	0.8219
0.9800	1.876	0.9638	0.77530	0.8484
		0.9864	0.77398	0.8732

Diffusion measurements were made using the Gouy technique.^{5,6} A twin-armed pycnometer was used to measure densities. Viscosities were obtained with a Cannon-Fenske viscometer. The self-diffusion coefficients quoted derive from Rayleigh measurements on the interdiffusion of the deuterated and ordinary hydrocarbons.⁷

In very dilute solutions, σ for the solute can be calculated precisely from measured binary diffusion coefficients since the term involving the solvent co-

efficient is very small and can be obtained from the linear approximation rule. Thus in dilute solutions the deviation of the solute frictional coefficient from the linear approximation can be determined. Calling

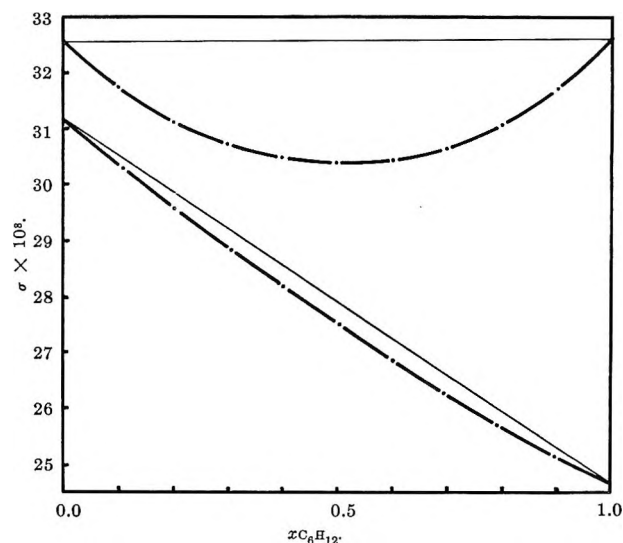


Figure 1. Frictional coefficients (σ) vs. mole fraction: upper curve, $\sigma_{C_6H_{12}}$; lower curve, $\sigma_{C_6H_6}$.

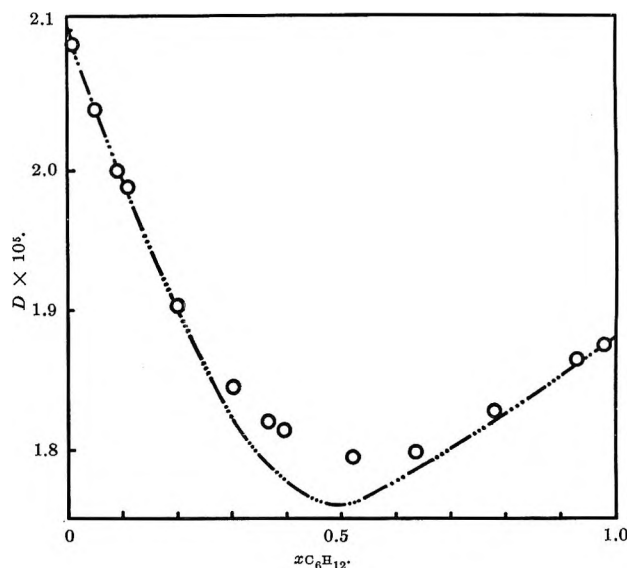


Figure 2. Diffusion curves; circles are measured values ($\pm 0.2\%$); broken curve represents values calculated from σ values in Table II.

(2) J. A. Harpst, Thesis, Yale University, 1962.

(3) M. V. Kulkarni, G. F. Allen, and P. A. Lyons, *J. Phys. Chem.*, **69**, 2491 (1965).

(4) L. Onsager, *Ann. N. Y. Acad. Sci.*, **46**, 241 (1945).

(5) L. G. Longworth, *J. Am. Chem. Soc.*, **69**, 2510 (1947).

(6) G. Kegeles and L. J. Gosting, *ibid.*, **69**, 2516 (1947).

(7) J. D. Birkett and P. A. Lyons, *J. Phys. Chem.*, **69**, 2782 (1965).

σ_{APP} the value predicted by the linear rule and $\Delta\sigma$ the deviation from the predicted value, the relative deviation $\Delta\sigma/\sigma_{\text{APP}}$ in dilute solutions is proportional to the corresponding quantity $\Delta\eta/\eta_{\text{APP}}$. (In the system $\text{C}_6\text{H}_6\text{-C}_6\text{H}_{12}$ the volume change on mixing is positive; the frictional coefficients are lower than the linear first-order approximation.)

If the dilute solution behavior, $\Delta\sigma/\sigma_{\text{APP}} = k\Delta\eta/\eta_{\text{APP}}$, is assumed to hold at all concentrations, values of σ_i for each component can be predicted at all concentrations; they are displayed in Figure 1 and listed in Table II.

These σ terms may be used in the Hartley-Crank equation to compute binary diffusion coefficients over the entire range of concentrations. The comparison with measured values is in Table II. The agreement, apparent in Figure 2, is very good, approaching the experimental accuracy of the thermodynamic term and optical self-diffusion data.

Table II

x_c	Q^a	η	$\sigma_c \times 10^8$	$\sigma_B \times 10^8$	$D_{\text{calc}} \times 10^6$	$D_{\text{obsd}} \times 10^6$
0.0	1.000	0.601	32.54	31.26	2.104	2.104
0.1	0.896	0.587	31.70	30.42	1.989	1.988
0.2	0.828	0.581	31.10	29.63	1.905	1.903
0.3	0.780	0.585	30.71	28.90	1.821	1.846
0.4	0.758	0.595	30.46	28.20	1.777	1.813
0.5	0.758	0.614	30.40	27.53	1.759	1.798
0.6	0.780	0.640	30.43	26.88	1.779	1.796
0.7	0.816	0.679	30.67	26.27	1.802	1.810
0.8	0.864	0.730	31.09	25.70	1.829	1.834
0.9	0.924	0.797	31.71	25.15	1.857	1.859
1.0	1.000	0.888	32.63	24.65	1.880	1.880

^a $Q = [1 + (\partial \ln f_i / \partial \ln x_i)]$.

The success of the second-order approximation for evaluating σ values is probably not as impressive as it appears at first glance. This empirical device only demonstrates the internal consistency of the diffusion data. It may be observed that the linear approximation predicts results fairly well, with a maximum discrepancy of about 6%; this second approximation cuts the discrepancy by a factor of three. Finally, despite the satisfactory numerical agreement there is a discernible trend in the data; calculated diffusion coefficients are slightly lower than measurements. It will, nonetheless, be a matter of some interest to discover the limit of the range of applicability of this simple rule.

Acknowledgment. This work was supported in part by Atomic Energy Commission Contract AT(30-1)-1375.

On the Compressibility of Molten Alkali Halides

by E. L. Heric

Department of Chemistry, University of Georgia, Athens, Georgia
(Received February 10, 1965)

Among similar compounds the isothermal compressibility, $\beta = -(1/V)(\partial V/\partial P)_T$, may vary considerably. Thus, among the alkali halides experimental values¹ range at 800° from 28.6 to 82.7 $\times 10^{-12}$ cm.² dyne⁻¹ for lithium chloride and cesium bromide, respectively. The work from which these values were obtained is unusually comprehensive. A number of the alkali halides were omitted, however, and the estimation of β for several of these from β vs. ion size plots is not feasible. There is, in general, a paucity of β data for molten salts, and a simple correlation between the values in a series of related compounds is desirable. Such a relationship is reported here for the alkali halides, being the ratio of β to the molal volume, V . Thus, the quantity is the compressibility per unit volume.

Table I lists the β/V ratios at 200° intervals for 12 alkali halides. Ten of these represent experimentally measured¹ values of β . RbCl and RbBr β values were obtained by the present author through interpolation from well-defined, isothermal plots of β vs. cation radius for alkali chlorides and bromides.¹ V values were obtained from the data of Jaeger,² except for LiBr from the data of Yaffe and Van Artsdalen.³ The temperatures included in Table I for the alkali halides cover the range of their fusion temperatures. Thus, many of the β/V values correspond to a supercooled liquid state. Those β values were obtained by interpolation of plots of compressibility vs. temperature. For this purpose the data of Bockris and Richards were combined with those of Bridgman⁴ at or near room temperature. The latter data are actually adiabatic compressibilities rather than isothermal, but at those low temperatures the difference between the two comparatively small values is not significant to the present conclusions.

It is evident from Table I that at a given temperature β/V is constant within an average deviation of

(1) J. O'M. Bockris and N. E. Richards, *Proc. Roy. Soc. (London)*, **A241**, 44 (1957).

(2) F. M. Jaeger, *Z. anorg. allgem. Chem.*, **101**, 1 (1917).

(3) I. S. Yaffe and E. R. Van Artsdalen, *J. Phys. Chem.*, **60**, 1128 (1956).

(4) P. W. Bridgman, *Proc. Am. Acad. Arts Sci.*, **67**, 345 (1932).

Table I: $10^{12} \beta/V$ in Ergs⁻¹ at the Indicated Celsius Temperatures

	400°	600°	800°	1000°
LiCl	0.48	0.66	0.85	1.03
LiBr	0.46	0.64	0.80	0.99
NaCl	0.43	0.58	0.76	1.01
NaBr	0.42	0.59	0.75	0.93
NaI	0.47	0.64	0.82	1.04
KCl	0.42	0.58	0.78	1.02
KBr	0.43	0.59	0.76	1.00
KI	0.44	0.62	0.84	1.12
RbCl ^a	0.39	0.55	0.75	0.99
RbBr ^a	0.45	0.63	0.82	1.09
CsCl	0.43	0.60	0.80	1.09
CsBr	0.48	0.68	0.92	1.28
Av. = av. dev.	0.44 ± 0.02	0.61 ± 0.03	0.80 ± 0.04	1.05 ± 0.06
		300°	500°	
LiNC ₃		0.50	0.69	
NaN ₃		0.40	0.56	
KNO ₃		0.36	0.51	

^a β not determined experimentally (see text).

about 5%, which is only a little greater than the maximum error of 3.5% in the β data.¹ While there is some disagreement between the density data in the two sources,^{2,3} the effect on β/V is negligible. Also assumed negligible is the uncertainty introduced by extrapolation of the density data to supercooled liquid temperatures.

There appears to be no consistent relationship between deviations from the mean β/V and the ratios of cation to anion radius. Moreover, the data of Bridgman⁴ show a well defined continuity between compressibility and anion radius for the halides of each alkali metal. Accordingly, it seems reasonable to assume that the alkali fluorides and the other four alkali halides missing in the data of Bockris and Richards have β/V values consistent with those of the remaining species listed in Table I.

The extent of constancy among the alkali halides in Table I reflects a similarity in the temperature coefficients of β and V . Whether this arises mainly from the similar electronic configuration of the ions or from their similar spherical shape is not clear. It is of interest to note, however, that among the several alkali nitrates^{1,2} included in Table I, less similarity in β/V is found. The temperature range over which the β/V constancy may be assumed is no doubt limited. Thus, for CsBr, for example, at 1000° the value is already over 20% above the average.

If a constancy in β/V is assumed, this, in combination with reasonable assumptions regarding certain mixing properties of molten alkali halides, leads to a prediction of symmetry in the contribution of volume effects to the Gibbs free energy of mixing.

Hildebrand and Scott⁵ have expressed the molar excess Gibbs free energy of mixing in binary systems, ΔG^E , as

$$\Delta G^E = x_1 x_2 w - x_1^2 x_2^2 w^2 / zRT - x_1^2 x_2^2 w^2 \beta / 2V \quad (1)$$

where x is the mole fraction of the indicated components 1 and 2, w is an interaction energy parameter characteristic of the system, and z is the coordination number. The terms in eq. 1 account for random interaction, nonrandom orientation of the mixed components, and volume effects, respectively. (Equation 1 may also be modified for mixtures of unequal-sized components by inclusion of an asymmetry term.⁶) Equation 1 represents a refinement of the s-regular model,⁷ which was originally formulated for nonelectrolyte systems. It has since been found that molten salt systems may be treated from a similar point.^{8,9} In nonelectrolyte systems the orientation and volume terms are usually neglected because of the relatively small w values in such systems.⁵ At the higher temperatures typical of molten salt systems, however, this assumption is commonly less valid. Thus, Aukrust, *et al.*,¹⁰ have found that in binary molten alkali halide mixtures w may exceed 4000 cal. mole⁻¹ at 800°. It can be shown^{1-3,11} that for a w that large, the ratio of the sum of the orientation and volume terms to the random term in eq. 1 is 0.15. Moreover, the ratio of the volume term to the orientation term is 0.40. The latter ratio becomes 0.80 in quasi-binary systems, where the denominator of the orientation term in eq. 1 becomes $2zRT$.⁹

While the random term in eq. 1 is symmetrical in x , the other terms generally are not because of variation in the concentration-dependent functions z , β , and V .⁵

In systems where the orientation and volume terms of eq. 1 are significant, neither β nor V individually would be additive functions although they should both depart from additivity in the same direction. These departures should be such,⁵ however, that the assumption of additivity in handling the rather small volume

(5) J. H. Hildebrand and R. L. Scott, "The Solubility of Nonelectrolytes," 3rd Ed., Reinhold Publishing Corp., New York, N. Y., 1950, Chapter 8.

(6) O. J. Kleppa, *J. Phys. Chem.*, **64**, 1937 (1960).

(7) E. A. Guggenheim, "Mixtures," Oxford University Press, London, 1952, Chapter 4.

(8) M. Blander, "Molten Salt Chemistry," Interscience Publishers, Inc., New York, N. Y., 1964, pp. 127-237.

(9) B. R. Sundheim "Fused Salts," McGraw-Hill Book Co., Inc., New York, N. Y., 1964, Chapter 2.

(10) E. Aukrust, B. Björge, H. Flood, and T. Førlund, *Ann. N. Y. Acad. Sci.*, **79**, 830 (1960).

(11) H. A. Levy, P. A. Agron, M. A. Bredig, and M. D. Danford, *ibid.*, **79**, 762 (1960).

term introduces negligible error therein. If, then, additivity in β/V is adopted, for alkali halide mixtures β/V is constant at a constant temperature, and the volume term in eq. 1 is symmetrical in concentration.

While the present hypothesis on mixing has been framed in terms of binary (or quasi-binary) mixtures, it is evident that a constancy of β/V throughout the alkali halides means that this quantity may also be considered constant for mixtures containing any number of those components.

The Association of Cesium Chloride in Anhydrous Methanol at 25°

by Robert L. Kay

Mellon Institute, Pittsburgh, Pennsylvania 15213

and James L. Hawes¹

Metcalf Research Laboratory, Brown University, Providence 12, Rhode Island (Received February 23, 1965)

An analysis of the precise conductance measurements of Gordon and co-workers^{2,3} for the alkali halides in anhydrous methanol solutions by the Fuoss–Onsager conductance theory⁴ indicated that lithium, sodium, and potassium halides are unassociated electrolytes.⁵ On the other hand, the data of Frazer and Hartley^{6,6} indicated that CsCl has an association constant of 15 ± 7 in methanol solution. Recent data for CsCl in an ethanol–water mixture⁷ and a dioxane–water mixture⁸ with the same dielectric constant as that of anhydrous methanol indicate a value of K_A of about 27. These conductance measurements were undertaken in order to clarify this situation.

Experimental

All measurements were carried out using a guarded electrode conductance cell fitted with a salt cup dispensing device. Full details concerning the cell, bridge, purification of CsCl, and experimental procedure have been outlined elsewhere.⁷

Methanol was purified by fractional distillation after a 24-hr. reflux over magnesium methoxide and had a specific conductance of less than 3×10^{-8} ohm⁻¹ cm.⁻¹ and a density of 0.78659 g. ml.⁻¹.

Considerable difficulty was encountered in making measurements with anhydrous methanol as solvent. The resistances which drifted by as much as 0.1% over

a period of several hours were influenced by stirring, and the frequency dependence was large and in an abnormal direction. We attribute this effect to an oxidation reaction of the methanol at the platinized electrodes. The effect can be accentuated if a fused porous platinum paste is used on the electrodes. Also, if the cell is rinsed and filled with water after a measurement in methanol, it is found that the abnormal frequency dependence persists although reduced in magnitude. Only prolonged cleaning with fuming nitric acid returned the slightly platinized electrodes to their original condition. The effect can be eliminated by the scrupulous exclusion of oxygen from the solvent and cell atmosphere. The salt-dispensing device was most effective in this respect.

The data were analyzed by the Fuoss–Onsager equation⁴ in the form

$$\Lambda = \Lambda_0 - S(C\gamma)^{1/2} + EC\gamma \log C\gamma + JC\gamma - K_A C\gamma \Lambda^2 \quad (1)$$

and also in the form for unassociated electrolytes

$$\Lambda = \Lambda_0 - SC^{1/2} + EC \log C + JC \quad (2)$$

All calculations were made on an I.B.M. 7090 computer.⁷ A dielectric constant⁹ of 32.64 and viscosity¹⁰ of 0.5445 cp. were used for methanol at 25°. The densities of the solutions were assumed to follow the linear relationship $d = 0.78659 + 0.169\bar{m}$ obtained from density measurements on the most concentrated solutions studied. Here \bar{m} is the concentration in moles per 1000 g. of solution.

Results

The equivalent conductances of CsCl in anhydrous methanol at 25° are given in Table I along with $\Delta\Lambda$, the difference between Λ measured and that calculated from eq. 1.

The results of a computer analysis of the data by eq. 1 are given in Table II along with the results of

(1) Adopted, in part, from a Ph.D. thesis submitted to Brown University, 1962.

(2) J. P. Butler, H. I. Schiff, and A. R. Gordon, *J. Chem. Phys.*, **19**, 752 (1951).

(3) R. E. Jervis, D. R. Muir, and A. R. Gordon, *J. Am. Chem. Soc.*, **75**, 2855 (1953).

(4) R. M. Fuoss and F. Accascina, "Electrolytic Conductance," Interscience Publishers, Inc., New York, N. Y., 1959.

(5) R. L. Kay, *ibid.*, **82**, 2099 (1960).

(6) J. E. Frazer and H. Hartley, *Proc. Roy. Soc. (London)*, **A109**, 351 (1925).

(7) J. L. Hawes and R. L. Kay, *J. Phys. Chem.*, **69**, 2420 (1965).

(8) J. Justice and R. M. Fuoss, *ibid.*, **67**, 1707 (1963).

(9) P. S. Albright and L. J. Gosting, *J. Am. Chem. Soc.*, **68**, 1061 (1946).

(10) G. Jones and H. J. Fornwalt, *ibid.*, **60**, 1683 (1938).

Table I: Conductance of CsCl in Anhydrous Methanol at 25°

10 ⁴ C	Λ	$\Delta\Lambda$
7.164	105.688	+0.004
13.089	102.973	-0.005
19.210	100.828	-0.003
25.314	99.067	+0.000
30.521	97.761	-0.004
35.603	96.634	+0.004
42.842	95.209	+0.013
48.526	94.184	-0.011

Table II

	Eq. 2	Eq. 1	Frazer and Hartley ^{5a}
Δ_0	112.85 ± 0.05	113.19 ± 0.02	113.42 ± 0.08
\bar{d}_J	2.59 ± 0.04	3.70 ± 0.07	4.5 ± 1.5
K_A		8.9 ± 0.5	15 ± 7
σ_A	0.07	0.009	0.03

treating CsCl as an unassociated electrolyte and the results of a recalculation of the data of Frazer and Hartley.⁶ The standard deviation of the individual points σ_A is also included and shows the much better fit obtained when association was taken into account (eq. 1).

There seems to be no doubt that CsCl is associated in methanol solution presumably owing to the low solvation energy of the large Cs cation. Within the precision of their measurements, the results of Frazer and Hartley agree with our results from eq. 1 with the possible exception of Λ_0 where the difference is almost three standard deviations. The association constant of 8.9 results in a decrease in Λ of 2.3 units at the highest concentration studied and indicates that CsCl is about 2.5% associated at 0.005 *M*. This is about one-third as much as would be predicted from the association constant of CsCl in either an ethanol-water⁷ or a dioxane-water mixture⁸ with the same dielectric constant as methanol. It is difficult to explain this difference simply by an appeal to ion solvation since it would require stronger interaction in methanol than in a solvent mixture containing a considerable portion of water. A more likely explanation possibly lies in considering the ion-pair association to be a multistep process involving a different number and, possibly, type of solvent molecules in each step.^{11,12}

Acknowledgment. This work was supported by the U. S. Atomic Energy Commission under Contract AT (30-1)-2727.

(11) M. Eigen and K. Tamm, *Z. Elektrochem.*, **66**, 93, 107 (1962).

(12) G. Atkinson and S. K. Kor, *J. Phys. Chem.*, **69**, 128 (1965).

Solubility Behavior of Polyoxyethylene

Nonylphenol Ethers in Cyclohexane and the Effect of Water by a Light-Scattering Method

by Ayao Kitahara

Tokyo College of Science, Kagurazaka, Shinjuku-ku, Tokyo, Japan
(Received April 24, 1964)

Micelle formation of some oil-soluble nonionic surfactants in nonaqueous solvents has been studied.¹ The solubility behavior of other nonionic surfactants in nonaqueous solvents is worthy of investigation, because the general behavior of their solubility has not yet been clarified.

Micelle formation of an ionic surfactant (sodium dioctyl sulfosuccinate) in nonaqueous solutions was reported by the author and others.² A comparative study of the solubility of a nonionic surfactant and that of an ionic one is of interest.

Some oil-soluble polyoxyethylene nonylphenol ethers show an interesting solubility behavior. The effect of water on the solubility and on the micellar weight of the nonionic surfactants is considerably different from the effect of water on these properties of an ionic one.

Experimental

Materials. Polyoxyethylene nonylphenol ethers were synthesized at the Research Laboratory of Kao Soap Co. and that of Lion Oil and Fat Co. in Japan. The by-product, polyethylene glycol, and the remaining salts were eliminated with a countercurrent distribution method using a solvent system of water-*n*-butyl alcohol.³ Water and *n*-butyl alcohol were removed by drying the samples at 40–50° and 2–3 mm.

The properties of the three samples used are listed in Table I. The absence of polyethylene glycol in the samples listed above was ascertained by thin layer chromatography.⁴

Apparatus and Method. The solubility behavior was investigated by a light-scattering method. The light scattered was observed by a Shimadzu photoelectric light-scattering photometer.² A hydrous or an anhydrous concentrated solution was originally prepared

(1) P. Debye and W. Prins, *J. Colloid Sci.*, **13**, 86 (1958); S. Ross and J. P. Olivier, *J. Phys. Chem.*, **63**, 1671 (1959); P. Becher, *ibid.*, **64**, 1221 (1960); P. Debye and H. Coll, *J. Colloid Sci.*, **17**, 220 (1962).

(2) A. Kitahara, T. Kobayashi, and T. Tachibana, *J. Phys. Chem.*, **66**, 363 (1962).

(3) K. Nagase and Y. Sakaguchi, *Kogyo Kagaku Zasshi*, **64**, 635 (1961).

(4) S. Hara, *Bunseki Kagaku*, **12**, 199 (1963).

Table I: Properties of Samples

Mean polymerized degree of ethylene oxide added	OH value	Mol. wt.	Abbreviation of names
4.17	139.1	403	NPE-4
6.12	114.7	489	NPE-6
9.70	87.0	649	NPE-10

and filtered with a very fine glass filter made by Corning Glass Co. Each solution was prepared by successive addition of an aliquot of the original solution to a quantity of the solvent filtered previously. The intensity of the light scattered at the direction of 0, 45, 90, and 135° from each solution was measured to determine the dissymmetry and the reduced scattering intensity. The measurement of the refractive index increment and the calculation of the micellar weight were similar to those in the preceding paper.² The temperature of the interior of the sample box was $29 \pm 2^\circ$.

Results and Discussion

Solubility Behavior and the Effect of Water. Rectangular diagrams of the solubility of anhydrous and hydrous systems of cyclohexane solutions of NPE-4, NPE-6, and NPE-10 are depicted in Figures 1, 2, and 3, respectively. The ordinate shows the mole fraction of water and the abscissa that of a surfactant. The meaning of the symbols used in Figures 1-3 is as follows: a solid circle indicates a transparent solution in which the dissymmetry (Z_{45}) is nearly equal to 1; an open circle, a clear solution in which $Z_{45} > 1$; a triangle, a solution in which $Z_{45} \gg 1$; and a cross mark, a turbid solution.

In the anhydrous system of NPE-10, the solution is transparent at a very low concentration, but becomes turbid as the concentration increases. The solution clears again at higher concentration. A recovery of the clearness of the solution was not found over the concentration range observed in the anhydrous system of NPE-4. There was no appearance of turbidity in the anhydrous system of NPE-6. The appearance of turbidity followed by clearness, as seen in the case of anhydrous NPE-10, was observed in anhydrous systems of cyclohexane solutions of other polyoxyethylene alkylphenol ethers which have a certain ratio of the number of oxyethylene groups to the number of carbons in the alkyl groups.

All of the hydrous samples used here showed a recovery of clearness after the appearance of turbidity. The recovery of clearness in the hydrous systems at a higher concentration may be ascribed to solubilization of water by micelles formed at that concentration.

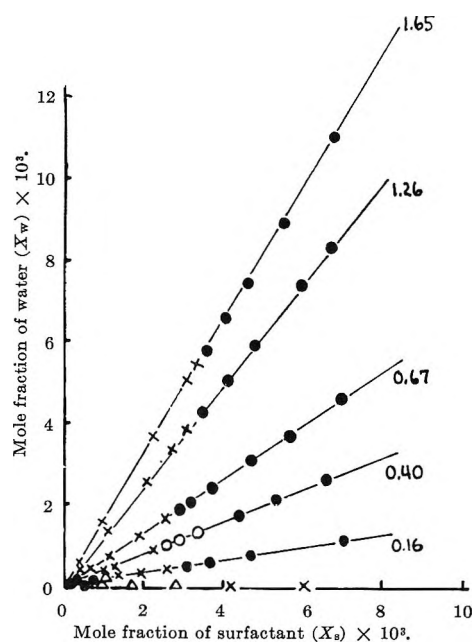


Figure 1. Solubility diagram of NPE-4.

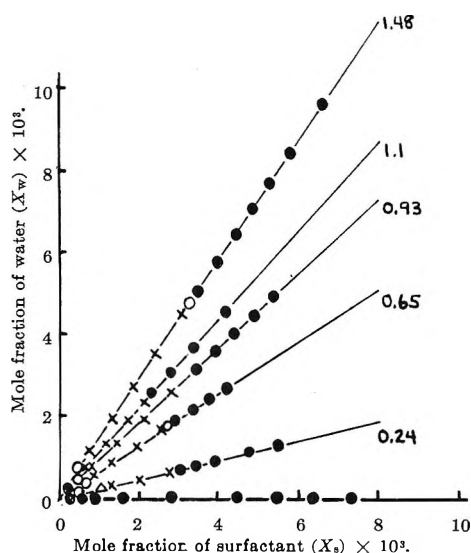


Figure 2. Solubility diagram of NPE-6.

The effect of traces of water, which may be present in the anhydrous systems, on the solubility needs to be checked before the cause of the solubility behavior can be discussed. The following experiment was conducted for this purpose. The glass-made apparatus depicted in Figure 4 was employed. Nonaqueous stopcock grease was thinly used for stopcocks (C_1 , C_2) and the joints.

A sample of a surfactant was put into vessel B and dried by evacuation from D. Cyclohexane, purified and dried previously, and phosphorus pentoxide were

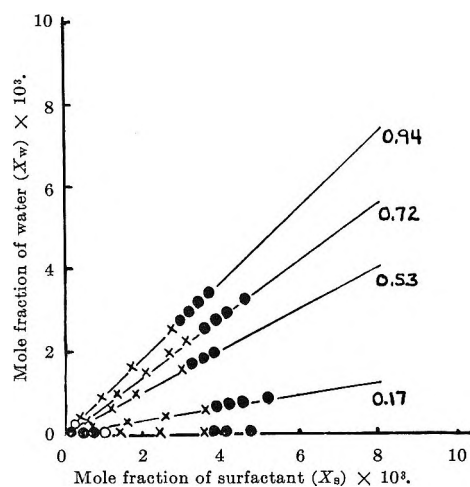


Figure 3. Solubility diagram of NPE-10.

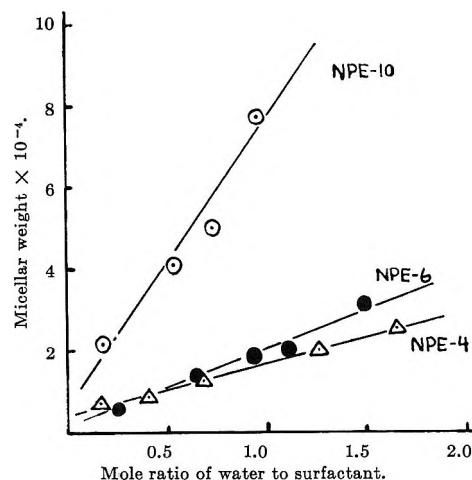


Figure 5. Effect of water on micellar weight.

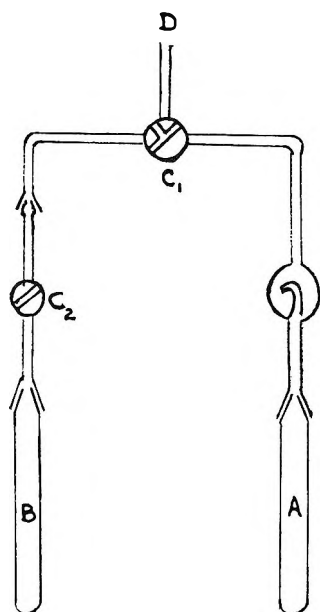


Figure 4. Apparatus used for preparing a dry solution.

put into vessel A and left there for a period of time with intermittent shaking. The cyclohexane thus dried was distilled from A, which was heated gently, to cold B. The clearness of the dry solution prepared in B was checked by Tyndall light at a definite temperature. Turbidity still appeared at a definite concentration of the dry solution, though the temperature at which the turbidity appeared decreased a little in the case of NPE-10. The preceding fact that no turbidity was observed in anhydrous NPE-6 may be due to the low temperature producing turbidity or to the low content of traces of water.

Why turbidity appears, followed by clearness, or whether or not the turbidity would disappear by perfect

drying will be answered by further study of a dry solution.

Micellar Weight and the Effect of Water. The number at the end of each line in Figures 1-3 shows the mole ratio of water to a surfactant. A group of clear solutions is indicated on the same line by solid circles. The micellar weight of these solutions, calculated from the values of their scattered light intensity, was depicted *vs.* the mole ratio of water to a surfactant in Figure 5. The micellar weight increases linearly with the mole ratio. The effect of water on the micellar weight is more marked in the case of a higher content of ethylene oxide.

A similar effect of water on the micellar weight and a similar solubility behavior were observed in the cases of polyoxyethylene nonylphenol ethers from which polyethylene glycol and salts had not been removed.

On the other hand, anhydrous or hydrous solutions of Aerosol OT (sodium dioctyl sulfosuccinate) in cyclohexane were transparent over a similar concentration range. The micellar weight of hydrous systems was nearly equal to that of anhydrous systems in the cases of 2.7 and 5.5 mole ratio of water to a surfactant.

This marked difference in the effect of water on the micellar weight of Aerosol OT and that of polyoxyethylene nonylphenol ethers seems to result from the difference between the micellar structure of both surfactants. The interior of the micelle of Aerosol OT is firmly bonded because of its ionic nature, and solubilized water probably has no effect on the structure and the size of the micelle. On the other hand, the interior of the micelle of polyoxyethylene nonylphenol ether is loose because of hydrogen bonding, and solubilized water increases the micellar size by bonding more surfactant molecules to the original micelle with increased hydrogen bonding.

Acknowledgment. The author wishes to thank Mr. Chuhei Asakawa for taking part in the measurements of light scattering and Mr. Haruhiko Arai for carrying out the purification of the samples.

The Proton Magnetic Resonance Study of the Protonation of Pyrazine

by Hirotake Kamei

Physics Division, Electrotechnical Laboratory, Tanashi-machi, Kitatama-gun, Tokyo, Japan (Received May 18, 1964)

During the course of an investigation of the electric properties of pyrazine and its derivatives, it became desirable to study the behavior of pyrazine in the presence of a proton donor. While some work has been done on the spectroscopic studies of the protonation of pyrazine in sulfuric acid,¹⁻⁴ little attention has been paid to the behavior of the protonation at different pyrazine-acid compositions. Nuclear magnetic resonance (n.m.r.) methods⁵ are suited to such an investigation.

In the present investigation, the protonation of pyrazine by trifluoroacetic acid was studied by n.m.r. techniques. One of the advantages of using trifluoroacetic acid as solvent is that an internal reference may be employed. When the internal reference is used, the solvent effects⁶ can be dealt with fairly readily.

Experimental

Reagent grade pyrazine was fractionally distilled under dry nitrogen and purified by sublimation *in vacuo* at liquid nitrogen temperature just before use. Reagent grade trifluoroacetic acid and cyclohexane were dried over phosphorus pentoxide and purified by fractional distillation under dry argon. Reagent grade concentrated sulfuric acid was used without further purification.

Samples consisting of approximately 0.5 ml. of solution in each n.m.r. sample tube were prepared in a glove box under an atmosphere of dry nitrogen. The sample tubes containing the solutions were stoppered with a rubber tube and stopcock and then removed from the glove box. The tubes were immersed in liquid nitrogen, evacuated, and sealed. The compositions of all solutions were determined by weight.

The n.m.r. spectra were obtained with a Japan Electron Optics Laboratory JNM-3 instrument operating at 40 Mc./sec. which was equipped with a tempera-

ture control device. Measurements were made at 23.5 ± 0.2 and $-35 \pm 1^\circ$. The resonance spectrum of aromatic protons in pyrazine consists of a single line with a chemical shift depending on concentration. This indicates that the lifetime of an exchanging species is short. The chemical shifts were determined by linear interpolation between two bracketing side bands generated by modulating the magnetic field. Ten to twelve measurements of the chemical shift were averaged for each sample. The resulting average deviations were approximately 0.004 p.p.m.

Results and Discussion

Chemical Shift of Protonated Pyrazine. It is apparent from the ultraviolet absorption spectra¹ that pyrazine dissolved in 60% and concentrated sulfuric acid forms monoprotonated and diprotonated species, respectively. The observed proton resonance shifts of pyrazine were measured at low concentrations in 64.4% and concentrated (95%) sulfuric acid. The experimental data are plotted in Figure 1. The chemical shifts of monoprotonated and diprotonated pyrazine were determined from the infinite dilution shifts obtained by graphical extrapolation of curves a and b in Figure 1, respectively. These observed shifts must be corrected for the solvent effects.

The bulk susceptibility shift, σ_b , is given by $^{2/3} \pi \Delta\chi_v$, where $\Delta\chi_v$ is the difference in the volume susceptibilities of the solvent and benzene. The values of χ_v ($\times 10^6$) for benzene, 64.4% sulfuric acid, and concentrated sulfuric acid are taken to be -0.617 ,⁷ -0.803 ,³ and -0.777 ,⁸ respectively.

The magnitude of the perturbation shifts arising from other solvent effects is not directly obtainable from the experimental data of the pyrazine-sulfuric acid system. It may be assumed that the magnitude of the solvent effects shift, σ_0 (except polar effect), of protonated pyrazines is equal to that of benzene. Benzene has no electric moment, and its molecular shape

(1) F. Halverson and R. C. Hirt, *J. Chem. Phys.*, **19**, 711 (1951).

(2) L. F. Wiggins and W. S. Wise, *J. Chem. Soc.*, 4780 (1956).

(3) D. A. Keyworth, *J. Org. Chem.*, **24**, 1355 (1959).

(4) A. S. Chia and R. F. Trimble, Jr., *J. Phys. Chem.*, **65**, 863 (1961).

(5) J. A. Pople, W. G. Schneider, and H. J. Bernstein, "High Resolution Nuclear Magnetic Resonance," McGraw-Hill Book Co., Inc., New York, N. Y., 1959.

(6) A. D. Buckingham, T. Schaefer, and W. G. Schneider, *J. Chem. Phys.*, **32**, 1227 (1960).

(7) V. C. G. Trew, *Trans. Faraday Soc.*, **49**, 604 (1953).

(8) By assuming Wiedemann's additivity law for the systems, these values were calculated from molar susceptibility, χ_M . The values of χ_M ($\times 10^6$) for water and H_2SO_4 are taken to be -12.97 and -39.8 , respectively ("Handbook of Chemistry and Physics," Chemical Rubber Publishing Co., Cleveland, Ohio, 1963).

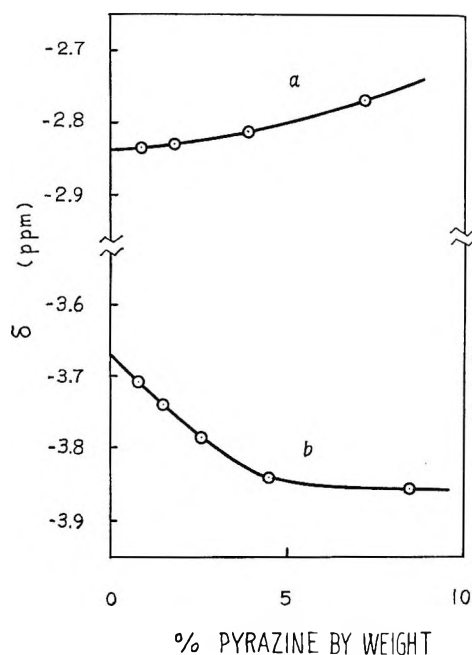


Figure 1. The chemical shift of pyrazine (relative to external benzene reference) as a function of concentration in sulfuric acid: a, 64.4%; b, 95%.

is analogous to that of protonated pyrazines. At infinite dilution the resonance shift of benzene in concentrated sulfuric acid (corrected for the bulk susceptibility) has a lower field shift of 0.745 p.p.m. relative to gaseous benzene. This value corresponds to the solvent effects shift of diprotonated pyrazine. When 64.4% sulfuric acid is used as solvent, the signal of benzene cannot be observed because it overlaps with the signal of the acid protons. The stoichiometric mole fraction of H_2SO_4 in 64.4% sulfuric acid is 0.25. The solvent effects shift of monoprotated pyrazine may be given by $0.745 \times 0.25 = 0.186$ p.p.m.

The polar effect shift, σ_E , is approximately proportional to the solvent parameter, $(\epsilon - 1)/(\epsilon + 1)$, where ϵ is the dielectric constant of the solvent. This perturbation shift is also involved in the observed shift which was measured in trifluoroacetic acid using the internal reference. The values of $(\epsilon - 1)/(\epsilon + 1)$ for sulfuric acid and trifluoroacetic acid are 0.97 and 0.95, respectively. Therefore, σ_E in sulfuric acid has approximately the same value as in trifluoroacetic acid, and the correction for this effect may be unnecessary.

The observed chemical shifts corrected for solvent effects, δ_{cor} , are given in Table I, along with the solvent effects parameters needed for these corrections.

Protonation of Pyrazine by Trifluoroacetic Acid. The chemical shift of pyrazine in trifluoroacetic acid

Table I: Aromatic Proton Chemical Shift of Pyrazine and Its Protonated Species in P.p.m. Relative to Cyclohexane and Solvent Effects Parameter

Species	σ_b	σ_a	δ_{cor}
Pyrazine			-7.075 ^a
Monoprotated	0.389	0.186	-7.567 ^b
Diprotated	0.334	0.745	-7.894 ^b

^a This value is the infinite dilution shift of pyrazine in carbon tetrachloride relative to the internal cyclohexane reference.

^b These values were obtained by considering the chemical shift of pure benzene relative to cyclohexane, -5.305 p.p.m.

was measured as a function of pyrazine mole fraction, x . The internal reference was approximately 1 mole % cyclohexane. The results are given in Table II.

Table II: Proton Chemical Shift of Pyrazine in Trifluoroacetic Acid in P.p.m. Relative to Internal Cyclohexane Reference

Mole fraction of pyrazine	δ , p.p.m.	Mole fraction of pyrazine	δ , p.p.m.
0.0170	-7.899	0.2158	-7.981
0.0315	-7.911	0.2444	-7.963
0.0554	-7.922	0.2734	-7.934
0.0914	-7.940	0.3011	-7.905
0.1203	-7.953	0.3446	-7.844
0.1557	-7.964	0.3957	-7.779
0.1839	-7.973		

In the presence of aromatics, the signal position of the internal reference compound is markedly altered. For this reason, correction for the shift of cyclohexane must be applied to the observed shift of pyrazine. Since the precise volume susceptibility of the solutions is not known, the internal reference shift cannot be determined with respect to external reference. Fortunately, as the temperature is lowered a new resonance signal of cyclohexane appears at a lower field. The chemical shift of the new peak is a few tenths p.p.m. relative to the signal which appears at room temperature. Under this condition the Tyndall phenomenon was observed, corresponding to the formation of a colloidal solution. Spherical particles are dispersed in the medium which has approximately the same composition of pyrazine and trifluoroacetic acid as that at room temperature. Cyclohexane is the main component of the dispersed particle, and the concentration of pyrazine in it is very low. Solvent effects on the resonance shift of dispersed cyclohexane are negligible. The particle corresponds to a spherical

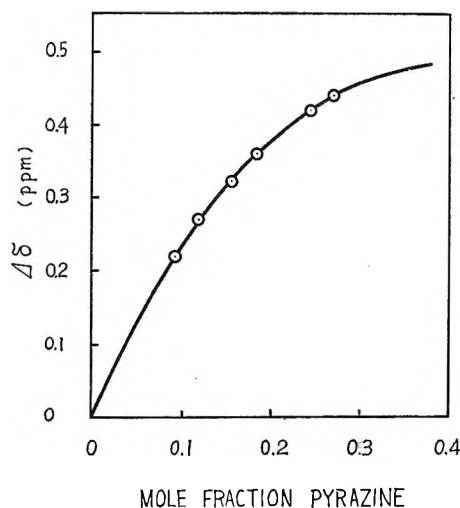


Figure 2. Plot of $\Delta\delta$ vs. concentration of pyrazine at -35° .

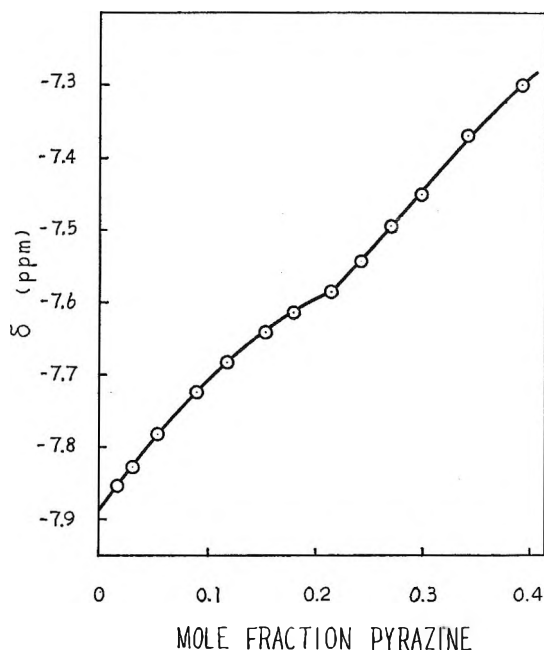


Figure 3. The chemical shift of pyrazine as a function of concentration in trifluoroacetic acid. Chemical shifts are corrected for reference shift and referred to the internal cyclohexane signal.

external cyclohexane reference and gives a low-field signal. The separation, $\Delta\delta$, of this signal from the high-field signal may be the internal reference shift. The results obtained at -35° are shown in Figure 2 as a function of pyrazine concentration. The shift of cyclohexane was determined at low temperature only and is assumed to be the same for room temperature.

The chemical shifts, corrected for the reference shift, are plotted in Figure 3. The chemical shift at infinite

dilution, -7.889 p.p.m., is in good agreement with that of diprotonated pyrazine, -7.894 p.p.m. There is a hump in the curve at a concentration $x = 0.22$. The chemical shift at this concentration, -7.58 p.p.m., is in good agreement with the shift of monoprotated species, -7.567 p.p.m.

These results indicate that monoprotation is incomplete at concentrations $x > 0.22$ and that this reaction approaches completion at $x = 0.22$. Diprotation occurs at $x < 0.22$, at which concentrations unprotonated species do not exist. At very low concentration pyrazine exists largely as diprotonated species. That the two protonation reactions do not overlap is attributed to the stabilization of monoprotated pyrazine.

The Behavior of the Silver-Silver Iodide Electrode in the Presence of Tetraalkylammonium Ions

by R. Fernández-Prini and J. E. Prue

Department of Chemistry, University of Reading, Reading, Berkshire, England (Received August 5, 1964)

Measurements of e.m.f. of the cell $\text{Ag}|\text{AgI}|\text{NR}_4\text{I}(\text{c})|\text{KCl}(\text{satd.})|\text{KI}(\text{c})|\text{AgI}|\text{Ag}$ were recently reported.¹ Mean ionic activity coefficients for tetraalkylammonium iodides were calculated from the results, but it was soon pointed out² that the values were absurdly high and in conflict with those already reported in the literature. New measurements by the isopiestic technique^{3,4} have confirmed Stokes' conclusion. Like other workers,^{3,5} we can confirm that the e.m.f. values reported in the original work¹ are approximately correct. Frank⁶ has maintained that meaningful values of the ratio of the activity coefficients of the iodide ion in the two solutions can be obtained from the results (e.g., he calculates $f_{\text{I}^-(\text{NR}_4\text{I})}/f_{\text{I}^-(\text{KI})} = 14.7$ when $c = 0.3 M$), but by inserting experimental mean ionic activity coefficients and reasonable estimates of transport numbers in an exact formula⁷ we have satis-

(1) M. A. V. Devanathan and M. J. Fernando, *Trans. Faraday Soc.*, **58**, 784 (1962).

(2) R. H. Stokes, *ibid.*, **59**, 761 (1963).

(3) V. E. Bower and R. A. Robinson, *ibid.*, **59**, 1717 (1963).

(4) S. Lindenbaum and G. E. Boyd, *J. Phys. Chem.*, **68**, 911 (1964).

(5) J. C. Rasaiah, quoted in ref. 6.

(6) H. S. Frank, *J. Phys. Chem.*, **67**, 1554 (1963).

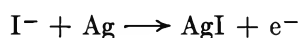
fied ourselves that the surprisingly large e.m.f. values observed must have some origin other than an "ideal" diffusion potential or a "salt effects" potential.⁷ Instead, we believe that tetraalkylammonium ions have an effect on the electrode reaction.

Silver-silver iodide electrodes were prepared in the normal way.⁸ The cell e.m.f. values only became steady when the cells were left overnight and were not very reproducible. Electrodes which had been immersed in tetraalkylammonium iodide changed from the usual yellow color to white, and after several hours immersion they were found to have a potential of several millivolts when they were returned to potassium iodide solution and their e.m.f. was measured against an electrode not so treated.

If 0.1 *M* tetraethylammonium iodide is added to 0.1 *M* silver nitrate, the yellow precipitate of silver iodide initially formed changes to white when excess of iodide is added. The white precipitate from a known amount of silver nitrate when filtered off and dried *in vacuo* had a weight which corresponded to the composition 2AgI·NEt₄I. The compound had an infrared spectrum (Nujol mull) with the same lines as NEt₄I and a melting point of 224°, in agreement with that reported⁹ for the same compound many years ago. Similar compounds have also been reported¹⁰ for other tetraalkylammonium iodides. In the presence of sufficient tetraalkylammonium iodide the electrode reaction in the cell will therefore be

$$\frac{1}{2}\text{NR}_4^+ + \frac{3}{2}\text{I}^- + \text{Ag} \longrightarrow \frac{1}{2}(2\text{AgI}\cdot\text{NR}_4\text{I}) + \text{e}^-$$

rather than



It is interesting that tetraalkylammonium compounds similar to those with silver iodide have been reported for other metal iodides such as mercury. A black layer was formed on the surface of mercury-mercurous iodide electrodes (prepared as recommended by Vosburgh¹¹) when they were immersed in tetraethylammonium iodide. When both silver-silver iodide electrodes in the concentration cell were replaced by mercury-mercurous iodide electrodes, the e.m.f. values were of opposite sign! Clearly tetraalkylammonium ions have a large specific effect on one or both electrodes. The potential difference between a silver-silver iodide and a mercury-mercurous iodide electrode immersed in 0.03 *M* tetraethylammonium iodide solution was about 62 mv. different from that predicted from the known E° values. With potassium iodide solution the expected e.m.f. was obtained.

To confirm the suggestion that the electrode reaction is changed in the presence of tetraalkylammonium

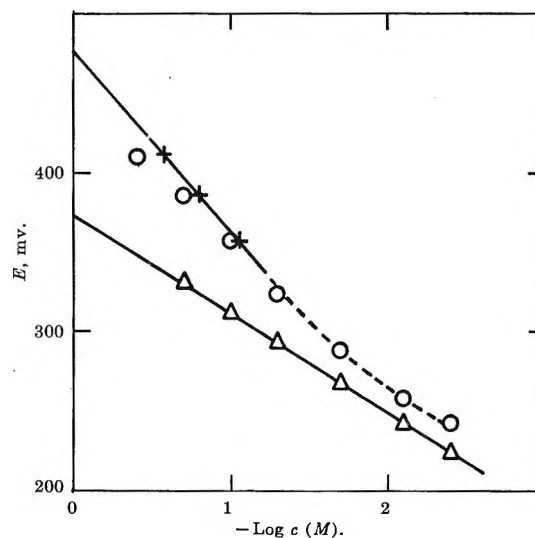
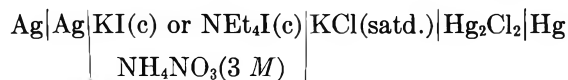


Figure 1. E vs. $-\log c$: Δ , KI; \circ , NEt₄I; $+$, NEt₄I (allowing for association).

ions, we made some measurements (25°) with the cell



If the ammonium nitrate keeps ionic activity coefficients and junction potentials constant, the e.m.f. for measurements with potassium iodide should be given by

$$E = E'_{\text{ref}} + (RT/F) \ln c \quad (1)$$

where E'_{ref} is constant. In the case of tetraethylammonium iodide the e.m.f. should be given by

$$E = E''_{\text{ref}} + (2RT/F) \ln c \quad (2)$$

if the suggested change of cell reaction occurs. The results are plotted in Figure 1. The slope from the KI results is 62 mv. which is not far from the ideal value of 59 mv. The results for NEt₄I in sufficiently dilute solution are seen to approach those¹² for KI, but the slope for the results with more concentrated solutions is almost twice as great. A rough estimate of the degree of association of tetraethylammonium iodide based on Bower and Robinson's data³ leads to corrected free iodide concentrations which give the

(7) E. A. Guggenheim, *J. Phys. Chem.*, **34**, 1758 (1930); A. Unmack and E. A. Guggenheim, *Kgl. Danske Videnskab. Selskab, Mat.-Fys. Medd.*, **10**, No. 8, 1 (1930).

(8) G. J. Janz in "Reference Electrodes," D. J. G. Ives and G. J. Janz, Ed., Academic Press, New York, N. Y., 1961, p. 209.

(9) D. Strömholm, *Fer.*, **36**, 142 (1903).

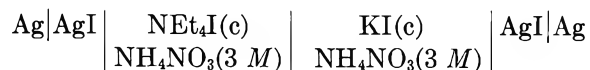
(10) R. L. Datta and T. Gosh, *J. Am. Chem. Soc.*, **36**, 1017 (1914).

(11) W. C. Vosburgh, *ibid.*, **50**, 2386 (1928).

(12) The residual difference was probably because the electrodes had originally been used in more concentrated solutions of NEt₄I.

full line in the figure with a slope of 116 mv. compared with an ideal value of 118 mv.

Our measurements also give e.m.f. values for the cell



We compare in Table I interpolated values with those reported by Devanathan and Fernando¹ for the same cell with no swamping medium. The slight effect of the swamping medium on the e.m.f. values

Table I

<i>c</i> , <i>M</i>	0.003	0.01	0.03	0.1	0.3
<i>E</i> (NH ₄ NO ₃), mv.	9	16	27	44	64
<i>E</i> (ref. 1), mv.	7.8	20.5	27.3	48.1	69.1

confirms our conclusion that no significant information about ratios of ionic activity coefficients can be obtained from Devanathan and Fernando's data.

Acknowledgment. R. F.-P. is grateful to the Consejo Nacional de Investigaciones Científicas y Técnicas (Argentina) for a grant.

Effects of Experimental Parameters on the (n,γ)-Activated Reactions of Bromine with Liquid Cyclohexane

by Joseph A. Merrigan¹ and Edward P. Rack

Avery Chemistry Laboratory, The University of Nebraska, Lincoln, Nebraska (Received December 18, 1964)

In recent years much emphasis has been placed on developing kinetic and mechanistic models for chemical reactions activated by nuclear transformations, such as the Estrup-Wolfgang model for tritium-hydrocarbon systems^{2a-c} and the Geissler-Willard Auger electron reaction hypothesis for liquid state halogen reactions.^{2d} Since various models are semiempirical, a premium is placed on data representing the true hot-atom reactions.

This paper presents results of a study of the influence of various experimental parameters on the reactions of Br^{80m} and Br⁸², activated by the (n,γ) reaction, with liquid cyclohexane. We found the determinations of bromine organic retentions (per cent of radiobromine stabilized in organic combination) were complicated

by postactivation thermal reactions which occurred readily during and after thermal neutron irradiations.

Experimental

Materials. Phillips research grade cyclohexane (99.99 mole % purity) was used without further treatment. It was tested by adding 10⁻³ ml. of elemental bromine containing a high specific activity of Br⁸² (36 hr.) to 10 ml. of the liquid. The solution was allowed to stand in the dark up to 6 hr., following which the Br₂ was extracted with 0.5 *M* aqueous sulfite, and the radioactivity in the aqueous and organic layers was determined. Less than 0.5% reaction was traced, indicating that no more than 10⁻⁶ mole fraction of thermally reactive impurities was present. Bromine prepared from Mallinckrodt reagent grade K₂Cr₂O₇, KBr, and H₂SO₄ was used after three distillations over Fisher reagent grade P₂O₅, collecting middle fractions. Eastman C₂H₅Br was purified by washing with sulfite solution, drying over silica gel, and doubly distilling. Iodine was sublimed from a mixture of Mallinckrodt reagent grade I₂ and KI and collected on a cold glass surface.

Sample Preparation. Reaction mixtures of bromine and cyclohexane were prepared immediately before introducing them into quartz bulblets. All operations were done with the exclusion of light. Extreme care was employed in preparing reaction systems for neutron irradiations. Quartz bulblets were attached to a quartz-Pyrex graded-seal assembly, which was then cleaned by successive washings with concentrated nitric acid, dilute base, and (four washings) distilled water. The quartz bulb assembly was then evacuated on a vacuum line and flamed to remove any adsorbed water. Reaction mixtures were introduced into the cooled bulblets and degassed four or more times. The bulblets were sealed while frozen under vacuum, wrapped in aluminum foil to prevent possible light-induced reactions, and stored under liquid nitrogen prior to neutron irradiations.

Neutron Irradiations. Samples were irradiated in the Omaha, Neb., V.A. Hospital Triga reactor at a thermal neutron flux of 10¹¹ neutrons cm.⁻² sec.⁻¹ and an accompanying γ-radiation flux of 3 × 10¹⁷ e.v. g.⁻¹ min.⁻¹. Samples were rotated in the lazy susan sample holder to ensure uniformity of flux. Irradiations were performed at 25° and varied from 3 sec. to 3 hr. All samples were frozen in liquid nitrogen

(1) Receipt of Monsanto Fellowship is gratefully acknowledged

(2) (a) P. J. Estrup and R. Wolfgang, *J. Am. Chem. Soc.*, **82**, 2661 (1960); (b) P. J. Estrup and R. Wolfgang, *ibid.*, **82**, 2665 (1960); (c) R. Wolfgang, *J. Chem. Phys.*, **39**, 2983 (1963); (d) P. R. Geissler and J. Willard, *J. Phys. Chem.*, **67**, 1675 (1963).

within 20 sec. after irradiation, suppressing post-activation thermal reactions. Light was excluded during and after irradiations.

Extraction and Counting. In order to minimize post-activation thermal reactions, bulblets containing the irradiated systems in the *frozen state* were extracted in two-phase mixtures of CCl_4 plus Br_2 carrier and 0.5 *M* aqueous Na_2SO_3 . The organic fraction was separated from the inorganic and dried over anhydrous CaCl_2 . Samples (10 ml.) of each fraction were counted using a γ -ray, well-type scintillation detector. Experimentally, it was found that neither coincidence loss nor density corrections were necessary for the measured counting rates. Before counting, solutions were allowed to stand long enough for any Br^{80} (18 min.) produced by the (n, γ) reaction to decay. In all studies of the $\text{Br}^{79}(n, \gamma)\text{Br}^{80\text{m}}$ -activated reactions, counting solutions were allowed to stand 2 to 3 hr. following extraction, before counting, to allow $\text{Br}^{80\text{m}}$ (4.4 hr.) to re-establish equilibrium with the Br^{80} (18 min.) daughter and Br^{80} activity which had reacted as a result of isomeric transition to decay. Samples were checked for radiochemical purity using a single-channel radiation analyzer. The per cents $\text{Br}^{80\text{m}}$ and Br^{82} organically combined were readily determined by counting the samples approximately 7 to 8 ($\text{Br}^{80\text{m}}$ plus Br^{82} activity) and 50–60 hr. (Br^{82} activity) after irradiation.

By making proper corrections for Br^{82} activity at the time of the first count, $\text{Br}^{80\text{m}}$ data were obtained. Two or more experiments were accomplished for each condition tested and the results given in the tables are averages of values obtained. The maximum absolute experimental errors in organic retentions were $\pm 0.5\%$.

Radiation-Induced Reactions. Liquid mixtures of I_2 tagged with I^{131} in cyclohexane were irradiated in the reactor in radiation damage studies. Carrier-free Oak Ridge iodide-131 was oxidized by H_2O_2 to I_2^{131} , extracted into the cyclohexane-iodine system in the dark, washed, and dried over silica gel. The I^{131} as organic was always less than 2% prior to neutron irradiations. Organic retentions after irradiations were corrected for these preirradiation organic retentions.

Results and Discussion

In our study of the extent of $\text{Br}^{80\text{m}}$ and Br^{82} reactions in cyclohexane as a function of irradiation time, we found a general increase in both organic retentions with length of irradiation. Table I illustrates this effect which is common to all systems but diminishes with increasing scavenger concentrations. A pseudo-isotope effect (more pronounced the lower the Br_2 concentration) was found for irradiations longer than 1 or 2 min. because of higher rates of increase in Br^{82} organic

Table I: Organic Retentions of $\text{Br}^{80\text{m}}$ and Br^{82} Formed by (n, γ) Activation of Bromine-Cyclohexane^a Solution as a Function of Length of Irradiation

Irradiation time, sec. ⁵	Organic retention, % ^c	
	Br^{82}	$\text{Br}^{80\text{m}}$
1820	38.2	29.0
1100	36.7	28.0
740	34.8	27.5
500	32.7	27.0
200	29.0	26.1
140	27.3	25.0
80	26.0	24.8
50	25.0	24.5
30	24.2	24.0
0 ^d	23.5	23.5

^a Bromine present: 6.31×10^{-3} mole fraction. ^b Twenty seconds is added to actual irradiation times to allow for thermal reactions occurring between the end of irradiation and freezing in liquid nitrogen. ^c Results are within ± 0.5 experimental error. Statistical errors were negligible. ^d Zero time was obtained by extrapolating a plot of organic retention vs. irradiation time to zero irradiation time.

retentions with irradiation time. This rate of reaction variation between $\text{Br}^{80\text{m}}$ and Br^{82} could not be due to the longer average lifetime³ of Br^{82} in such short irradiations. In light of the discovery of $\text{Br}^{82\text{m}}$ (5–6 min.) reported independently by Anders⁴ and Emery,⁵ the differences between the Br^{82} and $\text{Br}^{80\text{m}}$ data in Table I may be related to the fact that the final stabilization of part of the Br^{82} occurs as a result of the isomeric transitions from the $\text{Br}^{82\text{m}}$ state to the ground state of Br^{82} , whereas the $\text{Br}^{80\text{m}}$ results completely from the (I, γ) process. If this is true, consideration of the data is complicated by the fact that part of the Br^{82} ground-state products of those samples irradiated for only a few minutes may have been formed while the sample was in the solid state.

The general increase in organic retention with irradiation time described above could be caused by various factors such as presence of thermally reactive impurities in chemicals used, light-induced reactions, and radiation damage. As shown in the Experimental section, no impurities reactive to Br_2 were present, and exposure to light was minimized for all systems. Radiation damage was extensively studied. By measuring the extent of radiation-induced I_2 reactions traced with I^{131} at low concentrations (below 5×10^{-3} *M*)

(3) F. S. Rowland and W. F. Libby, *J. Chem. Phys.*, **21**, 1495 (1953).

(4) O. U. Anders, Abstracts, 148th National Meeting of the American Chemical Society, Chicago, Ill., Aug. 1964, p. 10R.

(5) J. F. Emery, Abstracts, 148th National Meeting of the American Chemical Society, Chicago, Ill., Aug. 1964, p. 10R.

in cyclohexane, using the G value found by Schuler and Fessenden⁶ of 5.66 ± 0.25 molecules of RI produced/100 e.v., we determined the radiation dose rate to be 3×10^{17} e.v. g.⁻¹ min.⁻¹. This dose rate is the same as found by Fricke dosimetry.⁷ The radiation-induced organic retention followed the equation $O.R. = DGTW/2n$, where $O.R.$ is the per cent organically bound I¹³¹, D is the dose rate in e.v. g.⁻¹ min.⁻¹, G is the number of molecules of RI produced per 100 e.v., T is time of irradiation in min., W is the weight of solvent in grams, n is the number of I₂ molecules present in the solvent, and 2 is the number of molecules of RI produced per molecule of I₂. For a given dose, the radiation-induced organic retention should be a hyperbolic function of the concentration of I₂. For a dose rate of 3×10^{17} e.v. g.⁻¹ min.⁻¹ we calculated expected radiation-induced organic retentions which agreed well with experimental results.

The extent of radiation-induced reactions in the iodine-cyclohexane system at a dose rate of 3×10^{17} e.v. g.⁻¹ min.⁻¹ and 30-min. irradiations became negligible (below 1%) at concentrations of I₂ above 3×10^{-3} mole fraction. With decreasing I₂ concentration below 3×10^{-3} mole fraction the radiation-induced organic retentions approach 100%.

We performed experiments designed to show the relative scavenging abilities of Br₂ and I₂ in cyclohexane. I₂ and Br₂ were shown to have excellent scavenging abilities⁸ and similar scavenging powers in C₂H₅Br and CCl₃Br.⁹ We also found this to be true in cyclohexane, using similar techniques. Since Br₂ and I₂ scavenging abilities were found similar in cyclohexane, we could calculate the radiation-induced organic retentions in the Br₂ system using the equation previously given. Thus, for irradiations of 30 min. or less and Br₂ concentrations above 3×10^{-3} mole fraction, radiation-induced organic retentions were negligible. Therefore, the increase of organic retentions, especially at high scavenger concentrations (greater than 0.1 mole fraction), with irradiation time was not a result of radiation-produced reactions.

We investigated the organic retention as a function of "thermal time" after the sample had been taken from the reactor. From Table II it is evident that thermal reactions occurred during the irradiations as well as after samples were taken from the reactor. By comparing columns C and B, a rise in organic retention from 1 to 5 min. of neutron irradiations is observed. Comparing columns C and A, it is evident that reactions contributing to an increase in organic retention occur after irradiations as well as during irradiations.

The average lifetime of the radioactive atoms in the solutions measured after 5-min. irradiations would

Table II: Organic Retentions of Br⁸² Formed by (n,γ) Activation of Bromine-Cyclohexane Solution as a Function of Time at 25° during and after Irradiation

Mole fraction of Br ₂	Organic retention, % ^a		
	A (1 + 4 min.)	B (5 min.)	C (1 min.)
0.082	16.0, 16.1	14.5, 14.3	13.4, 13.1
0.137	14.3, 14.5	13.1, 13.2	12.1, 12.2
0.256	12.6, 12.5	10.7, 11.0	9.7, 9.8
0.451	9.1, 9.1	8.5, 8.6	7.5, 7.9

^a Column A refers to samples irradiated in the reactor for 1 min. and allowed to stand at 25° for 4 min. before quenching thermal reactions by freezing under liquid nitrogen. Column B refers to samples irradiated for 5 min. with immediate quenching of thermal reactions using liquid nitrogen. Column C refers to samples irradiated 1 min. with immediate quenching of thermal reactions by freezing in liquid nitrogen.

be shorter than that of radioactive atoms produced in 1-min. irradiations and allowed to stand in the system for 4 additional min. Therefore, with thermal reactions occurring, organic retentions for samples irradiated in the reactor for 5 min. should be lower than organic retentions of equivalent samples irradiated for 1 min. and allowed to stand for 4 min. at 25°. A comparison of columns A and B in Table II illustrates this effect.

In separate experiments at 4×10^{-2} mole fraction of Br₂ in cyclohexane, we found that following a 5-min. neutron irradiation, the organic retention of Br⁸² increased with the time the sample was allowed to stand at 25° before extracting. When samples were extracted immediately after a 5-min. irradiation, the organic retention was 17.9%. When equivalent samples were allowed to stand at 25° for 25 min. following a 5-min. irradiation, the organic retention increased to 25.5%. When they were allowed to stand for 4 hr., the organic retention increased to 28.0%. Thus, a long-lived reactive species was produced in the irradiation, which continued to exist and to influence organic retentions until the sample was frozen or extracted. This necessitated inclusion of the 20-sec. "thermal time" between irradiation and freezing of samples in our interpretations.

Presence of an "olefin-like" species formed by γ-radiation, as postulated by Willard and Chien¹⁰ to be

(6) R. H. Schuler and R. W. Fessenden, *J. Am. Chem. Soc.*, **79**, 273 (1957).

(7) Determined by W. K. Ellgren of this laboratory, 1964.

(8) (a) G. Levey and J. E. Willard, *J. Am. Chem. Soc.*, **74**, 6161 (1952); (b) S. Goldhaber and J. E. Willard, *ibid.*, **74**, 318 (1952); (c) J. F. Hornig and J. E. Willard, *ibid.*, **75**, 461 (1953).

(9) S. Aditya and J. E. Willard, *ibid.*, **79**, 3367 (1957).

(10) J. C. W. Chien and J. E. Willard, *ibid.*, **77**, 3441 (1955).

produced in long neutron irradiations of *n*-propyl bromide, was checked by irradiating, in the reactor, separate degassed samples of Br₂ and cyclohexane for 15 min. and immediately mixing 1.8×10^{-4} mole of the Br⁸² tagged Br₂ (specific activity 20 mcuries g.⁻¹) with 1 ml. of the irradiated cyclohexane. In our studies of Br⁸² organic retention as a function of length of neutron irradiation at this concentration (0.02 mole fraction of Br₂), we found the organic retention following a 15-min. irradiation increased 14.5% over the zero-time irradiation retention. If the long-lived reactive species were formed in pure cyclohexane by radiation in the reactor, it should have reacted with the added tagged Br₂ giving at least 14.5% organic retention after standing for 15 min. or longer at 25°. This would be expected since the thermal reactions were shown to occur outside as readily as inside the reactor (Table II). However, less than 0.5% reaction of radiobromine was found after the mixture remained at room temperature in darkness for 2 to 4 hr. This indicated that significant quantities of the reactive species were formed only when bromine was present in the cyclohexane.

If I¹²⁸ were produced in cyclohexane, it might be expected to show phenomena similar to bromine. In a time study of the iodine-cyclohexane system, no increase in I¹²⁸ organic retention with irradiation time was found.

A total of 250 separate experiments was performed in studying the effects of irradiation time on organic retention of Br^{80m} and Br⁸² at 14 different concentrations. Plots of irradiation times *vs.* organic retentions (similar to Table I) showed the highest rate of increase for short irradiations. Organic retentions varied little for irradiations of 30 min. or more; thus, a plateau was reached on which we observed reproducible, but not totally hot-atom organic retentions. Since irradiations shorter than 10 sec. were not feasible, we extrapolated the plots to zero irradiation time and interpreted these organic retentions as due to hot-atom reactions other than postactivation thermal reactions. The organic retentions at extrapolated zero-time, 30-sec., and 30-min. (plateau region) irradiations are illustrated in Table III.

The differences between organic retentions resulting from 30-min. and zero-time irradiations vary between 20% for very low and 3% for very high Br₂ concentrations. However, the ratio of the fraction fixed immediately to the fraction fixed slowly is nearly constant. If the scavenger curve, *i.e.*, organic retention as a function of mole fraction of Br₂, for Br⁸² after 30-min. irradiations is plotted, a nonlinear function is found with rather good correlation to data published

by Milman¹¹ for Br⁸⁰ (18 min.) using irradiations of 20–40 min. The experimentally determined Br⁸² scavenger curve for 30-sec. irradiations is much lower than the 30-min. curve and linear from 0.1 to 1.0 mole fraction of Br₂. The zero-time Br⁸² scavenger curve coincides with that of Br^{80m} within $\pm 1\%$ and is linear from 0.07 to 1.0 mole fraction of Br₂ with a slope of

Table III: Organic Retentions of Br⁸² and Br^{80m} in Liquid Cyclohexane as a Function of Br₂ Scavenger Concentration and Irradiation Time^a

Mole fraction of Br ₂	Organic retention, % ^b		
	Br ^{80m} and Br ⁸² , zero time	Br ⁸² , 30 sec.	Br ⁸² , 1820 sec.
0.001	30.0	36.6	50.1
0.002	29.0	32.6	44.8
0.004	28.0	30.2	42.3
0.006	23.5	24.0	38.2
0.013	20.0	21.5	34.1
0.019	18.5	19.6	32.0
0.031	16.4	17.1	27.8
0.051	13.0	14.1	23.8
0.071	11.2	13.5	21.8
0.137	10.5	12.4	19.0
0.256	9.15	10.7	14.6
0.451	6.80	7.35	11.7
0.604	5.30	5.41	8.52
0.729	3.70	3.73	6.46

^a Twenty seconds is added to actual irradiation times to allow for thermal reactions occurring between the end of irradiation and freezing in liquid nitrogen. Zero time was obtained by extrapolating a plot of organic retention *vs.* irradiation time to zero irradiation time. ^b Results are within $\pm 0.5\%$ experimental error. Statistical errors were negligible.

–12.5%. The low scavenger concentration region below 0.07 mole fraction of Br₂ shows a marked increase in Br^{80m} and Br⁸² organic retentions, possibly due to diffusive reactions of unscavenged radicals as originally postulated by Hornig and Willard.^{8c} Study in the low scavenger concentration region was facilitated by using zero-time extrapolations since the radiation-produced organic retentions were minimized by short irradiations and eliminated by proper extrapolations.

The extrapolation of the linear portion of the zero-time scavenger curve to zero Br₂ mole fraction is $12.5 \pm 0.5\%$ as compared to $17.5 \pm 0.5\%$ for the 30-min. irradiation curve, the same value obtained by Milman

(11) M. Milman, *Radiochim. Acta*, 2, 180 (1964).

for Br^{80} . We found that Milman's¹¹ application of the Estrup-Wolfgang kinetic model^{2a-c} to the liquid bromine-cyclohexane system, assuming hot bromine atom reactions with cyclohexane molecules, did not correlate with our zero-time bromine data. In fact, the linearity of the scavenger curve supports a radical-type model^{8c} such as the random fragmentation model,¹² the Auger radiation model,^{2d} or a combination of both.

The Auger radiation hypothesis was given increased support by the work of Thompson and Miller¹³ which shows that in condensed media, certain recoiling atoms rarely develop a charge prior to loss of initial kinetic energy. If Auger radiation alone were responsible for the final chemical state of the Br^{80m} and Br^{82} one might expect an isotope effect due to a different per cent of internal conversion.¹⁴ However, if Auger radiation led to the same per cent organic combination as random fragmentation, no isotope effect would be expected. Since none was observed (in the absence of postactivation thermal reactions), the Br^{80m} and Br^{82} hot-atom yields in Br_2 -scavenged cyclohexane may be explained by the random fragmentation model or a combination of random fragmentation and Auger radiation models.

The nature of the reactive species, its control, and the possible role of Br^{82m} are being extensively studied. If a long-lived, thermally reactive species is formed as a consequence of isomeric transition reactions as well as by (n, γ) reactions, the observed pseudo-isotope effect may be due to an increase in the concentration of the species formed by the Br^{82m} isomeric transition reaction. Preliminary results indicate that such species may be formed in *n*-hexane, 2,2-dimethylbutane, 2,3-dimethylbutane, 2-methylpentane, and 3-methylpentane. Ellgren¹⁵ has found postactivation thermal reactions of Br_2 in CCl_4 with an increase in the organic retentions of Br^{80m} and Br^{82} with length of irradiation. If such long-lived reactive species are formed by radiobromine atoms in all organic solvents, it may call for a re-evaluation of most liquid bromine hot-atom chemistry data.

Acknowledgment. We thank Alan J. Blotcky and the personnel of the Omaha V.A. Hospital who assisted us in the many reactor irradiations. This research was supported in part by funds made available by the University of Nebraska Research Council.

Hydrogen Bonding of Amide Groups in Dioxane Solution

by H. Susi

Eastern Regional Research Laboratory, Eastern Utilization Research and Development Division, U. S. Department of Agriculture, Agricultural Research Service, Philadelphia, Pennsylvania 19118 (Received February 1, 1966)

Lactams frequently have been used as model compounds to investigate amide to amide hydrogen bonding because the *cis* arrangement of C=O and N-H groups leads to dimerization exclusively and prevents complications arising from multiple equilibria between hydrogen-bonded chain polymers.¹⁻³ Various authors have employed infrared methods to investigate the dimerization of lactams in carbon tetrachloride, a solvent which is virtually inert from the standpoint of hydrogen bonding.¹⁻⁴ Relatively little work has been reported in solvents which are themselves capable of hydrogen-bond formation. Such studies lead to a net energy difference between initial and final states characterized by amide groups bonded to the solvent and to each other, respectively. The results are of interest in assaying the role of hydrogen bonds in the secondary structure of proteins under conditions where amide-amide bonds can compete with amide-solvent bonds. The energy of interaction of even weak proton donors, such as chloroform, with an amide has been estimated at 2 kcal./mole.²

This communication reports a study of the dimerization of δ -valerolactam in a proton-accepting solvent, dioxane, by methods of infrared spectroscopy. One of the principal difficulties encountered in work with complex systems is proper evaluation of the temperature dependence of the absorption coefficients of various species.⁵ For the investigated system, a procedure involving some approximations is proposed which takes into account both solvent-solvent and solvent-solute interactions and which leads to internally consistent results over a wide range of temperature and concentration.

- (12) J. E. Willard, *Ann. Rev. Nucl. Sci.*, **3**, 193 (1953).
- (13) J. L. Thompson and W. W. Miller, *J. Chem. Phys.*, **38**, 2477 (1963).
- (14) S. Wexler and T. H. Davies, *ibid.*, **20**, 1688 (1952).
- (15) W. K. Ellgren, private communication, this laboratory, 1964.

- (1) M. Tsuboi, *Bull. Chem. Soc. Japan*, **24**, 75 (1951).
- (2) W. Klemperer, M. W. Cronyn, A. H. Maki, and G. C. Pimentel, *J. Am. Chem. Soc.*, **76**, 5846 (1954).
- (3) R. C. Lord and T. J. Picro, *Z. Elektrochem.*, **64**, 672 (1960).
- (4) H. E. Affsprung, S. D. Christian, and J. D. Worley, *Spectrochim. Acta*, **20**, 1415 (1964).
- (5) G. C. Pimentel and A. L. McClellan, "The Hydrogen Bond," W. H. Freeman and Co., San Francisco, Calif., 1960, p. 77.

Experimental

δ -Valerolactam (Aldrich Chemical Co.⁶) was purified by distillation to remove traces of water. Dioxane (Fisher Certified Reagent) was refluxed with dilute hydrochloric acid for 12 hr., then refluxed over sodium for 24 hr. and distilled.⁷ Absorption spectra from 6000 to 7000 cm^{-1} were obtained with a Cary Model 14 instrument. Sample concentrations ranged from 0.1 to 0.8 mole/l. The absorption of each sample was investigated at 25, 45, and 65°. A water-jacketed controlled-temperature absorption cell of conventional design¹ and 25-mm. path length was employed.

Only one temperature-dependent absorption band of appreciable intensity, centering close to 6690 cm^{-1} ($\sim 1.495 \mu$), was observed in the investigated range. This band was assigned to the first overtone of the NH stretching mode of amide groups not involved in amide-amide H-bonding, on the basis of its temperature dependence and by comparison with spectra obtained in various other solvents (CCl_4 , CCl_3H) and the spectrum of the pure lactam. It should be pointed out that neither in dioxane solution nor in any other investigated solvent (or in the spectrum of the pure lactam) were bands of appreciable intensity found which could be assigned to overtones of NH stretching fundamentals of groups involved in amide-amide bonding. Although the corresponding fundamentals are very intense,¹⁻³ the overtones must be extremely weak. Figure 1A gives the observed peak absorbance of the investigated absorption band as a function of temperature and concentration, as observed in a 25-mm. cell.

Evaluation of Experimental Results

If no higher polymers are formed and if the solvent is inert, then the following relations hold

$$K'_x = \frac{C - M}{2M^2} \left(\frac{C + M}{2} + C_s \right) \quad (1)$$

$$M = A/\epsilon d \quad (2)$$

$$K'_x = \frac{C - A/\epsilon d}{2(A/\epsilon d)^2} \left(\frac{C + A/\epsilon d}{2} + C_s \right) \quad (3)$$

where K'_x is the dimerization constant in mole fraction units; C is the total solute concentration in moles per liter; C_s is the solvent concentration in moles per liter; M is monomer concentration in moles per liter; A is the absorbance of monomers; ϵ is the absorptivity of monomeric species; and d is the path length.

Rearrangement of (3) leads to

$$C_s/A = (\epsilon d/A^2)(C^2/2 + C_s C) - (4K'_x + 1)/2\epsilon d \quad (4)$$

The unknowns K'_x and ϵ can be obtained by setting

$$y = C_s/A \quad (4a)$$

$$x = (1/A^2)(C^2/2 + C_s C) \quad (4b)$$

and by plotting y vs. x . ϵd is given by the slope and K'_x is calculated from the intercept. The necessity to evaluate ϵ by extrapolation is eliminated.

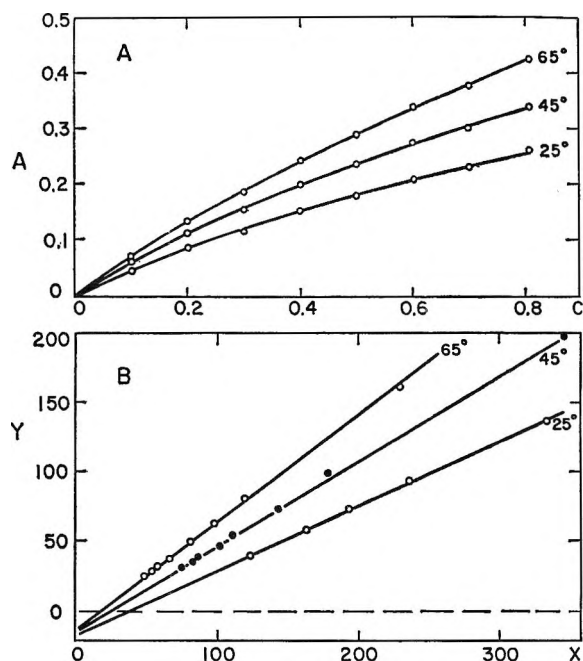


Figure 1. A: Observed absorbance of δ -valerolactam in dioxane solution at 1.495μ ; path length: 25 mm. B: Graphical evaluation of absorptivity and dimerization constant; $y = C_s/A$; $x = (1/A^2)(C^2/2 + C_s C)$.

Figure 1B presents the results of the described graphical procedure. It is immediately obvious that the slope of the obtained lines varies with temperature, *i.e.*, that the observed absorptivity [$\epsilon_{\text{obsd}} = (dA/dC)_{T,C \rightarrow 0}$] is strongly temperature dependent. An inspection of Figure 1A leads to the same conclusion.

If the monomer is heavily bonded to the solvent, then dimerization occurs by breaking up this complex and forming the dimer and two solvent molecules. In this case, eq. 1 holds for the dimerization of initially solvent-bonded monomers. Previous infrared studies have shown that amides are very strongly bonded to ethers,⁸ *i.e.*, the monomer-solvent association constant

(6) Mention of specific firms and products does not imply endorsement by the U. S. Department of Agriculture over others of a similar nature not named.

(7) K. Hess and H. Frahm, *Ber.*, **71**, 2627 (1938).

(8) S. Mizushima, M. Tsuboi, T. Shimanouchi, and Y. Tsuda, *Spectrochim. Acta*, **7**, 100 (1955).

has a high value. If the association constant for solute-solvent interaction is much higher than the solvent-solvent association constant, eq. 3 is also applicable to the dimerization of initially solvent-bonded monomers, provided the temperature dependence of the apparent absorptivity is taken into consideration.

Figure 1B leads to the following numerical values: $T = 298^\circ\text{K}$., $\epsilon_{\text{obsd}} = 0.184 \text{ l. mole}^{-1} \text{ cm.}^{-1}$, $K'_z = 4.1 \text{ (mole fraction)}^{-1}$; $T = 318^\circ$, $\epsilon_{\text{obsd}} = 0.246$, $K'_z = 4.2$; $T = 338^\circ$, $\epsilon_{\text{obsd}} = 0.295$, $K'_z = 4.0$.

The variation of K'_z is within experimental accuracy. Standard methods lead to: $\Delta H = 0 \pm 0.5 \text{ kcal./mole}$, $\Delta S^\circ = +3 \pm 0.5 \text{ e.u.}$ for the dimerization of initially solvent-bonded monomers. The entropy value refers to a standard state defined in mole fractions.

Discussion

The results suggest that the energy required to break amide-ether hydrogen bonds is approximately equal to the energy of formation of amide-amide bonds. The relatively high value of the association constant is thus a consequence of a positive standard entropy change upon dimerization. While the system is far too complex for a detailed discussion of entropy relations, a brief qualitative consideration might provide some insight. The "monomeric" system involves two particles schematically represented by: $2 \times (\text{amide-dioxane})$. Upon dimerization, one amide-amide dimer (with two H bonds) and two free solvent molecules are formed, *i.e.*, the total number of particles is increased. At sufficiently high concentration, the positive value of ΔS° results in a considerable number of $\text{NH}\cdots\text{O}=\text{C}$ bonds being formed without a net change in enthalpy. The value of K'_z reported here is about 1/725 times the value given by Tsuboi¹ for dimerization of δ -valerolactam in carbon tetrachloride solution ($K_{\text{C}(\text{CCl}_4, 25^\circ)} = 280 \text{ moles/l.}$; $K_{\text{z}(\text{CCl}_4, 25^\circ)} = 2900 \text{ (mole fraction)}^{-1}$), reflecting the strong competition between dimerization and solvent interaction in the studied system.

The experimental data, as presented in Figure 1A, re-emphasize the necessity^{3,5} to determine the temperature dependence of apparent absorptivity values if thermodynamic quantities are deduced from absorbance measurements in complex systems. Our results also lend support to the conclusion⁹ that the anharmonicity of XH stretching fundamentals is reduced by hydrogen bonding.¹⁰

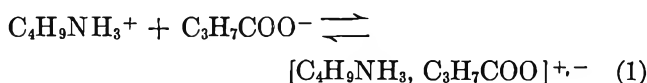
Ion-Pair Formation in Aqueous Solutions of Butylammonium Isobutyrate¹

by Irving M. Klotz and Henry A. DePhillips, Jr.²

Department of Chemistry, Northwestern University, Evanston, Illinois (Received February 8, 1965)

Among the noncovalent bonds which may participate in the fixation of conformation in protein molecules one must include the possibility of electrostatic interactions between pendant $-\text{NH}_3^+$ and $-\text{COO}^-$ side chains. From the physicochemical behavior of simple ions in aqueous solution there are indications³ that ion-pair formation, such as $[-\text{NH}_3^+\cdots-\text{OOC}-]$, does not occur to any detectable extent except at very high concentrations. Nevertheless, no direct measurements have been available for a system of an ammonium and carboxylate groups suitable as a model for potential interactions among protein side chains. We have now found that optical measurements in the near-infrared, similar to those used previously to study amide hydrogen bonds,⁴ do give an insight into ion-pair formation between *n*-butylammonium and isobutyrate ions.

In essence we have used the overtone infrared region to measure the equilibrium constant for the reaction



From the equilibrium constant, established at three temperatures, the free energy, enthalpy, and entropy of ion-pair interactions may be calculated.

Experimental

Preparation of Solutions. Spectra were examined in the region of 1.5μ rather than in the fundamental range so as to minimize complications due to the absorption by water, the solvent. As in previous work a reference cell was prepared containing the same amount of water as the sample cell but with a solute,

(1) This investigation was supported in part by a grant (GM-09280) from the National Institute of General Medical Sciences, Public Health Service. It was also assisted by support made available by a Public Health Service Training Grant (No. 5T1-GM-626) from the National Institute of General Medical Sciences.

(2) Predoctoral Fellow of the U. S. Public Health Service, 1961-1963.

(3) I. M. Klotz, *Brookhaven Symp. Biol.*, **13**, 25 (1960).

(4) I. M. Klotz and J. S. Franzen, *J. Am. Chem. Soc.*, **84**, 3461 (1962).

(9) See ref. 5, p. 114.

(10) The overtone frequency in dioxane solution is very close to the overtone frequency in CCl_4 solution. The fundamental frequency is substantially lower in dioxane solution.

optically transparent at the wave length of interest, in place of the butylammonium butyrate in the sample cell.

A series of reference solutions of potassium isobutyrate in water was prepared, their densities were determined, and their water concentrations were calculated. A graph of density (or composition) *vs.* water content of the reference solutions was then drawn. Thereafter a sample solution was made from accurately known weights of *n*-butylammonium butyrate and water; the density of this solution was determined and the concentration of water therein was calculated. Inspection of the graph for reference solutions then revealed what composition to create to have an accurately balanced filler for the reference cell.

Densities. Measurements were made with a Weld-type pycnometer of 7-cc. volume. Samples were introduced with a hypodermic needle. All densities were determined at $25.00 \pm 0.05^\circ$.

Spectra. Absorption spectra in the 1.4–1.7- μ range were recorded with a Cary spectrophotometer, Model 14R. The cell compartment in the spectrophotometer was thermostated and the temperature within the absorption cells was checked periodically with a thermistor probe. Quartz absorption cells were used.

Materials. *n*-Butylamine and isobutyric acid of reagent grade were purchased from Fisher Scientific Co. The salt butylammonium isobutyrate was obtained by slowly mixing amine and acid in a large beaker with rapid stirring. A slight excess of amine was used to assure complete reaction. Dry nitrogen was bubbled through the liquid for 2 hr. to remove excess amine. A spectrum of the final product revealed no absorption at 1.53 μ , where pure butylamine exhibits an intense absorption. Potassium isobutyrate was prepared by neutralizing isobutyric acid with potassium hydroxide. Carbon tetrachloride was Fisher Spectranalyzed grade.

Results

Water itself shows a broad region of absorption in the near-infrared with a peak at about 1.46 μ at room temperature. Addition of *n*-butylammonium isobutyrate to water changes the absorption spectrum. Such a change may reflect two contributions, however: (1) the solute absorbs in this region; and (2) the solute changes the absorption spectrum of water because it perturbs the structure of the solvent.⁵

To compensate for the second effect we have used potassium isobutyrate in the reference cell. This salt, being present at approximately the same concentration as the butylammonium isobutyrate in the sample cell, should have approximately the same ionic

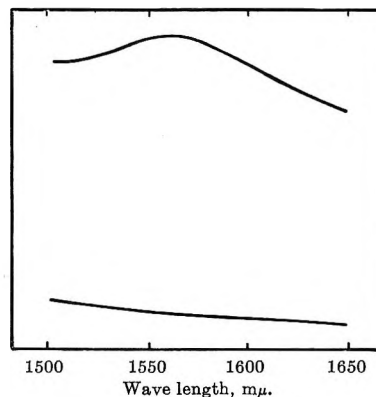


Figure 1. The upper curve is the difference spectrum in the near-infrared region. (1510–1650 $m\mu$) for an aqueous solution of *n*-butylammonium isobutyrate *vs.* an aqueous solution of potassium isobutyrate containing the same molarity of water: concentration of butylammonium isobutyrate, 3.389 *M*; temperature, 25.0° . The lower line shows the balance between cells with identical contents.

perturbing effect on the solvent. A typical difference spectrum is illustrated in Figure 1 and shows a peak at 1.56 μ . Since this is the general range in which the overtone absorption of N–H groups usually appears, it seems reasonable to assume that the intensity of the difference spectrum at 1.56 μ reflects the concentration and state of the $\text{CH}_3\text{CH}_2\text{CH}_2\text{CH}_2\text{NH}_3^+$ group. If there is no charge in state, the molecular extinction coefficient should be essentially constant. If a large change in extinction coefficient is observed it seems reasonable to attribute it to ion-pair formation. On this basis one can measure the equilibrium constant from changes in absorbance at 1.56 μ .

For the equilibrium of eq. 1, an association constant, *K*, may be written as

$$K = \frac{1 - \alpha}{\alpha^2} \frac{1}{C_t} \quad (2)$$

where α is the fraction of total butylammonium isobutyrate in the form of free ions and C_t is the total molar concentration of salt. (Strictly speaking this equation gives only the equilibrium quotient since activity coefficients are not included). Spectrophotometric measurements provide the information for the evaluation of α . In a solution containing free ions and ion pairs, the absorbance, *A*, may be expressed as

$$A = (\epsilon_{\text{ions}}C_{\text{ions}} + \epsilon_{\text{ion pair}}C_{\text{ion pair}})l \quad (3)$$

where ϵ represents the extinction coefficient and *l* is the optical path length. In view of the definition of α , it follows that

(5) That salts affect the infrared spectrum of water has long been known in the literature. For a recent description of some of these effects see I. M. Klotz, *Federation Proc.*, 24, S-24 (1965).

$$A = lC_t[\epsilon_{\text{ions}}\alpha + \epsilon_{\text{ion pair}}(1 - \alpha)] \quad (4)$$

$$= lC_t\epsilon_{\text{obsd}}$$

from which we obtain

$$\alpha = \frac{\epsilon_{\text{obsd}} - \epsilon_{\text{ion pair}}}{\epsilon_{\text{ions}} - \epsilon_{\text{ion pair}}} \quad (5)$$

The value of ϵ_{obsd} , which is in essence defined by the second part of eq. 4, is obtained from the measured value of A for a solution of known C_t of butylammonium butyrate. Since in increasingly dilute solutions, ion pairs would tend toward complete dissociation, ϵ_{ions} can be evaluated from

$$\lim_{C_t \rightarrow 0} \epsilon_{\text{obsd}} = \epsilon_{\text{ions}} \quad (6)$$

Such an extrapolation is illustrated in Figure 2. The values found for ϵ_{ions} were 524, 413, and 310 $\text{cm}^2 \text{mole}^{-1}$ at 1.3, 25.0, and 49.8°, respectively. The determination of $\epsilon_{\text{ion pair}}$ is generally more difficult. However, butylammonium isobutyrate is a liquid at room temperature, and we have assumed that

$$\lim_{C_t \rightarrow \infty} \epsilon_{\text{obsd}} = \epsilon_{\text{ion pair}} = \epsilon_{\text{pure liq}} \quad (7)$$

The spectrum of the pure liquid was examined at each temperature, with potassium isobutyrate mixed with carbon tetrachloride in the reference cell. The extinction coefficient calculated at 1.56 μ is small, 25 $\text{cm}^2 \text{mole}^{-1}$. Since this is near zero, and there is some uncertainty in regard to compensation by the contents of the reference cell, we have arbitrarily set $\epsilon_{\text{ion pair}}$ equal to zero. The uncertainty in K due to this procedure is about 5%.

Knowing ϵ at the extrema, α and then the apparent association constant K may be computed from experimental values of ϵ_{obsd} vs. C_t . As is evident from Figure 2, most of the salt exists as ions until the concentration of water is greatly reduced so that ion pairs must be formed. In the range of 1–3 M butylammonium isobutyrate, α varies from 0.96 to 0.7, *i.e.*, the salt is overwhelmingly present as ions. Association constants are thus very uncertain but vary from about 0.02 at low concentrations to 0.2 near 3 M . At 25° a rough extrapolation to infinite dilution was attempted and it led to $K = 0.03$.

From an equilibrium constant alone one cannot tell much about the nature of the interaction in these ion

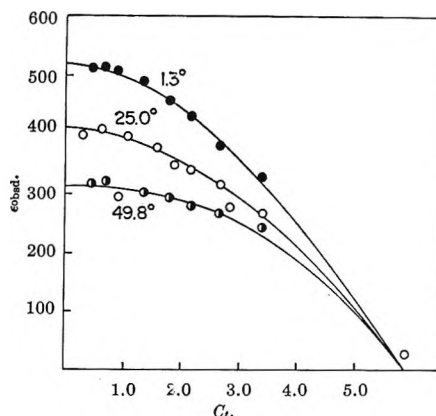


Figure 2. Observed extinction coefficients at 1.56 μ as a function of total (molar) concentration of *n*-butylammonium isobutyrate in water.

pairs. Nevertheless, since the observed K is an order of magnitude greater than that for an $\text{N}-\text{H}\cdots\text{O}=\text{C}$ hydrogen bond in an aqueous solvent,⁴ it seems likely that electrostatic interactions are contributing to the stability of the ion pair.

The uncertainty in association constant was too great to permit a direct computation of ΔH° from the temperature dependence of $\ln K$. However, by a procedure analogous to that used previously for hydrogen-bonding amides in water⁴ one can show that

$$\left(\frac{\partial \ln C_{\text{ions}}}{\partial T}\right)_{P,\alpha} = -\frac{\Delta H^\circ}{RT^2} \quad (8)$$

i.e., one can compute the enthalpy from the temperature dependence of C_{ions} at constant α . By this method a ΔH° of $-1 \text{ kcal. mole}^{-1}$ was obtained. In summary then, for the ionic association of eq. 1, at 25°

$$\Delta F^\circ = 2.1 \text{ kcal. mole}^{-1}$$

$$\Delta H^\circ = -1 \text{ kcal. mole}^{-1}$$

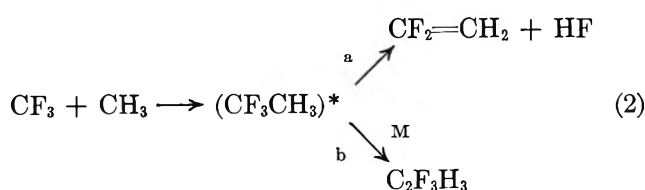
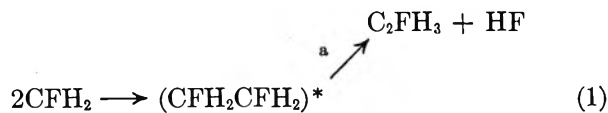
$$\Delta S = -10 \text{ gibbs mole}^{-1}$$

As one might expect from other ion associations, ΔS° has a negative value, presumably because some water molecules are released, and ΔH° is near zero. It is no surprise then that ΔF° for ion-pair formation is unfavorable. As the results in Figure 2 show most directly, only at high molar concentrations of butylammonium isobutyrate, where the water concentration is severely reduced, do the ions tend to become appreciably associated.

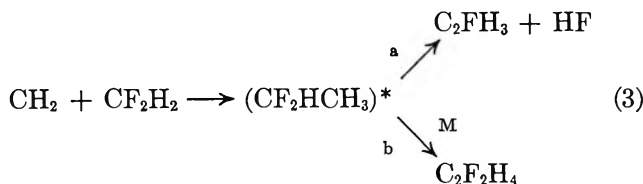
COMMUNICATIONS TO THE EDITOR

The Reaction of Methylene with CF_2H_2

Sir: The formation of vibrationally excited fluorethanes *via* radical combination may result in the elimination of HF from the vibrationally excited species^{1,2}

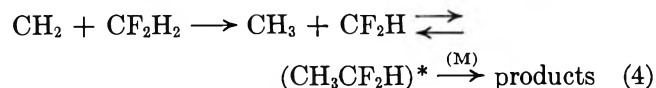


before complete collisional stabilization occurs. We have now produced similar eliminations, using the insertion reaction of methylene into C-H bonds



by photolyzing ketene in the 3000–3800-Å spectral region in the presence of CF_2H_2 . The results are presented in Table I.

The absence of products in the presence of O_2 indicates an abstraction mechanism



followed by combination, and the participation of triplet methylenes at the longer wave lengths (>3400 Å)^{3,4} which are scavenged, together with any mono radicals formed, by O_2 . Some very recent work on the reactions of CH_2 with CH_3Cl and CH_2Cl_2 strongly favors an abstraction mechanism⁵ (Cl \gg H atom), although the exclusive formation of CD_3CDH_2 in the system⁶ $\text{CH}_2 + \text{CD}_4 + \text{O}_2$ clearly demonstrates that insertion occurs.

Secondary evidence for the presence of monoradicals in our system was not conclusive. CH_4 and C_2H_6 were formed, but they were also present when ketene was photolyzed alone. We did not identify any $\text{CF}_2\text{HCF}_2\text{H}$, and $\text{C}_2\text{F}_3\text{H}$ would not be expected.⁷ However, a major fate of the monoradicals produced in (4) would also be addition at $>\text{C}=\text{C}<$. Further, the dissociation step

Table I^c

Temp., °K.	Reactants, cm.		Products, ^b			% reaction ^d	$\text{C}_2\text{H}_4/\text{CO}^e$
	CH_2CO	CF_2H_2	C_2FH_3	$\text{C}_2\text{F}_2\text{H}_4$	$\text{CF}_2\text{HCH}_3^f$		
305	0.86	5.50	1.16	0.716	1.62	4.7	0.25
354	1.16	4.96	1.86	1.14	1.64	5.7	0.24
397	0.82	6.38	1.49	0.793	1.88	7.2	0.22
431	0.92	7.48	2.01	0.622	3.23	6.5	0.18
477	1.22	13.10	2.64	0.569	4.65	6.6	0.16
528	0.86	9.46	1.57	0.268	5.86	4.5	0.11
518 ^f	0.92	7.14	Trace	None

^a Reaction time and volume, 1 hr. and 156 cc., respectively.

^b Analysis by v.p.c. on 2-m. 3% squalane on alumina column.

^c Vinyl fluoride was also identified by mass spectrometry.

^d $(\text{C}_2\text{FH}_3 + \text{C}_2\text{F}_2\text{H}_4)/\text{CO} \times 100$. Large conversion (>50%) of ketene were used. ^e V.p.c. indicated increasing C_2 's with temperature, from $\text{CH}_2 + \text{C}_2\text{H}_4$. ^f O_2 added (1.66 cm.).

in (4) must be included for reaction sequence 3, so that the presence of radicals does not invalidate (3).⁸

The $\text{C}_2\text{FH}_3/\text{C}_2\text{F}_2\text{H}_4$ ratios in Table I are similar in magnitude and show the same temperature dependence for those reported earlier¹ in the photolysis of $(\text{CFH}_2)_2\text{CO}$, at a total pressure of 2 cm. Although the reaction of CH_2 with vinyl fluoride is rapid,⁹ we assume little is lost, on concentration grounds. The results may be rationalized by taking a relative over-all efficiency of 0.2 to 0.3 for energy transfer for the reaction mixture, compared to the ketene as unity.¹⁰ The results do not favor the abstraction over the insertion mechanism, as the excess energy that CH_2 carries into its reactions¹¹ would be insufficient to alter markedly the HF elimination ratios in reaction sequence 3.^{12,13}

(1) G. O. Pritchard M. Venugopalan, and T. F. Graham, *J. Phys. Chem.*, **68**, 1786 (1964).

(2) W. G. Alcock and E. Whittle, *Trans. Faraday Soc.*, **61**, 244 (1965); R. D. Giles and E. Whittle, *ibid.*, **61**, 1425 (1965).

(3) S. Y. Ho, I. Unger, and W. A. Noyes, Jr., *J. Am. Chem. Soc.*, **87**, 2297 (1965).

(4) We used a B.T.H. ME/D high-pressure mercury arc (no filter) with intense emission at longer wave lengths.

(5) D. W. Setser, R. Littrell, and J. C. Hassler, *J. Am. Chem. Soc.*, **87**, 2062 (1965).

(6) J. A. Bell and G. B. Kistiakowsky *ibid.*, **84**, 3417 (1962).

(7) G. O. Pritchard and J. T. Bryant, *J. Phys. Chem.*, **69**, 1085 (1965).

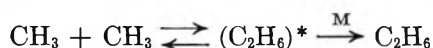
(8) Setser's product data⁹ on $\text{CH}_3(\text{A}) + \text{CH}_2\text{Cl}(\text{B})$ cross (disproportionation + combination) ratios, $R_{\text{AB}}^2/R_{\text{AA}}R_{\text{BB}}$, should give ≈ 4 . The two low pressure runs give values of 4.5 and 3.9, but the remainder yield an average value of 2.1, which may indicate complications.

(9) F. Casas, J. A. Kerr, and A. F. Trotman-Dickenson, *J. Chem. Soc.*, 1141 (1965).

(10) Setser's HCl elimination data⁹ from the vibrationally excited chloroethanes give $\text{C}_2\text{H}_3\text{Cl}/\text{C}_2\text{H}_4\text{Cl}_2 \approx 1.9$ and $\text{C}_2\text{H}_4/\text{C}_2\text{H}_5\text{Cl} \approx 20$, reflecting a decrease in effective oscillators in $\text{C}_2\text{H}_5\text{Cl}^*$.

(11) J. A. Bell, *Progr. Phys. Org. Chem.*, **2**, 1 (1964).

Omitting the experiment at 305° K., the remaining data give a good Arrhenius plot¹⁴ of $E_a - E_b$ (for reaction 3) = 2.7 kcal. mole⁻¹. Whittle² finds $E_a - E_b$ (for reaction 2) = 1.9 kcal. mole⁻¹. Similar temperature dependencies have been found¹⁵ for the dissociation/stabilization ratio for $(C_2H_6)^*$



It appears that energy transfer is less efficient with increasing temperature.¹³

A similar series of experiments was conducted with CF_3H , but the expected products, $CF_2=CH_2$ and CF_3-CH_3 , were not detected, indicating that no reaction occurred. Recent bromination studies¹⁶ indicate that $D(CF_3-H) - D(CF_2H-H) \simeq 2$ kcal. mole⁻¹, which is a contributing factor. It has also been found⁹ that the reactivity of CH_2 toward ethylene, both with regard to addition and insertion, decreases markedly with increasing fluorination. Benson⁷ has proposed that methylene insertion processes of high cross section probably occur *via* very loose transition states to which ionic states, $CH_2 \cdots \overset{+}{H} \cdots (R)$, make a major contribution. Increasing the number of highly electronegative F atoms in the R group thereby reduces the reaction probability.¹⁸

Acknowledgments. We are indebted to Dr. E. Whittle for communication of unpublished data, and to the National Science Foundation for a grant-in-aid.

(12) We may estimate that the excited species in sequence 3 is ~ 90 kcal. vibrationally excited at 3000 Å., compared to 85 kcal. in sequence 4. The transfer of 10–20 kcal. of excess vibrational energy may occur per collision.¹³

(13) B. S. Rabinovitch and M. C. Flowers *Quart. Rev. (London)*, **18**, 122 (1964).

(14) Over an extended temperature range, linear plots are not obtained.¹

(15) R. E. Dodd and E. W. R. Steacie, *Proc. Roy. Soc. (London)*, **A223**, 283 (1954); S. Toby and B. H. Weiss, *J. Phys. Chem.*, **68**, 2492 (1964).

(16) A. M. Tarr, J. W. Coomber, and E. Whittle, *Trans. Faraday Soc.*, **61**, 1182 (1965).

(17) S. W. Benson, *Advan. Photochem.*, **2**, 1 (1964).

(18) This is equally applicable to an insertion or an abstraction mechanism, as Benson¹⁷ postulates that insertion is really abstraction followed by recombination of the radicals which are in very close proximity.

DEPARTMENT OF CHEMISTRY
UNIVERSITY OF CALIFORNIA
SANTA BARBARA, CALIFORNIA

G. O. PRITCHARD
J. T. BRYANT
R. L. THOMMARSON

RECEIVED JUNE 3, 1965

The Radiolysis of Monodisperse Colloidal Sulfur

Sir: Absorption by gross heterogeneous mixtures of sulfur and water at 33° of ionizing radiation correspond-

ing to 5.5×10^{20} e.v./ml. produces sulfate and sulfide in small but measurable quantities. A species is formed which has an absorption peak in the ultraviolet at 210 m μ and is qualitatively similar to that obtained by heating to 90–100° mixtures of sulfur and water. The latter product has been described as consisting of sulfide and sulfur oxyanions.¹ These products are not formed after comparable exposure at 33° in the absence of radiation.

Since colloidal sulfur essentially monodisperse with regard to particle size may be readily prepared and the particle size determined by light scattering measurements,² the radiolysis of such systems affords an unusual opportunity for the study of heterogeneous radiation kinetics. This communication describes preliminary results obtained from such experiments.

Sulfur hydrosols having a very narrow range of particle size (La Mer sols) were prepared by mixing dilute sodium thiosulfate and hydrochloric acid solutions under conditions of careful temperature control and extreme precautions to exclude foreign particulate matter. When the particles had reached a desired stage of growth, the reaction was stopped by titration with saturated aqueous bromine. The colloidal systems were irradiated in a Co⁶⁰ source at dose rates which varied from 2.90 to 2.75×10^{19} e.v./ml. hr. over the period of the experiments.

Particle sizes were determined by the polarization ratio method using a Brice-Phoenix light scattering photometer. Typical spectra are shown in Figure 1 in which ratios of horizontally to vertically polarized intensities are plotted as a function of scattering angle for a colloid before and after irradiation. From the positions of the maxima and minima, particle sizes were obtained using the tabulations in ref. 2.

Curves A, B, and C in Figure 2 show the effect of radiation in aerated colloids of several different initial sizes of particles. In these systems the initial reactant concentrations were 0.0015 *M* thiosulfate and 0.0030 *M* acid. They differ only in the extent to which the reaction has occurred to form the different sized particles and in the amount of bromine added to stop the reaction. In each case there is a linear relationship between the fifth power of the radius and total dose to at least as small a radius as 0.15 μ . Such a relationship is consistent with a rate expression $-dv/dt = k/a$ in which v represents the particle volume (or mass of sulfur) and a the surface area; k includes the dose rate and is constant for a given suspension.

(1) W. A. Pryor, "Mechanisms of Sulfur Reactions," McGraw-Hill Book Co., Inc., New York, N. Y., 1962.

(2) M. Kerker and V. K. La Mer, *J. Am. Chem. Soc.*, **72**, 3516 (1950).

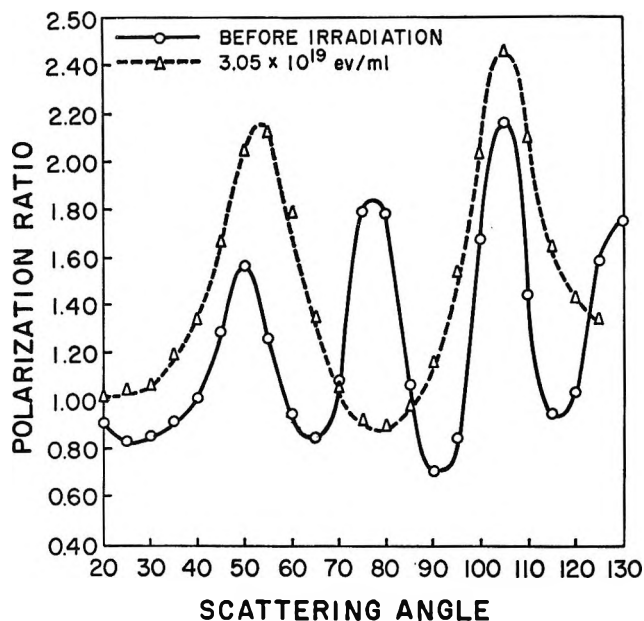


Figure 1. Polarization ratio spectra of a sulfur hydrosol before and after exposure to ionizing radiation. The initial spectrum corresponds to particles of $0.30\text{-}\mu$ radius. After receiving a dose corresponding to 3.05×10^{19} e.v./ml. the radius has been reduced to 0.19μ .

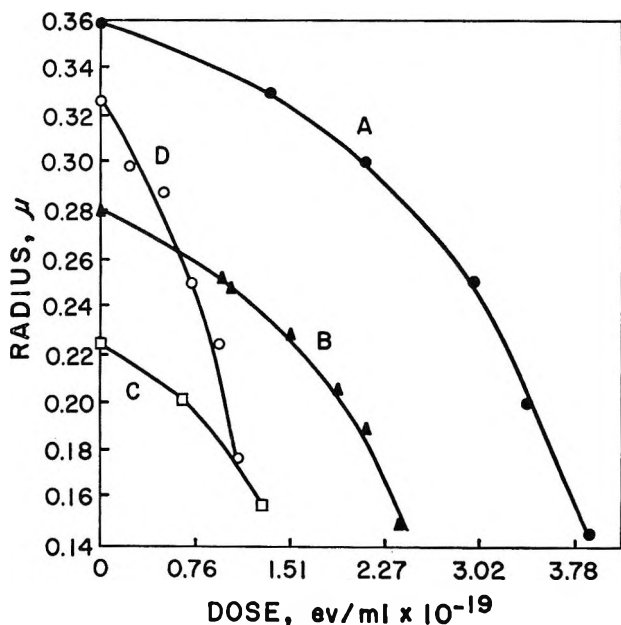


Figure 2. Effect of ionizing radiation on particle size in monodisperse sulfur hydrosols. The series represented by curve D was $0.16 M$ in *n*-propyl alcohol.

Within the framework of the usual picture of radiation-induced reactions in dilute aqueous systems, one may consider two limiting cases. (1) The rate of disappearance of elemental sulfur depends on the surface area exposed to a constant radical "flux."

For such a process, $dv/dt = -ka$ and the particle radius would decrease linearly with dose. (2) A constant rate of reaction, for particles above a certain size, would correspond to a linear change in volume with dose.

The observed particle size-dose relationships indicate that a more complex mechanism is involved and that there is an increasing reactivity of the colloidal material with a decrease in particle size.

In the series represented by curve D the colloidal system was made $0.16 M$ in *n*-propyl alcohol before irradiation. Since the alcohol is an efficient scavenger for both H and OH radicals, the marked acceleration in the rate seems most likely due to a modification in the interfacial properties of the sulfur-water system.

The colloidal suspensions do not respond well to the usual degassing techniques and bubbling with gas evidently disrupts the narrow particle size distribution. Results in deaerated systems at this time are qualitative, but in every case the rate was faster than in the systems exposed to the atmosphere.

Current experiments are concerned with a more detailed study of the kinetics and include measurements of salt effects and those of additives which alter the interfacial characteristics of the colloidal system.

Acknowledgment. This work was supported by a grant from the Division of Radiological Health of the U. S. Public Health Service. Appreciation is expressed to the Department of Food Science for the use of their facilities and light scattering photometer.

DEPARTMENT OF CHEMISTRY
THE UNIVERSITY OF GEORGIA
ATHENS, GEORGIA 30601

F. J. JOHNSTON

RECEIVED JUNE 18, 1965

Evidence for Bromine-82m Isomeric Transition Activated Reactions in Saturated Hydrocarbons and Alkyl Halides

Sir: Discovery of the $\text{Br}^{82\text{m}}(\text{IT})\text{Br}^{82}$ nuclear reaction ($T_{1/2}$ 5-6 min.)^{1,2} has helped to resolve apparent discrepancies in the literature concerning experimentally correct values of $\text{Br}^{80\text{m}}$ and Br^{82} organic retentions resulting from the radiative neutron-capture reactions in condensed organic systems.³ Isotope separations of

(1) O. U. Anders, Abstracts, 148th National Meeting of the American Chemical Society, Chicago, Ill., Sept. 1964, p. 10R.

(2) J. F. Emery, *ibid.*, p. 10R.

(3) For a review of hot atom reactions in condensed phases, see J. E. Willard, *Nucleonics*, 19, No. 10, 61 (1961); *Ann. Rev. Phys. Chem.*, 6, 141 (1955).

$\text{Br}^{80\text{m}}$ and Br^{82} attributable to $\text{Br}^{79}(\text{n},\gamma)\text{Br}^{80\text{m}}$ and $\text{Br}^{81}(\text{n},\gamma)\text{Br}^{82}$ reactions in several liquid and solid organic systems have been reported and refuted by various authors.⁴ The disagreement may be due in part to $\text{Br}^{82\text{m}}(\text{IT})\text{Br}^{82}$ reactions.

We studied the systems listed in Table I with particular attention given to experimental parameters. The detailed experimental procedures and equipment used were described previously.⁵ All thermal neutron irradiations were performed at a flux of 10^{11} n. cm.⁻² sec.⁻¹ in the Triga reactor at the Omaha, Neb., V. A. Hospital. One-milliliter samples were frozen by immersing in liquid nitrogen, resulting in opaque crystalline solids in the saturated hydrocarbon- Br_2 and CCl_4 - Br_2 mixtures, and glasses in the alkyl bromides. All samples were irradiated for 3 sec. in the frozen state.

Unusual and totally unexpected results were that neither $\text{Br}^{80\text{m}}$ nor Br^{82} organic retentions were over 1% in saturated C_6 hydrocarbons and CCl_4 when the samples were kept frozen and extracted directly from the frozen state into organic and inorganic phases (Table I). When the samples were melted and maintained at 25° for 10 min. immediately following irradiation, Br^{82} organic retentions increased markedly while those of $\text{Br}^{80\text{m}}$ remained below 1%. When samples were kept frozen for 5 hr. after irradiation (allowing decay of $\text{Br}^{82\text{m}}$ before thawing) and then thawed and left at 25° for 10 min., both $\text{Br}^{80\text{m}}$ and Br^{82} organic retentions remained below 1%. Similar experiments showed that Br^{80} (18 min.) in cyclohexane acted exactly as $\text{Br}^{80\text{m}}$.

In the alkyl halides studied (Table I), $\text{Br}^{80\text{m}}$ and Br^{82} organic retentions were finite in the pure systems and decreased when Br_2 scavenger was added. An isotope separation was noted in the solid systems with Br^{82} organic retentions being greater than those of $\text{Br}^{80\text{m}}$. However, when the samples were melted immediately after irradiation (as described above) $\text{Br}^{80\text{m}}$ organic retentions remained constant while those of Br^{82} were lowered. When the samples were kept frozen 5 hr. following irradiation, before melting, Br^{82} organic retentions remained constant.

Thermal reactions were shown not to produce a change in organic retentions, as noted by the constancy of $\text{Br}^{80\text{m}}$ retentions while Br^{82} retentions changed. Since the changes in Br^{82} organic retentions only occurred when samples were liquefied *immediately* after irradiation, we conclude that the $\text{Br}^{82\text{m}}(\text{IT})\text{Br}^{82}$ reaction produced Br^{82} retention changes. It is interesting that $\text{Br}^{82\text{m}}(\text{IT})\text{Br}^{82}$ reactions did not cause any chemical reactions in the frozen state.

Obviously, $\text{Br}^{80\text{m}}$ and Br^{82} isotope separations (or lack of them) in liquid organic systems may partially

Table I: Organic Retentions^a of $\text{Br}^{80\text{m}}$ and Br^{82} in Solid Saturated Hydrocarbons and Alkyl Halides Produced in 3-Sec. Thermal Neutron Irradiations at -196°

	Mole fraction of Br_2	—Av. organic retention, %—			
		Frozen after irradiation ^b		Thawed after irradiation ^c	
		$\text{Br}^{80\text{m}}$	Br^{82}	$\text{Br}^{80\text{m}}$	Br^{82}
$c\text{-C}_6\text{H}_{12}$	0.137	0.6	0.6	0.6	7
$\text{CH}_3(\text{CH}_2)_4\text{CH}_3$	0.096	0.7	0.7	0.7	12
$(\text{CH}_2)_3\text{CCH}_2\text{CH}_3$	0.120	0.3	0.3	0.3	12
$(\text{CH}_2)_2\text{CHCH}(\text{CH}_3)_2$	0.106	0.6	0.6	0.6	8
$\text{CH}_3\text{CH}_2\text{CH}(\text{CH}_3)\text{-CH}_2\text{CH}_3$	0.107	0.8	0.8	0.8	10
$(\text{CH}_3)_2\text{CHCH}_2\text{CH}_2\text{CH}_3$	0.074	0.7	0.8	0.7	10
CCl_4	0.172	1.0	1.0	1.0	19
CCl_3Br	...	74	85	74	75
CCl_2Br	0.179	43	57	43	40
$\text{CH}_3\text{CH}_2\text{CH}_2\text{Br}$...	63	80	63	64
$\text{CH}_3\text{CH}_2\text{CH}_2\text{Br}$	0.164	26	36	26	25
$\text{CH}_3\text{CH}_2\text{Br}$...	61	79	61	48
$\text{CH}_3\text{CH}_2\text{Br}$	0.140	39	53	39	25

^a Maximum experimental error was ± 0.5 . ^b Samples were stored under liquid nitrogen before and after irradiation. They were melted into the extraction mixture while extracting. ^c Samples were thawed immediately after irradiation and brought to 25° for 10 min. before extraction.

result from $\text{Br}^{82\text{m}}$ isomeric transition reactions. The combination of the short half-life of $\text{Br}^{82\text{m}}$ (5-6 min.) and relatively long half-life of Br^{82} (35.9 hr.) makes it impossible to obtain, directly, absolute data for $\text{Br}^{81}(\text{n},\gamma)\text{Br}^{82}$ and $\text{Br}^{81}(\text{n},\gamma)\text{Br}^{82\text{m}}$ activated reactions. The $\text{Br}^{82\text{m}}$ isomeric transition activated reactions must be prevented or evaluated to obtain data for the (n,γ) activated reactions. In the case of $\text{Br}^{80\text{m}}$ data, one can eliminate contributions from $\text{Br}^{80\text{m}}$ isomeric transition reactions by proper counting techniques.⁵ The magnitude of observed isotope separations should be a function of the time of irradiation and time between irradiation and extraction. Even in solid systems this reaction may affect isotope separations when samples are thawed before the $\text{Br}^{82\text{m}}$ has decayed.

Acknowledgment. This work was supported by the Minnesota Mining and Manufacturing Company through a research fellowship.

- (4) (a) F. S. Rowland and W. F. Libby, *J. Chem. Phys.*, **21**, 1495 (1953); (b) M. S. Fox and W. F. Libby, *ibid.*, **20**, 487 (1952); (c) J. C. W. Chien and J. E. Willard, *J. Am. Chem. Soc.*, **76**, 4735 (1954); (d) R. H. Schuler and C. E. McCauley, *ibid.*, **79**, 821 (1957).
 (5) J. A. Merrigan and E. P. Rack, *J. Phys. Chem.*, **69**, 2795 (1965).

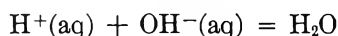
DEPARTMENT OF CHEMISTRY
 UNIVERSITY OF NEBRASKA
 LINCOLN, NEBRASKA

JOSEPH ANDREW MERRIGAN
 EDWARD PAUL RACK

RECEIVED JUNE 10, 1965

The Volume Change on Neutralization of Strong Acids and Bases

Sir: We recently reported¹ a limiting apparent molal volume of $-5.25 \text{ ml. mole}^{-1}$ for aqueous sodium hydroxide at 25° . From this value and those for hydrochloric acid and sodium chloride given by Harned and Owen² we obtained a volume change at zero ionic concentration of 21.86 (sign error in ref. 1) ml. mole^{-1} for the reaction



Dr. Redlich has kindly pointed out³ that the limiting value for the apparent molar volume for hydrochloric acid listed in ref. 2 is based on an incorrect extrapolation to zero concentration. Accordingly, we have re-determined apparent molal volumes of hydrochloric acid at five concentrations from 0.002 to 0.024 M by the dilatometric method.¹ The results confirm the theoretical limiting slope⁴ and extrapolate to $\phi_v^\circ(\text{HCl}) = 17.82 \pm 0.02 \text{ ml. mole}^{-1}$. Our results are in excellent agreement with the earlier work of Redlich and Bigeleisen,⁵ but are not in agreement with the results of Geffcken and Wirth or the ϕ_v° values (18.20 and 18.07) quoted by Harned and Owen² that are based on extrapolations with limiting slopes considerably smaller than the theoretical slope.

Combination of $\phi_v^\circ(\text{HCl}) = 17.82 \text{ ml. mole}^{-1}$, $\phi_v^\circ(\text{NaOH}) = -5.25 \text{ ml. mole}^{-1}$ from our previous work,¹ $\phi_v^\circ(\text{NaCl}) = 16.61 \text{ ml. mole}^{-1}$ from the work of Kruis⁶ (obtained by extrapolation based on the correct limiting slope), and the molar volume of water leads to $\Delta V^\circ = 22.11 \text{ ml. mole}^{-1}$ for the neutralization reaction represented above. The change from our previous value arises entirely from the revision in $\phi_v^\circ(\text{HCl})$ from the values reported by Harned and Owen.²

(1) L. G. Hepler, J. M. Stokes, and R. H. Stokes, *Trans. Faraday Soc.*, **61**, 20 (1965).

(2) H. S. Harned and B. B. Owen, "The Physical Chemistry of Electrolytic Solutions, 3rd Ed., Reinhold Publishing Corp., New York, N. Y., 1958, p. 361.

(3) O. Redlich, personal communication to L. G. H., 1965.

(4) O. Redlich and D. M. Meyer, *Chem. Rev.*, **64**, 221 (1964).

(5) O. Redlich and J. Bigeleisen, *J. Am. Chem. Soc.*, **64**, 758 (1942).

(6) A. Kruis, *Z. physik. Chem.*, **34B**, 1 (1936).

PHYSICAL CHEMISTRY DEPARTMENT
UNIVERSITY OF NEW ENGLAND
ARMIDALE, N.S.W., AUSTRALIA

L. A. DUNN
R. H. STOKES

DEPARTMENT OF CHEMISTRY
CARNEGIE INSTITUTE OF TECHNOLOGY
PITTSBURGH, PENNSYLVANIA

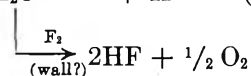
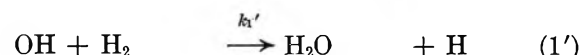
L. G. HEPLER

RECEIVED JUNE 14, 1965

A Suggested Mechanism for the Hydrogen-Fluorine Reaction. II. The Oxygen-Inhibited Reaction

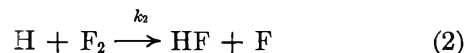
Sir: Recently, Levy and Copeland have studied the rate of reaction between hydrogen and fluorine, first in a flow system diluted with nitrogen¹ and secondly in a static system, in the presence of oxygen² in the temperature range $122\text{--}162^\circ$. A previous communication³ suggested a mechanism for reaction in the absence of oxygen; the present communication indicates how that mechanism can be expanded to describe the oxygen-inhibited reaction.

Levy and Copeland² found that small amounts of oxygen greatly decrease the reaction rate but that soon the rate reaches a limiting value and is unaffected by further oxygen addition. The limiting rate was found to be approximately proportional to the fluorine concentration and the square root of the hydrogen concentration. This result can be explained by the reactions



The numbering of the last three reactions, indicated by primes, conforms to the numbering frequently used for these hydrogen-oxygen chain reaction steps.⁴

When small amounts of oxygen are added to hydrogen-fluorine mixtures, reaction 6 competes with the step



At large oxygen concentrations reaction 2 is over-

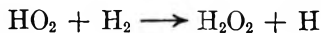
(1) J. B. Levy and B. K. W. Copeland, *J. Phys. Chem.*, **67**, 2156 (1963).

(2) J. B. Levy and B. K. W. Copeland, *ibid.*, **69**, 408 (1965).

(3) R. S. Brokaw, *ibid.*, **69**, 2488 (1965).

(4) B. Lewis and G. Von Elbe, "Combustion, Flames, and Explosions of Gases," Academic Press Inc., New York, N. Y., 1951.

whelmed. Reaction 6 is well known from studies of the hydrogen-oxygen reaction; it inhibits so that hydrogen and oxygen will not combine at atmospheric pressure and temperatures much below 500°, except in the presence of a suitable catalyst. Although the HO₂ radical is sufficiently stable that it inhibits hydrogen-oxygen below ~500°, at higher temperatures chains may be continued through the slow reaction



Since the hydrogen-fluorine reaction continues, albeit at a reduced rate, it seems reasonable that HO₂ must react with fluorine, as in reaction 7. Reaction 8 is a reasonable bimolecular chain-termination step, while reactions 2', 3', and 1' are familiar links from the hydrogen-oxygen branched chain. (Reactions 1', 2', and 3' must be included to account for the fact that in the presence of a large amount of oxygen the reaction rate is independent of oxygen concentration.) Water is not detected as a reaction product since it further reacts to yield HF and oxygen.⁵

By applying the steady-state approximation to the concentrations of hydrogen, fluorine, and oxygen atoms and also the OH and HO₂ radicals and remembering that $k_6[M_{(6)}] \gg k_2'$, the following rate expression is obtained

$$\frac{d[\text{HF}]}{dt} \cong 2 \frac{k_1 k_2' k_7}{k_6 k_8} \frac{[\text{H}_2][\text{F}_2]}{[M_{(6)}]}$$

Actually the various third-body efficiencies in reaction 6 should be considered

$$k_6[M_{(6)}] = k_{6,\text{H}_2}([\text{H}_2] + 0.43[\text{N}_2] + 0.35[\text{O}_2] + f_{\text{F}_2}[\text{F}_2] + f_{\text{HF}}[\text{HF}])$$

Here f_{F_2} and f_{HF} are the third-body efficiencies of F₂ and HF relative to hydrogen (the efficiencies for nitrogen and oxygen are from Lewis and Von Elbe⁴). We might guess that $f_{\text{F}_2} \sim 0.3$ (by analogy with nitrogen and oxygen); based on this assumption an analysis of the data of Levy and Copeland's² Figure 3 indicates that $f_{\text{HF}} \sim 1$. Thus, the mechanism predicts a rate proportional to about the first power of the fluorine concentration and a somewhat lower order with respect to hydrogen. An over-all rate constant can be obtained by equating the theoretical rate expression with the empirical formula of Levy and Copeland

$$k_{\text{over-all}} = \frac{k_1 k_2' k_7}{k_6 k_8} = k_{1/2} \frac{[\text{H}_2] + 0.43[\text{N}_2] + 0.35[\text{O}_2]}{[\text{H}_2]^{1/2}}$$

Values so calculated are shown in Table I. The over-all rate constants show slightly less variation, percentage-wise, than the empirical 1.5-order rate constants.

Table I: Rate Constants for the Hydrogen-Fluorine Reaction at 132°^a

Initial mole fractions				Rate constants	
F ₂	H ₂	O ₂	N ₂	$k_{1/2}$, a.u. ^{-1/2} min. ⁻¹ (ref. 2)	$k_{\text{over-all}}$, min. ⁻¹
0.032	0.032	0.794	0.142	0.14	0.38
0.066	0.066	0.659	0.209	0.14	0.28
0.129	0.129	0.659	0.084	0.14	0.22
0.066	0.132	0.659	0.143	0.16	0.25
0.132	0.066	0.659	0.143	0.15	0.29
0.066	0.264	0.659	0.011	0.18	0.23
0.066	0.396	0.527	0.011	0.20	0.24
0.066	0.527	0.396	0.011	0.26	0.31
				Av. 0.17 ± 0.03	0.27 ± 0.04

^a Total pressure 695 torr; from Table III of ref. 2.

In summary, the mechanism proposed here seems to provide an adequate description of the oxygen-inhibited reaction between hydrogen and fluorine. The experimental data for smaller oxygen additions can perhaps help to elucidate further the combination of the mechanisms set forth here and in the preceding communication.³

(5) V. A. Slabey and E. A. Fletcher, N.A.C.A. Technical Note 4374, Sept. 1958.

LEWIS RESEARCH CENTER
NATIONAL AERONAUTICS AND SPACE
ADMINISTRATION
CLEVELAND, OHIO 44135

RICHARD S. BROKAW

RECEIVED JUNE 22, 1965

Parachor and Surface Tension of Amorphous Polymers

Sir: Knowledge of the surface tension of polymers is of interest, on the one hand, as a means of elucidating the nature of the bulk and surface structure of polymeric liquids¹ and, on the other hand, because of its controlling influence on such practical applications of polymers as spinning, adhesion, and stability of dispersions. The critical surface tension γ_c of wetting of solid polymers, obtainable from contact angle data by a procedure proposed by Zisman,² has often been employed as an estimate of the surface free energy of polymers, but there always remained the question of the precise relation between γ_c and the true surface free energy. For this reason, there has recently been a growing interest

(1) H. W. Starkweather, Jr., *SPE Trans.*, 5, 5 (1965).

(2) W. A. Zisman, "Advances in Chemistry Series," No. 43, American Chemical Society, Washington, D. C., 1964, p. 1.

Table I: Parachor and Surface Tension of Polymers

Polymer	γ at 150°, dynes/cm.	$-d\gamma/dT$	γ at 20° (extrapolated)	Parachor/repeat unit	Parachor/ mol. wt.	d at 20°, g./cm. ³	γ at 20° (calcd.)
Poly(ethylene oxide)	33.2	0.073	42.8	99.8	2.265	1.142	44.7
Linear Polyethylene	28.3	0.053	35.3	80.0	2.852	0.855	35.4
Atactic polypropylene	22.1	0.056	29.6	116.3	2.764	0.861	32.0
Poly(dimethyl)siloxane	13.6	0.055	20.6	154.4	2.082	0.975	17.0

in direct measurements of surface tension of amorphous (or molten) polymers.^{3,4} We have now developed a method of measuring the surface tension of highly viscous polymers by a further refinement⁵ of the pendant drop method⁶ and have determined the values of the surface tension of a number of polymers as a function of temperature. Full details of the results and the experimental procedures will be published elsewhere. In this communication we report the finding that the parachor can be a useful means of estimating surface tensions of not only ordinary low molecular weight liquids but probably also of polymers.

In Table I, columns 2-4 summarize our surface tension measurements on four polymers. The polyethylene oxide is Union Carbide's Carbowax 6000, purified by extraction with ethyl ether; the linear polyethylene is Alathon 7050 of melt index 20; the polypropylene is the atactic fraction, melt index 1000, extracted from isotactic polypropylene; the crystallinity of the atactic fraction is estimated to be about 5% (m.p. 156°); and the poly(dimethyl)siloxane is the Dow Corning Silicone 200 fluid of viscosity 10⁶ centistokes. The values of parachor per repeat unit given in the table were computed by use of the atomic parachor values recommended by Quayle⁷: 9.0 for C, 15.5 for H, 19.8 for O, 31 for Si, and -3.7 for a branching point. The density values at 20° given in the seventh column were obtained by extrapolating the liquid density from above the melting point. The surface tension γ in dynes per centimeter was calculated from the parachor P by

$$\gamma = (Pd/M)^4 \quad (1)$$

where M is the molecular weight and d is the density in g./cm.³. The calculated values of γ are very sensitive to errors in P and d since γ depends on the fourth

power of these two quantities. Yet the agreement between the calculated γ values and the values obtained by extrapolation of experimental data to 20° is entirely satisfactory. Another interesting observation is that the ratio F/M for poly(ethylene oxide) is lower than for polyethylene and polypropylene, and therefore the higher surface tension for the former polymer arises solely from its higher density. In fact, the density of a liquid is an important parameter determining its surface tension, as manifested in such empirical relationships as McLeod's equation. For example, the ratio P/M for *n*-hexane is 3.144, and yet its surface tension at 20° is 18.4 dynes/cm., much lower than that of polyethylene, because of its lower density—0.659 as compared to 0.855 g./cm.³ for the latter. Similarly,⁴ the much lower temperature coefficients, $-d\gamma/dT$, observed for all the polymers studied here, as compared to those of ordinary liquids, appear to arise largely from the lower thermal expansion coefficients of polymer and only to a lesser extent from the difference in the conformational freedoms of polymer segments at the surface and in the bulk.¹

(3) R. E. Johnson, Jr., and R. H. Dettre, presented at the Gordon Research Conference on Adhesion, New Hampton, N. H., Sept. 1964.

(4) (a) H. Schonhorn and L. H. Sharpe, *J. Polymer Sci.*, **3A**, 569 (1965); (b) *Polymer Letters*, **3**, 235 (1965).

(5) R.-J. Roe and V. L. Bacchetta, to be published.

(6) J. M. Andreas, E. A. Hauser, and W. A. Tucker, *J. Phys. Chem.*, **42**, 1001 (1938); E. Fordham, *Proc. Roy. Soc. (London)*, **A194**, 1 (1948); D. O. Niederhauser and F. E. Bartell, "Fundamental Research on Occurrence and Recovery of Petroleum, 1948-1949," American Petroleum Institute, Baltimore, Md., 1950, p. 114.

(7) O. R. Quayle, *Chem. Rev.*, **53**, 439 (1953).

ELECTROCHEMICALS DEPARTMENT
E. I. DU PONT DE NEMOURS & CO., INC.
NIAGARA FALLS, NEW YORK

RYONG-JOON ROE

RECEIVED JUNE 28, 1965